
**Towards a new Lateglacial to early Holocene varve
chronology for the Swedish Timescale using
microfacies analysis and tephrochronology**



Rachel Mary Devine

**Submitted in accordance with the requirement for the degree of
Doctor of Philosophy**

Royal Holloway, University of London

December 2019

Declaration of Authorship

I, Rachel Devine, hereby declare that this thesis and the work presented in it is entirely my own. Where I have consulted the work of others, this is always clearly stated.

Signed: _____

Date: _____

Acknowledgements

First of all, I would like to thank my supervisors Adrian Palmer, Ian Matthews, Alison McLeod and Stefan Wastegård. Their unwavering support throughout the entire PhD has been incredible, especially during these final few months (and days!).

I am also incredibly grateful to the London NERC DTP for providing me with the opportunity to undertake this PhD, and NERC for funding the project. I am also extremely grateful to Miros Charidemou, Millie Watts and Suzanne Maclachlan at the BOSCORF Laboratory, National Oceanography Centre, Southampton, for scanning all of the cores from this thesis on the Itrax Core Scanner. I would also like to thank Chris Hayward at the Tephra Analysis Unit, University of Edinburgh for help with tephra analysis.

Thank you to Lars Brunnberg for providing the original varve count data for the Östergötland varve chronology and for help with site selection...you were right about tephra in Asplången! I will always remember your support, kind words and eagerness to help in any way possible, especially our many discussions in the Swedish Varve Museum. I am also grateful to Bö Strömberg for help and support in the early phase of this PhD and for the interesting discussions about the Swedish Timescale.

I would like to thank the staff and students at Royal Holloway, University of London for help with laboratory work and production of specialist reports. In particular: Katy Flowers for help with tephra preparation; Poppy Harding-Blockley for production of diatom slides, identification, analysis and specialist summary report; Chris Francis for chironomid preparation and identification; Marta Perez-Fernandez for macrofossil preparation, identification and specialist summary report, and; Joanna Tindall for ostracod identification.

Finally, I would like to thank my family and friends for their unwavering support throughout the past 5 years. Mum, Dad and Michael, you are devoted and selfless in your support and I could not have done this without you. Dad, you were the best fieldwork assistant and we had such an incredible time. What an adventure! We made so many memories that I will never forget. The pizza, porridge and hut dancing were personal highlights, oh and the science too!

I also thank Rebecca Smith and David Arnold for your help on fieldwork in July 2016 and for your constant support. You bring a new meaning to the word 'friend'. To Lizzy Peneycad and Julian Martin thank you for being great housemates and for your friendship. Ash Abrook and Chris Francis thank you for being great friends and letting me stay with you in the final few months, and Chris for that last minute lift to

Southampton when my car broke down! To Joshua Pike, Jacob Bendle and Celia Martin-Puertas for the many varve and thin section chats, and Kristy Holder for the many phone calls, you have been a constant support. I'd also like to thank Dorothy Weston and Alice Carter-Champion for your companionship in the early hours on the probe in Edinburgh and for your friendship over the last 7 years at Royal Holloway.

Tom, thank you for your support, you are the best. I can't wait to be your wife.



For Lasse Brunberg

Abstract

The Swedish Timescale (STS) is a composite varve chronology that spans the last ca 14,000 years and comprises over 1,000 individual varve thickness records. It has primarily been used to reconstruct the deglaciation of the Fennoscandian Ice Sheet but has also been used to derive age estimates for Baltic Ice Lake drainage events. Several researchers have suggested that there may be up to 900 varve years missing during the Lateglacial and Holocene periods. This research presents the results of microfacies analysis and tephrochronology from three sites in Östergötland to test the existing regional varve chronology and timing of deglaciation.

Comparison between macro and microscale analyses of varves indicate that the analytical precision of μ XRF, X-radiograph and macroscale sedimentology do not allow for accurate characterisation of sediments. Up to 40% more varves were identified under thin section than from macroscale counts which is the traditional means of varve analysis within the STS. Microfacies analysis enabled reconstruction of local sediment processes that are fundamental for the construction of accurate varve chronologies. These results suggest that there may be fundamental flaws within the STS that stem from a lack of detailed sediment descriptions and sediment process information.

The identification of tephra at all three sites demonstrates the potential to independently correlate and date varve records within the STS. Bayesian age modelling integrates the varve count data and tephra ages and has: 1) enabled more precise age estimates of the tephra; 2) anchored the varve chronologies to a calendar-year timescale; and 3) provided calendar year estimates for deglaciation. The identification of the Askja-S tephra within glacial varves at Asplången indicates that the site became ice-free around $11,044 \pm 43$ cal. yrs BP which is in disagreement with the published Younger Dryas age for site deglaciation. Critically, this suggests that the Baltic Ice Lake existed during the early Holocene. The presence of proximal varves in Östergötland during the early Holocene suggests that the ice margin was in the Middle Swedish End Moraine Zone at its pre-drainage position at Mt Billingen during this time. Therefore, it is proposed that the final drainage of the Baltic Ice Lake occurred sometime after $11,044 \pm 43$ cal. yrs BP. These results do not support the current timing for the final Baltic Ice Lake drainage which at present is dated to the Younger Dryas-Preboreal transition ca 11,500 cal. yrs BP. If this inference is correct, the final Baltic Ice Lake drainage may have impacted early Holocene climatic cooling events.

Table of Contents

Chapter 1. Introduction.....	22
1.1 Quaternary climate change.....	22
1.2 The Last Glacial to Interglacial Transition (LGIT) in the North Atlantic	23
1.3 Synchronising climate records during the LGIT	26
1.4 Varve records and the Swedish Timescale.....	27
1.5 Research Aims	29
1.6 Research Objectives	30
1.7 Thesis structure.....	30
Chapter 2. North Atlantic Climate and the Fennoscandian Ice Sheet	32
2.1 Introduction	32
2.1.1 Driving mechanisms of North Atlantic climate	32
2.1.2 Phasing of palaeoclimatic events across the North Atlantic during the LGIT.....	34
2.1.3 Summary	37
2.2 The Fennoscandian Ice Sheet (FIS).....	38
2.2.1 Geomorphological evidence	38
2.2.2 Lithostratigraphic evidence	42
2.2.3 Biostratigraphic evidence.....	42
2.2.4 Chronostratigraphic evidence	42
2.3 Deglaciation chronology	52
2.3.1 24-16 ka BP.....	52
2.3.2 16-14 cal. ka BP	55
2.3.3 14-12.7 cal. ka BP	56
2.3.4 12.9-11.7 ka BP.....	59
2.3.5 Baltic Ice Lake (BIL) drainage events.....	65
2.3.6 Yoldia Sea Stage 11.7-10.7 ka BP.....	66
2.3.7 Ancylus Lake stage 10.7-9.8 ka BP	67
2.4 Summary.....	68
Chapter 3. The Swedish Timescale.....	69
3.1 Overview	69
3.2 Origins and early construction	70
3.2.1 Varve composition and thickness measurements	72

3.2.2	Composite chronology structure	73
3.2.3	Early applications.....	75
3.3	Revising and extending the Swedish Timescale	76
3.3.1	Postglacial chronology	77
3.3.2	Finiglacial chronology	77
3.3.3	Gotiglacial chronology.....	79
3.4	Efforts to date the STS	83
3.4.1	Radiocarbon dating.....	83
3.4.2	Synchronisation with ice-core records.....	84
3.4.3	Tephrochronology.....	85
3.5	Current state of play	87
Chapter 4.	Glaciolacustrine varves.....	92
4.1	Introduction	92
4.2	Glaciolacustrine varve processes	93
4.2.1	Sediment transport	93
4.2.2	Temporal controls on sediment transport.....	95
4.2.3	Depositional processes.....	95
4.2.4	Other glaciolacustrine processes and structures.....	96
4.3	Glaciolacustrine varve structures.....	98
4.3.1	Proximal varves	98
4.3.2	Distal varves	100
4.3.3	Spatial distribution of varved sediments.....	102
4.3.4	Summary of varve structures	103
4.4	Varve analytical techniques	105
4.4.1	Macroscale sedimentology	105
4.4.2	Particle size analysis	105
4.4.3	Digital image analysis	106
4.4.4	X-ray radiography	107
4.4.5	μ XRF analysis	108
4.4.6	Microfacies analysis.....	110
4.4.7	Micro-CT scanning.....	114
4.5	Varve chronology development	114
4.5.1	Error estimation	115
4.6	Tephra analysis.....	116
4.6.1	Application in varve research.....	116
4.7	Summary.....	117

Chapter 5. Methodology	118
5.1 Introduction	118
5.2 Site selection	119
5.2.1 Regional Geology	123
5.2.2 Svinstadsjön location	125
5.2.3 Asplången location and background	125
5.2.4 Glottern location and background	125
5.3 Field methods.....	127
5.3.1 Sediment depth sounding and bathymetric surveys	127
5.3.2 Sediment extraction	128
5.4 Macroscale sedimentological methods	130
5.4.1 Sediment description	130
5.4.2 Sediment imaging.....	130
5.4.3 Macroscale varve analysis from core surface	130
5.4.4 Particle size analysis	131
5.5 Microscale sedimentological methods	132
5.5.1 X-ray radiography	132
5.5.2 Micro-XRF core scanning	135
5.5.3 Thin section production.....	137
5.6 Geochronological methods	141
5.6.1 Constructing site varve chronologies	141
5.6.2 Tephrochronology.....	141
5.6.3 Geochemical analysis (EPMA).....	144
5.7 Statistical Analyses	144
5.7.1 Bayesian Age Modelling	144
5.8 Palaeoecological proxies.....	146
5.8.1 Diatom preparation	146
5.8.2 Plant macrofossil, ostracod and chironomid preparation	147
5.9 Summary.....	147
Chapter 6. Results - Svinstadsjön	149
6.1 Core recovery and basin survey	151
6.2 Macroscale sedimentology and stratigraphy	153
6.2.1 Sediment units.....	153
6.2.2 Sedimentology of laminated couplets in LF1-3.....	157
6.2.3 Interpretation of varve formation	160
6.2.4 Non-varved sediments	161

6.2.5	Varve ^{MAC} chronology	161
6.3	X-radiograph image analysis	164
6.3.1	Description of X-radiograph images	164
6.3.2	Varve ^{XRAD} chronology	166
6.4	μXRF analysis	170
6.4.1	Pre-analysis data treatment	170
6.4.2	Multivariate analysis and grain size estimation	170
6.4.3	Varve ^{XRF} chronology	174
6.5	Thin section analysis	177
6.5.1	Microscale description of the laminated sediments in LF1-3	177
6.5.2	Deformation structures	183
6.5.3	Sediment process interpretation for the Lamination Sets	184
6.5.4	Interpretation of the Lamination Sets as glaciolacustrine varves	185
6.5.5	Varve ^{TSA} chronology	186
6.6	Synthesis of varve identification and counting methods	190
6.6.1	Differences in varve texture	190
6.6.2	Differences in varve structure	191
6.6.3	Differences between description of non-varved sediments	193
6.6.4	Varve count differences between methods	193
6.6.5	Summary and revised protocol for varve identification and counting	196
Chapter 7.	Results - Asplången	197
7.1	Core recovery and basin survey	197
7.2	Macroscale sedimentology and stratigraphy	199
7.2.1	Sediment units	199
7.3	Sedimentology of laminations in LF1 and LF2	202
7.3.1	Lamination Types and Lamination Sets	203
7.3.2	Deformation structures	205
7.3.3	Sediment process interpretation for the Lamination Sets	205
7.3.4	Interpretation of the Lamination Sets as varves	209
7.4	Palaeoecological proxies	209
7.4.1	Summary of palaeoecological proxy results	209
7.5	Varve ^{TSA} chronology	212
7.6	Summary	215

Chapter 8. Results - Glottern.....	216
8.1 Core recovery and basin survey	216
8.2 Macro and microscale sedimentology and stratigraphy	218
8.2.1 Sediment units.....	218
8.2.2 Sedimentology of laminated couplets (LF1 and LF2)	220
8.2.3 Lamination Types and Lamination Sets	221
8.2.4 Deformation structures.....	223
8.2.5 Sediment process interpretation for the Lamination Sets	223
8.2.6 Deformation zones.....	225
8.2.7 Interpretation of the Lamination Sets as varves	230
8.3 Varve ^{TSA} chronology	230
8.4 Summary.....	233
Chapter 9. Tephra results.....	234
9.1 Svinstadsjön tephrostratigraphy	234
9.2 Svinstadsjön tephra classification	236
9.3 Asplången tephrostratigraphy.....	236
9.3.1 ASP 1160	236
9.3.2 Samples from 510-540 cm.....	236
9.3.3 ASP 537 and ASP 536.....	237
9.3.4 ASP 530	237
9.3.5 ASP 524	237
9.3.6 ASP 516	237
9.3.7 ASP 410 and ASP 402.....	237
9.4 Asplången tephra classification	242
9.4.1 ASP 1160	243
9.4.2 ASP 537 and ASP 536.....	243
9.4.3 ASP 530 and ASP 524.....	243
9.4.4 ASP 516	243
9.4.5 ASP 410	243
9.4.6 ASP 402	243
9.5 Glottern tephrostratigraphy	244
9.5.1 GLO 304 and GLO 305.....	244
9.6 Glottern tephra classification	248
9.6.1 GLO 304 and GLO 305.....	249
9.7 Tephra correlations	249
9.7.1 Correlations within and between sites.....	249

9.7.2 Correlations to known tephras	251
9.8 Implications for published tephra ages	264
9.9 Chapter summary.....	265
Chapter 10. Bayesian age modelling	267
10.1 Introduction	267
10.2 Data selection.....	267
10.3 Model assumptions	269
10.4 Model 1 – Asplången.....	270
10.4.1 Model 1 input	270
10.4.2 Model 1 output	272
10.5 Model 2 – Svinstadsjön	275
10.5.1 Model 2 input	275
10.5.2 Model 2 output	278
10.6 Summary.....	279
Chapter 11. Discussion	282
11.1 Introduction	282
11.2 Microfacies analysis	282
11.2.1 Lamination Types.....	283
11.2.2 Lamination Sets	285
11.2.3 Lamination Set Assemblages.....	285
11.2.4 Comparisons between sites	289
11.2.5 Comparisons with Ringberg and Erlström (1999)	293
11.2.6 Implications for constructing a composite varve chronology.....	295
11.3 Comparison of the varve records in this thesis with the existing varve records	296
11.3.1 Glottern	296
11.3.2 Asplången.....	299
11.3.3 Summary	303
11.4 Assessing the correlation between the Svinstadsjön and Asplången varve records.....	304
11.4.1 Summary	306
11.5 Tephrochronology	306
11.5.1 Bayesian age modelling of tephras	307
11.5.2 Absolute dating of varve sequences.....	308
11.5.3 Tephra and varve thickness correlations in this thesis.....	312

11.6	Deglaciation chronology and timing of BIL drainage	315
11.6.1	Overview of the final BIL drainage.....	315
11.6.2	Lithostratigraphic evidence.....	317
11.6.3	Dating the final BIL drainage	323
11.6.4	Pollen analysis and synchronisation of varve and GRIP ice-core records.....	324
11.6.5	Implications for the deglaciation chronology in Östergötland.....	331
11.6.6	Proposed timing of final BIL drainage.....	332
11.6.7	Potential implications for the Yoldia Sea dates.....	335
11.6.8	Comparison with existing deglaciation chronology	337
11.6.9	Early Holocene climatic events.....	342
11.7	Summary.....	342
Chapter 12.	Conclusions	346
12.1	Introduction	346
12.2	Key findings.....	346
12.3	Ideas for future work:.....	351
12.3.1	Target area 1 – Refining the absolute chronology and identifying the ‘missing’ years in the STS (12.5 to 11 ka) using the northern Kristiansson (1986) varve records.....	352
12.3.2	Target area 2 – Extending the ‘known’ tephra lattice in varve records from sites north of Asplången (<11 ka).....	353
12.3.3	Target area 3 – Constraining the timing of changes in state of the BIL from varve records in the Baltic Proper	353
12.3.4	Target area 4 – Accurate and precise timing of the final BIL drainage using varved sediment records in the MSEMZ	354

Table of Figures

Figure 1-1. The $\delta^{18}\text{O}$ record from the NGRIP Greenland ice-core showing the Lateglacial event stratigraphy and the stratigraphic subdivision of the Lateglacial in Sweden.	25
Figure 2-1. Time-transgressive climatic change during the Younger Dryas.....	34
Figure 2-2. Lateglacial isotherm maps based on chironomid-inferred summer air temperatures.....	35
Figure 2-3. The Fennoscandian Ice Sheet margin during the Younger Dryas.	39
Figure 2-4. Prominent eskers and ice-margin positions of the FIS between 22-10.8 ka BP. From Stroeven et al. (2016) pp. 98.	40
Figure 2-5. Locations of OSL, radiocarbon, and cosmogenic nuclide exposure samples included in the Stroeven et al. (2016) deglaciation chronology.....	43
Figure 2-6. Baltic Ice Lake varve sites.	49
Figure 2-7. Locations of Lateglacial and Holocene tephtras in southern Sweden.	51
Figure 2-8. Major end moraine zones in southern Sweden.	54
Figure 2-9. Map of the MSEMZ in the Mt Billingen area.	63
Figure 2-10. Radiocarbon and OSL ages from the MSEMZ.	64
Figure 2-11. Reconstruction of the area north of Mt Billingen before (A) and after (B) BIL drainage.....	65
Figure 3-1. Geographical distribution of regional varve chronologies in the STS.	70
Figure 3-2. Gerard De Geer demonstrating varved sediments in Essex Junction, US, 1920 (De Geer, 1940).	71
Figure 3-3. Gerard De Geer measuring clay varves in the traditional way at an open section.	73
Figure 3-4. The Swedish Timescale (STS).....	75
Figure 3-5. Attempted varve correlations in Sweden and America.	76
Figure 4-1. Flow types within ice-contact and ice-distal lakes.	94
Figure 4-2. Schematic of deformed varved clay due to push-moraine formation in Gullhammar, Sweden. Modified from Johnson et al. (2019).	97
Figure 4-3. Example of a dropstone with bending of the lowermost and onlap of the uppermost laminations (Devine and Palmer, 2017).	98
Figure 4-4. Ice-proximal varves identified by Ridge et al. (2012).....	99
Figure 4-5. Lamination Set Assemblages proposed by Palmer et al. (2019).	101
Figure 4-6. Schematic of theoretical proximal-distal sediment processes within an ice-contact valley lake.	103

Figure 4-7. Lamination Types proposed by Palmer et al. (2019) pp. 13.	113
Figure 5-1. Site locations in this study.....	120
Figure 5-2. Schematic showing the currently proposed ages of the varve records in this research alongside the Mullsjön and Gropviken records.	122
Figure 5-3. Geological map of Östergötland county in south-eastern Sweden.	124
Figure 5-4. Map of south eastern Sweden showing site locations.	125
Figure 5-5. Sediment core extraction from lake margins in the snow during May 2017 fieldwork. R. Devine and B. Devine.	128
Figure 5-6. Overlapping cores extracted from the Glottern site.	129
Figure 5-7. X-radiograph core preparation.	133
Figure 5-8. X-radiograph image processing in Adobe Photoshop™.	134
Figure 5-9. Example of \geq cm-scale varves in an X-radiograph image and corresponding core surface image.	135
Figure 5-10. Key stages of thin section preparation.	138
Figure 5-11. A revised extraction methodology for cryptotephra.....	143
Figure 6-1. Approach undertaken to evaluate different methods of varve identification and counting.....	150
Figure 6-2. Sediment depth survey result and site map.	152
Figure 6-3. Sediment log, core image and particle size data.	154
Figure 6-4. Core surface images for LF1, LF2, LF3 and LF4.....	155
Figure 6-5. Core surface images and varve ^{MAC} thickness plotted against depth.	163
Figure 6-6. Core surface images, X-radiograph images and particle size data.....	165
Figure 6-7. Examples of anomalously large grains in LF1 and LF2 observed from X-radiographs.	166
Figure 6-8. X-radiograph images and varve ^{XRAD} thickness plotted against depth.	169
Figure 6-9. Principal Component Analysis (PCA) of μ XRF data.	172
Figure 6-10. Core surface images with corresponding X-radiographs and μ XRF In(Ca/Fe) data.	174
Figure 6-11. Varve ^{XRF} thickness record with example μ XRF In(Ca/Fe) plots from LF2 and LF3.	176
Figure 6-12 Lamination Types (LT) and sets (LS) in the Svinstadsjön sequence alongside sediment logs.....	179
Figure 6-13. Deformation structures from LF1 observed under thin section.	183
Figure 6-14. Core surface image, varve ^{TSA} thickness and varve ^{TSA} microfacies ...	188
Figure 6-15. Normalised varve thickness record plotted alongside Varve Quality, Lamination Sets and occurrence of IRD/dropgrains.	189

Figure 6-16. Varve thickness record for each methodology alongside varve counts in each lithofacies unit.	194
Figure 7-1. Asplången sediment depth survey and site map.	198
Figure 7-2. Core image, Sediment log, lithofacies units and particle size data.	201
Figure 7-3. Core surface images from LF1, LF2, LF3 and LF4, particle size data for LF2 and LF3.	202
Figure 7-4. Lamination Types (LT) and sets (LS) in the Svinstadsjön sequence alongside micro sediment logs.	207
Figure 7-5. Normalised varve thickness record plotted alongside Varve Quality and Lamination Sets.	214
Figure 8-1. Site location map and sediment depth survey.	217
Figure 8-2. Core image, sediment log, lithofacies units, and particle size data for Glottern.	219
Figure 8-3. Images of \geq cm-scale laminations in LF1 (A) and $<$ cm-scale laminations in LF2 (B).	220
Figure 8-4. Examples of deformation structures in the Glottern sequence.	225
Figure 8-5. Lamination Types and Lamination Sets observed in the Glottern sequence.	226
Figure 8-6. Normalised varve thickness record plotted alongside Varve Quality, Lamination Sets and occurrence of IRD and deformation.	232
Figure 9-1. Svinstadsjön tephrostratigraphy.	235
Figure 9-2. Asplången tephrostratigraphy.	238
Figure 9-3. Asplången tephra classification.	242
Figure 9-4. Glottern tephrostratigraphy.	245
Figure 9-5. Glottern tephra classification.	248
Figure 9-6. Harker variation plots for the Asplången and Glottern tephras.	250
Figure 9-7. The $\delta^{18}\text{O}$ record and event stratigraphy from the NGRIP for the LGIT (Rasmussen et al., 2006, 2014) alongside key tephras from the Icelandic and Eifel volcanic centres that have been identified across the North Atlantic region. Modified from Timms et al. (2019).	251
Figure 9-8. Harker variation diagrams for rhyolitic Lateglacial-early Holocene tephras and tephras from the Asplången and Glottern sites.	253
Figure 9-9. Asplången tephra chemistry data alongside published data for the Askja-S and early Holocene Borrobol-type tephras.	256
Figure 9-10. Asplången stratigraphic log from 480-1246 cm with identified tephra layers.	257
Figure 9-11. Diagram showing published ages of the Askja-S and Fosen tephras and the Asplången varve record.	259
Figure 9-12. Asplången tephra chemistry data and published data for early Holocene Borrobol-type, Vedde Ash, Suđuroy and AF555 tephras.	261

Figure 9-13. Glottern tephra chemistry data alongside published data for the Askja-S tephra.	263
Figure 10-1. Schematic showing the new ages of the sites in this study alongside the Gropviken and Mullsjön varve records.	268
Figure 10-2. Schematic diagram showing the overlap between the Asplången and Lake Czechowskie varve records.	272
Figure 10-3. Model 1 OxCal output.	274
Figure 10-4. Varve thickness correlation between Svinstadsjön and Asplången.	275
Figure 10-5. Schematic overlap between Asplången and Svinstadsjön varve records.	277
Figure 10-6. Model 2 OxCal output.	279
Figure 10-7. Model 1 and Model 2 output: Asplången and Svinstadsjön varve chronologies presented on a modelled cal. yrs BP timescale.	280
Figure 11-1. Lamination Set Assemblages in this study.	288
Figure 11-2. Lamination Sets and Lamination Set Assemblages in the Glottern sequence.	290
Figure 11-3. Lamination Sets and Lamination Set Assemblages in the Svinstadsjön sequence.	291
Figure 11-4. Lamination Sets and Lamination Set Assemblages in the Asplången sequence.	292
Figure 11-5. Glottern varve chronologies from this study and Wohlfarth et al. (1998).	297
Figure 11-6. Example of a deformation zone observed from the core surface, under X-ray and under thin section.	298
Figure 11-7. Asplången varve thickness record from this study and Brunberg (unpublished).	300
Figure 11-8. Example of varves in Lamination Set A in the Asplången sequence.	301
Figure 11-9. Hypothetical varve correlations using varve thickness wiggle matching (top) and colour changes (bottom).	302
Figure 11-10. Lamination Sets in the Svinstadsjön and Asplången sequences aligned using the link varve (dashed line).	305
Figure 11-11. Schematic of the expected and new ages of the varve chronologies.	309
Figure 11-12. Location of “missing” varves between the Glottern and Svinstadsjön site in relation to the Kristiansson (1986) varve records.	312
Figure 11-13. Hypothesised tephra correlations using varve spacing between Tephra 1 and Tephra 2 in the Svinstadsjön sequence.	314
Figure 11-14. The Lateglacial-Holocene event stratigraphy for eastern middle Sweden.	316

Figure 11-15. Location of sites in this thesis in relation to the BIL drainage and marine ingression ice margin lines (in De Geer years).	318
Figure 11-16. Pollen diagram from the Baltic Proper varve record from Andrén et al. (1999).	325
Figure 11-17. Correlation of the 5-yr mean varve thickness in the northwestern Baltic Proper and the 5-yr mean $\delta^{18}\text{O}$ record from the GRIP ice-core. Modified from Andrén et al. (1999).	326
Figure 11-18. Strömberg (1994) and Brunnberg (1995) ice lines in relation to the sites in this study and Mt Billingen.	331
Figure 11-19. Event stratigraphy for the Lateglacial-Holocene transition in eastern middle Sweden alongside the chronology presented in this thesis. Modified from Björck et al. (2002).	334
Figure 11-20. Deglaciation ages for the Svinstadsjön and Asplången sites proposed in this thesis in comparison to the deglaciation chronology proposed by Stroeven et al. (2016).	337
Figure 11-21. Map of the remaining dates after filtering the Stroeven et al. (2016) dataset.	340
Figure 11-22. Deglaciation ages from the Stroeven et al. (2016) filtered dataset.	341
Figure 12-1. Target areas for future research on the STS.	351

Table of Tables

Table 2-1. Modern radiocarbon ages of seawater in the Bornholm Basin and Øresund area (DeltaR) and error (DeltaR Error).....	46
Table 2-2. Radiocarbon dates from marine molluscs from the Ra and Ås Moraines in Norway.	59
Table 2-3. ¹⁰ Be surface exposure ages from the Salpausselkä I moraine.....	60
Table 2-4. Radiocarbon dates from the MSEMZ from Johnson and Ståhl (2010).	64
Table 3-1. Examples of discrepancies in the varve chronology for specific sections of the STS.....	78
Table 3-2 Varve colour changes and associated depositional environment and chronostratigraphical information. Modified from Björck et al. (2002).	82
Table 3-3. Lake Mullsjön radiocarbon sample data from Wohlfarth et al. (1993).	86
Table 3-4. Summary of the methodologies used to construct the key regional varve chronologies that comprise the Lateglacial and early-Holocene STS.....	90
Table 4-1. Varve structure in ice-proximal varves (Ridge et al., 2012)	99
Table 5-1. Site information from the Glottern sequence.	126
Table 5-2. Boreholes and extracted sediment cores at each site.	129
Table 5-3. Particle size analysis sampling strategy	131
Table 5-4. Varve Quality Index (VQI) criteria.....	140
Table 5-5. Key methodologies that were used for varve identification and counting.	148
Table 6-1. Lithofacies summary displayed from oldest to youngest.	159
Table 6-2. Summary of breaks in varve ^{MAC} sedimentation.....	162
Table 6-3. Summarised varve ^{MAC} thickness characteristics in each lithofacies.....	162
Table 6-4. Summary of breaks in varve ^{XRAD} sedimentation.	167
Table 6-5. Summarised varve ^{XRAD} thickness characteristics in each lithofacies....	168
Table 6-6. Summary of key μ XRF elements and correlation with PC-1.....	171
Table 6-7. Summary of breaks in varve ^{XRF} sedimentation.	175
Table 6-8. Summarised varve ^{XRF} thickness characteristics in each lithofacies.	175
Table 6-9. Sedimentological properties of the Lamination Types (LT) observed in the microfacies of the glaciolacustrine sediments within the Svinstadsjön sequence.	178
Table 6-10. Lamination Sets identified within the Svinstadsjön sequence.....	178
Table 6-11. Lithofacies summary based on macro and microscale analyses.	181

Table 6-12. Summary of breaks in varve ^{TSA} sedimentation.	187
Table 6-13. Summarised varve ^{TSA} thickness characteristics in each lithofacies. ..	188
Table 6-14. Summary of the accuracy of each methodology with respect to varve description, interpretation, and number of varves counted per lithofacies unit.	192
Table 6-15. Varve counts for each methodology per 100 cm.	194
Table 7-1. Sedimentological properties of the Lamination Types (LT) observed in the microfacies of the glaciolacustrine sediments within the Asplången sequence.	203
Table 7-2. Lamination Sets identified within the Svinstadsjön sequence.	204
Table 7-3. Summary of the different laminated lithofacies identified at Asplången including specific attributes, interpretation of sedimentary processes and inferred depositional environment.	208
Table 7-4. Summary of lithofacies attributes, sediment process interpretation and depositional environment for non-laminated lithofacies	211
Table 7-5. Summary of breaks in varve ^{TSA} sedimentation.	212
Table 7-6. Summarised varve thickness characteristics in each lithofacies.	213
Table 8-1. Sedimentological properties of the Lamination Types (LT) observed in the microfacies of the glaciolacustrine sediments within the Glottern sequence.	221
Table 8-2. Lamination Sets identified within the Glottern sequence.	222
Table 8-3. Glottern lithofacies summary including specific attributes, interpretation of sedimentary processes and inferred depositional environment.	228
Table 8-4. Summary of breaks in varve ^{TSA} sedimentation.	231
Table 8-5. Summarised varve thickness characteristics in each lithofacies.	231
Table 9-1. Raw and mean chemical data for Asplången, values expressed as weight % oxide.	239
Table 9-2. Chemical data for GLO 304 and GLO 305, values expressed as weight % oxide.	246
Table 9-3. Summary of the tephra layers identified in the Asplången sediment record	262
Table 10-1. Model 1 output.	273
Table 10-2. Model 2 output.	278
Table 11-1. Sedimentological properties of the Lamination Types (LT) observed in the microfacies of the glaciolacustrine sediments within this study.	284
Table 11-2. Lamination Sets identified within the Glottern, Svinstadsjön and Asplången sequences.	285
Table 11-3. Lamination Sets that were identified at each site.	289
Table 11-4. Microfacies descriptions of Baltic Ice Lake varves by Ringberg and Erlström (1999).	294

Table 11-5. Glottern varve count comparison	297
Table 11-6. Asplången varve counts from this study and Brunnberg.....	299
Table 11-7. Correlation between this study and the Brunnberg Asplången varve chronologies.	301
Table 11-8. Radiocarbon data from the Mullsjön site (Wohlfarth et al., 1993).	309
Table 11-9. Radiocarbon sample information from Glottern. Modified from Wohlfarth et al. (1998).....	311
Table 11-10. Possible correlations for unknown tephra layers in the Svinstadsjön sequence.	313
Table 11-11 Summary of differences between brown and grey varves.	321
Table 11-12. Summary of radiocarbon samples from Brunnberg and Possnert (1992).	335
Table 11-13. Conversion of the STS to cal. yrs BP in Stroven et al. (2016).....	338
Table 11-14. Criteria for selecting deglaciation dates from the Stroeven et al. (2016) dataset.....	339

Chapter 1. Introduction

1.1 Quaternary climate change

The Quaternary, the most recent geological period, spans the last 2.58 Ma and has long been considered the 'Glacial Epoch' (Gibbard *et al.*, 2010). The most distinctive features of the Quaternary are the oscillations between cold (glacial) and warm (interglacial) climatic events (Ruddiman *et al.*, 1988). These cycles are identified in long and relatively undisturbed marine archives which have been used as a global climatic framework of glacial-interglacial cycles (Shackleton and Opdyke, 1973; Lisiecki and Raymo, 2005). The climatic cyclicity identified in marine archives has since been corroborated by the high-resolution analyses of ice-cores from Greenland and Antarctica (Rasmussen *et al.*, 2014). The key driving mechanism of this climatic cyclicity is considered to be due to changes in the Earth's orbital cycles such as the eccentricity (100 ka cycles), the obliquity of the ecliptic (41 ka cycles) and the precession of the equinoxes (21 ka cycles) i.e. the Milankovitch hypothesis (Hays *et al.*, 1976; Imbrie and Imbrie, 1979; Imbrie *et al.*, 1993; Maslin and Ridgwell, 2005). Despite evidence for orbital forcing over long-term climate cycles from marine sediments (Lisiecki and Raymo, 2005), coral reefs (Mesolella *et al.*, 1969; Siddall *et al.*, 2007), loess sequences (Sun *et al.*, 2006, 2015), pollen records (Magri and Tzedakis, 2000; Torres *et al.*, 2013) and ice-cores (Petit *et al.*, 1999), the timing and frequency of glaciations does not consistently coincide with predicted astronomical variations (Ruddiman *et al.*, 1986; Ruddiman, 2006a). It appears that additional elements in the climate system such as greenhouse gases (CO₂, CH₄) (Pisias and Shackleton, 1984; Ruddiman, 2006b), tectonic activity (Ruddiman and Kutzbach, 1991; Ruddiman, 1997), and the complex feedback mechanisms of the ocean-atmosphere-cryosphere realms, amplify the effects of astronomical forcing (Muschitiello *et al.*, 2015).

Superimposed on orbitally-driven cycles are millennial to decadal-scale climatic events often referred to as 'sub-Milankovitch' events (e.g. Bond *et al.*, 1993; Rasmussen *et al.*, 2006; Steffensen *et al.*, 2008). These events are short-lived abrupt climatic transitions that are preserved in a range of climatic archives such as ice-core, marine and terrestrial records (Alley and Ágústsdóttir, 2005; Steffensen *et al.*, 2008; Dokken *et al.*, 2013; Rasmussen *et al.*, 2014) and have enabled further sub-division of the Quaternary into 'stadial' (cold) and 'interstadial' (warm) periods (Blockley *et al.*,

2012; Lowe and Walker, 2015). These events are also referred to as Abrupt Climatic Events (ACEs) and are of particular importance to the palaeoclimate community since they are considered to be ideal analogues for future abrupt climatic change.

1.2 The Last Glacial to Interglacial Transition (LGIT) in the North Atlantic

A key time period for the study of ACEs is the Last Glacial to Interglacial Transition (LGIT) (16-8 ka BP) (Björck *et al.*, 1998; Walker *et al.*, 1999, 2012). In the northern hemisphere, multiple warm and cold events are recorded throughout this period and were most prominently expressed in the North Atlantic region (Björck *et al.*, 1996; Lowe *et al.*, 2008). During the LGIT, two prominent periods of cold climate have been identified; the Oldest Dryas (>14,700 yrs BP) and the Younger Dryas (*ca* 12,900-11,700 yrs BP). The warmer interstadial between these two cold climatic periods is the Bølling-Allerød (*ca* 14,700-12,900 yrs BP) which derives its name from the Scandinavian pollen stratigraphy (Iversen, 1954; Mangerud *et al.*, 1974). The Bølling-Allerød is also interrupted by a short-lived cold climatic period called the Older Dryas (*ca* 13,400-13,200 yrs BP).

Following climatic cooling during the Younger Dryas, warmer climate conditions returned and prevailed into the early Holocene. In the North Atlantic the early Holocene was highly variable and is characterised by several short-lived, cooling events (Bond *et al.*, 1997). For example the Preboreal Oscillation (PBO; 11,500-11,400 b2k; Rasmussen *et al.*, 2007); the 11,100 cal. yrs BP event (Blockley *et al.*, 2018), Erdalen events (10,100-10,05 and 10,000-9,850 cal. yrs BP; Dahl *et al.*, 2002) and the 9,300 cal. yrs BP and 8,200 cal. yrs BP cooling events (Nesje *et al.*, 2001; Marshall *et al.*, 2007; Rasmussen *et al.*, 2007) have been identified in terrestrial and ice-core records.

Evidence from multi-proxy analysis of terrestrial, marine and ice-core archives, and from climate models, suggests that ACEs occurred largely due to ice-ocean feedbacks during the final retreat of northern hemisphere ice sheets (Mayewski *et al.*, 2004; Tarasov *et al.*, 2012; Rach *et al.*, 2014; Muschitiello *et al.*, 2015; Schenk *et al.*, 2018). In the North Atlantic region, the Fennoscandian Ice Sheet (FIS) played a major role in influencing sub-millennial climate events by modulating atmospheric and North Atlantic Ocean circulation (Li *et al.*, 2010; Dokken *et al.*, 2013; Singh *et al.*, 2014). Several authors suggest that:

- 1) the FIS caused atmospheric blocking of cold westerly winds over Fennoscandia (Lane *et al.*, 2013; Muschitiello and Wohlfarth, 2015; Schenk *et al.*, 2018; Schenk and Vinuesa, 2019),
- 2) feedbacks between the atmosphere, ocean and sea-ice in the Nordic Seas led to periods of enhanced climatic cooling (Bakke *et al.*, 2009; Li *et al.*, 2010; Rach *et al.*, 2014; Muschitiello *et al.*, 2015), and
- 3) meltwater from the FIS, in particular the drainage of the ice-dammed Baltic Ice Lake (BIL), impacted North Atlantic Deep Water (NADW) formation (Stocker and Wright, 1991), leading to slowdown of the Atlantic Meridional Overturning Circulation (AMOC) and subsequent climatic cooling (e.g. Björck *et al.*, 1996; Muschitiello *et al.*, 2015, 2016).

As well as past AMOC weakening, it has been shown that the AMOC has been weakening in recent years (Srokosz and Bryden, 2015; Thornalley *et al.*, 2018) and the IPCC state that “it is *very likely* that the AMOC will weaken further over the 21st century” (Collins *et al.*, 2013 pp. 1093). Therefore, understanding the driving mechanisms and environmental responses to ACEs is fundamental to mitigate the impact of future change.

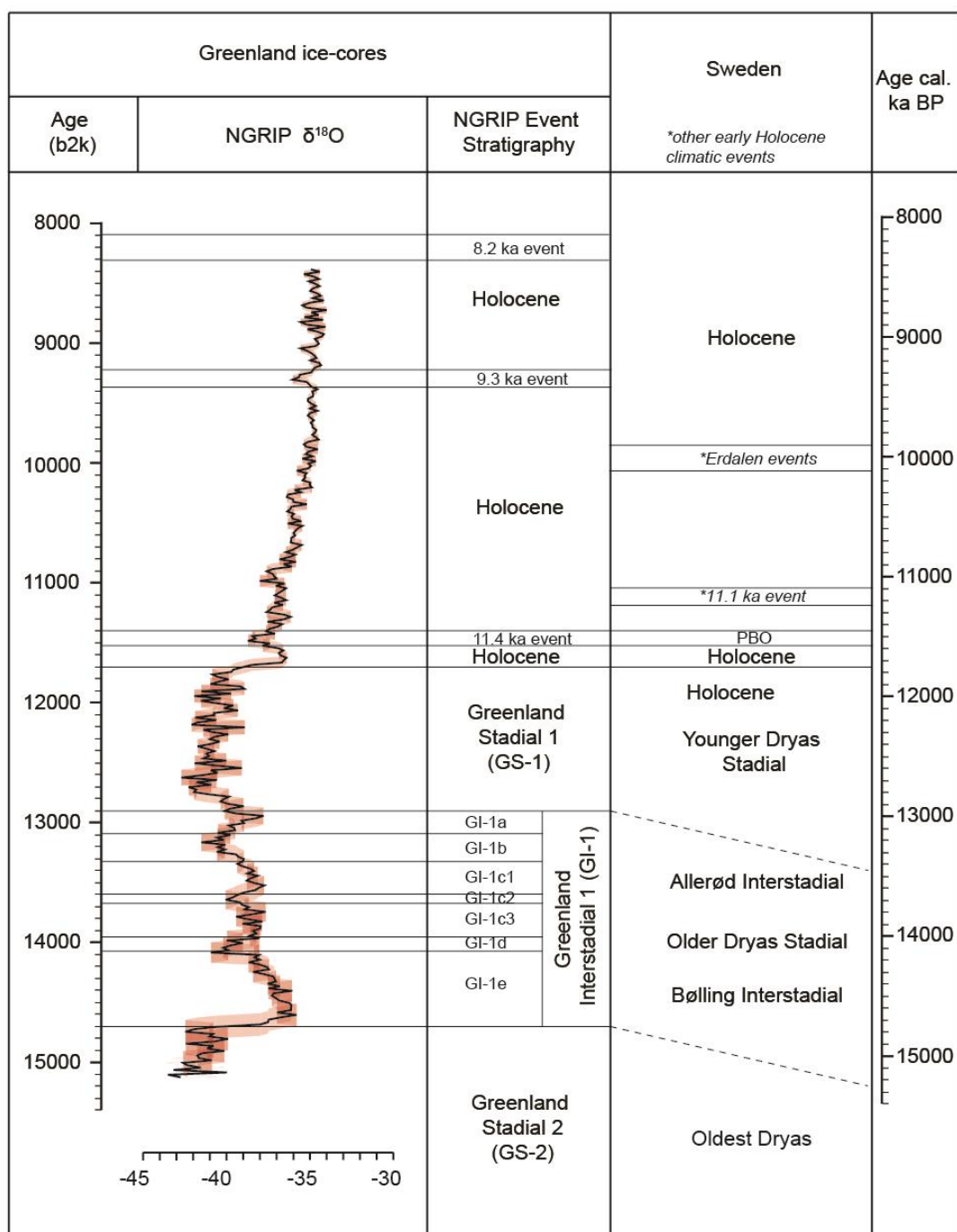


Figure 1-1. The $\delta^{18}\text{O}$ record from the NGRIP Greenland ice-core showing the Lateglacial event stratigraphy and the stratigraphic subdivision of the Lateglacial in Sweden.

The isotopic record is based on the NGRIP GICC05 ice-core chronology. Calibrated radiocarbon year timescale is also shown. Modified from Lowe and Walker (2015) with the Swedish event stratigraphy from Björck et al. (2001). Early Holocene climatic events that are identified outside Sweden are also highlighted with an asterisk and include the 11.1 ka BP event (Blockley et al., 2018) and Erdalen events (10.1-10.0 and 10.0-9.85 cal. ka BP BP; Dahl et al., 2002).

1.3 Synchronising climate records during the LGIT

In order to understand the driving mechanisms of ACEs it is essential that high-resolution, independent age estimates for these events are derived. This enables the synchronicity/asynchronicity of ACEs to be tested and an assessment to be made about leads and lags in the climate system across regional to hemispheric scales (e.g. Lane *et al.*, 2013; Muschitiello and Wohlfarth, 2015; Blockley *et al.*, 2018).

Whilst abundant research exists that demonstrates the impact of the FIS on North Atlantic systems, the chronologies that underpin these studies are often based on:

- 1) radiocarbon dates with large or unaccountable uncertainties such as bulk and/or marine radiocarbon samples, or
- 2) 'tuning' or 'wiggle matching' records to expected climatic events that are observed in the Greenland ice-core chronology (e.g. Björck *et al.*, 1996; Andrén *et al.*, 1999; Ringberg *et al.*, 2003).

This approach assumes that climatic change occurs synchronously in Greenland and Scandinavia and that the proxy records represent the same climatic forcing mechanism. This prohibits assessment of any leads and lags in the climate system. To overcome this, independent means of correlating records are required so that assumed climatic synchronicity can be tested. In recent years the development of tephrochronology (the use of volcanic ash layers as isochronous marker layers to correlate between records) has improved the chronological precision of LGIT records and enabled a more robust test of climatic synchronicity/asynchronicity (e.g. Lane *et al.*, 2013).

In addition to independently-dated records, climatic archives must be of sufficiently high (annual-decadal) resolution to fully understand the timing, duration and phasing of ACEs. For example, the high-resolution isotopic records from the Greenland ice-cores illustrate that, during the LGIT, ACEs largely operated at decadal timescales (Rasmussen *et al.*, 2006; Steffensen *et al.*, 2008). However, many lacustrine and marine sediment records do not have the same level of stratigraphic resolution as the Greenland ice-core records. This restricts highly precise assessments of the amplitude and rapidity of climatic transitions beyond Greenland. Other incremental dating records include annually laminated (varved) sediments, which can be used to assess climatic change at sub-annual to decadal scales i.e. a resolution that is comparable to the Greenland ice-core records. Thus, varved sediments have the potential to aid understanding of the driving mechanisms and responses to ACEs.

1.4 Varve records and the Swedish Timescale

There are several detailed varve sediment records from the LGIT (e.g. Brauer *et al.*, 1999; Hang, 2003; MacLeod *et al.*, 2011; Palmer *et al.*, 2012; Lane *et al.*, 2013; Ott *et al.*, 2016) but arguably the most widely known is the Swedish glacial varve chronology, commonly known as the Swedish Timescale (STS) (De Geer, 1912, 1940). The STS is based on cross-correlation of numerous clastic varve records and has been used to constrain the timing and duration of climatic phases during the LGIT (Ringberg, 1979; Ringberg and Rudmark, 1985; Strömberg, 1985; Björck and Digerfeldt, 1986; Kristiansson, 1986; Wohlfarth *et al.*, 1993; Andrén *et al.*, 1999).

The STS is also the primary dating technique for reconstructing the past ice margin position during deglaciation of the FIS during the LGIT (e.g. De Geer, 1940; Kristiansson, 1985; Brunnberg, 1995; Wohlfarth *et al.*, 1998). From *ca* 14 ka BP a combination of sea level changes and isostatic movements led to isolation of the Baltic Sea from the North Atlantic, and the Baltic became the ice-dammed Baltic Ice Lake (BIL) (Andrén *et al.*, 2011). Following retreat of the FIS during the Late Allerød-Younger Dryas transition (*ca* 12.9 ka BP) (Muschitiello *et al.*, 2016), the ice-dammed Baltic Ice Lake catastrophically drained and released large volumes of freshwater into the North Atlantic causing abrupt climatic cooling (Björck *et al.*, 1996; Muschitiello *et al.*, 2015). Subsequent readvance of the FIS blocked the drainage pathway and the BIL was ice-dammed again during the Younger Dryas period. Climatic warming during the Younger Dryas-Preboreal transition (*ca* 11.7 ka BP) (Andrén *et al.*, 1999) led to FIS retreat, opening up the drainage pathway for a second time (Björck *et al.*, 2002). This final drainage event delivered *ca* 7,800 km³ of freshwater to the North Sea (Jakobsson *et al.*, 2007) together with rapid meltwater from the Fennoscandian, Barents Sea and Laurentide Ice Sheets (Björck *et al.*, 1996). It has been estimated that the final BIL drainage occurred *ca* 300 yrs before the Preboreal Oscillation (Brunnberg, 1995; Andrén *et al.*, 2002), a period of climatic cooling during the early Holocene (Björck *et al.*, 2002). However, little attention has been given to a possible link between the final BIL drainage event and early Holocene climatic cooling events.

Given the importance of freshwater forcing from FIS meltwater and BIL drainage, the Swedish Timescale provides an invaluable, high-resolution, record to investigate the driving mechanisms and climatic responses to these events at a resolution comparable with the Greenland ice-core records. Recent research, however, demonstrates that there are inconsistencies in the construction and chronological precision of the STS (Wohlfarth *et al.*, 1997; Andrén *et al.*, 1999; Björck *et al.*, 2001). In what was considered a 13,300-year continuous varve chronology, up to 700-900

varve years are missing either during the Younger Dryas-Preboreal period, the early Holocene or the mid-Holocene (Björck *et al.*, 1996; Wohlfarth *et al.*, 1997, 1998; Andrén *et al.*, 1999). There are several potential reasons for the missing varves in the STS that form the fundamental basis for this thesis;

- 1) it is often assumed that varve thickness is driven by the relative position of the ice margin and so varve records can be linked in order to build a composite varve chronology (e.g. De Geer, 1940; Kristiansson, 1986; Strömberg, 1994; Wohlfarth *et al.*, 1998),
- 2) it is also assumed that other sediment features such as colour changes (Brunnberg, 1995; Andrén *et al.*, 1999), ice-rafted debris (Andrén *et al.*, 2002), deformation zones (Kristiansson, 1986), or distinct sand layers (De Geer, 1940; Strömberg, 1989) were deposited synchronously or near-synchronously across the Baltic Basin. This provides the basis for using these sedimentological features as definitive “pinning points” to link varve records and/or provide chronological links to climatic events,
- 3) the traditional means of identifying and counting annual sediment layers relies solely on macroscale sedimentological analysis of laminations which can be unclear, indistinct, extremely thin (<cm thickness) and difficult to identify with the naked eye.

Difficulties identifying and linking varve records that are constructed at the macroscale are described throughout almost all varve research in the STS (e.g. Kristiansson, 1985; Strömberg, 1985; Brunnberg, 1995; Ringberg *et al.*, 2002). Yet outside of the STS it is commonplace for researchers to verify macroscale varve counts with microscale analyses (e.g. Brauer, 2004; Francus, 2004; Palmer *et al.*, 2010; Lapointe *et al.*, 2012; Marshall *et al.*, 2012; Bendle *et al.*, 2017). In varve research outside the STS it is routine to first understand the internal seasonal succession of annual laminations in order to develop a varve depositional model (e.g. Lamoureux, 2001; Palmer, 2005). It is widely accepted that to do so requires examination of varve texture and structure at the microscale (Brauer, 2004; Zolitschka *et al.*, 2015; Palmer *et al.*, 2019). Microscopic analyses include thin section micromorphology, scanning electron microscopy (SEM) and micro-X-ray fluorescence (μ -XRF) techniques (e.g. Brauer *et al.*, 2008; MacLeod *et al.*, 2011; Martin-Puertas *et al.*, 2012). Analysing varved sediments at the microscale is therefore fundamental for generating robust varve chronologies but this approach has not been routinely applied to the STS. However, it is important to recognise that almost all work on the STS was undertaken before the 1990's when microstratigraphical methods were not accessible or in their infancy. In light of the recent advances in microscale analyses of varved sediments,

this presents an excellent opportunity to test the macroscale approaches that have been applied to the STS and improve the reliability of the varve chronologies.

There have been attempts to independently date and correlate varve records in the STS using radiocarbon dating of macrofossils (e.g. Brunnberg and Possnert, 1992; Wohlfarth *et al.*, 1995, 1998; Wohlfarth and Possnert, 2000; Björck *et al.*, 2001; Muschitiello *et al.*, 2016). Yet radiocarbon dates from the STS have yielded large errors (e.g. Brunnberg and Possnert, 1992; Wohlfarth and Possnert, 2000) and conflicting dates from the same varve interval have been reported (Wohlfarth *et al.*, 1993, 1998). These problems are likely due to the low abundance of fossil material in glaciolacustrine varve sequences and problems associated with the radiocarbon plateau during the LGIT (Björck *et al.*, 1996). In some instances, even terrestrial plant macrofossils, which are often considered to be somewhat “superior” to bulk sediment samples, can suffer from the effect of fossil recycling, resulting in apparent older ages (Lowe and Walker, 2000).

In the absence of material for radiocarbon dating, the approach taken by many researchers is to use macroscale varve analysis and distinctive sediment features to link individual varve records in order to create a composite varve chronology (Kristiansson, 1986; Strömberg, 1989, 1994; Brunnberg, 1995; Andrén *et al.*, 1999). This method has been largely successful at extending the timescale across most of southern Sweden, but it does not enable testing of the timescale. Consequently, independent correlation methods, in combination with high precision (microscale) varve analysis, must be sought if the STS is to be fully utilised for accurate reconstruction of FIS retreat and accurate dating of BIL drainage events. This in turn can improve our understanding of abrupt climatic events identified in the North Atlantic and those that have been linked to the drainage of the Baltic Ice Lake.

1.5 Research Aims

Due to the aforementioned links between the BIL drainage and abrupt climatic events, this research will focus on the part of the STS that covers the final drainage of the Baltic Ice Lake; The Younger Dryas-early Holocene (ca 12.7-11.5 cal. ka BP) (Andrén *et al.*, 1999; Björck *et al.*, 2002).

This research utilises the combined application of microscale sediment analysis and tephrochronology to construct a highly precise and independently dated varve chronology to address the following research aims:

- 1) Test the traditional macroscale-based methodological approaches that have been employed when creating the STS.
- 2) Refine the timing of Fennoscandian Ice Sheet retreat during the Younger Dryas-early Holocene in order to independently test the deglaciation chronology.
- 3) Critically assess the age of the final drainage of the Baltic Ice Lake and propose links to climate shifts across the North Atlantic region.

1.6 Research Objectives

To achieve these aims a series of objectives will be undertaken:

- 1) Develop and implement refined protocols for identifying and analysing glaciolacustrine varves in the STS that utilises microscale sediment techniques.
- 2) Develop a detailed understanding of lake processes in the BIL through microfacies analysis and compare the new varve chronologies to published data and assess disparities between the datasets.
- 3) Identify and chemically analyse tephra layers within the varved sediments and correlate to known tephtras.
- 4) Develop an absolutely-dated composite varve chronology through varve counting and tephrochronology using Bayesian age modelling techniques.

1.7 Thesis structure

This thesis is divided into twelve chapters (not including references or appendices). **Chapter 2** provides an overview of North Atlantic climate during the LGIT with specific emphasis on the role of the Fennoscandian Ice Sheet and Baltic Ice Lake drainage. **Chapter 3** summarises the Swedish Timescale including methodologies of construction, chronological precision and application to Quaternary climate and environmental research. The chapter concludes with a summary of current independent dating techniques in the STS including radiocarbon and tephrochronology. **Chapter 4** summarises the sedimentological processes that occur in glaciolacustrine systems and the processes that lead to varve formation. The chapter also provides an overview of key methodological approaches for varve identification that are adopted in the wider research community and which are employed in this thesis. Particular focus is given to macroscale varve analysis, micro X-ray Fluorescence (μ XRF) analysis, X-radiograph image analysis and thin section micromorphology. **Chapter 5** outlines the key methodological approaches utilised in

this thesis including site selection. **Chapter 6** presents a critical evaluation of varve counting methodologies using a case study example from the first of three sites included in this thesis. The main lithological results and varve counts are presented. The chapter summarises with a revised protocol for varve analysis for other sites in this thesis and for subsequent varve analysis in the STS. **Chapters 7 and 8** present the main lithological and varve count results from Site 2 and 3 in this thesis using the protocol outlined in Chapter 6. **Chapter 9** presents the tephra results from each site including correlations to published tephras. Implications for published ages of these tephras given the varve count data are also highlighted. **Chapter 10** integrates all chronological information from each site to produce Bayesian age-models for two of the three sites in this thesis. The site chronologies are placed on an absolute timescale. **Chapter 11** presents the local-scale palaeoenvironmental reconstructions using the varve structures identified in Chapters 6, 7 and 8 and discusses the implications of these findings for the construction of site and composite varve chronologies in the STS. The chapter also compares the new varve records with existing varve data and comparisons are drawn between the traditional macroscale-based varve chronologies and the new thin section-derived chronologies in this thesis. The tephra data are also critically evaluated and the potential of tephrochronology for the construction of accurate and reliable composite varve chronologies is also explored. The implications of the tephra-based varve chronologies for the published ages of the varve sites is also discussed. The latter half of this chapter includes a re-evaluation of the deglaciation of the FIS and also discusses the potential implications for BIL drainage. Possible links to freshwater forcing and/or climatic cooling events are also presented alongside the relevance of these findings for North Atlantic climate during the LGIT. **Chapter 12** summarises the main conclusions of this work and discusses directions for future research.

Chapter 2. North Atlantic Climate and the Fennoscandian Ice Sheet

2.1 Introduction

This first part of this chapter provides further detail on the driving mechanisms of ACEs with particular focus on the North Atlantic region. The spatial and temporal variability in climatic change throughout the LGIT is also presented. The second part of this chapter focuses on the Fennoscandian Ice Sheet (FIS) and presents a summary of the lithostratigraphic, biostratigraphic and chronostratigraphic evidence for deglaciation. The final part of this chapter presents a summary of the FIS deglaciation chronology since the Last Glacial Maximum (*ca* 23-21 ka BP; Hughes *et al.*, 2016) including Baltic Ice Lake (BIL) drainage events and subsequent Baltic Sea stages during the early Holocene.

2.1.1 Driving mechanisms of North Atlantic climate

In addition to long-term climatic variations, the Quaternary is characterised by short-lived, decadal to millennial-scale abrupt climatic events (ACEs). In the North Atlantic region, these events have been observed in high-resolution ice-core records from Greenland, in particular the NGRIP record, which is dated by annual layer counting (Rasmussen *et al.*, 2006). These archives indicate that temperature change between interstadial and stadial periods was rapid and could occur within decades (Rasmussen *et al.*, 2006). Factors that contribute to short-lived climatic change include variations in greenhouse gases (Ruddiman, 2006), solar variability (e.g. Wooling *et al.*, 2010; Martin-Puertas *et al.*, 2012), volcanic eruptions (Robock, 2000) and the complex feedback mechanisms between the ocean, ice and atmospheric realms (Lowe and Walker, 2014). All of these factors in isolation or in combination could have driven ACEs, however, the rapidity and magnitude of ACEs is thought to largely reflect instability in the climate-ocean systems of the North Atlantic (Clement and Peterson, 2006).

It has been proposed that the key driving mechanism of North Atlantic climate is the North Atlantic ocean which is highly sensitive to variations in temperature and salinity (Jessen *et al.*, 2008; Thornalley *et al.*, 2018). Even small amounts of freshwater can have a large effect on thermohaline circulation (Clark *et al.*, 2001; Rahmstorf *et al.*, 2005). Several authors have concluded that during the last glacial cycle ocean

circulation in the North Atlantic was highly variable in strength and direction (Duplessy *et al.*, 1988; Clark *et al.*, 2002; Rahmstorf, 2002), and abrupt climatic change was likely driven by variations in the salinity and strength of the Atlantic Meridional Overturning Circulation (AMOC) (Alley, 2007). It has been proposed that freshwater inputs to the North Atlantic either from ice-sheet collapse or catastrophic outbursts from ice-dammed lakes (Gherardi *et al.*, 2009; Thornalley *et al.*, 2010) led to temporary shutdown of the AMOC (Clark *et al.*, 2001). This triggered widespread changes in the ocean-atmosphere systems and led to abrupt climatic cooling (Bond *et al.*, 1993; Björck *et al.*, 1996), thus impacting terrestrial systems in northwest Europe (e.g. Coope *et al.*, 1998; Brooks and Langdon, 2014).

The favoured explanation for freshwater forcing prior to the Younger Dryas is a catastrophic meltwater outburst from Lake Aggasiz which was dammed by the Laurentide Ice Sheet (LIS) (Broecker *et al.*, 1989; Murton *et al.*, 2010). It is widely accepted that thousands of cubic kilometres of freshwater from the melting LIS suppressed the AMOC, triggering abrupt climate change (Licciardi *et al.*, 1999; Teller *et al.*, 2002; Broecker, 2006). Recent research also suggests a northwest LIS outlet to the Arctic Ocean during the mid-Younger Dryas (Breckenridge, 2015). Whilst abundant research demonstrates that the LIS provided the main source of freshwater forcing to the North Atlantic prior to the Younger Dryas, additional freshwater sources have been proposed. These include the Antarctic Ice Sheet (AIS) (MacAyeal, 1992; Deschamps *et al.*, 2012) and more recently, the Fennoscandian Ice Sheet (FIS) (Muschitiello *et al.*, 2016).

Freshwater from the AIS has been linked to the 'bipolar seesaw' hypothesis (Blunier *et al.*, 1998; Broecker, 1998). This hypothesis is based on the principle that deep-water ocean systems play a major role in heat re-distribution around the globe (Hegerl and Bindoff, 2005). If freshwater is released into the North Atlantic, this would interrupt the production of North Atlantic Deep Water (NADW), leading to cooling in the North Atlantic (Flower *et al.*, 2000). This would in turn drive the migration of the polar front and influence heat transfer in the ocean which would also impact Atlantic Bottom Water (ABW) production, ultimately leading to warming in the south (Rahmstorf, 2002). However, discrepancies in the timing of temperature change between the poles (e.g. Capron *et al.*, 2010) demonstrate that, similar to Milankovitch cycles, other factors such as the location, timing and volume of freshwater input, influence atmospheric processes and amplify the effects of ocean circulation changes. More recently, it has been proposed that meltwater fluxes from the FIS and the catastrophic drainage of the BIL may have triggered the onset of cold climate conditions at the start of the Younger Dryas (Muschitiello *et al.*, 2016).

Although the exact controls on climate variability throughout the last glacial cycle remain uncertain, there is common agreement that weakening of the AMOC during the LGIT, in particular during the early Younger Dryas, caused abrupt climatic cooling in the North Atlantic (McManus *et al.*, 2004; Jennings *et al.*, 2006; Bakke *et al.*, 2009). In addition to the multiple drivers of climatic change, the evolution of key climatic phases during the LGIT was spatially complex. With recent improvements in geochronological methods, researchers have suggested that the seasonal expression of climatic change during the LGIT likely occurred asynchronously (Figure 2-1) (Lane *et al.*, 2013; Muschitiello and Wohlfarth, 2015; Blockley *et al.*, 2018).

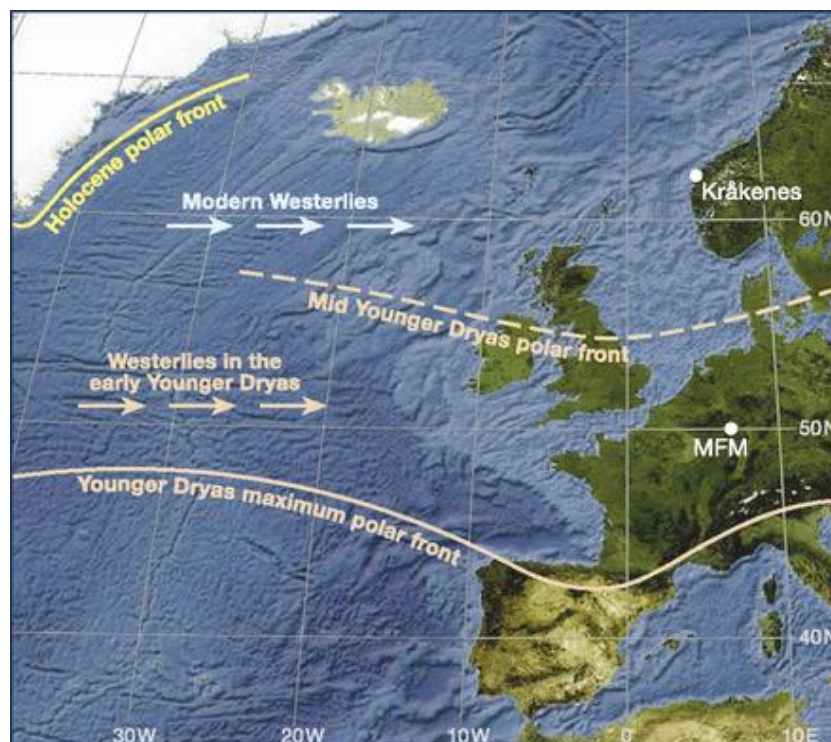


Figure 2-1. Time-transgressive climatic change during the Younger Dryas. Location of the Kråkenes and Meerfelder Maar sites that contain high-resolution proxy records of GS-1 (Younger Dryas Stadial) and inferred positions of the Polar Front. From Lane *et al.* (2013).

2.1.2 Phasing of palaeoclimatic events across the North Atlantic during the LGIT

The oscillations between cold and warm climatic events during the LGIT are recorded in many different palaeoclimatic archives across the North Atlantic (e.g. Coope and Lemdahl, 1995; Coope *et al.*, 1998; Rasmussen *et al.*, 2006; Brooks and Langdon, 2014). In particular, temperature reconstructions from fossil chironomids across northwest Europe demonstrate temperature variations on an east-west (Van Asch *et al.*, 2012) and a north-south gradient (Brooks and Langdon, 2014).

During the Interstadial (Bølling-Allerød), chironomid-inferred summer temperatures (C-IT) vary on an east-west gradient from $\sim 11.5^{\circ}\text{C}$ in the British Isles to $\sim 13.5^{\circ}\text{C}$ in continental northwest Europe, compared to summer temperatures during the Younger Dryas which vary from $\sim 7.5^{\circ}\text{C}$ in the British Isles to $\sim 11.0^{\circ}\text{C}$ in continental northwest Europe (Figure 2-2).

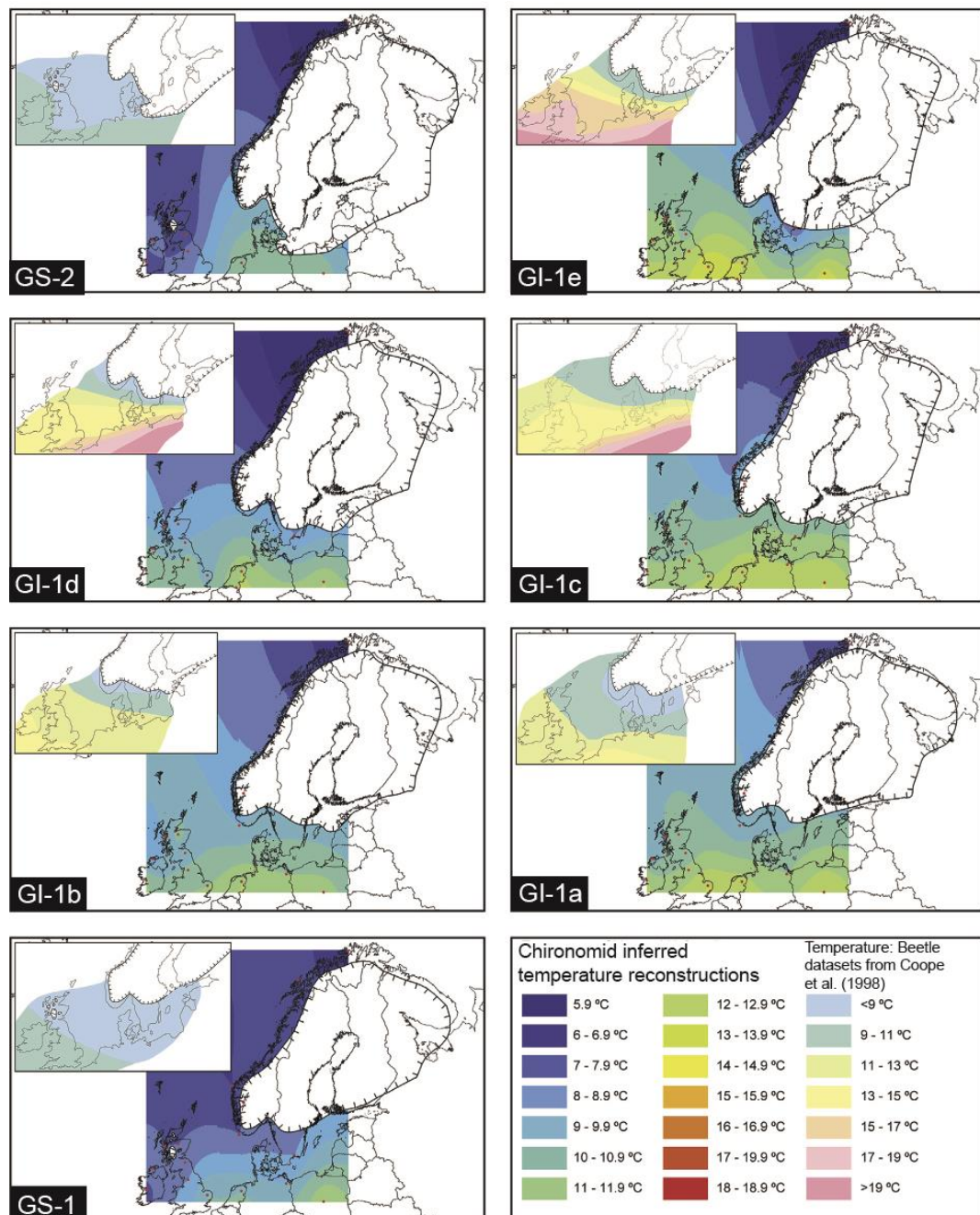


Figure 2-2. Lateglacial isotherm maps based on chironomid-inferred summer air temperatures.

Summer air temperatures were estimated using the Norwegian temperature calibration dataset. Coleoptera-inferred MCR temperature estimates of the warmest month are shown in the inset map in the top left of each diagram. Note the east-west temperature gradient. The north-south gradient appears strongest on continental Europe than in the British Isles as indicated by the narrower isotherm bands in continental Europe. Modified from Brooks and Langdon (2014).

The east-west gradient has been attributed to the influence of the North Atlantic, in particular the thermohaline circulation (Brooks and Langdon, 2014). During warm periods (GI-1e, GI-1c and GI-1a), the north-south gradient appears strongest on continental Europe than in the British Isles (Figure 2-2). The north-south temperature gradient has been attributed to the influence of the FIS which controlled the position of the Polar Front during the LGIT (Lane *et al.*, 2013). Moreover, it has been proposed that cold katabatic winds from the FIS also influenced air temperature at sites in close proximity to the ice margin (Muschitiello and Wohlfarth, 2015; Schenk *et al.*, 2018).

Until recent years, it has been difficult to determine whether abrupt climatic changes during the LGIT that are observed in many proxy records, were regionally synchronous or whether significant leads and lags existed between the atmosphere, marine, terrestrial and cryosphere realms. This is generally because the dating techniques that have been applied to such proxy records do not have sufficient temporal resolution to assess the precise timing and duration of individual climatic events (Lowe and Walker, 2015). However, in recent years, there have been several studies that demonstrate a temporal lag in climatic change across the North Atlantic region during the Younger Dryas and early-Holocene periods (e.g. Lane *et al.*, 2013; Muschitiello and Wohlfarth, 2015; Blockley *et al.*, 2018). In Germany, geochemical evidence from annually-laminated lake sediments at Meerfelder Maar (MFM) indicate an increase in stormy conditions at the onset of the Younger Dryas (Brauer *et al.*, 2008). This is attributed to the strength of the AMOC, which enabled North Atlantic sea ice to expand, driving the oceanic Polar Front southwards, and diverting strong westerly winds across central Europe (Lane *et al.*, 2013). This has been precisely dated to 12,679 (MFM) varve years, which post-dates the onset of the Younger Dryas in Greenland by *ca* 200 years (Figure 2-1) (Lane *et al.*, 2013). In Norway at Lake Kråkenes, evidence from lake sediment geochemistry indicates that the Nordic seas were permanently frozen during the Younger Dryas. As the Polar Front retreated northwards, sea ice conditions deteriorated, with ice-free conditions occurring prior to 12.5 ka BP. This pre-dates the Younger Dryas by *ca* 200 years in comparison to the Greenland ice-cores (Bakke *et al.*, 2009). More recently, research by Muschitiello and Wohlfarth (2015) demonstrates a mean temporal lag of *ca* 290 years in the proxy response to climatic change during the Younger Dryas across sites in northwest Europe. The authors suggest that this lag was partly driven by the expansion of sea ice in Norway and cold katabatic winds from the FIS.

The key stratigraphic marker for these events is the Vedde Ash dated to 12,140±40 MFM yrs in the Meerfelder Maar varve chronology (Brauer *et al.*, 2008), 12,023±86 cal. yrs BP (2 σ) (Bronk Ramsey *et al.*, 2015), 12,171±114 b2k (Rasmussen *et al.*,

2006). Tephrochronology has enabled the assumed synchronicity of Younger Dryas climate to be tested through correlation of multiple climatic archives of comparable chronological resolution. Critically, by establishing a robust independently dated chronology it has been possible to assess temporal and spatial changes in climate and further understand the impacts on marine, terrestrial and cryosphere systems.

2.1.3 Summary

The factors that controlled the climate of the Quaternary are complex and interconnected. Nevertheless, a series of abrupt climate events punctuate the Late Quaternary and are recorded within terrestrial, marine and ice-core sequences. It is likely that orbital forcing controls the major climate oscillations over glacial-interglacial cycles, but abrupt millennial and centennial-scale climatic changes are largely driven by complex feedback mechanisms between ice sheets, ocean circulation and migrating Polar Fronts. In particular the LGIT is characterised by rapid high magnitude shifts in climate that have been linked to meltwater from northern and southern hemisphere ice sheets, with most recent attention focussed on the role of the FIS.

Recent research has focussed on freshwater forcing from the FIS in relation to the first drainage of the Baltic Ice Lake at the onset of Younger Dryas cooling (Muschitiello *et al.*, 2015, 2016). However little attention has been given to possible freshwater forcing related to the final drainage of the BIL at the Younger Dryas-Preboreal transition. The current limitation for resolving the effect of freshwater forcing from the final BIL drainage on climatic change is the chronological link between climatic events, ice-sheet deglaciation and meltwater events. This thesis aims to provide an independently dated, high-resolution varve chronology for the Younger Dryas-Preboreal transition in order to provide a more precise estimate of the final BIL drainage event.

The following section summarises the evidence for FIS retreat during the last deglaciation followed by the current deglaciation chronology. The final part of this section provides a summary of BIL drainage events and the subsequent early Holocene Baltic Sea stages.

2.2 The Fennoscandian Ice Sheet (FIS)

Since the LGM three large ice sheets covered northern Europe: The British-Irish Ice Sheet, the Barents Ice Sheet and the Fennoscandian Ice Sheet. The following sections of this chapter focus on the retreat of the FIS after separation from the other ice sheets following the LGM (Clark *et al.*, 2012).

The retreat pattern of the FIS has been linked to key climatic phases during the LGIT that have been primarily inferred from pollen stratigraphical analyses and radiocarbon dating (Björck and Digerfeldt, 1984, 1986). The major end-moraines are associated with cooling during the Younger Dryas and mark the final retreat and decay of the ice sheet prior to climatic warming during the Holocene period. As well as climatic drivers, it has also been proposed that local topographic factors (e.g. Johansson, 1982; Ronnert, 1989) and proximity to the sea (Sørensen, 1992; Lohne *et al.*, 2007) were important factors in driving the rate of FIS retreat. The complex and dynamic behaviour of the FIS during deglaciation is observed through differences in retreat rates across the ice sheet inferred from glacial landforms. Generally, marine margins experienced faster retreat rates, with slower retreat rates observed at terrestrial ice margins (Duphorn *et al.*, 1979; Stroeven *et al.*, 2016).

2.2.1 Geomorphological evidence

Reconstruction of FIS deglaciation is primarily based on ice-marginal and sub-glacial landforms. These include ice-dammed lakes, moraines, glaciofluvial deposits, meltwater channels, eskers, drumlins and striae. The following sections provide a brief summary of these landforms and their use in FIS reconstructions.

2.2.1.1 Ice-dammed lakes

Palaeoshorelines and delta deposits from ice-dammed lakes have been used to map the deglaciation of the FIS (e.g. Lundqvist, 1972; Borgström, 1989; Longva and Thoresen, 1991). The drainage of these lakes occurred when the ice margin retreated and opened up the natural drainage pathway of the lake catchments (Lundqvist, 1972). Drainage deposits have also been found in clay varve records as prominent sand layers that have been used as evidence for high-magnitude, basin-wide drainage events (De Geer, 1940; Strömberg, 1989, 1994). The most widely known ice-dammed lake in the Baltic Sea basin is the Baltic Ice Lake, which at its maximum capacity had a volume of 29,300 km³ (Jakobsson *et al.*, 2007).

2.2.1.2 Moraines and glaciofluvial deposits

Sediment landforms such as moraines and glaciofluvial deposits have been used to reconstruct ice margin retreat and readvances. These deposits have been found across the extent of the FIS in Poland, Denmark, Germany, Russia, Norway and the Baltic countries but are more commonly found at the eastern and southern ice-limits (Sørensen, 1992; Houmark-Nielsen and Kjær, 2003; Fredin *et al.*, 2012; Houmark-Nielsen *et al.*, 2012). The most prominent of these landforms have been linked to the Younger Dryas and are thought to mark the last glacial stillstand before final deglaciation during the early Holocene (Björck and Digerfeldt, 1984; Saarnisto and Saarinen, 2001). Moraines deemed to be of Younger Dryas age are found in Sweden, Norway and Finland (Figure 2-4) (Donner, 2010; Stroeven *et al.*, 2016). Post-Younger Dryas ice-marginal landforms are more rare and are used to guide deglaciation reconstructions throughout the early Holocene until ice-free conditions in northern Sweden ca 10,500 cal. yrs BP (Hughes *et al.*, 2016; Stroeven *et al.*, 2016).

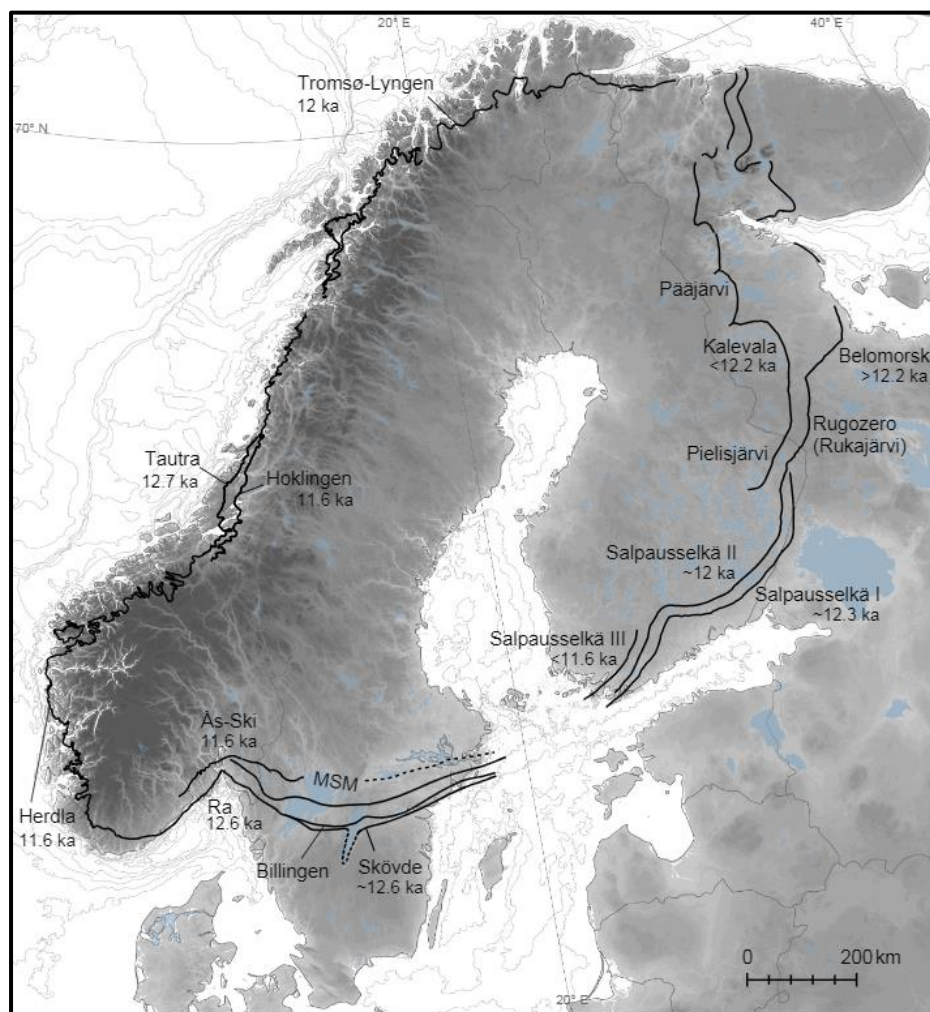


Figure 2-3. The Fennoscandian Ice Sheet margin during the Younger Dryas. Modified from Hughes *et al.* (2016).

2.2.1.3 Eskers

With their characteristic coarse-grained sorted sediments and long and winding ridge-like structure, eskers are distinctive sediment landforms that are deposited in meltwater streams that form at the base of an ice sheet. Since eskers typically form in close proximity to the ice margin (Kleman, 1972; Hebrand and Åmark, 1989), and because the long axis of an esker tracks the flow direction of an ice sheet, their morphology has been used to map the former position of the FIS (e.g. Stroeven *et al.*, 2016). Their prominence across Fennoscandia alongside their recognisable and sizeable structure has led to extensive and accurate mapping from both aerial photographs and LiDAR imagery (Lundqvist, 1959; Hättestrand, 1998; Hättestrand and Clark, 2006b). Stroeven *et al.* (2016) summarise the well-developed pattern of esker systems and glacial lineations across Fennoscandia since the LGM (Figure 2-4). Their reconstruction suggests that in southern Sweden ice-basal conditions were mostly warm-based but parts of northern Sweden likely remained cold-based up until final deglaciation.

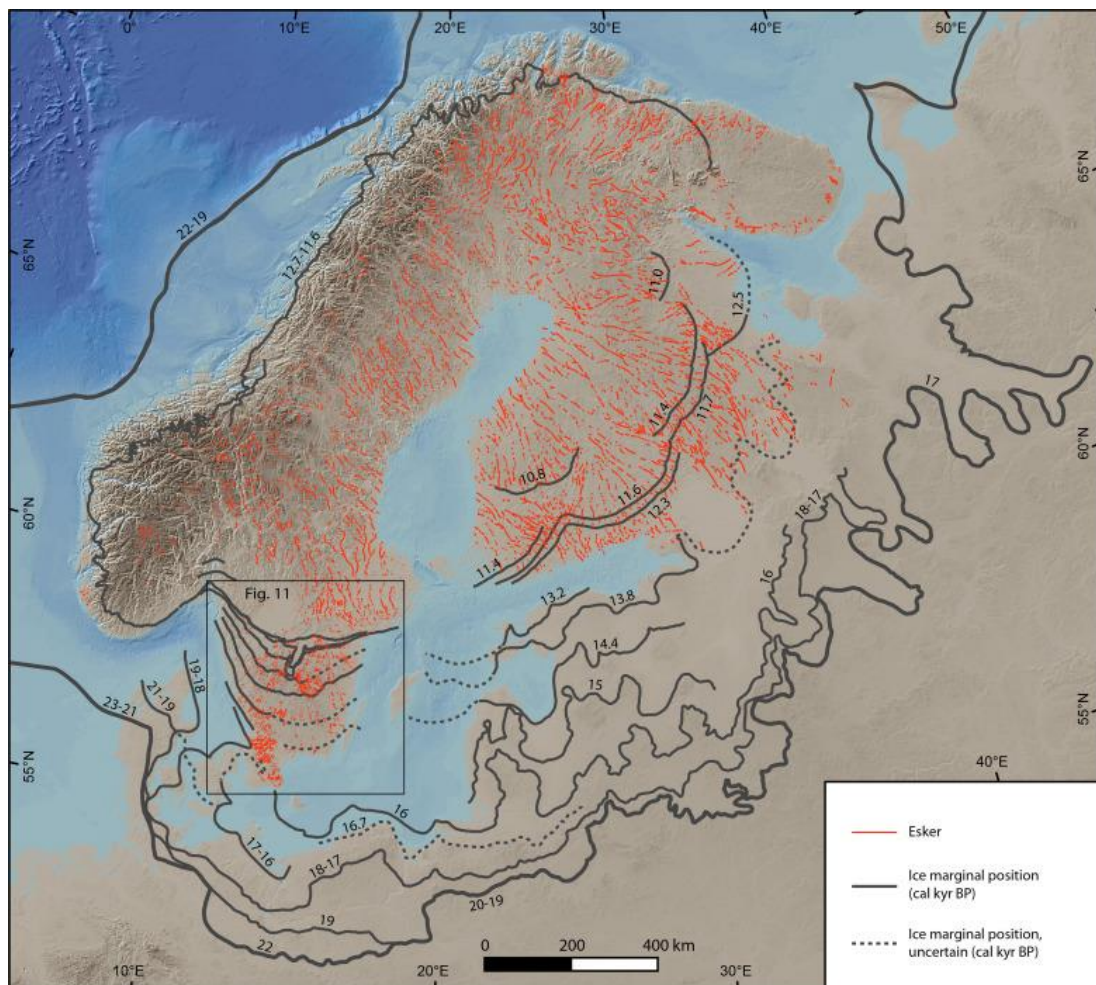


Figure 2-4. Prominent eskers and ice-marginal positions of the FIS between 22-10.8 ka BP. From Stroeven *et al.* (2016) pp. 98.

2.2.1.4 Meltwater channels

Marginal meltwater channels form when meltwater from the glacier runs parallel to the glacier margin and erodes underlying bedrock/sediment. These channels are typically tens of meters deep, meters wide, and hundreds of meters long and can form in cold-based or warm-based glacier conditions (Stroeven *et al.*, 2016). Meltwater channels have been used to reconstruct the deglaciation of the FIS (e.g. Kleman, 1972, 1994; Hättestrand and Stroeven, 2004; Stroeven *et al.*, 2016) and are particularly prominent in northern Sweden where the final deglaciation of the FIS took place (Hättestrand and Clark, 2006a; Hättestrand *et al.*, 2007).

2.2.1.5 Hummocks, hummock tracts and hummock corridors

Hummocks are individual landforms with irregular topography that display large variations in size and relief. A large area which comprises multiple hummocks is a “hummock tract” and when hummock tracts occupy an elongated zone that is clearly distinct this is referred to as a “hummock corridor” (Peterson and Johnson, 2018; Peterson *et al.*, 2018). These landforms have been identified across southern Sweden (Gavelin and Munthe, 1907; Stolpe, 1911; Johnsson, 1956; Lundqvist and Wohlfarth, 2001), mid and northern Sweden (Hättestrand, 1997) and more recently in southwest Finland (Mäkinen *et al.*, 2017). Generally, hummocks are interpreted to have formed due to collapse of supraglacial debris that forms on stagnant ice but can also form in proglacial and subglacial environments (Johnson and Clayton, 2003; Peterson and Johnson, 2018). Using LiDAR-based digital elevation models, Peterson *et al.* (2017) identified two distinct types of hummock tracts: 1) v-shaped hummocks with a gentle up-ice and steep down-ice slope and; 2) semi-ordered ridge systems that are traverse to ice flow, and which are morphologically similar to “ribbed moraine” (Johnsson, 1956; Möller, 1987, 2010). Hummock tracts and corridors are a major feature of the landscape and have been used to map the former ice-flow direction of the FIS (Hättestrand, 1997; Peterson *et al.*, 2017, 2018).

2.2.1.6 Drumlins and striae

Drumlins, also referred to as ‘lineations’, are elongated sediment landforms that form parallel to the ice direction and have been widely utilised for FIS reconstructions (Kleman *et al.*, 1997; Putkinen *et al.*, 2011; Stroeven *et al.*, 2016). They are often found in “swarms” that can be up to hundreds of kilometres in length. In contrast, glacial striae represent the smallest-scale evidence of ice-flow on bedrock. The orientation of glacial striae has been utilised for FIS reconstructions since the early 20th century (e.g. De Geer, 1909; Caldenius, 1942). Together, drumlins and striae

have been used to reconstruct ice flow direction across Fennoscandia (e.g. Lundqvist, 2007; Hughes *et al.*, 2016; Stroeven *et al.*, 2016).

2.2.2 Lithostratigraphic evidence

Lithostratigraphy provides a framework for deglaciation through linking sediment units across regions (e.g. Lagerlund, 1987). For example, the location of glaciolacustrine sediments has enabled reconstruction of the areas above and below the highest shoreline of the Baltic Ice Lake. In Denmark, six dated lithostratigraphical levels of inter-till sediments provide the framework for the Danish deglaciation chronology (Houmark-Nielsen and Kjær, 2003). In northern Denmark the Kattegat Till pre-dates a series of glaciotectonic structures and in northern Sjælland the Kattegat Till overlies the Klintholm Till (Houmark-Nielsen, 1987; Lagerlund and Houmark-Nielsen, 1993). In southern Sweden the complex series of deformed sediments between moraines that forms the Middle Swedish End Moraine Zone (MSEMZ) has been reconstructed from detailed lithostratigraphy and geomorphological mapping (Johansson, 1926; Björck and Digerfeldt, 1984; Johnson *et al.*, 2019).

2.2.3 Biostratigraphic evidence

The biostratigraphic subdivision of the Lateglacial in Sweden uses the following terminology; the Oldest Dryas, the Bølling Interstadial, the Older Dryas, the Allerød Interstadial, the Younger Dryas and the Holocene (Jessen, 1935; Iversen, 1973; Mangerud *et al.*, 1974). These terms are derived from pollen analysis in a number of lacustrine sediment records in Denmark, southern Sweden and Norway, as well as elsewhere in Europe. Pollen analysis from lake sediment sequences located between ice-marginal landforms provides a framework for the different phases of FIS retreat (Mangerud *et al.*, 1974; Hillefors, 1979; Björck and Digerfeldt, 1991; Berglund, 1995). Throughout reconstructions of the FIS, biostratigraphy is often used interchangeably as a chronostratigraphic tool. Phases of FIS retreat and glacial landforms that were originally correlated to pollen zones have subsequently been assigned ages through correlation with the Greenland ice-core event stratigraphy (e.g. Stroeven *et al.*, 2016). For example, the moraines that are associated with the Younger Dryas pollen zone have been dated to ca 12.9-11.7 ka BP i.e. the age of GS-1 in the Greenland ice-cores (Rasmussen *et al.*, 2014). The use of biostratigraphy as a chronostratigraphic tool is described further in section 2.2.4.4.

2.2.4 Chronostratigraphic evidence

Geomorphological mapping has allowed the retreat history of the FIS to be placed within a morphostratigraphic framework that has been corroborated by

lithostratigraphy. However, evidence can be fragmentary due to spatial discontinuity of glacial landforms. Understanding the dynamics and rates of ice-sheet deglaciation and the potential sensitivity of the FIS to climatic events requires the development of accurate and precise chronologies. For the FIS a range of geochronological techniques have been applied to reconstruct deglaciation (Figure 2-5). Efforts have focussed on: 1) cosmogenic nuclide exposure dating of moraine boulders and ice-scoured bedrock; 2) luminescence dating of outwash sands and moraine sediments; 3) radiocarbon dating of samples from lacustrine and marine sediments; 4) biostratigraphy; and 5) development of local and regional varve chronologies. The following sections present these dating techniques in more detail.

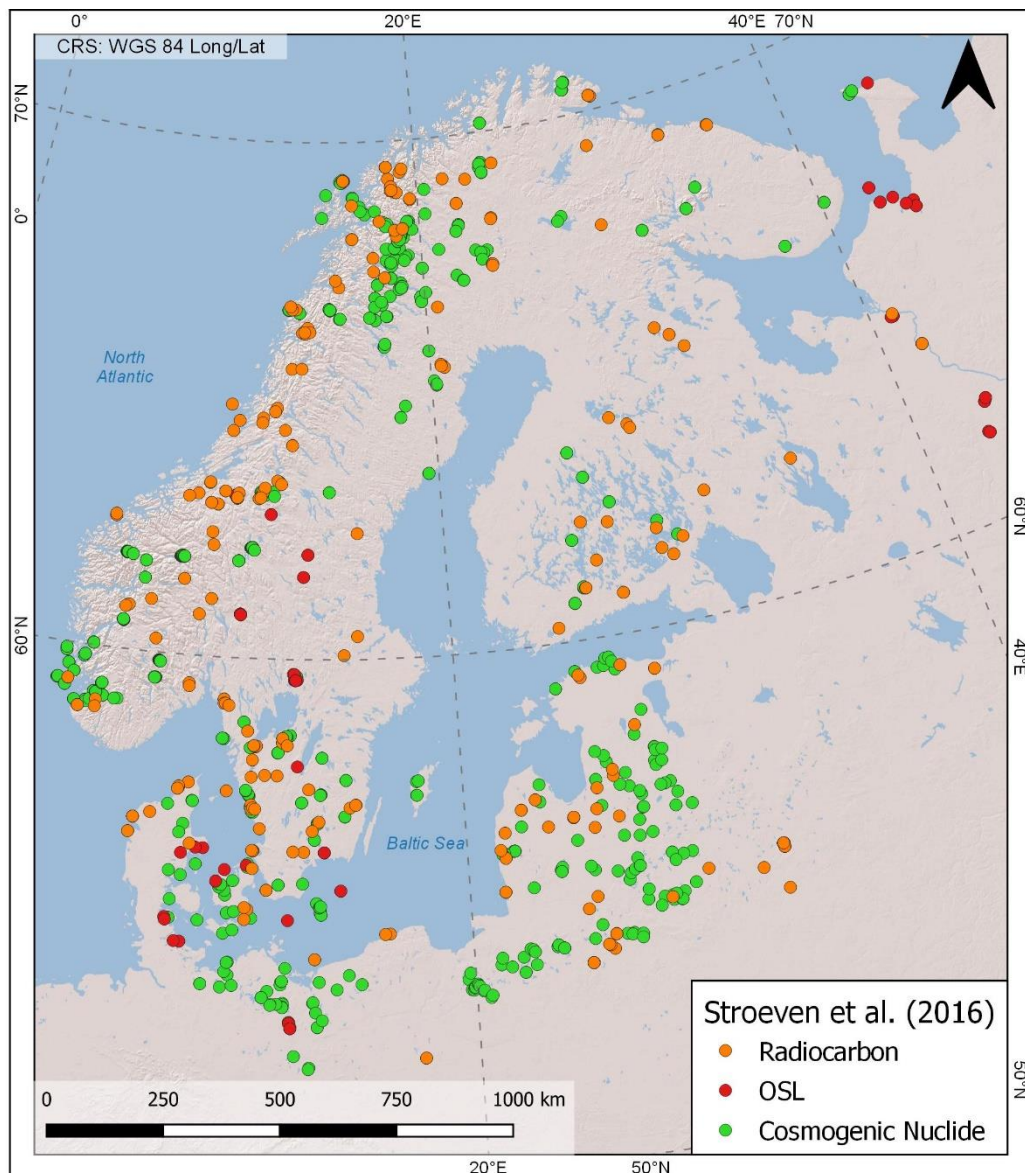


Figure 2-5. Locations of OSL, radiocarbon, and cosmogenic nuclide exposure samples included in the Stroeve et al. (2016) deglaciation chronology.

2.2.4.1 Cosmogenic nuclide (CN) exposure dating

Cosmogenic nuclide (CN) surface exposure dating uses samples taken from bedrock or boulders and typically, quartz minerals are exposed to cosmic rays. Four nuclides are produced, one stable (^{21}Ne) and three radioactive (^{10}Be , ^{26}Al , and ^{14}C). Arguably, the most reliable nuclide is ^{10}Be which has mainly been used in recent decades for reconstructing FIS retreat (Figure 2-5) (Rinterknecht *et al.*, 2004, 2005, 2006; Heine *et al.*, 2009).

CN exposure ages typically yield *ca* $\pm 10\%$ uncertainties (e.g. Li *et al.*, 2005; Larsen *et al.*, 2012; Anjar *et al.*, 2014). During the LGIT this often equates to uncertainties in the order of thousands or hundreds of years. Therefore, this dating technique provides a broad chronostratigraphic framework for the deglaciation chronology but lacks the precision to define events over the time period in question within this thesis. Comprehensive reviews of CN dates for the FIS are presented by Stroeven *et al.* (2016) and Hughes *et al.* (2016).

2.2.4.2 Optically Stimulated Luminescence (OSL) dating

Optically Stimulated Luminescence (OSL) dating is based on the build-up of a luminescence signal in quartz grains that are shielded from sunlight during burial (Walker, 2005). In theory, OSL dating can potentially yield accurate minimum ages of deglaciation, but some OSL ages are older than the expected deglaciation age due to incomplete bleaching of sand grains (e.g. Johnson and Ståhl, 2010). Nevertheless, OSL dating has been used to reconstruct FIS deglaciation (e.g. Heine *et al.*, 2009; Alexanderson and Murray, 2012; Saks *et al.*, 2012) and provides a broad chronostratigraphic framework. Since OSL dates frequently contain errors that are too large to alone resolve deglaciation chronologies at centennial-decadal scales, other dating techniques are required to test and refine OSL-based chronologies (e.g. Bendle *et al.*, 2017).

2.2.4.3 Radiocarbon (^{14}C) dating

Radiocarbon dating has been used extensively for estimating the timing of FIS retreat and is mostly based on samples from lacustrine and marine environments (e.g. Hillefors, 1975; Björck and Håkansson, 1982; Björck and Digerfeldt, 1989; Wohlfarth *et al.*, 1993; Berglund, 1995; Björck *et al.*, 1996; Wohlfarth, 1996; Wastegård *et al.*, 1998; Wohlfarth and Possnert, 2000; Johnson and Ståhl, 2010). Whilst the application of radiocarbon dating is widespread in FIS research, there are a number of limitations that must be considered when interpreting radiocarbon-based age estimates from these depositional environments.

In lacustrine environments it is logical to assume that following deglaciation there was a delay in the stabilisation of soils and the establishment of vegetation on the landscape. Therefore, radiocarbon dates from organic matter in lacustrine records from glacial environments provide minimum age estimates for deglaciation. Contamination can also be problematic for bulk sediment samples from glacial environments since older carbon may have been transported to the area by the glacier thus producing apparently older ages (Walker *et al.*, 2001). This is known as the mineral carbon offset and can become incorporated within bulk samples due to reworked older carbon from the surrounding catchment or erosion of older carbon within bedrock (Walker, 2005). For macrofossil samples from lacustrine environments plants that photosynthesise sub-aquatically (e.g. aquatic mosses) can sequester older carbon from the lake water, which is then incorporated into animals which feed on these plants and on each other. This is termed the 'hard-water effect' and can add up to 1,200 years to the apparent radiocarbon age of a sample (Peglar *et al.*, 1989). To overcome the hard water effect, bulk sediment samples should be avoided, or at the very minimum unquantifiable errors associated with the mineral carbon error and/or the hard water effect should be acknowledged. Instead single-species terrestrial macrofossils (e.g. seeds and leaves) should be used to construct radiocarbon-based age models (Walker, 2005; Lowe and Walker, 2014).

Arguably, the most reliable lacustrine radiocarbon age model for the FIS is the varve chronology proposed by Muschitiello *et al.* (2016). The authors remodelled radiocarbon ages from the Wohlfarth *et al.* (1998) regional varve chronology within a Bayesian framework. Muschitiello *et al.* (2016) applied rejection criteria to the original radiocarbon ages and omitted ages from: 1) bulk sediment samples; 2) samples reported to have been contaminated by fungi; and 3) samples that yielded conflicting ages from the same varve interval. The chronology covers the period from the Allerød to the early Younger Dryas *ca* 13,200-12,400 cal. yrs BP and has been used to constrain the timing of deglaciation in southern Östergötland and the first Baltic Ice Lake drainage event (Muschitiello *et al.*, 2016).

In marine environments, radiocarbon ages from samples such as shells, fish and algae are typically several hundreds of years older than in terrestrial settings (Walker, 2005). This age difference is due to the large carbon reservoir of the oceans. At the ocean surface, exchange of CO₂ between the atmosphere and the ocean means that ¹⁴C becomes incorporated into sea water as dissolved carbonate. After surface waters sink to intermediate and deep water depths, the ocean water decays and takes on an apparent age. A correction is necessary to compare marine and terrestrial samples, but this correction varies over relatively short distances due to complex

ocean circulation patterns. A correction value to account for the apparent age of sea water is typically applied to radiocarbon dates on fossil samples which used dissolved carbonate to build their shells (e.g. foraminifera, molluscs). In the Baltic Sea and North Atlantic, measurements on present-day molluscs show that the ocean water has an average apparent age of around -400 ^{14}C yrs (Bard *et al.*, 1991) and hence radiocarbon dates from fossil molluscs from Fennoscandia have been corrected by this value (e.g. Lundqvist and Wohlfarth, 2001). However, when looking at a much smaller area of the Baltic Sea, for example in the Bornholm Basin and the Øresund area, the ageing effect of modern water samples varies from between ca 250-900 years (Heier-Nielsen *et al.*, 1995; Lougheed *et al.*, 2013) (Table 2-1).

Table 2-1. Modern radiocarbon ages of seawater in the Bornholm Basin and Øresund area (DeltaR) and error (DeltaR Error).

Ages have been corrected by -400 ^{14}C yrs to account for the regional seawater age offset. Information taken from www.calib.org/marine.

Longitude	Latitude	DeltaR	DeltaR Error	Locality	Sub region	Reference
13.400	55.000	407	55	Arkona Basin	Baltic Sea	Lougheed <i>et al.</i> (2013)
12.783	55.317	657	55	Arkona Basin	Baltic Sea	Lougheed <i>et al.</i> (2013)
13.817	55.167	337	51	Arkona Basin	Baltic Sea	Lougheed <i>et al.</i> (2013)
12.367	54.767	347	55	Arkona Basin	Baltic Sea	Lougheed <i>et al.</i> (2013)
12.630	55.950	422	54	Vedbaek Øresund (15-18 m)	Øresund	Heier-Nielsen <i>et al.</i> (1995)
14.217	55.183	247	55	Arkona Basin	Baltic Sea	Lougheed <i>et al.</i> (2013)
12.550	56.070	391	59	Øresund off Hellebaek	Øresund	Heier-Nielsen <i>et al.</i> (1995)
12.050	55.670	905	56	Roskilde Fjord by Roskilde	Denmark	Heier-Nielsen <i>et al.</i> (1995)
14.560	55.270	292	55	Bornholm Basin	Baltic Sea	Lougheed <i>et al.</i> (2013)
14.567	55.083	357	51	Arkona Basin	Baltic Sea	Lougheed <i>et al.</i> (2013)

Though modern variations in the marine reservoir effect can be quantified globally, research suggests that the marine reservoir effect has changed over time (Bard *et al.*, 1994; Austin *et al.*, 1995; Bjorck *et al.*, 2003; Mangerud *et al.*, 2006). For example, Waelbroeck *et al.* (2001) suggest that during the Younger Dryas, North Atlantic

surface water ages may have varied by up to 1,350 ^{14}C yrs though Bard *et al.* (1994) and Austin *et al.* (1995) propose it was around 700-800 yrs. At the Younger Dryas-Preboreal transition, the North Atlantic marine reservoir offset may have dropped rapidly to *ca* 300-400 yrs (Mangerud *et al.*, 2006) and could have been up to 700 yrs during the Preboreal (Haflidason *et al.*, 2000). Quantifying the past marine reservoir offset remains a challenge in the palaeoclimate community.

Nevertheless, marine radiocarbon dates are used for FIS reconstructions and have been obtained from: 1) bulk marine sediments that underlie or are located in front of moraines (e.g. Björck and Håkansson, 1982; Berglund, 1995); 2) shells that are located in sediments in front of a moraine (e.g. Blake and Olsen, 1999); and 3) from shells in reworked marine sediments that have become incorporated within moraines (e.g. Fernlund, 1988, 1993, Johnson and Ståhl, 2010). Marine radiocarbon dates form a fundamental part of the deglaciation chronology and are used in the most recent reconstruction of FIS retreat (Hughes *et al.*, 2016; Stroeven *et al.*, 2016).

As well as problems related to depositional environment (e.g. marine/lacustrine), long-term variations in ^{14}C production is also a major problem in radiocarbon dating as atmospheric ^{14}C varies over time (Lowe and Walker, 2014). The Lateglacial and early Holocene, is characterised by several radiocarbon 'plateau'. For example the Preboreal is characterised by a plateau at 10,000 ^{14}C yrs BP (Björck *et al.*, 1996) and radiocarbon dates from this time period are highly sensitive to the marine reservoir effect. Therefore, dates between 11,000-10,500 ^{14}C yrs BP could yield an age of *ca* 10,000 ^{14}C yrs BP if a marine reservoir effect of 700-800 yrs is applied (Björck *et al.*, 2002).

2.2.4.4 Using biostratigraphy as a chronostratigraphic tool

Pollen stratigraphies have also been used to date key moraine belts across Fennoscandia (Lundqvist and Wohlfarth, 2001). For example, the Middle Swedish End Moraine Zone (MSEMZ), the Ra moraines in Norway and the Salpausselkä I and II moraines in Finland were initially correlated to the Younger Dryas period using pollen analysis (Donner, 1951, 2010; Björck and Digerfeldt, 1984; Lundqvist, 1995; Mangerud *et al.*, 2011). The Younger Dryas (12.9-11.7 ka BP) age of the moraines has since been verified by radiocarbon dating (e.g. Johnson and Ståhl, 2010), ^{10}Be exposure dating (e.g. Tschudi *et al.*, 2000) and/or correlation with the Greenland ice-core chronology (Stroeven *et al.*, 2016).

It has been recognised that the age correlation of glacial moraines using pollen stratigraphies was based on the assumption that the moraines in Sweden, Norway and Finland were deposited synchronously, and that the vegetation record, as

reflected in the pollen stratigraphy, reflects the same forcing mechanism that led to moraine emplacement (Björck *et al.*, 2002). The correlation of the Swedish and Finish end moraines to the Younger Dryas is still generally accepted after 70 years of detailed study (Donner, 2010). These moraines are considered to represent the last major stillstands of the FIS before climatic amelioration during the early Holocene. As such many models of ice retreat across Fennoscandia consider these moraines as a key chronostratigraphic marker in the deglaciation chronology (e.g. Andrén *et al.*, 2011; Hughes *et al.*, 2016; Stroeven *et al.*, 2016). The significance of these moraines, in particular the timing of their emplacement, is particularly important for Baltic Ice Lake drainages which are considered in section 2.3.5.

2.2.4.5 Evidence from glacial varves

Glacial varved clays were deposited during the BIL stage of the Baltic Sea and have been used to track the retreat of the FIS in southern Sweden. These varves are located in the modern Baltic Sea, along the current Baltic coast and in south eastern Sweden (Figure 2-6).

De Geer (1912) developed the first varve model and proposed that light-coloured silt and dark-coloured clay laminations deposited in the Baltic Basin were deposited within a year (a varve). The basal varve which is deposited on top of the underlying bedrock or glacial till represents the minimum age of deglaciation and therefore the former position of the ice margin (De Geer, 1884, 1912, 1940; Sauramo, 1918, 1923). De Geer also proposed that the thickness of each varve was primarily driven by the position of the ice margin and as such, varve records in close proximity could be correlated using varve thickness patterns in order to create a composite varve record. It is important to note that later work by other researchers (e.g. Ringberg, 1984; Kristiansson, 1986; Brunnberg, 1995; Ringberg *et al.*, 2003) suggests that additional processes may control varve thickness, and these are discussed further in Chapters 3 and 4. By constructing varve-thickness diagrams and correlating overlapping records from successive glacially-eroded basins from south to north, De Geer established a varve chronology in the Stockholm area and along the Swedish east coast (De Geer, 1884, 1912, 1940). His chronology represented the pioneering first steps in estimating the timing and rate of ice recession. Since the initial work by De Geer (De Geer, 1884, 1896, 1912, 1940) the Swedish varve chronology or 'Swedish Timescale' (STS) has been continuously revised and now extends to the present day (Strömberg, 1985, 1994; Kristiansson, 1986; Cato, 1987; Andrén, 1990; Brunnberg, 1995; Wohlfarth *et al.*, 1998).

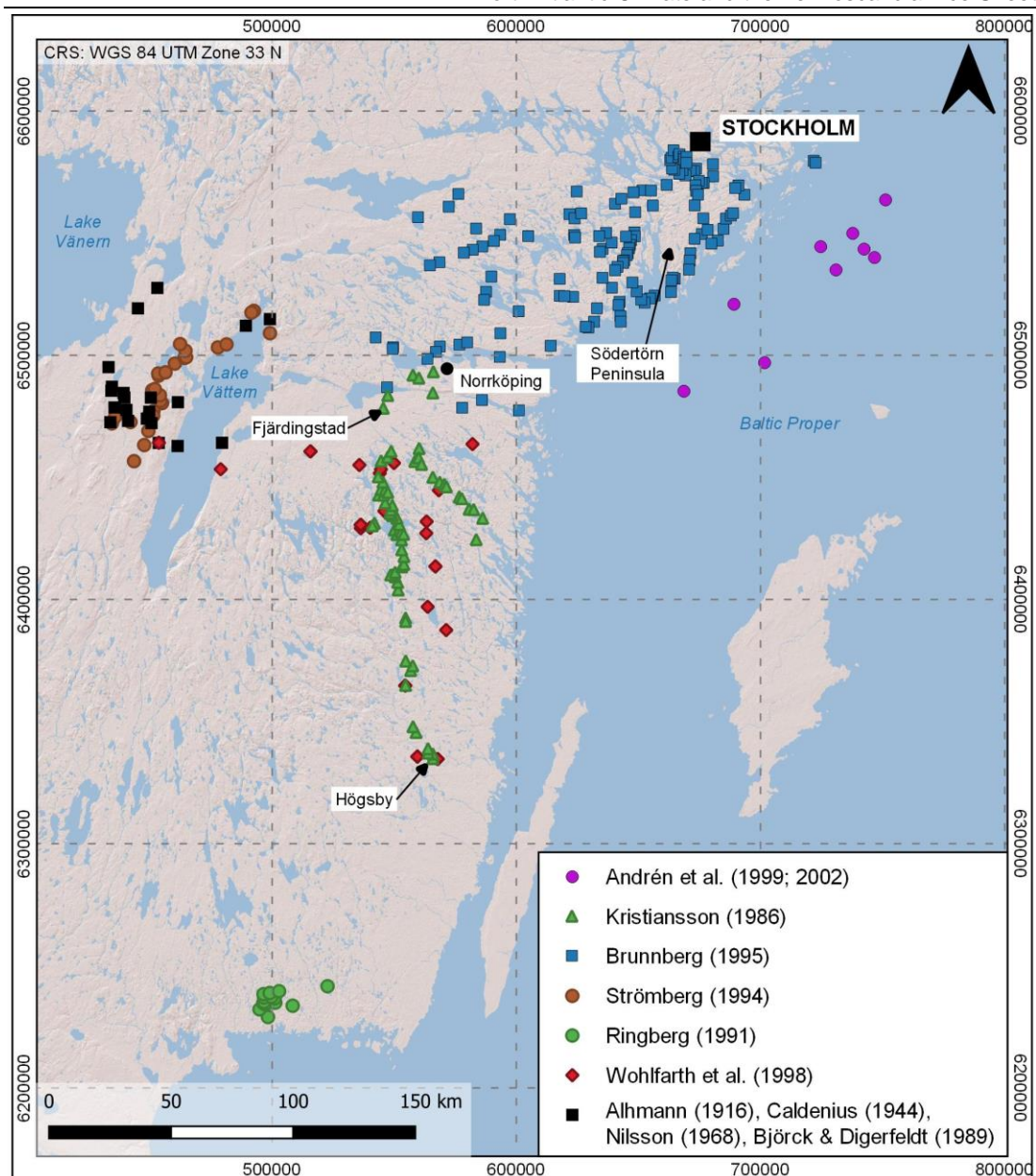


Figure 2-6. Baltic Ice Lake varve sites.

Site locations were digitised using a combination of grid references and by georeferencing maps provided in the original publication.

Despite the efforts of many researchers over the last century, correlation of the STS with the Greenland GRIP ice-core chronology (Andrén *et al.*, 1999, 2002; Ringberg *et al.*, 2003) and correlation with tree ring data (Björck *et al.*, 1996) indicate that hundreds of varves are missing in the STS (Andrén *et al.*, 2002). It is generally accepted that about 700-900 varves are missing during the Lateglacial, early or mid-Holocene periods (Andrén *et al.*, 2002; Strömberg, 1994; Wohlfarth *et al.*, 1997). Further details on the construction and chronological issues in the STS are presented in Chapter 3.

2.2.4.6 Tephrochronology

The identification of tephra in sediment archives across Fennoscandia provides further chronological constraint for deglaciation. The age of the lowermost tephra layer within lacustrine sediment records provides a minimum age of deglaciation. Fennoscandia is ideally located for the distribution and deposition of distal Icelandic tephtras during the Lateglacial. Firstly, the distance is within the dispersal range of major and medium-sized Icelandic eruptions and secondly, the prominent wind direction is towards Scandinavia (Wastegård, 2005). To date, several Lateglacial and Holocene tephtras have been identified in non-varved sediments above the highest shoreline of the Baltic Ice Lake (Figure 2-7).

In southern Sweden, the Borrobol, Hässeldalen and Askja-S tephtras were identified in the Hässeldala port sediment record from Blekinge. At the sites of Fågelmossen and Högstorpssmossen, Björck and Wastegård (1999) report the presence of Icelandic ash, which was preliminarily assigned to the Lateglacial Vedde Ash (12,023±86 cal. yrs BP (2σ); Bronk Ramsey *et al.*, 2015). More recently, the Laacher See Tephra (LST) from the Laacher See volcano in the East Eifel Volcanic Field in western Germany (*ca* 12,900 cal. yrs BP; Bronk Ramsey *et al.*, 2015) has been identified and chemically analysed from Korslättamossen fen, in southernmost Sweden (Larsson and Wastegård, 2018).

Although rare, tephra has also been identified in varved sediment records from the Lateglacial and Holocene (Zillén *et al.*, 2002; MacLeod *et al.*, 2014). For Lateglacial varve records, volcanic glass shards were found but not chemically analysed in the varve record from Lake Mullsjön (Figure 2-7, site 9) (Wohlfarth *et al.*, 1993), though recently, tephra has been chemically analysed from the Gropviken site in Östergötland and correlated to the Lateglacial Vedde Ash (Figure 2-7, site 1) (MacLeod *et al.*, 2014). For the Holocene period, Zillén *et al.* (2002) identified three mid-Holocene tephra layers in west central Sweden. The identification of tephra in varved sediments demonstrates the potential to identify other Lateglacial and early Holocene tephtras within varved sediments. Critically, the combination of tephra and varve chronology enables more precise age estimates for ice-sheet deglaciation with errors typically of decadal/centennial-scale (e.g. Bendle *et al.*, 2017). However, this is, at present, an underutilised chronological technique in FIS reconstructions.

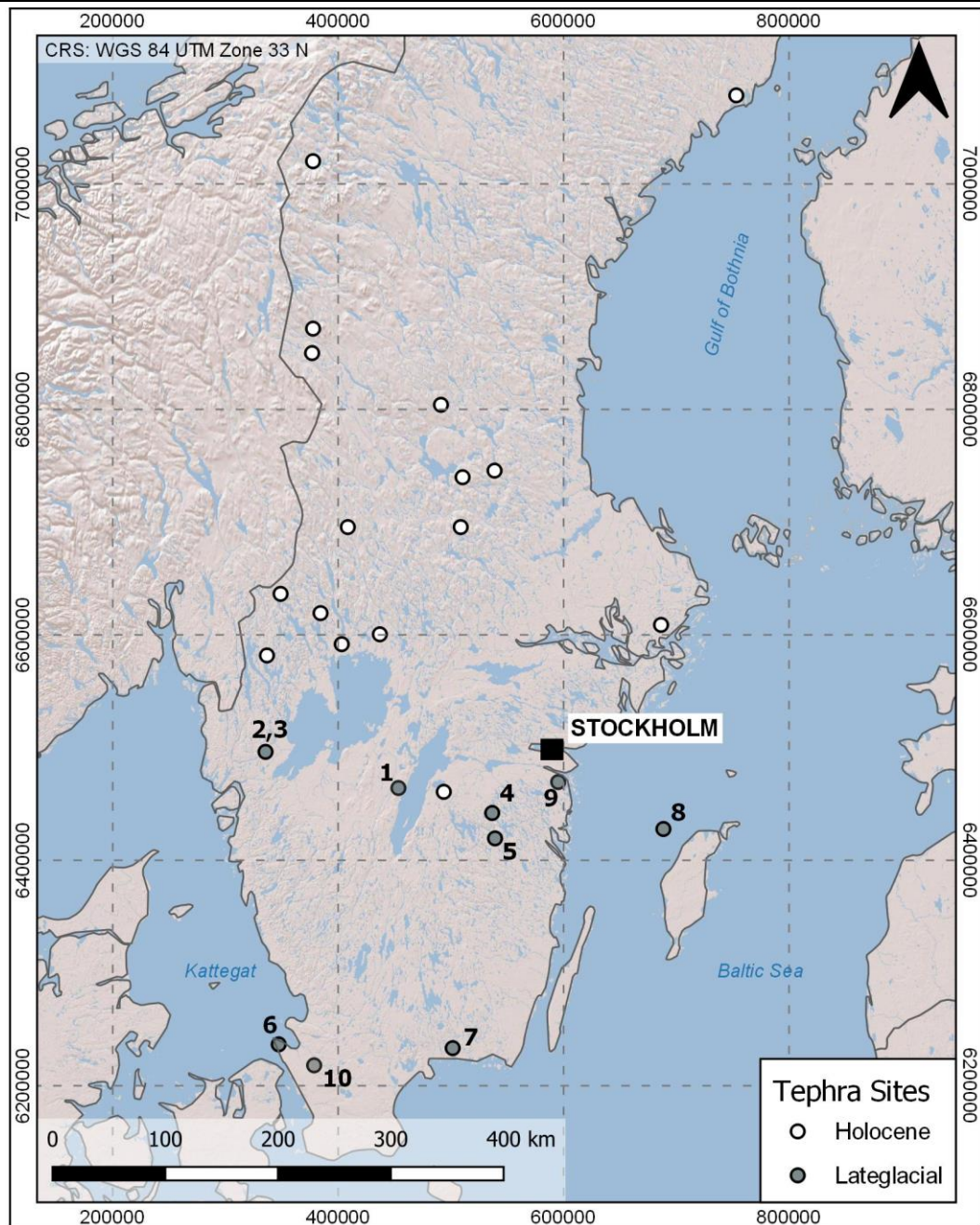


Figure 2-7. Locations of Lateglacial and Holocene tephras in southern Sweden.

1) Lake Mullsjön (Wohlfarth et al., 1993); 2) Lake Madtjärn (Wastegård et al., 1998); 3) Lake Götesjön (Schoning, 2001, 2002); 4) Fågelmossen (Björck and Wastegård, 1999); 5) Högstorpsmossen (Björck and Wastegård, 1999; Björck et al., 2002); 6) Lake Kullatorpssjön (Sandgren et al., 1999; Wastegård et al., 2000); 7) Hässeldala port (Davies et al., 2003); 8) NW Gotland (Påhlsson and Bergh Alm, 1985); 9) Gröpviken (MacLeod et al., 2014). 10) Korslätmamossen fen (Larsson and Wastegård, 2018). Holocene tephras are cited in (Wastegård, 2005).

2.3 Deglaciation chronology

Using the lines of evidence detailed in section 2.2, a Fennoscandian Ice Sheet deglaciation chronology has been established. Here, key phases of the ice-sheet retreat are presented to provide a framework for discussion of the FIS reconstructions in Sweden that are pertinent to the thesis.

2.3.1 24-16 ka BP

During the LGM (*ca* 24-21 ka BP) the FIS reached its maximum extent in Scandinavia and northern Europe (Houmark-Nielsen and Kjær, 2003). The southernmost extent has been mapped using the Brandenburg moraine in Germany (Lippstreu *et al.*, 1995; Lüthgens and Böse, 2011), the Leszno moraine in Poland (Tylmann *et al.*, 2019) and the Mid-Danish till in Denmark (Larsen *et al.*, 2009). At the LGM the FIS also advanced into Latvia (Saks *et al.*, 2012), Lithuania (Baltrūnas *et al.*, 2007; Lasberg and Kalm, 2013) and Russia (Kjær *et al.*, 2003; Stauch and Gualtieri, 2008). The exact position and timing of maximum ice extent in Russia is uncertain and different reconstructions place the LGM several hundred kilometres and several thousands of years apart (Stauch and Gualtieri, 2008; Hughes *et al.*, 2016). Arguably, the best age estimate of the LGM in Russia is *ca* 17-15 ka BP (Larsen *et al.*, 1999; Lyså *et al.*, 2014) which is considerably later than other parts of the ice sheet (Stroeven *et al.*, 2016).

After the LGM, a series of advances and retreat phases across the southernmost limit of the FIS occurred (see summary by Houmark-Nielsen and Kjær, 2003), though it is generally accepted that the Baltic Sea was deglaciated *ca* 17 ka BP (Lagerlund and Houmark-Nielsen, 1993; Sandgren *et al.*, 1999) and southernmost Sweden was ice-free by *ca* 16 ka BP (Andrén *et al.*, 2011). In southern Sweden, ¹⁰Be exposure ages from the island of Bornholm, yield ages of *ca* 20-17 ka BP (Houmark-Nielsen *et al.*, 2012), implying deglaciation of the southwest Baltic Sea by *ca* 17 ka BP. However, some CN exposure ages from boulders within the Halland Coastal Moraine, north of Bornholm in southwestern Sweden, yield ages of 19-15 ka BP (Larsen *et al.*, 2012), the older of which contradict the *ca* 17 ka BP deglaciation age that has been proposed for the Baltic Sea (Kramarska, 1998).

By *ca* 17 ka BP the FIS had started to retreat from its maximum position in Russia (Lunkka *et al.*, 2001; Baltrūnas *et al.*, 2007) and eastern Europe (Svendsen *et al.*, 2004; Lasberg and Kalm, 2013). During initial deglaciation of the Baltic (*ca* 17-16 ka BP), the sea was connected to the marine waters in the Kattegat (Lagerlund and Houmark-Nielsen, 1993; Sandgren *et al.*, 1999). This is evidenced by ringed seal

(*Pocha hispida*) and polar cod (*Gadus polaris*) fossils within brackish clays in the northern Øresund area (Lagerlund and Houmark-Nielsen, 1993). During this time the Øresund strait between Sweden and Denmark was the main drainage area of the FIS (Andrén *et al.*, 2011). Following isostatic rebound of the Øresund region, which was faster than the rate of sea level rise, the Baltic was uplifted above sea level. This initiated the ponding of freshwater and the Baltic Ice Lake began to form at ca 16 ka BP (Lagerlund and Houmark-Nielsen, 1993; Andrén *et al.*, 2011).

The following sections summarise the deglaciation chronology from ca 16-8 ka BP with a particular focus on FIS retreat in Sweden. Comprehensive reviews of the deglaciation chronology outside Sweden are provided by Svendsen *et al.* (2004), Demidov *et al.* (2006), Hughes *et al.* (2016) and Stroeve *et al.* (2016).

2.3.1.1 Halland Coastal Moraines (HCM) (17.4-16.0 cal. ka BP)

The Halland Coastal Moraines (HCM) comprise the oldest moraine belt in Sweden (Caldenius, 1942). The HCM are different to other moraine belts in Sweden in that there are multiple parallel moraines that cover a ca 15 km wide zone (Fernlund, 1993). The HCM can be traced across the Kattegat coast and the westernmost moraines continue onto the Kattegat floor (Figure 2-8) (Mörner, 1969; Lundqvist and Wohlfarth, 2001). In places the HCM can form a series of small moraines with deltas and individual moraines have been deposited on top of drumlins and eskers (Caldenius, 1942; Berglund, 1979; Fernlund, 1988, 1993). The internal structure of the HCM is complex and individual moraines consist of alternating units of diamicton and sorted silts and gravel (Fernlund, 1988, 1993). Marine clay and mollusc shells are also incorporated within the HCM and indicate formation as push moraines during FIS readvance (Berglund, 1979; Fernlund, 1988, 1993).

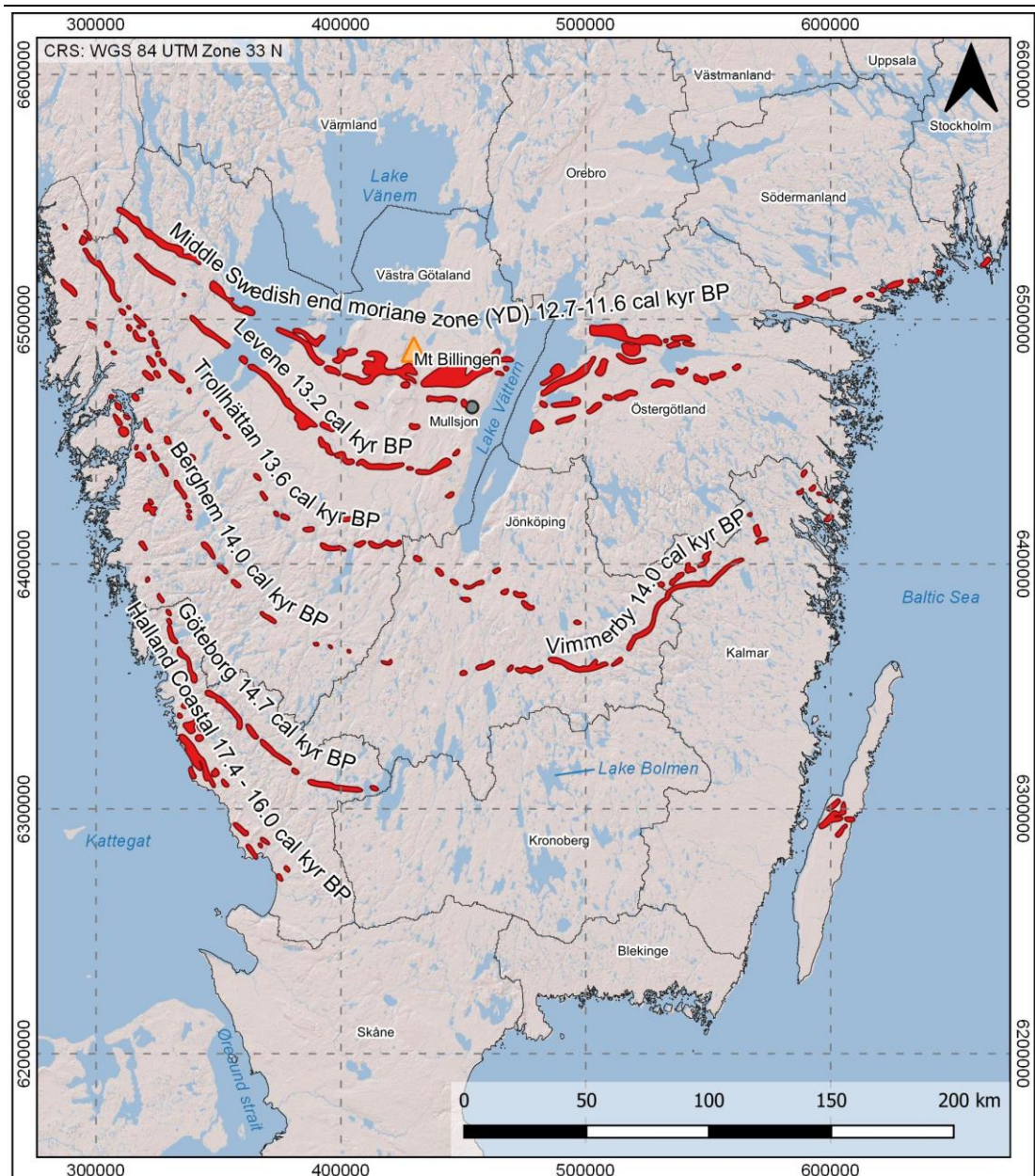


Figure 2-8. Major end moraine zones in southern Sweden.

The age assignments (in cal. ka BP) are based on radiocarbon dates (Lundqvist and Wohlfarth, 2001), CN exposure dates (Larsen et al., 2012; Anjar et al., 2014), and, primarily, correlations with the Greenland ice-core event stratigraphy (Rasmussen et al., 2014). Modified from Stroeven et al. (2016).

There is longstanding debate surrounding the age of the HCM which has been dated by: 1) radiocarbon dating mainly of fossil mollusc shells incorporated within the moraines; 2) CN exposure dating; and 3) pollen stratigraphy. Radiocarbon dates from mollusc shells suggest the HCM formed ca 14-13 ^{14}C ka BP (Berglund, 1979; Påsse, 1992) whereas Björck et al. (1988) suggest the HCM are older than 12.9 ^{14}C ka BP and Fernlund (1988, 1993) proposed ages of 12.7-12 ^{14}C ka BP. More recently, Berglund (1995) correlated the lake sediments from between the innermost and outermost moraines to the Bølling pollen zone. Radiocarbon dates from aquatic

mosses and bulk sediment samples from these lakes yielded ages between 12.9-12.3 ^{14}C yrs BP for the Bølling pollen zone (Berglund, 1995). Lundqvist and Wohlfarth (2001) accepted and calibrated the ages proposed by Berglund (1995) with a resulting age of ca 15.55-14.55 cal. ka BP (using the IntCal98 curve; Stuiver *et al.*, 1998). However, the calibrated age falls in the Oldest Dryas pollen zone. Nevertheless, since the radiocarbon dates are from sediment sequences between the innermost and outermost moraine, by inference the HCM must be older than the Berglund (1995) radiocarbon dates. Therefore, the HCM were assigned an age of ca 18-16 ka BP (Lundqvist and Wohlfarth, 2001). In recent years, Larsen *et al.* (2012) reported ^{10}Be ages from the HCM that range between 20-14.7 ka BP which broadly supports the ca 18-16 ka BP age proposed by Lundqvist and Wohlfarth (2001). Moreover, Stroeven *et al.* (2016) propose an age of 17.4-16 ka BP based on one-to-one matching with cold phases in the Greenland ice-core record. An age of ca 18-16 ka BP for the formation of the HCM is used in the most recent reconstructions of FIS retreat (e.g. Hughes *et al.*, 2016; Stroeven *et al.*, 2016).

2.3.2 16-14 cal. ka BP

Several radiocarbon dates indicate that by 15 ka BP the FIS had retreated further onto the Norwegian coast (Goehring *et al.*, 2008) and at the beginning of the Bølling Interstadial, the Skagerrak sea was a calving bay that released icebergs into the Norwegian channel (Andersen, 1979). On the eastern margin of the FIS, the ice margin has been mapped using the Haanka and Luga moraines in Russia (Demidov *et al.*, 2006; Stauch and Gualtieri, 2008; Fredin *et al.*, 2012) and the North Lithuanian moraine (Baltrūnas *et al.*, 2007; Kalm, 2012).

2.3.2.1 Göteborg Moraine (GM) (14.7 cal. ka BP)

After formation of the HCM in southwest Sweden, the Göteborg Moraine (GM) formed further inland and to the north (Figure 2-8). The GM is composed of a series of discontinuous ridges which are up to 50 m high (Wedel, 1971; Hillefors, 1975, 1979). The eastern extension of the moraine is debated and has been traced to Blekinge in southern Sweden (Björck *et al.*, 1988) and further east towards Lake Bolmen (Andersson, 1998). The GM is typically composed of diamict and sorted sands and gravel (Hillefors, 1979) though the western extension is composed of till units that overly marine sediments (Lundqvist and Wohlfarth, 2001). The GM has been correlated with the Oldest Dryas pollen zone (Berglund, 1995) and radiocarbon ages from marine molluscs and marine vertebrate bones range from 12.9-12.5 ^{14}C ka BP (Hillefors, 1975, 1979; Berglund, 1979, 1995; Björck and Håkansson, 1982; Björck *et al.*, 1988) which equates to 15.4-14.5 cal. ka BP (Lundqvist and Wohlfarth, 2001).

Recently, Larsen *et al.* (2012) and Anjar *et al.* (2014) reported ^{10}Be exposure ages between ca 18.8-13.8 ka BP which broadly support the existing radiocarbon ages and pollen stratigraphy. The GM has also been dated to 14.7 ka BP by correlation with GS-2 in the Greenland ice-core chronology (Stroeven *et al.*, 2016). The 14.7 ka BP age is used in the most recent reconstructions of FIS retreat (Hughes *et al.*, 2016; Stroeven *et al.*, 2016).

2.3.3 14-12.7 cal. ka BP

At ca 14 ka BP the FIS had retreated from the northern and western Norwegian coasts (Mangerud *et al.*, 2011) and from southernmost Sweden (Kjær *et al.*, 2006; Johnsen *et al.*, 2009). The radiocarbon dated varve chronology from Lake Onega in Finland also indicates ice-free conditions by ca 14 ka BP (Saarnisto and Saarinen, 2001; Hang *et al.*, 2019). Between ca 14-12.7 ka BP the central Baltic became ice-free and rapid isostatic rebound of coastal areas led to formation of the “highest shoreline” (Svensson, 1989; Andrén *et al.*, 2011). The retreat across southern Sweden between ca 14-12.7 ka BP is characterised by several stillstands and minor readvances as indicated by several moraine belts that are located to the west of Lake Vättern (Lundqvist and Wohlfarth, 2001); the Berghem Moraine (ca 14 ka BP), Trollhätan Moraine (ca 13.6 ka BP) and the Levene Moraine (ca 13.2 ka BP). To the east of Lake Vättern, there is only one prominent moraine belt, the Vimmerby Moraine (ca 14 ka BP) (VM) (Agrell *et al.*, 1976; Johnsen *et al.*, 2009). By ca 13 ka BP the Baltic Ice Lake was uplifted ca 10 m above sea level (Björck, 2008).

2.3.3.1 The Berghem Moraine (BM) (14.0 cal. ka BP)

To the east of the northernmost extent of the GM are numerous moraines and deltas that comprise the Berghem Moraine (BM) (Figure 2-8) (Caldenius, 1942; Hilldén, 1979). The BM has been mapped northward across the Koster Islands (Johansson, 1982) and to the southeast (Hilldén, 1979). Using LiDAR elevation data Dowling *et al.* (2013) show a clear morphological continuation between the easternmost part of the BM and the Vimmerby Moraine in south eastern Sweden.

A series of double ridges that comprise the BM likely represent readvance or oscillations of the ice margin (Björnsjö, 1949; Mörner, 1969; Lundqvist and Wohlfarth, 2001). Detailed geomorphological mapping and stratigraphy indicate that the ice margin oscillations were likely driven by the local topography (Johansson, 1982; Ronnert, 1989), and were therefore likely to have been highly sensitive to climatic fluctuations (Lundqvist and Wohlfarth, 2001).

The BM has been dated through pollen stratigraphy and radiocarbon dating of lacustrine and marine fossil material that were deposited in close proximity to the moraine. Ages range between ca 12.1-11.1 ^{14}C ka BP (Fredén, 1988; Pässe, 1992; Sørensen, 1992; Berglund, 1995). Pollen stratigraphy from basal lake sediments deposited to the east of the BM were initially correlated to the Bølling pollen zone (Hilldén, 1979), but were later correlated to the Older Dryas pollen zone (Berglund, 1995). Bulk radiocarbon dates from these lake sediments yielded ages of ca 12.2-11.8 ^{14}C ka BP (Hilldén, 1979), and were later calibrated to 14.1-13.9 cal. ka BP (Björck and Håkansson, 1982). The radiocarbon ages contradict the Bølling pollen zone interpretation by Hilldén (1979) but are in agreement with the Older Dryas pollen zone assignment by Berglund (1995). Radiocarbon dates have also been acquired from mollusc shells deposited in marine clays on the northern side of the BM and provide a minimum age constraint of ca 12.35-12.25 ^{14}C ka BP or ca 14.4-14.2 cal. ka BP (Fredén, 1988). These dates support formation of the BM during the Bølling pollen zone (Lundqvist and Wohlfarth, 2001).

Since the BM has been linked to the Vimmerby Moraine in south eastern Sweden (Dowling *et al.*, 2013) it has been proposed that these moraine belts were deposited synchronously (Stroeven *et al.*, 2016). The BM has also been correlated to GI-1d in the Greenland ice-core chronology on the basis of a ca 14 ka BP age of formation (Stroeven *et al.*, 2016).

2.3.3.2 The Vimmerby Moraine (VM) (14.0 cal. ka BP)

The Vimmerby Moraine is the most prominent ice marginal landform in south eastern Sweden and can be traced for ca 100 km (Figure 2-8) (Johnsen *et al.*, 2009). The age of the moraine is constrained by the Östergötland-Småland varve chronology which is located slightly north of the VM (Wohlfarth *et al.*, 1998). The southernmost sites that comprise the regional varve chronology contain terrestrial macrofossils that have been radiocarbon dated to ca 13.2 cal. ka BP (Wohlfarth *et al.*, 1998; Muschitiello *et al.*, 2016). Furthermore, pollen analysis from these varve records place the oldest part of the regional varve chronology in the Bølling pollen zone (Kristiansson, 1986).

More recently, ^{10}Be exposure ages from boulders within the VM yield mean ages of ca 14.6-14.5 ka BP (Anjar *et al.*, 2014). Correlation of the VM with the BM (and GI-1d) support an age of ca 14 ka BP (Stroeven *et al.*, 2016).

2.3.3.3 The Trollhättan Moraine (TM) (13.6 cal. ka BP)

Northeast of the Berghem Moraine is the Trollhättan Moraine (TM) (Figure 2-8) (Johansson, 1982). The TM has been traced on land and also extends onto the

present-day sea floor in the Skagerrat (Sørensen, 1992). The TM is characterised by multiple moraines that can be narrow and can contain deformed or glaciotectonised sediments indicative of an oscillating ice margin (Fredén, 1990; Björck and Digerfeldt, 1991). The TM has also been linked to the Hvaler Moraine in Norway which has an estimated age of *ca* 12.0-11.8 ka BP (Mangerud *et al.*, 2011).

Many researchers have attempted to date the TM using radiocarbon dating from a range of sample material. Radiocarbon samples include bulk lacustrine sediments, seal and whale bones, bulk marine sediment and marine shells. Ages from these samples range from 12.2-11.6 ¹⁴C yrs BP (Fredén, 1975, 1988; Berglund, 1979, 1995; Björck *et al.*, 1988). Radiocarbon dating of marine algae from basal lake sediments adjacent to the TM indicate that the area became ice free between 14.2-13.45 cal. ka BP (Björck and Digerfeldt, 1982). Pollen analysis also places these sediments during the early Allerød pollen zone (Björck and Digerfeldt, 1982; Lundqvist and Wohlfarth, 2001). The smaller size of the TM in comparison to other moraine belts in southern Sweden has been associated with GI-1c2 in the Greenland ice-cores (Stroeven *et al.*, 2016) which was a short-lived and low-magnitude cold event that has been dated to *ca* 13.6 ka BP (Rasmussen *et al.*, 2014). The *ca* 13.6 ka BP age is used in the most recent reconstructions of FIS retreat (Hughes *et al.*, 2016; Stroeven *et al.*, 2016).

2.3.3.4 Levene Moraine (LM) (13.2 cal. ka BP)

The Levene Moraine (LM) is located between the Trollhättan Moraine to the southwest and the Middle Swedish End Moraine Zone (MSEMZ) to the north (Figure 2-8) (Strömberg, 1969; Johansson, 1982). The LM can be traced for >250 km from Lake Vänern in southern Sweden into Norway (Strömberg, 1969) where it has been linked to the Onsøy Moraine (Sørensen, 1979). The easternmost part of the LM has also been linked to the Vimmerby Moraine in south eastern Sweden (Johnsen *et al.*, 2009).

The LM is composed of well-defined, long ridges (Johansson, 1982) and close to Lake Vänern marine clays overly some moraine ridges (Lundqvist and Wohlfarth, 2001). However, the sedimentology of the rest of the LM is less well studied and is assumed to be diamict and sorted sediments (Lundqvist and Wohlfarth, 2001).

Early palynological studies from adjacent lakes suggest formation of the LM during the Older Dryas (Berglund, 1979), but later investigations from other lake sequences suggest correlation to the Allerød pollen zone (Björck and Digerfeldt, 1982, 1991; Björck *et al.*, 1998). There are no radiocarbon dates from sediments or fossils that have been incorporated within the LM and so radiocarbon ages are derived from

adjacent lake sequences (e.g. Björck and Digerfeldt, 1984, 1986). Samples of marine algae have been dated from the basal lake sediments and returned ages between ca 14.1-13.1 cal. ka BP. Since the lake sediments are located outside of the LM the radiocarbon dates are considered a minimum age estimate. It was therefore assumed that the moraines formed after the mid-Allerød (Lundqvist and Wohlfarth, 2001). Further pollen and radiocarbon stratigraphies from basal lake sediments inside the LM complex have been assigned to the late-Allerød and yield ages between ca 13.43-12.94 cal. ka BP (Björck and Digerfeldt, 1984). More recently, ^{10}Be ages from the LM yield ages between ca 14.6-12.7 cal. ka BP (Larsen *et al.*, 2012; Anjar *et al.*, 2014) which broadly support the radiocarbon age estimates of ca 14.1-13.1 cal. ka BP. The LM has also been dated by correlation to GI-1b in the Greenland ice-cores (Stroeven *et al.*, 2016) at ca 13.2 ka BP (Rasmussen *et al.*, 2014). The 13.2 ka BP age for the LM is used in the most recent deglaciation chronologies (Hughes *et al.*, 2016; Stroeven *et al.*, 2016).

2.3.4 12.9-11.7 ka BP

The Younger Dryas (ca 12.9-11.7 ka BP) ice-margin position has been mapped almost continuously around Fennoscandia (Figure 2-3). In Norway two prominent moraines, the Ra Moraine and the Ås Moraine, have been identified that are associated with the start and the end of the Younger Dryas (Mangerud *et al.*, 2011). ^{14}C dates from marine molluscs indicate that the Ra Moraine formed ca 12.6 cal. ka BP and the Ås Moraine formed later in the Younger Dryas ca 11.9 cal. ka BP (Table 2-2). It has also been suggested that in other locations in Norway the ice-margin line oscillated.

Table 2-2. Radiocarbon dates from marine molluscs from the Ra and Ås Moraines in Norway. ^{14}C ages from Andersen *et al.* (1995) calibrated using IntCal13 (Reimer *et al.*, 2013).

Moraine	Sample code	^{14}C yrs BP	cal. yrs BP ($\mu+\sigma$)
Ra	T-8522	10,570 \pm 110	12,477 \pm 156
Ra	T-8523	10,680 \pm 100	12,606 \pm 96
Ra	TUa-144	10,630 \pm 160	12,493 \pm 200
Ra	TUa-145	10,680 \pm 170	12,549 \pm 207
Ra	T-424	10,760 \pm 200	12,643 \pm 237
Ås	TUa-296	10,215 \pm 95	11,915 \pm 212

In Finland the succession of three parallel ridges; the Salpausselkä I, II and III moraines, formed during the Younger Dryas and early Holocene periods. The existing chronology for these moraines is based mainly on varve chronology, biostratigraphy, ^{14}C dating and CN dating. For the Salpausselkä I and II moraines, correlation of the

Finnish and Swedish varve chronologies places these landforms within the Younger Dryas period (Strömberg, 1990) and within a 600 yrs bracket (Sauramo, 1923, 1929). More recently, varve counts, ^{14}C dating and palaeomagnetic measurements of lake sediments from Lake Onega in Russia (and correlation of these varves with the Finnish varve chronology) suggest that the Salpausselkä I and II moraines formed between 12,250-11,590 ± 100 cal. yrs BP (Saarnisto and Saarinen, 2001). The 660 yrs bracket is in agreement with the 600 yrs reported in the original Finnish varve chronology by Sauramo (1929).

CN exposure ages from boulders within the Salpausselkä I moraine also support a Younger Dryas age (Tschudi *et al.*, 2000). Rinterknecht *et al.* (2004) also reported an error-weighted mean from nine ^{10}Be exposure ages of 12.4 ± 0.7 ^{10}Be ka for the Salpausselkä I moraine. However, given the large uncertainties on the dates, an early Holocene age is also possible (Table 2-3).

Table 2-3. ^{10}Be surface exposure ages from the Salpausselkä I moraine. Further details on these dates are provided by the original authors.

Reference	Sample code	^{10}Be ka BP
(Rinterknecht <i>et al.</i> , 2004)	FIN-1	13.0 \pm 1.1
	FIN-2	11.8 \pm 1.1
	FIN-3	10.9 \pm 1.0
	FIN-4	12.0 \pm 1.1
	FIN-5	13.2 \pm 1.1
	FIN-6	11.8 \pm 1.0
	FIN-7	13.5 \pm 1.2
	FIN-8	13.5 \pm 1.2
	FIN-9	13.1 \pm 1.1
(Tschudi <i>et al.</i> , 2000)	Sal 1	13.3 \pm 1.1
	Sal 3	12.4 \pm 1.0
	Sal 4b	12.1 \pm 1.0
	Sal 5	12.6 \pm 1.1

It has been suggested that the Salpausselkä III moraine formed *ca* 300 yrs after the onset of the Holocene (Björck *et al.*, 1997). This inference is based on a correlation that has been made between the Finnish and Swedish varve chronologies (Donner, 2010). Brunnberg (1995) suggested that the brackish water ingression of the Yoldia Sea stage in Sweden occurred at the same time as the formation of the Salpausselkä III moraine, equating to *ca* 11.6 ka BP (Donner, 2010).

2.3.4.1 The Middle Swedish End Moraine Zone (MSEMZ) (12.9-11.7 cal. ka BP)

The MSEMZ describes the moraines that were formed at the southern margin of the FIS in southern Sweden during the Younger Dryas (Figure 2-8). These moraines have been a long-standing focus of FIS research (Strömberg, 1969; Björck and Digerfeldt, 1984; Johnson and Ståhl, 2010; Stroeve *et al.*, 2016; Johnson *et al.*, 2019), in part because they represent the last oscillation of the ice margin prior to the final drainage of the BIL. The number and morphology of the moraines is different across the MSEMZ reflecting different patterns of deglaciation.

To the east of Mt Billingen the geomorphology of the moraines and the varve chronology indicate a slow ice margin retreat with minor oscillations (Strömberg, 1994). In Lake Vättern there is sedimentological evidence for two readvances that have been attributed to the Younger Dryas (Waldermarson, 1986), however the varved-pollen record from lake sediments at Lake Mullsjön on the western coast of Lake Vättern shows a Late Allerød-Younger Dryas vegetation succession. This suggests that this site was ice-free and never over-ridden by a glacial readvance during the Younger Dryas (Björck and Digerfeldt, 1989). More recently, Wohlfarth *et al.* (1993) obtained radiocarbon dates from fragments of *Salix*, *Betula* and *Dryas octopetala* leaves from the Lake Mullsjön sediment sequence. However, the samples yielded much younger ages than were expected from the Younger Dryas pollen-stratigraphy. The samples yielded ages of $9,640 \pm 190$ and $9,945 \pm 115$ ^{14}C yrs BP and when calibrated using IntCal13 these ages equate to $10,984 \pm 281$ and $11,484 \pm 194$ cal. yrs BP respectively. The authors attribute the unexpected younger ages of these samples to problems with sample storage and analysis that may have incorporated younger carbon, such as fungi growth. As such, the ^{14}C ages from Lake Mullsjön were deemed unreliable and correlation to the Younger Dryas is based on pollen stratigraphy and the presence of so-called typical Lateglacial macrofossils such as *Dryas octopetala* (Wohlfarth *et al.*, 1993).

It has since been proposed that a prominent but narrow ice lobe existed in Lake Vättern, which may explain why the Mullsjön site was not over-ridden by glacial ice during the Younger Dryas (Wohlfarth and Possnert, 2000; Björck *et al.*, 20015). An alternative explanation is that the original Younger Dryas age of the Lake Vättern readvances, proposed by Waldermarson (1986) and later adopted by Lundqvist and Wohlfarth (2001), is incorrect. More recently, Greenwood *et al.* (2015) obtained a 74 m sediment record alongside geophysical data from Lake Vättern. After integration of these new data with regional geomorphological evidence, the authors proposed an

alternative hypothesis; that multiple readvances in the southern Vättern basin occurred prior to the Younger Dryas. The authors also suggest that a Younger Dryas ice advance may have occurred but was composed of thin or floating ice and did not penetrate the full length of the lake (Greenwood *et al.*, 2015).

In western Sweden there is evidence of a readvance during the Younger Dryas which has been linked to two prominent deltas; the Dal's Ed and the Ödskölt's Moar delta (Björck and Digerfeldt, 1991). Direct dating of these deltas is at present lacking, but their Younger Dryas age is based on correlation to the Ra and Ås moraines in Norway and the Skovde-Billingen moraines in southern Sweden (Lundqvist and Wohlfarth, 2001). The Ödskölt's Moar delta is located ca 15 km SE of the Dal's Ed delta and the presence of clays which underlie outwash plain sediments at the Ödskölt's Moar delta (Johansson, 1982) suggest the ice margin may have retreated and readvanced (Johansson, 1982; Björck and Digerfeldt, 1991).

In central Sweden to the west of Mt Billingen there are seven prominent moraines that differ in morphology and composition from east to west (Figure 2-9) (Björck and Digerfeldt, 1984; Johnson and Ståhl, 2010; Johnson *et al.*, 2019). In the west, the moraines are typically composed of deformed glaciomarine clay whereas in the east the moraines are composed of fluvial sands and gravel (Johnson *et al.*, 2019). Earlier in the deglaciation this area was submerged below sea level with relative sea level between 120-130 m a.s.l (Björck and Digerfeldt, 1984; Strömberg, 1992). Johnson *et al.* (2019) interpret the seven ridges as push moraines whereby glaciomarine clay that was deposited during ice-margin retreat from the southernmost end moraine (Skara) was pushed, up-thrusted and deformed during ice margin oscillation. The northernmost ridge at Gullhammar represents the last glacial stillstand before the ice margin retreated north of Mt Billingen opening up the drainage pathway of the BIL causing catastrophic drainage (Figure 2-9) (Strömberg, 1992, 1994). This means that by inference, the formation of the MSEMZ in this area occurred before the final BIL drainage.

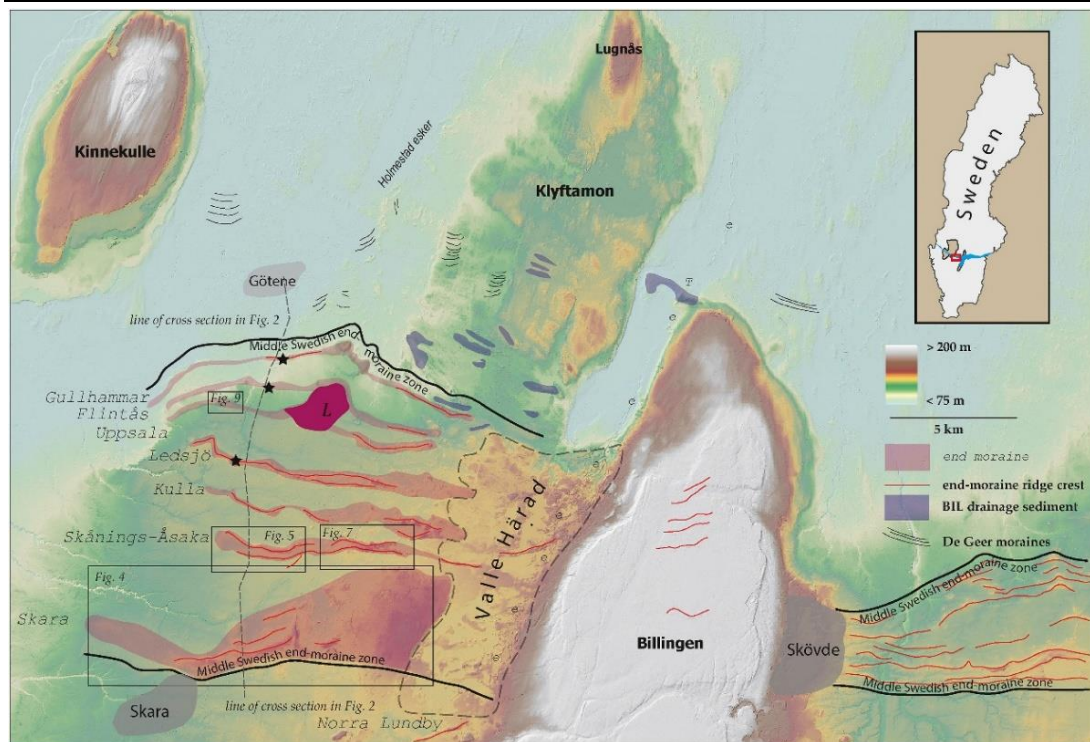


Figure 2-9. Map of the MSEMZ in the Mt Billingen area.

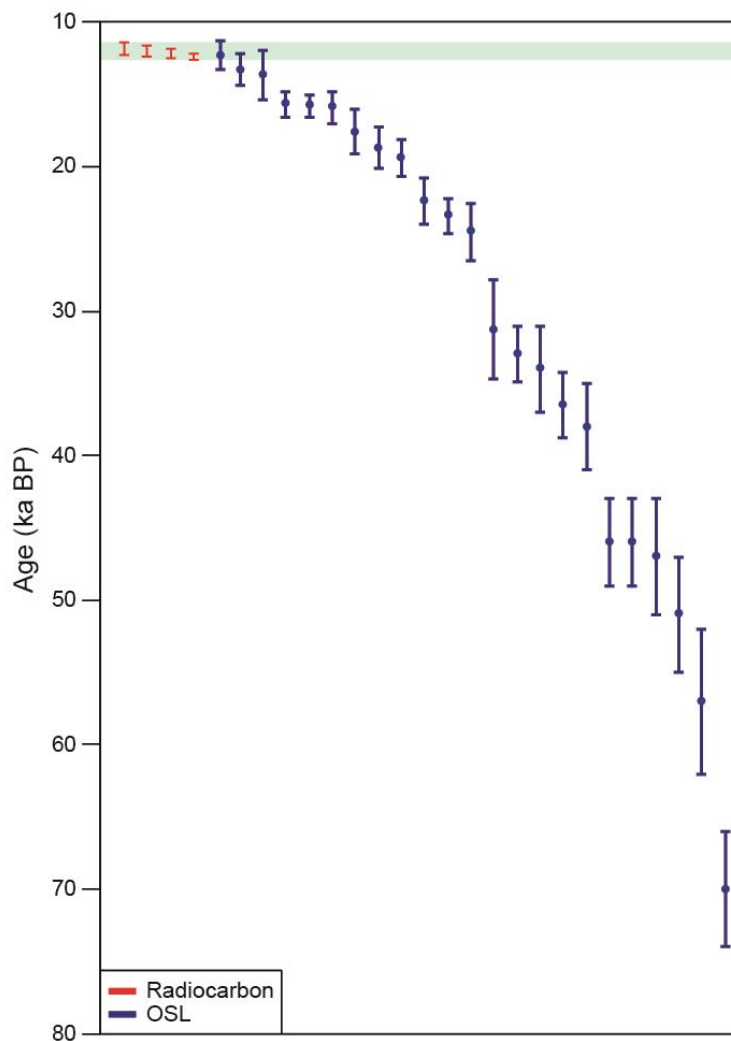
Inset shows map location between Lake Vänern (to the west) and Lake Vättern (to the east) as well as the position of MSEMZ across Sweden (in blue). The names of the end moraines are shown west of Billingen. 'e' = prominent eskers. 'T' = Timmersdala ridge. 'L' = Ledsjömo, an ice-contact delta built up at the Uppsala and Flintås ice-margin positions. The Gullhammar and Skara end moraines that are referred to in the main text are also shown. From Johnson et al. (2019) pp.2.

The MSEMZ has primarily been dated by radiocarbon dating of marine foraminifera and ostracods (Johnson and Ståhl, 2010). Samples were corrected by 500 or 800 years (depending on the location of the moraine) to account for the marine reservoir effect. Radiocarbon ages range from ca 13.0-11.4 cal. ka BP (Table 2-4) (Johnson and Ståhl, 2010). It was initially suggested that the clay in the moraine ridges was originally deposited during the Allerød but was deformed and incorporated within the moraine ridges during ice advance in the Younger Dryas (Björck and Digerfeldt, 1984; Björck, 1995).

Table 2-4. Radiocarbon dates from the MSEMZ from Johnson and Ståhl (2010).

Calibrated using IntCal04 (Reimer et al., 2004).

Sample code	Dated Material	Sample quantity ($\mu\text{g C}$)	^{14}C yrs BP	cal. yrs BP (95.4%)
LuS 7406	Benthic foraminifers	515	11,200 \pm 100	12,140–12,595
LuS	Benthic ostracods	130	10,915 \pm 140	11,665–12,390
LuS	Benthic foraminifers	285	11,070 \pm 130	11,910–12,530
LuS	Benthic ostracods	115	10,815 \pm 170	11,415–12,350
Ua-32596	<i>Astarte borealis</i> (?) or <i>Macoma calcaria</i> (?)	-	14,420 \pm 80	12,690–13,000

**Figure 2-10.** Radiocarbon and OSL ages from the MSEMZ.

The age range of the radiocarbon dates is highlighted in green and 3 OSL dates overlap with these ages. Johnson and Ståhl (2010) provided data for 23 of the 25 OSL ages. The 23 OSL ages with corresponding sample data are plotted here. Modified from Johnson and Ståhl (2010).

OSL ages have also been obtained from clay deposited within the push moraines but samples yielded ages ranging from 11 to 70 ka BP, with errors ranging from 900-5,000 years per sample (Johnson and Ståhl, 2010). In total 25 samples were dated by OSL dating and only 3 of these were of Younger Dryas age and overlap in age with the radiocarbon dates from the MSEMZ (Figure 2-10). The other ages were considered too old due to insufficient bleaching of sand grains (Johnson and Ståhl, 2010). The MSEMZ has also been dated to the Younger Dryas period by correlation with GS-1 in the Greenland ice-core chronology (Stroeven *et al.*, 2016) and this age is used in the most recent deglaciation chronologies (Hughes *et al.*, 2016; Stroeven *et al.*, 2016).

2.3.5 Baltic Ice Lake (BIL) drainage events

Due to isostatic uplift, the BIL was ca 25 m above the sea level during the Younger Dryas. During this period the ice margin blocked the natural drainage pathway of the BIL at Mt Billingen (Figure 2-11). After the ice margin retreated past the northernmost moraine in the MSEMZ and past the end of Mt Billingen, the drainage pathway opened and the BIL catastrophically drained into the sea (Björck and Digerfeldt, 1986; Björck, 1995).

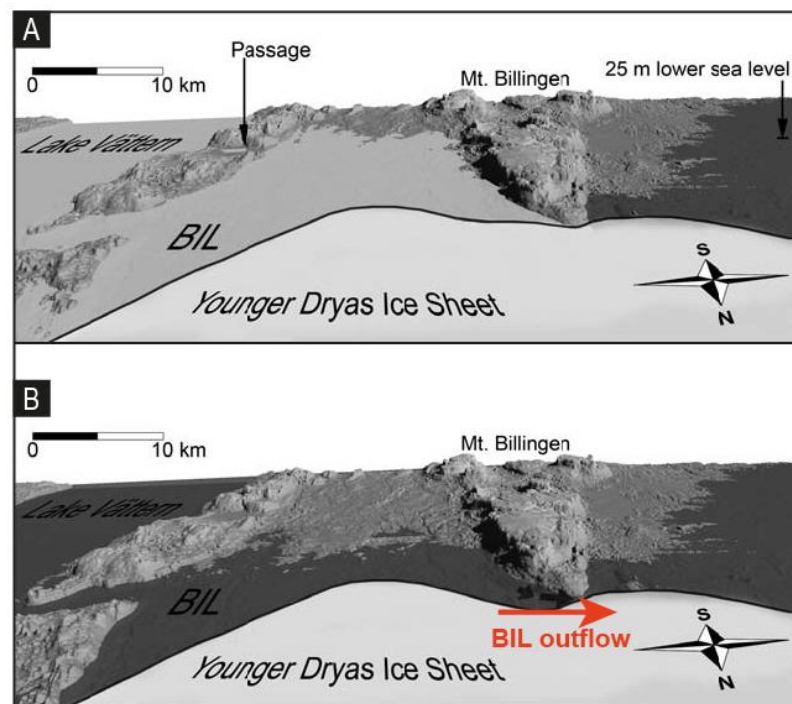


Figure 2-11. Reconstruction of the area north of Mt Billingen before (A) and after (B) BIL drainage.

Diagram based on a 50 × 50 m Digital Terrain Model (DTM). The BIL level is shown with light grey shading and the sea level which was 25 m lower in comparison to the BIL is shown with a darker grey shading. Diagram is facing southwards. Modified from Jakobsson *et al.* (2007).

The first drainage is thought to have lowered the lake level by 5-10 m before a phase of ice readvance blocked the drainage pathway for a second time (Björck, 1995). Evidence of a readvance is only clear on the western side of Mt Billingen (Björck and Digerfeldt, 1984) where glaciotectonised sediments and till deposits within the moraines in the MSEMZ indicate that the ice margin fluctuated (Johnson *et al.*, 2019). On the eastern side of Lake Vättern detailed varve studies by Caldenius (1942) and Strömberg (1994) show no clear evidence of a readvance during any part of the Younger Dryas cold period, and that the drainage pathway at Mt Billingen remained ice-dammed. It has been suggested that after a few hundred years the ice margin receded from Mt Billingen for a second time and the final drainage of the BIL occurred (Björck and Digerfeldt, 1989; Strömberg, 1992; Andrén *et al.*, 2002) which lowered the lake level by a further 15-20 m (Björck *et al.*, 1998; Björck *et al.*, 2002). Jakobsson *et al.* (2007) estimate that at its maximum capacity, the BIL contained 29,300 km³ of freshwater, and over 26% of its volume (7,800km³) catastrophically drained into the North Atlantic during the final drainage.

Understanding the precise timing of BIL drainages during the Lateglacial is vital to resolve the potential impacts of freshwater forcing on North Atlantic climate. The first drainage has been dated to the end of the Allerød interstadial (Björck, 1995) which has been supported by varved sediments in Lake Vättern that show evidence of a marine ingression during the early Younger Dryas (Swärd *et al.*, 2016). More recently, the drainage has been precisely dated to 12,700±52 cal. yrs BP using Bayesian age modelling (Muschitiello *et al.*, 2016). The authors remodelled a series of radiocarbon dates that were obtained from macrofossils within varved sediments in Småland and Östergötland (Wohlfarth *et al.*, 1998) and use a rapid drop in varve thickness as a 'proxy' for BIL drainage. This age is consistent with a ca 13 cal. ka BP age that has previously been proposed (Björck and Digerfeldt, 1989; Björck, 1995; 2008). The second drainage has been linked to a colour change from brown to grey varves in the varve records in south eastern Sweden and the Baltic Proper (e.g. Brunnberg, 1995; Andrén *et al.*, 1999, 2002). This has been dated to the Younger Dryas-Preboreal transition at ca 11.7 ka BP just prior to the onset of the Holocene (Andrén *et al.*, 1999; Björck *et al.*, 2002). Further evidence on these specific elements and the final drainage of the BIL, which is a key focus of this thesis, are provided in Chapter 3.

2.3.6 Yoldia Sea Stage 11.7-10.7 ka BP

After final BIL drainage, the Baltic entered the Yoldia Sea stage which was characterised by a complex pattern of relative sea level changes and ingression of saline water into the Baltic (S Björck, 1995; Björck *et al.*, 2001; Andrén *et al.*, 2002).

Immediately after the final BIL drainage, a further *ca* 300 years of freshwater conditions prevailed in the BIL and this is termed the 'first freshwater phase of the Yoldia Sea Stage' (Björck *et al.*, 2001). In varve sediment sequences from Östergötland and the Baltic Proper, this freshwater phase of the Yoldia Sea is represented by *ca* 300 grey varves which overly brown BIL varves (Brunnberg, 1995; Andrén *et al.*, 2002).

By *ca* 11.3 ka BP the Yoldia Sea entered a brackish phase which is identified in numerous sediment cores around the Baltic Basin. The brackish phase is evidenced by a lithological change in varve records from Östergötland, the Baltic Proper, the Södertörn Peninsula and the Stockholm area by a change from grey freshwater varves to reddish colour brackish varves (Brunnberg, 1995; Andrén *et al.*, 2002). These reddish varves have been identified in the western and south eastern Baltic Sea and contain marine calcareous fossils and diatoms (Svensson, 1989; Brunnberg, 1995; Schoning and Wastegård, 1999; Andrén *et al.*, 2002). The duration of the brackish Yoldia Sea stage has been estimated between *ca* 60-200 yrs (Wastegård *et al.*, 1995; Andrén *et al.*, 2002), however the precise timing of marine influx is still debated. Radiocarbon dates from shell fragments, foraminifera and the bivalve *Portlandia arctica* were acquired from samples taken from west of the Närke Strait at Lake Vibysjön. Dates from *Portlandia arctica* yielded an age of $10,580 \pm 75$ ¹⁴C yrs BP and dates from foraminifera returned an age of $10,985 \pm 140$ ¹⁴C yrs BP (Wastegård *et al.*, 1998). These ages were considered older than expected, however, there are questions regarding the marine reservoir offset during the Yoldia Sea stage which has been estimated at 1,000-1,500 years (Wastegård and Schoning, 1997) and 800-1,000 years (Wastegård *et al.*, 1998).

Despite the challenges associated with calculating the marine reservoir offset it has been proposed that by *ca* 11 ka BP the Yoldia Sea entered a second freshwater phase. Due to the high uplift rate in south central Sweden, the Øresund Strait became shallower which prevented the inflow of marine water to the Baltic.

2.3.7 Ancyclus Lake stage 10.7-9.8 ka BP

After complex isostatic uplift across southern Sweden, the Baltic became isolated from the sea, creating the freshwater Ancyclus Lake at *ca* 9.2 ka BP (Bennike and Jensen, 1998). By *ca* 8.0 ka BP sea-level rise enabled marine water to enter the Baltic through the Øresund Strait threshold, marking the end of the Ancyclus Lake and the start of the modern Baltic Sea phase (Jensen *et al.*, 1999).

2.4 Summary

Despite differences in the FIS retreat rate, several extensive moraine belts across Fennoscandia and Europe indicate standstills and readvances since the LGM (Lundqvist and Wohlfarth, 2001; Svendsen *et al.*, 2004; Mangerud *et al.*, 2011). Glacial landforms represent a series of specific ice marginal positions and provide a relative chronology of events. Throughout early investigations of the FIS, the deglaciation chronology was built using pollen stratigraphy and radiocarbon dating, with samples derived from marine fossils or bulk lacustrine sediment (Hillefors, 1975, 1979; Björck and Digerfeldt, 1984, 1986; Berglund, 1995). With the advent of other dating techniques such as CN and OSL dating, there have been recent attempts to re-appraise the deglaciation chronology (e.g. Larsen *et al.*, 2012; Anjar *et al.*, 2014), however, the large uncertainties (often thousands of years) associated with these techniques has served only to corroborate, rather than test the deglaciation chronology. For example, this has led to correlation of the major moraine belts to cold climatic events within the Greenland ice-core chronology which does not enable the deglaciation chronology to be tested.

At present, errors in the dates are frequently too large (centuries to millennia) to enable reliable chronological constraints on short-lived (century-decadal scale) ice margin fluctuations. As such, the current deglaciation chronology remains a framework that should be tested. Indeed Stroeven *et al.* (2016) suggest that their deglaciation chronology likely contains uncertainties of between 500-2,000 years in the pre-Younger Dryas part and between 100-500 years in the post Younger-Dryas part. The level of stratigraphic resolution is key to unravelling the chronological complexities of ice sheet dynamics during the LGIT and the timing of BIL drainage events. This is especially important as the different phases of FIS retreat have been linked to distinct climatic events throughout the LGIT. One such dating technique that enables high-resolution ice sheet reconstruction is the use of varve chronologies, which provides a high-precision record. Accurate, independent fixing of the varve chronology can be achieved through combining varve chronology with tephrochronology. With respect to the FIS retreat there is a unique opportunity to provide more precise and accurate tests of the current deglaciation models, through the underutilised approach of varve and tephrochronology. The following chapter provides an overview of the annually resolved chronology that has been used for FIS reconstructions, and which is the key focus of this thesis, The Swedish Timescale.

Chapter 3. The Swedish Timescale

3.1 Overview

The Swedish varve chronology or the ‘Swedish Timescale’ (STS) is a composite sediment record which largely represents the melting and retreat history of the Fennoscandian Ice Sheet (FIS). It is composed of glacial and postglacial varves with *ca* 4,000 clastic glacial varves and *ca* 10,000 deltaic postglacial varves. The STS was constructed by visually correlating over 1,000 overlapping varve thickness diagrams from successive glacially eroded basins from southern to northern Sweden. The glacial varves with distinct alternations between silt-dominated summer and clay-dominated winter layers, represent seasonal sediment input to the Baltic Basin throughout several stages of its history. The oldest glacial varves were deposited in the ice-dammed Baltic Ice Lake (BIL), with the youngest glacial varves deposited during the Yoldia Sea and Ancylus Lake stages. During the postglacial part of the chronology varves were deposited in the Littorina Sea in northern Sweden (Cato, 1987; Wohlfarth *et al.*, 1996). Today glacial varved sediments from the BIL can be found along the Baltic Sea coast, in the Baltic Sea, and in western Östergötland and eastern Västergötland of southern Sweden (De Geer, 1940; Strömberg, 1985; Kristiansson, 1986; Cato, 1987; Ringberg, 1991; Brunnberg, 1995; Wohlfarth *et al.*, 1998).

Considered a “count down from the top” chronology, the younger part of the STS consists of postglacial deltaic sediments in the estuary of the River Ångermanälven in northern Sweden (Cato, 1987; Wohlfarth *et al.*, 1996), whilst the oldest part of the varve chronology is found in north eastern Skåne and Blekinge in southernmost Sweden and extends back to >14,000 varve years before present (vyr BP) (Ringberg and Rudmark, 1985; Ringberg, 1991; Wohlfarth and Possnert, 2000; Ringberg *et al.*, 2002) (Figure 3-1). Several researchers have demonstrated inconsistencies in the construction and chronological precision of the STS. Research shows that in what was considered a continuous varve chronology, up to 700-900 varve years are missing during the Younger Dryas, early Holocene and/or mid-Holocene (Wohlfarth *et al.*, 1997; Andrén *et al.*, 2002). This chapter provides a review of the construction of the STS, examples of its application to Quaternary science research and explanations for chronological uncertainties.

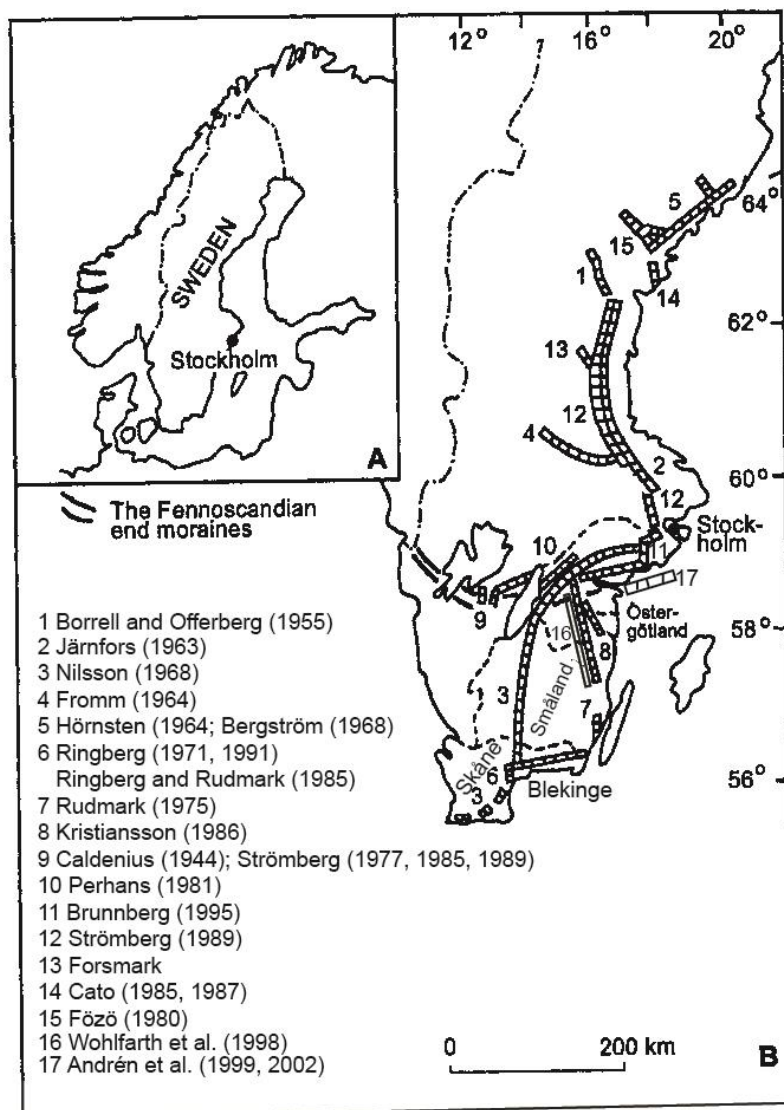


Figure 3-1. Geographical distribution of regional varve chronologies in the STS. Modified from Wohlfarth et al. (1995).

3.2 Origins and early construction

In 1862, the Swedish Geological Survey used the term “hvarfvig lera” to describe laminated glaciolacustrine sediments on one of the first Geological maps of Sweden (Karlsson, 1882). The Swedish geologist Gerard De Geer later described these sediments using the term “varve” to represent the annual process of sediment deposition. A varve consisted of a dark-coloured fine-grained winter layer, and a light-coloured coarse-grained summer layer (De Geer, 1884) (Figure 3-2). At the International Congress in Stockholm in 1910 De Geer explained how he discovered varves: “Indeed, it seems to me quite as improbable that the melting-season of the land-ice should not put its stamp upon the annual sediment...” (De Geer, 1926; pp. 256). As the main geochronological framework at the time was the simplistic model of sediment age

increasing with depth, “varves” were a significant advancement in understanding the age of geological deposits. By pioneering the term “varve”, De Geer also created a new depositional model in geology and established the term “geochronology”.



Figure 3-2. Gerard De Geer demonstrating varved sediments in Essex Junction, US, 1920 (De Geer, 1940).

After first identifying varves in 1878 at individual open sections, it wasn't until 1904 that De Geer “happened to get a very good correlation between two clay sections 1 km apart from each other...” (De Geer, 1926; pp. 256). This formed the basis for creating a composite varve chronology from multiple varve records. After extensive fieldwork in the Stockholm area, it became apparent that sites in close proximity could be correlated and a composite varve chronology could be constructed (De Geer, 1912, 1940). To create a composite varve chronology De Geer cross correlated sediment sequences by wiggle-matching thickness patterns between sites in close proximity and using specific marker horizons such as coarser grained ‘drainage varves’ (De Geer, 1912, 1926, 1940). De Geer was able to track the ice margin position from Stockholm to Jämtland and estimated a retreat time of 1,073 years (De Geer, 1912).

3.2.1 Varve composition and thickness measurements

Across Sweden, individual varve sequences are broadly similar in composition in that both grain size and varve thickness typically increase with depth. These characteristics are thought to be related to the extent and behaviour of the FIS, with thicker varves at ice-proximal locations and thinner varves at ice-distal locations. Summer laminations in basal ice-proximal varves are typically composed of coarse-grained (sand-silt) often with multiple laminations within one summer component (e.g. Ringberg, 1984; Ringberg and Erlström, 1999) and winter laminations are typically fine-grained (fine silt to clay). In contrast the uppermost varves within an individual varve sequence are usually composed of silty summer laminations and fine-silt to clay winter laminations.

It is widely assumed that the clay-rich laminations that cap coarse-grained summer laminations formed during the winter months when the lake surface froze. This prohibited internal mixing from surface winds and turbidity currents enabling finer grained material to settle from suspension in the water column. Therefore, the seasonal changes between the melt season (spring and summer) and the non-melt season (autumn and winter) underpin the annual nature of De Geer's varve model. Critically, the STS is based on the principle that as the FIS retreated, successive glacially eroded basins became exposed and accumulated varved sediments. Therefore, the oldest/basal varve represents the minimum age of deglaciation. After extensive fieldwork and geomorphological mapping, De Geer (and later Bergström (1968) and Strömberg (1994)) noted that the basal varve at each site was deposited stratigraphically above bedrock, till or subglacial landforms such as eskers. The orientation of eskers, subglacial striae and moraine ridges were then used to construct the direction of ice retreat, with glacial varves used to determine the timing of retreat between prominent landforms (De Geer, 1940).

Initially varve records were observed and recorded in open pits (Figure 3-3), though later measurements were also made from sediment cores. Open pits enable the lateral continuity of laminations to be assessed and more accurate determination of the basal varves. Varve sequences obtained from open pits are typically very short, though longer (>100 yrs) continuous varve sequences have been extracted using sediment coring equipment. In particular, the "Swedish Foil Piston Corer" enables retrieval of undisturbed terrestrial sequences up to 11 m length (e.g. Järnefors, 1963; Brunnberg, 1995). Depending on the depth and moisture content of clay varve sequences different methods are practised in the field. For example, in the Mt Billingen area the uppermost 3-4 m of varves are dry and difficult to core so were sampled in open sections (Strömberg, 1983, 1989). Traditionally, varves in the STS were measured by rolling a paper strip over the

section or core surface, marking each individual varve on the paper strip and measuring varve thickness with a ruler (Figure 3-3).



Figure 3-3. Gerard De Geer measuring clay varves in the traditional way at an open section. The traditional method of using a paper strip and pencil is widely adopted in the STS. Photo taken in Beckomberga, Stockholm, 1931 by Ebba Hult De Geer, courtesy of Lars Brunnberg and Stefan Wastegård.

Varve thickness diagrams were then constructed and used to correlate sites by wiggle matching patterns in the varve thickness records (Figure 3-5). Marker-varves such as thick, silty varves were sometimes used for correlations (Caldenius, 1944; Nilsson, 1968) as were non-varved sections such as sand beds and zones of deformation (De Geer, 1940; Wohlfarth *et al.*, 1998) or colour changes (Strömberg, 1994; Brunnberg, 1995; Andrén *et al.*, 2002).

3.2.2 Composite chronology structure

The STS is built upon three key phases defined by De Geer (1912;1940), the Gotiglacial, Finiglacial and Postglacial (Figure 3-4). The Gotiglacial and Finiglacial are composed of glaciolacustrine varved clays, with some ‘symmict’ or brackish water varves deposited in the Finiglacial, whereas the youngest varves in the Postglacial are deltaic sediments.

Several researchers have since extended the varve chronology beyond De Geer's initial timescale, as is shown in Figure 3-4. The longest part of the timescale, the Postglacial, started after the drainage of ice-dammed lakes and the Centraljämmtska Issjön in central Sweden (De Geer, 1912; Lidén, 1913, 1938). This is marked by a thick varve in the Indalsälven river (De Geer, 1912) which represents "varve-zero" in the De Geer timescale. This varve acted as an anchor point for the STS and subsequent varve chronologies have been reported in varve years before and after varve-zero (e.g. Strömberg, 1985, 1990, 1994; Kristiansson, 1986; Brunnberg, 1995; Wohlfarth *et al.*, 1998).

Initial investigations by Lidén (1913; 1938) suggested 7,522 postglacial varves were deposited after varve zero in the fluvial deposits along the River Ångermanälven. The Postglacial chronology enabled the rest of the STS to be fixed to the present-day and varve years were then reported in *vyr*s BP 1950, often also referred to as *vyr*s BP.

The oldest part of the chronology is the Gotiglacial between varve -1,073 and *ca* -4,000 (De Geer years). De Geer (1912, 1940) constructed the younger part of the Gotiglacial chronology with the older part constructed decades later (e.g. Ringberg and Rudmark, 1985; Kristiansson, 1986; Strömberg, 1989, 1994; Brunnberg, 1995; Wohlfarth *et al.*, 1998) (Figure 3-4). De Geer's (1940) varve -1,073 represented the onset of the Finiglacial period (Figure 3-4) and signifies the marine incursion at the start of the Yoldia Sea stage. The Finiglacial, or early Holocene, part of the chronology is between varve zero and -1,073 De Geer years, and is the shortest part of the timescale representing the first 1,073 years after the drainage at Mt Billingen. The onset of the Postglacial varve chronology was later revised to 9,237 *vyr*s BP 1950 (Cato, 1985, 1987) and was considered to be synonymous with the Holocene (Figure 3-4).

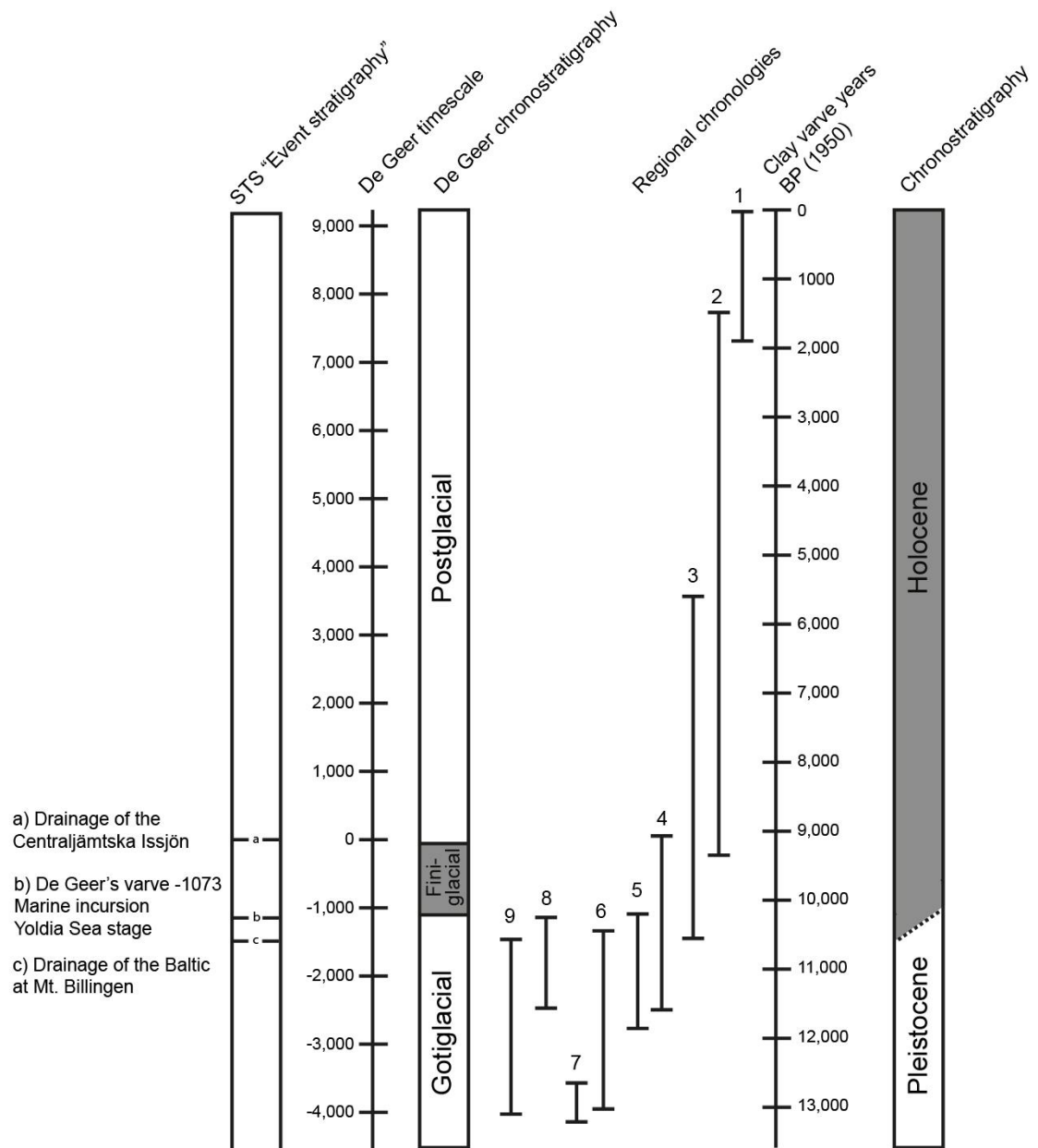


Figure 3-4. The Swedish Timescale (STS).

Comparison between De Geer chronostratigraphy and conventional chronostratigraphy with the De Geer timescale and clay-varve years before 1950. The main STS chronologies are also highlighted: 1) Cato, (1985; 1987), 2) Lidén, (1913, 1938), 3) De Geer, 1940, 4) Strömberg, (1989, 1994), 5) Brunnberg, (1995), 6) Kristiansson, (1986), 7) Ringberg and Rudmark (1985), 8) Andrén et al. (1999, 2002), 9) Wohlfarth et al. (1998). Modified from Brunnberg (1995).

3.2.3 Early applications

As well as creating and expanding the STS, De Geer (1940) also attempted to correlate the STS with varve records in North America. He suggested that solar activity was the controlling factor on long term varve thickness trends and as such records across wide regions could be correlated (Figure 3-5). However, these so-called “teleconnections” were heavily criticised and are now considered to be flawed. It is now accepted that varve

thickness can be driven by several different processes that operate across a range of temporal and spatial scales. Therefore, synchronising varve records across hemispheric scales was considered inaccurate (Antevs, 1931, 1935, 1954).

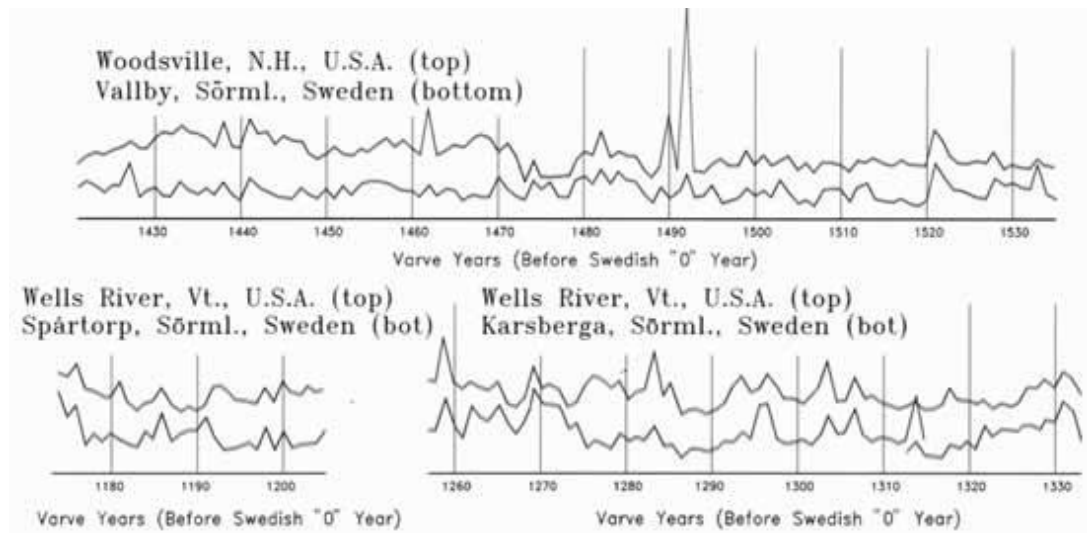


Figure 3-5. Attempted varve correlations in Sweden and America. Northern Connecticut Valley of New England, USA (De Geer, 1912) tufts.edu/varves/NAVC.

In addition to reconstructing the chronology of FIS retreat, the STS was also used for other palaeoenvironmental reconstructions. For example, by extending the varve chronology into northernmost Sweden using varve deposits from a succession of river deltas, Lidén (1938) was able to reconstruct the relative land uplift in vrys BP. This research formed an important basis for understanding isostatic rebound in Sweden (Mörner, 1979; Svensson, 1989). However, with the advent of radiocarbon dating (Arnold and Libby, 1949), the application of varve analysis as a dating tool was side-lined. Varve studies were deemed inaccurate and unreliable due to their floating chronology and many glaciolacustrine varve sequences lacked organic material suitable for radiocarbon dating (e.g. De Geer, 1912, 1927; Antevs, 1931). Efforts switched from glacial varves to chronologies from continuous, non-glacial lake records.

3.3 Revising and extending the Swedish Timescale

The following sections present an overview of the revisions that have been made to the STS. This section is not structured in geological order i.e. from the Gotiglacial to the Postglacial but in the chronological order that the revisions were made. This section begins by briefly explaining the revisions that were made to the Postglacial and Finiglacial chronologies as they anchor the timing of the Gotiglacial. The Gotiglacial

period will be more extensively discussed as this relates directly to the period investigated in this thesis.

3.3.1 Postglacial chronology

Revisions to the STS were published from the 1960's onwards. In the Postglacial part of the chronology Cato (1985, 1987) revised the youngest part of Lidén's (1913, 1938) chronology and extended the Postglacial timescale from 7,522 to 9,266 varves. Initially, the older part of Lidén's chronology was validated by comparing the shore-line displacement curves derived from deltaic varves along the River Ångermanälven with shore-line displacement curves derived from the isolation of lake basins (Renberg and Segerström, 1981). However, Cato (1992) established an offset of ca 300 vyrs between 4,000 and 7,000 vyrs BP between the varve chronology and the shore-line displacement curves. This was initially attributed to the different locations of the lake-isolation studies which were located both inside and outside of the River Ångermanälven valley and which may have experienced differing eustatic sea-level movements (Cato, 1992). However, Wohlfarth *et al.* (1997) suggest that the ca 300 vyrs offset between the curves could be interpreted in terms of an error in the chronology. Indeed, radiocarbon dates from seeds and catkin scales of *Betula* suggest a possible discrepancy of 300-1,000 vyrs in the Holocene varve chronology between 2,000 and 5,000 vyrs BP (Wohlfarth *et al.*, 1997).

3.3.2 Finiglacial chronology

Strömberg (1989) connected the early Holocene "Finiglacial" varves to the oldest Postglacial varves using prominent drainage varves. He revised the original estimate for the duration of the Finiglacial period of 1,073 vyrs (De Geer, 1912, 1940) to 1,191 vyrs. Potential errors in the construction of the late Finiglacial/early Postglacial chronology are described by Strömberg (1989, pp.177) who suggests that "difficulties in delimiting annual varves sometimes occur but are only a minor problem". He suggests that errors in the chronology are "due to the fact that several hundred varve series have to be correlated with each other in order to get a complete late Finiglacial and Postglacial Swedish Timescale, and correlation mistakes are a human factor difficult to avoid entirely" (Strömberg, 1989; pp.177). Strömberg (1994) estimated that errors due to inaccurate correlations amount to a minimum of an additional 120 vyrs in the early part of the Postglacial chronology, but errors associated with delimiting varves due to human error are not quantified.

In De Geer's original chronology, the ingress of sea water at varve -1,073 was thought to have occurred immediately after the final drainage of the Baltic Ice Lake at Mt Billingen. However, revisions to the STS suggest that approximately 300 vyrs of freshwater

conditions occurred after the final drainage and before marine ingression in the Stockholm area (Strömberg, 1992; Brunnberg, 1995; Andrén *et al.*, 2002). The evidence for a 300 kyr freshwater phase is largely based on distinct colour changes that occur in numerous varve records across Östergötland, Södermanland, the Södertörn peninsula and Stockholm. However, there is evidence for marine conditions immediately after the drainage but before the marine ingression in the Lake Vättern basin (Björck *et al.*, 2001). There are also discrepancies between individual estimates for the precise duration of the post-drainage freshwater phase (Table 3-1).

Table 3-1. Examples of discrepancies in the varve chronology for specific sections of the STS. Discrepancies that relate to a specific varve year which marks a chronostratigraphic change are highlighted with an asterisk.

Section of the STS	Description	Number of yrs	References
Postglacial	Revision to the youngest part of the chronology (Lidén 1913;1938) Revision between 37- 1978 AD extended chronology from 7,522 to 9,266 (up to 1979 AD)	+1,744	Lidén (1913, 1938), Cato (1985, 1987)
	Offset between 7,000 and 4,000 yrs BP	ca 300	Cato (1992)
	Offset between 5,000 and 2,000 yrs BP after radiocarbon dating	300-1,000	Wohlfarth <i>et al.</i> (1997).
Finiglacial	From De Geer zero varve to De Geer's varve -1073	1,073	De Geer (1940)
		1,190 +/- 40	Strömberg (1985)
		1,092	Järnefors (1963)
	Deglaciation from Stockholm to Uppsala. Indistinct 'symmict' varves deposited in brackish water conditions during the Yoldia Sea stage	150	De Geer (1940)
		175	Strömberg (1985)
		70-120	Wastegård <i>et al.</i> (1995)
		240	Andrén <i>et al.</i> (2002)
10-50	Björck <i>et al.</i> (2001)		
Gotiglacial	Time between the drainage of Mt Billingen and ingression of sea water (Yoldia Sea stage)	None	De Geer (1912)
		292	Sauramo (1923)
		262 or 309	Strömberg (1992)
		310	Brunnberg (1995)
	Time between the drainage at Mt Billingen and the Younger Dryas/Preboreal pollen shift	40	Andrén <i>et al.</i> (1999)
		120	Andrén <i>et al.</i> (2002)
	Beginning of the Younger Dryas	*Local vyr 1,700	Kristiansson (1986)
		*Local vyr 1,510-1,660	Wohlfarth <i>et al.</i> (1998)

3.3.3 Gotiglacial chronology

Strömberg (1989; 1994) connected the Gotiglacial to the Finiglacial chronology through overlapping varve thickness diagrams in east central Sweden extending the STS from ca 10,400 vrs BP to ca 11,500 vrs BP (Figure 3-1). The STS was then extended further south into Östergötland, Småland, Blekinge and Skåne through the Younger Dryas, Allerød, Older Dryas and Bølling periods via a continuous chain of varve chronologies (e.g. Ringberg, 1971, 1979, 1991; Ringberg and Rudmark, 1985; Kristiansson, 1986). In Östergötland and Småland the composite varve chronology by Kristiansson (1986), which consisted of 107 varve diagrams spanning 2,310 vrs, covered the area from Högsby (most southerly site) to Norrköping (most northerly site). Initially this regional chronology was not correlated to Strömberg's (1985) chronology in the north and was 'floating'. Kristiansson (1986) therefore reported varve records on a local varve year timescale that spanned 2,825 to 515 vrs.

The most southerly sites from Kristiansson's chronology were tentatively correlated by Björck and Möller (1987) to varve chronologies further south in NE Skåne and Blekinge (Ringberg, 1979, 1991) using common varve thickness patterns. The overlap occurs between local varve years 2,560-2,700 (on the Kristiansson timescale). Ringberg's (1979, 1991) composite chronology in southern Sweden is comprised of 185 varve diagrams, while in eastern Blekinge and southeastern Småland, the Ringberg and Rudmark (1985) composite varve chronology is based on 6 diagrams. Initially, these two regional chronologies comprised the southern Sweden varve chronology which spanned 640 vrs, but additional varve records extended the chronology by 54 vrs (Wohlfarth *et al.*, 1993). Collectively, the chronologies in Blekinge and Småland span 694 vrs and cover the Bølling and Older Dryas pollen zones (Wohlfarth *et al.*, 1994).

After the correlation between Kristiansson's and Ringberg's regional varve chronologies was established, Björck and Möller (1987) utilised pollen data from varve records in southern Sweden to date Kristiansson's varve chronology. Using characteristically thin varves from Kristiansson's chronology in the Högsby area, Björck and Möller (1987) linked to the thin varves that were deposited during the Older Dryas in southernmost Sweden. The overlap between southernmost and south eastern Sweden was placed between the local varve years 2,560-2,800 on the Kristiansson timescale. The deposition of thick varves around local varve year 2,550-2,560 was then dated to the beginning of the Allerød period using the assumption that thicker varves would likely be deposited during warmer climatic conditions (Björck and Möller, 1987). Using the occurrence of deformation structures and the overall decrease in varve thickness, Kristiansson (1986) dated the Allerød/Younger Dryas boundary at local varve year 1,760. During the first

ca 200 vyrs of the Younger Dryas as defined in the varve chronology, Kristiansson (1986) reported varve records with disturbances, such as folded varves that are overlain by sand and glacial till. These records have been attributed to a readvance and oscillation of the ice margin which is consistent with other studies in the Vimmerby area (e.g. Berglund, 1979).

In the younger part of the Kristiansson (1986) varve chronology, at local varve years 707-708 in the Fjärdingstad site, there is a marked colour change from brown to grey coloured varves. Kristiansson (1986) attributed the colour change to oxidation as a result of modern-day groundwater conditions. He suggested that light-coloured red/brown summer layers can be caused by more pronounced oxidation of iron within the sediments and dark-coloured or black winter layers can be caused by reduction conditions (Kristiansson, 1986). Whilst the colour change coincided with a change in texture in the varve series, Kristiansson (1986) argued that the colour changes could also occur due to the presence of different minerals within the sediments. In addition, when using varve thickness patterns and marker varves to link site varve chronologies, Kristiansson noted that the position of the colour change was not consistent and could “jump” between boundaries (Kristiansson, 1986). For these reasons Kristiansson states that “using colour to correlate different sites cannot be correct unless it is known exactly what has caused the colours” (Kristiansson, 1986, pp. 40) and that if varve thickness changes are due to local processes then they are useless for correlation.

Despite the recommendations by Kristiansson (1986), Brunnberg (1995) used the same colour change from brown to grey varves within his regional chronology to link to the Kristiansson (1986) chronology. This correlation connected the Kristiansson (1986) chronology to the main part of the STS and enabled the colour change at local varve years 707-708 in the Kristiansson (1986) chronology to be dated to 10,712-10,726 vyrs BP. Due to the existing correlation between the Kristiansson (1986) chronology and the varve chronologies in southernmost Sweden, the STS was extended into the Bølling and Older Dryas periods.

The Brunnberg (1995) regional chronology consists of 201 varve diagrams, of which 160 were new sites and 41 from other sources (26 from De Geer (1932, 1940), 4 from Nilsson (1968), 9 from Kristiansson (1986), and 2 unpublished). The chronology spans -1,042- to -2,513 vyrs (De Geer years) which corresponds to 10,280-11,751 vyrs BP 1950. Varve records are located in Östergötland, the Södertörn peninsula, Södermanland and Stockholm. There are two distinct colour changes within the Brunnberg regional varve chronology that play an important role in the deglaciation chronology (Table 3-2). The varve records across this region appear to transition from brown to grey to red across

the southernmost to the northernmost sites. In the southern sites in Östergötland and Södermanland, varves transition from basal brown varves to grey varves. This colour change occurs between the local vyrs 1,474 to 1,501 (De Geer timescale) and sites in Södermanland have been correlated using a combination of varve thickness and the colour change to sites on the Södertörn peninsula. In sites south of Stockholm and the Södertörn peninsula there are approximately 300 grey varves within the individual site chronologies, however Brunnberg (1995) describes difficulties correlating grey varves between sites due to considerable variations in varve thickness.

The colour change from brown to grey varves has also been found further west (Strömberg, 1994) and in the Baltic Proper (Andrén *et al.*, 1999) and has been interpreted as the final drainage of the Baltic Ice Lake, which is thought to mark the end of the Younger Dryas period (Strömberg, 1994). It is generally accepted that the presence of ca 300 grey glacial varves stratigraphically above brown glacial varves represents the duration of a freshwater Baltic phase. This short-lived freshwater phase occurred immediately after the drainage of the Baltic Ice Lake at Mt Billingen, but prior to the ingression of marine water in the Stockholm area (Strömberg, 1994; Brunnberg, 1995; Andrén *et al.*, 2011). It is often referred to as the first freshwater sub-stage of the Yoldia Sea stage (Svensson, 1989).

The transition from a freshwater phase to a marine/brackish phase has been linked to the stratigraphic change in varve colour from grey glaciolacustrine varves to red glaciomarine/symmict varves in sites in the Stockholm area and western Södermanland (Brunnberg, 1995; Andrén *et al.*, 2002). The glaciomarine environment has been long established through finds of the marine arctic mollusc *Portlandia (Yoldia) arctica* within the varved sediments (e.g. De Geer, 1913, 1940; Brunnberg and Possnert, 1992) and more recently by findings of marine foraminifera and ostracods (e.g. Schoning and Wastegård, 1999). In the Brunnberg (1995) chronology the transition from the older grey glaciolacustrine clay to the red glaciomarine clay occurs asynchronously over a 12 kyr period (ca 1,190-1,187 local vyrs). Brunnberg (1995) proposed that the phasing of the colour change is due to several factors such as local differences in topography, the altitude of each sampling site or the current conditions at the lake bottom. A marine signal has also been reported in other areas across south eastern Sweden and the duration of the marine phase ranges from 10 years (Björck *et al.*, 2001) to 250 vyrs (Brunnberg, 1995) (Table 3-1). Despite these differences, it has been estimated that symmict clays were deposited in the vicinity of Uppsala ca 240 years after the marine ingression in Stockholm (Strömberg, 1989), but it is not yet clear whether this lag is a “true” lag or whether the sedimentological expression of this event varies between sites. It is likely

that there was a weak and decreasing salinity in the Baltic Basin after the brackish water phase but there is no evidence in the fossil record.

Table 3-2 Varve colour changes and associated depositional environment and chronostratigraphical information. Modified from Björck et al. (2002).

Varve colour	Depositional Environment	Baltic event stratigraphy	De Geer "chrono-stratigraphy"	Pollen stratigraphy
Red	Symmict/ glaciomarine	Yoldia Sea stage (brackish water)	Finiglacial	PBO
Colour change from grey to red	Glaciolacustrine/ glaciomarine transition	Onset of the brackish phase of the Yoldia Sea	Gotiglacial/ Finiglacial	Preboreal
Grey	Glaciolacustrine	First freshwater sub-stage of the Yoldia Sea Stage post-drainage	Gotiglacial	Preboreal
Colour change from brown to grey	Glaciolacustrine	Final drainage of the BIL	Gotiglacial	Younger Dryas/Preboreal boundary
Brown	Glaciolacustrine	Baltic Ice Lake, pre-drainage	Gotiglacial	Younger Dryas
Brown	Glaciolacustrine (freshwater)	Baltic Ice Lake	Gotiglacial	Allerød

3.3.3.1 Statistical correlations

The correlations proposed by Ringberg (1971, 1991), Ringberg and Rudmark (1985) and Kristiansson (1986) for the southern Sweden chronology were investigated by statistical methods in the late 1990's. Holmqvist and Wohlfarth (1998) applied cross correlation analysis to overlapping varve diagrams and found only 78 out of 363 varve connections "fulfilled the statistical requirements for a perfect match" pp. 35. Furthermore, in 96 cases, the published link was different to the link proposed by statistical correlation (Holmqvist and Wohlfarth, 1998). Whilst this research highlights that there are potentially fundamental flaws in the construction and correlation of site chronologies, statistical correlations can provide false-positive results (Kristiansson, 1986).

Despite a significant period of revision and extension to De Geer and Lidén's original varve chronologies, errors remain in the revised chronology. This is demonstrated by the conflicting estimates for the number of yrs within each section of the STS and the duration of specific events (Table 3-1). Furthermore, statistical methods appear to invalidate the approach taken by many researchers to rely on wiggle-matching varve thickness records to create a composite varve chronology. Allied to this is the assumption that marker zones such as colour changes in the varved sediments occurred synchronously across the Baltic Ice Lake basin and can be used to link regional varve chronologies (e.g. Kristiansson, 1986; Strömberg, 1994; Brunnberg, 1995). These

problems initiated another phase of revision to the STS and from the 1990's onwards researchers attempted to independently date varve records.

3.4 Efforts to date the STS

The idea that the STS represented a continuous varve chronology was challenged in the late 1990's. To overcome problems in the correlation of varve records and derive calendar year ages there were several attempts to independently date the STS that included: wiggle-matching ^{14}C dates from varve records with ^{14}C dates from other lake records such as the Lake Gosciarz varve record in Poland (e.g. Goslar *et al.*, 1999) and synchronising varved-pollen stratigraphies to the Greenland ice-core chronology (e.g. Björck *et al.*, 1996; Andrén *et al.*, 1999). Radiocarbon dates derived from terrestrial macrofossils in varved clays from southernmost to northernmost Sweden were calibrated by wiggle matching the ^{14}C ages to the Lake Gosciarz varve record in Poland (Wohlfarth and Possnert, 2000). The authors suggest that there is an offset between previously derived vrs BP and calibrated yrs BP age estimates. The offset is estimated at >2,000 vrs in the oldest part of the chronology, around 1,300 vrs at the Bölling/Older Dryas boundary, >800 vrs at the Younger Dryas/Holocene boundary and either 650 vrs or 900-940 vrs at the Allerød/Younger Dryas transition (Wohlfarth and Possnert, 2000). However, the approaches that were employed to independently date the STS using radiocarbon-based methods could be considered somewhat dubious.

3.4.1 Radiocarbon dating

To test the aforementioned problems in the Kristiansson (1986) chronology, Wohlfarth *et al.* (1998) produced a radiocarbon dated varve chronology from core material at sites in close proximity to some of Kristiansson's sites. Wohlfarth *et al.* (1998) aimed to connect to and extend the Kristiansson chronology to provide a more comprehensive overlap with the Ringberg (1971, 1979) varve chronology in the south. Wohlfarth *et al.* (1998) report that of 25 investigated sites, only 9 sites contained terrestrial plant remains for radiocarbon dating. The plant macrofossils included mainly leaves and leaf fragments of *Dryas octopetala*, *Betula nana* and *Salix polaris*, but also leaves of *Armeria*, *Silene*, *Salix reticulata* and *Ericaceae*. Fragments of flower stems, seeds and fruits were also found but were very rare. In total, 24 radiocarbon dates were reported and their reliability was assessed by comparison with the composite varve chronology. Wohlfarth *et al.* (1998) report 4 samples with distinctly older ages than the varve chronology that were interpreted as having been composed of reworked plant material, and 2 samples that yielded too young ages that had been affected by fungi.

The final radiocarbon dated varve chronology indicates several revisions to the Kristiansson (1986) chronology. For example, radiocarbon ages suggested the Allerød/Younger Dryas boundary occurred *ca* 100-250 yrs earlier than proposed by Kristiansson (1986) and that deglaciation across the sites took approximately 1,300-1,700 yrs which is considerably longer than the 900-1,000 yrs proposed by Kristiansson (1986). The Wohlfarth *et al.* (1994, 1998) composite varve chronology is 806 yrs long, covers 55 sites from Småland and Östergötland, and represents one of the first steps towards providing independent age estimates for the STS. However, the radiocarbon calibration method employed by Wohlfarth *et al.* (1998) is questionable. The authors synchronise radiocarbon chronologies from Lake Madtjärn (Sweden), Lake Gosciarz (Poland) and the Swedish varves using the radiocarbon plateau at the Allerød/Younger Dryas boundary (Goslar *et al.*, 1999) rather than using more precise radiocarbon calibration methods that were available at the time (e.g. Stuiver *et al.*, 1998). In recent years this composite varve chronology, also known as the Småland–Östergötland chronology, has been updated and radiocarbon ages have been recalibrated using the IntCal13 calibration curve (Reimer *et al.*, 2013), within a Bayesian age model (Muschitiello *et al.*, 2015). The revised chronology, which spans *ca* 12,400-13,200 cal. yrs BP is now considered to represent the most robust independently dated part of the STS, in part due to the lack of disturbed varves and the high correlation between individual varve records.

3.4.2 Synchronisation with ice-core records

In other varve sequences that have not been revised, radiocarbon age estimates can appear several hundreds of years younger than the yrs BP age (e.g. Brunnberg and Possnert, 1992). To understand whether this offset is due to errors in the STS or the radiocarbon dates, researchers have relied on synchronising varve records to the GRIP ice-core chronology using pollen stratigraphies as an independent dating tool STS (e.g. Andrén *et al.*, 1999; Ringberg *et al.*, 2003). For example, pollen boundaries and varve spacing have been used to derive age estimates for specific pollen zones (Wohlfarth *et al.*, 1994; Andrén *et al.*, 1999; Björck *et al.*, 2002). Varve thickness records have been aligned to the GRIP record and age-information transferred from the ice-core record to the STS (Andrén *et al.*, 1999; Ringberg *et al.*, 2003; Stroeven *et al.*, 2016). In some instances aligned varve thickness and ice core records have been compared with radiocarbon ages (e.g. Björck *et al.*, 1996; Wohlfarth and Possnert, 2000).

Synchronisation of varved pollen records suffers from several fundamental assumptions: 1) that the vegetation record derived from pollen analysis in Sweden represents the same climatic signal that is recorded in the $\delta^{18}\text{O}$ record from Greenland; 2) that varve thickness

is primarily controlled by climate and can be wiggle-matched to the $\delta^{18}\text{O}$ climatic record from Greenland and; 3) that climatic changes in Greenland and Sweden occurred synchronously and there is no lag in the proxy response to those changes throughout the investigated time period. Recently, Muschitiello and Wohlfarth (2015) demonstrated that there is a mean temporal lag of ca 290 years in the proxy-inferred climatic change between sites in Denmark and southern Sweden during the Younger Dryas. Moreover, several researchers have demonstrated that varve thickness in glaciolacustrine environments may be controlled by several factors that are not necessarily related to climatic changes (Chapter 4). Despite the aforementioned assumptions, varve records have been tuned to the GRIP ice-core record using pollen stratigraphy and further revisions to the STS have been made on this basis (Andrén *et al.*, 1999, 2002).

In the late 1990's the STS was also extended into the north western Baltic Proper and the local varve chronology, which consists of 10 overlapping records, spans the time from ca 10,250- 11,550 yrs BP (Andrén *et al.*, 1999). The link between the Baltic Proper varves and south-eastern Sweden is again based on the colour changes similar to those observed in terrestrial varve sequences (e.g. Kristiansson, 1986; Strömberg, 1994; Brunnberg, 1995). Pollen analysis also places the Baltic Proper varve chronology within the Younger Dryas and Preboreal pollen zones between 10,630-10,690 yrs BP 1950. By using the Younger Dryas-Preboreal transition period in the GRIP $\delta^{18}\text{O}$ ice-core chronology as an anchor point, Andrén *et al.* (1999) synchronised the varve thickness record to the ice-core record. This suggested that the final drainage of the BIL, defined by the colour change, occurred ca 40 yrs before the Younger Dryas-Preboreal climate shift, though this was later revised to 120 yrs (Andrén *et al.*, 2002). The authors also proposed that at least 875 yrs are missing from the STS in the part younger than ca 10,300 yrs BP. Again, this approach may have been successful in identifying a potential error in the STS but approaches such as aligning the STS with the GRIP ice-core records assumes climatic synchronicity between Greenland and Sweden, and that the vegetation response as recorded by the pollen stratigraphy, represents a climatic signal. As such, independent correlation methods are required such that the timing, duration and synchronicity of climatic change and the associated proxy or ice-sheet response can be more accurately assessed.

3.4.3 Tephrochronology

In recent years, tephra layers have been found within mid-Holocene varved sediments from West central Sweden (Zillén *et al.*, 2002) and from Younger Dryas varve sediments in southern Sweden (Wohlfarth *et al.*, 1993; MacLeod *et al.*, 2014). It has been proposed that the Vedde Ash was deposited in the varve record from Lake Mullsjön which is

located to the west of Lake Vättern in Västergötland (Wohlfarth *et al.*, 1993). Tephra shards from Lake Mulsjön varves were identified under thin section and were not chemically analysed. Instead, correlation to the Vedde Ash at Mulsjön is based on radiocarbon dating of macrofossils within the varve sequence that are biostratigraphically associated to the Younger Dryas period. Species identification appears uncertain however, as only fragmentary remains were found (Table 3-3).

Table 3-3. Lake Mulsjön radiocarbon sample data from Wohlfarth *et al.* (1993).
L=leaves, ff=fragments, ?=uncertain species identification.

Sample number	Lab. No.	No. of yrs	vyr interval	Expected chronozone	Macrofossils submitted	AMS ¹⁴ C age BP
AMS-12	Ua-2741	105	510-615	Younger Dryas	? <i>Dryas octopetala</i> (L, ff)	9640±190
AMS-16, 17	Ua-2744	50	210-260	Younger Dryas	? <i>Betula</i> (L, ff), ? <i>Salix</i> (L, ff)	9945±115

Wohlfarth *et al.* (1993) suggested that since no other major ash bed is found in north western Europe in the middle of the Younger Dryas, correlation to the Vedde Ash at Lake Mulsjön should be accepted. However, recent research in Scotland suggests that the Abernethy tephra, which has the same chemical profile as the Vedde Ash, represents a separate volcanic eruption that occurred after deposition of the Vedde Ash (Matthews *et al.*, 2011; MacLeod *et al.*, 2015). Subsequent age modelling indicates that the age difference between the Vedde Ash and Abernethy tephra is *ca* 500 cal. yrs BP (Bronk Ramsey *et al.*, 2015) confirming that the tephra are from two separate eruptions.

The only other identification of the Lateglacial Vedde Ash in Swedish varves is reported by MacLeod *et al.* (2014) from the Gropviken site in Östergötland. Chemical analyses were obtained for the tephra layer and correlation to the Vedde Ash has been made on this basis. Whilst it is theoretically possible that these correlations could be incorrect and the tephra layers at Gropviken and Mulsjön could be correlated to the Abernethy tephra, this tephra has thus far not been found outside of Scotland. Moreover, given that the Abernethy tephra is preceded by the Vedde Ash in several sites in Scotland, and only one tephra layer is identified at both Mulsjön and Gropviken, correlation to the Vedde Ash at these sites seems the most likely correlation given the available evidence.

More recently, Pike (2015) conducted detailed sedimentological and tephrostratigraphical analysis of the Svärsklova varve record from Östergötland which was originally investigated by Brunnberg (1995). Volcanic glass shards were identified but shard concentrations were extremely low and chemical analyses were not obtained (Pike, 2015).

The identification of the Lateglacial Vedde Ash within the Gropviken and Mullsjön varve records demonstrates the potential to find tephra within other varve records in the STS. However, the use of tephra as an independent marker horizon to link varve records has not been fully exploited in the STS despite evidence for tephra preservation within non-varved sediments across Sweden during the Lateglacial and Holocene periods (Wastegård *et al.*, 1998; Björck and Wastegård, 1999; Davies *et al.*, 2003; Wohlfarth *et al.*, 2006; Lind *et al.*, 2013).

3.5 Current state of play

The STS provides an annually resolved record of FIS retreat across a time interval that contains multiple periods of abrupt climate change (e.g. Rasmussen *et al.*, 2006; Walker *et al.*, 2012). However, there are several errors in the construction and dating of the varve records that prohibit confidence in their precision and accuracy. Several authors have proposed that there are errors in the links between site records and also between regional chronologies, and at present it is not clear whether the resulting missing years are due to errors in the identification of the varved sediments, the construction of composite chronologies or the independent dating methodologies.

Whilst De Geer (1940) initially proposed that varve thickness variations in the BIL are related to the extent and behaviour of the FIS, with thicker varves at ice-proximal locations and thinner varves at ice-distal locations, many researchers have since proposed that varve thickness variations in the STS were driven by other processes. For example, varve thickness variations have been linked to climatic changes (Kristiansson, 1986; Ringberg *et al.*, 2003), lake drainage events (Brunnberg, 1995; Wohlfarth *et al.*, 1998), and the length of the summer season (Ringberg, 1984). Indeed, varve studies outside of the STS indicate that thickness variations may be driven by a number of local and regional factors such as: variations in sediment availability, precipitation, glacier melt, catchment instability and air temperature (Ohlendorf *et al.*, 1997; Huguen *et al.*, 2000; Lamoureux and Gilbert, 2004; Tomkins *et al.*, 2008; Amann *et al.*, 2014; Devine and Palmer, 2017). Thus, variations in varve thickness may be driven by a combination of ice proximity, hydroclimatic variability and within-basin sediment processes (Chapter 4). These complexities likely explain the difficulties that have been described by several researchers when correlating varve records in close proximity and even varve cores from the same site can display different varve thickness patterns (Strömberg, 1985, 1989; Kristiansson, 1986; Brunnberg, 1995). The apparent problems linking varve records are further exemplified by unsuccessful statistical correlations between varve records in close proximity (Holmqvist and Wohlfarth, 1998; Wohlfarth *et al.*, 1998).

Several authors have also argued that using only varve thickness variations does not always produce reliable results (e.g. Sauramo, 1923; Caldenius, 1924; Järnefors, 1963; Kristiansson, 1986). For example, Caldenius (1924) and Järnefors (1963) suggest that proximal varves are largely influenced by local conditions and are of limited use for correlations, whereas Antevs (1922) suggests that the most distal varves, with insignificant variations are also of little use for site correlations. Authors have also expressed difficulties in determining if the composition of a varve is influenced locally or by basin-wide conditions (e.g. Kristiansson, 1985; Brunnberg, 1995). To determine if varve thicknesses and/or marker beds are driven by local or regional processes, the approach adopted by almost all STS varve researchers is to sample many varve sites in close proximity to create multiple overlapping varve thickness measurements. This approach, whilst time consuming, appears largely successful across Sweden however, there are regions where it is difficult to create a robust composite varve chronology. In particular, researchers have described difficulties correlating varve sequences across Östergötland and up to the Stockholm area (e.g. Kristiansson, 1986; Brunnberg, 1995; Wohlfarth, 1998).

Difficulties demonstrating robust statistical correlations between sites can also be explained by the lack of precision in varve thickness measurements, since varves in the STS are traditionally measured at the macroscale. In modern varve analyses, it is commonplace for researchers to analyse laminated sediments at the microscale to ascertain the internal sediment characteristics and processes of deposition before assigning an annual (varved) signal to the laminations (Brauer, 2004; Palmer *et al.*, 2010; Bendle *et al.*, 2017). It appears that researchers have accepted that laminations are varves using the simplistic descriptive frameworks developed by, for example, De Geer, (1912, 1940) and Antevs, (1931) without rigorous analysis of the varve structures at each site. It is important to recognise, however, that most investigations on the STS were undertaken at a time when microscopic investigations of varves were in their infancy.

Whilst breaks within varve sequences have been identified at the macroscale (e.g. Kristiansson, 1986; Strömberg, 1989; Wohlfarth *et al.*, 1998), non-annual laminations that are only discernible at the microscale may exist within the varve records. With the exception of Ringberg and Erlström (1999) microscopic sedimentological methods have not been routinely applied to the STS. Microscopic investigations of varved sediments in the STS would: 1) enable the current methodological approach of analysing varves at the macroscale to be tested; 2) permit an accurate assessment of varve count error, which at present is lacking throughout many sequences in the STS (Table 3-4); and 3)

allow greater precision of varve thickness measurements, which may improve the number of statistically significant correlations.

As well as varve thickness correlations, some varve chronologies have been linked using distinct marker horizons such as drainage varves (De Geer, 1912; Strömberg, 1994), deformation zones (Kristiansson, 1986), particularly thick or thin varves (Kristiansson, 1986; Wohlfarth *et al.*, 1998), or colour changes (Brunnberg, 1995; Andrén *et al.*, 2002). Whilst these techniques are widespread, they are inconsistently applied in the construction of composite varve chronologies, nor are they consistently applied to link regional chronologies (Table 3-4). Fundamentally, the use of so-called “marker horizons” to correlate varve records assumes that marker horizons were deposited synchronously across the Baltic Basin and without independent means of dating the varve records these assumptions cannot be tested. The approaches employed to correlate varve records and link regional varve chronologies have instead been reinforced by other lines of evidence such as tuning varved-pollen records to the Greenland ice-core chronology (e.g. Andrén *et al.*, 1999) and/or using pollen stratigraphy as a chronostratigraphic tool (e.g. Kristiansson, 1986)

Despite questions regarding its construction, the STS has been used to determine the timing and duration of key palaeoclimatic and palaeoenvironmental events. For example, in recent years the STS has been used to constrain the deglaciation chronology (Hughes *et al.*, 2016; Stroeve *et al.*, 2016), infer the timing of BIL drainage (Muschitiello *et al.*, 2016) and exceptionally thick varves have been linked to enhanced ice-sheet melting induced by volcanic activity (Muschitiello *et al.*, 2017). However, the methods employed to identify, measure, correlate and date varve records require revision to be able to maximise the full potential of the STS.

Table 3-4. Summary of the methodologies used to construct the key regional varve chronologies that comprise the Lateglacial and early-Holocene STS.

Regional varve chronology	Number of varve diagrams and overall length of chronology	Methods used to link individual site chronologies	Methods used to link to other regional varve chronologies	Timescales used	Varve count error
Strömberg (1989; 1994)		<ul style="list-style-type: none"> • Visual correlations between varve thickness diagrams • Exceptionally thick varves 	<p>Visual correlations between varve thickness diagrams and exceptionally thick varves are used to link to the Brunnberg (1995) chronology.</p> <p>Drainage varves are used to link to the Cato (1985) chronology since the varves can be indistinct and thicknesses are extremely thin due to lack of clay in the brackish water/symmict varves between Uppsala and Stockholm deposited during the Yoldia stage of the Baltic</p>	<ul style="list-style-type: none"> • De Geer vyrs • vyrs BP 	Error reported for certain sections e.g. deglaciation from Stockholm to Uppsala lasted about 175 years with an error of 10 vyrs, but error in the Swedish end moraine zone could be as high as 200-300 vyrs (Strömberg, 1985).
Brunnberg (1995)	201 varve diagrams spanning 1,471 vyrs from 1,042-2,513 vyrs before De Geer's zero varve	<ul style="list-style-type: none"> • Visual varve thickness links are strong in some locations but weak in others • Colour changes are used to guide varve thickness-based overlaps 	<p>Brunnberg (1995) used the colour change in varve records in Östergötland to link to varves at 707-708 vyrs in the Kristiansson (1986) chronology.</p> <p>Visual correlations between varve thickness diagrams and drop in varve thickness is used to correlate terrestrial varve sites Tottnäs and Hästdammen to the Baltic Sea chronology.</p>	<ul style="list-style-type: none"> • Local vyrs • vyrs BP 	Unquantified varve count errors but difficulties correlating sites
Andrén <i>et al.</i> (1999, 2002)	14 varve diagrams spanning 1,280 vyrs from 11,530-10,250 vyrs BP	<ul style="list-style-type: none"> • Visual correlations between varve thickness diagrams • Exceptionally thick varves • Position of colour changes used to verify overlap 	<p>Visual correlations between varve thickness diagrams and drop in varve thickness is used to correlate sites in the Baltic Sea to terrestrial records in the Brunnberg (1995) chronology.</p> <p>Pollen stratigraphy and synchronisation to GRIP ice-core chronology used to verify correlation to terrestrial sequences.</p>	<ul style="list-style-type: none"> • Local vyrs • vyrs BP • Ice core yrs BP • Radiocarbon yrs BP 	No errors reported in the varve counts but Baltic Sea chronology was extended by 105 years by Andrén <i>et al.</i> (2002) after a new correlation was proposed to the previous correlation by Andrén <i>et al.</i> (1999)
Kristiansson (1985;1986)	107 varve diagrams, total of 2,310 vyrs, spanning ca 1,600 vyrs	<ul style="list-style-type: none"> • Visual varve thickness links • Exceptionally thick varves 	Björck and Möller (1987) used thin varves in the southern sites to link to the varve chronologies in southernmost Sweden by (Ringberg, 1971).	<ul style="list-style-type: none"> • Local vyr timescale 	±1 year for each 100 or 200 varves. This is based on the opinion of the

Regional varve chronology	Number of varve diagrams and overall length of chronology	Methods used to link individual site chronologies	Methods used to link to other regional varve chronologies	Timescales used	Varve count error
		<ul style="list-style-type: none"> • Exceptionally thin varves • Distinct varve thickness packages 	Brunnberg (1995) used the colour change at 707-708 v. yrs to link to varve records in Östergötland.	<ul style="list-style-type: none"> • v. yrs BP was used after link to Brunnberg (1995) chronology 	author. Difficulties correlating sites
Wohlfarth <i>et al.</i> (1998)	55 varve diagrams spanning 658 v. yrs	<ul style="list-style-type: none"> • Visual correlations between varve thickness diagrams • Exceptionally thick varves • Exceptionally thin varves • Position of distinct colour changes used to verify overlap • Statistical analyses used to support visual correlations • Especially thick clayey winter layers. 	<p>Characteristic thick clayey varves in the site Glottern 2 were used to link to Kristiansson's sites 41 Afsinge and 42b Rimforsa at local varve years 1938-1941.</p> <p>Correlation not possible with Ringberg (1971) sites in southernmost Sweden. But radiocarbon dates from Toregöl consistent with radiocarbon dated pollen records from southernmost Sweden indicate area was ice free between the late Bølling/Older Dryas/early Allerød.</p>	<ul style="list-style-type: none"> • Local v. yrs from the Kristiansson (1986) timescale are used • Radiocarbon v. yrs 	No error in the varve chronology reported
Ringberg (1979;1991)	185 varve diagrams spanning 640 v. yrs from local v. yr -325 to +315	<ul style="list-style-type: none"> • Visual correlations between varve thickness diagrams • Exceptionally thick varves 	Correlation to Wohlfarth <i>et al.</i> (1998) not possible but radiocarbon dates from Toregöl consistent with radiocarbon dated pollen records from southernmost Sweden and indicate area was ice free between the late Bølling/Older Dryas/early Allerød.	<ul style="list-style-type: none"> • Local v. yrs BP • Radiocarbon v. yrs 	No error in the varve chronology reported
Ringberg and Rudmark (1985)	6 diagrams	<ul style="list-style-type: none"> • Visual correlations between varve thickness diagrams • Exceptionally thick varves 		<ul style="list-style-type: none"> • Local v. yrs BP 	No error in the varve chronology reported

Chapter 4. Glaciolacustrine varves

4.1 Introduction

Varved sediments provide high-resolution archives of past environmental and climatic change at sub-seasonal to decadal timescales (Brauer and Casanova, 2001; Brauer *et al.*, 2009; Zolitschka *et al.*, 2015). Annually-laminated sediments are found in a range of depositional environments and are composed of different proportions of biogenic, clastic and chemical-precipitate material depending on the factors controlling limnological processes. Due to their high temporal resolution, varve chronologies can be used in combination with other independent dating techniques to produce highly accurate and precise age-depth models. Since varve chronologies are of comparable temporal resolution to tree rings and often contain terrestrial plant macrofossils suitable for ^{14}C dating, varve chronologies have also been used to calibrate radiocarbon chronologies (Goslar *et al.*, 1999, 2000; Bronk Ramsey *et al.*, 2012). Varve chronologies are also valuable for tephrochronology, particularly where multiple tephras are found within a single varve sequence and, provided there are no hiatuses, the time interval between volcanic ash layers can be estimated with annual to decadal precision (e.g. Blockley *et al.*, 2014; Lane *et al.*, 2015; Ott *et al.*, 2016). The generation of accurate varve chronologies is contingent upon the development of a robust varve depositional model (Zolitschka *et al.*, 2015). This requires full understanding of the processes that control seasonal sedimentation patterns that are often complex. For example, sedimentation patterns can relate to local-scale processes such as proximity to the lake edge/valley sides (Devine and Palmer, 2017) and broader basin-wide processes such as precipitation (Amann *et al.*, 2014), temperature (Hardy *et al.*, 1996), lake level changes (Palmer *et al.*, 2010), and solar activity (Haltia-Hovi *et al.*, 2007).

This thesis is concerned with the analysis of glaciolacustrine sediments that are almost entirely composed of minerogenic material and this chapter presents a review of the sedimentological processes that lead to glaciolacustrine varve formation. A summary of key analytical methodologies used in varve research is also presented. Allied to this and fundamental to the approach taken within this thesis is the use of tephrochronology and tephrostratigraphy, and the final part of this chapter discusses the use of tephrochronology specifically in varve research.

4.2 Glaciolacustrine varve processes

Glaciolacustrine varves accumulate in cold climate conditions in proglacial ice-contact or glacier distal lakes. The high sediment yields commonly associated with glacial systems causes large quantities of minerogenic material to be released into lakes mainly during the melt season directly from the glacier. Significant contributions of minerogenic material can also be transported to the basin via meltwater streams and/or nival meltwater sources. The lack of vegetation on the landscape, periglacial activity and seasonal changes in peak discharge means that large volumes of minerogenic material are eroded and transported into the lake basin. The high minerogenic content of the sediment supply typically means that glacial lakes are nutrient poor (Zolitschka *et al.*, 2015).

Glacial varves are formed due to the identification of consistent structures driven by seasonal patterns in sediment supply to a lake basin. During the melt season (spring/summer), sediment is delivered to the lake basin either directly from the glacier margin or from external (to the lake water) sources (Ashley, 1975; Smith and Ashley, 1985; Cockburn and Lamoureux, 2008). These sediment-laden flows can be composed of sand and gravel, as well as silts and clays (Bennett *et al.*, 2002). Due to internal currents generated by the flows and wind-driven surface mixing, fine-grained clay sediments are kept in suspension during the melt season and coarser-grained material is deposited. In the non-melt season (autumn/winter), the lake waters freeze over and inhibit the formation of surface currents allowing the finer clay fraction to be deposited from suspension in the water column. Glaciolacustrine varves are therefore composed of distinctive layers: a coarser-grained "summer" and a finer-grained "winter" layer. The method of sediment delivery to a basin is a key element of creating varve sediments and this is given more detailed consideration in the following section.

4.2.1 Sediment transport

In glaciolacustrine systems, sediment enters the lake via several pathways. In ice-contact lakes, sediment can enter the body of water directly from the glacier margin via 1) sub-glacial and supraglacial streams (Ashley, 1975; Smith and Ashley, 1985; Mulder and Alexander, 2001; Bennett *et al.*, 2002), 2) snow-melt related run-off (Francus *et al.*, 2002; Cockburn and Lamoureux, 2008; Ridge *et al.*, 2012), 3) iceberg rafting (Thomas and Connell, 1985), and 4) aeolian transport (Lewis *et al.*, 2002). In ice-distal lakes, sediment is usually transported within stream channels that drain catchment snow-melt or within meltwater streams that originate from a glacier that is located in the catchment but not in direct contact with the lake (Sturm, 1979). Aeolian transport can also occur in

distal glacial lakes where sediment from the surrounding catchment is blown into the lake basin and falls from suspension in the water column (Lewis *et al.*, 2002).

Sediment flows that are sourced directly from the glacier enter a lake body as supra- and englacial flows or from subglacial meltwater sources (Benn, 1996; Bennett *et al.*, 2002). Slumps that occur at the ice margin or on higher angle slopes of subaqueous ice-marginal fans can also generate surge-type flows. Depending on the density of the flow and the density of the lake water (which is a product of temperature and/or sediment concentration), sediment-laden flows enter the lake basin and travel at different depths within the lake. Density flows and cohesive flows tend to dominate in proximal locations where sediment concentration is greater than 10% whereas turbidity currents dominate as the flows evolve toward distal locations when the sediment concentration falls below 10% (Mulder and Alexander, 2001). When inflows enter a stratified water body they occur as either overflows, interflows or underflows (Smith and Ashley, 1985). Often in glacial systems, the sediment concentrations drive density differences between the inflowing water and lake water. If the inflowing water has a higher sediment concentration (higher density than the lake water), then the flow will travel as an underflow across the lake bottom. If the flow has a lower sediment concentration (lower density than the lake water) then the flow will travel as an overflow in the higher part of the water column (Figure 4-1). If there is a thermocline within the lake body and the inflowing water is the same density as the lake water, then the inflow will travel as an interflow across the thermocline (Figure 4-1).

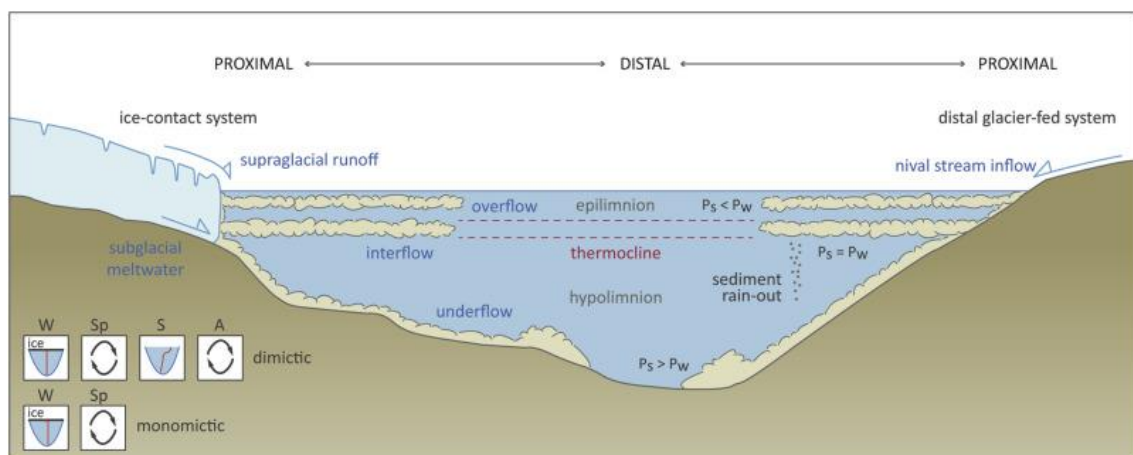


Figure 4-1. Flow types within ice-contact and ice-distal lakes.

Thermally stratified lake with density differences occur during the summer period. The depth of the flow within the lake water is driven by the relative density of the sediment inflow (P_s) and the lake water (P_w) leading to underflows, interflows and/or overflows. Temperature stratification in dimictic and monomictic lakes across the winter (W), spring (Sp), summer (S) and autumn (A) is summarised in the left-hand corner of the figure. From Palmer *et al.* (2019), pp.4.

Assuming that similar density differences between the lake and the stream water exists then underflows can also develop during periods of nival melt. The different flow types

experienced within different parts of glacial lakes can be distinguished by monitoring of modern lake systems. This has revealed that all three types of flow can exist simultaneously, with flow velocities ranging between $>10 \text{ cms}^{-1}$ for underflows and $5\text{-}10 \text{ cms}^{-1}$ in overflows and interflows (Crookshanks and Gilbert, 2008).

4.2.2 Temporal controls on sediment transport

The timing of sediment delivery to ice-contact and distal glacial lakes is primarily driven by the annual freeze-thaw cycle with most sediment delivered to the lake during the melt season (Gustavson, 1975; Lamoureux, 2001; Lewis *et al.*, 2002; Cockburn and Lamoureux, 2008). For ice-contact lakes ablation of the ice mass delivers sediment to the lake directly from the glacier, whilst ice-contact and distal glacial lakes can also receive sediment during the spring as significant nival melt that also transports minerogenic material to the lake basin. During the summer, precipitation events can also cause high discharge (flood) events to transport sediment to the basin. Church and Gilbert (1975) estimated that up to 50% of the annual sedimentation load during the summer months can be sourced from single run-off events. During the melt season (spring/summer), finer grained material is recirculated in the water column due to internal mixing and wind-driven surface currents. In the non-melt season, the surface waters of the lake are frozen, and the finer grained material settles from suspension to the lake bottom.

Seasonal sediment delivery is a major control on sedimentation patterns within glacial lakes and is an important component of glaciolacustrine varves. However, there are stochastic events that deliver material to the lake basin at subseasonal scales. Diurnal fluctuations in flow can occur and reflect changes in meltwater release due to fluctuating air temperatures. Stochastic events, such as slump deposits will also be recorded within sediment sequences (Smith, 1978).

4.2.3 Depositional processes

Deposition of grains from flows will be dependent on the grain sizes of the material transported within the flow, the flow velocity and changes in flow velocity as it propagates into the basin. As an example of these relationships, For interflows and overflows, which have a velocity between 5 and 10 cms^{-1} , deposition of grains $<250 \mu\text{m}$ is initiated after only a small decline in flow velocity (Palmer *et al.*, 2019).

For underflows, the flow velocity will decrease with progression of the flow across the lake basin due to two key reasons: 1) coarser grains are deposited first which reduces the sediment concentration and thus the velocity of the flow; and 2) friction at the base of the flow and between the lake water causes the flow velocity to decline. The

concentration of sediment within an underflow decreases with increasing distance from the point at which the flow enters the lake. As the flow moves across the lake floor the head of the flow mixes with the lake water with the coarser grains deposited first via traction/bedload whereas finer grains (fine silts and clays) are distributed higher in the water column. During the summer the finer grains are kept in suspension until the winter when suspension settling processes dominate.

For overflow and interflows, again the flow velocity decreases with progression through the lake waters though sediments are deposited exclusively from suspension settling. Again, coarser grains are deposited closer to the point of inflow, possibly within deltas or subaqueous fans and finer grains (fine sand, silts and clays) are distributed more widely across the lake basin. During the summer the finer grains that originated from interflows and overflows are kept in suspension in the water column due to internal mixing and surface winds. During the winter when the lake waters freeze, the lake waters are calm, and this allows the fine grained sediment to fall from suspension. It is the seasonal controls on sediment transport and deposition which ultimately lead to the formation of glaciolacustrine varves with their characteristic fine-grained (clay) “winter layer” and coarse grained (sand to silt) “summer layer”.

4.2.4 Other glaciolacustrine processes and structures

Other depositional processes occur in glacial lakes that are driven by different processes, and these create different sediment structures than those preserved by the more persistent sediment processes delivering material to the basin described above. These single comparatively short-lived events can cause deformation of discrete parts of the sediment sequence or cause more pervasive deformation of the sediment stack and can cause difficulties in determining the original flow processes from sediment records. These processes include slumping, load deformation, seismic activity, glacial readvance and iceberg rafting. Soft sediment deformation due to slumping is common in proximal areas of glacial lake basins where subaqueous outwash fans accumulate (Cheel and Rust, 1986) or in subaqueous zones on valley sides (e.g. Devine and Palmer, 2017). Slump facies can occur due to: 1) uneven loading of a fan surface due to preferential accumulation from different fan-channels; 2) melting of buried glacial ice within a fan (Cheel and Rust, 1986); and 3) an uneven basin bathymetry. The bathymetry of the lake basin can be uneven due to the underlying geology or geomorphological landforms such as eskers or moraines that were deposited prior to lake formation (e.g. Strömberg, 1994). Water escape structures are also common in glaciolacustrine sediments and are indicative of load deformation (Bennett *et al.*, 2002; Talling *et al.*, 2012; Bendle *et al.*, 2017) that can be driven by high aggradation rates on outwash fans

or deltas (Cheel and Rust, 1986). Load deformation can occur, for example, during periods of turbidite emplacement (Talling *et al.*, 2012).

The triggering of these surge-type deposits (e.g. Mörner, 2011) can be caused by seismic activity, during periods of glacial unloading (e.g. Tröfthen and Mörner, 1997) or in response to geological earthquakes (Monecke *et al.*, 2004; Avşar *et al.*, 2016). Seismic shaking leads to the liquefaction, re-suspension and rapid deposition of glaciolacustrine sediments as “seismites” (Mörner, 1996, 2011). These sediments can be characterised by either load structures, convolute bedding, rip up clasts of silt and clay within a fine matrix, or massive graded thick beds of sand and silt (Johnsen and Brerand, 2006). Deformation of glaciolacustrine sediments can also be caused by oscillation of the ice margin (Kristiansson, 1986; Waldemarson, 1986). This commonly impacts the proximal zone of the glaciolacustrine system with up-thrusted beds or vertical/sub-vertical laminations that form during push-moraine formation due to ice margin readvance (e.g. Johnson *et al.*, 2019) (Figure 4-2).

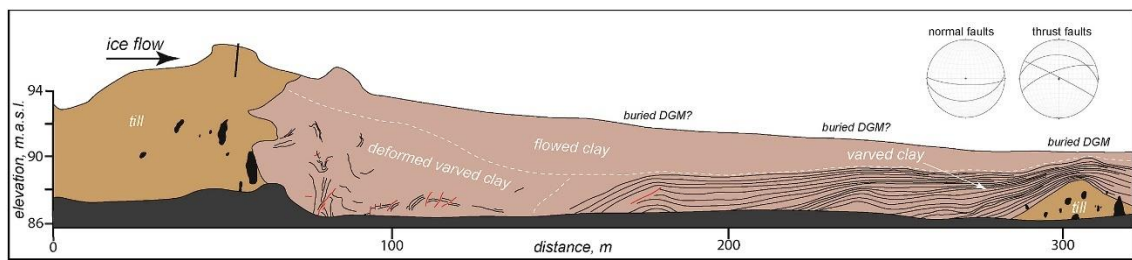


Figure 4-2. Schematic of deformed varved clay due to push-moraine formation in Gullhammar, Sweden. Modified from Johnson *et al.* (2019).

At a finer scale, the deposition of anomalously large grains or clasts interpreted as ice-rafted debris (IRD) (Thomas and Connell, 1985) can cause deformation of previously deposited sediments (Ovenshine, 1970; Bendle *et al.*, 2017; Devine and Palmer, 2017). Deformation consists of penetration and/or bending of laminations at the bottom contact and bending/on-lap of the upper contact (Figure 4-3). Deposition of aeolian grains which are typically $<200\ \mu\text{m}$ and sink into laminations can also cause deformation to delicate sediment structures, though this is rarely described (Ringberg and Erlström, 1999).

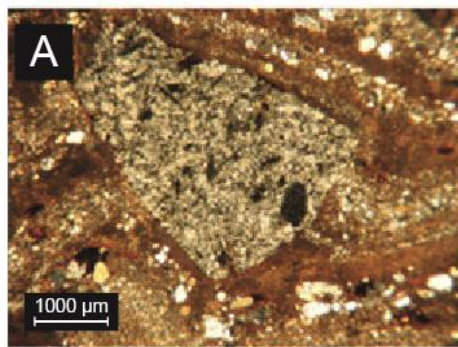


Figure 4-3. Example of a dropstone with bending of the lowermost and onlap of the uppermost laminations (Devine and Palmer, 2017).

The following section presents the different varve structures that are observed across a lake basin with focus on proximal and distal varves.

4.3 Glaciolacustrine varve structures

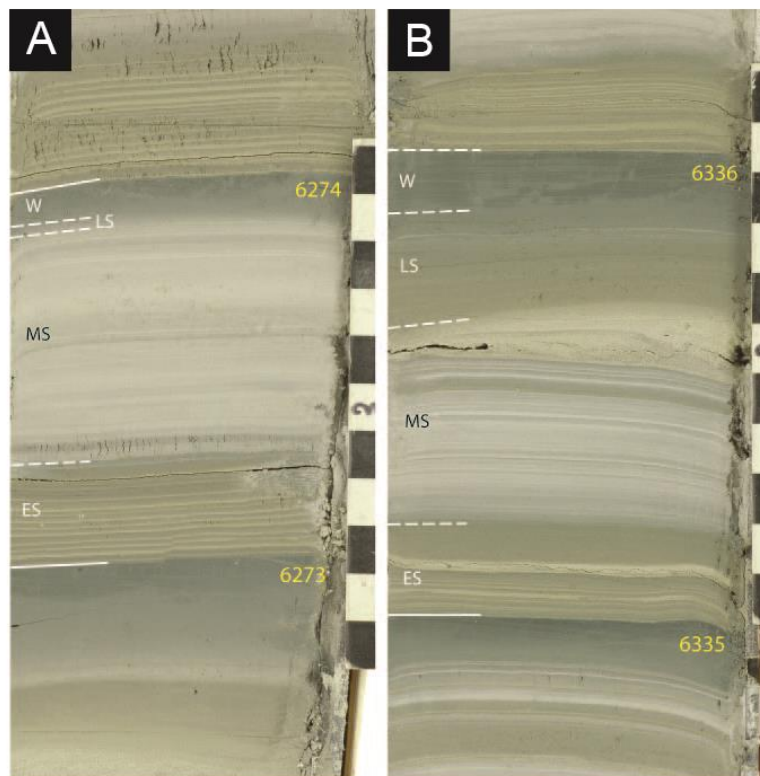
There are several fundamental characteristics that are considered common to glaciolacustrine varves; 1) winter layers are composed almost entirely of clay (Ashley, 1975; Ridge *et al.*, 2012); 2) there are sharp contacts between the winter layer and overlying summer layer; and 3) the contact between the winter layer and the underlying summer layer can be gradational, diffuse or sharp (Ashley, 1975), and 3) summer layers can be internally complex with multiple graded units (Ringberg and Erlström, 1999; Ridge *et al.*, 2012), or can be composed of a single unit (Palmer *et al.*, 2019). There are, however, differences in varve structure, texture and thickness across a lake basin and these differences are largely driven by proximity to the point of sediment input.

4.3.1 Proximal varves

Glacial varves that are deposited relatively close to a receding ice margin are typically thicker (\geq cm-scale) and the summer component is usually complex with multiple laminations. Ridge *et al.* (2012) describe the internal structure of proximal varves that formed close to the retreating ice margin of the Laurentide Ice Sheet in the Connecticut Valley (New England, USA). These proximal varves display thicknesses of >80 mm, and the summer (melt season) component can be subdivided into three units that are related to different stages of the melt season. Table 4-1 summarises the varve structures and depositional processes and Figure 4-4 shows examples of these structures.

Table 4-1. Varve structure in ice-proximal varves (Ridge et al., 2012)

Summer component Unit	Description	Process interpretation
Early melt season	<ul style="list-style-type: none"> • Darker colour due to higher clay content • Composed of rhythmically graded clayey silt laminae 	Diurnal meltwater fluctuations.
Main melt season	<ul style="list-style-type: none"> • Lighter colour laminations than the other summer units • Composed of rhythmically graded fine sand or very coarse silt of irregular thickness. • The first graded lamination is commonly the coarsest sediment in the entire summer component 	Often these layers form the coarsest sediment in the melt season and reflect high sedimentation during periods of high subglacial discharge, as well as nival flooding and/or larger rainfall events.
Late melt season	<ul style="list-style-type: none"> • Darker colour than the main melt season unit below due to higher clay content • Composed of rhythmically graded clay-rich laminae. • Laminae are less well-defined than in the early and main melt season units, and commonly fine upwards • The upper contact grades into the winter layer above with occasional interruptions by silt or fine sand 	<p>Late melt season laminations are finer grained than the main melt season and reflect waning meltwater discharge</p> <p>The occasional silt or fine sand grains may represent late summer to early fall runoff or melting events that briefly reinvigorate bottom currents after clay deposition has begun.</p>

**Figure 4-4.** Ice-proximal varves identified by Ridge et al. (2012).

Subunits of the summer layer by early (ES), main (MS), and late (LS) melt season (summer). Numbers on winter clay units (W) indicate local varve years. Early and late melt season units are darker than the main melt season unit because of higher clay content. The lighter main melt season unit has a higher silt and fine-sand content. Winter units are composed of nearly pure clay and have a dark greenish grey colour. (A) Varve 6274 shows a highly rhythmic early melt season unit while the late melt season unit is very thin and indistinct. Varve 6273 shows a gradational contact between the summer and winter layers. (B) Varve 6336 shows rhythmic beds in the early melt season unit and very faint rhythmic layers in the late melt season unit. Each black or white box = 1 cm.

The multiple laminations within the summer component of varves are also described by Heideman *et al.* (2015) in a varve record from Lillooet Lake, Canada which is predominantly fed by nival melt. Thick flood deposits within the melt season layers were also identified and the mean varve thickness is between 20-30 mm. Proximal varves with multiple melt season layers have also been identified in the Baltic Ice Lake and the number of melt season laminations has been linked to the length of the melt season (Ringberg, 1984). Other structures in proximal varves include erosional contacts between laminations and clay intraclasts (Ashley, 1975; Ridge *et al.*, 2012).

4.3.2 Distal varves

Glacial varves that are deposited in distal locations to a receding ice margin are thinner (<cm-scale) than proximal varves. The summer component of distal varves can also be complex with multiple laminations but there are usually fewer laminations and the overall varve thickness is thinner than for ice-proximal varves. The summer component can also be simpler in structure with only one or two laminations. The most recent review of distal glaciolacustrine varve facies is presented by Palmer *et al.* (2019). The authors provide a comprehensive review of published macroscale and micromorphological descriptions of glaciolacustrine varves from Europe, North America and South America. Distal varves are categorised into five groups called “Lamination Set Assemblages” that are related to the proximal-distal relationship within the lake basin: 1) Proximal Intermediate; 2) Intermediate-Distal Lake Bottom; 3) Distal Delta/Subaqueous Fan Bottomset; 4) Distal Lake Bottom; and 5) Ultra Distal/Nival. Figure 4-5 summarises the characteristics of distal glaciolacustrine varves including varve thickness, particle size, structure and nature of contacts between the melt season and non-melt season. The basinward sediment transport processes are also highlighted alongside the sediment source and example microfacies sediment logs.

Lamination Set Assemblage	Varve Thickness (mm)	Melt Season (MS)			Non-Melt Season (NMS)		
		Particle Size (Sorting)	Structure	Upper Contact	Particle Size	Structure	Upper Contact
1	20 - 600 MS > NMS	VCZ - MZ (WS)	multi-lamination; f.u. (CZ-MZ); turbidites f.u. (CS-VFS)	sharp	C (VFZ) (WS)	graded: VFZ f.u. to clay from the first part of the lamination	sharp
2	2 - 20 MS ≥ NMS	VFS; CZ; MZ (WS)	multi-lamination; 1st input MZ; later f.u. (CZ-MZ)	sharp	C (VFZ) (WS)	graded: VFZ f.u. to clay from the first part of the lamination	sharp
3	0.5 - 5 MS ≥ NMS	FS; VFS; VCZ (WS)	normally single, massive lamination or double lamination; contains clay rip-up clasts	sharp	C (VFZ) (WS)	graded: VFZ f.u. to clay from the first part of the lamination	sharp
4	1 - 5 MS ≤ NMS	MZ; CZ (WS)	multiple laminations; alternations of CZ and MZ; CZ sometimes single grain lineations	sharp	C (VFZ) (WS)	graded: VFZ f.u. to clay from the first part of the lamination	sharp
5	<1 MS ≤ NMS	MZ (PS)	single lamination or multi lamination; single grain lineations of CZ	appears graded	C (VFZ) (WS)	graded appearance due to contact from MZ layer; f.u. to clay	sharp

MS = Melt Season; NMS = Non Melt Season; FS = fine sand; VFS = very fine sand; VCZ = very coarse silt; CZ = coarse silt; MZ = medium silt; VFZ = very fine silt; C = clay; WS = well sorted; PS = poorly sorted; f.u. = fining upwards; QS = Quasi Steady; ST = surge type

Lamination Set Assemblage	Basinward Transport	Sediment Source	Lamination Set Assemblage Name	Microfacies Schematic
1	MS: QS underflow & ST for turbidites NMS: suspension settling	All glacier sourced sediment	Proximal Intermediate	
2	MS: QS underflow 1st input lower energy (spring melt from catchment) than subsequent laminae.	High glacier sourced sediment	Intermediate / Distal Lake Bottom	
3	NMS: suspension settling MS: QS underflow (traction load) NMS: suspension settling	High fluvial (nival)/glaciofluvial; low direct glacier sourced sediment	Distal Bottom-set (delta/subaqueous fan)	
4	MS: QS underflow; only high discharge events recorded; element of suspension deposition. NMS: suspension settling	High fluvial (nival)/glaciofluvial; low ice contact glacial component	Distal Lake Bottom	
5	MS: QS underflow; flow velocity is low providing only suspended load. Some mixing of higher flow events NMS: suspension settling	High fluvial (nival) glaciofluvial; no ice contact component	Ultra Distal / Nival	

Key:
MS = Melt Season; NMS = Non Melt Season; QS = Quasi Steady; ST = surge type; sg = single grain

Melt season
 massive
 normally graded
 normally graded
 inverse graded

Non Melt season
 grading at the very first part of the lamination
 grading distributed evenly through the lamination

Thickness range of the microfacies (mm) 0 2-20
 Grain size on each log: c (clay); fz (fine silt); mz (medium silt); cz (coarse silt); vfs (very fine silt)

Figure 4-5. Lamination Set Assemblages proposed by Palmer et al. (2019). Characteristics of Lamination Set Assemblages, sediment source and dominant basinward transport mechanism.

In distal glaciolacustrine settings, non-annual varve-like structures have also been identified in the clay component of varves (Shaw and Archer, 1978; Lambert and Hsü, 1979). These so-called “false varves” contain coarse grained deposits within the winter layers. For example, the varved sediments at Kickininee Park, Okanagan Valley, British Columbia contain cross-laminated sands within the clay component that are interpreted as short-lived, high energy flow events in the winter season (Shaw and Archer, 1978). In Switzerland, lake monitoring and sediment trap analysis at Lake Walensee indicates that turbidity currents generated by hyperpycnal inflow occurred sporadically throughout the year producing “false varves” (Lambert and Hsü, 1979). Since the winter season is typically considered a period of low sedimentation rates in glacial lakes (Ashley, 1975; Ridge *et al.*, 2012), these structures may cause over-counting when constructing a varve chronology. In extant lakes it is possible to observe sediment processes and quantify the occurrence of false varves, however this is not always possible, and cannot be achieved in palaeoglaciolacustrine settings. In the absence of modern lake-monitoring, varve counts should be verified by independent dating techniques such as radiocarbon or tephrochronology (section 4.5 and 4.6).

4.3.3 Spatial distribution of varved sediments

An important consideration is that the point at which sediment enters a lake basin can be described as proximal or distal irrespective of whether the sediment is sourced from a glacier or from streams that enter the lake basin from the surrounding catchment (Ashley, 1975) (Figure 4-6). Where glaciolacustrine varves are deposited in restricted valley systems, turbidity currents can also be sourced from ablation of distal glacier ice, or from precipitation events or snowmelt in the catchment that can lead to the formation of subaqueous fans (Ashley, 1975; Palmer *et al.*, 2010; Devine and Palmer, 2017). Therefore, sediment processes and thus varve thicknesses and structure are heavily influenced by the position of the sampling location relative to a sediment source, rather than just the position of the ice margin (Figure 4-6). Consequently, the sediment structures may display equifinality when comparing material deposited from flows propagated from the ice in comparison to those structures deposited from streams within the lake catchment. Indeed, relatively coarse sediments in the melt season layers and thick varves can be deposited across delta surfaces with decreases in varve thickness toward the toe end of the delta (Devine and Palmer, 2017).

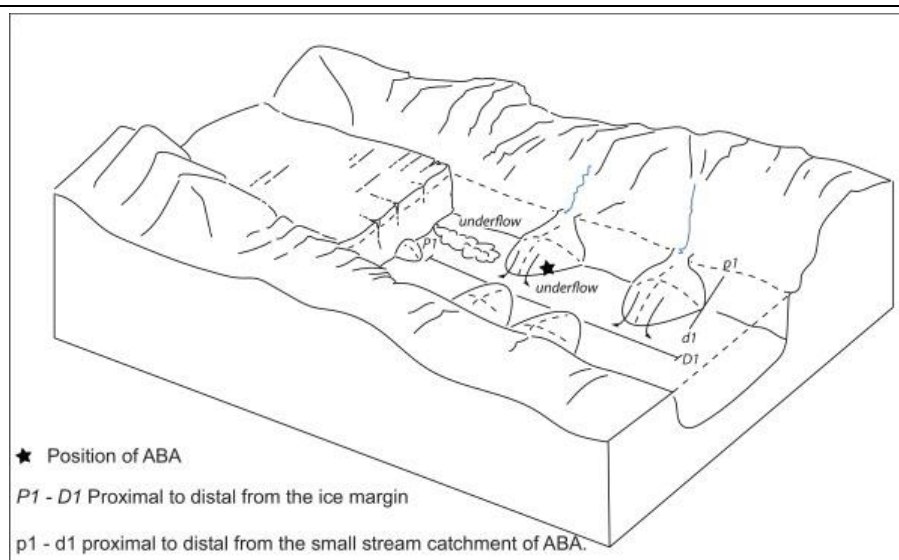


Figure 4-6. Schematic of theoretical proximal-distal sediment processes within an ice-contact valley lake.

Sediment is transported into the lake waters directly from the ice with progressively thinner varves developing with greater distance from the ice margin (P1–D1). Proximal to distal thinning of varve thickness across fan surfaces (p1-d1) also occurs when sediment is transported to the basin via alluvial transport from small mountain catchments. From Devine and Palmer (2017) pp. 143.

It is also important to note the spatial disparity in varve formation across a lake basin. Since nival melt can be restricted to certain parts of the catchment, not all flows are pervasive across a lake basin. This means that some years are not accounted for in the sediment record leading to “missing varves”. Multiple cores across a lake basin are preferred in order to test the spatial extent of laminations that comprise individual varves (Lamoureux, 2001) although in palaeoglaciolacustrine systems access to such sequences is not always available.

4.3.4 Summary of varve structures

Varve structures decrease in thickness and the melt season component decreases in complexity from proximal to distal locations within a lake basin. This is related to the number of high velocity/ high sediment concentration flows that can reach distal locations of the basin. In distal parts of the lake basin five varve microfacies have been identified; Proximal Intermediate, Intermediate-Distal Lake Bottom, Distal Delta/Subaqueous Fan Bottomset, Distal Lake Bottom, and Ultra Distal/Nival. There are several sedimentological properties that are common to all glaciolacustrine varves which are summarised by Palmer *et al.* (2019):

- 1) The contact between the clay (non-melt season) layer and the overlying coarser (melt season layer) is always sharp.

- 2) The melt season layer is generally composed of very fine sand and silt units with variations in structure and thickness. These units comprise either multiple graded or massive laminae. Coarse sediments are commonly observed at or just below the contact to the non-melt season (clay) layer.
- 3) When observed at the macroscale, there is a sharp contact between the melt season layer and the overlying non-melt season layer, though at the microscale this can be graded.
- 4) At the macroscale the non-melt season layer is composed almost entirely of clay, but at the microscale it can grade from very fine silt to clay.

Whilst this thesis is primarily concerned with glaciolacustrine varves, it is important to emphasise that glacial varves do not always form within lake basins or in all parts of the glaciolacustrine systems. For example, clastic varves may form due to seasonal processes in delta (Cato, 1985; Wohlfarth *et al.*, 1997), glaciofluvial (Bennett *et al.*, 2002; Crookshanks and Gilbert, 2008) or glaciomarine (Stevens, 1985; Johnson *et al.*, 2013) environments. Shallower water depths in the littoral zone of a lake may be prone to continuous mixing in the water column and so finer-grained material, that is characteristic of the non-melt season may not be deposited. Alternatively, the variable topography of lake basins may prevent the progression of turbidity currents across the lake basin (e.g. Gustavson, 1975). For example, an esker, glacial boulder or a moraine may cause “blocking” of sediment density flows (e.g. Lundqvist, 1957), thus leading to “missing varves” in the sediment record. Varve sedimentation can also be interrupted by stochastic events which can cause deformation and/or breaks in the varve record (section 4.2.4). Consequently, it is important that the geomorphological context of the basin is understood, as well as the factors that might favour varve formation, including the likely cause of non-varve deposition. In certain circumstances, the presence of non-varve beds or laminations can act as marker layers within a particular basin aiding the development of the varve chronology by correlation between cores (see section 4.5). Provided the succeeding and/or preceding varves around deformation or a turbidite can be correlated with other varve records from the same lake basin, it is possible to determine the geographical extent of, for example, a seismic event (e.g. Bendle *et al.*, 2017). However, this is more difficult when examining sediment cores rather than sediment outcrops which enable the lateral continuation of deformation structures to be assessed. The following section examines the core techniques that have been used to understand sediment transport and depositional processes in the formation of varves and also strategies used for the development of a glaciolacustrine varve chronology that are pertinent to this thesis.

4.4 Varve analytical techniques

To maximise the potential of varve records complete sediment sequences must be recovered. Thorough investigation of the sampling area is necessary to determine a suitable coring site. Sediment depth surveys can aid in such efforts as they allow for assessment of the underlying topography to identify a flat area of the basin that minimises the influence of slump deposits. Understanding the local and regional geomorphological context may also help to identify suitable varve sampling locations to avoid areas that are prone to deformation from, for example, push-moraines (Figure 4-2). For extant lakes, it is necessary to extract the uppermost varve at the sediment-water interface to establish modern depositional processes and develop a varve model. However, in palaeoglaciolacustrine settings this is not possible and so researchers rely on descriptive frameworks to objectively characterise lamination sedimentology (Ashley, 1975; Smith and Ashley, 1985; Ridge *et al.*, 2012). Accurate varve identification requires scrutiny of the internal texture and structure of laminations to determine a seasonal cycle (Zolitschka *et al.*, 2015). This is typically achieved through visual observations of colour and grain size between individual laminations. For thick varves (\geq cm-scale) this is sometimes possible (e.g. Ridge *et al.*, 2012; Bendle *et al.*, 2017) but it is now considered necessary to use microscopic techniques for varves that are <cm-scale (Lamoureux, 2001; Brauer, 2004). The following sections summarise key methodologies that are used to analyse varved sediments across a range of analytical resolutions from the macro to microscale.

4.4.1 Macroscale sedimentology

The most direct method of analysing varved sediments at the macroscale is via inspection of outcrops or open core surfaces. To enhance the visual distinction between laminations sediment cores can be left to air dry (e.g. Wohlfarth *et al.*, 1998; Ridge *et al.*, 2012; Bendle *et al.*, 2017). Varve counting is conducted either by marking individual varves with coloured pins or marking varves directly onto tape that is rolled alongside sediment cores or vertically down the varved outcrop (e.g. De Geer, 1912; Caldenius, 1932; Brunnberg, 1995; Andr n *et al.*, 1999; Hang, 2003; Ridge *et al.*, 2012; Hang *et al.*, 2019). Whilst varves can be identified at the macroscale measurement precision is restricted to *ca* 1 mm which can be insufficient to accurately delimit lamination boundaries (Brauer, 2004; Zolitschka *et al.*, 2015).

4.4.2 Particle size analysis

In varve research, particle size analysis can be used to validate field and laboratory observations in order to support the interpretation of varve formation. Typically, grain

size analysis is conducted via visual estimations from sediment samples at the macroscale (Antevs, 1931; De Geer, 1940; Hang, 2003; Brauer *et al.*, 2009; Ridge *et al.*, 2012), though measurements can be made under thin section (Ringberg and Erlström, 1999; Palmer *et al.*, 2010, 2019; Bendle *et al.*, 2017) or from high-resolution image analysis (e.g. Francus *et al.*, 2002; Ojala and Francus, 2002). In recent years, laser diffraction analysis has enabled precise quantification of particle sizes and generation of grain size distribution curves (Bendle *et al.*, 2017; Maurycy Źarczyński *et al.*, 2019; Regnéll *et al.*, 2019). Grain size data can be used to characterise different varve types (e.g. Źarczyński *et al.*, 2019) and reconstruct catchment processes that may be related to climate (e.g. Francus *et al.*, 2002; Lamoureux and Gilbert, 2004; Lapointe *et al.*, 2012).

4.4.3 Digital image analysis

Analysis of high-resolution images of split core surfaces has become a prominent tool in varve research (e.g. Andrén *et al.*, 2002; Francus *et al.*, 2002; Marshall *et al.*, 2012; Nakagawa *et al.*, 2012). Acquisition of digital images is fast and non-destructive, and files can be readily shared between analysts. Characterisation of laminations can be performed either manually or via semi-automated statistical analysis of images. For manual analysis, sediments are typically characterised using visual grain size estimation and distinctions between lamination colour. Several computer programs are available that allow analysts to store sediment images, mark lamination boundaries and record varve thickness data (e.g. Cybis Coordinate Recorder, Peak Counter, Image Pro Express, Adobe Photoshop). However, manual analysis can be somewhat subjective and varve identification is dependent on the skills and experience of the analyst. To account for user-bias Zolitschka *et al.* (2015) recommend that at least two researchers carry out varve measurements.

In recent years, there have been developments in semi-automated image analysis of varves (Rupf and Radons, 2004; Weber *et al.*, 2010; Marshall *et al.*, 2012; Schlolaut *et al.*, 2012). For example, the BMPix macro, developed by Weber *et al.* (2012) extracts red, green, blue (RGB) and grey values on any bitmap image at pixel resolution. Colour and grey-scale data can be derived from both core surface images and transmitted light images (e.g. thin sections and X-radiographs). The macro calculates the average RGB or grey value across a pre-defined pixel width and the resultant data are plotted against depth. Pixel width can be adjusted to reduce noise, but this involves subjective decisions and/or prior knowledge of lamination thickness. Settings can also be adjusted to account for changes in sediment colour as varve characteristics may vary throughout the sequence. Following extraction of these data, the PEAK tool can be used to produce semi-automatic varve counts and measurements (Weber *et al.*, 2010). A major

advantage of semi-automated analysis is the faster generation of repeat varve counts that may improve varve chronologies (Zolitschka *et al.*, 2015). However, Kinder *et al.* (2013) found that for thicker varves with a complex internal structure, automated methods overestimate varve counts. The authors also report that turbidites were erroneously identified as varves and thin, mm-scale, laminations were not identified from image analysis but were identifiable under thin section. Whilst image analysis allows faster varve counts, image resolution is typically insufficient for accurate grain size estimation and precise measurement of thin (<mm-scale) laminations. In addition, images provide limited data for the chemical composition of laminae. These limitations prohibit accurate assessment of annual and non-annual structures which is fundamental for the generation of accurate varve chronologies.

4.4.4 X-ray radiography

X-ray radiography is a fast and non-destructive technique that is used for scanning and recording density differences within sediment cores. It is based on the X-ray absorption properties of different materials and can be performed on split sediment cores or resin-impregnated blocks (Lamoureux, 2001). X-ray radiography allows comparison of lithostratigraphy between cores and for correlation of overlapping cores to create composite sediment profiles. It can also be used to highlight internal sedimentological properties that are not visible at the core surface. Features such as bioturbation, hidden clasts, deformation structures, unconformities and macrofossils such as shells or bones can appear distinct under X-ray. These factors make X-ray radiography a useful technique for the characterisation of sediments in addition to other sediment analysis techniques.

Samples are typically scanned on an Itrax Core Scanner which collects optical and X-radiograph images by moving the sample incrementally through an X-ray beam (Croudace *et al.*, 2008; Marshall *et al.*, 2012). The absorption of the X-rays depends on sediment thickness, the elemental composition of the sample and sediment density (Francus *et al.*, 2015). Sediment density can be a product of various factors including water content, grain size, sediment porosity and the relative proportions of minerogenic matter, organic matter and biogenic silica (Ojala and Francus, 2002; Tiljander *et al.*, 2002; St-Onge *et al.*, 2007). X-radiographs are particularly useful in varve research as they enable the analysis of thin (<1 mm) laminations that are difficult to identify and characterise from macroscale observations. In a single varve, the composition and therefore the density of individual laminations varies between each seasonal lamination. The regular and repeating cycle of laminations, each with different density properties, appears on an X-radiograph image as alternations between light and dark laminations.

In bio-clastic varves, dense clastic layers absorb more X-rays than organic layers and appear lighter in X-radiograph images (e.g. Tiljander *et al.*, 2002; Martin-Puertas *et al.*, 2012; Neugebauer *et al.*, 2014). In glaciolacustrine varves the same principle applies whereby clay/winter layers show a lighter colour in the X-radiograph image than coarser silt/summer layers that appear darker (e.g. Weber *et al.*, 2010; MacLeod *et al.*, 2011). This is because clay/winter layers have a lower porosity and therefore higher water content than silt/summer layers. Clay-rich laminations therefore have a greater ability to absorb X-rays than silt/sand laminations which have a lower water content and a higher porosity. As a consequence, X-radiographs can be used to estimate the relative grain-size differences between individual laminations and can be used to develop a varve depositional model.

For varve thickness measurements, greyscale values can be acquired from digital image processing. There are several computer programs and Excel macros that can be used to extract grey value data from X-radiograph images (e.g. DendroScan, PeakCounter, BMPix) (Tiljander *et al.*, 2002; Haltia-Hovi *et al.*, 2007; Weber *et al.*, 2010; Marshall *et al.*, 2012). Although computer-generated varve counting provides more objective results, Tiljander *et al.* (2002) suggests that it should never be used in isolation for varve counting. It is now considered standard practice to integrate X-radiograph analysis with other varve analytical methodologies such as thin section analysis, μ XRF data and particle size data (Lamoureux, 2001; Saarnisto and Saarinen, 2001; Haltia-Hovi *et al.*, 2007; MacLeod *et al.*, 2011; Muschitiello *et al.*, 2016).

4.4.5 μ XRF analysis

Micro X-ray fluorescence (μ XRF) analysis is a rapid and non-destructive method of measuring the chemical composition of wet, frozen or resin-impregnated sediment cores (Croudace *et al.*, 2008). Measurements are acquired by incrementally moving the sample through an X-ray beam and scanners are commonly set at 100 μ m, 200 μ m and 500 μ m resolutions. μ XRF scans are usually taken on an Itrax Core Scanner at the same time as X-radiograph and optical image scans (Bloemsmas *et al.*, 2018). Data are expressed as element intensities in kilo counts per second (kcps) and are somewhat proportional to the chemical concentration of the sediment at a particular sampling point. The relationship between element intensity and concentration is not straightforward and analyses have revealed that element intensities from XRF core scanners are non-linearly related to element concentration (Weltje and Tjallingii, 2008). This can be explained by the influence of sediment characteristics that are unrelated to sediment chemistry such as water and organic content (L wemark *et al.*, 2011; Boyle *et al.*, 2015), as well as

external factors such as the X-ray parameters (Tjallingii *et al.*, 2007). These factors should be taken into consideration when analysing element intensity data.

Whilst XRF scanners can measure a wide range of elements from Aluminium to Uranium, many lighter elements that are outside of the measuring range of the XRF detector are present within sediment cores and cannot be detected (Lövemark *et al.*, 2011). Higher quantities of elements such as nitrogen, carbon and oxygen cause dilution effects resulting in lower counts for heavier elements and *vice versa*. This is known as the 'closed sum effect' (Weltje and Tjallingii, 2008; Lövemark *et al.*, 2011; Boyle *et al.*, 2015) and is a consideration when analysing correlations between individual elements. To resolve difficulties associated with closed-sum data Aitchison (1982) proposed that compositional data (e.g. percentages, ppm, element intensities), are first expressed as logarithms of ratios. This approach is now standard practice for XRF data and it is now recommended to transform element intensity data into log-ratios (Weltje and Tjallingii, 2008; Weltje *et al.*, 2015). The transformed data can then be used for statistical analyses and characterisation of sediments.

In varve research, μ XRF data are used to chemically characterise varve structure and produce a varve depositional model (e.g. MacLeod *et al.*, 2011; Marshall *et al.*, 2012; Martin-Puertas *et al.*, 2012; Dulski *et al.*, 2015; Słowiński *et al.*, 2017; Tylmann *et al.*, 2017). Whilst some elements and element ratios have been widely used in μ XRF studies of varved sediments, (e.g. Ti as an indicator of clastic input: Martin-Puertas *et al.* (2012); Tylmann *et al.* (2017)), specific elements should not be taken as universally applicable. This is largely due to the fact that several elements can produce a similar or varying signal depending on lake-specific conditions such as the mineralogy of the catchment, sediment sources and/or climatic setting (Davies *et al.*, 2015). Additionally, since there are no guidelines to suggest which elements to use for log-ratios an objective statistical methodology is required. Principal Component Analysis (PCA) is ideally suited for compositional data and it enables an assessment of elements which account for the greatest variation in element intensities (MacLeod, 2010; Słowiński *et al.*, 2017; Żarczyński *et al.*, 2019). Those elements that account for the greatest variation are considered useful for delimiting varve boundaries and the resultant log-ratio plots can be used for varve counting (e.g. Marshall *et al.*, 2012).

New developments in the analysis of varved sediments via μ XRF core scanning enables the superposition of chemical data on digital images of varves from thin sections, split core surfaces or X-radiographs (Marshall *et al.*, 2012). The analyst determines varve boundaries by integrating several lines of evidence and assigning a 'Varve Quality' score for each individual varve based on the number of criteria that are met (Nakagawa *et al.*, 2012). The Varve Quality score can also be used to estimate varve count uncertainty.

Marshall *et al.* (2012) recommend that at least 10 measurements should be made across a single varve in order to provide sufficient data for every seasonal layer, however, this is not always possible since the number of data points per varve is dependent on the analytical resolution of the Itrax Scanner and varve thickness. To determine the accuracy of μ XRF varve counts, researchers can compare log-ratio plots with corresponding thin sections or X-radiographs (MacLeod *et al.*, 2011; Nakagawa *et al.*, 2012; Neugebauer *et al.*, 2012; Dulski *et al.*, 2015; Schlolaut *et al.*, 2018). Varve counts from μ XRF data are not typically the sole method of generating varve counts and are commonly used in combination with other methodologies. It is necessary to verify that variations in the chemical data accurately reflect the composition of seasonal laminations rather than non-annual laminations such as turbidites or “event layers”. However, when comparing the accuracy of different varve counting methodologies, μ XRF varve counts can be conducted in isolation (e.g. Marshall *et al.*, 2012).

4.4.6 Microfacies analysis

Microfacies analysis is increasingly being applied to the analysis of varved sediments (e.g. Brauer *et al.*, 2008; Palmer *et al.*, 2008; Coven *et al.*, 2010; Martin-Puertas *et al.*, 2012; Van Daele *et al.*, 2014). A key advantage of this methodology is the ability to identify sediment structures that are not visible at the macroscale. Macroscopic techniques enable identification of biogenic or clastic laminations at an analytical resolution from millimetre to centimetre scale. Several researchers have identified microstructures such as sub-seasonal laminations within varved sediments (Dean *et al.*, 1999; Brauer, 2004). These so-called “sub-laminations” can be of less than millimetre scale and can be misidentified as intercalated “event” layers when examined macroscopically (e.g. Czymzik *et al.*, 2013). Where lamination boundaries appear indistinct at the macroscopic level, boundaries can appear clear under thin section allowing accurate delineation of laminations. Thin section analysis is therefore required to accurately delimit lamination boundaries and determine whether or not laminated sediments preserve an annual (varve) signal (Brauer *et al.*, 1999; Brauer and Casanova, 2001; Brauer, 2004).

In the past few decades there have been technical improvements in thin section production (e.g. Lamoureux, 1994; Lotter and Lemcke, 1999) particularly for clay-rich glaciolacustrine sediments (e.g. Palmer *et al.*, 2008). However, production is often time consuming and labour-intensive taking up to 12 weeks for the generation of thin sections. When varved sediments are sampled in the field, subsamples for thin section are usually extracted from sediment outcrops using kubiens tins with 2-3 cm overlap between each sample (e.g. Ringberg and Erlström, 1999; Palmer, 2005; Bendle *et al.*, 2017). Thin

section subsamples can be taken from wet sediment cores by using a z-shaped cutter to create an overlap between samples (Palmer *et al.*, 2010) or using foil tins to extract overlapping samples that are usually 8 cm in length and 2-4 cm wide (Brauer *et al.*, 1999; Martin-Puertas, Brauer, *et al.*, 2012; Devine and Palmer, 2017). Before impregnation with resin, sediment samples must first be dried. Samples can be left to air-dry in kubiena tins (Bendle *et al.*, 2017) or can be freeze dried (Merk, 1971) but these approaches can produce cracks due to shrinkage during drying. An alternative technique is the use of acetone which replaces pore-water and keeps sediments wet, thus minimising textural damage during shrinkage (Lotter and Lemcke, 1999; Lamoureux, 2001). Once samples are dry, an epoxy resin replaces the acetone, fills the pore-water spaces and impregnates the sample (Lamoureux, 1994). The initial impregnation process may also take place under vacuum to ensure complete infiltration of the resin between individual grains (Palmer *et al.*, 2008). For clay-rich glaciolacustrine varves, the resin-impregnated samples are left to cure for 6-8 weeks with a final cure undertaken at 60°C. The hardened sediment samples are cut and polished using the same process as for rock-based thin sections. Thin sections are then analysed with a petrographic microscope under plane and cross-polarised light to examine lamination composition (Brauer, 2004).

Thin section analysis is commonly applied to biogenic, endogenic and mixed varves as seasonal laminations are usually of mm-scale and require microscopic analysis (e.g. Zolitschka *et al.*, 2000; Brauer and Casanova, 2001; Ojala and Francus, 2002; Martin-Puertas *et al.*, 2012; Neugebauer *et al.*, 2012, 2014; Scholaut *et al.*, 2018). Due to their greater (cm-scale) thicknesses glaciolacustrine varves are not commonly analysed under thin section and are instead analysed macroscopically or from digital images (De Geer, 1940; Strömberg, 1994; Francus *et al.*, 2002; Hang, 2003; Ridge *et al.*, 2012). A major disadvantage of these approaches is the inability to distinguish between annual and non-annual sedimentation such as turbidites, deformation zones or “event” layers (Brauer *et al.*, 2009; Czymzik *et al.*, 2013). Macroscopic techniques also restrict accurate identification of mm-scale and sub-mm-scale laminations that can accumulate in glaciolacustrine environments (Ringberg and Erlström, 1999; MacLeod, 2010; Palmer *et al.*, 2010).

In order to develop robust varve chronologies researchers have developed descriptive protocols for the objective classification of glaciolacustrine sediments under thin section (Ringberg and Erlström, 1999; Palmer, 2005; Palmer *et al.*, 2012). These protocols focus on the internal composition and structure of laminations using subtle variations in particle size, sorting, structures and the nature of contacts between laminations. Recently, Palmer *et al.* (2019) formalised and expanded existing descriptive frameworks to include sediment sorting, deformation structures, dropgrains, intraclasts, and the plasmic fabric

of grains. Their descriptive scheme is based on the identification of individual Lamination Types that can be categorised as those that are deposited by 1) persistent flow, 2) variable flow, or 3) low energy suspension settling (Figure 4-7).

Individual Lamination Types are then grouped into Lamination Sets based on common cycles in sedimentation (Figure 4-5). It is important to note that the term Lamination Set may be used to describe non-annual as well as varved sediments since varves are composed of at least two Lamination Types (Palmer, 2005; Palmer *et al.*, 2010, 2019). Using a combination of sediment description, lamination thickness and the ratio of coarse-grained to fine-grained components, Palmer *et al.* (2019) propose five distinct varve microfacies or “Lamination Set Assemblages”: 1) Proximal Intermediate; 2) Intermediate-Distal Lake Bottom; 3) Delta/Sub-aqueous Fan Bottomset; 4) Distal Lake Bottom; and 5) Ultra Distal/Nival (Figure 4-5). These varve microfacies allow reconstruction of the relative position of sediment input to former lake basins and builds on previously proposed models of glaciolacustrine varve processes (e.g. Ashley, 1975; Smith and Ashley, 1985; Ringberg and Erlström, 1999; Palmer, 2005; Palmer *et al.*, 2010).

Varve descriptive models are essential for the development of robust varve chronologies. The classification proposed by Palmer *et al.* (2019) permits reconstruction of local and larger scale sediment processes through application of the scheme across multiple locations within a lake basin and integration with geomorphological evidence. The descriptive scheme enables the reconstruction of the former position of the glacier margin as well as lake level changes through time (e.g. Palmer *et al.*, 2010; Bendle *et al.*, 2017). These processes can then be assessed to determine the relative climatic control on varve sedimentation (e.g. Palmer *et al.*, 2012).

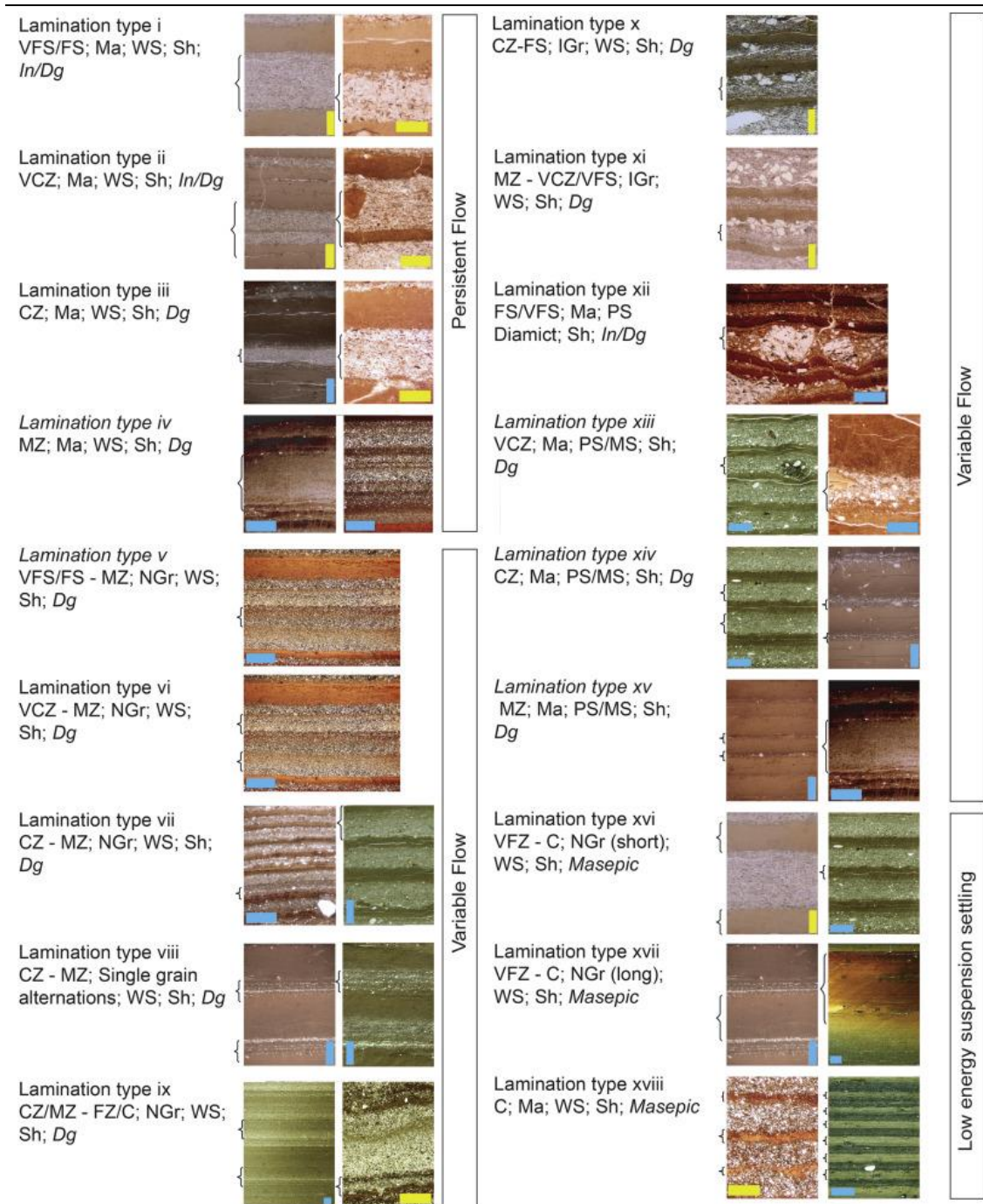


Figure 4-7. Lamination Types proposed by Palmer et al. (2019) pp. 13.

Lamination Types observed within glaciolacustrine varve microfacies are classified as Variable Flow, Persistent Flow and Low energy suspension settling. Lamination Types i to xv have grain sizes ranging between medium silt and fine sand whilst Lamination Types xv to xvii are very fine silt and clay. All images are under plane polarised light. Yellow bars represent 0.5 mm, blue bars represent 1 mm. FS = fine sand; VFS = Very fine sand; VCZ = very coarse silt; CZ = coarse silt; MZ = medium silt; VFZ = very fine silt and C = clay. Ma = massive; IGr = inverse grading; NGr = normal grading; WS = well sorted; MS = moderately sorted; PS = poorly sorted. Sh = sharp contact; Dg = dropgrain; In = intraclast.

4.4.7 Micro-CT scanning

Three-dimensional X-ray computed tomography (CT) scans or micro CT-scans (mCT) provide a fast, precise and cost-effective means of determining density variations within sediment sequences (Fortin *et al.*, 2013). mCT scans are particularly useful for the identification of deformation structures, erosional features or “hidden laminations” in sediment cores (Bendle *et al.*, 2015). The technique is similar to X-ray radiography and is based on the attenuation of X-rays which is closely related to the density and composition of sediments (Orsi *et al.*, 1994; Mees *et al.*, 2003). Multiple X-ray radiograms are compiled to create a 3D volumetric model of the sediment sample which enables the researcher to assess the spatial relationship between grains, visualise the internal structure of a sample and determine the optimum location for a thin section sample (Bendle *et al.*, 2015). The technique is particularly useful in varve research as the production of thin sections requires large volumes of material that once lithified in resin cannot be used for other forms of analysis (e.g. ecological proxies, radiocarbon dating and tephra analysis). Moreover, thin sections are a 2D representation of 3D structures that are complex and interrelated (Bendle *et al.*, 2015). The use of CT-scanning in varve research is in its infancy but has the potential to improve the identification of sediment features in a non-destructive way, although access to CT-scanning equipment can be difficult in the geosciences (Zolitschka *et al.*, 2015).

4.5 Varve chronology development

Once a varve depositional model is determined, varve counts and thickness measurements are conducted in order to create a varve chronology. Irrespective of the methodological approach used to identify varves (e.g. macroscale, X-radiographs, thin sections), marker varves such as anomalously thick or thin varves, and deformation/slump structures can be used to provide overlaps between sequences. The extraction of multiple parallel cores across a lake basin enables cross-correlation of varve records that may minimise or “bridge” gaps due to deformation, ultimately extending the varve chronology (Pettersen *et al.*, 1993; Lamoureux, 2001). Event deposits are not always pervasive across the lake basin and can be avoided by targeting an area of the basin that is less likely to be prone to such deposits. When event deposits cannot be “bridged” via overlapping cores, interpolation of the number of varves across the interval of homogenised or indistinct laminations can be applied (e.g. Scholaut *et al.*, 2018). This is achieved by applying the mean sedimentation rate (varve thickness) from the underlying varves across the non-varved section. However, this approach introduces

uncertainty to the varve chronology due to the assumption that the sedimentation rate is consistent across the interval and is comparable to the underlying varved sediments.

Replicate varve counts are essential in order to test the internal validity and replicability of the varve chronology. Zolitschka *et al.* (2015) recommend that at least two analysts should carry out varve counts and measurements independently. An assessment of varve preservation or “Varve Quality” should also be undertaken in order to identify sections of the varve record that may be prone to varve count errors (e.g. Lotter and Lemcke, 1999; Brauer and Casanova, 2001; Żarczyński *et al.*, 2018).

4.5.1 Error estimation

Repeat varve counts from independent analysts must be undertaken and where there are discrepancies between analysts individual varves should be assigned a count error (Ojala and Saarnisto, 1999; Brauer and Casanova, 2001; Zolitschka *et al.*, 2015). Varve count errors are cumulative with increasing age or depth (Ojala *et al.*, 2015). Inconsistencies in varve counts between analysts can be related to indistinct laminations or poor Varve Quality (e.g. Bendle *et al.*, 2017) but can also be related to changes in varve composition throughout the varve sequence (Marshall *et al.*, 2012; Scholaut *et al.*, 2012). Varve count errors can be classified as Type 1 errors (over counting), or Type 2 errors (missing or unrecognised varves) (Lamoureux and Bradley, 1996). There are different approaches to determining the varve count error such as calculating the maximum and minimum deviations from the mean (Lotter and Lemcke, 1999) and assigning a ± 1 varve year (Bendle *et al.*, 2017), or a ± 0.5 varve year (Regnéll *et al.*, 2019) error. Some authors have also used tie points as marker horizons to estimate the error for individual sections (Bendle, 2017) and/or the entire record (Lamoureux, 2001).

Cross correlation of multiple varve records from the same site/basin is also recommended by Lamoureux (2001). This enables an assessment of the different types of error which can be related to: 1) misidentification of varves during measurement; 2) inconsistent distribution of sediment across the lake basin which can lead to “missing” varves at some localities; and 3) localised disturbance or erosion of varve structures. Once correlated, the internal varve count error for each varve record within a lake basin should be combined to create an overall varve count error for the composite varve record (e.g. Bendle, 2017). It should be recognised that varve count error provides an assessment of the precision of varve counts, rather than the chronological error (accuracy) of the age depth model. In order to test the precision of varve counts, independent means of dating varve records should be adopted such as radiocarbon dating (Wohlfarth *et al.*, 1993, 1995; Ridge *et al.*, 2012) or tephrochronology (MacLeod *et al.*, 2011; Lane *et al.*, 2015; Ott *et al.*, 2016).

4.6 Tephra analysis

Tephrochronology involves the use of discrete volcanic ash horizons as isochronous marker layers to correlate and/or date sediment sequences (Lowe, 2011). Tephra deposits are preserved in terrestrial, marine and ice-core records and provide an invaluable means with which to independently correlate different climate and environmental archives. Tephra deposits must be physically and chemically characterised in order to be correlated with known eruptions (Davies, 2015). When known eruptions have reliable ages, chemical characterisation of tephras and correlation allows age information to be transferred between sediment records.

There have been considerable technological advances within tephrochronology (e.g. Blockley *et al.*, 2005; Lowe, 2011; Hayward, 2012) that have enabled the identification and chemical characterisation of non-visible tephras known as “cryptotephras”. Such cryptotephras can be deposited thousands of kilometres away from their eruptive source (Zillén *et al.*, 2002; Lane *et al.*, 2011, 2013; Blockley *et al.*, 2012; Regnéll *et al.*, 2019) and are increasingly used for correlations between sediment sequences across large geographic areas (Blockley *et al.*, 2014). Critically, cryptotephra deposits can be used to constrain the timing and duration of palaeoenvironmental events and assess leads and lags in the climate system (e.g. Lane *et al.*, 2013; Rach *et al.*, 2014).

4.6.1 Application in varve research

The combined application of tephrochronology and varve chronology enables the timing and duration of palaeoenvironmental events to be precisely constrained (Litt *et al.*, 2009; Wulf *et al.*, 2013; Neugebauer *et al.*, 2014; Van Daele *et al.*, 2014). The rapid deposition of volcanic glass in lake systems that support varve formation means that tephras are typically confined to a narrow stratigraphic range and are often located within a single varve (e.g. Ott *et al.*, 2016; Bendle *et al.*, 2017). Since varved sediments are usually deposited in anoxic bottom waters with minimal bioturbation, tephra deposits are rarely prone to post-depositional reworking that can distribute tephra shards across several varve years.

Another advantage of tephrochronology within varve records is that the number of varves between successive tephra layers indicates the number of varve years between volcanic eruptions (e.g. Brauer *et al.*, 1999; Zillén *et al.*, 2002; Van Daele *et al.*, 2014; Lane *et al.*, 2015; Ott *et al.*, 2016). As such, varve records yield the potential to constrain existing age estimates of known tephras (e.g. Ott *et al.*, 2016) in a manner similar to what has been achieved from annual layer counting between tephras in ice-core records (Abbott and Davies, 2012; Cook *et al.*, 2018). Tephra layers can also be used to check the

internal validity of composite varve chronologies through independent means of correlating individual varve records (Wulf *et al.*, 2013; Bendle *et al.*, 2017). Varve count error can also be assessed by using a tephra layer(s) as an independent marker layer (Zillén *et al.*, 2002; Brauer *et al.*, 2008), thus improving the accuracy and precision of varve chronologies. However, tephrochronology has yet to be widely applied within glaciolacustrine varve contexts (MacLeod *et al.*, 2014; Bendle *et al.*, 2017).

4.7 Summary

Varved sediments provide high-resolution archives of past environmental and climatic change at sub-seasonal to decadal timescales (Brauer and Casanova, 2001; Brauer *et al.*, 2009; Zolitschka *et al.*, 2015). The generation of accurate varve chronologies requires development of a robust varve depositional model (Zolitschka *et al.*, 2015). Controls on varve sedimentation are often complex and can be related to local-scale and larger scale basin-wide processes. In the context of the STS these processes appear not to have been considered and this is largely due to the restricted level of analytical precision afforded by the macroscale techniques that are traditionally employed to analyse the varved sediments. A key objective of this thesis is to understand the depositional processes that lead to the formation of varves in the STS in order to develop a robust varve depositional model and increase varve count accuracy. The application of tephrostratigraphy and tephrochronology will enable the varve records to be independently dated and also for the varve counts to be independently validated.

Chapter 5. Methodology

5.1 Introduction

The aim of the thesis is to re-investigate the precision and accuracy of the Swedish Timescale. This will be achieved by comparing the macroscale description and microfacies analysis of glaciolacustrine varve sediments at sites that span the Younger Dryas to Preboreal part of the timescale. For Lateglacial Swedish varves, there has been only one study (Ringberg and Erlström, 1999) that has provided a detailed microfacies examination of glaciolacustrine varve structures, with the results of the study aimed primarily at understanding lake basin processes and the position of the ice margin rather than challenging the chronostratigraphy of the Swedish Timescale. Otherwise the model for the timing of ice retreat using varve structures is based upon macroscale measurements and counts and linking sites with varve thickness measurements and marker-beds. This approach does not take into account the impact of sedimentation of a non-annual nature, such as turbidites or slump deposits, or exploit the potential of distal glaciolacustrine varve structures. In addition, independent testing of the age of these sequences has been provided through radiocarbon, cosmogenic and optically stimulated luminescence dates that enable the sequences to be placed on an absolute timescale (Chapter 3). However, the role of tephrochronology has yet to be fully exploited, and this will be a key element of this thesis.

To examine this in more detail three sites were selected that theoretically were depositing varve sediments during the Younger Dryas period and up to the final drainage of the Baltic Ice Lake. In this chapter, the rationale for site selection are presented (section 5.2), the field methods that were adopted are outlined (section 5.3), and the laboratory analytical procedures are described (sections 5.4 – 5.8). Emphasis is placed on the sedimentological description of core sequences that were extracted from the three basins because detailed sedimentological analysis at a range of scales forms a fundamental part of this thesis. The four key methods of varve analysis presented in this research are: 1) macroscopic sediment descriptions; 2) X-ray radiography; 3) μ XRF analysis; and 4) thin section micromorphology. These methods allow for comprehensive description and measurement of laminations ranging from the macroscale (\geq cm-scale) to microscale analysis of thin sections (<cm-scale) and have been applied in the analysis of varved sediments (Chapter 4). Alongside sediment descriptions at the macro and microscale, X-ray radiography and μ XRF analyses provide quantitative assessments of

density and chemical variations within and between individual laminations. These approaches are coupled with tephrochronology and ecological proxies.

5.2 Site selection

In order to extract and analyse varved sediments that span the time period of interest, site selection was targeted at varve records that were most likely to contain volcanic ash that was deposited during the late Younger Dryas and/or early Holocene. The presence of tephra horizons within the varve sequences would also enable the records to be: 1) independently dated and fixed in absolute time; 2) independently correlated to produce a composite varve chronology; and 3) the composite varve chronology could be used to test the existing deglaciation chronology. Using the occurrence of the Vedde Ash (12,023±86 cal. yrs BP (2 σ); Bronk Ramsey *et al.*, 2015) within varved sediments at the Gropviken site (MacLeod *et al.*, 2014) and the purported Vedde Ash at the Mullsjön site (Wohlfarth *et al.*, 1993) as known points, the ice margin lines proposed by Brunnberg (1995) and Strömberg (1994) were traced towards Lake Roxen (Figure 5-1). This approach was chosen for two reasons. First, the new sites could be cross correlated with the Gropviken record thus constraining the timing of deglaciation further inland from the Swedish east coast. Second, the new 'Vedde Ash target area' is geographically located in the region where the varve chronologies of Brunnberg (1995) and Kristiansson (1986) overlap. This would provide a firm correlation between these regional chronologies in a part of the STS that is considered to contain errors (Chapter 3).

To further maximise the potential to find volcanic ash, long varve sequences (>100 yrs) were targeted. The Svinstadsjön site was chosen in this regard as the site is located within the target area and contains a long varve record. It was expected that the Vedde Ash would be found within the uppermost varves of the 9 m sequence, of which 7.46 m are varved sediments.

After initial macroscale observations of the varved sequence at Svinstadsjön, a minimum of 500 varves were identified. Using the assumption that the Vedde Ash would be located towards the top of the Svinstadsjön sequence, it was estimated that the base of the sequence was at least *ca* 12,500 cal. yrs BP or older. Therefore, it was anticipated that the base of the Svinstadsjön sequence would overlap in age with one or more of the northernmost varve records within the Wohlfarth *et al.* (1998) chronology. The northernmost sites within this chronology were radiocarbon dated to *ca* 12,400-12,500 cal. yrs BP (Wohlfarth *et al.*, 1998; Muschitiello *et al.*, 2016). To extend the Svinstadsjön site chronology and link to the radiocarbon-dated varve chronology by Wohlfarth *et al.* (1998) the Glottern sequence was chosen. This site is part of the Wohlfarth *et al.* (1998)

regional varve chronology and radiocarbon dates from the uppermost 100 varves yield an age of ca 12,500 cal. yrs BP (Muschitiello *et al.*, 2016). If the sites overlap in age varve thickness correlation between the Svinstadsjön and Glottern records could be possible.

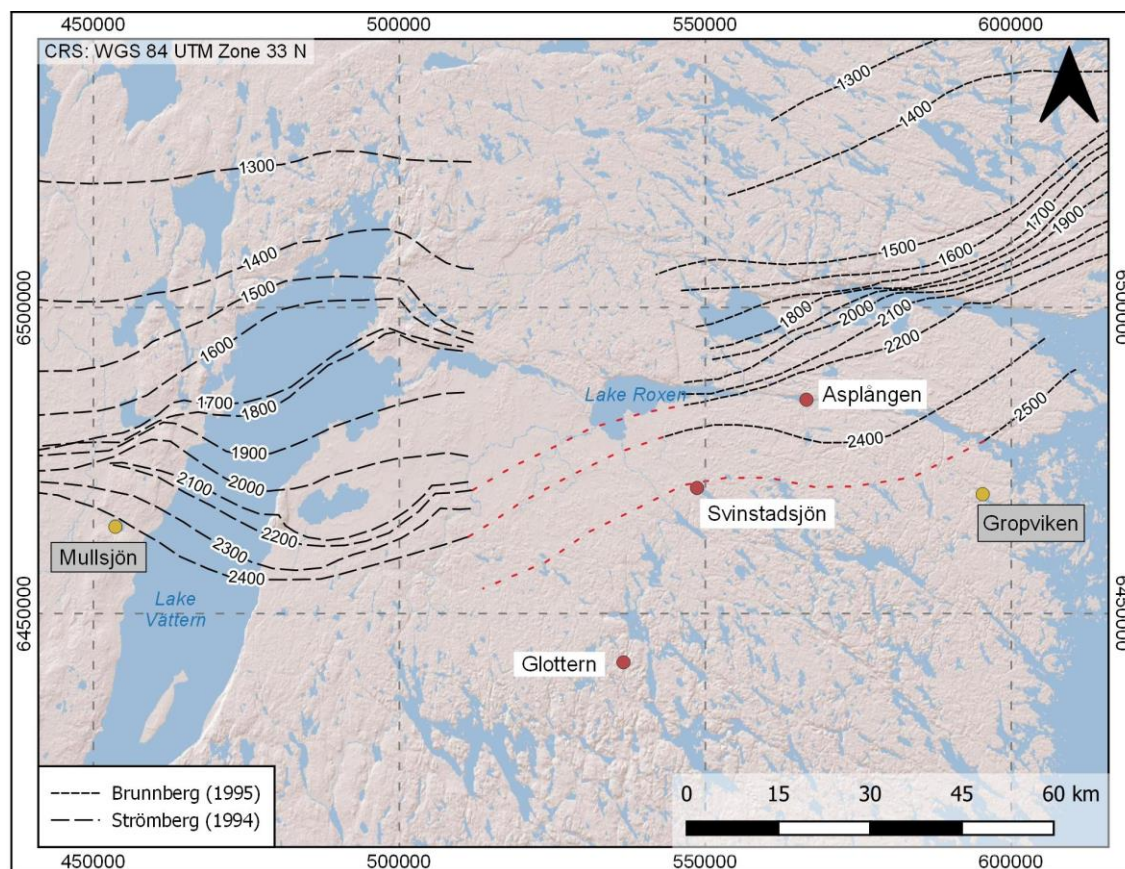


Figure 5-1. Site locations in this study.

Site locations in relation to 1) the ice margin lines proposed by Strömberg (1994) and Brunenberg (1995) and 2) the location of the Gropviken (MacLeod *et al.*, 2015) and Mullsjön (Wohlfarth *et al.*, 1993) sites that contain the Vedde Ash. Dashed red lines are inferred links between sites and are shown for illustrative purposes only.

The third and final site was chosen in order to extend the Svinstadsjön chronology further north and into sediments younger than the Vedde Ash. The ice margin lines proposed by Brunenberg (1995) were traced north by approximately 200 varve years. To give the best possible chance of finding the Vedde Ash in the base of the final site varve chronology, the varve record had to be longer than 200 yrs and located on or near to the ice margin line that is located 200 yrs younger (north) of Svinstadsjön. The Asplången site was chosen since it fulfilled these criteria and previous analysis yielded a 609 yr sequence (Brunenberg, unpublished). Using the published ice margin lines, it was estimated that the Asplången sequence deglaciated ca 200 years after the Svinstadsjön site and that the Asplången varve record would extend into the early Holocene. It was anticipated that the non-varved sediments stratigraphically above the

uppermost varves in the Asplången record may contain early Holocene tephras such as the Abernethy Tephra ($11,462 \pm 144$ (2σ); Bronk Ramsey *et al.*, 2015) or the Hässeldalen Tephra ($11,316 \pm 124$ (2σ); Wastegård *et al.*, 2018).

In summary, the chosen sites, Asplången, Svinstadsjön and Glottern were selected based on: 1) the likely presence of the Vedde Ash with the potential to find the Abernethy or Hässeldalen tephras at Asplången; 2) the current ice margin lines and existing radiocarbon dates which suggest that Svinstadsjön and Glottern should overlap in age; and 3) that the Vedde Ash would be found within the top of the Svinstadsjön sequence and in the lowermost varves at Asplången and could be used to create a link between these sites. In addition, the presence of the Vedde Ash within the Gropviken varve chronology (MacLeod *et al.*, 2014) could also be used to strengthen the link between the Asplången and Svinstadsjön chronologies to form a composite varve chronology which spans *ca* 12,700 cal. yrs BP – *ca* 11,500 cal. yrs BP (Figure 5-2). The resulting composite varve chronology would be the first step towards a tephra lattice within the STS and could be used to test the existing deglaciation chronology for the region.

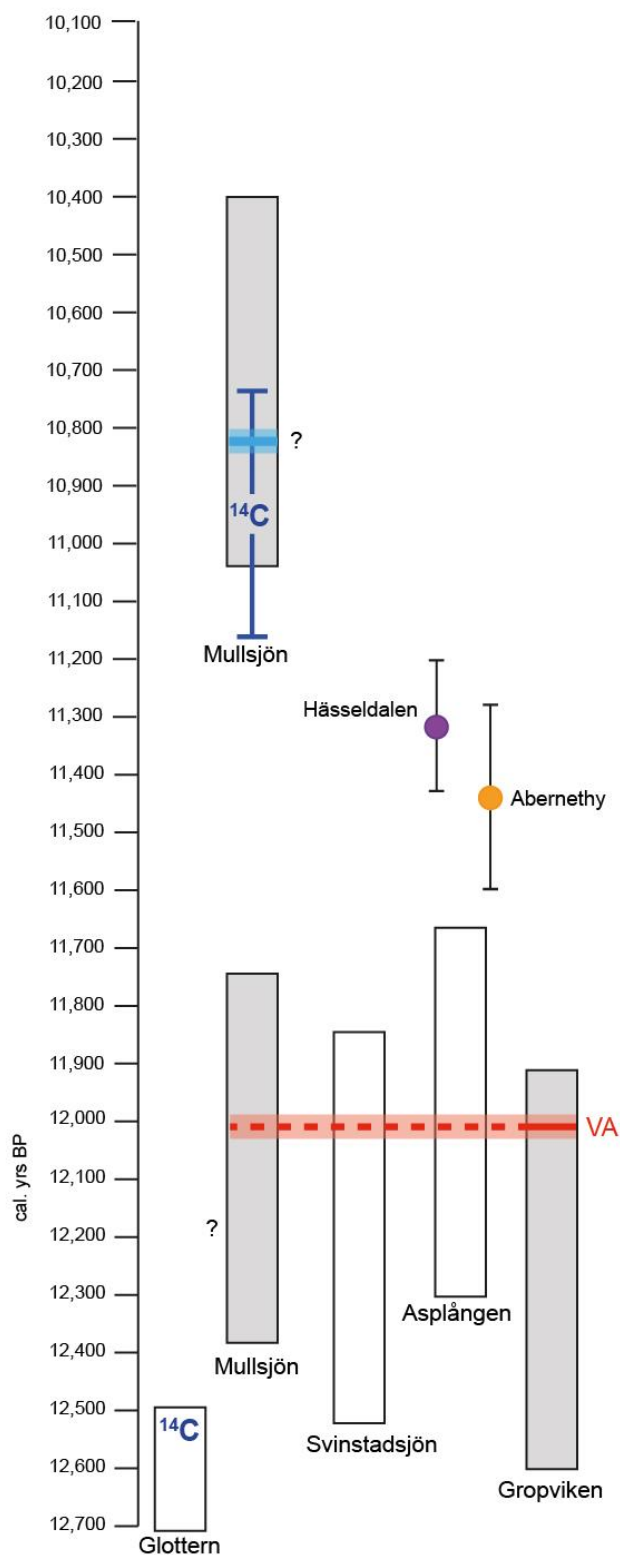


Figure 5-2. Schematic showing the currently proposed ages of the varve records in this research alongside the Mullsjön and Gropviken records.

The Vedde Ash (VA) is shown on the Gropviken record with a solid red line. The Vedde Ash will be used as a tie-point to link the records from Asplången, Svinstadsjön and Gropviken. The ^{14}C age from the Glottern sequence by Wohlfarth et al. (1998) places the uppermost 100 varves at ca 12,500 cal. yrs BP. Two possible ages are presented for the Mullsjön sequence based on the purported correlation of the tephra layer to the Vedde Ash and calibration of a radiocarbon date that is ca 200 yrs beneath the tephra layer (see section 5.2.4 for further details). Other key LGIT tephras are also shown.

5.2.1 Regional Geology

The sites are located within the Östergötland county of south eastern Sweden. The region is mostly underlain by acid intrusive rocks including granites, granodiorite and monazite, with some units showing porphyritic textures or augen-bearing. Approximately 40 km northwest of Svinstadsjön the geology consists of carbonate-rich rocks including limestone, dolomite and marble, as well as quartz-feldspar rich sandstones and greywackes, mica-rich shales and sandstones. There are also rare volcanic components, ranging from acid to ultrabasic composition, and including rhyolite, dacite and gabbro (Figure 5-3). The rocks are typically between 2.85 and 1.87 Ga or 1.88 and 1.74 Ga and formed as part of the Svecokarelian orogeny. As a result, many of these rocks have undergone metamorphism and show a varying intensity of gneissic textures. The sedimentary rocks are between 850 Ma and 34 Ma and have been much less affected by metamorphism.

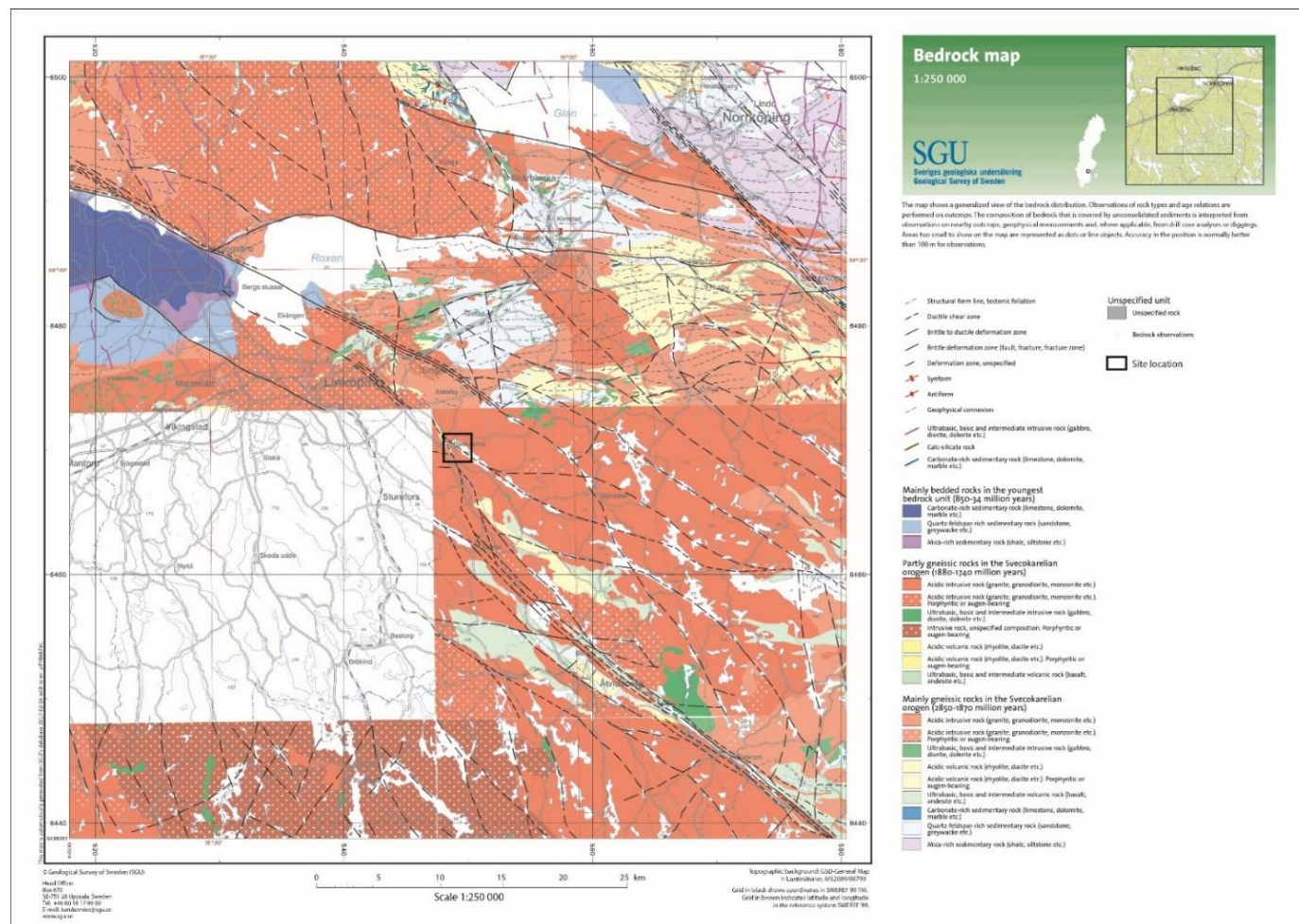


Figure 5-3. Geological map of Östergötland county in south-eastern Sweden. Map obtained from SGU.se map generator software.

5.2.2 Svinstadsjön location

Svinstadsjön (58°29'58"N, 16°08'27"E) is located approximately 170 km south-west of Stockholm. The site is situated 70 km west of Lake Vättern and 14 km south of Lake Roxen (Figure 5-4). Cores were taken from the northern shore of the present-day freshwater lake to the west of Bankekind village.

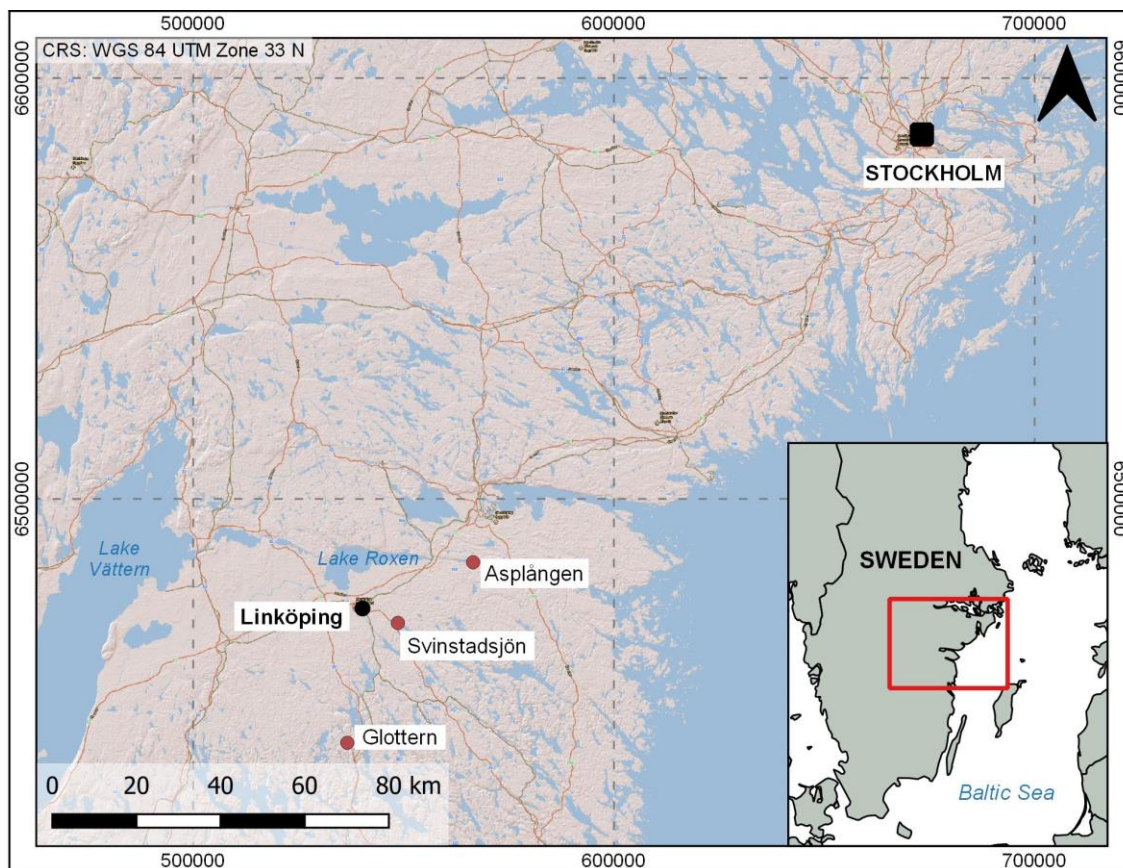


Figure 5-4. Map of south eastern Sweden showing site locations.

5.2.3 Asplången location and background

Asplången (58°22'21"N, 15°49'53"E) is located approximately 140 km south-west of Stockholm. The site is situated 80 km west of Lake Vättern and 10 km east of Lake Roxen along the Göta Kanal (Figure 5-4). Cores were taken from the southern shore of the present-day lake. The site was investigated previously by Dr Lars Brunnberg who identified 609 yrs at the site (unpublished).

5.2.4 Glottern location and background

Glottern (58°07'09"N, 15°37'17"E) is located approximately 200 km south-west of Stockholm. The site is situated 60 km west of Lake Vättern and 40 km south of Lake Roxen (Figure 5-4). Cores were taken from the south eastern shore of the present-day lake.

The site has been investigated previously by Wohlfarth *et al.* (1998) and is located in the northern part of an 800-year long regional varve chronology which is composed of over 50 varve records from south-eastern Sweden (Wohlfarth *et al.*, 1998). During the Baltic Ice Lake phase Glottern was situated within an archipelago (Wohlfarth *et al.*, 1998). The archipelago experienced isostatic rebound following deglaciation during the Late Allerød and Younger Dryas periods which led to the isolation of the area from the Baltic Ice Lake. Sediment sequences within the archipelago are characterised by glacial varves overlain by homogenous clays and organic lacustrine sediments. Three varve sequences of 159, 198 and 150 yrs were extracted from the site (Table 5-1) and the uppermost 100 yrs from site 2 were initially radiocarbon dated to ca 12,600 cal. yrs BP by synchronising the regional varve thickness chronology to the Lake Gosciadz varve record in Poland (Wohlfarth *et al.*, 1998). The radiocarbon age estimates for the regional varve chronology were later revised by Muschitiello *et al.* (2016) using Bayesian age modelling. The section of the regional varve chronology attributable to the Glottern site chronology is now dated to ca 12,400 cal. yrs BP (Muschitiello *et al.*, 2016).

Table 5-1. Site information from the Glottern sequence.

Varve data and radiocarbon dates (Wohlfarth *et al.*, 1998) L- leaf, Lf – leaf fragment, S – seed. + indicates that the base of the sediment sequence was not reached by coring

Varve data				
Coordinates	Height a.s.l	Varve count	Age of bottom varve (local yrs)	Age of bottom varve in calendar years BP
Glottern1 N 58°07'20" E 15°37'15"	111 m	159	1995+	12,645+
Glottern 2 N58°07'20" E15°37'15"	111 m	198	2003	12,653
Glottern 3 N58°07'20" E15°37'15"	111 m	150	1954+	12,604+
Radiocarbon data				
Lab code	Local varve years	Material	AMS 14C date yr BP	Estimated cal yr BP
Ua-4496	1856±50	Salix/Betula (Lf)	10 585±465	12,506
Ua-10180	1872±66	Empetrum (L), Salix indet (Lf), Salix/Betula (Lf), Dryas oct. (L), Arenaria (S), insects	11,550±300	12,522

5.3 Field methods

5.3.1 Sediment depth sounding and bathymetric surveys

An auger survey was carried out at each site to map the bathymetry and identify a suitable coring location. Due to lack of ice cover during the winter months and access to a coring raft, auger surveys were taken at lake margins rather than from locations within the present-day lake basin at each site (Figure 5-5). Sediment depth measurements were undertaken using 1.0 m extension rods and a systematic transect-based sampling approach. Transects were spaced 10 m apart and depth probes were undertaken every 10 m. This approach was successful at the Glottern and Svinstadsjön sites but was difficult to implement at Asplången. The first target area at Asplången consisted of impenetrable dry clays in the upper 1-2 m, therefore the auger survey focussed on a second area of the lake margin. Auger survey results are reported in individual site chapters (Chapter 6: Svinstadsjön, Chapter 7: Asplången: Chapter 8: Glottern).



Figure 5-5. Sediment core extraction from lake margins in the snow during May 2017 fieldwork. R. Devine and B. Devine.

5.3.2 Sediment extraction

Sediment sequences were extracted using a 1.0 m length and 5 cm diameter 'Russian' corer (Jowsey, 1966). Overlapping cores were obtained from adjacent boreholes at each site. The overlapping sequence is vital to obtain due to the 10 cm nosecone at the base

of the coring chamber that disturbs sediment 10 cm beneath each 1.0 m sample. An overlap of 50 cm was extracted at each site (Figure 5-6).



Figure 5-6. Overlapping cores extracted from the Glottern site. Common marker layers between cores are highlighted with red dashed lines.

Sediments were photographed in the field using a Nikon digital camera. The overall stratigraphy was noted during field observations with more detailed sediment descriptions performed in the laboratory. Table 5-2 summarises the boreholes and sediment depths at each site.

Table 5-2. Boreholes and extracted sediment cores at each site.

*Asterisks denotes cores that were not scanned on the iTRAX core scanner.

Asplången		Svinstadsjön		Glottern	
Borehole	Cores (cm)	Borehole	Cores (cm)	Borehole	Cores (cm)
2A	500-600	3A	0-100	1A	0-100*
	600-700		100-200		100-200*
	700-800		200-300		200-300*
	800-900		300-400		300-400
	900-1000		400-500		400-500
	1000-1100		500-600		600-700
	1100-1200		600-700		700-800
2B	50-150*	3B	150-250	1C	50-150*
	150-250		250-350		150-250*
	250-350		350-450		250-350*
	350-450		450-550		350-450
	450-550		550-650		450-550
	550-650				550-650
	650-750				650-750
	750-850				750-850
	850-950				
	950-1050				
1050-1150					
2C	1146-1246	3C	700-800 800-900	1B	800-900
2D	0-100*	3D	650-750		
	100-200*		740-840		
	200-300				
	300-400				
	400-500				

5.4 Macroscale sedimentological methods

5.4.1 Sediment description

Prior to conducting further sediment descriptions, cores were cleaned using a scalpel horizontally across the core to prevent vertical contamination. The cleaned sediment surfaces were described in detail in the laboratory using standard lithological techniques (e.g. Evans and Benn, 2004). Descriptions focussed on sediment composition, grain size, sorting, structures, contacts between sedimentological units, and Munsell colours. Sediment logs were created for each site and are presented in individual results chapters.

5.4.2 Sediment imaging

Each of the cleaned sediment cores was digitally imaged in the laboratory using a Canon 600D DSLR camera mounted to a camera stand. Individual photographs of the core sections were manually stitched together using Adobe Photoshop™ to produce whole core images. Composite core images are presented alongside sediment logs to show the relationship between lithological changes and other proxy information collected.

5.4.3 Macroscale varve analysis from core surface

In Baltic Ice Lake varve research, varve counts are typically produced from macroscale sediment analysis of open sections or from open cores (e.g. Brunnberg, 1995; Wohlfarth *et al.*, 1998; Andrén *et al.*, 2002; Hang, 2003). For the Glottern and Asplången records original varve counts were undertaken in laboratory conditions by Wohlfarth *et al.* (1998) and Brunnberg (unpublished) respectively. Both researchers used a paper strip to mark the thickness of each summer and winter layer following the methodology of De Geer (1912, 1940). This traditional varve counting methodology was replicated across all sites in this thesis in order to make complete comparisons between different varve counting methods. When inspecting flat core surfaces, varved sediments were identified using a descriptive framework derived from existing glaciolacustrine varve research (e.g. Hang, 2003; Ridge *et al.*, 2012). Macroscale descriptions focused on particle-size, sorting, structure, and the nature of contacts between laminations. When laminations were too thin to discriminate accurately, the sediments were described as “unclear laminations” and a gap in varve sedimentation was noted. The following criteria were used for macroscale identification of varves: 1) The coarse component (normally silt or very fine sand) must be overlain by finer, clay sediment; 2) the light-coloured silt/sand lamination must be clearly distinguishable from the dark-coloured clay lamination; 3) the coarse component can have multiple laminations, either with two or more distinct laminations;

4) the coarse component can be well, moderately or poorly sorted, whereas the fine component is well-sorted; 5) laminations in the coarse component can be normally graded or massive whereas the fine component is massive; and 5) the contact between silt and overlying clay can be sharp or graded, non-erosive and almost without any grading. The contacts between clay and overlying silt can be sharp, erosive or irregular. All contacts can be horizontal or undulating.

5.4.4 Particle size analysis

Particle size analysis of laminated sediments was used to verify grain size estimations from macroscale, μ XRF, X-radiograph and thin section analyses. Grain size analysis was undertaken for each lithofacies unit that consisted of lamination couplets. Sub-samples were taken from cores using a 3 mm wide spatula. For lithofacies units that consist of \geq cm-scale lamination couplets, three couplets were sampled, and analyses were obtained for each individual lamination. For lithofacies units that comprise <cm-scale lamination couplets, three 5 cm long bulk samples were analysed. Bulk sampling was used due to the difficulties of sub-sampling individual mm-scale laminations in the laboratory with a 3 mm width spatula. Table 5-3 summarises the particle size sampling strategy for each site and each lithofacies unit.

Table 5-3. Particle size analysis sampling strategy

Site	Lithofacies	Couplet thickness	Sample type	Cores sampled
Svinstadsjön Asplången Glotten	LF1	cm-scale	Individual laminations	SVIN3D 8-9m SVIN3C 7.4-8.4m ASP2A 11-12 m GLO1B 8-9 m
Svinstadsjön Asplången Glotten	LF2	cm-scale	Individual laminations	SVIN3B 3.5-4.5 m SVIN3B 1.5-2.5 m ASP2B 7.5-8.5 m GLO1A 5-6 m
Svinstadsjön	LF3	mm-scale	Bulk 5 cm sample	SVIN3A 1-2 m

The particle-size characteristics of laminations was determined using a Malvern Mastersizer 3000 laser diffraction system with a Hydro MU sampler. Prior to analysis, samples were mixed with 0.5% sodium hexametaphosphate and placed within an ultrasonic bath for 30 seconds to ensure complete disaggregation of particles. During a single sample run, three measurements were obtained during a 1-minute run time and the mean grain sizes are quoted for each sample run.

5.5 Microscale sedimentological methods

5.5.1 X-ray radiography

X-ray radiography is a fast and non-destructive technique that uses the different X-ray absorption properties of sediments to highlight density differences within sediment sequences (Croudace *et al.*, 2008; Francus *et al.*, 2015). In this research, X-ray images were used to validate macroscale-based core overlaps, detect hidden clasts that were not visible at the core surface and for microscale examination of varved sediments (e.g. Haltia-Hovi *et al.*, 2007; Marshall *et al.*, 2012).

Sediment cores were scanned at the British Ocean Sediment Core Research Facility (BOSCORF) of the National Oceanography Centre (NOC) at the University of Southampton using an Itrax XRF Core Scanner from Cox Analytical Systems. All 16 of the extracted cores from Svinstadsjön, 21 of 23 extracted cores from Asplången and 10 of 16 extracted cores from Glottern were scanned on the Itrax core scanner (see Table 5-2 for details). X-radiograph images were generated using a Molybdenum tube set at 55 kV and 50 mA with a step size of 200 µm and a dwell time of 15 seconds. Ojala and Francus (2002) recommend that a constant slab thickness of 1 cm or less generates the best results for X-radiographic imaging due to even exposure. As such, in the initial stage of this research 1 cm thick u-channel sub-samples were taken for Itrax scans (cores SVIN3B 550-650 cm and SVIN3A 600-700 cm). These cores were turned onto a flat surface and a white plastic u-channel (2.4 cm width, 1 cm depth, 100 cm length) was pressed into the curved side of the core. A 'cheese wire' was dragged along the underside of the u-channel to separate the sediment sub-sample from the rest of the sediment core. The u-channel was lifted from the core to create the sub-sample. The sediment surface of the sub-sample was cleaned flat with a scalpel horizontally and the sample was wrapped in plastic. Due to the nature of glaciolacustrine sediments, the presence of hidden clasts made sub-sampling with a u-channel and 'cheese wire' problematic. There were several granule-sized (2-3 mm) clasts within the two cores and it was difficult to avoid dragging the clasts through the core when sub-sampling. As such, minor deformation was likely imparted on the sediment, and as such X-radiograph images from u-channels were examined with caution.

It was also likely that the top 2-3 mm of the new sediment surface was also disturbed during the removal of the u-channel. To account for this, approximately 2-3 mm of sediment was cleaned back from the new surface of the sediment core (Figure 5-7). Due to these difficulties, and the risk of deforming delicate varve structures, the u-channel

method was not used for the remaining cores. Instead sediment cores remained intact and the flat surface was scanned.

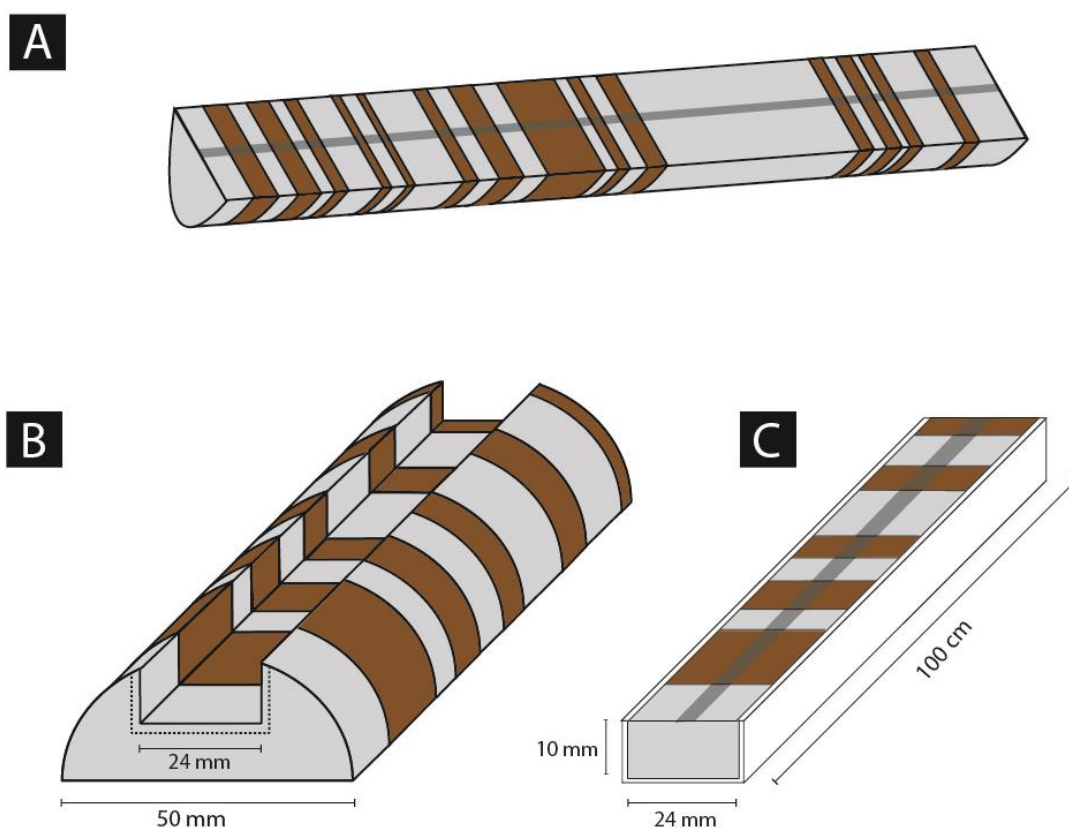


Figure 5-7. X-radiograph core preparation.

Diagram A shows the cleaned flat surface of a sediment core and the area of sediment scanned by the Itrax core scanner (grey line). Diagram B shows the remaining sediment after u-channel subsampling. Diagram C shows the u-channel subsample and the area of sediment scanned by the Itrax core scanner (grey line). U-channels were only taken from two cores: SVIN3B 550-650 cm and SVIN3A 600-700 cm. The dashed line on diagram B delineates the 2-3 mm of sediment that was cleaned back to remove any potential deformation incurred during u-channel subsampling. Figure adapted from Pike (2015).

Cores were cleaned perpendicular to the long core axis to avoid cross-contamination and to make the sediment surface as flat as possible. A flat surface is essential to ensure reliable results are obtained from the Itrax core scanner (Bloemsma *et al.*, 2018). Extra precautions were taken to ensure that cores were adequately sealed and did not dry out. Where possible, cores were scanned on the Itrax prior to sub-sampling for other analyses (e.g. tephra, thin sections and microfossils) to avoid exposure to air. It was apparent during initial sediment description and core logging that some cores dried out quicker than others. This was noted and these cores were covered with 3 μm thickness polypropylene film prior to X-ray scanning to reduce drying. The following cores were covered with polypropylene film: ASP2B 250-350 cm, ASP2D 200-300 cm, SVIN3A 200-300 cm, SVIN3B 150-250 cm, SVIN3B 250-350 cm, SVIN3C 800-900 cm.

For the Asplången sequence only, sub-samples for tephra analysis were taken from the curved under-side of 9 out of 21 sediment cores prior to X-ray scanning. Of these cores, five were sampled in the middle 20 cm (Figure 5-8) and four were sampled the entire length of the core. As such, there are changes in the thickness of the sediment across the core width. This is visible in Figure 5-8, where the X-ray shadows appear lighter where a tephra sub-sample was taken from the core. This has been compensated for by applying a brightness filter to a select area of the X-radiograph image in Adobe Photoshop™. Included in the appendices are details of the X-radiograph images that were affected by tephra sub-sampling.

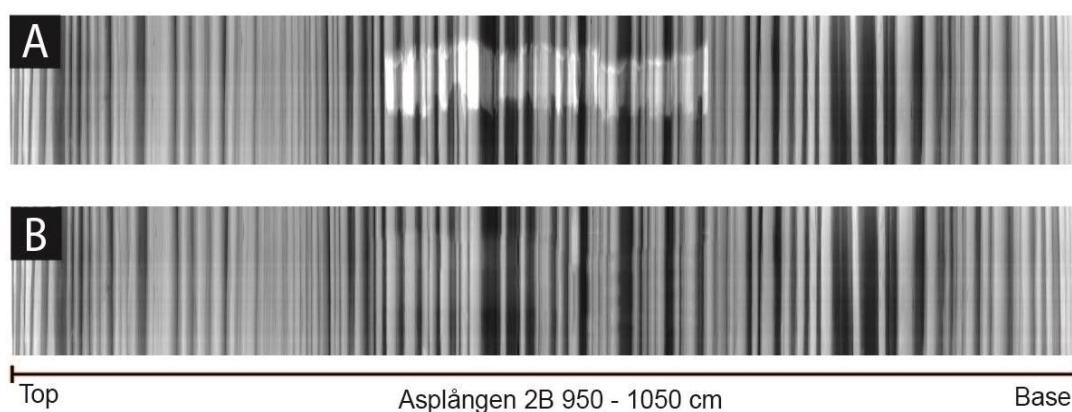


Figure 5-8. X-radiograph image processing in Adobe Photoshop™. Example of an X-radiograph image before (A) and after (B) processing in Adobe Photoshop to remove lighter shadowing caused by tephra subsampling.

5.5.1.1 Varve identification from X-radiograph images

In this research, X-radiographs were used for varve identification and counting and to highlight hidden clasts and deformation that were not visible at the sediment surface (e.g. Weber *et al.*, 2010; MacLeod *et al.*, 2011). Prior to varve counting, X-radiographs were re-sized to the precise length of each core in Adobe Photoshop™ and overlapping images were aligned using distinct lamination patterns. Figure 5-9 shows an example of varves identified from an X-radiograph image alongside the corresponding core surface image. Particle size data were used to verify grain size interpretations and the following descriptive criteria were used to classify light and dark lamination couplets as varves: 1) the dark (coarse-grained) lamination must be overlain by a lighter (clay) lamination; 2) the contact between a light lamination and the following dark lamination must be sharp; 3) the darker lamination can have multiple laminations, either with two distinct laminations, or more than two laminations; and 4) where laminations appear pixelated and varve boundaries cannot be accurately delineated, sediments were described as “unclear laminations” and a gap in varve sedimentation was noted.

It is important to note that laminations classed as unclear in X-radiograph images may be unclear due to inherent sedimentological properties or due to limitations of the X-ray resolution. For example, any lamination <200 μm thickness appeared unclear under X-ray but could still be a varve. All varve thickness measurements were made using Adobe Photoshop™ and stored in an excel spreadsheet. Any clasts or zones of deformation were also noted and compared to macroscale sediment descriptions.

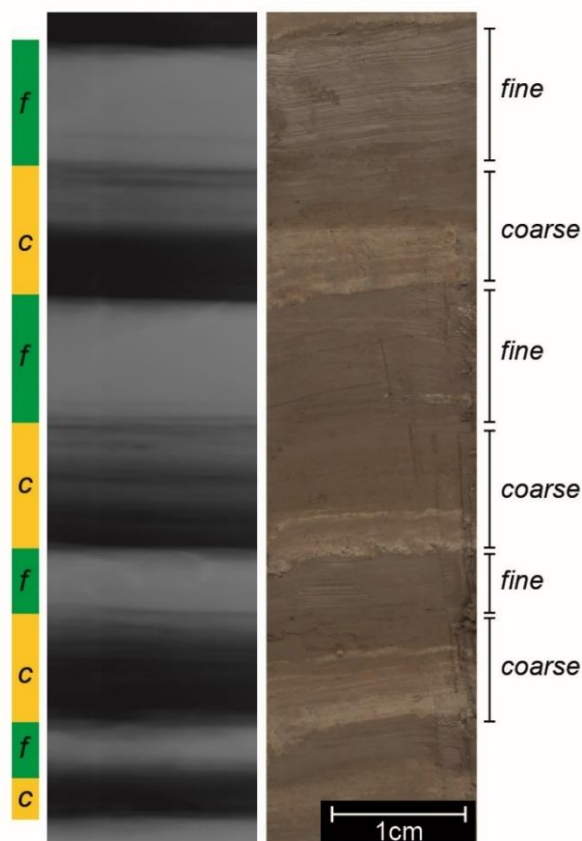


Figure 5-9. Example of $\geq\text{cm}$ -scale varves in an X-radiograph image and corresponding core surface image. Coarse laminations appear dark and fine laminations appear lighter under X-ray.

5.5.2 Micro-XRF core scanning

Micro X-ray fluorescence (μXRF) scanning provides a high-resolution record of the chemical composition of sediment cores. Measurements are expressed as element intensities in total kilo-counts per second (kcps) and are proportional to the chemical concentrations within the sediment at a particular sampling interval (Croudace *et al.*, 2008). μXRF data were acquired using a Molybdenum tube set at 30 kV and 50 mA and a dwell time of 30 s. The μXRF records provide 1-20 measurements per varve depending on the resolution of μXRF measurements and varve thickness. Fieldwork was completed in two stages, and in July 2016 cores were collected from Svinstadsjön from 0-700 cm. In May 2017 the full sediment sequences from Asplången and Glottern were extracted

and a further 2 m from 700-900 cm at Svinstadsjön. For the 0-700 cm Svinstadsjön sequence obtained in July 2016, measurements were carried out at 500 µm resolution with the Itrax µXRF core scanner. Cores collected in May 2017 from Svinstadsjön (700-900 cm) and cores from Asplången and Glottern (marked with an asterisk in Table 5-2) were scanned at 200 µm resolution.

5.5.2.1 µXRF data processing

In total, 37 elements were detected at each site during µXRF analysis (Al, Si, P, S, Cl, Ar, K, Ca, Ti, V, Cr, Mn, Fe, Ni, Cu, Zn, Ga, As, Se, Br, Rb, Sr, Y, Zr, Cs, Ba, Ce, Pr, Nd, Yb, Ta, W, Ir, Pt, Pb, Bi), but most of those elements were inconsistently detected. Datasets for each 1 m core profile were screened for elements that were inconsistently detected. A detection threshold of 95% was used to remove elements that were detected in less than 95% of measurements (e.g. Davies *et al.*, 2015), and varves with fewer than 3 measurements per lamination were also removed from the dataset. Zero values and some trace elements were also removed: Nd, Ir, V, W, Y.

Since µXRF measurements are sensitive to other sediment characteristics that are unrelated to chemistry such as water content variations (e.g. the closed sum effect; Chapter 4, section 4.4.5), raw kcps µXRF data require normalisation (Tjallingii *et al.*, 2007; Weltje and Tjallingii, 2008). First, the centred log-ratio (clr) transformation (e.g. Aitchison, 1982) was applied to raw element intensity data, and then log ratios of two elements were calculated for each measurement interval (e.g. Croudace *et al.*, 2008; Weltje and Tjallingii, 2008; Boyle *et al.*, 2015; Rothwell and Croudace, 2015). The *clr* formula is presented below, where lij is the element intensity of element i in measurement j , and gmj is the geometric mean of all elements analysed at measurement j .

$$clr\ lij = \ln(lij / gmj)$$

To determine which elements to use in log ratio plots, Principal Component Analysis (PCA) was applied to the *clr*-transformed dataset (e.g. Martin-Puertas *et al.*, 2012).

5.5.2.2 Principal component analysis (PCA) of µXRF data

As all µXRF data derived from Itrax core scanners are multivariate, PCA was used to examine all elements simultaneously to determine which elements demonstrated the greatest variation (e.g. MacLeod, 2010; Poraj-Górska *et al.*, 2017). Elements with the greatest variation were deemed useful for detecting grain size changes between the coarse-grained (summer) and fine-grained (winter) lamination within a single varve. To verify interpretations from PCA, the µXRF datasets were categorised by sedimentary units using a combination of macroscale sediment descriptions and X-radiograph

images. In a separate Excel column, each individual μ XRF measurement was assigned a number that corresponds to a particular sedimentary facies. For example, μ XRF measurements that correspond to a clay lamination were given a score of 1, silt/sand laminations a score of 2, lake gyttja, 3. This enabled lamination thicknesses to be derived from μ XRF data and for each individual μ XRF measurement to be colour-coded a PCA bi-plot.

5.5.2.3 Varve identification from μ XRF scanning data

When using μ XRF data for varve counting, element intensities from topsoil and gyttja sediments were removed from each dataset. Sediment classified as “unclear laminations” during analysis of core surfaces and from X-radiograph images were also removed from each μ XRF dataset. Manual varve counting was performed using the freely available *PeakCounter* software (available from <http://polsystems.rits-palaeo.com/>) (Marshall *et al.*, 2012). Log ratio plots were analysed, and the number of peaks were counted. For consistency in the identification process manual varve counts had to fulfil two pre-defined criteria: 1) Within each varve, a minimum of 3 measurements must be made per seasonal lamination to enable clear identification of each varve; and 2) each varve must be easily distinguishable from either macroscale observations or X-radiograph images. Couplets of light and dark laminations that did not fulfil both criteria were classified as “unclear laminations” and a gap in varve sedimentation was noted.

5.5.3 Thin section production

Thin section micromorphology is applied in this research to: 1) ascertain whether or not the laminations preserve an annual (varve) signal; 2) assess varve count errors; and 3) provide a means of assessing other counting methodologies. All laminated sediments at all sites were prepared for thin sections. Sediment sub-samples (8 cm long, 2-3 cm wide) were taken using a z-shaped cutter with a 2 cm overlap (Figure 5-10). Samples were dried using acetone replacement, impregnated with an epoxy resin under vacuum and left to cure for 8-10 weeks. To maximise the amount of surface area for the thin section, rather than slicing cured resin-impregnated samples in half, the lowermost 2-3 mm of the flat surface of the blocks were sliced with a circular saw and removed (Figure 5-10). All thin sections were prepared by R. Devine and A. Palmer using standard protocols for clay-rich unconsolidated sediments (Palmer *et al.*, 2008).

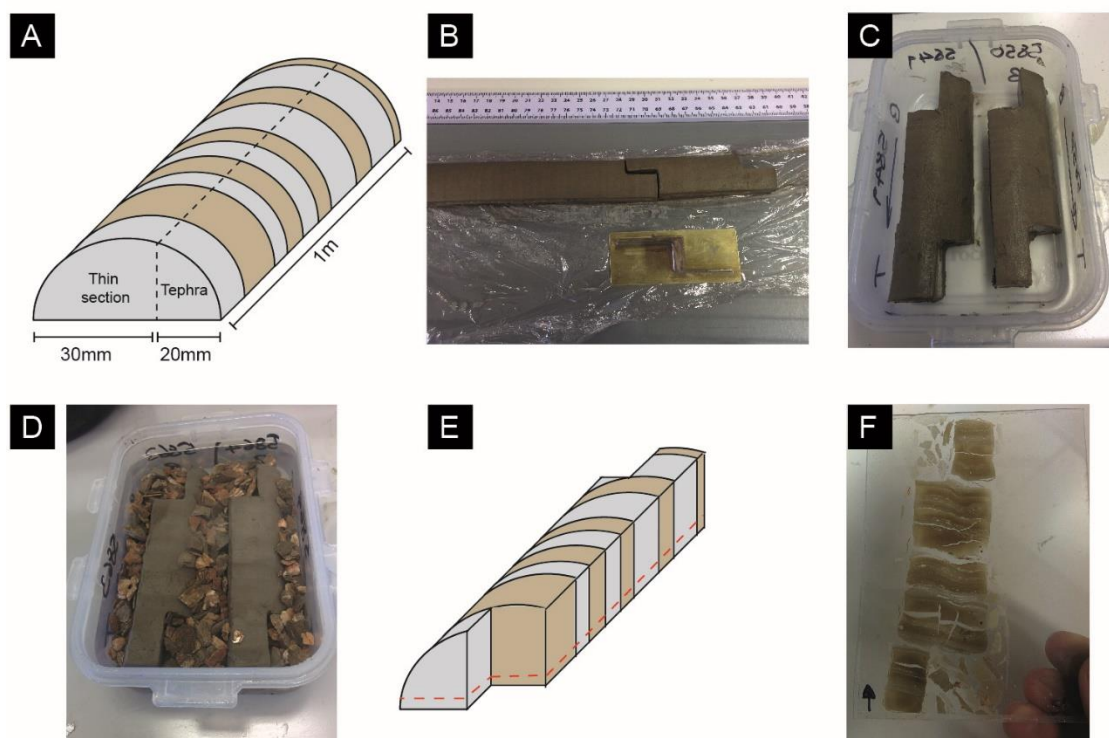


Figure 5-10. Key stages of thin section preparation.

(A) Schematic drawing showing the proportion of core material retained for thin sections and tephra analysis. (B) Z-shaped cutter used to sub-sample for thin sections. (C) Sediment subsamples within a labelled tupperware box, (D) Sediment samples in acetone with gravel packing within a labelled Tupperware box, (E) Schematic showing where the resin-cured samples were cut to maximise thin section surface area, (F) thin section.

5.5.3.1 Thin section micromorphology and varve identification

Thin sections were first inspected on a light box to verify overlaps between slides and identify marker layers. Sediments were then analysed under plane and cross polarised light and detailed microfacies descriptions were undertaken following the methodologies developed by Ringberg and Erlström (1999), Palmer (2005) and Palmer *et al.* (2012). Each individual lamination was described with a focus on particle-size, sorting, texture, structure, and the nature of contacts between laminations. Where possible, counts were made following a vertical transect along each thin section, though in some instances, slides were traversed to avoid areas of sediment that were polished too thinly during thin section production. Thin section slides were examined using a Leica™ M205-C petrological microscope. Images were captured using a Pixera 600es camera and measurements were made using the software package Image-Pro Express.

The following descriptive criteria, developed by Palmer (2005) and Palmer *et al.* (2010) were used to classify lamination couplets as varves:

- 1) The coarse component (normally silt or very fine sand) must be overlain by finer sediment (clay). The coarse component can be massive, normally graded, or

inversely graded, and where a coarse lamination is massive it can be well, moderately or poorly sorted. The coarse component can have multiple laminations, either two distinct laminations or more than two laminations. The fine component can be initially grade from very fine silt to clay, but the dominant grainsize is clay, or can be massive.

- 2) The contact between silt and overlying clay can be graded or sharp. The contact between clay and overlying silt must be sharp.
- 3) Under cross-polarised light, clay laminae must display maeseptic fabric.

Laminations with common sedimentological properties were categorised into distinct Lamination Types using the descriptive scheme outlined by Palmer *et al.* (2019). Lamination Types occur as regularly repeating groups and were analysed to ascertain whether they represent annual cycles of sedimentation i.e. varves. Where identified, varves were categorised into five distinct varve microfacies based on the stratigraphic arrangement of Lamination Types. The distinction of discrete varve microfacies enabled reconstruction of glaciolacustrine sediment processes over time (e.g. Palmer *et al.*, 2012; Devine and Palmer, 2017). Thin section analysis also enabled an assessment of varve preservation using the Varve Quality Index (VQI). Each varve was assigned a score of 1, 2 or 3 using criteria adapted from published literature (e.g. Lotter and Lemcke, 1999; Brauer and Casanova, 2001; Żarczyński *et al.*, 2018) (Table 5-4).

Table 5-4. Varve Quality Index (VQI) criteria.

Information taken from published literature and presented alongside an adapted version that is used in this thesis.

VQI	Lotter and Lemcke (1999)	Brauer and Casanova (2001)	Żarczyński <i>et al.</i> (2018)	This thesis
0		very low preservation (15% counting uncertainty)		
1	homogeneous sediment, no varve visible, no counts possible		low quality, boundaries interrupted, counting difficult	low quality: boundaries are unclear and irregular across thin section, counting difficult
2	varves often interrupted by turbidites or bioturbated, upper and/or lower limit not clearly present, no reliable counts, only estimates possible		high quality, regular varves, boundaries slightly interrupted, counting reliable	high quality: regular varves, boundaries unclear but regular across thin section, counting reliable
3	upper and lower limit of the varve clearly present, only a few disturbances, reliable counts possible	very well preserved (1% counting uncertainty)	perfect quality, regular varves, boundaries parallel, counting reliable	perfect quality: regular varves, boundaries clear, counting reliable
4	standard varve, reliable counts			

All varve thickness data were standardised to allow comparison of varve thickness records within and between sites. Varve thickness differences between sites are likely to be driven by the relative proximity of a site to the sediment source. This means that sites within the same basin can have variable varve thicknesses for a given varve year, depending on proximity to the glacier margin (e.g. Ashley, 1975; Gustavson, 1975; Heideman *et al.*, 2015) or the lake margin (e.g. Devine and Palmer, 2017). As such, varve thicknesses were normalised using the log-transformation and then standardised by the z-score values (Desloges and Gilbert, 1994; Heideman *et al.*, 2015). Z-scores were calculated using the equation below where V_{zy} is the standardised varve thickness for that year (y), V_y is the log-transformed varve thickness, \bar{V}_y is the mean log-transformed varve thickness, and SD is the standard deviation.

$$V_{zy} = \frac{(V_y - \bar{V}_y)}{SD}$$

To test the visual overlap between varve records, Pearson's product moment correlation was applied to the varve thickness records (e.g. Palmer *et al.*, 2010; Bendle *et al.*, 2017).

5.6 Geochronological methods

5.6.1 Constructing site varve chronologies

For the Svinstadsjön varve record an independent varve chronology was constructed using two independent repeat counts; one made by R. Devine and one by A. Palmer. Varve counts were compared and discrepancies between counters were noted (e.g. Lamoureux and Bradley, 1996; Bendle *et al.*, 2017). Varve counting discrepancies were typically located in zones of poor Varve Quality and were recorded as ± 0.5 varve years (vyrs) (e.g. Regnéll *et al.*, 2019) following the annual layer counting uncertainty that is applied to the Greenland Ice Core Chronology (Rasmussen *et al.*, 2006). Mean varve thickness was then derived from the repeat counts to produce a composite varve chronology. For the Asplången and Glottern records a single varve count was conducted by R. Devine and a second varve count is pending. Varve count errors are therefore not reported for these sequences.

5.6.2 Tephrochronology

Tephrochronology provides an alternative means of establishing an independently dated chronology in the absence of material suitable for radiocarbon dating. Although tephra has been detected in some glacial lake varves (MacLeod, 2010; MacLeod *et*

al., 2014; Bendle *et al.*, 2017), this approach is more commonly applied in biogenic varve research. In this thesis, varve chronology and tephrochronology are combined to achieve several key objectives: 1) Provide absolute age estimates for varve deposition; 2) test varve count accuracy and compare different varve counting methodologies; 3) link varve sequences together independent of varve thickness data; and 4) provide a chronostratigraphic framework for paleoenvironmental interpretations (e.g. changes in glaciolacustrine processes, rate of ice sheet retreat, evolution of the Baltic Ice Lake).

5.6.2.1 Tephra sampling and preparation

Entire core sequences from each site were scanned for tephra content by taking 10 cm-long scan samples. Sample length was increased or decreased so that a known number of whole varve years could be incorporated within each sample (e.g. MacLeod *et al.*, 2014). Scan samples were processed using the method outlined by Blockley *et al.* (2005) with a few minor modifications: 1) Samples were not combusted before processing due to the high clay content which when furnaced became difficult and time consuming to sieve; 2) the sieved size range was increased from 25-80 μm to 15-125 μm since technical improvements in the EPMA analysis process enable analysis of smaller grains (Hayward, 2012) and thus maximises shard concentrations; 3) dilute detergents were not required for disaggregating material since samples were of low organic content; and 4) due to the low amount of organic matter only a single cleaning float of heavy liquid (2.0 g/cm^3) was needed. Where tephra was detected samples were refined to varve scale and processed in the same manner as for scan samples, however when shards were prepared for geochemical analysis, they were not subjected HCl treatment. A revised flow chart of the methodological approach is presented in Figure 5-11.

Preparation of tephra shards for geochemical analysis via wavelength dispersive electron probe microanalysis (WDS-EPMA) followed the procedures outlined by Timms (2016) and Lane *et al.* (2014). Individual tephra shards were handpicked using a micromanipulator and gas chromatography syringe and mounted on a probe stub using Specifix-40 epoxy resin (Lane *et al.*, 2014). The shards were hand polished using a 0.10 μm Al_2O_3 paste to create polished sections for chemical analysis (Timms, 2016). Stubs were cleaned in an ultrasonic bath before carbon coating.

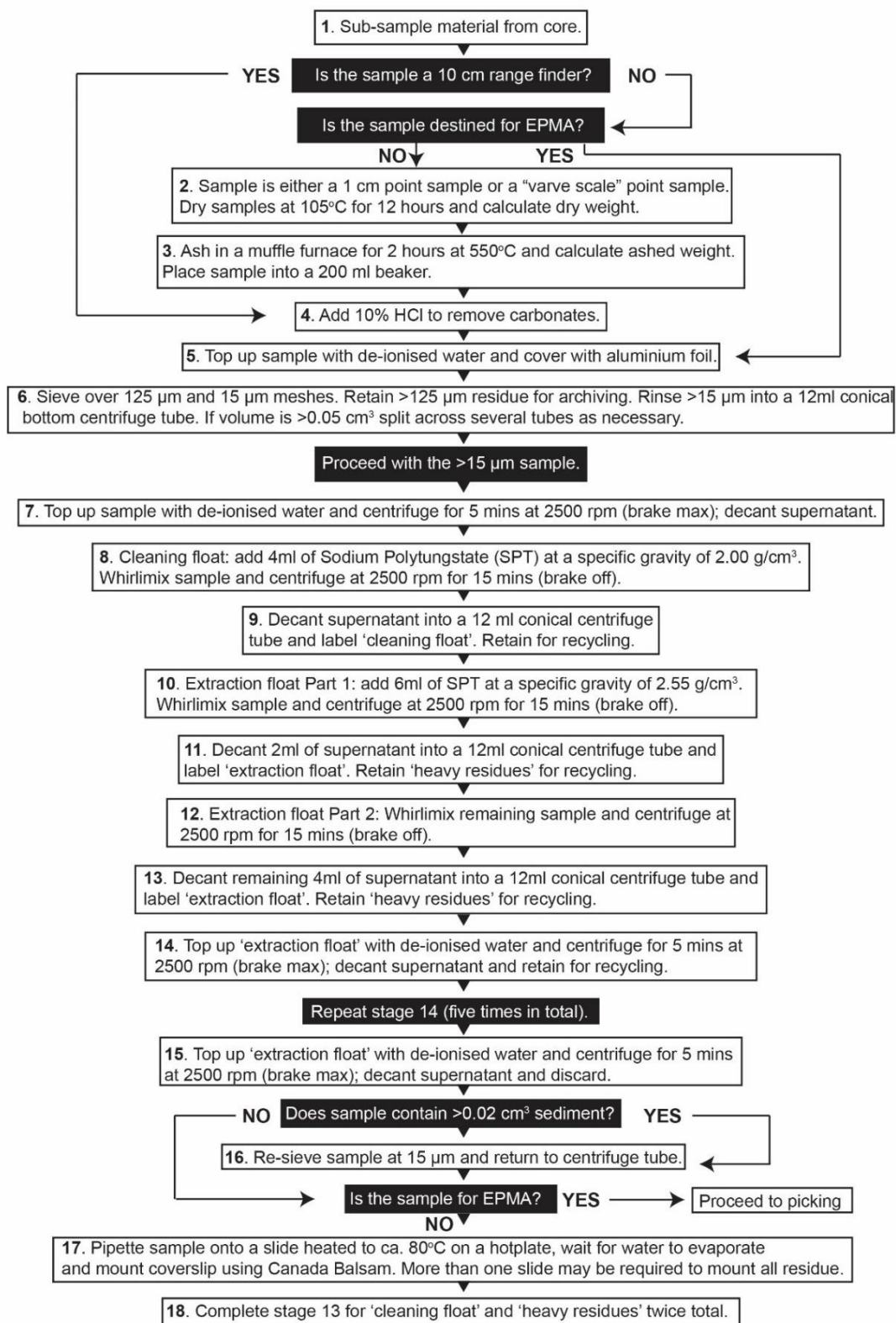


Figure 5-11. A revised extraction methodology for cryptotephra. Methodology based on Blockley et al. (2005) and Timms (2016). This modified technique was applied to all tephra samples in this research.

5.6.3 Geochemical analysis (EPMA)

All chemical analyses were conducted at the School of Geosciences, University of Edinburgh on a Cameca SX100 electron probe microanalyser. All samples were analysed using a 3 µm beam and machine settings followed the protocol outlined by Hayward (2012). To check for machine drift standards were run prior to and after analyses were undertaken. All standards are presented in the appendices. For all samples the major elements Si, Ti, Al, Fe, Mn, Mg, Ca, Na and K were analysed. Cl was also analysed in samples from Asplången (ASP1160, ASP537, ASP536, ASP530, ASP524, ASP516, ASP410, ASP402). All analyses are reported as wt% oxide.

5.6.3.1 Data filtering and tephra correlations

Prior to data processing the geochemical datasets were first 'filtered' to eliminate measurements from non-tephra objects such as minerogenic material and biogenic silica. All geochemical tephra correlations are based on filtered non-normalised datasets (Hunt and Hill, 1993). Correlations are made using element biplots using the software Geochemical Data Toolkit (GCDkit) v 3.0 (Janoušek *et al.*, 2006). Whilst it has become standard practice in Europe to reject analyses which display totals lower than 98% (e.g. Matthews, 2008) or 95% (e.g. Hunt and Hill, 1993; Pollard *et al.*, 2006) it can be argued that these values are somewhat arbitrary and cannot be universally applied across all tephra. For example, there are several Borrobol-type tephra within the Lateglacial and early Holocene that consistently display totals less than 95% (Timms *et al.*, 2017). Therefore, the 95% rule was instead used to guide the data filtering process rather than acting as a strict protocol. Published chemical data are used for tephra correlations and are provided in the Appendices.

5.7 Statistical Analyses

5.7.1 Bayesian Age Modelling

Bayesian age modelling is used in this thesis as it offers the ability to integrate tephra-based ages and varve data to produce robust, independently dated varve chronologies. All records were modelled within OxCal v4.3 (Bronk Ramsey, 2009) using the simplest model possible, the *Sequence* model and using interval spacing to include the varve data. The model uses the varve spacing as a gap function including varve count uncertainties and makes only the assumption that age increases with depth. All data were entered as Gaussian distributions and errors were propagated. The model codes are provided in the appendices.

It is important to note that if a sediment sequence is composed of continuous varves and constrained with multiple ^{14}C ages then a *U_Sequence* or a *P_Sequence* model are also appropriate (Bronk Ramsey, 2008). For certain stratigraphic sequences the *U_Sequence* and *P_Sequence* models can reduce uncertainties providing better chronological control than the more widely used *Sequence* model. Whilst the *U_Sequence* model generates high precision outputs, it can be deemed somewhat rigid as it assumes that sedimentation rates year to year, or the numbers of varves laid down should be uniform (Blockley *et al.*, 2008). The *P_Sequence* model can incorporate stratigraphical information in a less rigid way using a prior based on the Poisson distribution (Bronk Ramsey, 2008). This process recognises that sediment deposition is a series of events and each event can be related to another as well as to the overall stratigraphy (Blockley *et al.*, 2008). When using these models, the depth of each sediment unit is typically used, but when applied to varve studies the depth can be converted to varve year. Therefore, the *U_Sequence* and *P_Sequence* models can be used in the same way as a *Sequence* model which uses a gap function for varve interval spacing.

Blockley *et al.* (2008) explored the effect of using different age models on the radiocarbon dated Soppensee varve chronology which is dated to the Younger Dryas and early Holocene periods. The authors deemed the *P_Sequence* model to be more successful at identifying outlier radiocarbon dates and reducing uncertainties than the *Sequence* model. The *U_Sequence* model was also applied but this approach was deemed too stringent for the varve record.

Whilst the *U_Sequence* and *P_Sequence* models can reduce uncertainties (e.g. Blockley *et al.*, 2008), these approaches are better suited to stratigraphic sequences with superior age control such as the Soppensee varve chronology which is constrained by 89 AMS radiocarbon ages (Hajdas *et al.*, 1993). In contrast, the composite varve chronology presented in this thesis is constrained by 3 tephra ages. Therefore, the use of a *P_Sequence* or a *U_Sequence* model would likely have negligible effect on the uncertainties and be of limited use for identifying outliers in the varve chronologies presented in this thesis. If, however, radiocarbon ages were obtained for the varve records, and if the tephra ages were non-normal distributions, the *P_Sequence* or *U_Sequence* models may then create some forcing of the model away from the mid-point. Therefore, use of a *Sequence* model is deemed appropriate for the tephra-based varve chronologies presented in this thesis and follows the approach adopted by Bendle *et al.* (2017).

5.8 Palaeoecological proxies

A limited number of samples were prepared for palaeoecological proxies from Asplången. Samples were not contiguously spaced but were targeted around the transition from the uppermost glacial varve into blue/grey homogenous clays to provide crude contextual information of palaeoenvironmental conditions during the time of sediment deposition. Palaeoecological information is primarily used to substantiate sedimentological interpretation of a non-varved unit as a turbidite. The turbidite is located stratigraphically above varved sediments and below deposition of a tephra layer (see Chapter 7 for details). The interpretation of a turbidite enabled appropriate age assignment to this stratigraphic unit (i.e. instantaneous deposition) during Bayesian age modelling of the sediment sequence (see Chapter 10 for details). Therefore, results from palaeoecological proxies form a minor part of this thesis. The sampling resolutions were determined by the author whereas laboratory processing and analyses were conducted by other analysts (see acknowledgements). Samples were processed for diatoms, chironomids, ostracods and plant macrofossils.

5.8.1 Diatom preparation

Diatom analysis has been used in this study to provide an indication of lake water salinity across a key sediment boundary in the Asplången record only. Seven samples were prepared for diatom analysis from the ASP2A sequence at Asplången, following Battarbee *et al.* (2001) digestion procedure. For each sample, ~0.1g of wet sediment were placed into a centrifuge tube with 5ml 30% H₂O₂ and then placed into a water bath. Samples were heated to 80°C until all organic material was removed. After this, a few drops of 50% HCl were added to each sample, and samples were topped up with distilled water. The samples were centrifuged at 1200 rpm for 4 minutes and then the supernatant liquid decanted. The samples were then refilled with distilled water and the washing process was repeated 4 times. In the last rinse, a few drops of weak NH₃ were added to prevent diatom clumping. The samples were pipetted onto cover slips, covered, and left to evaporate overnight. Following this, slides were made by heating a hotplate to 130°C in a fume cupboard, a drop of Naphrax mounting medium (refractive index 1.65) was placed on the slide and the cover slip was inverted. The slide was heated to drive the toluene off the Naphrax, allowing the refractive index to rise to 1.73, making it ideal for diatom slides.

Samples were studied at x1000 magnification using a Lecia DMBL. Identifications followed (Krammer and Lange-Bertalot, 1986, 1988, 1991a, 1991b) supplemented with Lange-Bertalot (2001), Krammer (2002) and web-based resources such as

<https://diatoms.org> (Diatoms of North America) and Algalbase; (Guiry and Guiry, 2018). Diatom data are presented against sediment depth and diatom assemblage zones are identified.

5.8.2 Plant macrofossil, ostracod and chironomid preparation

The sediment sequence at Asplången was also sampled for plant macro-fossils but only 6 samples were taken from the sediments that cover the boundary from glaciolacustrine varves to blue/grey homogenous clays. This approach was undertaken to provide further contextual information about the depositional environment in addition to diatom analysis. Individual 1 cm³ of sediment were disaggregated and passed through a 125 µm sieve mesh with all materials retained for identification. All macrofossil remains were identified in deionised water using a low powered binocular stereomicroscope. During plant macrofossil identification, ostracods were also found but were not cleaned. Ostracod identifications were made to genus level using Fuhrmann (2012). A limited number of chironomid remains were also identified in 2 of the 6 macrofossil samples. Chironomids were picked in deionised water and mounted using warm 10% KOH and Euparal slide mountant. The head capsules were identified using a compound microscope at 100-400x magnification, with reference to Brooks *et al.* (2007).

5.9 Summary

A key aim of this thesis is to challenge the existing chronology of the Swedish Timescale by determining if traditional macroscale analysis of Baltic Ice Lake sediment sequences produces accurate varve chronologies. If macroscale analysis leads to consistent misidentification of varves, this may account for, or at least partly account for, the “missing years” in the Swedish Timescale. In order to test the accuracy of macroscale analysis, the laminated sediment sequences presented in this research were analysed using: 1) macroscale analysis of split core surfaces; 2) X-radiograph image analysis; 3) µXRF data analysis; and 4) thin section micromorphology (Table 5-5). The resultant varve counts from each methodology were compared to evaluate varve count differences between the different methodologies and analytical resolutions (Chapter 6).

From this point forward, the following abbreviations are used to describe varves that were identified using the different methodological approaches in this research.

varve^{MAC} Varves that are identified at the macroscale

varve^{XRAD} Varves that are identified from X-radiograph images

varve^{XRF} Varves that are identified from μ XRF data

varve^{TSA} Varves that are identified from Thin Section Analysis

Table 5-5. Key methodologies that were used for varve identification and counting. Note that particle size analysis was used to verify grain size interpretations from other methodologies rather than for the generation of varve counts.

Methodology	Analytical precision	Application
Particle Size Analysis	Lamination scale ~1 mm	<ul style="list-style-type: none"> To validate grain size observations from core surface To validate grain size interpretation from X-radiograph images To validate grain size interpretation from μXRF data
Macroscale analysis of sediment surface	1 mm	<ul style="list-style-type: none"> Sediment description To determine varve classification scheme Generate varve counts
X-ray radiography	200 μ m	<ul style="list-style-type: none"> Sediment description To determine varve classification scheme Generate varve counts
μ XRF	200 μ m (500 μ m at Svinstadsjön from 0-700 cm)	<ul style="list-style-type: none"> Sediment description To determine varve classification scheme Generate varve counts
Thin section micromorphology	63 μ m	<ul style="list-style-type: none"> Sediment description To determine varve classification scheme Generate varve counts

In addition to microscopic analyses of varved sediments, the identification of volcanic ash within varve records will enable site varve chronologies to be independently dated. Given that site selection is primarily based on tracing the published ice-margin lines to find sediment records that likely contain volcanic ash, the results from tephra analysis hold the potential to revise the existing deglaciation model if the tephra results do not align with the expected tephra horizons within the site varve chronologies. A third expected outcome of the tephra data is to independently link site varve chronologies. This will also enable the current methodologies that are used to correlate site records within the STS such as varve thickness wiggle-matches, statistical methods and use of marker horizons, to be tested.

It is important to note that this research was conducted in several sequential phases such that the results from Svinstadsjön (Chapter 6) were used to refine the methodological approach that was applied to Asplången (Chapter 7) and Glottern (Chapter 8). Therefore, it is recommended that the results chapters are read in the order that they are presented in this thesis and should not be taken as stand-alone chapters.

Chapter 6. Results - Svinstadsjön

This chapter presents the results from Svinstadsjön and is the site that was used to evaluate the accuracy of traditional macroscale analysis through comparison with microscale techniques. Following evaluation of different varve count methodologies, a revised protocol for identification of varves at Svinstadsjön is presented. This protocol is applied to the sediment sequences at Asplången (Chapter 7) and Glottern (Chapter 8) to test its replicability at other sites in the Baltic Ice Lake.

The approach to description of the laminated sediments from Svinstadsjön was based on establishing the fidelity of different descriptive methods to establish whether the sediments were annually laminated and also develop accurate chronologies. In the first instance, macroscale description and counts were made in order to replicate the methodological approach widely applied to the construction of the Swedish Timescale. These counts were then applied to analytical techniques now more commonly used (e.g. particle size analysis, X-ray radiography, thin section analysis and geochemical characterisation using μ XRF). This enabled direct comparison to and interrogation of the traditional approach to varve identification. As such, the sediments at Svinstadsjön were first classified as varves using only macroscale analysis (verified by particle size data). This macroscale count is then used as a benchmark which was subsequently validated using descriptions and counts from the microscale techniques: 1) X-radiograph images; 2) peaks in μ XRF data; and 3) thin section analysis. The varve counts and sedimentology results from each methodology are presented separately before comparisons between methods are drawn and revisions to the traditional macroscale methodology are presented. Figure 6-1 summarises the approach undertaken at Svinstadsjön and how the results from this chapter are used to inform the approach in subsequent results chapters.

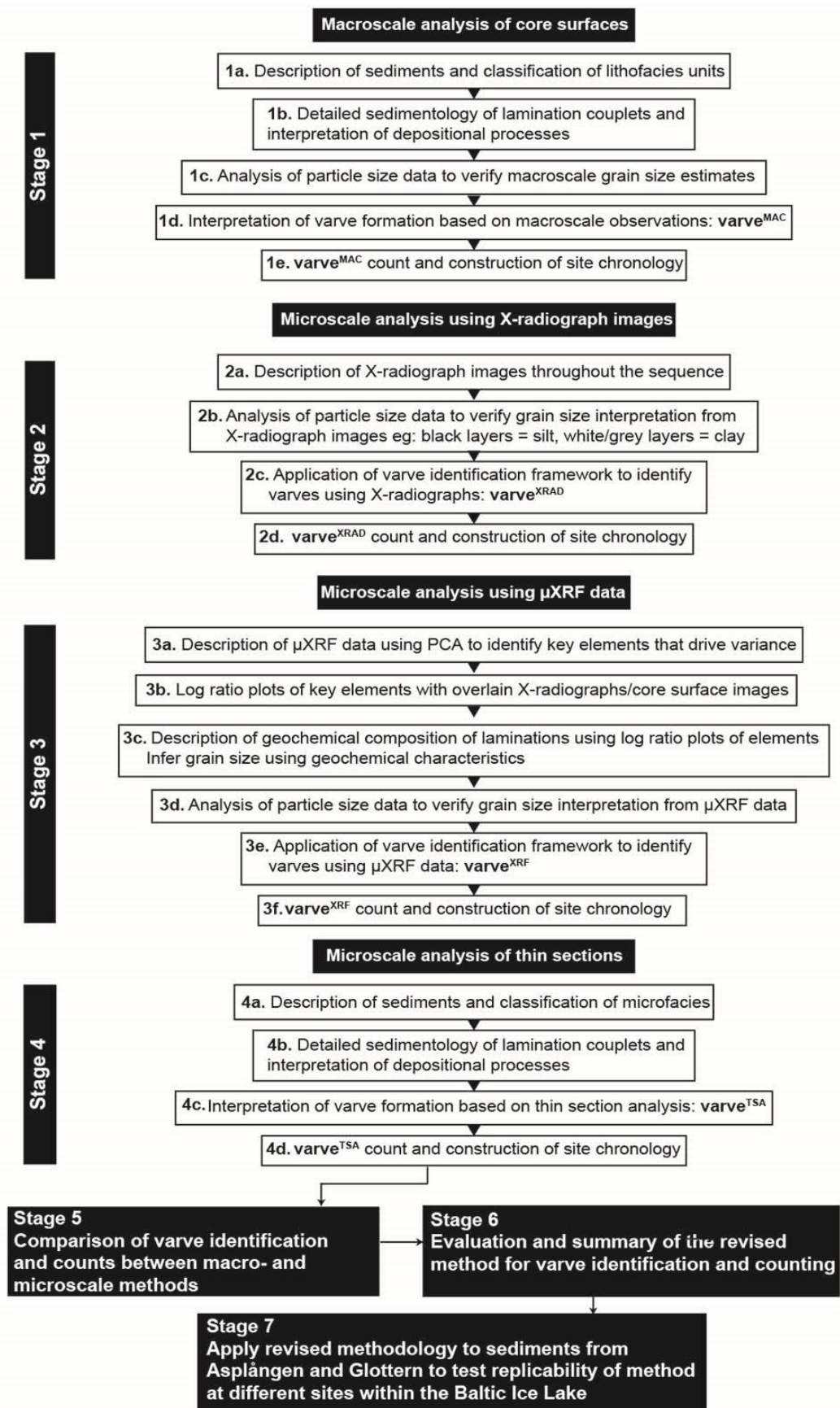


Figure 6-1. Approach undertaken to evaluate different methods of varve identification and counting.

6.1 Core recovery and basin survey

An auger survey of the north-western shore of Svinstadsjön was carried out in July 2016 to map the bathymetry of the field site (Figure 6-2). The basin topography at the site is uneven with a prominent hollow that is 9.8 m deep, toward the northern end of the site and is flanked by two shallow mounds to the north and south which are areas *ca* 2-3 m higher in relief than the basin. The distance between the hollow and each mound is approximately 10 m with a 17° slope. Despite this hollow being one of the deepest points within the basin, it is in a steep area that may be prone to local mass movement. Similarly, although the southern area of the basin is the deepest at 11 m (dark blue area), the basin appears to shelf from east-west and therefore may also be prone to mass movement processes. Figure 6-2 shows the location of each depth probe and the coring location which is in the flattest part of the site that also maximised depth.

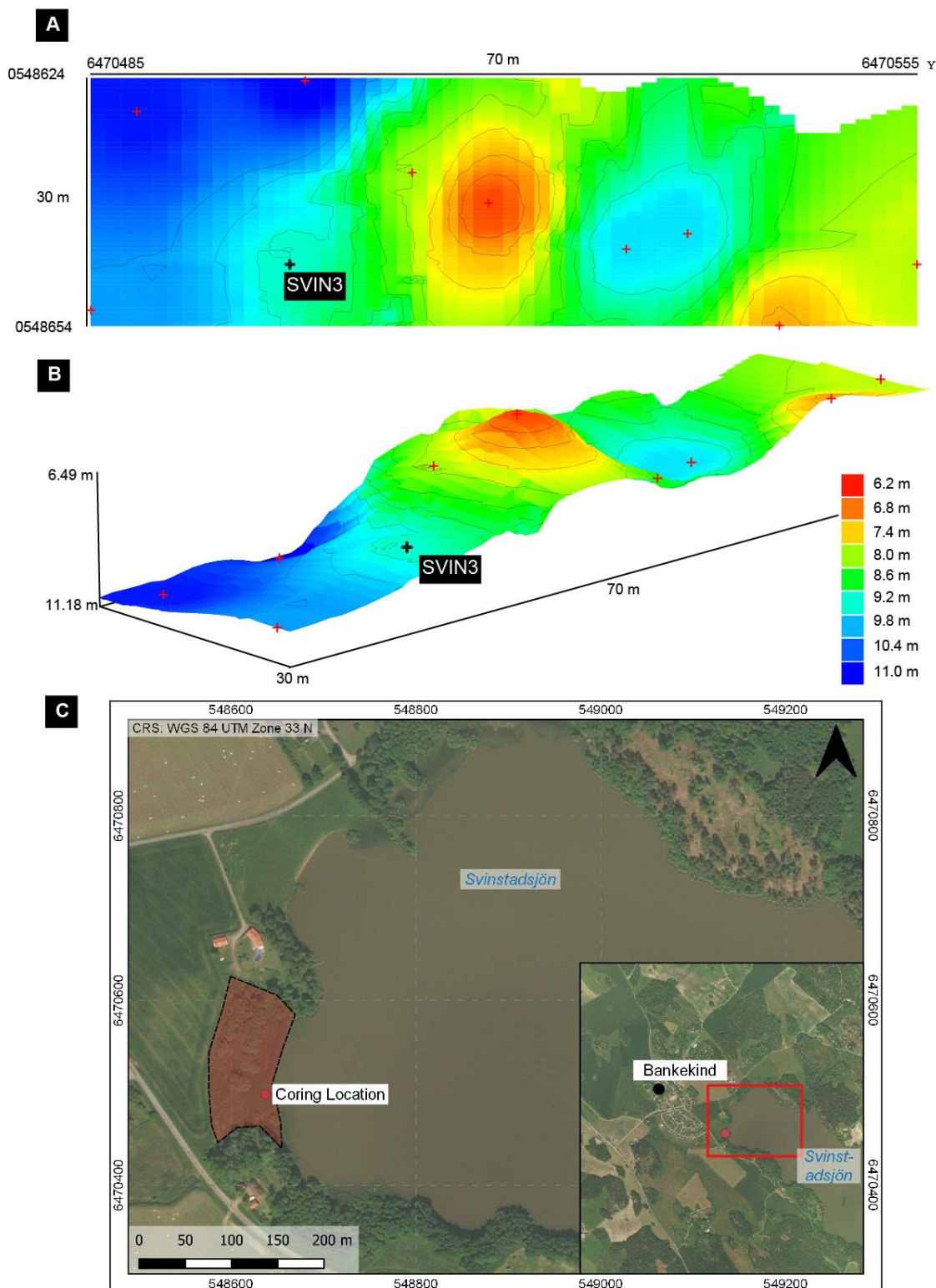


Figure 6-2. Sediment depth survey result and site map. (A) Sediment depth survey in 2D and (B) in 3D. Red crosses mark depth probe locations and the black cross marks the coring location 58°22'21"N, 15°49'53"E. Depth surveys were plotted in QuickGrid. (C) Site map showing the area covered by the sediment depth survey in red.

6.2 Macroscale sedimentology and stratigraphy

This section focusses on the identification and description of key lithofacies units, and detailed sedimentological description of the laminated sediments to determine whether the sediments preserve an annual signal.

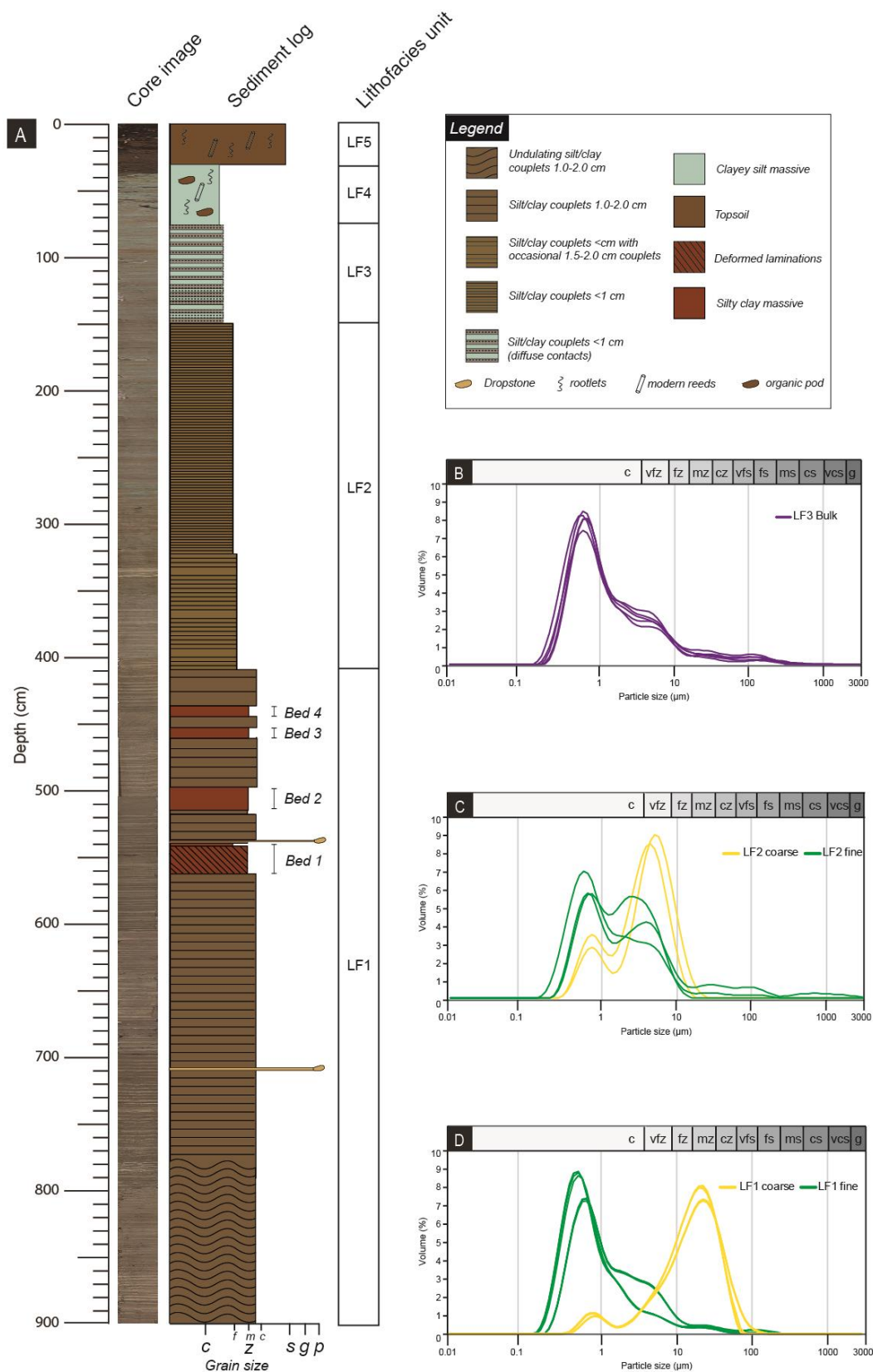
6.2.1 Sediment units

The sequence is 9 m long and contains 7.465 m of well-defined laminated silts and clays overlain by 0.79 m of weakly laminated silty clay and 0.41 m of clayey silt. The sequence is capped by 0.335 m of topsoil. During depth probing, the coring rods hit a solid basal surface and when recovering the basal Russian corer, the cone of the corer turned through sands and gravel, but these were not retrieved. It is assumed that the sands and gravel have a thickness of at least 10 cm.

Five lithofacies (LF) units were identified from the extracted sediment at Svinstadsjön: 1) brown clearly laminated couplets of silt and clay \geq cm-scale thickness; 2) brown clearly laminated couplets of silt and clay $<$ cm-scale thickness; 3) grey and blueish grey diffusely laminated silt and clay couplets <0.5 cm thick; 4) massive blueish grey clayey silt with dark brown pods of organic material; and 5) topsoil.

LF1 (900-410 cm) is split into two sub-units. Sub-unit 1a (900-780 cm) comprises undulating laminated silts and clays, and sub-unit 1b (780-410 cm) comprises horizontally bedded laminated silts and clays with isolated gravel- to pebble-sized clasts (Figure 6-3). In LF1, couplets of silt (coarse) and clay (fine) are \geq cm thickness with the silt laminations being 10 YR 7/1 light grey and composed of medium silts whereas clay laminations are 10 YR 4/2 dark greyish brown. LF1 is also punctuated by four beds that interrupt the deposition of silt and clay lamination couplets. Bed 1 (561-542.5 cm) is comprised of sub-horizontal/deformed laminations overlain by a 4.3 cm thick silt massive bed. Beds 2, 3 and 4 are composed of massive silt: Bed 2 at 518.4-495 cm, Bed 3 at 461.3-451 cm and Bed 4 at 442.5-434.7 cm (Figure 6-3 and Figure 6-4).

LF2 (410-153.5 cm) is composed of horizontally bedded laminated silt and clay couplets that are typically $<$ cm-scale. Silt laminations are composed of very fine silts and are 10 YR 4/3 brown and clay laminations are 10 YR 4/2 dark greyish brown (Figure 6-3). Whilst most lamination couplets are $<$ cm-scale thickness, occasional couplets of 1.5-2.0 cm thickness are observed between 410-322 cm (Figure 6-3).



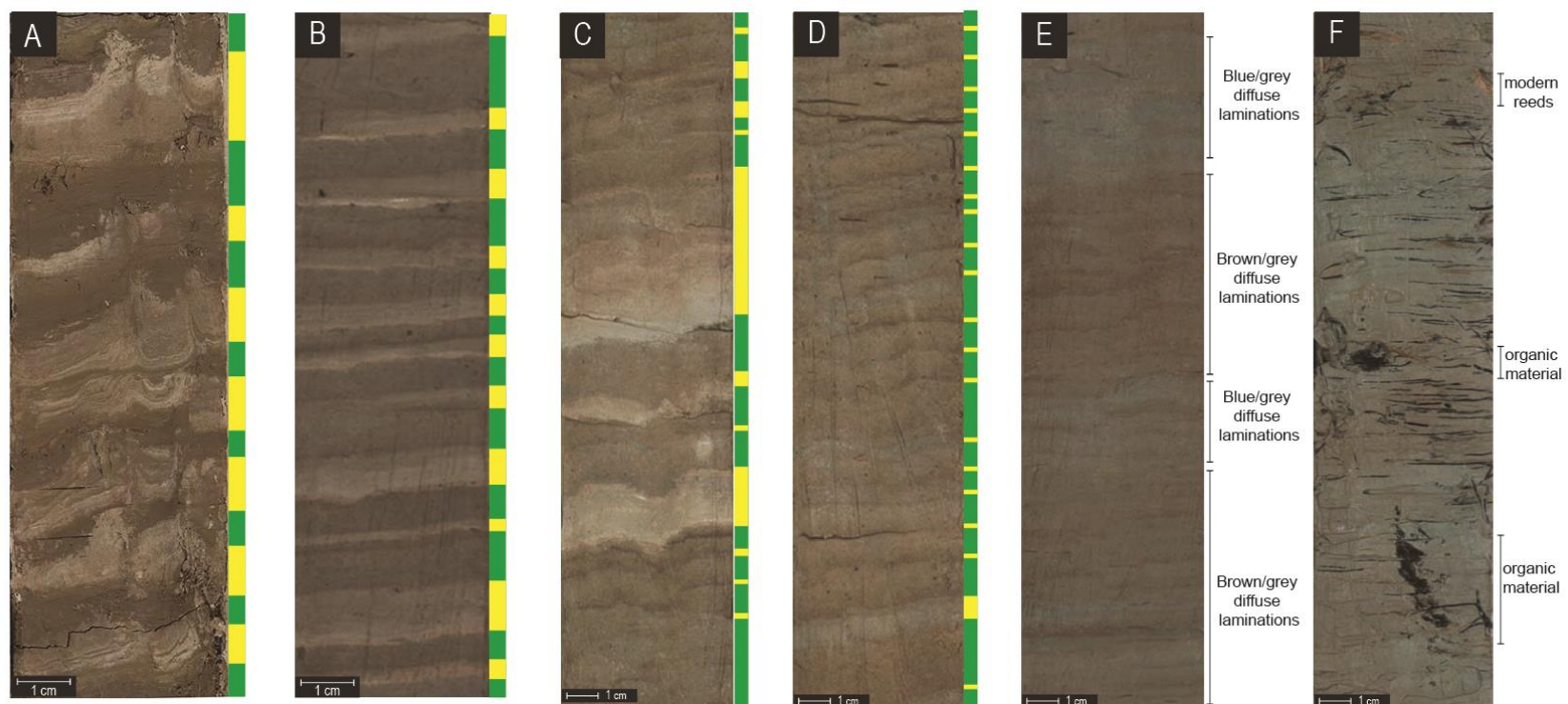
LF3 (153.5-74.5 cm) is composed of horizontally bedded, diffusely laminated silts and clays. The laminated sediments are grouped into two distinct colour types; those that are reddish grey and those that are blueish grey. In the reddish grey lamination couplets, the silt component is 10 YR 4/3 brown and the clay component is 10 YR 3/1 dark reddish grey. In the blueish grey laminations, the silt component is 10 YR 4/3 brown and the clay component is 7.5YR 5/0 grey. Couplets of silt and clay laminations are typically <0.5 cm thickness and are very difficult to delimit (Figure 6-4). Particle size analysis shows that the modal grain size is clay with a minor component of very fine silt.

LF4 (74.5-33.5 cm) is a massive silty-clay bed that is 7.5YR 5/0 grey, contains 1 mm thick black rootlets, pods of organic material and modern-day reeds.

LF5 (33.5-0 cm) is topsoil and is composed of organic silty sand that is 10 YR 3/3 very dark brown with present-day reeds and rootlets.

Figure 6-4. Core surface images for LF1, LF2, LF3 and LF4.

Next page. (A) Undulating lamination couplets of silt and clay in LF1a. (B) Horizontally bedded laminations in LF1b. Laminations in LF1 are \geq cm-scale thickness. (C and D) Examples of horizontally bedded lamination couplets in LF2 (410-153.4 cm) which are composed of fine silt and clay. Most lamination couplets are <cm-scale but occasional \geq cm-scale lamination couplets are observed at the base of LF2 from 422-310 cm. (E) Examples of diffuse laminations in LF3 (153.4-74.5 cm) which are composed of very fine silt and clay. Laminations appear as distinct packages of blue/grey and brown/grey laminations. (F) Sediment from LF4 (74.5-33.5 cm) which is composed of blue/grey clayey silt and thin <1 mm black rootlets. Pods of organic material and roots from modern reeds were also observed. (G) Bed 1 which is in LF1 and is composed of deformed laminations and a pebble-sized dropstone. Coarse-grained laminations are highlighted with yellow boxes and fine-grained laminations are highlighted with green boxes.



6.2.2 Sedimentology of laminated couplets in LF1-3

Description of the laminated sediments (LF1-3) combines macroscale observations and particle size data. Irrespective of thickness, the laminated couplets are characterised by a brown coarse component (silt) that is overlain by a darker brown, grey, or reddish grey, fine component that is normally graded from very fine silt to clay. Couplets can be subdivided based on the internal structure and thickness of the coarse component and the colour of the fine component: 1) those which are \geq cm-scale with either 1, 2 or 3 laminations in the coarse component and a dark brown fine component (LF1); 2) those which are <cm-scale with a single coarse component layer that is normally graded or massive and a dark brown fine component (LF2); and 3) those which are <cm-scale with a single lamination in the coarse component and a grey or reddish colour fine component (LF3). The contact between the fine component and the succeeding coarse component is always sharp in LF1 and LF2 but is diffuse in LF3.

6.2.2.1 LF1 (\geq cm-scale brown laminations)

In LF1, 45% of couplets contain 2-3 layers in the coarse component and appear massive with sharp basal contacts (Figure 6-4). These laminations are composed of well-sorted silt with grain sizes from 10 to 30 μ m (Figure 6-3). For the other couplets in LF1, the coarse component is massive and comprised of well-sorted medium silt. The fine component has a gradational lower contact and when observed at the macroscale is composed of massive clay. However, particle size data indicate that the fine component is graded from very fine silt to clay. Larger clasts that deform the underlying laminations are also observed (Thomas and Connell, 1985), and are of pebble-size when observed at the macroscale.

6.2.2.2 LF2 and LF3 (<cm-scale brown laminations)

In LF2 silty clay couplets that are <cm-scale usually contains a single lamination within the coarse component that is overlain by the clay lamination. The silt component is typically composed of well-sorted fine silt and each clay component has a sharp contact with the overlying silt lamination. Like LF1, the fine component has a gradational lower contact and when observed at the macroscale is composed of massive clay. However, particle size data suggest that the fine component is graded from very fine silt to clay (Figure 6-2). Isolated granule- to gravel sized clasts are also observed.

In LF3, couplets are <cm-scale, always contain a single lamination within the coarse component and the fine component is always overlain by the succeeding silt lamination. The contacts between laminations are always diffuse however, due to the thickness of

laminations, it is not possible to ascertain if the fine component is massive or graded. Since silt laminations are typically <1 mm thickness and the boundary between overlying clay laminations is diffuse, it is difficult to accurately delimit each lamination at the macroscale. Additional bulk particle size distributions indicate that each lamination is normally graded from very fine silt to clay (Figure 6-3). The regular alternation between silt and clay laminations, as demonstrated by particle size data (Figure 6-3), permit further investigation of these sediments to characterise their internal structure and origin of deposition.

The sediments described in LF1, LF2 and LF3 are consistent with sedimentation in a subaqueous environment. Further interpretation of depositional processes within each lithofacies are provided in Table 6-1.

Table 6-1. Lithofacies summary displayed from oldest to youngest.
Specific attributes, interpretation of sedimentary processes and inferred depositional environment.

Litho facies	Attribute	Process interpretation	Environment	Reference
LF1	<ul style="list-style-type: none"> • cm-scale rhythmically bedded medium silts and clays • multiple laminations in the coarse (silt) component • Isolated gravel- to pebble-sized clasts • Deformed laminations e.g. folding, contorting, shearing or homogenisation of laminations • 2:1 or 3:1 coarse:fine thickness ratio 	Silt-sized sediment sourced from ice-proximal sediment density flows; fine laminations formed from suspension settling; clasts deposited from iceberg rafting. Deformation due to localise slumping	Proximal glaciolacustrine	Ashley (1975); Smith and Ashley (1985); Mulder and Alexander (2001); Talling <i>et al.</i> (2012)
LF2,	<ul style="list-style-type: none"> • mm-scale rhythmically bedded very fine silts and clays • single lamination in the coarse (silt) component • Occasional cm-scale lamination couplets (only in LF2a). • Sporadic granule-gravel sized clasts • 1:1 or 1:2 coarse:fine thickness ratio 	<p>Silt laminations formed mostly from suspension settling of reworked sediments but could also be the result of density flows, but in a more distal location than LF1. Clay laminations deposited from suspension settling. Thicker cm-scale couplets in LF2a from one-off high velocity/high sediment load density currents</p> <p>Isolated granule-gravel sized clasts consistent with IRD/aeolian deposition.</p>	Distal glaciolacustrine; distal to glacier margin and distal to lake edge	Palmer <i>et al.</i> (2019)
LF3	<ul style="list-style-type: none"> • mm-scale rhythmically bedded very fine silts and clays • Diffusely laminated and difficult to define • Alternations between red and grey packages of laminations • 1:2 or 1:3 coarse:fine thickness ratio 	Silt laminations formed mostly from either suspension settling of reworked sediments in the water column, or a continuum of density flows. Clay lamination deposited from suspension settling.	Ultra-distal glaciolacustrine; distal to glacier margin and distal to lake edge	Palmer <i>et al.</i> (2019); Strömberg (1994); Brunnberg (1995)
LF4	<ul style="list-style-type: none"> • Clayey silt massive • Pods of organic material • Macrofossils e.g. Seeds, leaves, rootlets 	Clastic sediment sourced from suspension settling of reworked/flocculated sediments. Organic material and macrofossils transported from erosion of the catchment and/or littoral zone due to drop in lake level.	Ultra-distal glaciolacustrine	Interpretation
LF5	<ul style="list-style-type: none"> • Dark brown silty sand with macrofossils and modern reeds 	Well-drained soil	Present-day lake edge	Interpretation

6.2.3 Interpretation of varve formation

The description of the rhythmically laminated silts and clays in LF1 and LF2 are consistent with glaciolacustrine varves that have been identified at the macroscale (De Geer, 1912; Ashley, 1975; Smith and Ashley, 1985; Ridge *et al.*, 2012). During the melt season (spring/summer), sediment enters the lake basin as an underflow or overflow. After the flow enters the lake body it loses velocity and coarser-grained material is deposited almost instantly. Therefore, the melt season is represented by the coarser component of the lamination couplets. At Svinstadsjön, summer laminations can be composed of multiple laminations of fine/medium silt that may represent individual pulses of sediment that entered the lake basin. The fine (clay) component remains in suspension during the melt season due to currents within the lake and wind-driven surface currents (Ashley, 1975; Smith and Ashley, 1985). During the non-melt season (winter/autumn) the lake waters freeze and inhibit the formation of surface currents allowing the finer-grained clays and very fine silts to be deposited from suspension in the water column.

6.2.3.1 LF 1 (\geq cm-scale brown varves)

In all lamination couplets, the sharp contact between the fine-grained lamination and the following coarse-grained lamination suggests a rapid change in the style of sedimentation. This is interpreted as the transition between the melt season and non-melt season. The multiple laminations with sharp contacts that are observed in the coarse (silt) component are characteristic of deposition from underflows with high sediment concentration (Ashley, 1975; Mulder and Alexander, 2001) and were likely deposited during the peak melt season (Gustavson, 1975; Ridge *et al.*, 2012). Due to the relatively fine grain size of the coarse component (medium-fine silt) it was difficult to accurately characterise the internal lamination structure that may provide more detail on the nature and timing of sub-seasonal melt. However, it is possible that internal lamination structure could be observed at the microscale. Results from thin section analysis of these sediments are presented in section 6.5. Overall, the structures observed within the laminated couplets in LF1, and their depositional processes indicate that the sediments are glaciolacustrine varves that were deposited in proximal-to distal locations within an ice-contact lake (Ashley, 1975; Smith and Ashley, 1985; Ridge *et al.*, 2012).

6.2.3.2 LF 2 (<cm-scale brown varves with sharp contacts)

In all lamination couplets there is a sharp contact between the coarse-grained layer and the underlying fine-grained layer which is indicative of a rapid switch in the style of sedimentation. This is consistent with a transition between melt season and non-melt

season sedimentation. The melt season layer is deposited either from the continuation of sediment underflows or from suspension settling of re-worked sediments. Non melt season (clay) layers were deposited from suspension settling in quiescent lake waters (e.g. Ringberg and Erlström, 1999; Palmer *et al.*, 2010). Isolated grains are interpreted as IRD (Thomas and Connell, 1985). The overall structure and composition of the laminations, and their depositional processes are typical of ice-distal glaciolacustrine varves deposited in an ice-contact lake (Ashley, 1975; Palmer *et al.*, 2010, 2019).

6.2.3.3 LF3 (<cm-scale grey varves with diffuse contacts)

The structures described in LF3 are less commonly associated with glaciolacustrine varves, primarily due to their diffuse boundaries. However, similar structures are found in sediment sequences from the Baltic and which are classified as glaciolacustrine varves (e.g. Strömberg, 1994; Brunnberg, 1995). For LF3, the diffuse boundaries with a very fine silt/fine silt coarse component are difficult to delimit at the macroscale and so accurate assessment of lamination structure was difficult. However, some varves were identifiable within this unit.

6.2.4 Non-varved sediments

Within LF1 there are sections of the sediment sequence that interrupt the deposition of annually laminated sediments and represent different depositional processes. Firstly, the presence of deformed laminations in LF1 that display folding and shearing may be due to slumping or displacement of varves over short distances (e.g. Devine and Palmer, 2017). This is likely due to the uneven basin bathymetry at the Svinstadsjön site (Figure 6-2). The massive silt beds within LF2, which have no obvious laminated structure at the macroscale, probably represent fine-grained glaciolacustrine sedimentation. It is also important to note that the basal contact of each massive silt bed is sharp and non-erosive, therefore, it is unlikely that these sediments are turbidites. Multiple sediment cores would help ascertain the lateral continuity of these beds and clarify depositional process.

6.2.5 Varve^{MAC} chronology

Individual varve chronologies were produced for each core using the varve description criteria outlined in section 5.3.3 and a composite site varve^{MAC} chronology was produced by averaging varve^{MAC} thickness for each year across repeat measurements between overlapping cores. Prominent marker layers such as the disturbed zone in Bed 1 and silt massive Beds 2-4 were used as definitive 'pinning-points' between cores (e.g. Lamoureux, 2001; Palmer *et al.*, 2008, 2010; Bendle *et al.*, 2017). In the absence of pinning-points to link cores, sediment depths were used. Core overlap details are

presented in the appendices. The location of breaks in the otherwise continuous thickness sequence are identified and categorised as either: 1) deformed varves; 2) silt massive sediments; or 3) unclear lamination couplets (Table 6-2). Within LF1, Beds 1 to 4 interrupt otherwise continuous varve sedimentation. The stratigraphic arrangement of these beds is also displayed alongside a site varve^{MAC} chronology in Figure 6-5. It is important to distinguish between breaks which are due to a gap in geological time (e.g. deformation or slump deposits) that indicate a hiatus in the varve chronology, versus breaks that may be due to low analytical precision (e.g. unclear laminations) that may lead to under-counting or missed varves. For the other varve identification methodologies that are presented in this chapter (X-radiograph, μ XRF and thin section analysis), the type and number of breaks are also presented. This allows for comparisons between methodologies with the results evaluated in section 0.

Table 6-2. Summary of breaks in varve^{MAC} sedimentation.

Lithofacies	Depth (cm)	Type of break			
		Deformation	Silt massive bed	Unclear lamination couplets	Total
LF1	900-410	1 (Bed 1)	3 (Beds 2, 3, 4)	0	4
LF2	410-153.5	0	0	0	0
LF3	153.5-74.5	0	0	0	0
	Total	1	3	0	4

In total 619 varves^{MAC} and 4 sections of non-varved sediment were identified during macroscale analysis. The varve thickness characteristics of the Svinstadsjön record are presented for each lithofacies (Table 6-3). In LF1 there are 210 varves^{MAC} with an average thickness of 17.5 mm. The ratio of coarse to fine laminations fluctuates between 1:2 and 2:1 throughout the unit. The minimum varve^{MAC} thickness measurement in LF1 is 4 mm with a maximum of 46 mm. In LF2, there are 361 varves^{MAC} with a mean thickness of 8 mm. Melt season layers are typically thinner than non-melt season layers but can be approximately equal. Finally, in LF3, 49 varves^{MAC} were identified which have an average thickness of 6.6 mm. Melt season layers are approximately equal to, or thinner than non-melt season layers.

Table 6-3. Summarised varve^{MAC} thickness characteristics in each lithofacies.

Lithofacies	Depth (cm)	Varve number	Varves (n)	Mean (mm)	St dev	Min (mm)	Median (mm)	Max (mm)	Coarse:Fine
LF1	900-410	1-210	210	19.8	8.5	3	15	46	2:1
LF2	410-153.5	211-571	361	8.0	3.5	2	9	28	1:1
LF3	153.5-74.5	571-619	48	6.6	3	2	5	21	1:2

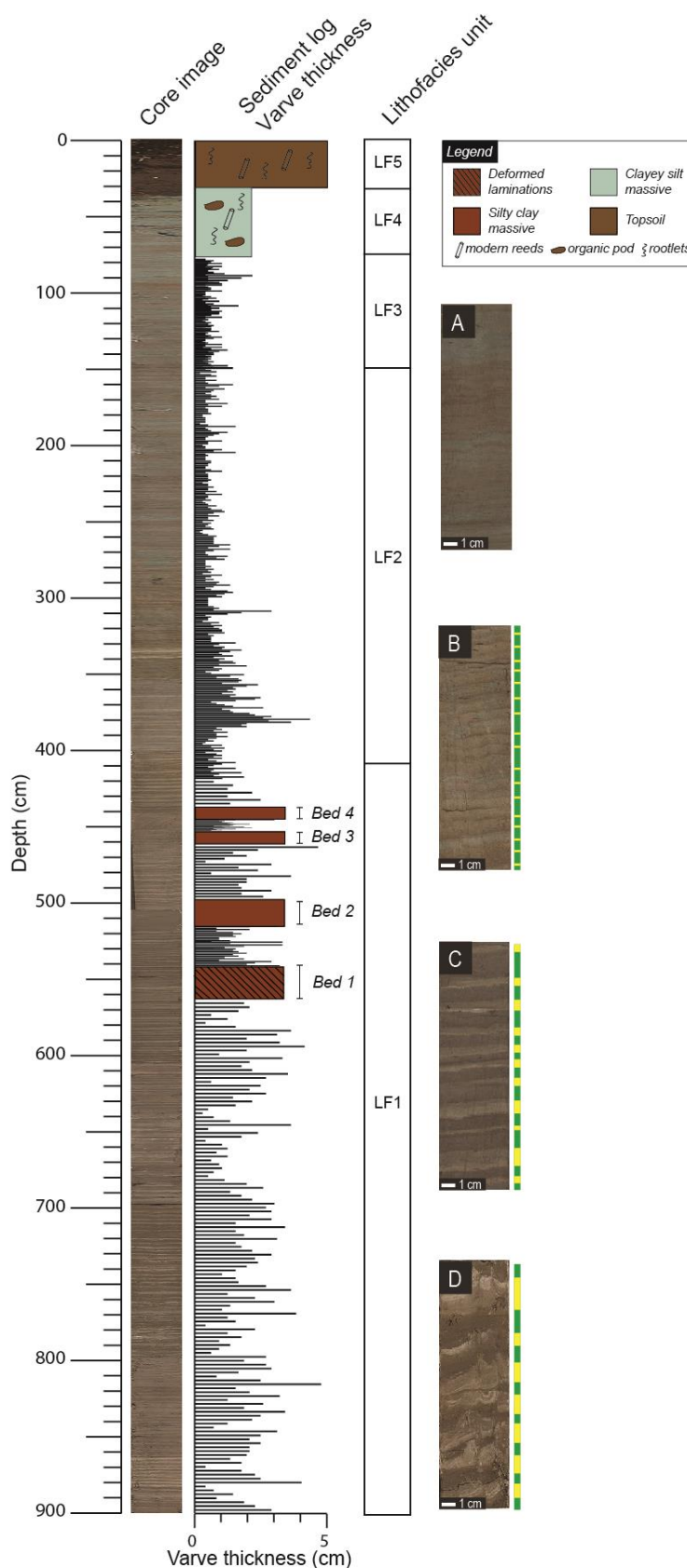


Figure 6-5. Core surface images and varve^{MAC} thickness plotted against depth. Breaks in the site varve^{MAC} sequence are either deformed laminations or silt massive beds. Example core surface images of <cm-scale varves in LF3 (A), <cm-scale varves in LF2 (B), and ≥cm-scale varves^{MAC} in LF1 (C and D). Yellow boxes highlight coarse-grained laminations and green boxes highlight fine-grained laminations.

6.3 X-radiograph image analysis

This section uses X-radiograph images and builds on macroscale description and interpretation of the laminated sediments as varves focussing on: 1) description and interpretation of key lithofacies units that contain laminated sediments; 2) description of varve^{XRAD} structure; and 3) construction of a varve^{XRAD} chronology.

6.3.1 Description of X-radiograph images

The lithofacies identified at the macroscale are broadly comparable to changes identified in the X-radiograph images. Particle size analysis at the macroscale indicates that the dark layers in the X-radiographs represent coarse (silt) laminations and light grey layers represent fine (clay) laminations (Figure 6-6). Further detailed description of these changes within lithofacies units 1-3 are presented below.

6.3.1.1 LF1 (>cm-scale laminations)

In LF2, laminations are horizontally bedded throughout the unit with sharp boundaries between light (clay) layers and succeeding dark (coarse) layers. The contact between light layers and the following dark layer is almost always sharp but can occasionally be slightly diffuse. Within the dark layers, subtle variations are observed that could represent sub-seasonal laminations within the coarse component, though boundaries between these layers are difficult to define. Clay layers typically contain a <1 mm thickness dark grey layer that grades to a lighter grey colour or can be composed of a single shade of light(er) grey. Within LF1, there are also elliptical/circular-shadows within the coarse component. These shadows have an a-axis approximately 300-600 μm and are located towards the top of the dark lamination (Figure 6-7). These anomalous shadows are interpreted as dropgrains/IRD (Thomas and Connell, 1985) and their occurrence in the upper part of the coarse component is consistent with iceberg calving in the late melt season.

6.3.1.2 LF2 (<cm-scale laminations)

In LF2, laminations are horizontally bedded with a sharp contact between each light layer and the succeeding dark layer. The contact between the dark (silt) layer and the following light (clay) layer is slightly diffuse. This is due to the 200 μm resolution of the X-radiograph image such that a silt lamination that is <1mm thickness is represented by fewer than 5 pixels. In contrast, occasional $\geq\text{cm}$ -scale thickness laminations at the base of LF2 (410-322 cm) have sharp contacts under X-ray. Within LF2, there are also elliptical/circular-shadows within the coarse component with an a-axis approximately 200-400 μm (Figure 6-7). Unlike LF1 these shadows are in sections of the sequence with

unclear/pixelated laminations. It is therefore not possible to determine if these grains are derived from IRD such as those in LF1, but they are nevertheless categorised as anomalously large grains.

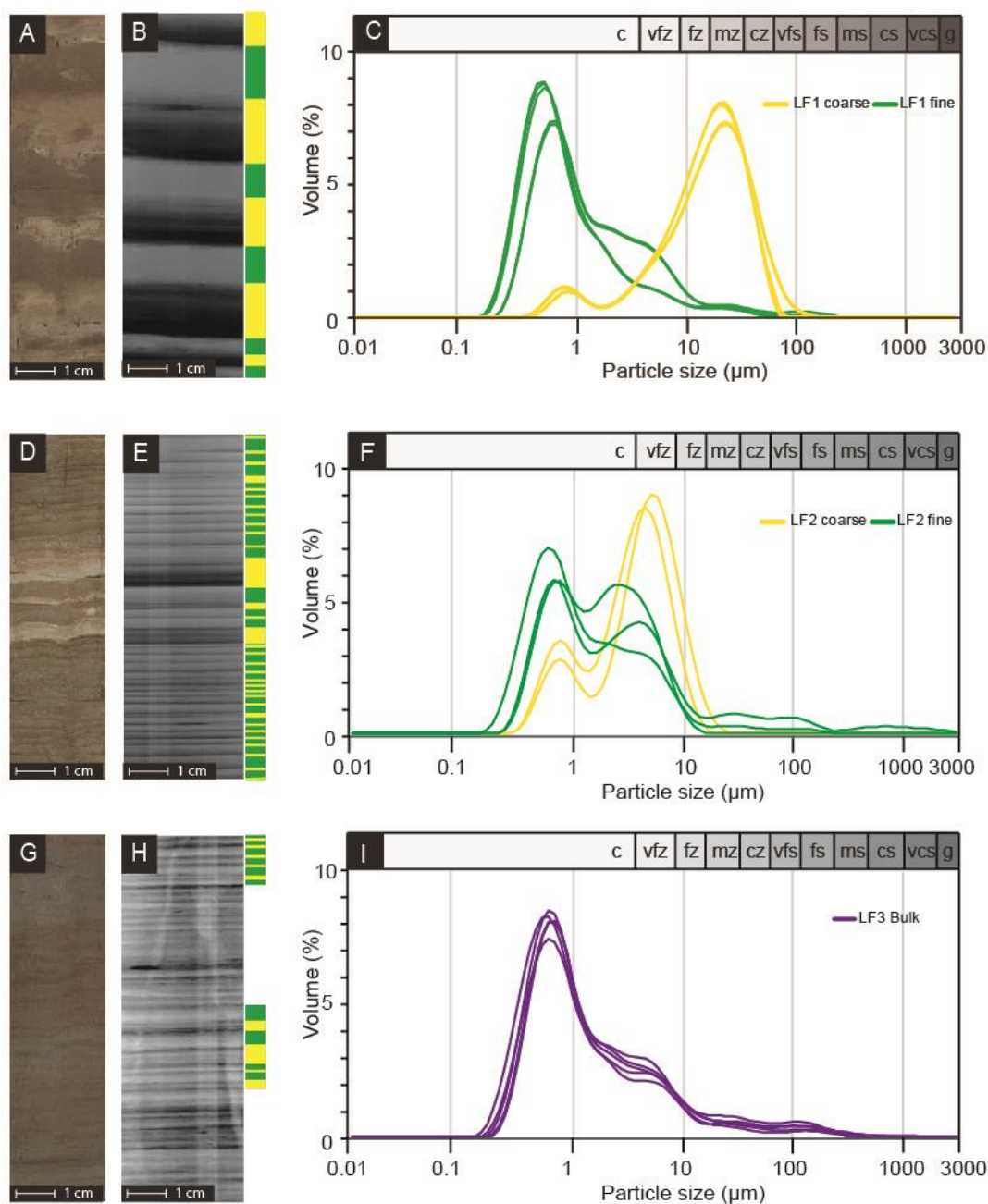


Figure 6-6. Core surface images, X-radiograph images and particle size data. Examples of clearly identifiable varve^{MAC} and varve^{XRAD} alongside particle size information in LF1 (A-C) and LF2 (D-F). The coarse (silt) component is represented by yellow boxes/curves and the fine (clay) component is represented by green boxes/curves. In LF3 (G-I), laminations appear more clearly in the X-radiograph image (H) than macroscale observations from the core surface (G) but are still less diffuse than X-radiograph images from LF1 and LF2. In LF3, boundaries between laminations are typically pixelated but on occasion clearly defined laminations punctuate the otherwise continuous sequence of pixelated laminations (H). Particle size data for LF3 are also presented (I).

6.3.1.3 LF3 (<cm-scale laminations)

These sediments appear to be laminated but boundaries between laminations are typically pixelated and unclear. This is likely due to the (200 μm) analytical resolution of the X-radiograph image that is insufficient to be able to clearly delineate laminations of a comparable thickness. There are however sections of the sequence where lamination couplets with clear boundaries punctuate the otherwise continuous sequence of diffuse/pixelated laminations that dominate LF3 (Figure 6-7).

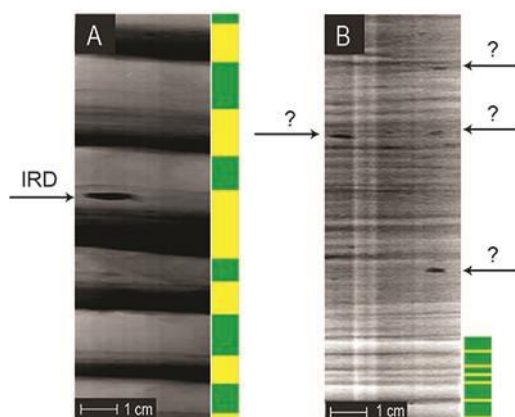


Figure 6-7. Examples of anomalously large grains in LF1 and LF2 observed from X-radiographs. (A) Larger grains in LF1 interpreted as IRD. (B) Larger grains in LF2 interpreted as either IRD or aeolian deposits as indicated by a question mark. Yellow boxes highlight coarse-grained and green boxes highlight fine-grained laminations.

Since the structures recorded in the X-radiographs broadly mirror those identified in LF1 at the macroscale, varve counts were conducted from X-radiographs. Particle size analysis was also used to verify grain size interpretations. It is recognised that varves cannot be defined using only X-radiograph images and so macroscale inspections of the cores were, to some extent, used to guide the X-radiograph varve counts.

6.3.2 Varve^{XRAD} chronology

This section presents a varve^{XRAD} thickness record based on the X-radiograph criteria for the definition of varve boundaries at Svinstadsjön (section 5.5.1.1). Overlapping X-radiograph images were aligned in Adobe PhotoshopTM using prominent marker layers such as extremely thick varves and disturbed zones as ‘pinning points’ (e.g. Lamoureux, 2001; Palmer *et al.*, 2010; Bendle *et al.*, 2017). Sediment depths were used as a final means of linking cores if prominent marker layers were not present. Core overlap details are presented in the appendices. Varve^{XRAD} thickness measurements were conducted on each individual X-radiograph image. To form a composite chronology, mean varve

thickness measurements were calculated for each varve using repeat measurements between overlapping X-radiograph core images.

Within LF1-3, 31 small breaks were identified and categorised. The same categories were used for breaks identified from X-radiograph images as for breaks identified at the macroscale: 1) deformed varves; 2) silt massive sediments; and 3) pixelated/unclear lamination couplets (Table 6-4). Breaks in the varve^{XRAD} sequence due to deformed laminations appear only in LF1 whereas breaks due to unclear/pixelated laminations occur in LF2 and LF3. After analysis of X-radiograph images the silt massive beds identified during macroscale analysis (Beds 2, 3 and 4), appeared to be extremely thick (dark) silt layers which have a sharp contact to a succeeding (grey) clay lamination. As a result, Beds 2, 3, and 4 were re-interpreted as extremely thick varves measuring 20.13 cm, 10.43 cm and 11.42 cm respectively (Figure 6-8). The stratigraphic arrangement of breaks in the varve^{XRAD} record are displayed alongside a site varve^{XRAD} chronology in Figure 6-8.

Table 6-4. Summary of breaks in varve^{XRAD} sedimentation.

Lithofacies	Depth (cm)	Type of break			
		Deformation	Silt massive bed	Unclear lamination couplets	Total
LF1	900-410	3	0	2	5
LF2	410-153.5	0	0	18	18
LF3	153.5-74.5	0	0	8	8
	Total	3	0	28	31

In total 488 varves^{XRAD} and 31 sections of non-varved sediment were identified from X-radiograph images. The varve^{XRAD} thickness characteristics of the Svinstadsjön record are presented for each lithofacies (Table 6-5). The varve^{XRAD} thickness record is divided based on lithofacies units 1-3 however, there are thickness variations within each unit (see appendices for varve thickness characteristics for each 100 cm). In LF1 there are 257 varves^{XRAD} with an average thickness of 18 mm. The average thickness, however, decreases from 19 mm to 17.4 mm from base to top of the unit. It is important to note the occurrence of three extremely thick varves^{XRAD} between 440-500 cm that inflate mean varve^{XRAD} thickness within LF1. The ratio of coarse to fine laminations remains constant at approximately 2:1, except for varves^{XRAD} in 500-600 cm which have a ratio of 1:2. The minimum varve^{XRAD} thickness measurement in LF1 is 4.1 mm with a maximum of 201.3 mm. In LF2, there are 197 varves^{XRAD} with an average thickness of 7.5 mm. The average thickness decreases from 7.5 mm to 5.5 mm from base to top of the unit. Melt season layers are typically thinner than non-melt season layers but can be approximately equal. The ratio of coarse to fine laminations fluctuates between 1:2 and

1:1 throughout this unit. Finally, in LF3, 34 varves^{XRAD} were identified which have an average thickness of 5.5 mm. Melt season layers are approximately equal to, or thinner than non-melt season layers.

Table 6-5. Summarised varve^{XRAD} thickness characteristics in each lithofacies.

Lithofacies	Depth (cm)	Varve number	Varves (n)	Mean (mm)	St dev	Min (mm)	Median (mm)	Max (mm)	Coarse:Fine
LF1	900-410	1-257	257	18	8.59	3.40	15.18	48.20	2:1
LF2	410-153.5	258-454	197	7.5	5.14	1.45	6.00	33.25	1:1
LF3	153.5-74.5	454-488	34	5.5	2.29	2.60	4.80	12.90	1:2

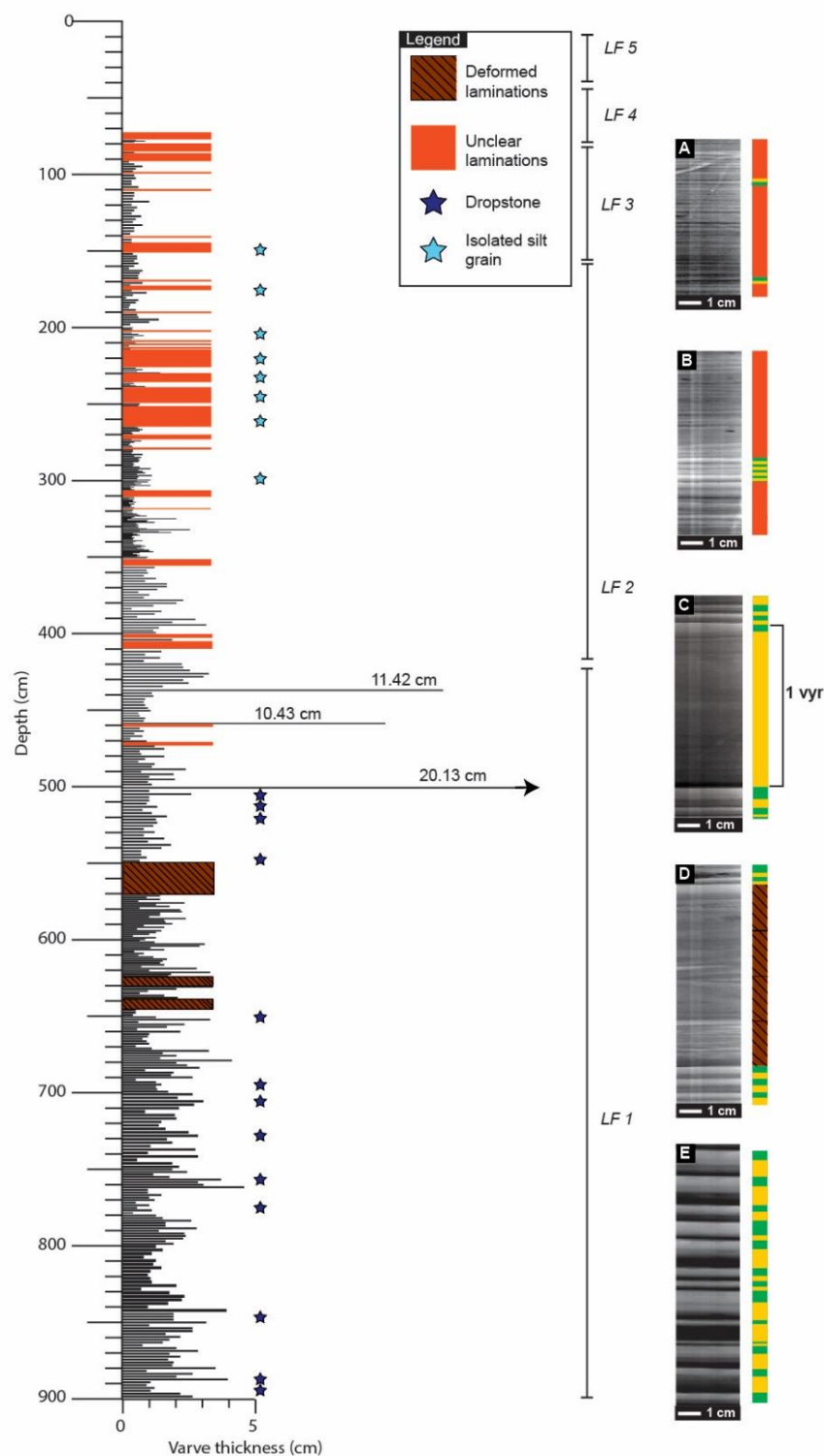


Figure 6-8. X-radiograph images and varve^{XRAD} thickness plotted against depth. Extremely thick varves are labelled alongside their thickness. Bars for the three extremely thick varves^{XRAD} are not to scale. Breaks in site varve^{XRAD} series indicate sections with deformed or pixelated laminations. Dark blue stars indicate IRD and light blue stars indicate anomalously large grains that cannot be attributed as IRD due to their occurrence within unclear laminations. Yellow boxes highlight coarse-grained laminations and green boxes highlight fine-grained laminations. (A) Examples of X-radiograph images from LF3. Occasional clear laminations interrupt continuous pixelated laminations. (B) Example X-radiograph image from LF2 depicting unclear laminations. (C) Example of an extremely thick varve^{XRAD}. (D) Deformed laminations in LF1, Bed 1. (E) Clearly laminated \geq cm-scale thickness varves^{XRAD} in LF1.

6.4 μ XRF analysis

This section uses μ XRF data and builds on macroscale description and interpretation of the laminated sediments as varves focussing on: 1) selection of key elements for log ratio calculations; 2) determining if log-ratio plots can be used as a proxy for grain size changes within and between laminations; 3) description of varve^{XRF} structure; and 4) construction of a varve^{XRF} chronology.

6.4.1 Pre-analysis data treatment

Prior to analysis of μ XRF data, varves with fewer than 3 measurements per seasonal lamination were removed from the dataset, equating to 25.3% of the total measurements (2,558 of 10,093 measurements) and measurements with zero values were also removed. The element intensities of Ca, Cu, Fe, K, Mn, Pb, Rb, Si, Sr, Ti, Zn, Zr were taken forward for analysis.

6.4.2 Multivariate analysis and grain size estimation

Since the main purpose of μ XRF analysis in this research is for grain-size estimation and generation of varve counts, it was necessary to determine which elements explain the variation within the dataset. Figure 6-9 shows the result of PCA of the μ XRF data with the primary component, PC-1, plotted against component PC-2. The first three components explain more than 88.8% of the total variability: PC-1 – 61.6%, PC-2 – 17.8%, PC-3 – 9.5% and the results suggest a strong signal from PC-1. The PCA bi-plot shows that K, Ti, Fe, Rb, Zr and Sr are located along the positive direction of PC-1 and Ca, Mn and Si in the negative direction.

Several authors have demonstrated that certain elements are enriched in specific grain-size fractions. In the Svinstadsjön sequence, both Fe and Rb are positively correlated with PC-1 and this may reflect a higher clay content. For example, Rb tends to display strong sorption to clay minerals (e.g. Oldfield *et al.*, 2003; Boës *et al.*, 2011; Kalugin *et al.*, 2013), and Cuven *et al.* (2010) describe elevated concentrations of Fe in the clay component of clastic varves. However, Zr also shows a positive correlation (0.45) with PC-1 but is typically concentrated in the silt and sand fractions of lacustrine environments (e.g. Oldfield *et al.*, 2003; Kalugin *et al.*, 2013). At Svinstadsjön, Sr, Ti, and Zr are also positively correlated with PC-1 alongside elements that are typically enriched in the clay fraction (Fe, K, Rb), but Kalugin *et al.* (2013) and Alexandrin *et al.* (2018) found the coarse component of clastic varves in Siberia to be enriched in Sr, Ti and Zr. In the Svinstadsjön sequence, Ca and Si, which are located along the negative direction of PC-1 can be enriched in either the clay or the sand-size fraction (e.g. Cuven *et al.*, 2010; Balascio *et al.*, 2011; Moreno *et al.*, 2011).

The results from PCA suggest that the relationship between grain size and the chemical composition of the laminated sediments at Svinstadsjön is not straightforward. This is exemplified in the PCA biplot where measurements from clay (green dots) and silt/sand (yellow dots) are widely spread across the vector space (Figure 6-9). Therefore, it is not possible to associate every element to a specific grain size fraction, but those elements with the strongest correlation with PC-1 could be related to sediment grain size. Table 6-6 summarises the environmental interpretations of key elements and their correlation with PC-1.

Table 6-6. Summary of key μ XRF elements and correlation with PC-1. Environmental interpretations from published literature are also presented. Modified from Davies et al. (2015).

Element	Correlation with PC-1	Environmental interpretation (higher values)	Reference
Ca	-0.99	Derived from plagioclase increased allochthonous lithoclastic material	Balascio <i>et al.</i> (2011)
Si	-0.28	Derived from quartz in clay or sand layers	Cuven <i>et al.</i> (2010); Moreno <i>et al.</i> (2011)
Sr	0.18	silt/sand	Kalugin <i>et al.</i> (2013)
Ti	0.19	silt/sand, increased glacial meltwater, silt-rich facies, clay-rich sediment, fine-grained detrital material, aeolian deposition	Cuven <i>et al.</i> (2010); Martin-Puertas <i>et al.</i> (2012); Czymzik <i>et al.</i> (2013); Kalugin <i>et al.</i> (2013); Bakke <i>et al.</i> (2009)
Zr	0.45	Coarse silt and sand	Oldfield <i>et al.</i> (2003); Cuven <i>et al.</i> (2010); Kalugin et al, (2013)
K	0.09	Derived from orthoclase, clay-rich layers in varved sediments, fine-grained detrital inputs	Cuven <i>et al.</i> (2010); Kylander <i>et al.</i> (2011)
Fe	0.80	Present in most clay minerals and associated with clay-rich sediments	Cuven <i>et al.</i> (2010)
Rb	0.77	Low environmental mobility owing to strong adsorption to clay minerals	Boës <i>et al.</i> (2011); Kylander <i>et al.</i> (2011)

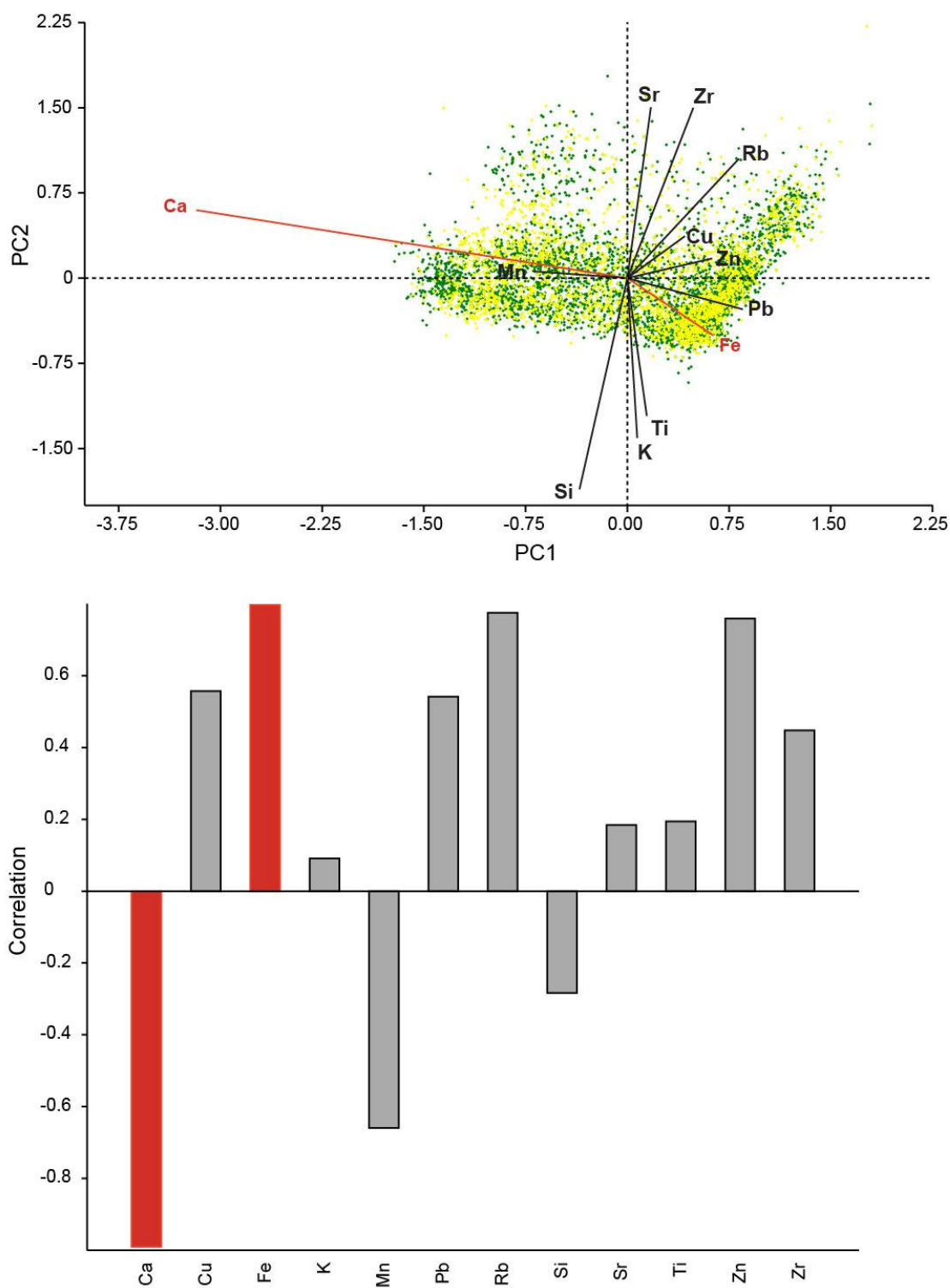


Figure 6-9. Principal Component Analysis (PCA) of μ XRF data.

(Top) PCA biplot of μ XRF data from Svinstadsjön. Primary component PC-1 plotted against PC-2. Ca and Fe display a similar direction along PC-1 and are highlighted in red. Data points from coarse-grained sediment are yellow and those from fine-grained sediments are green. (Bottom) PC-1 loadings, Ca and Fe are highlighted in red and display the strongest correlations with PC-1 (Ca: -0.99, Fe: 0.80).

Following PCA, two elements, one with negative correlation and one with positive correlation with PC-1, were chosen for log ratio calculation to be used as a grain size proxy. However, there are no set rules that determine which elements to use, or which element should be the numerator and which element the denominator (Weltje and Tjallingii, 2008). This is primarily due to site-specific factors that influence the chemical composition of sediments such as bedrock geology, organic content, and catchment weathering (Davies *et al.*, 2015). Nonetheless, changes in lake sediment grain-sizes have been inferred from several elemental ratios such as Ti-K (increase = larger grain size; e.g. Marshall *et al.*, 2012) and Zr/Rb (increase = smaller grain size; e.g. Kylander *et al.*, 2011). In glaciolacustrine varve studies, the ratios of K/Ti, Zr/Rb and Ca/Fe have been used as a varve counting tool (Cuven *et al.*, 2010; MacLeod *et al.*, 2011; Muschitiello *et al.*, 2016). However, the ratio of K/Ti proved unreliable at Svinstadsjön since K and Ti are both positively correlated with PC-1. In addition, the ratio of Zr/Rb also proved unreliable even though Zr is typically associated with the coarse fraction and Rb with clay-rich sediments. This is likely because both elements are also positively correlated with PC-1. At Svinstadsjön, the element with the strongest negative correlation with PC-1 is Ca (-0.99), and the element with the strongest positive correlation is Fe (0.80). These elements therefore drive the greatest variability within the dataset, demonstrating their suitability for grain size estimation. Therefore, the log ratio of Ca/Fe was calculated for each μ XRF measurement and plotted against depth. Particle size data were used to verify grain size interpretations from $\ln(\text{Ca/Fe})$.

The $\ln(\text{Ca/Fe})$ data were used for varve^{XRF} identification with peaks observed in the coarse component and troughs in the fine component. The coarse component is likely enriched in Ca due to the presence of plagioclase and orthoclase, whereas the fine component is enriched in iron since most clay-bearing minerals are iron-rich. However, the results were inconsistent throughout the Svinstadsjön sediment sequence. After initial analysis, the $\ln(\text{Ca/Fe})$ profile appears to mirror varve structure in LF1 where varves are \geq cm-scale. However, in LF2 and LF3 where varves are $<$ cm-scale, the $\ln(\text{Ca/Fe})$ peaks are inconsistent. This is likely due to the number of μ XRF measurements per lamination afforded by 500 μ m resolution in LF2 and LF3 (Figure 6-11). Nevertheless, a site varve^{XRF} chronology was constructed and is presented in the following section.

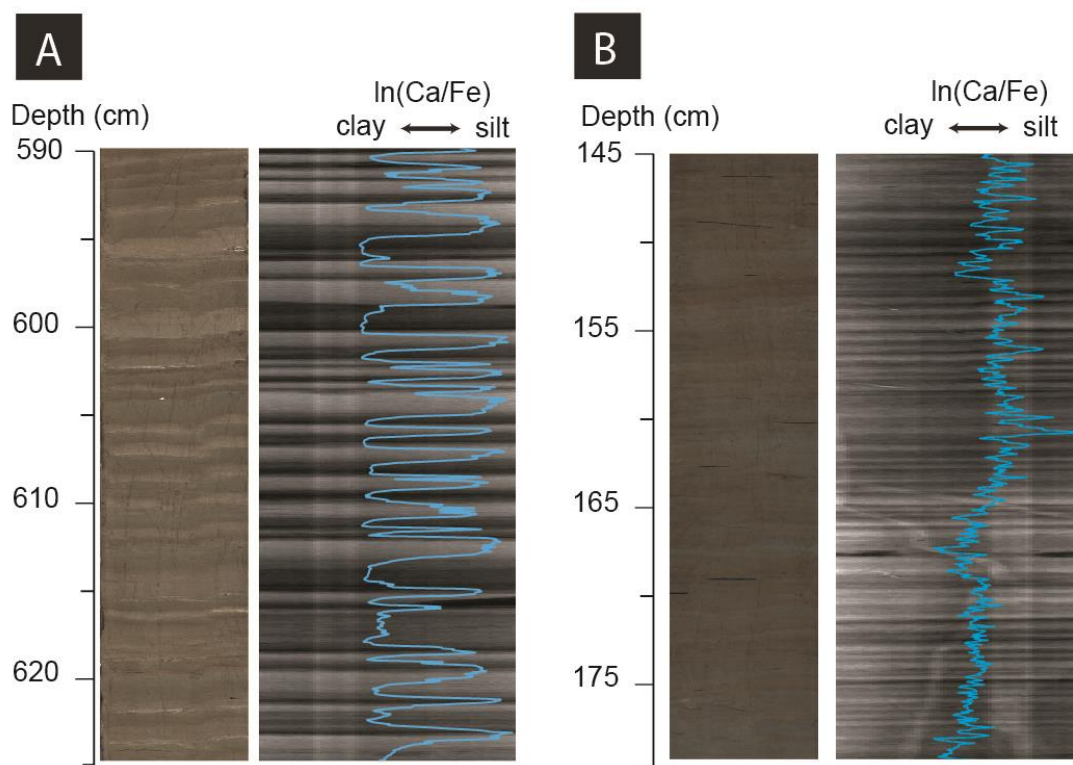


Figure 6-10. Core surface images with corresponding X-radiographs and μ XRF $\ln(\text{Ca}/\text{Fe})$ data. Example $\ln(\text{Ca}/\text{Fe})$ plots overlay on X-radiograph images from LF1 (A) and LF2 (B) with core surface images. (A) $\ln(\text{Ca}/\text{Fe})$ profile shows a peak in the coarse/dark laminations and a trough in the fine/light laminations. (B) $\ln(\text{Ca}/\text{Fe})$ profile is indistinct in LF2.

6.4.3 Varve^{XRF} chronology

This section presents a varve^{XRF} thickness record based on μ XRF criteria for the identification of varve boundaries at Svinstadsjön (section 5.5.2.3). Individual varve chronologies were produced for each 100 cm core and overlain on X-radiograph core images. A composite varve^{XRF} chronology was produced by averaging varve^{XRF} thickness for each varve across overlapping cores using X-radiograph core images as a guide.

Within LF1-3, 37 breaks were identified and categorised (Table 6-7). Two categories were identified from μ XRF $\ln(\text{Ca}/\text{Fe})$ data and used to classify breaks in varve sedimentation: 1) varves with fewer than 3 measurements per seasonal lamination; and 2) sections of the μ XRF $\ln(\text{Ca}/\text{Fe})$ profile with a “flat-line” structure that tend to occur in zones of deformed sediments. Breaks due to a ‘flat line’ μ XRF $\ln(\text{Ca}/\text{Fe})$ profile appear only in LF1 in zones of deformation whereas breaks due to thin varves with fewer than 3 μ XRF measurements occur in LF2, and varves were not identified in LF3. The stratigraphic arrangement of breaks in the varve^{XRF} record are displayed alongside a site varve^{XRF} chronology in Figure 6-11.

Table 6-7. Summary of breaks in varve^{XRF} sedimentation.

Lithofacies	Depth (cm)	Type of 'gap'		
		Flat line	Varves with fewer than 3 measurements per lamination	Total
LF1	900-410	3	1	4
LF2	410-153.5	0	27	27
LF3	153.5-74.5	0	6	6
	Total	3	34	37

In total 336 varves^{XRF} and 37 sections of non-varved sediment were identified from μ XRF analysis. The varve^{XRF} thickness characteristics of the Svinstadsjön record are presented for each lithofacies (Table 6-8). Thickness characteristics in each 100 cm are included in the appendices. The varve^{XRF} thickness record is divided based on lithofacies units 1-3, however it was not possible to count any varves in LF3. This is because the coarse components in LF3 are often <1 mm thickness resulting in a maximum of 1 μ XRF data point per lamination. Similarly, considerably fewer varves were observed in LF2 and LF1 than from macroscale analysis.

Table 6-8. Summarised varve^{XRF} thickness characteristics in each lithofacies.

Lithofacies	Depth (cm)	Varve number	Varves (n)	Mean (mm)
LF1	900-410	1-252	252	15.8
LF2	410-153.5	252-336	84	8.8
LF3	153.5-74.5	N/A	0	N/A

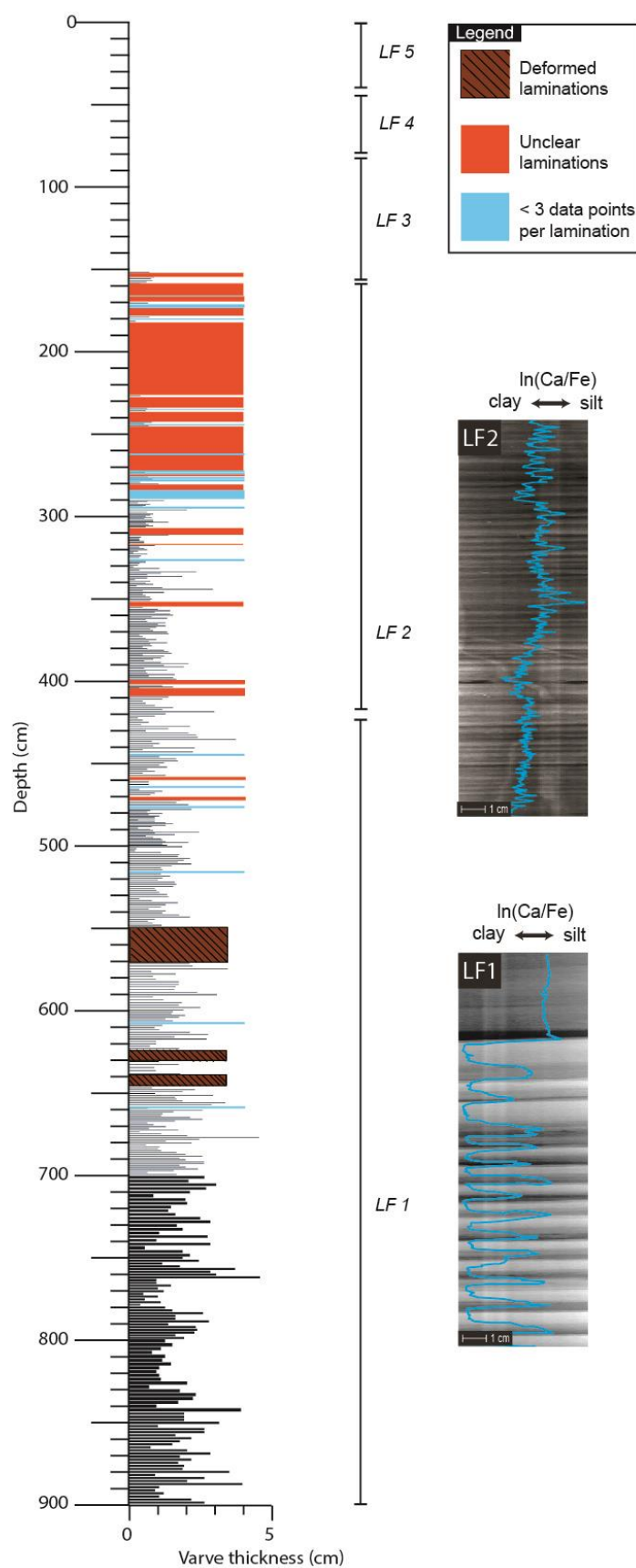


Figure 6-11. Varve^{XRF} thickness record with example μ XRF In(Ca/Fe) plots from LF2 and LF3. Breaks in varveXRF sedimentation are also highlighted in orange and blue.

6.5 Thin section analysis

This section uses thin section analysis and develops macroscale description and interpretation of the laminated sediments as varves. Thin section analysis has enabled: 1) further (micro)sedimentological description of the laminated sediments through identification of discrete Lamination Types; 2) description of key Lamination Sets; 3) interpretation of varve^{TSA} sedimentation; 4) refinement of varve identification criteria; and 5) construction of a varve^{TSA} chronology. The sediments were described using a microfacies approach and individual laminations were classified by their microscale sediment characteristics (e.g. Brauer, 2004; Palmer *et al.*, 2010, 2012, 2019; Bendle *et al.*, 2017). The descriptive terminology follows the protocol outlined by Palmer *et al.* (2019). The term “couplet” is avoided when discussing the microscale properties of the sediments since individual coarse component laminations may contain more than one Lamination Type (LT) at the microscale. Lamination Types are coded by roman numerals. Repeating packages of Lamination Types are referred to as Lamination Sets (LS) (Palmer *et al.*, 2019) and are coded alphabetically. Following the identification of discrete Lamination Types and sets, sediment process interpretations are proposed which include the relative timing of sediment transport and deposition to the lake floor. Using lamination characteristics, including lamination thicknesses, Lamination Sets are interpreted as varves. In Chapter 11 Lamination Sets are categorised into “Lamination Set Assemblages” that relate to specific parts of the lake basin (Palmer *et al.*, 2019).

6.5.1 Microscale description of the laminated sediments in LF1-3

Microscale sediment description of the laminated sediments combines microfacies and particle size data. The sequence is characterised by distinct alternations between coarse (silt) components that can contain one or multiple laminations types, and fine (clay) components that are normally graded from very fine silt to clay. Lamination Types identified within the Svinstadsjön sequence are presented in Table 6-9.

Table 6-9. Sedimentological properties of the Lamination Types (LT) observed in the microfacies of the glaciolacustrine sediments within the Svinstadsjön sequence.

Descriptions follow the format of Palmer et al. (2019). *asterisks denotes laminations types that are not identified by Palmer et al. (2019) and are unique to the Svinstadsjön record.

C = clay; VFZ = very fine silt; FZ = fine silt; MZ = medium silt; CZ = coarse silt; FS = fine sand. Ma = massive; NGr = normally graded. WS = well sorted; MS = moderately sorted; PS = poorly sorted. Sh = sharp; Gr = gradational. Dg = dropgrain; In = intraclast; WD = well-developed.

Lamination Type (LT)	Grain size (dominant)	Structure	Sorting	Upper Contact	Other
i	VFS/FS	Ma	WS	Sh	In/Dg
v	VFS/FS-MZ	NGr	WS	Sh	Dg
vi	VCZ-MZ	NGr	WS	Sh	Dg
vii	CZ-MZ	NGr	WS	Sh	Dg
viii	CZ-MZ	Single grain alternations	WS	Sh	Dg
ix	CZ/MZ-FZ/C	NGr	WS	Sh	Dg
xiv	CZ	Ma	PS/MS	Sh	Dg
xv	MZ	Ma	PS/MS	Sh	Dg
xvi	VFZ-C	NGr (short)	WS	Sh	Masepic WD
xix*	VFZ	Ma	WS	Gr	Dg

Repeating groups of Lamination Types were also identified and classified into distinct Lamination Sets (Table 6-10). Further details on the different Lamination Types (LT), and sets (LS) are outlined in the following section.

Table 6-10. Lamination Sets identified within the Svinstadsjön sequence.

Lamination Set (LS)	Coarse-grained component LT	Fine-grained component LT
A	xix	xvi
B	xiv	xvi
C	xv	xvi
D	viii	xvi
E	vii, viii	xvi
F	i, v, ix	xvi

6.5.1.1 \geq cm-scale brown Lamination Sets in LF1

Microscale sediment analysis has enabled the detection of four distinct Lamination Sets within LF1 (LS C, D, E, F) (Figure 6-12). In LF1 97% of coarse components are internally complex containing multiple (3-10) Lamination Types that vary in grain size from fine silt to fine sand (Figure 6-12). The laminations within coarse components can be massive or normally graded, and well or moderately sorted. In LS E, a coarse silt input often caps the whole lamination after a succession of normally graded coarse and medium silt laminations. In LF1, 3% of coarse components are composed of a single lamination of

moderately sorted medium silt (LS C). Fine components are normally graded from very fine silt to clay (LT xvi) and under cross-polarised light display masepic fabrics.

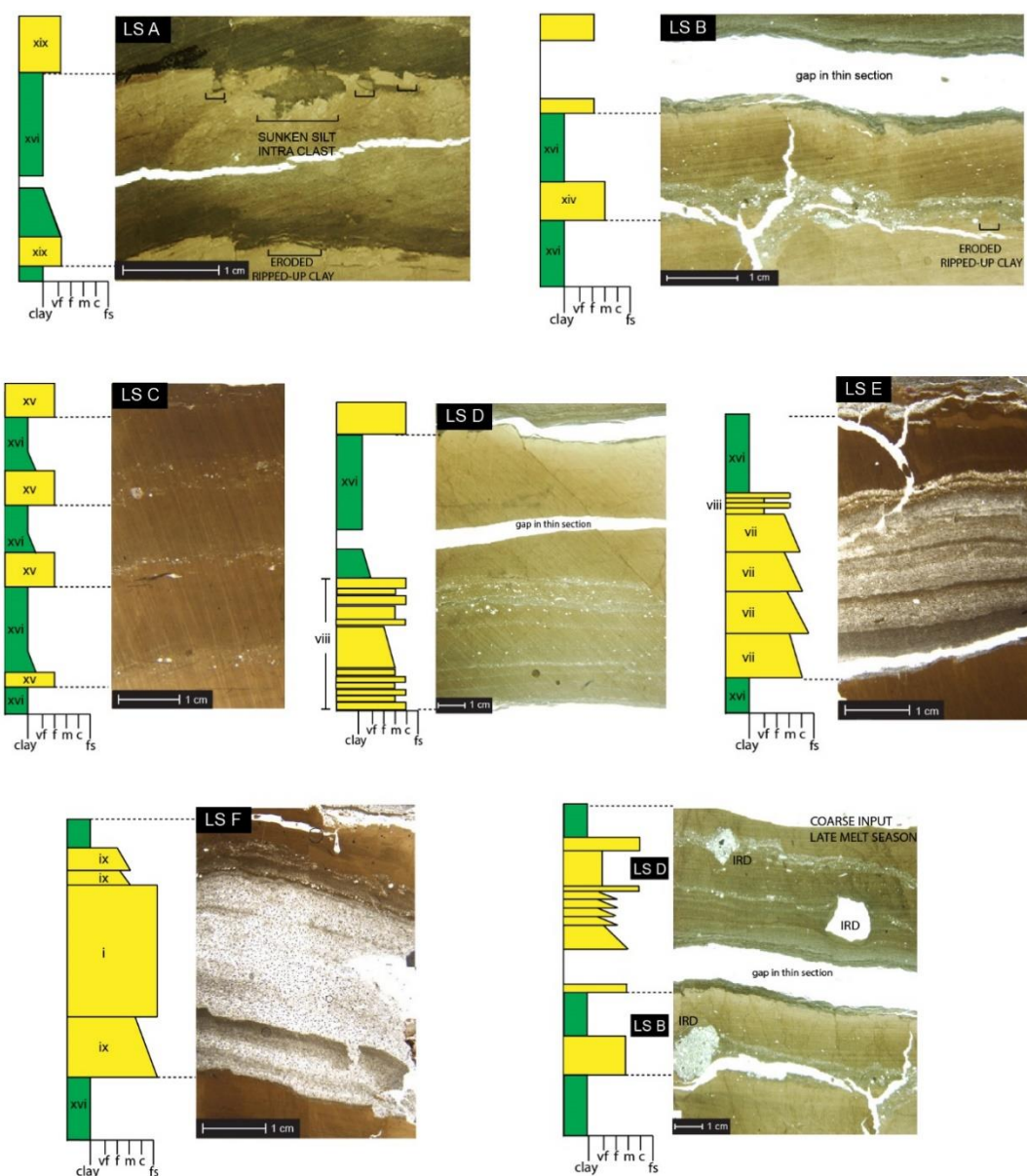


Figure 6-12 Lamination Types (LT) and sets (LS) in the Svinstadsjön sequence alongside sediment logs.

Examples of <cm-scale varves (LS A, B and C) and \geq cm-scale varves (LS D, E and F). All Lamination Sets (LS) are labelled with Lamination Types (LT) and contain a coarse-grained component (yellow) that is overlain by a fine-grained component (green). The following statements describe the coarse component only. LS A is composed of LT xix: well sorted massive very fine silt to fine silts with a sharp lower contact and a graded contact between the coarse and fine component. Pockets of silt and individual coarse silt/fine sand grains that have sunk into the underlying clay component are common. Eroded, ripped up clay is often observed in the base of the coarse component. LS B is composed of LT xiv: moderately sorted massive medium to coarse silts with occasional fine sand grains with a sharp upper and lower contact. LS C is composed of LT ix: moderately sorted, massive, fine to medium silt with occasional coarse silt grains and is typically <1 mm thickness. LS D composed of LT viii: multiple single grain alternations of massive medium silt to coarse silt laminations (continued next page)

LS E is composed of LT vii and viii: multiple graded and/or massive medium silt to coarse silt laminations with sharp upper and lower contacts. LS F is composed of LT v, i and ix: a package of multiple graded and/or massive coarse silt to fine sand laminations with sharp upper and lower contacts. Within this LS coarser inputs are observed in the late melt season. Dropstones commonly occur in the mid and late melt season of LS E and LD F and cause bending and onlap of coarse material. In all LS the fine-grained component has high birefringence under cross polarised light and is LT xvi.

6.5.1.2 <cm-scale laminated couplets in LF2

In LF2, Lamination Sets are <cm-scale and contain a single lamination in the coarse component. The coarse laminations are one of two laminations types LT xiv and LT xix. LT xiv has sharp contacts and is composed of moderately sorted massive medium to coarse silts with occasional fine sand grains with a sharp upper and lower contact. For LT xix: the contact between silt and the overlying clay lamination is gradational and therefore difficult to delineate, even at the microscale. The upper boundaries of clay components in LF2 can be eroded and occasionally have gradational lower contacts but are almost always sharp. Clasts of clay are often located towards the base of silt laminations. The fine component of each lamination set grades from very fine silt to clay and under cross-polarised light displays masepic fabrics. There are also coarse silt- to fine sand sized grains which have partially or totally sunk into the clay (e.g. Ringberg and Erlström, 1999) (Figure 6-12). Clasts of gravel to pebble size can be located in the middle or top of the coarse component and deform underlying laminations.

6.5.1.3 <cm-scale laminated couplets in LF3

Lamination Sets in LF3 are <cm thickness and the coarse component is always sharply truncated by the succeeding silt lamination. The coarse laminations are composed of well sorted fine- to very fine silt and the lamination is often <200 µm thick (LT xix) (Figure 6-12). The contact with the overlying fine component is gradational and difficult to delineate. The fine component of each lamination couplet grades from very fine silt to clay and under cross-polarised light displays masepic fabrics. Again, the top of the clay layers can show evidence of erosion, though this is not consistent throughout the lithofacies unit. Table 6-11 summarises the Lamination Sets that were identified from thin section analysis within each lithofacies unit.

Table 6-11. Lithofacies summary based on macro and microscale analyses.

Additional attributes that were identified under thin section but were not observed at the macroscale are highlighted in **bold**. Interpretation of depositional processes are presented alongside an inferred depositional environment.

Lithofacies	Lamination Sets	Attribute	Process interpretation	Environment	Reference
LF1	C, D, E, F	<ul style="list-style-type: none"> • ≥cm-scale rhythmically bedded medium silts and clays • Multiple (3-10) laminations in the coarse (silt) component • Sporadic gravel- to pebble-sized clasts • Deformed laminations e.g. folding, contorting, shearing or homogenisation of laminations • Silt rip-up intra-clasts • Boudinage and water escape features 	<p>Glaciolacustrine setting that receives silt-sized sediment from ice-proximal sediment density flows (LT B-E); fine laminations (LT A) formed from suspension settling; clasts deposited from iceberg rafting;</p> <p>Silt rip-up intra-clasts formed by subaqueous concentrated sediment density flows that are of high velocity/high sediment load and erode previously deposited material.</p> <p>Boudinage and water escape features are consistent with ductile deformation, and are likely due to sediment loading</p>	Proximal/distal glaciolacustrine	Ashley (1975); Smith and Ashley (1985); Mulder and Alexander (2001); Talling <i>et al.</i> (2012)
LF2,	A, B, C	<ul style="list-style-type: none"> • <cm-scale rhythmically bedded very fine silts and clays • Single lamination in the coarse (silt) component; either (LT F) well sorted fine/very fine silt with additional coarse silt/fine sand grains or (LT G) well sorted fine/very fine silt • Occasional ≥cm-scale lamination couplets (only in LF2a). • Sporadic granule-gravel sized clasts 	<p>Distal lacustrine setting; distal to glacier margin and distal to lake edge; silt laminations of composition (LT F) formed mostly from suspension settling of reworked sediments, but composition (LT G) are likely the result of density flows, but in a more distal location than LF1. Clay lamination deposited from suspension settling. Thicker cm-scale couplets in LF2a from one-off high velocity/high sediment load density currents. Isolated granule-gravel sized clasts consistent with IRD and aeolian deposition. Those at the base of the coarse component are likely aeolian, those in the middle/top are IRD.</p> <p>Rip-up clasts of clay formed by erosive sediment density flows</p>	Distal glaciolacustrine	Ringberg and Erlström (1999), Palmer <i>et al.</i> (2019)

Litho-facies	Lamination Sets	Attribute	Process interpretation	Environment	Reference
		<ul style="list-style-type: none"> • Clay ripped up and deposited at the base of silt laminations 			
LF3	A, B	<ul style="list-style-type: none"> • <cm-scale rhythmically bedded very fine silts and clays • Diffusely laminated (macroscale) • Sharp basal contact at the microscale • Graded contact between silt and overlying clay • Alternations between red and grey packages of laminations • Some clay laminations show erosive upper contacts 	<p>Ultra-distal lacustrine setting; distal to glacier margin and distal to lake edge; silt laminations formed from either a) sediment density underflows as evidenced by erosive upper contacts in some clay layers, b) suspension settling of reworked sediments in the water column, c) settling of aeolian sediments that form on the ice surface in the winter and fall form suspension in the early melt season. Clay lamination deposited from suspension settling.</p>	Ultra-distal glaciolacustrine	Ringberg and Erlström (1999), Palmer <i>et al.</i> (2019)

6.5.2 Deformation structures

Microfacies analysis has enabled the identification of non-varved sediments and deformation structures that were not observable at the macroscale. These include water escape features, boudinage, silt rip-up clasts, diamicton, faults, recumbent folds, silt intra-clasts and inverted varves (Figure 6-13). The location of non-varved sediments within the Svinstadsjön sequence are highlighted in (Figure 6-14).

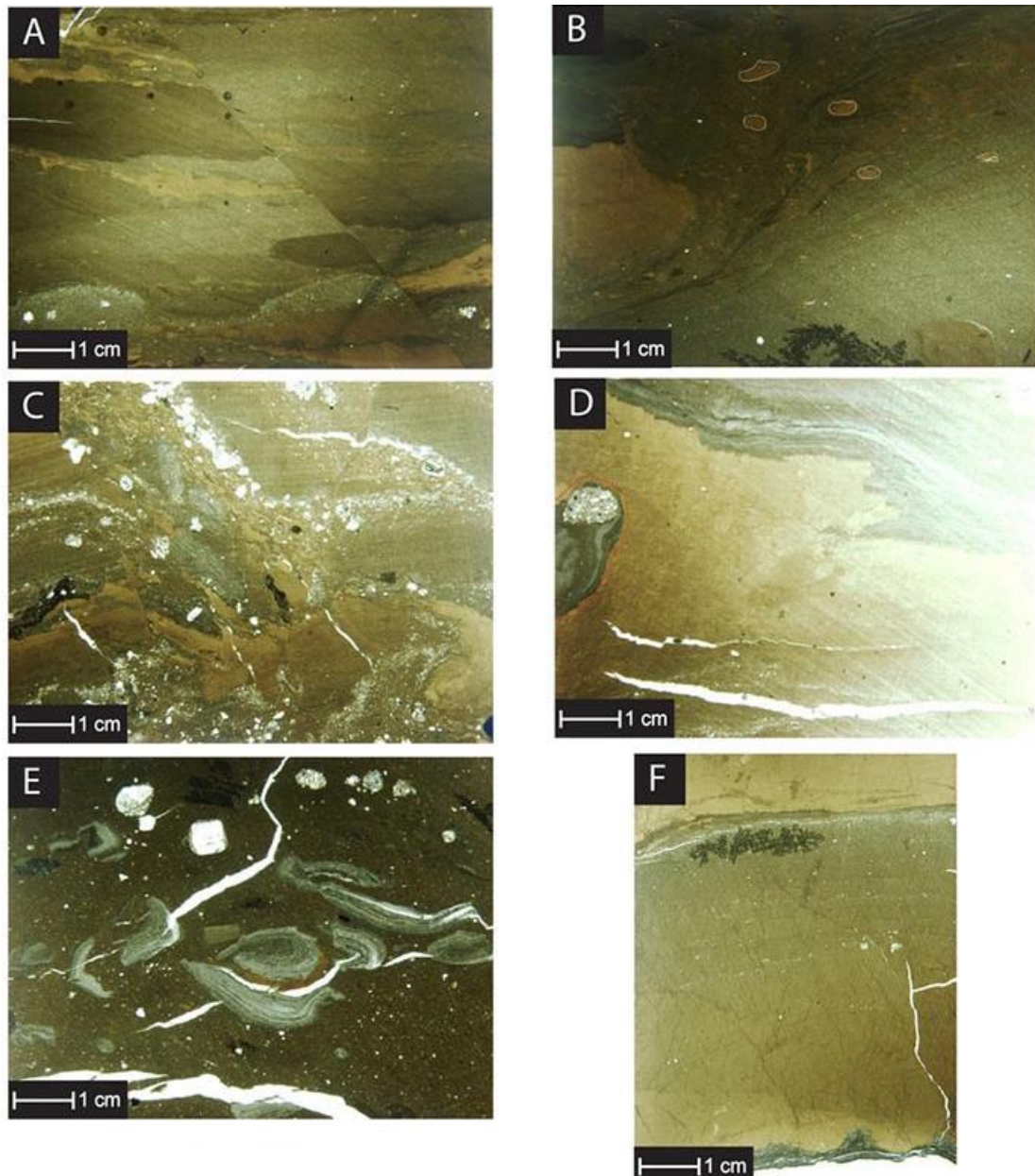


Figure 6-13. Deformation structures from LF1 observed under thin section. (A) Laminated silts and clays that display boudinage and are normally faulted at 657-660 cm. (B) Recumbent fold with pockets of ripped up clay at 550-560 cm. (C) water escape structure at 454-462 cm. (D) Silt intraclast that has sunken into the fine component of the previous clay lamination. (E) Ripped up silt laminations set within a diamicton at 796-800 cm. (F) Example of an inverted varve in a series of 8 observed at 624-629 cm that are interpreted to be part of a larger recumbent fold structure.

6.5.3 Sediment process interpretation for the Lamination Sets

This section provides an interpretation of the sediment processes for each lamination set with particular focus on whether the sediments were deposited as underflows or from suspension settling.

6.5.3.1 LF 1 (\geq cm-scale brown Lamination Sets)

The multiple sediment pulses within coarse components in LS D, E and F that exhibit sharp contacts suggest that sediment was primarily delivered to the lake basin as underflows (Mulder and Alexander, 2001). This is supported by the occasional presence of rip-up clasts within the Lamination Types (e.g. Bendle *et al.*, 2017). Sediment grain size can vary between individual sediment pulses and likely reflects several individual underflows or a single underflow with a variable sediment concentration (Ashley, 1975; Gustavson, 1975). Coarser-grained inputs often cap coarse laminations and represent the final underflows that entered the lake basin during the late melt season after settling of finer-grained material (e.g. Bendle *et al.*, 2017). Occasional larger clasts of gravel to pebble-size that deform the underlying laminations are interpreted as IRD (Thomas and Connell, 1985).

6.5.3.2 LF 2 (<cm-scale brown Lamination Sets with sharp contacts)

In LF2 the presence of clasts of clay that are often located towards the base of coarse components are likely eroded from the underlying clay lamination and redeposited as a result of current action during the melt season (e.g. Ringberg and Erlström, 1999). The fine component of each Lamination Set grades from very fine silt to clay and under cross-polarised light displays masepic fabrics and is consistent with sediment deposition during the winter/non-melt season. There are also coarse silt- to fine sand sized grains which have partially or totally sunk into the clay (e.g. Ringberg and Erlström, 1999). Grains that are sunk into clay laminations likely reflect aeolian deposits that were initially deposited on the frozen lake surface during summer/melt season but fell through the water column during the early spring after the frozen lake surface melted (Lewis *et al.*, 2002). Clasts of gravel to pebble size can be located in the middle or top of the coarse component, deform underlying laminations and are consistent with IRD (Thomas and Connell, 1985).

6.5.3.3 LF3 (<cm-scale grey Lamination Sets with diffuse contacts)

In LF3, the sharp contacts between the fine component and coarse component are consistent with a rapid switch in sedimentation style consistent with seasonal changes in sedimentation. The top of the clay layers can show evidence of erosion consistent with underflows that are associated with current action during the melt season (e.g. Ringberg and Erlström, 1999), but this is not consistent throughout the lithofacies unit. Where

erosion of clay is not evident, the coarse component is likely deposited through suspension settling of re-worked fine-grained sediments in the water column throughout the melt season/summer. Further suspension settling of clay particles occurs during the winter/non-melt season when the lake waters are still.

6.5.4 Interpretation of the Lamination Sets as glaciolacustrine varves

Thin section analysis indicates that the Lamination Sets from Svinstadsjön are typical of glaciolacustrine varves observed at the microscale (Ringberg and Erlström, 1999; Brauer, 2004; Palmer, 2005; Bendle *et al.*, 2017; Palmer *et al.*, 2008, 2010, 2019). During the winter/non-melt season the lake waters are still, and the fine-grained LT xvi is deposited via suspension settling. During the summer/melt season the coarser-grained Lamination Types are deposited either from: 1) sediment density underflows; 2) suspension settling of reworked lake-bottom sediments; or 3) suspension settling of aeolian sediments. The increased analytical resolution afforded by microfacies analysis has enabled more precise descriptions of intra-lamination structures in the varved sediments. Subsequently, additional interpretations of glaciolacustrine processes are possible at sub-seasonal scale which has led to refinement of varve identification criteria. Table 6-11 summarises the Lamination Sets that were identified from thin section analysis within each lithofacies unit.

After thin section analysis, several revisions were made to the Svinstadsjön sequence. Firstly, the dominant lithofacies units observed at the macroscale remain the same, but several microfacies were observed within each lithofacies that were not possible to describe at the macroscale. Microfacies analysis enabled description of subtle differences in texture and structure within individual laminations that provide additional insight into sub-seasonal processes.

The structures observed in LF1 are consistent with glaciolacustrine varves in a proximal-to distal location. A key difference between macroscale and thin section analysis is the number of deformation zones (1 zone in macroscale, 5 zones under thin section), and the style of deformation observed. Under thin section, there are deformation structures associated with load deformation e.g. water escape features and boudinage, and there are several deformation structures associated with slope collapse e.g. folds, faults and inverted varves. In particular, the presence of 8 inverted varves that were not observed during macroscale analysis suggests the sediments are part of a larger fold structure and were therefore omitted from varve counts.

Thin section analysis has also enabled high-resolution analysis of sub-seasonal sedimentation. There are considerably more laminations identified within the coarse

component of varves than were identified during macroscale analysis (1-3 observed at the macroscale, 3-10 observed at the microscale), suggesting that more sediment density flows reached the coring location during the melt season than macroscale analysis seems to suggest.

In LF2 the structures observed under thin section are consistent with glaciolacustrine varves though there are now two microfacies within this unit. The presence of eroded clay that has been ripped up and deposited at the base of most coarse laminations, suggests sedimentation occurred mostly via sediment underflows. However, there are instances where clay erosion is not observed and these sediments were likely deposited from settling of silts that were in suspension in the water column. Another key finding from microfacies analysis is that it is now possible to identify aeolian drop grains (coarse sand-sized) that are sunken into coarse component laminations (e.g. Ringberg and Erlström, 1999).

The structures described in LF3 such as eroded clay that has been ripped up and deposited at the base of some coarse laminations, suggests that despite glacier retreat, sediments were still occasionally reaching the coring location via sediment underflows. Additionally, the presence of sunken sand grains and sunken packages of silt within the upper parts of winter layers, suggests aeolian sedimentation in the early melt season. Another key observation is that the boundaries between fine components and succeeding coarse layers are sharp when observed under thin section, though at the macroscale, laminations appeared diffuse. These properties suggest a rapid switch in deposition style between laminations consistent with glaciolacustrine varve deposition (e.g. Ringberg and Erlström, 1999; Palmer, 2005; Palmer *et al.*, 2010; 2019 Bendle *et al.*, 2017). The fine-grained sediments (very fine silt and fine silts) that dominate the coarse components indicate sedimentation in an ultra-distal glaciolacustrine environment (e.g. Palmer *et al.*, 2019).

6.5.5 Varve^{TSA} chronology

This section presents a varve^{TSA} thickness record and chronology based on the refined criteria for the definition of varve^{TSA} boundaries at Svinstadsjön (section 5.5.3.1). A composite site varve^{TSA} chronology was produced by averaging varve^{TSA} thickness for each varve^{TSA} measurement between overlapping thin sections and cores. Prominent marker layers such as deformed zones and extremely thick varves^{TSA} were used as definitive “pinning-points” between cores (e.g. Lamoureux and Bradley, 1996; Lamoureux, 2001; Palmer *et al.*, 2010; Bendle *et al.*, 2017). In the absence of pinning-points to link cores, sediment depths were used. Thin section overlaps are provided in the appendices. Varve^{TSA} count uncertainties were quantified from two separate counts

undertaken by RD and APP. Counting errors occur in zones of low varve^{TSA} quality and were recorded as ± 0.5 year uncertainties.

Within LF1-3, nine breaks were identified and categorised. The same categories were used for breaks identified from thin sections as for breaks identified at the macroscale: 1) deformed varves; 2) silt massive sediments; and 3) unclear laminations (Table 6-12). Gaps in the varve^{TSA} sequence due to deformed laminations appear only in LF1 whereas gaps due to silt massive beds occur only in LF3. The stratigraphic arrangement of breaks in the varve^{TSA} record are displayed alongside a site varve^{TSA} chronology in Figure 6-14 and Figure 6-15

Table 6-12. Summary of breaks in varve^{TSA} sedimentation.

Lithofacies	Depth (cm)	Type of break			
		Deformation	Silt massive bed	Unclear laminations	Total
LF1	900-410	6	0	0	6
LF2	410-153.5	0	0	0	0
LF3	153.5-74.5	0	3	0	3
	Total	0	3	0	9

In total 987 ± 23 varves^{TSA} and 9 sections of non-varved sediment were identified from thin sections. The varve^{TSA} thickness characteristics of the Svinstadsjön record are presented for each lithofacies (Table 6-13). The varve^{TSA} thickness record is divided based on lithofacies units 1-3 however, there are thickness variations within each unit. Thickness characteristics in each 100 cm are included in the appendices. In LF1 there are 295 varves^{TSA} with an average thickness of 13.53 mm. The average thickness, however, decreases from base to top of the unit. It is important to note the occurrence of three extremely thick varves^{TSA} between 500-440 cm that inflate mean varve^{TSA} thickness within LF1. The ratio of coarse to fine laminations remains constant at approximately 2:1. The minimum varve^{TSA} thickness measurement in LF1 is 1.42 mm with a maximum of 171.34 mm. In LF2, there are 523 varves^{TSA} with an average thickness of 4.1 mm. The average thickness decreases from base to top of the unit. The minimum varve^{TSA} thickness measurement in LF2 is 0.68 mm with a maximum of 23.6 mm. Melt season layers are typically thinner than non-melt season layers but can be approximately equal. The ratio of coarse to fine laminations fluctuates between 1:3, 1:2 and 1:1. Finally, in LF3, 169 varves^{TSA} were identified which have an average thickness of 3.22 mm. The average thickness decreases from base to top of the unit. The minimum varve^{TSA} thickness measurement in LF2 is 1.09 mm with a maximum of 11.40 mm. Melt season layers are thinner than non-melt season layers and the ratio of coarse to fine laminations is 1:2.

Table 6-13. Summarised varve^{TSA} thickness characteristics in each lithofacies.

Lithofacies	Depth (cm)	Varve number	Varves (n)	Mean (mm)	St dev	Min (mm)	Median (mm)	Max (mm)	Coarse:Fine
LF1	900-410	1-295	295	13.56	12.83	1.42	11.12	171.34	2:1
LF2	410-153.5	296-818	523	4.09	2.86	0.68	3.32	23.60	1:1
LF3	153.5-74.5	819-987	169	3.22	1.35	1.09	2.92	11.40	1:2

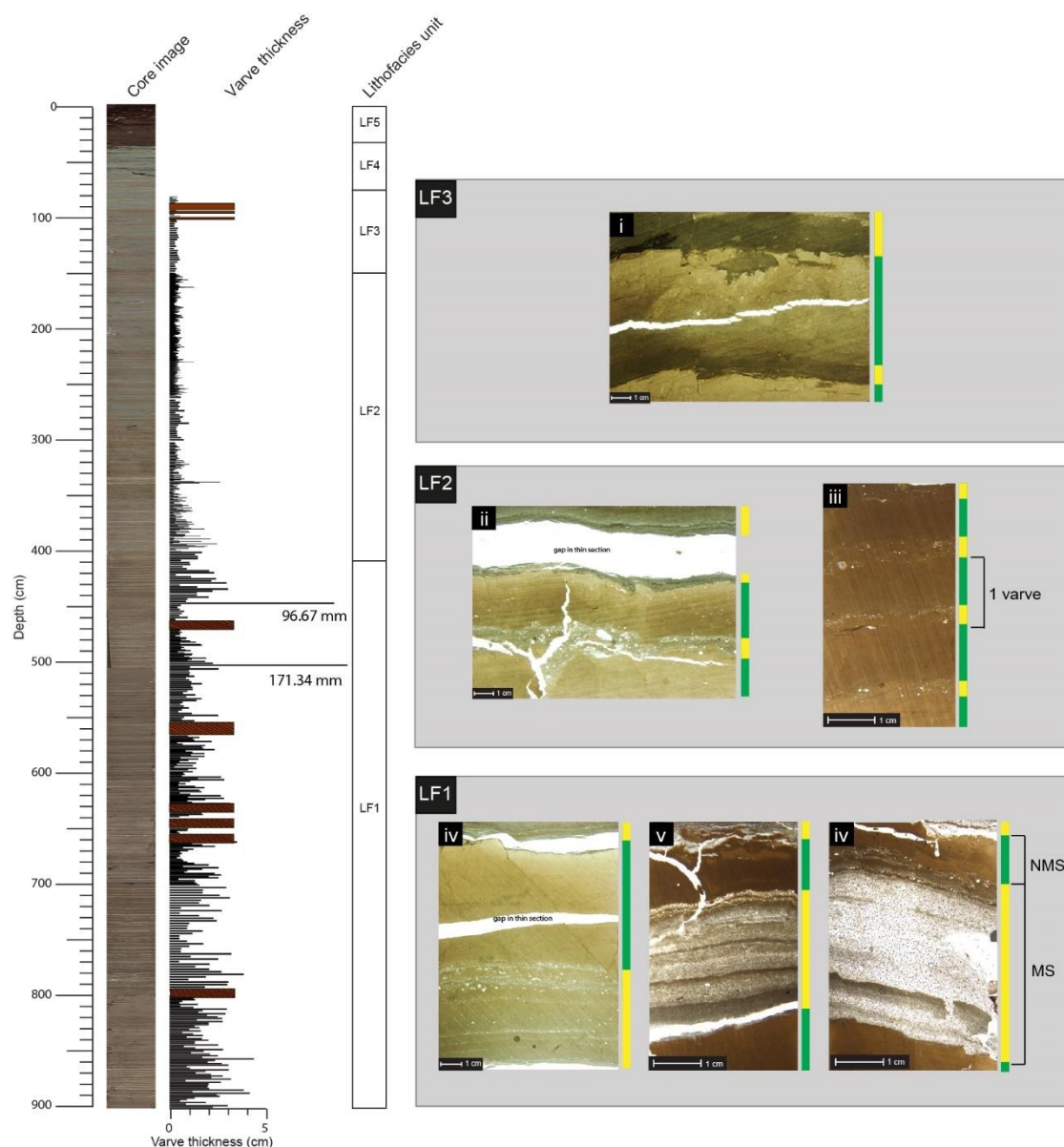


Figure 6-14. Core surface image, varve^{TSA} thickness and varve^{TSA} microfacies (i) LS A, (ii) LS B, (iii) LS C, (iv) LS D, (v) LS E and (vi) LS F. The melt season (MS) layer and non-melt season (NMS) are also labelled on LS F. Non-varved sediments are highlighted in the varve thickness graph with brown boxes.

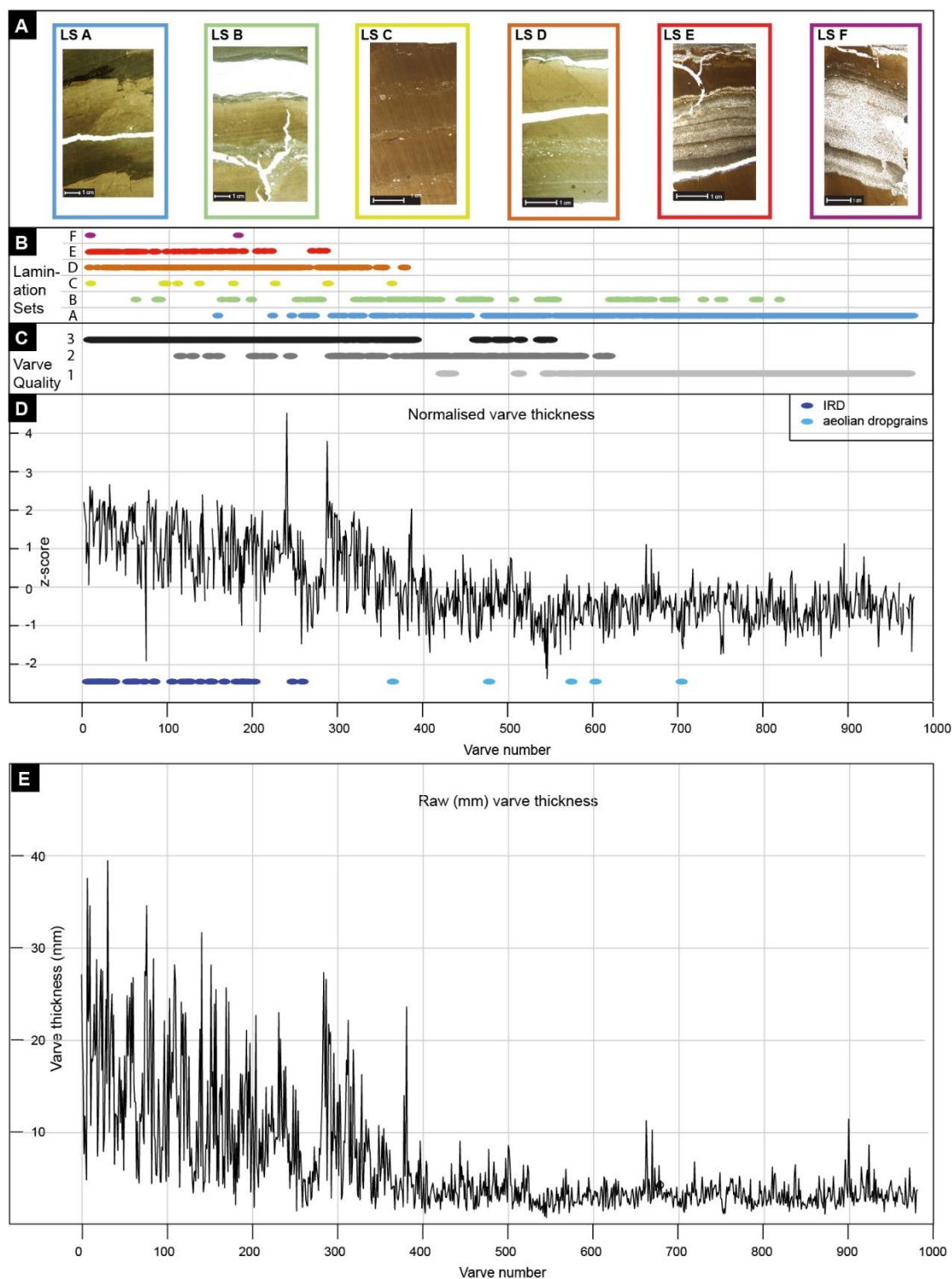


Figure 6-15. Normalised varve thickness record plotted alongside Varve Quality, Lamination Sets and occurrence of IRD/dropgrains.

(A) Varve microfacies images, (B) varve microfacies distribution throughout the sequence, (C) Varve Quality, (D) Normalised varve^{TSA} thickness record with occurrence of IRD (dark blue) and aeolian dropgrains (light blue) highlighted. The three extremely thick varves that measure 20.13 cm, 10.43 cm and 11.42 cm have been removed from the varve thickness diagram for illustrative purposes. (E) Raw (mm) varve thickness. Varve 1 is at the base of the sequence such that the diagram should be read from left to right as from base-to-top.

The basal ca 300 varves are composed of coarser-grained, multi-laminated summer components (LS D, LS E and LS F) whereas the uppermost varves are finer grained and composed of single lamination summer components (LS A, LS B and LS C). All varves were analysed under thin section and 387 (39%) were assigned a VQ score of 3, 193 (20%) were assigned a VQ score of 2, and 407 (41%) were assigned a VQ score of 1. The lower VQ scores are located in the upper part of the varve record and are typically associated with varves of Lamination Sets A, B and C (Figure 6-15).

6.6 Synthesis of varve identification and counting methods

This section provides a critical analysis of the methods that were used for varve identification and counting and concludes by suggesting a protocol that maximises varve count accuracy. Although varved sediments were either identified and/or delineated by each method, there were several differences in the data provided by each method that resulted in substantially different varve counts. To evaluate the results and develop a protocol, the results that were produced from sedimentological analysis were compared between methodologies. A qualitative approach was undertaken whereby each method was rated according to how accurately the following attributes were described: 1) varve texture; 2) varve structure; and 3) deformation zones. Table 6-14 summarises this approach including interpretations of depositional environment and varve counts. In the following sections, key differences between methods are described. Full details of the differences between each methodology are included in the appendices.

6.6.1 Differences in varve texture

There are several differences between methodologies for textural analysis of varves. From macroscale analysis three dominant grain size fractions were observed: clay, silt and fine sand, whereas at the microscale a full spectrum of grain sizes from clay to fine sand was observed: clay, very fine silt, fine silt, medium silt, coarse silt, fine sand. For X-radiograph and $\ln(\text{Ca}/\text{Fe})$ data, only relative grain sizes were derived that were later verified by particle size analysis. A key limitation of varve^{XRAD} and varve^{XRF} analyses is that neither method can identify subtle variations in grain size that are evident under thin section, nor is it possible to characterise sediment sorting. Despite descriptions of sediment sorting at the macroscale, in LF1 and LF2, some laminations that were classified as moderately or well sorted, are poorly sorted when observed at the microscale.

6.6.2 Differences in varve structure

Contacts between laminations varied by methodology and lithofacies. For $\ln(\text{Ca}/\text{Fe})$ data, it was not possible to determine the nature of contacts between laminations since the first measurement within each lamination is inconsistently positioned at the base/transition between laminations. Therefore, it is only possible to determine the chemical composition of whole laminations, rather than define the nature of contacts. This is exemplified by the μXRF PCA biplot (Figure 6-9) which shows no clear distinction between coarse-grained and fine-grained laminations across the vector space. For sediments in LF1 and LF2, contacts between fine-grained laminations and the succeeding coarse components appeared sharp when analysed by all other methodologies, however, for LF3, the contact between lamination couplets appeared diffuse at the macroscale, pixelated in X-radiographs but sharp under thin section. The diffuse/pixelated appearance of varves in LF3 is likely due to the subtle difference in grain size between exceptionally thin (<1 mm) laminations that were only visible under thin section. The diffuse/pixelated contacts in LF3 also prohibited accurate varve^{MAC} and varve^{XRAD} counts and only under thin section were accurate varve counts possible.

There were also differences in the structure of coarse component layers. At the macroscale, thin (ca 5-10 mm) graded beds were occasionally identified in coarse laminations in LF1. However, when observed at the microscale, considerably more graded beds were observed. Beds that were massive at the macroscale, were often normally graded, or contained multiple, normally graded silt beds under thin section. When analysing $\ln(\text{Ca}/\text{Fe})$ profiles, additional peaks were sometimes observed in complex coarse component layers, but results were inconsistent. As a result, varves were either over- or under-counted from $\ln(\text{Ca}/\text{Fe})$ data. In LF1 and LF2, X-radiograph and μXRF analyses permit delimitation of glaciolacustrine varve structures however, only macroscale and microscale sedimentology enable the sedimentology to be interpreted and varves to be classified as ice-proximal or ice-distal. This is because the texture and structure of coarse component layers, consistent with sediment density underflows, are only identified from traditional sedimentological analyses.

Table 6-14. Summary of the accuracy of each methodology with respect to varve description, interpretation, and number of varves counted per lithofacies unit. Varve descriptions are split by texture, structure and deformation zones and rated as either highly accurate (dark green), accurate (light green), somewhat accurate (amber) or inaccurate (red). During μ XRF analysis, fewer than 3 measurements were obtained per lamination in LF3 and so varves were not described and thus are coloured grey.

		varve ^{MAC}			varve ^{XRAD}			varve ^{XRF}			varve ^{TSA}				
LF1	Description	Texture	Structure	Deformation	Texture	Structure	Deformation	Texture	Structure	Deformation	Texture	Structure	Deformation	Highly accurate	
	Interpretation	Ice-proximal/ice distal glaciolacustrine varves			glaciolacustrine varves			glaciolacustrine varves			Ice-proximal/ice distal glaciolacustrine varves			Accurate	
	Varve count	210			257			252			295			Somewhat Accurate	
															Inaccurate
LF2	Description	Texture	Structure	Deformation	Texture	Structure	Deformation	Texture	Structure	Deformation	Texture	Structure	Deformation		
	Interpretation	Ice-distal glaciolacustrine varves			glaciolacustrine varves			glaciolacustrine varves			Ice-distal glaciolacustrine varves				
	Varve count	361			197			84			523				
LF3	Description	Texture	Structure	Deformation	Texture	Structure	Deformation	Texture	Structure	Deformation	Texture	Structure	Deformation		
	Interpretation	Ultra-distal glaciolacustrine varves, or brackish/marine varves			glaciolacustrine varves			N/A			Ultra-distal glaciolacustrine varves				
	Varve count	49			34			0			169				

6.6.3 Differences between description of non-varved sediments

There were several discrepancies between methods when describing deformation zones. Except for the deformed laminations in Bed 1 that were identified by every method (Figure 6-16), zones of deformation were identified from thin section analysis that were not identified when using any of the other methodologies. Similarly, at the macroscale, Beds 2, 3 and 4 were characterised as massive silts, however after analysis of X-radiograph images and thin sections, they were interpreted as extremely thick varves. Additionally, in LF1, a package of 8 inverted varves was also observed at the microscale and interpreted as part of a recumbent fold structure. The sediments were therefore classified as a zone of deformation and excluded from the varve^{TSA} count. The increased precision afforded by microfacies analysis enabled quantification of varve count error between methodologies. Counting errors were classified as either Type A: varves that were missed, or Type B: erroneously identified varves (e.g. Lamoureux and Bradley 1996). Varve counts were compared between methods, by depth (Table 6-15) and by lithofacies unit (Figure 6-16).

6.6.4 Varve count differences between methods

The total varve counts were considerably different between varve count methods with 619 vyrs counted from macroscale analysis, 488 vyrs counted from X-radiographs, 336 vyrs from μ XRF $\ln(\text{Ca}/\text{Fe})$ data and 987 ± 23 vyrs from thin sections (Figure 6-16). Table 6-15 details varve counts for each methodology per 100 cm.

In LF1, more varves were counted from thin sections and the fewest were counted from the open core. Between 500-600 cm 17 more varves were counted in thin section than from the open core. However, 9 fewer varves were counted in thin section than from $\ln(\text{Ca}/\text{Fe})$ μ XRF data between 700-800 cm (Table 6-15). This is due to the complexity and thickness of summer laminations which led to erroneously identified varves from $\ln(\text{Ca}/\text{Fe})$ μ XRF peaks (Type B error; Lamoureux and Bradley, 1996). Yet overall, macroscale, X-radiograph and μ XRF analyses led to under-counting of varves in LF1.

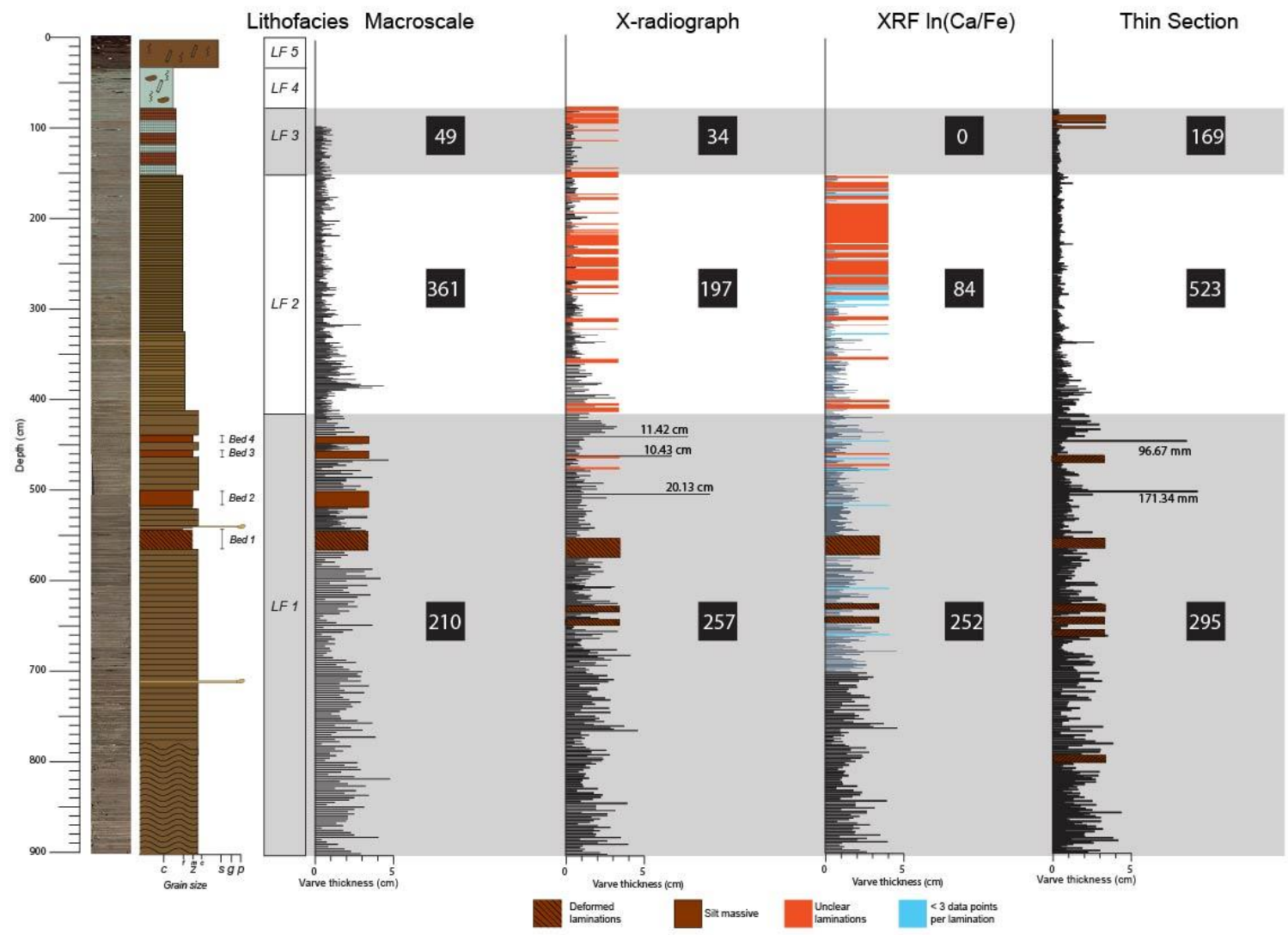
In LF2 approximately 30%, and in LF3 approximately 72% fewer varves were counted at the macroscale than from thin sections. Varves that were missed during macroscale analysis contained coarse laminations that are <1.5 mm thickness and are composed of fine silt. These characteristics made varve identification from open cores extremely difficult and explain the poor varve count accuracy achieved during varve^{XRAD} and varve^{XRF} analyses.

Table 6-15. Varve counts for each methodology per 100 cm.

Lithofacies	Depth (cm)	Macroscale	X-radiographs	μ XRF In(Ca/Fe)	Thin sections
LF1	800-900	49	50	54	71
LF1	700-800	55	54	51	42
LF1	600-700	57	59	55	64
LF1	500-600	42	50	49	59
LF1/LF2	400-500	56	50	47	66
LF2	300-400	92	103	53	141
LF2	200-300	135	60	16	279
LF2/LF3	100-200	133	50	11	251
LF3	0-100	0	12	0	14
	Total	619	488	336	987±23

Figure 6-16. Varve thickness record for each methodology alongside varve counts in each lithofacies unit.

Next page. Breaks in each varve record are highlighted and include deformed laminations, silt massive beds, zones of unclear laminations and in the varve^{XRF} record zones where fewer than 3 measurements were made per lamination. The core image is also presented alongside a sedimentary log. Extremely thick varves were identified from X-radiograph images and from thin section analysis with their thicknesses labelled. Note their thickness is not to scale in the diagram.



6.6.5 Summary and revised protocol for varve identification and counting

The results demonstrate that for accurate characterisation of the textural and structural properties of sediments, microscale analysis offers the greatest precision and accuracy. Thin section analysis ultimately leads to accurate interpretation of depositional processes and varve counts. Although macroscale analysis provides a general description of the sediments, when compared against microscale analysis, descriptions of varves can be invalidated. As such, macroscale analysis can be used to produce sediment logs and provide a minimum varve count but should not be used to generate final varve counts. Whilst varve counts from X-radiographs and μ XRF data were more accurate for \geq cm-scale varves than for $<$ cm-scale varves, overall, varve counts were highly inaccurate. In addition, despite the increased resolution from 500 μ m to 200 μ m at 700-900 cm depth, varves were either over or under-counted when using μ XRF data. Nevertheless, X-radiograph and μ XRF data provide contextual information to bolster traditional sedimentological descriptions but only when verified by thin sections.

As such the following protocol was adopted for varve description and counting and was applied to the sediment sequences at Asplången and Glottern:

- 1) Describe sediments at the macroscale and produce a sediment log
- 2) If sediments satisfy macroscale criteria for varves, count the number of varves to produce a minimum varve count
- 3) Identify key lithofacies units and zones of unclear laminations
- 4) Make targeted thin sections from each lithofacies unit and unclear laminations to verify varve origin
- 5) If varved, make thin sections throughout the rest of the lithofacies units
- 6) Derive sediment descriptions and interpretations from macroscale and microfacies analysis and produce varve count

Chapter 7. Results - Asplången

This chapter presents the results from macro- and microscale sedimentology of the laminated sediments at Asplången to understand depositional processes and develop a varve chronology for this sequence. Prior to this research, a varve chronology has been constructed from macroscale analysis of Asplången sediments (Brunnberg, unpublished), however, the results from Svinstadsjön demonstrate that it is necessary to construct a new site varve chronology using microfacies analysis of thin sections. X-radiograph images, and μ XRF data were initially used to characterise the varved sediments, however at Asplången, these methodologies proved inaccurate when compared to sediment descriptions and varve counts from thin section analysis. As such, this chapter presents sediment descriptions through integrating macroscale, microfacies and particle size evidence. Samples that cover the transition from varved to non-varved sediments were analysed for diatom and macrofossil content in order to give a broad indication of the depositional environment.

7.1 Core recovery and basin survey

Due to access restrictions, auger surveys of two areas along the southern shore of Asplången were taken. The survey results were used to map the bathymetry of the site to identify a suitable coring location (Figure 7-1). In the western auger site depth probes hit stiff blue clays at ca 1.5 m that were impenetrable except for two locations with 6 m and 10.5 m depths. At the eastern auger site sediment depths were variable. Impenetrable blue clays were also recorded, but most depth probes hit what appeared to be bedrock. The maximum sediment depth at Asplången was 12.46 m but of 32 auger locations, bedrock was only reached 10 times due to the difficulties of hand augering through stiff blue clays. It was not possible to survey further inland from the lake edge since the surrounding area is farmland or private property. It should be noted that during the original extraction of these sediments in 1997 (Brunnberg, unpublished), several cores were extracted from further out onto the lake from ice during the winter months (Brunnberg *pers. comm.*). However, this was not possible during the course of this thesis due to lack of ice cover in the winter months.

Despite these challenges, a sediment sequence was extracted from Asplången in the eastern auger site. The coring location sits within a ca 50 m² area with consistent sediment depths of between 10 m and 12.46 m. This was considered the area of the basin least likely to be prone to local slope destabilisation.

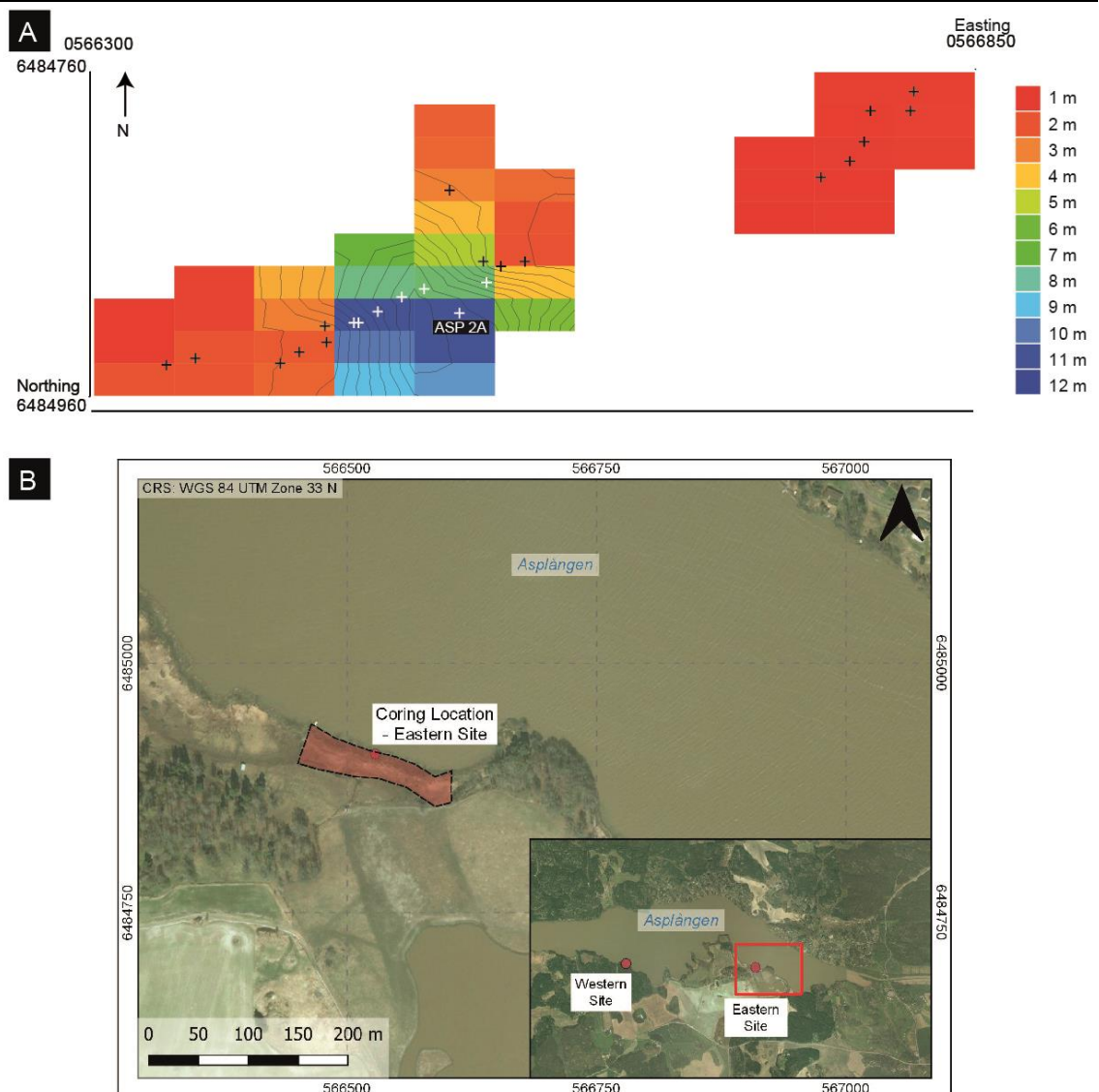


Figure 7-1. Asplången sediment depth survey and site map.

(A) Sediment depth survey of the eastern site in 2D. Black crosses mark depth probes that did not penetrate through the stiff blue clays. White crosses mark depth probes that reached bedrock. The ASP2A coring location is also marked at $58^{\circ}29'58''\text{N}$, $16^{\circ}08'27''\text{E}$. The sediment depth survey was plotted in QuickGrid. (B) Asplången site map showing the coring location in the eastern site.

7.2 Macroscale sedimentology and stratigraphy

This section focusses on the stratigraphic description of key sedimentary units and detailed sedimentological properties of the laminated glaciolacustrine sediments to determine their varved nature.

7.2.1 Sediment units

The sediment sequence is 12.46 m in length and contains 6.61 m of well-defined laminated silts and clays overlain by 0.33 m of dark blue, normally graded silty clay and 3.14 m of weakly laminated silty clay. The sequence is capped by 1.31 m of clayey silt massive, 0.27 m of brown gyttja and 0.25 m of reed peat. During depth probing, the coring rods hit a solid basal surface and when recovering the basal Russian corer, the cone of the corer turned through sands and gravel, but these were not retrieved. It is assumed that the sands and gravel have a thickness of at least 10 cm.

Seven lithofacies units were identified from the extracted sediment at Asplången: 1) brown clearly laminated couplets of silt and clay \geq cm-scale thickness; 2) brown clearly laminated couplets of silt and clay $<$ cm-scale thickness overlain by grey clearly laminated couplets of silt and clay $<$ cm-scale thickness; 3) Dark grey/blue normally graded silty clay; 4) alternating packages of reddish grey and blueish grey diffusely laminated silty clay; 5) light grey/blue clayey silt massive; 6) brown gyttja; and 7) reed peat (Figure 7-2).

LF1 (1246-895 cm) contains horizontally bedded lamination couplets of silt and clay that are \geq cm-scale thickness. Lamination couplets are composed of a 10 YR 7/1 light grey coarse lamination of medium- to coarse silt (modal grain size 20-30 μ m) overlain by a 10 YR 3/1 dark reddish grey clay lamination (Figure 7-3).

LF2 (895-585 cm) is composed of horizontally bedded laminated silt and clay couplets that are typically $<$ cm-scale. Throughout the unit, coarse laminations are composed of fine- to very fine silts. The unit is subdivided by the colour of lamination couplets. In sub-unit 2a (895-682 cm), silt laminations are 10 YR 4/3 brown and clay laminations are 10 YR 3/1 dark reddish grey. In sub-unit 2b (682-661 cm) silt laminations are 10 YR 4/3 brown but clay laminations alternate between 10 YR 3/1 dark reddish grey and Gley2 4/10BG dark greenish grey. In sub-unit 2c (661-585 cm), silt laminations are 10 YR 4/3 brown and clay laminations are exclusively Gley2 4/10BG dark greenish grey. Aside from colour, the texture and structure of lamination couplets is consistent between each sub-unit. Bed 1 (703.5-678 cm) interrupts the otherwise continuous deposition of laminated couplets in LF2 and is characterised by alternations between massive and weakly laminated silts and clays (Figure 7-3).

LF3 (585-552 cm) is a Gley2 3/5B very dark blueish grey unit of clayey silt. It has a sharp basal contact with underlying LF2 and grades from silty clay at the base to clayey silt at the top (Figure 7-3).

LF4 (552-238 cm) is composed of alternating packages of 5YR 5/0 grey and 10 YR 3/1 dark reddish grey clayey silt (Figure 7-3).

LF5 (238-107 cm) is massive clayey silt of Gley2 4/5B blueish grey.

LF6 (107-80 cm) is 10 YR 3/2 dark brown gyttja.

LF7 (80-55 cm) is 10 YR 3/3 very dark brown reed peat. The uppermost 55 cm of the sequence was not retrieved during coring due to high water content in the topsoil.

The following sections focus on the microfacies and sediment process interpretations for the laminated lithofacies (LF1 and LF2). In section 7.4 palaeoecological proxy data are presented for the transition from laminated (uppermost sediments in LF2) to non-laminated lithofacies (LF3 and LF4). Depositional processes and environmental interpretations are also presented for LF3 to LF7 by integrating macroscale sedimentology and palaeoecological proxy data. In section 7.5 a varve chronology for the Asplången is presented.

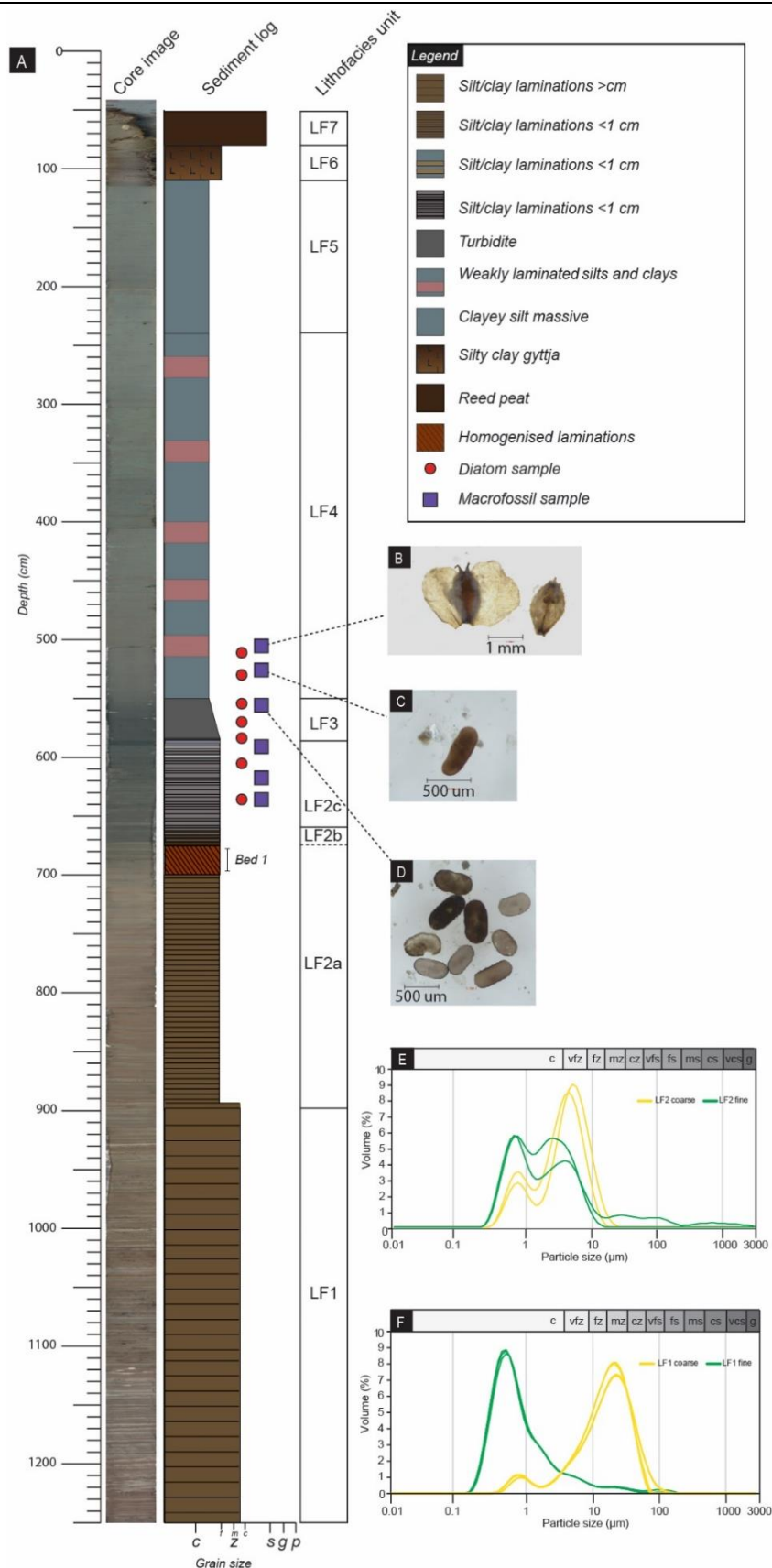


Figure 7-2. Core image, Sediment log, lithofacies units and particle size data. (A) Sediment core image and log with lithofacies units. (B) *Betula* seeds found in LF4, (C) *Herpetocypris* found in LF4, (D) *Candona* and *Herpetocypris* found in LF3, (E) particle size data for LF 2, (F) particle size data for LF 1. Yellow curves show data from the coarse lamination, green curves show data from the fine lamination.

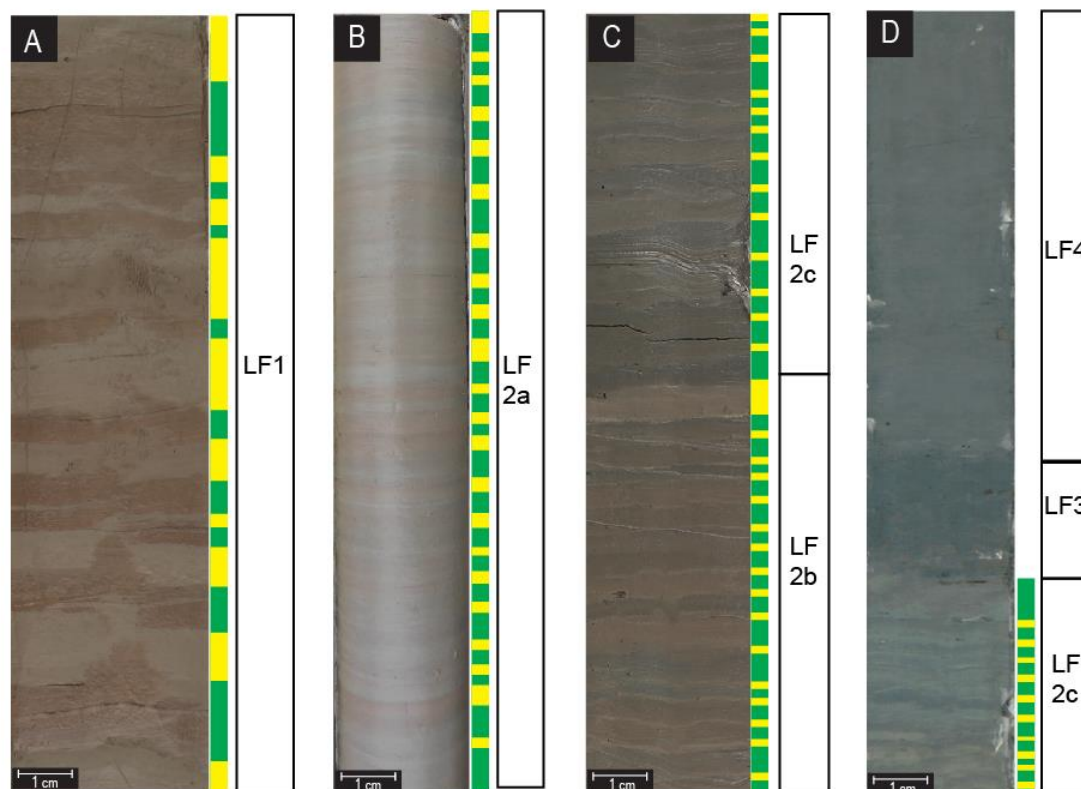


Figure 7-3. Core surface images from LF1, LF2, LF3 and LF4, particle size data for LF2 and LF3. (A) Examples of brown \geq cm-scale lamination couplets in LF1. (B) Examples of brown $<$ cm-scale lamination couplets in LF2. (C) Examples of brown $<$ cm-scale laminations in LF2b that are overlain by grey $<$ cm-scale laminations in LF2c. (D) Core 500-600 cm showing the transitions from LF2c grey $<$ cm-scale laminations to LF3 and LF4. (E) Particle size distributions for laminations in LF1. (F) Particle size distributions for laminations in LF2. Yellow = coarser-grained laminations, green = finer-grained laminations.

7.3 Sedimentology of laminations in LF1 and LF2

This section presents integration of macroscale and thin section descriptions alongside particle size data for the laminations in LF1 and LF2. Thin section analysis has enabled:

- 1) Microsedimentological description of the laminated sediments through identification of discrete Lamination Types;
- 2) description of key Lamination Sets;
- 3) interpretation of varve^{TSA} sedimentation; and
- 4) construction of a varve^{TSA} chronology.

The sediments were described using a microfacies approach and individual laminations were classified by their microscale sediment characteristics (e.g. Brauer, 2004; Palmer *et al.*, 2010, 2012, 2019; Bendle *et al.*, 2017). The descriptive terminology follows the protocol outlined by Palmer *et al.* (2019). The term “couplet” is avoided when discussing the microscale properties of the sediments since individual coarse component laminations may contain more than one Lamination Type (LT) at the microscale. Lamination Types are coded by roman numerals. Repeating packages of Lamination Types are referred to

as Lamination Sets (LS) (Palmer *et al.*, 2019) and are coded alphabetically. Following the identification of discrete Lamination Types and sets, sediment process interpretations are proposed in section 7.3.3 which include the relative timing of sediment transport and deposition to the lake floor. Using lamination characteristics, including lamination thicknesses, Lamination Sets are interpreted as varves (section 7.3.4). In Chapter 11 Lamination Sets are categorised into “Lamination Set Assemblages” (Palmer *et al.*, 2019) that relate to specific parts of the lake basin.

For both the \geq cm-scale laminations and the $<$ cm-scale laminations a silt component is overlain by a clay component. The contact between the clay laminations and the succeeding silt lamination is always sharp. Lamination Sets are subdivided based on the internal structure and thickness of the coarse component: 1) those which are \geq cm-scale with multiple laminations in the coarse component (LF1), 2) those which are $<$ cm-scale and which contain a single coarse component layer (LF2). In LF1 and the basal section of LF2 laminations are brown, whereas the uppermost laminations in LF2 are grey.

7.3.1 Lamination Types and Lamination Sets

The sequence is characterised by distinct alternations between coarse (silt) components that can contain one or multiple Lamination Types, and fine (clay) components that are normally graded from very fine silt to clay. Lamination Types identified within the Asplången sequence are presented in Table 7-1.

Table 7-1. Sedimentological properties of the Lamination Types (LT) observed in the microfacies of the glaciolacustrine sediments within the Asplången sequence.

Descriptions follow the format of Palmer *et al.* (2019). *asterisks denotes laminations types that are not identified by Palmer *et al.* (2019) and are unique to the Asplången record.

C = clay; VFZ = very fine silt; FZ = fine silt; MZ = medium silt; CZ = coarse silt; FS = fine sand. Ma = massive; NGr = normally graded. WS = well sorted; MS = moderately sorted; PS = poorly sorted. Sh = sharp; Gr = gradational. Dg = dropgrain; In = intraclast; WD = well-developed.

Lamination Type (LT)	Grain size (dominant)	Structure	Sorting	Upper Contact	Other
i	VFS/FS	Ma	WS	Sh	In/Dg
v	VFS/FS-MZ	NGr	WS	Sh	Dg
vi	VCZ-MZ	NGr	WS	Sh	Dg
vii	CZ-MZ	NGr	WS	Sh	Dg
viii	CZ-MZ	Single grain alternations	WS	Sh	Dg
ix	CZ/MZ-FZ/C	NGr	WS	Sh	Dg
xiv	CZ	Ma	PS/MS	Sh	Dg
xv	MZ	Ma	PS/MS	Sh	Dg
xvi	VFZ-C	NGr (short)	WS	Sh	Masepic WD
xix*	VFZ	Ma	WS	Gr	Dg

Repeating groups of Lamination Types were also identified under thin section and classified into distinct Lamination Sets (Table 7-2). The laminations types and sets are the same as those observed at Svinstadsjön. Further details on the different Lamination Types (LT), and sets (LS) are outlined in the following section.

Table 7-2. Lamination Sets identified within the Svinstadsjön sequence.

Lamination Set (LS)	Coarse-grained component LT	Fine-grained component LT
A	xix	xvi
B	xiv	xvi
C	xv	xvi
D	viii	xvi
E	vii, viii	xvi
F	i, v, ix	xvi

7.3.1.1 \geq cm-scale brown Lamination Sets in LF1

Microscale sediment analysis has enabled the detection of four distinct Lamination Sets within LF1 (LS C, D, E, F) (Figure 7-4). In LF1 63% of coarse components are internally complex containing multiple (3-10) Lamination Types that vary in grain size from fine silt to fine sand (Figure 7-4). The laminations within coarse components can be massive or normally graded, and well or moderately sorted. The basal contacts of laminations within the coarse component are sharp and horizontal with evidence of ripped-up silt. A single clayey-silt lamination can also cap the coarse component (LS E and LS F) and occurs after a succession of coarse-grained (coarse silt to fine sand) laminations. In LS E, a coarse silt input can also cap the whole lamination after a succession of normally graded coarse and medium silt laminations. In LF1, 37% of coarse components are comprised of a single lamination of moderately sorted medium silt (LS C). In \geq cm-scale Lamination Sets fine components are normally graded from very fine silt to clay (LT xvi) and under cross-polarised light display masepic fabrics.

7.3.1.2 $<$ cm-scale Lamination Sets in LF2

In LF2 there is a colour change from brown to grey Lamination Sets at 682 cm. There are no differences between the sediments based on microfacies descriptions apart from the distinct colour change. In $<$ cm-scale brown and grey Lamination Sets, coarse components are always sharply truncated by the succeeding clay lamination. The coarse laminations are one of two laminations types: LT xiv and LT xix. LT xiv has sharp contacts and is composed of poorly/moderately sorted coarse silts with occasional fine sand grains with a sharp upper and lower contact. LT xix has sharp contacts and is composed of poorly/moderately sorted medium silts with occasional coarse silt grains

with a sharp upper and lower contact. The upper boundaries of clay components in LF2 can be eroded and occasionally have gradational lower contacts but are almost always sharp. Unlike Svinstadsjön, there is no evidence of larger sand grains or silt clasts that are sunk into clay laminations. Isolated gravel-sized clasts that are anomalously large in comparison to the host sediment are rare. The fine component of each Lamination Set grades from very fine silt to clay and under cross-polarised light displays masepic fabrics.

7.3.2 Deformation structures

Other structures observed in \geq cm-scale Lamination Sets include occasional larger clasts that penetrate or deform the underlying laminations (Thomas and Connell, 1985), and are of pebble-size when observed at the macroscale. Diamict pellets that penetrate or deform the underlying laminations (e.g. Ovenshine, 1970) were also observed at the microscale. Bed 1 (703.5-678 cm) interrupts the otherwise continuous deposition of Lamination Sets in LF2 and is characterised by alternations between massive and weakly laminated silts and clays.

7.3.3 Sediment process interpretation for the Lamination Sets

This section provides an interpretation of the sediment processes for each Lamination Set with particular focus on whether the sediments were deposited as underflows or from suspension settling.

7.3.3.1 LF 1 (\geq cm-scale brown Lamination Sets)

Within \geq cm-scale Lamination Sets, coarse component layers display internal complexity and comprise multiple graded or massive laminations with sharp basal contacts. Multi-laminated coarse component layers are pervasive throughout \geq cm-scale Lamination Sets, and are composed of well-sorted fine, medium or coarse silt. The multiple sediment pulses within coarse components in LS D, E and F that exhibit sharp contacts suggest that sediment was primarily delivered to the lake basin as underflows (Mulder and Alexander, 2001; Talling *et al.*, 2012). This is supported by the occasional presence of rip-up clasts within the Lamination Types (e.g. Bendle *et al.*, 2017). The variable grain sizes of laminations either reflects the variable nature of several underflows entering the basin, or fluctuating sediment concentrations within a semi-continuous underflow (Ashley, 1975; Gustavson, 1975).

7.3.3.2 LF 2 (<cm-scale brown and grey Lamination Sets)

Silt clay Lamination Sets that are <cm-scale and contain a single lamination within the coarse component are always sharply truncated by the succeeding silt lamination. The coarse laminations are one of two laminations types: LT xiv moderately sorted fine- to

very fine silt with additional fine sand particles with sharp contacts, and LT xix well sorted fine- to very fine silt. For LT xix, the contact between silt and the succeeding clay lamination is gradational and indicative of sediments that have fallen from suspension in the water column. For LT xiv, the larger grain sizes and evidence of eroded and ripped up clay suggests that the sediments were transported to the lake as underflows. The upper boundaries of the succeeding clay components in LF2 can be eroded and have a gradational lower contact. Clasts of clay are likely eroded from the underlying clay layers and deposited in the lower parts of the silt layers as a result of erosion and redeposition during current action (e.g. Ringberg and Erlström, 1999). The fine component of each Lamination Set grades from very fine silt to clay and under cross-polarised light displays masepic fabrics. Anomalously large clasts located in the middle or top of the coarse component which deform underlying laminations are consistent with IRD (Thomas and Connell, 1985). A summary of the process interpretations for the laminated sediments in LF1 and LF2 is provided in Table 7-3.

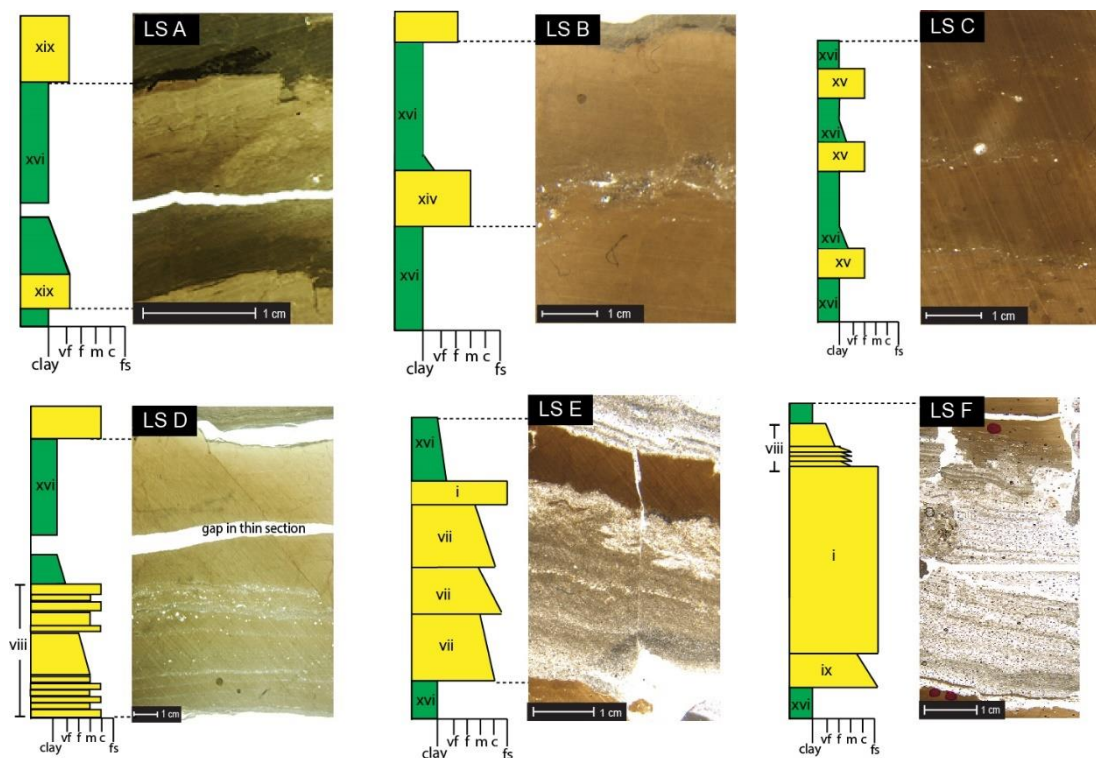


Figure 7-4. Lamination Types (LT) and sets (LS) in the Svinstadsjön sequence alongside micro sediment logs.

Examples of $< 1\text{ cm}$ -scale varves (LS A, B and C) and $\geq 1\text{ cm}$ -scale varves (LS D, E and F). All Lamination Sets (LS) are labelled with Lamination Types (LT) and contain a coarse-grained component (yellow) that is overlain by a fine-grained component (green). The following statements describe the coarse component only. LS A is composed of LT xix: well sorted massive very fine silt to fine silts with a sharp lower contact and a graded contact between the coarse and fine component. Pockets of silt and individual coarse silt/fine sand grains that have sunk into the underlying clay component are common. Eroded, ripped up clay is often observed in the base of the coarse component. LS B is composed of LT xiv: moderately sorted massive medium to coarse silts with occasional fine sand grains with a sharp upper and lower contact. LS C is composed of LT ix: moderately sorted, massive, fine to medium silt with occasional coarse silt grains and is typically $< 1\text{ mm}$ thickness. LS D composed of LT viii: multiple single grain alternations of massive medium silt to coarse silt laminations. LS E is composed of LT vii and viii: multiple graded and/or massive medium silt to coarse silt laminations with sharp upper and lower contacts. LS F is composed of LT v, i and ix: a package of multiple graded and/or massive coarse silt to fine sand laminations with sharp upper and lower contacts. Within this LS coarser inputs are observed in the late melt season. In all LS the fine-grained component has high birefringence under cross polarised light and is LT xvi.

Table 7-3. Summary of the different laminated lithofacies identified at Asplången including specific attributes, interpretation of sedimentary processes and inferred depositional environment.

Lithofacies	Lamination Sets	Attribute	Process interpretation	Environment	Reference
LF1	B, C, D, E, F	<ul style="list-style-type: none"> • \geqcm-scale rhythmically bedded medium silts and clays • Multiple (3-8) laminations in the coarse (silt) component, coarse and fine grained • Anomalous large clast • Silt rip-up intra-clasts 	<p>Glaciolacustrine setting that receives silt-sized sediment from ice-proximal sediment density flows; fine laminations formed from suspension settling; clast deposited from iceberg rafting; silt rip-up clasts formed by subaqueous concentrated sediment density flows that are of high velocity/high sediment load and erode previously deposited material</p>	Proximal/distal glaciolacustrine	Ashley (1975); Smith and Ashley (1985); Mulder and Alexander (2001); Talling <i>et al.</i> (2012)
LF2,	A, B, C	<ul style="list-style-type: none"> • <cm-scale rhythmically bedded very fine silts and clays • Either single lamination in the coarse (silt) component • Or multiple laminations (2 or 3) in the coarse component with a coarse upper lamination • Reddish brown Lamination Sets (sub-unit 2a) • Grey Lamination Sets (sub-unit 2b) • Dark grey Lamination Sets (sub-unit 2c) 	<p>Distal lacustrine setting; distal to glacier margin and distal to lake edge; silt laminations of LT xiv composition are likely the result of density flows, but in a more distal location than LF1. Clay lamination deposited from suspension settling. Coarse silt/fine sand laminations that cap the coarse components are from one-off high velocity/high sediment load density currents in the late melt season. Brown Lamination Sets (sub-unit 2a) receive sediment from similar source to LF1 such as from the glacier margin as underflows but also from suspension settling from localised reworking of lake-bottom sediments. Grey (sub-unit 2b) and dark grey Lamination Sets (sub-unit 2c) receive sediments mostly from erosion and transport of sediments from the lake-bottom within input from one-off high velocity density currents.</p>	Ice-contact distal glaciolacustrine with a transition to ultra-distal glaciolacustrine	Palmer <i>et al.</i> (2019)

7.3.4 Interpretation of the Lamination Sets as varves

The structures described in LF1 and LF2 are consistent with glaciolacustrine varves deposited in proximal- to distal locations within ice-contact lakes (Ashley, 1975; Smith and Ashley, 1985; Ringberg and Erlström, 1999; Ridge *et al.*, 2012). In all Lamination Sets, the sharp contact between the coarse layer and underlying fine layer indicates a rapid switch in the style of sedimentation that is consistent with a transition between non-melt season and melt season sedimentation. The structures described, especially the regular alternations of layers of silt and clay, are typical of glaciolacustrine varves observed at the macroscale (De Geer, 1912; Ashley, 1975; Smith and Ashley, 1985; Ridge *et al.*, 2012) and microscale (Ringberg and Erlström, 1999; Brauer, 2004; Palmer, 2005; Palmer *et al.*, 2008, 2010, 2019). At Asplången, the coarse component is deposited during the summer/melt season either from sediment density underflows or suspension settling of reworked lake-bottom sediments. During the summer, fine-grained (clay) sediments remain in suspension due to currents within the lake and wind-driven surface currents (Ashley, 1975; Smith and Ashley, 1985). During the non-melt season (winter/autumn) the lake water surface freezes and inhibits the formation of surface currents allowing the finer clay fraction to be deposited from suspension in the water column.

7.4 Palaeoecological proxies

The following section provides a summary of specialist reports that were provided for diatom and macrofossil analysis by Dr Poppy Harding-Blockley and Dr Marta Perez respectively (see appendices for reports). These reports have been expanded upon and integrated with lithostratigraphical data. Lake process interpretations are also proposed for LF2-LF4 using these data.

7.4.1 Summary of palaeoecological proxy results

Overall it appears the diatom and macrofossil remains from ASP2A show changing limnological conditions across LF2-LF4. The changing lake conditions appear to have increased the concentration and diversity of diatoms and potentially driven changes in the preservation of their frustules within the sediments. The core seems to demonstrate that the record is influenced by dissolution, and therefore further diatom analyses should be supported by quantification of the dissolution seen. There is some evidence from diatoms that waters may undergo changes in the salinity during this period but littoral zone chironomid species were found in the same sediment samples as the diatom

species that indicate brackish water conditions. This may indicate that these sediments are the result of reworking of littoral zone sediments rather than *in situ* sedimentation.

The lack of macrofossils in LF2 is unsurprising given microfacies analysis confirms that these sediments were deposited in a distal glaciolacustrine environment. The presence of some diatoms suggests that there were sufficient nutrients to support growth, though diatom numbers are low. Since glacial meltwater contains high nutrient concentrations (McClain *et al.*, 2003), some glacier-fed lakes can support diatom growth (Burpee *et al.*, 2018). However, some glaciolacustrine environments are nutrient poor due to limited chemical weathering and plant growth in the surrounding catchment (Zolitschka *et al.*, 2015), and this may account for, or partially account for the low number of diatoms in LF2. The sharp contact between LF2 and LF3 suggests that the transition from an ultra-distal glaciolacustrine environment to LF3 occurred quickly. The presence of *A. granulata* and its preference for turbulent, nutrient-rich lake water and the presence of *Paracladopelma* and *Pseudosmittia* suggest that LF3 was deposited in a cold, turbulent, freshwater lake. Microfacies analysis shows that LF3 consists of one normally graded bed suggesting deposition in a single event such as a turbidite or density flow. The interpretation of LF3 as a turbidite suggests that 33 cm of sediment were deposited almost instantaneously. Given the annual sedimentation rate (average varve thickness) prior to deposition of the turbidite is 3.56 mm, a large-scale event would have been required to deposit 33 cm of sediment. One explanation is a drop in lake level which would have exposed loose, fresh sediment at the lake edge that would have been prone to erosion and collapse. Subsequent in-wash and/or slumping of sediments would have increased turbidity within the lake creating an environment for *A. granulata* to thrive. Alternatively, the diatoms could represent reworked material as evidenced by the presence of littoral zone chironomid species of *Simuliidae* and *Ephemeroptera*.

In LF4, sediments are composed of silts and clays and microfacies analysis shows that glaciolacustrine varve sedimentation had ceased. In isolation, the presence of *H. holsatica*, *N. recens* and *R. acuminata* may indicate a change in environment to brackish water conditions. However, freshwater ostracods were also found in LF4 and so this unit may be indicative of reworking in the catchment. Alternatively, this unit could be interpreted as a transitional phase from glaciolacustrine (freshwater) to brackish. Depositional processes and environmental interpretations for the non-laminated lithofacies are summarised in Table 7-4. Higher resolution work in the future would be beneficial to confirm where diatoms and macrofossils are first documented in the record and to add further clarity to these findings.

Table 7-4. Summary of lithofacies attributes, sediment process interpretation and depositional environment for non-laminated lithofacies

Lithofacies	Attribute	Process interpretation	Environment
LF3	Dark grey normally graded silty clay, littoral zone chironomid species <i>A. granulata</i> , <i>Paracladopelma</i> and <i>Pseudosmittia</i>	Turbidite deposit. Drop in lake level that exposed loose sediment that would have been prone to collapse and in-wash to the basin. <i>A. granulata</i> diatoms inhabit turbulent, nutrient-rich lake water and the presence of <i>Paracladopelma</i> and <i>Pseudosmittia</i> suggest that LF3 was deposited in a cold, turbulent, freshwater lake	Turbid, freshwater lake
LF4	Alternations of reddish brown and blue/grey weakly laminated clayey silt Littoral zone chironomid species, freshwater ostracods Brackish water diatoms Freshwater algae <i>Characeae</i> and freshwater ostracod valves of the genus <i>Candona</i> and <i>Herpetocypris</i>	Shallower lake than in LF2 due to drop in lake level described in LF3. Low energy (high clay content). Brackish water diatoms likely reworked rather than <i>in situ</i> due to littoral zone chironomid species and freshwater algae/ostracods	Freshwater
LF5	Blue/grey clayey silt massive	Low energy (high clay content).	Freshwater?
LF6	Brown gyttja with abundant terrestrial macrofossils such as leaves, roots and seeds e.g. <i>Betula nana</i>	Shallow eutrophic lake with increased biogenic activity. Establishment of trees and shrubs in the surrounding catchment. Temperate/warm conditions.	Shallow lake, high productivity, warmer, forested catchment
LF7	Dark brown, organic-rich silts	Modern soil processes	Reed peat

7.5 Varve^{TSA} chronology

This section presents a varve^{TSA} thickness record and chronology for the Asplången sequence based on the refined criteria for the definition of varve^{TSA} boundaries (section 5.5.3.1). A composite site varve^{TSA} chronology was produced by averaging varve^{TSA} thickness for each varve^{TSA} measurement between overlapping thin sections and cores. Prominent marker layers such as disturbed zones and extremely thick varve^{TSA} were used as definitive “pinning-points” between cores (e.g. Lamoureux and Bradley, 1996; Lamoureux, 2001; Palmer *et al.*, 2010; Bendle *et al.*, 2017). In the absence of pinning-points to link cores, sediment depths were used. Thin section overlaps are provided in the appendices. A repeat varve count had not been undertaken at the time of submission. Only 1 break was identified in the Asplången sequence within LF2 (Bed 1) and is comprised of massive and weakly laminated silts and clays (Table 7-5).

Table 7-5. Summary of breaks in varve^{TSA} sedimentation.

Lithofacies	Depth (cm)	Type of break			
		Deformation	Silt massive bed	Unclear laminations	Total
LF1	1246-894	0	0	0	0
LF2	894-585	0	0	1	1
	Total	0	0	1	1

In total 827 varves and 1 section of non-varved sediment were identified from thin sections. The varve^{TSA} thickness characteristics of the Asplången record are presented for each lithofacies (Table 7-6).

The varve^{TSA} thickness record is divided based on lithofacies units 1 and 2 and LF2 is split by the colour change from brown to grey varves. However, there are thickness variations within each unit. Thickness characteristics in each 100 cm are included in the appendices. In LF1 there are 258 varves with an average thickness of 10.90 mm. The average thickness, however, decreases from base to top of the unit. The ratio of coarse to fine laminations changes from 3:1 between 1100-1200 cm, to 2:1 between 1000-1100 cm, then between 900-1000 cm melt season and non-melt season layers can be approximately equal, whereas at the top of LF1 between 800-900 cm the ratio of coarse to fine is 1:2. In LF1 the minimum varve thickness measurement is 1.21 mm with a maximum of 49.65 mm. In LF2, there are 569 varves^{TSA} with an average thickness of 3.77 mm. The ratio of melt season to non-melt season layers is 1:3 with a minimum varve thickness of 0.84 mm and a maximum of 13.12 mm. Table 7-6

shows varve data when LF2 is split by varve colour. There are 399 basal brown varves and 170 grey varves. The mean varve thickness is 3.58 mm in the brown varves and 4.20 mm in the grey varves. The minimum varve thickness is 0.84 mm in the brown varves and 1.21 mm in the grey varves. The maximum varve thickness is 10.74 mm in the brown varves and 13.12 mm in the grey varves. The ratio of coarse:fine components is 1:3 in both the brown and the grey varves. Normalised and raw (mm) varve thicknesses are presented in Figure 7-5 alongside Varve Quality and the distribution of Lamination Sets throughout the sequence.

Table 7-6. Summarised varve thickness characteristics in each lithofacies. LF2 is split by the colour change from brown to grey varves. Varve characteristics are similar between the varve colour types.

Lithofacies	Depth (cm)	Varve number	Varves (n)	Mean (mm)	St Dev	Min (mm)	Median (mm)	Max (mm)	Coarse:Fine
LF1	1246-895	1-258	258	10.90	8.25	1.40	8.32	49.65	2:1
LF2	895-585	259-827	569	3.77	1.69	0.84	3.52	13.12	1:3
LF2 split by colour (brown and grey varves)									
LF2 (brown)	895-703.5	259-657	399	3.58	1.56	0.84	3.39	10.74	1:3
LF2 (grey)	703.5-585	658-827	170	4.20	1.90	1.21	3.81	13.12	1:3

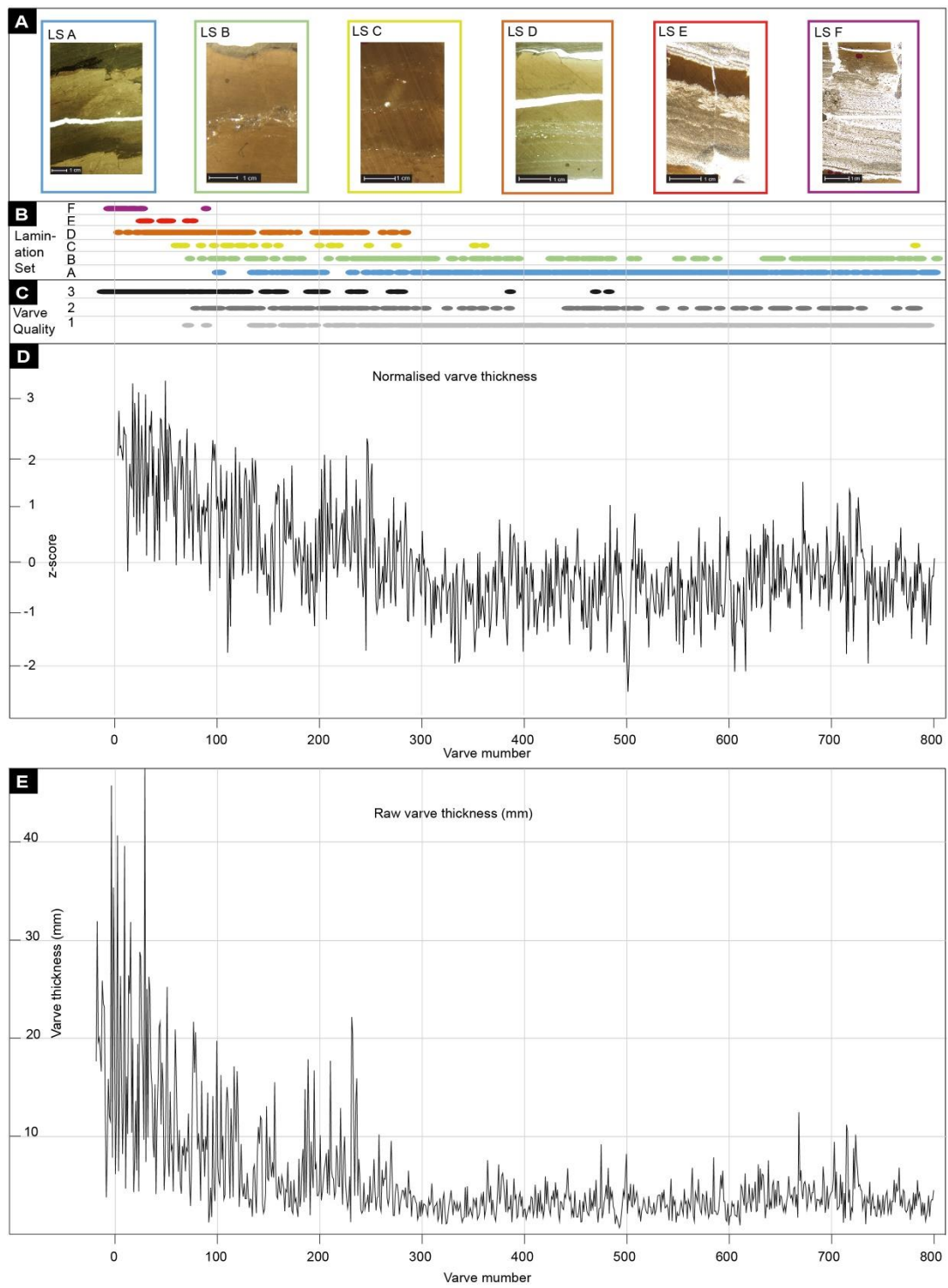


Figure 7-5. Normalised varve thickness record plotted alongside Varve Quality and Lamination Sets.

(A) Lamination Sets, (B) distribution of Lamination Sets throughout the sequence, (C) Varve Quality, (D) Normalised varve^{TSA} thickness record. (E) Raw (mm) varve thickness. Varve 1 is at the base of the sequence such that the diagram should be read from left to right as from base-to-top.

7.6 Summary

The revised methodology outlined in section 6.6.5 was successfully applied to the Asplången sediment sequence. Macroscale analysis provided a general description of the sediments and was used to produce sediment logs. Thin section analysis was used to refine sedimentological descriptions and interpretation of depositional processes which resulted in construction of an accurate varve chronology. The basal *ca* 130 varves are composed of coarser-grained, multi-laminated summer components (LS D, LS E and LS F) whereas the uppermost varves are finer grained and composed of single lamination summer components (LS A, LS B and LS C). All varves were analysed under thin section and 167 (20%) were assigned a VQ score of 3, 177 (21%) were assigned a VQ score of 2, and 483 (58%) were assigned a VQ score of 1. The lower VQ scores are located in the upper part of the varve record and are typically associated with varves of Lamination Sets A, B and C (Figure 7-5). A second varve count is pending though at present the Asplången varve record contains 827 yrs and 1 break in varve sedimentation. The following chapter presents the sedimentological data from the Glottern sequence.

Chapter 8. Results - Glottern

This chapter details the results from macro- and microscale sedimentology of the laminated sediments at Glottern to evaluate a potential varve origin and refine the existing varve chronology. Whilst a varve chronology has been constructed from macroscale analysis of Glottern sediments by Wohlfarth *et al.* (1998), the results from Svinstadsjön demonstrate that it is necessary to construct a new site varve chronology using microfacies analysis of thin sections. Like Svinstadsjön, X-radiograph images, and μ XRF data were initially used to characterise the varved sediments, however, these methodologies proved inaccurate when compared to sediment descriptions and varve counts from thin section analysis. As such, this chapter follows the approach taken for Asplången and presents sediment descriptions through integrating macroscale, microfacies and particle size evidence.

8.1 Core recovery and basin survey

Due to access restrictions, an auger survey of only the south-eastern shore of Glottern was undertaken. The survey results were used to map the bathymetry of the field site and identify a suitable coring location (Figure 8-1). Each depth probe hit bedrock and when twisted, the coring rods grated through coarse sands/gravel, however, when coring it was not possible to retrieve these sediments or ascertain the unit thickness. The basin topography at the site shallows from east to west and from south to north toward the current lake edge. Figure 8-1 shows the location of each depth probe and the coring location which is in the flattest part of the site that also maximised depth.

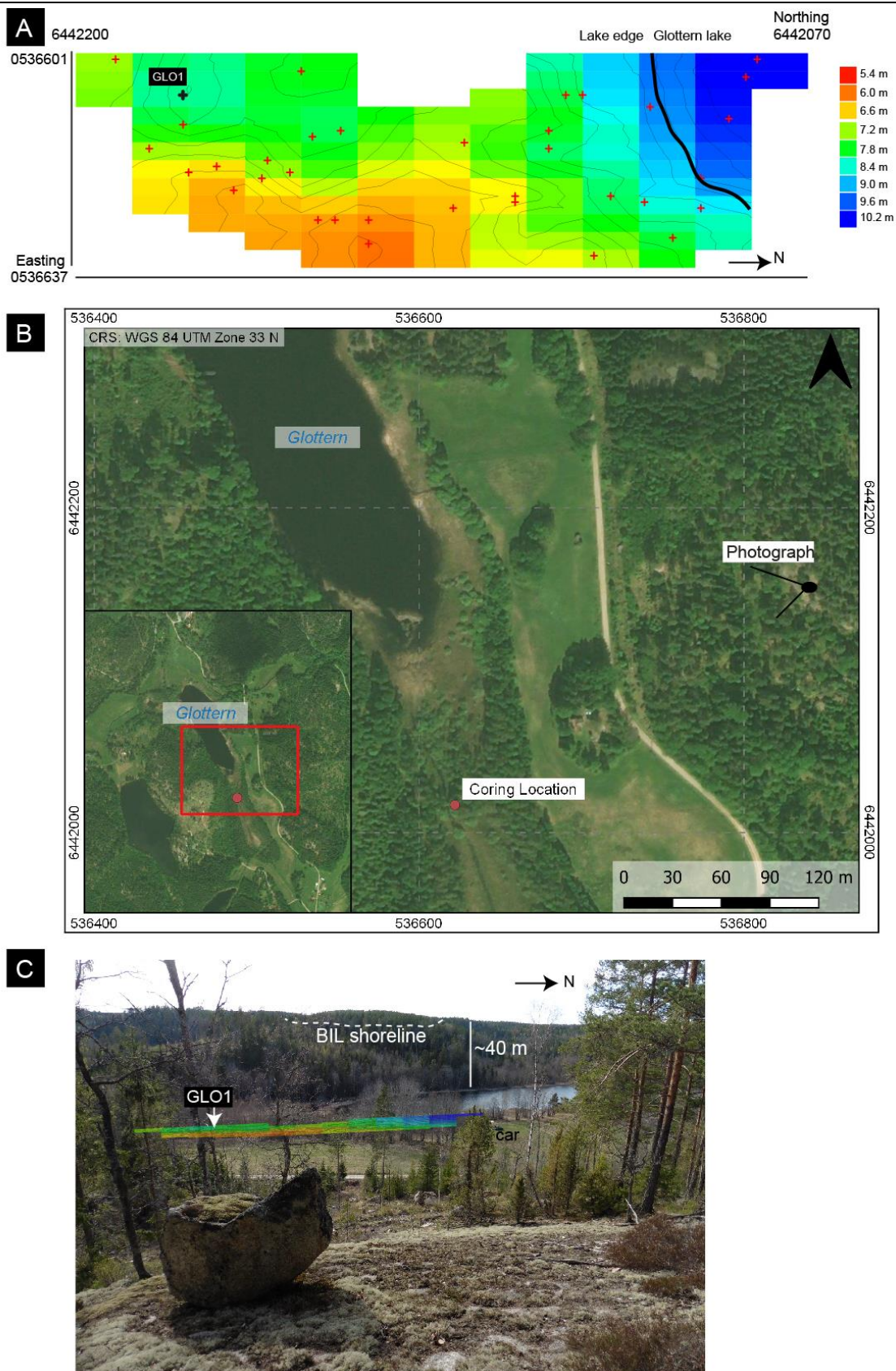


Figure 8-1. Site location map and sediment depth survey. (A) Sediment depth survey result from Glottern plotted in QuickGrid. Red crosses mark depth probe locations and the black cross marks the coring location. (B) Site map with coring location and location of photograph taken in image C. (C) Site photograph with auger survey, coring location and approximate altitude of the Baltic Ice Lake shoreline highlighted.

8.2 Macro and microscale sedimentology and stratigraphy

This section focusses on the stratigraphic description of key sedimentary units and detailed sedimentological properties of the laminated glaciolacustrine sediments to determine their varved nature.

8.2.1 Sediment units

The sediment sequence is 9 m in length and contains 4.3 m of well-defined silts and clays overlain by 1.02 m of silty clay. The upper part of the sequence is composed of 3.18 m of brown silty clay gyttja and is capped by 0.5 m of partially decomposed organic matter. Six lithofacies units were identified from the extracted sediment at Glottern: 1) brown clearly laminated couplets of silt and clay \geq cm-scale thickness; 2) brown clearly laminated couplets of silt and clay <cm-scale thickness; 3) brown silty clay with occasional sand layers and/or black banding; 4) transition from greyish brown silty clay to dark brown gyttja; 5) gyttja with abundant macrofossils; and 6) compacted and partially decomposed leaf litter (Figure 8-2).

LF1 (900-583 cm) contains horizontally bedded lamination couplets of silt and clay that are \geq cm-scale thickness. The lamination couplets in this unit are split into two sub-units based on sediment colour. Lamination couplets in sub-unit 1a (900-618 cm) are comprised of 10 YR 7/1 light grey coarse lamination of medium- to coarse silt (modal grain size 20-30 μ m) overlain by a clay lamination 10 YR 4/2 dark greyish brown. Sub-unit 1b (618-598 cm) contains lamination couplets of the same grain size and structure as sub-unit 1a, but clay laminations are 10 YR 3/1 dark reddish grey (Figure 8-3). In LF1, six zones of deformation interrupt the continuous deposition of silt and clay couplets. (Bed 1; 859.3-870.5 cm, Bed 2; 826.6-831cm, Bed 3; 811-825.5 cm, Bed 4; 787.7-801 cm, Bed 5; 672.3-687.9 cm, Bed 6; 646-663 cm). Beds 1-6 are composed of laminations that are faulted, folded and which have been ripped up and redeposited (Figure 8-4).

LF2 (583-470 cm) is composed of horizontally bedded laminated silt and clay couplets that are typically <cm-scale. Silt laminations are 10 YR 4/3 brown and clay laminations are 10 YR 4/2 dark greyish brown. Coarse laminations are composed of fine- to very fine silts (Figure 8-3).

LF3 (470-390 cm) is composed of light grey clayey silt that is interspersed by occasional sand beds and/or black organic-rich bands that are 1-4 mm thickness.

In LF4 (390-368 cm) there is a transition from 10 YR 6/1 grey clayey silt to 5YR 3/2 dark olive gray silty clay gyttja.

LF5 (368-50 cm) is composed of 10 YR 3/2 dark brown gytija with abundant terrestrial and aquatic macrofossils such as leaves, roots and seeds.

LF6 (50-0 cm) is topsoil and is composed of compacted, partially decomposed leaf litter. Interpretation of depositional processes within each lithofacies are provided in Table 8-3.

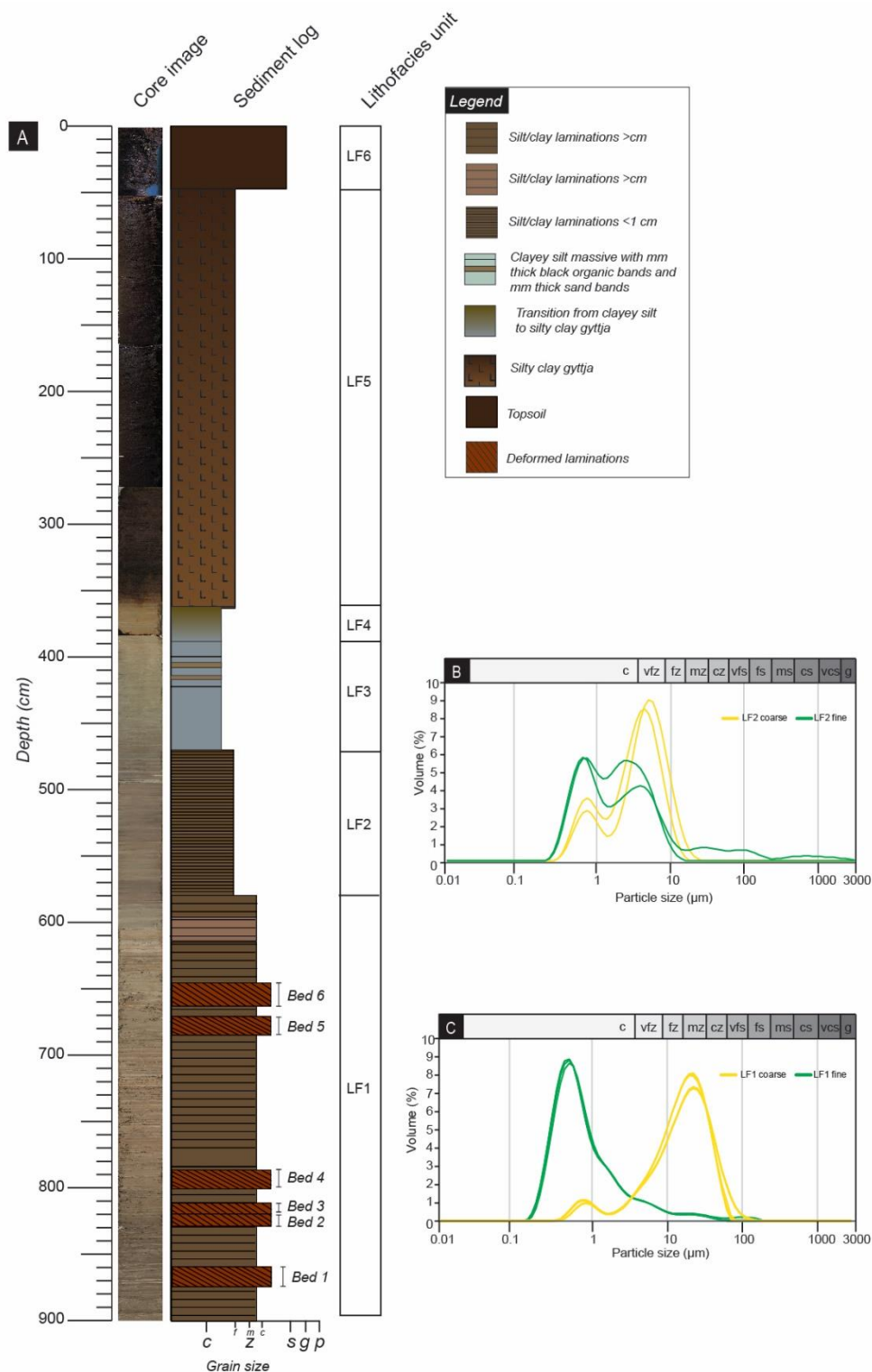


Figure 8-2. Core image, sediment log, lithofacies units, and particle size data for Glottern. (A) Sediment core image and log with lithofacies units. (B) Particle size data for LF 2, (C) particle size data for LF 1. Yellow curves show data from the coarse lamination, green curves show data from the fine lamination.

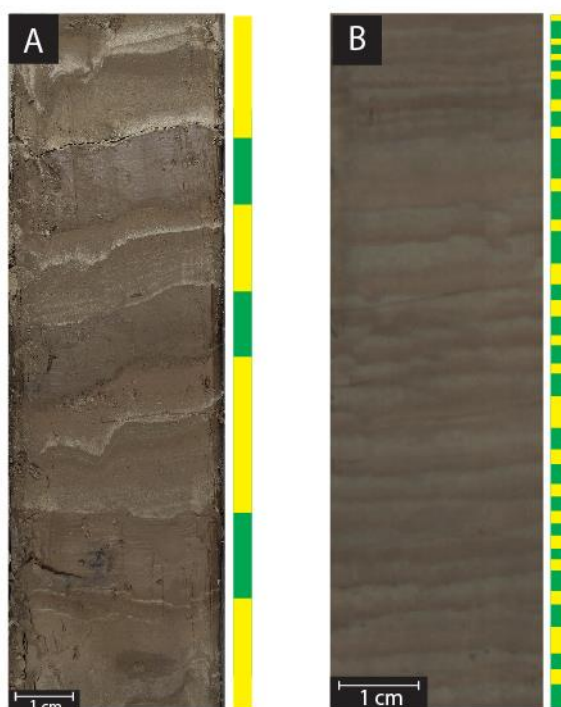


Figure 8-3. Images of \geq cm-scale laminations in LF1 (A) and $<$ cm-scale laminations in LF2 (B). All silt laminations are highlighted with yellow boxes and all clay laminations are highlighted with green boxes.

8.2.2 Sedimentology of laminated couplets (LF1 and LF2)

This section presents integration of macroscale and thin section descriptions alongside particle size data for the laminations in LF1 and LF2. Thin section analysis has enabled: 1) further (micro)sedimentological description of the laminated sediments through identification of discrete Lamination Types; 2) description of key Lamination Sets; 3) interpretation of varve^{TSA} sedimentation; and 4) construction of a varve^{TSA} chronology. The sediments were described using a microfacies approach and individual laminations were classified by their microscale sediment characteristics (e.g. Brauer, 2004; Palmer *et al.*, 2010, 2012, 2019; Bendle *et al.*, 2017). The descriptive terminology follows the protocol outlined by Palmer *et al.* (2019). The term “couplet” is avoided when discussing the microscale properties of the sediments since individual coarse component laminations may contain more than one Lamination Type (LT) at the microscale. Lamination Types are coded by roman numerals. Repeating packages of Lamination Types are referred to as Lamination Sets (LS) (Palmer *et al.*, 2019) and are coded alphabetically. Following the identification of discrete Lamination Types and sets, sediment process interpretations are proposed in section 8.2.5 which include the relative timing of sediment transport and deposition to the lake floor. Using lamination characteristics, including lamination thicknesses, Lamination Sets are interpreted as

varves (section 8.2.7). In Chapter 11 Lamination Sets are categorised into “Lamination Set Assemblages” (e.g. Palmer *et al.*, 2019) that relate to specific parts of the lake basin.

For both the \geq cm-scale laminations and the $<$ cm-scale laminations a silt component is overlain by a clay component. The contact between the clay laminations and the succeeding silt lamination is always sharp. Lamination Sets are subdivided based on the internal structure and thickness of the coarse component into those which are \geq cm-scale with 3 or more laminations in the coarse component (LF1), and those which are $<$ cm-scale and which contain 3 or fewer coarse component layers (LF2).

8.2.3 Lamination Types and Lamination Sets

The sequence is characterised by distinct alternations between coarse (silt) components that can contain one or multiple Laminations Types, and fine (clay) components that are normally graded from very fine silt to clay. Lamination Types identified within the Glottern sequence are presented in Table 8-1.

Table 8-1. Sedimentological properties of the Lamination Types (LT) observed in the microfacies of the glaciolacustrine sediments within the Glottern sequence.

* denotes laminations types that are not identified by Palmer *et al.* (2019) and are unique to the Glottern record. C = clay; VFZ = very fine silt; FZ = fine silt; MZ = medium silt; CZ = coarse silt; FS = fine sand. Ma = massive; NGr = normally graded. WS = well sorted; MS = moderately sorted; PS = poorly sorted. Sh = sharp; Gr = gradational. Dg = dropgrain; In = intraclast; WD = well-developed.

Lamination Type (LT)	Grain size (dominant)	Structure	Sorting	Upper Contact	Other
i	VFS/FS	Ma	WS	Sh	In/Dg
v	VFS/FS-MZ	NGr	WS	Sh	Dg
vi	VCZ-MZ	Ngr	WS	Sh	Dg
vii	CZ-MZ	Single grain alternations	WS	Sh	Dg
ix	CZ/MZ-FZ/C	NGr	WS	Sh	Dg
xiv	CZ	Ma	PS/MS	Sh	Dg
xv	MZ	Ma	PS/MS	Sh	Dg
xvi	VFZ-C	NGr (short)	WS	Sh	Masepic WD
xix*	VFZ	Ma	WS	Gr	Dg

Repeating groups of Lamination Types were also identified under thin section and classified into distinct Lamination Sets (Table 8-2). Further details on the different LT and LS are outlined in the following section.

Table 8-2. Lamination Sets identified within the Glottern sequence.

Lamination Set (LS)	Coarse-grained component LT	Fine-grained component LT
B	xiv	xvi
C	xv	xvi
D	viii	xvi
E	vii, viii	xvi
F	i, v, ix	xvi
G	xv, xix	xvi
H	ix,xv	xvi

8.2.3.1 LF 1 (\geq cm-scale Lamination Sets)

Microscale sediment analysis has enabled the detection of five distinct Lamination Sets within LF1 (LS B, E, F, G, H). In LF1 92% of coarse components are internally complex containing multiple (3-8) Laminations Types that vary in grain size from fine silt to fine sand (Figure 8-5). The Lamination Types within coarse components can be massive or normally graded, and well or moderately sorted. The basal contacts of laminations within the coarse component are sharp and can be horizontal or erosive with evidence of ripped-up silt. A single clayey-silt lamination can also cap the coarse component and occur after a succession of coarse-grained (coarse silt to fine sand) laminations. In \geq cm-scale Lamination Sets, the fine component has a sharp lower contact and fines upwards from very fine silt to clay. Under cross polarised light, clay layers display high birefringence consistent with well-developed masepic fabrics.

Throughout the Glottern sequence, only one anomalously large clast is observed at the top of a coarse lamination and diamict pellets that penetrate or deform the underlying laminations (e.g. Ovenshine, 1970) are absent. Lamination Types within coarse components often display faulting and/or shearing.

8.2.3.2 LF 2 (<cm-scale Lamination Sets)

In <cm-scale Lamination Sets, coarse components are always sharply truncated by the succeeding clay lamination. Four Lamination Sets are observed within LF2 (LS B, C, G and H), two that are composed of a single summer lamination (LS B and C), and two that are composed of a multi-laminated coarse component: (LS G and H).

For LS B and LS C the summer component is one of two laminations types: LT xiv and LT xix. LT xiv has sharp contacts and is composed of poorly/moderately sorted coarse silts with occasional fine sand grains with a sharp upper and lower contact. LT xix has sharp contacts and is composed of poorly/moderately sorted medium silts with occasional coarse silt grains with a sharp upper and lower contact. The upper boundaries

of clay components in LF2 can be eroded and occasionally have gradational lower contacts but are almost always sharp. Unlike Svinstadsjön, there is no evidence of larger sand grains or silt clasts that are sunk into clay laminations. Isolated gravel-sized clasts that are anomalously large in comparison to the host sediment are rare. The fine component of each Lamination Set grades from very fine silt to clay and under cross-polarised light displays masepic fabrics.

In LS G, the coarse component is composed of three laminations; a basal coarse-grained lamination of massive medium- to coarse silt, a very fine- to fine silt massive lamination, and an upper coarse-grained lamination of massive medium- to coarse silt. In LS H, the coarse component is composed of two laminations; a lower very fine- to fine silt massive lamination, and an upper coarse-grained lamination of massive medium- to coarse silt. The fine component of each Lamination Set grades from very fine silt to clay and under cross-polarised light displays masepic fabrics, whereas the other lamination types that compose the coarse component do not display masepic fabrics. LS G and LS H are pervasive throughout LF2 and account for 54.2% of the coarse Lamination Sets.

For LS B, LS C, LS G and LS H the summer layers appear darker than the winter layers under thin section (Figure 8-5), though at the macroscale summer layers appear lighter than winter layers (Figure 8-3). This is due to polishing of the thin section during production. For these Lamination Sets the boundaries between the coarse and fine component were easier to identify when the thin sections were slightly thicker than would normally be polished during production. The apparent dark colour of the summer layers is therefore a product of polishing and the slightly thicker sample on the slide. This reduced the amount of light transmitted through the summer laminations when observed microscopically.

8.2.4 Deformation structures

Other structures observed in \geq cm-scale couplets include occasional larger clasts that penetrate or deform the underlying laminations (Thomas and Connell, 1985), and are of pebble-size when observed at the macroscale. Diamict pellets that penetrate or deform the underlying laminations (e.g. Ovenshine, 1970) were also observed at the microscale. Six deformation zones were also observed in the Glottern sequence and interrupt the otherwise continuous deposition of Lamination Sets. All deformation zones are comprised of ripped up and folded laminations. Bed 1 occurs at 859.3-870.5 cm, Bed 2 occurs at 826.6-831cm, Bed 3 occurs at 811-825.5 cm, Bed 4 occurs at 787.7-801 cm, Bed 5 occurs at 672.3-687.9 cm and Bed 6 occurs at 646-663 cm. Deformation zones are only observed in LF1 and are absent in LF2.

8.2.5 Sediment process interpretation for the Lamination Sets

This section provides an interpretation of the sediment processes for each Lamination Set with particular focus on whether the sediments were deposited as underflows or from suspension settling.

8.2.5.1 LF 1 (\geq cm-scale Lamination Sets)

Within \geq cm-scale Lamination Sets, coarse component layers display internal complexity and are comprised of multiple graded or massive laminations with sharp basal contacts. Multi-laminated coarse component layers are pervasive throughout \geq cm-scale Lamination Sets, and are composed of well-sorted fine, medium or coarse silt.

Within coarse components the sharp contacts between multiple laminations and evidence of erosion (e.g. rip-up clasts) suggests that most sediment pulses were transported through the lake as underflows (Mulder and Alexander, 2001; Talling *et al.*, 2012). The variable grain sizes of laminations either reflects the variable nature of several underflows entering the basin, or fluctuating sediment concentrations within a semi-continuous underflow. For example, a single underflow can have variable sediment concentrations due to diurnal melt cycles or changes in meltwater fluxes across the melt season (Ashley, 1975; Gustavson, 1975).

A coarse-grained lamination with a sharp upper contact to overlying clay is often observed in \geq cm-scale varves. These coarse-grained laminations could represent a rapid transition to calm lake waters at the end of the melt season or could reflect a single surge event that entered a quiescent water body (Bendle *et al.*, 2017). Anomalously large clasts in LF1 are interpreted as IRD (Thomas and Connell, 1985).

8.2.5.2 LF 2 ($<$ cm-scale Lamination Sets)

The coarse component of $<$ cm-scale Lamination Sets is either composed of multiple laminations of (LS G and LS H) or a single lamination (LS B and LS C). In LF2, multiple coarse-grained laminations are the result of multiple influxes of sediment during the melt season (Palmer *et al.*, 2010, 2012). The sharp contacts between laminations within the coarse component suggest transport through the lake as underflows (Mulder and Alexander, 2001) with the upper and lower coarse-grained sediment pulses related to single influxes of sediment-laden meltwater at a given location (Palmer *et al.*, 2010, 2012). In some instances, a lower coarse-grained lamination is absent and instead only one coarser-grained lamination caps a clayey silt lamination. This suggests that in the early melt season either the velocity or number of underflows entering the lake basin was lower. The coarse component in the $<$ cm-scale Lamination Sets is composed of either poorly/moderately sorted massive medium silt with occasional coarse silt grains (LT xv) or poorly/moderately sorted massive coarse silt with occasional fine sand grains

(LT xiv). The contact with the underlying clay lamination can show evidence of erosion (e.g. ripped-up clay), though this is not consistent. This suggests that at Glottern, LT xv and LT xix were occasionally deposited as underflows, but where erosion of clay is not observed, the coarse component could have been deposited through suspension settling of re-worked sediments in the water column.

8.2.6 Deformation zones

Within LF1, it is important to note that there are breaks in the annually laminated sediments that reflect different mechanisms of sedimentation within the glaciolacustrine system. Microfacies analysis has enabled the identification of additional non-varved sediments and deformation structures that were not observable at the macroscale. These include silt rip-up clasts, faults and recumbent folds (Figure 8-4). The presence of deformed laminations which are folded or contorted may be caused by the slumping or displacement over short distances of previously deposited glaciolacustrine varve sediment (e.g. Devine and Palmer, 2017). Additional cores from the Glottern site would be required to assess the spatial distribution of deformation zones.

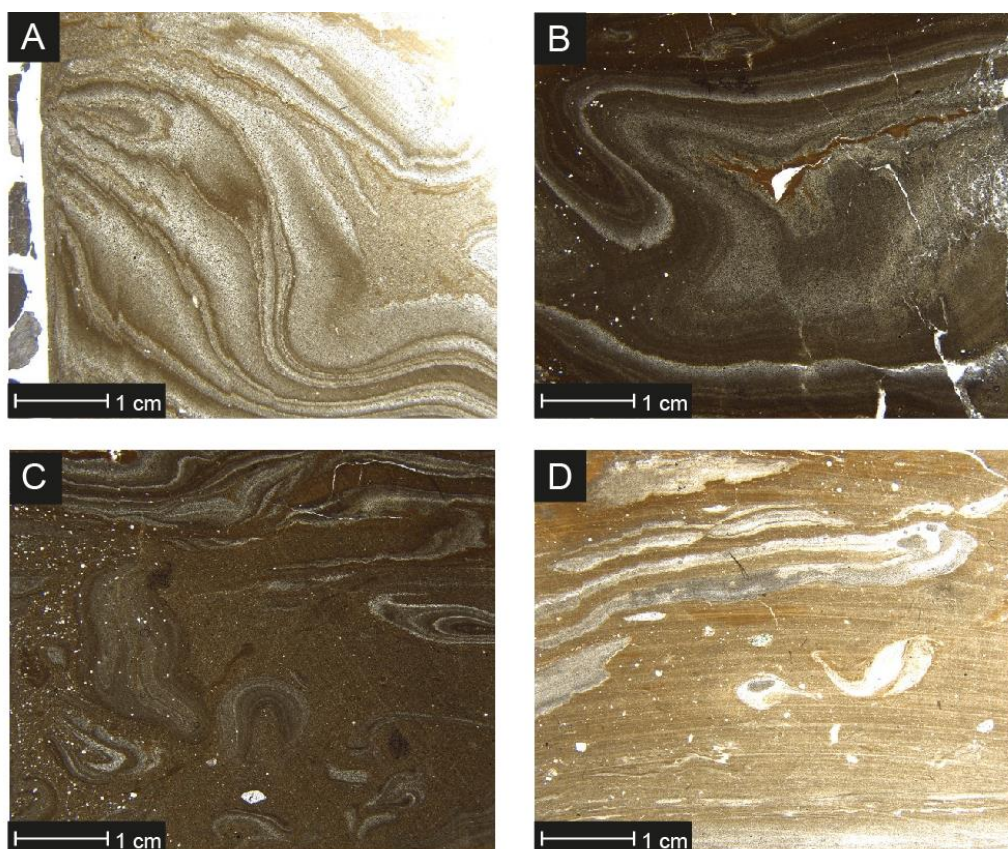


Figure 8-4. Examples of deformation structures in the Glottern sequence (A) Recumbent fold structure with shears in Bed 2, (B) Recumbent folding in Bed 3, (C) Folded and ripped up laminations that are set within a medium to coarse silt matrix in Bed 3, (D) Ripped up silt within a medium to coarse silt matrix in Bed 4.

A summary of the process interpretations for the laminated sediments in LF1 and LF2 is provided in Table 8-3 alongside interpretations for non-laminated sediments in LF3 to LF6.

Figure 8-5. Lamination Types and Lamination Sets observed in the Glottern sequence.

Next page. Examples of <cm-scale varves (LS B and C) and ≥cm-scale varves (LS E, F, G and H). All Lamination Sets (LS) are labelled with Lamination Types (LT) and contain a coarse-grained component (yellow) that is overlain by a fine-grained component (green). The following statements describe the coarse component only. LS B is composed of LT xiv: moderately sorted massive medium to coarse silts with occasional fine sand grains with a sharp upper and lower contact. LS C is composed of LT ix: moderately sorted, massive, fine to medium silt with occasional coarse silt grains and is typically <1 mm thickness. LS E is composed of LT vii and viii: multiple graded and/or massive medium silt to coarse silt laminations with sharp upper and lower contacts. LS F is composed of LT v, i and ix: a package of multiple graded and/or massive coarse silt to fine sand laminations with sharp upper and lower contacts. Within this LS coarser inputs are observed in the late melt season. LS G is composed of three laminations; a basal coarse-grained lamination of poorly/moderately sorted massive medium silt (LT ix), a middle very fine- to fine silt massive lamination (LT xix), and an upper LT ix. LS H is composed of two laminations; a lower well sorted lamination that grades from coarse silt/medium silt to fine silt/clay (LT ix) and an upper LT ix. In all LS the fine-grained component is LT xvi which grades from very fine silt to clay and has high birefringence under cross polarised light indicative of masepic fabric.

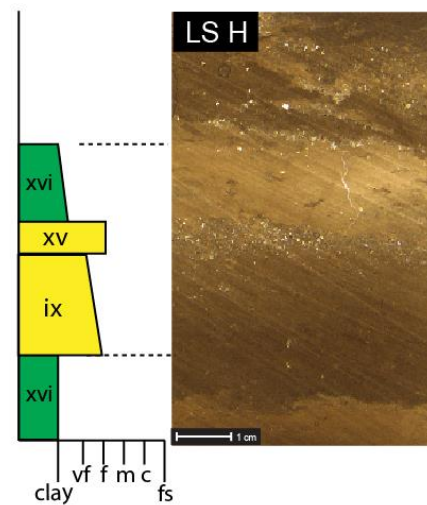
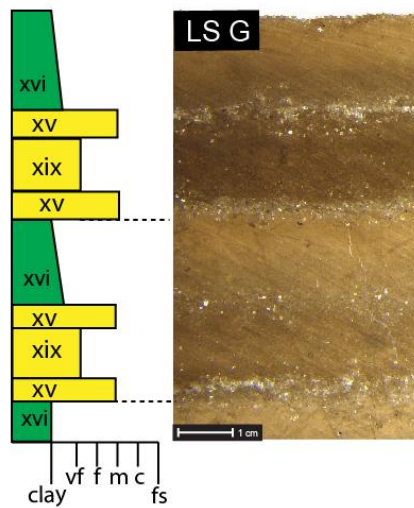
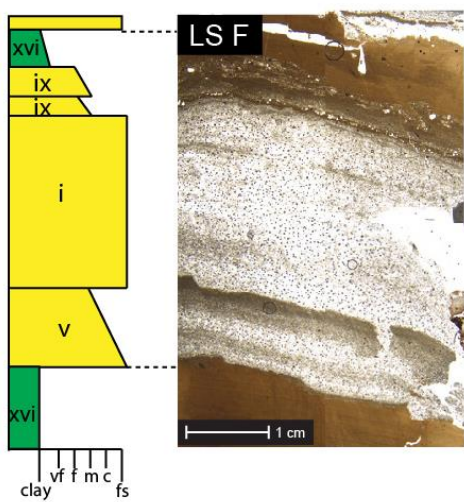
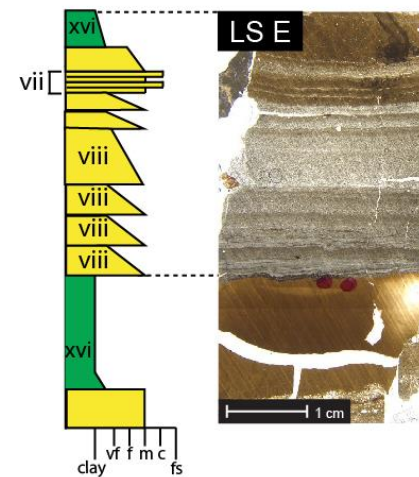
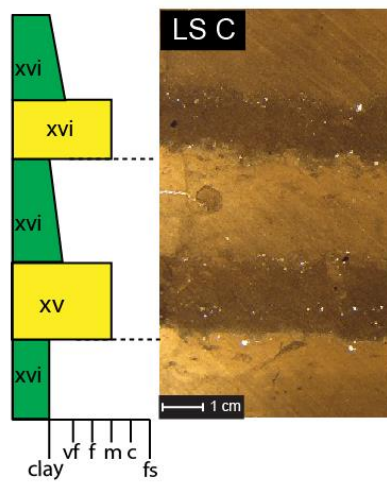
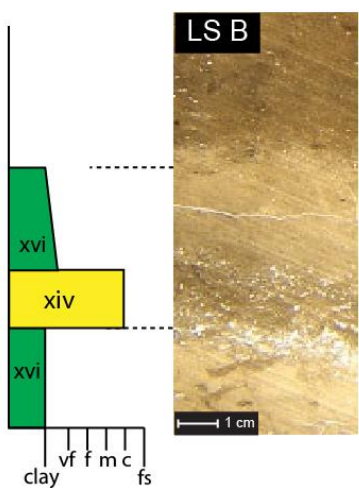


Table 8-3. Glottern lithofacies summary including specific attributes, interpretation of sedimentary processes and inferred depositional environment.

Lithofacies	Attribute	Process interpretation	Environment	Reference
LF1	<ul style="list-style-type: none"> • \geqcm-scale rhythmically bedded medium silts and clays • Multiple (3-8) laminations in the coarse (silt) component, coarse and fine grained • Anomalous large clast • Localised deformation (folding, contorting and shearing) of laminations • Silt rip-up intra-clasts 	<p>Glaciolacustrine setting that receives silt-sized sediment from ice-proximal sediment density flows (e.g. LS E and LS F); fine laminations formed from suspension settling; clast deposited from iceberg rafting;</p> <p>Silt rip-up clasts formed by subaqueous concentrated sediment density flows that are of high velocity/high sediment load and erode previously deposited material.</p> <p>Ductile deformation, likely due to sediment loading</p>	Proximal/distal glaciolacustrine	Ashley (1975); Smith and Ashley (1985); Mulder and Alexander, (2001); Talling <i>et al.</i> (2012)
LF2,	<ul style="list-style-type: none"> • <cm-scale rhythmically bedded very fine silts and clays • Either single lamination in the coarse (silt) component: (LS B and C), coarse grained upper lamination • Or multiple laminations (2 or 3) in the coarse component (LS G and H) with coarse upper lamination 	<p>Distal lacustrine setting; distal to glacier margin; coarse component laminations (LS G and H) are likely the result of density flows, but in a more distal location than LF1. Clay lamination deposited from suspension settling. Coarse silt laminations in LS G and LS H from one-off high velocity/high sediment load density currents in the late melt season.</p>	Distal glaciolacustrine	Palmer <i>et al.</i> (2019)

Lithofacies	Attribute	Process interpretation	Environment	Reference
LF3	<ul style="list-style-type: none"> • Clayey silt massive • Occasional sand beds and/or black organic-rich bands of 1-4 mm thickness 	Distal glaciolacustrine setting that receives fine-grained sediment from suspension settling in the water column. Lack of lamination couplets consistent with decreased seasonality, or shallow lake depth that allows constant lake water mixing. Coarser grained (sand) laminations and organic bands likely formed from erosion and transport of clastic and organic material from the littoral zone.	Distal glaciolacustrine, drop in lake level.	<i>interpretation</i>
LF4	<ul style="list-style-type: none"> • Transition from grey clayey silt to light brown silty clay gyttja. • Increase in organic matter and decrease in minerogenic material 	Transition from distal glaciolacustrine to temperate lacustrine environment with increased biogenic activity within the lake and in surrounding catchment. Climatic warming.	Temperate lacustrine setting with high biological productivity	Wohlfarth <i>et al.</i> (1998)
LF5	<ul style="list-style-type: none"> • Brown gyttja with abundant terrestrial and aquatic macrofossils such as leaves, roots and seeds e.g. <i>Betula nana</i>, <i>Potamogeton</i> 	Shallow eutrophic lake with increased biogenic activity. Establishment of trees and shrubs in the surrounding catchment. Temperate/warm conditions.	Shallow lake, high productivity, warmer, forested catchment	Wohlfarth <i>et al.</i> (1998)
LF6	<ul style="list-style-type: none"> • Compacted, partially decomposed leaf litter. 	Topsoil	Modern pine forest	<i>interpretation</i>

8.2.7 Interpretation of the Lamination Sets as varves

The structures described, especially the regular alternations of silt and clay Lamination Types, are typical of glaciolacustrine varves observed at the macroscale (De Geer, 1912; Ashley, 1975; Smith and Ashley, 1985; Ridge *et al.*, 2012) and microscale (Ringberg and Erlström, 1999; Brauer, 2004; Palmer, 2005; Palmer *et al.*, 2008, 2010, 2019). The structures described are also consistent with glaciolacustrine varves deposited in proximal- to distal locations within ice-contact lakes (Ashley, 1975; Smith and Ashley, 1985; Ringberg and Erlström, 1999; Ridge *et al.*, 2012). In all Lamination Sets, the sharp contact between the coarse layer and underlying fine layer indicates a rapid switch in the style of sedimentation that is consistent with a transition between non-melt season and melt season sedimentation.

At Glottern, the coarse component is deposited during the summer/melt season from sediment density underflows. During the summer, fine-grained (clay) sediments remain in suspension due to currents within the lake and wind-driven surface currents (Ashley, 1975; Smith and Ashley, 1985). During the non-melt season (winter/autumn) the lake water surface freezes and inhibits the formation of surface currents allowing the finer clay fraction to be deposited from suspension in the water column.

8.3 Varve^{TSA} chronology

A composite site varve^{TSA} chronology was produced by averaging varve^{TSA} thickness for each varve^{TSA} measurement between overlapping thin sections and cores. Prominent marker layers such as deformed zones and extremely thick varves^{TSA} were used as definitive 'pinning-points' between cores (e.g. Lamoureux and Bradley, 1996; Lamoureux, 2001; Palmer *et al.*, 2010; Bendle *et al.*, 2017). In the absence of pinning-points to link cores, sediment depths were used. Thin section overlaps are provided in the appendices. A repeat varve count had not been undertaken at the time of submission.

Whilst every attempt was made to conduct varve counts from thin sections throughout the entire sequence, varves from 616-692 cm and from 800-900 cm were counted at the macroscale. To account for possible counting uncertainties associated with macroscale counts, varve counts from all \geq cm thickness varves were compared between macroscale and thin sections. In total, 55 \geq cm thickness varves were counted from macroscale analysis and 56 from thin sections, equating to a 1.8% error. Therefore, a count error of 1.8% was applied to varved sections of the core that were analysed and counted at the macroscale. This equated to 36 varve^{MAC} \pm 1. The following tables summarise the varve chronology.

Six breaks were identified in the Glottern varve sequence within LF2 and LF1. These breaks are comprised of deformed laminations.

Table 8-4. Summary of breaks in varve^{TSA} sedimentation.

Lithofacies	Depth (cm)	Type of break			
		Deformation	Silt Bed	Unclear laminations	Total
LF1	900-598	6	0	0	6
LF2	598-470	0	0	0	0
	Total	6	0	0	6

In total 207 ±1 varves and 6 sections of non-varved sediment were identified from thin sections. The varve^{TSA} thickness characteristics of the Glottern record are presented for each lithofacies (Table 8-5).

The varve thickness record is divided based on lithofacies units 1 and 2, however there are thickness variations within each unit. Thickness characteristics in each 100 cm are included in the appendices. In LF1 there are 79 varves with an average thickness of 26.5 mm. The average thickness, however, decreases from the base to the top of the unit. The ratio of coarse to fine laminations remains constant at approximately 2:1 and the minimum varve thickness measurement is 6.5 mm with a maximum of 98.4 mm.

In LF2, there are 128 varves with an average thickness of 5.4 mm. Melt season layers are typically thicker than non-melt season layers but can be approximately equal. The ratio of coarse to fine laminations fluctuates between 2:1 and 1:1. The minimum varve thickness measurement in LF2 is 2.0 mm with a maximum of 14.3 mm.

Table 8-5. Summarised varve thickness characteristics in each lithofacies

Lithofacies	Depth (cm)	Varve number	Varves (n)	Mean (mm)	St dev	Min (mm)	Median (mm)	Max (mm)	Coarse:Fine
LF1	900-600	1-79	79	26.5	15.3	6.5	23.8	98.4	2:1
LF2	600-492	80-207	128	5.4	2.7	2.0	4.5	14.3	2:1/1:1

A summary of the Lamination Sets and Varve Quality (VQ) at Glottern are shown in Figure 8-6 alongside raw (mm) and normalised varve thickness.

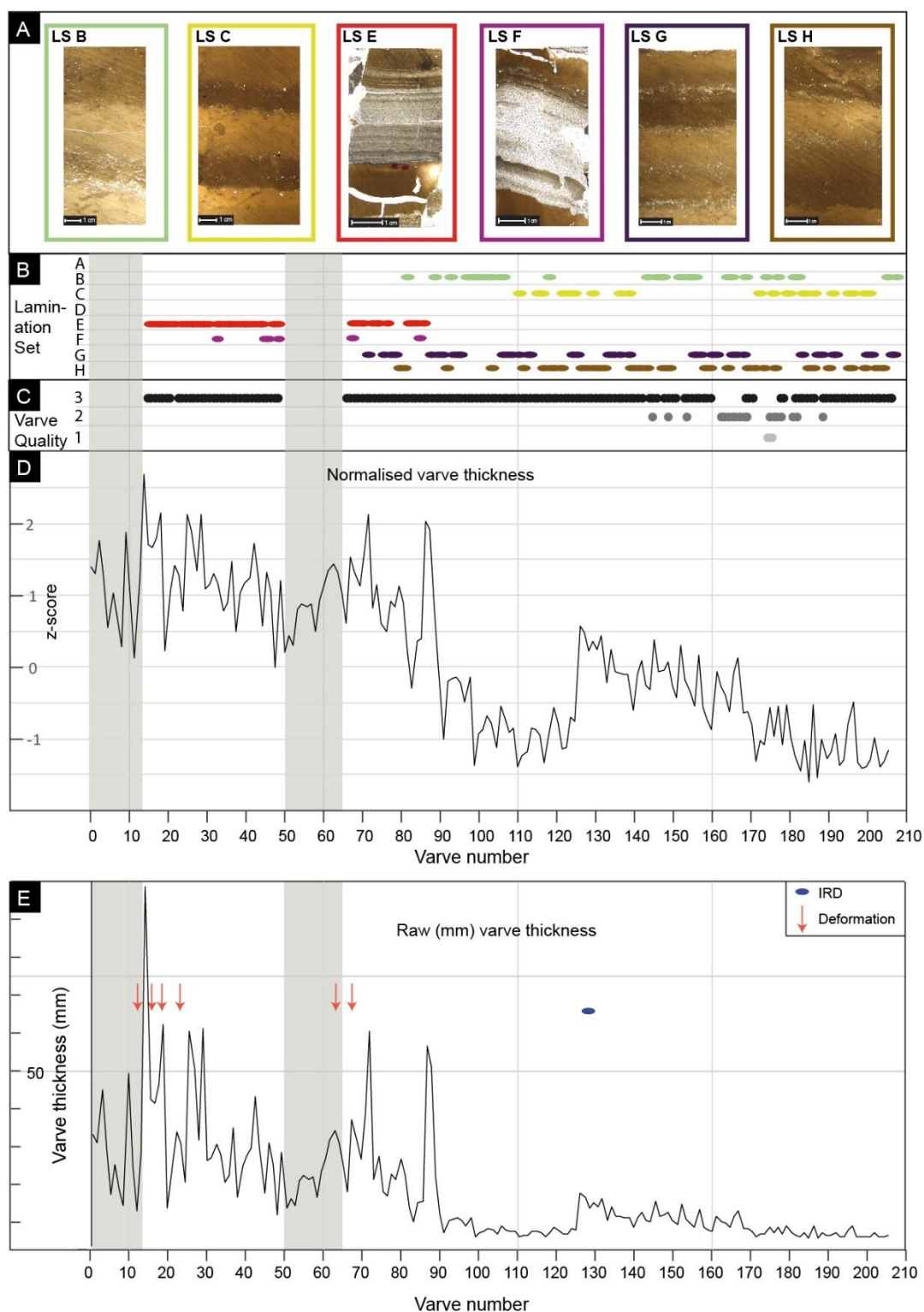


Figure 8-6. Normalised varve thickness record plotted alongside Varve Quality, Lamination Sets and occurrence of IRD and deformation.

(A) Lamination Sets, (B) distribution of Lamination Sets throughout the sequence, (C) Varve Quality, (D) Normalised varve^{TSA} thickness record, (E) Raw (mm) varve thickness. Varve 1 is at the base of the sequence such that the diagram should be read from left to right as from base-to-top. Grey boxes indicate sections of the varve sequence that were counted at the macroscale.

8.4 Summary

The revised methodology outlined in section 6.6.5 was successfully applied to the Glottern sediment sequence. Macroscale analysis provided a general description of the sediments and was used to produce sediment logs. Thin section analysis was used to refine sedimentological descriptions and interpretation of depositional processes which resulted in construction of an accurate varve chronology. The basal ca 80 varves are composed of coarser-grained, multi-laminated summer components (LS E and LS F) whereas the uppermost varves are finer grained and can be composed of single lamination summer components (LS B and LS C) or multi-laminated summer components (LS G and LS H). In total 173 of 207 varves were analysed under thin section and of these 156 (90%) were assigned a VQ score of 3, 15 (9%) were assigned a VQ score of 2, and 2 (1%) were assigned a VQ score of 1. The lower VQ scores are located in the upper part of the varve record and are typically associated with varves of Lamination Sets B, C, G and H (Figure 8-6). The Glottern varve record contains 207 ± 1 vyrs and 6 zones of deformation. A second varve count is pending though the ± 1 vyrs uncertainty was applied to the sequence to account for two sections of the varve record that were analysed macroscopically (section 8.3). The following chapter presents the tephra results from each site.

Chapter 9. Tephra results

This chapter presents the results of tephra analysis. Tephra shards were identified within the sediment sequences from all sites in this thesis, but chemical analyses were only possible for Asplången and Glottern. For the Svinstadsjön samples, difficulties were encountered during the stub polishing process with further details provided in section 9.2. Firstly, the stratigraphic position of the tephra layers is presented alongside descriptions of shard morphologies and shard concentrations for each site. Following this, chemical data are presented for each layer and classification of the tephra layers is made via total alkali vs silica diagrams (Le Bas *et al.*, 1986) and by K-series plots (Peccerillo and Taylor, 1976). Correlations are then made within and between sites followed by an overview of known tephras deposited in the North Atlantic region during the Lateglacial and early-Holocene. Correlations to known tephras are then proposed for each sample with published tephra data used for correlations presented in the appendices. The final part of this chapter discusses the implications of the results of this chapter for the published ages of the identified tephras. In Chapter 10, the varve spacing between the identified tephras at Asplången are used to re-model the ages of those tephras. The local and wider significance of these correlations for palaeoenvironmental and palaeoclimatic interpretations is discussed in Chapter 11.

9.1 Svinstadsjön tepthrostratigraphy

Subsamples taken from borehole A and C were processed for tephra at contiguous 10 cm intervals, whilst in boreholes B and D two 10 cm subsamples were extracted from the central 20 cm of each core to account for overlaps. Volcanic glass shards were found in two of the 10 cm samples from 400-410 cm depth and 800-810 cm depth. For sample 400-410 cm, which encompasses 5 varves^{TSA} (varve^{TSA} 297 to 301), one shard was identified (Figure 9-1). The shard measures approximately 25 µm along its a-axis and exhibits large open vesicles and smaller closed vesicles (Figure 9-1). All remaining sediments at 400-410 cm depth were re-sampled at varve scale for chemical preparation, but no additional shards were found. For sample 800-810 cm, one shard was identified in a scan sample that contained 8 varves^{TSA} (varve^{TSA} 65 to 72). The shard measures approximately 30 µm along its a-axis and has cusped edges and a large open vesicle (Figure 9-1). All remaining sediments at 800-810 cm depth were re-sampled to varve scale for chemical preparation, and three additional shards were extracted from

varve number 68. This tephra is comprised of small (20-30 μm), extremely thin shards with open and closed vesicles and cusped edges.

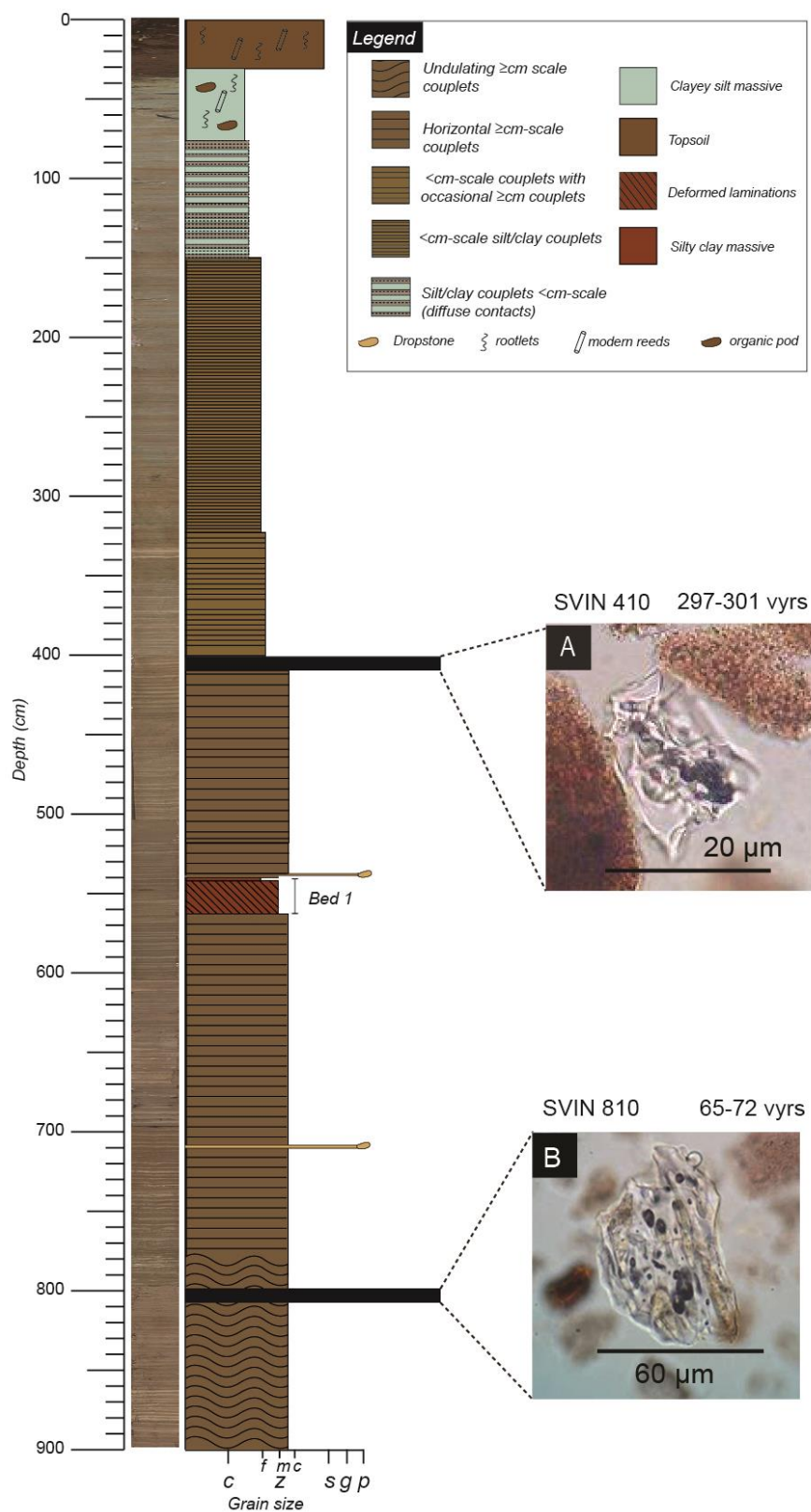


Figure 9-1. Svinstadsjön tephrostratigraphy. (A) Shard found in sample SVIN410 in varves 297-301, (B) Shard found in sample SVIN810 in varves 65-72.

9.2 Svinstadsjön tephra classification

Due to the exceptionally thin structure of these shards, difficulties were encountered during stub polishing. It is likely that the resin stubs were not sufficiently polished and so the thin shards in this sample were not exposed at the stub surface, thus yielding unsuccessful chemical analyses. At present it is not possible to chemically classify or correlate these tephras to known eruptions. However, possible tephra correlations are proposed in Chapter 11 using the results from Bayesian age modelling outlined in Chapter 10.

9.3 Asplången tephrostratigraphy

Subsamples taken from borehole A and D were processed for tephra at contiguous 10 cm intervals, whilst in boreholes B and C two 10 cm subsamples were extracted from the central 20 cm of each core to account for overlaps. Volcanic glass shards were found in several scan samples at 1150-1160 cm, 530-540 cm, 520-530 cm, 510-520 cm, 400-410 cm and 300-310 cm depth. Sample 1150-1160 cm is composed of varved sediments, samples 530-540 cm, 520-530 cm, 510-520 cm are located at the base of LF4 and samples 400-410 cm and 300-310 cm are located in the middle and top of LF4 respectively (Figure 9-2). In total eight samples were chosen for chemical analysis and analyses were obtained for all samples. Raw chemical data alongside mean and standard deviations are presented for each sample in Table 9-1.

9.3.1 ASP 1160

In scan sample 1150-1160 cm, which encompasses 5 varves^{TSA} (varve^{TSA} 31 to 35), one shard was identified (Figure 9-2). The shard measures approximately 25 μm along its a-axis and exhibits large open vesicles and smaller closed vesicles (Figure 9-2). All remaining sediments at 1150-1160 cm depth were re-sampled at varve scale for chemical preparation and 4 shards from varve 34 were picked and mounted.

9.3.2 Samples from 510-540 cm

Shard concentrations were calculated at 1 cm resolution between 510-540 cm. A distinct peak of 726 shards g^{-1} is observed at 535-537 cm followed by a 10 cm tail in shard numbers. A second smaller peak of 102 shards g^{-1} is observed within the tail at 530 cm. Two other peaks were observed at 524 cm and 516 cm with shard concentrations of 29 shards g^{-1} and 6 shards g^{-1} respectively (Figure 9-2). Across this interval shards exhibit cusped edges, open and closed vesicles, microlites and flutes with no obvious

differences between samples (Figure 9-2). Five samples were prepared for chemical analysis: ASP 537, ASP 536, ASP 530, ASP 524 and ASP 516.

9.3.3 ASP 537 and ASP 536

In total 100 shards (50 from each sample) were picked and mounted for chemical analysis with 23 analyses obtained (ASP 537 n=17, ASP 536 n=6).

9.3.4 ASP 530

In total 2 shards were picked and mounted for chemical analysis and 3 analyses from a single shard were obtained.

9.3.5 ASP 524

In total one shard was picked and mounted for chemical analysis with 2 analyses obtained.

9.3.6 ASP 516

In total 5 shards were picked and mounted for chemical analysis with 7 analyses obtained from 3 shards.

9.3.7 ASP 410 and ASP 402

Shard concentrations were calculated at 1 cm resolution between 400-410 cm. Two distinct peaks of 6 shards g⁻¹ at 410 cm and 11 shards g⁻¹ at 402 cm were identified. Shards exhibit cusped edges but are otherwise featureless. Both samples were prepared for chemical analysis. For ASP 410, 3 shards were picked and mounted with 4 analyses obtained from 2 shards.

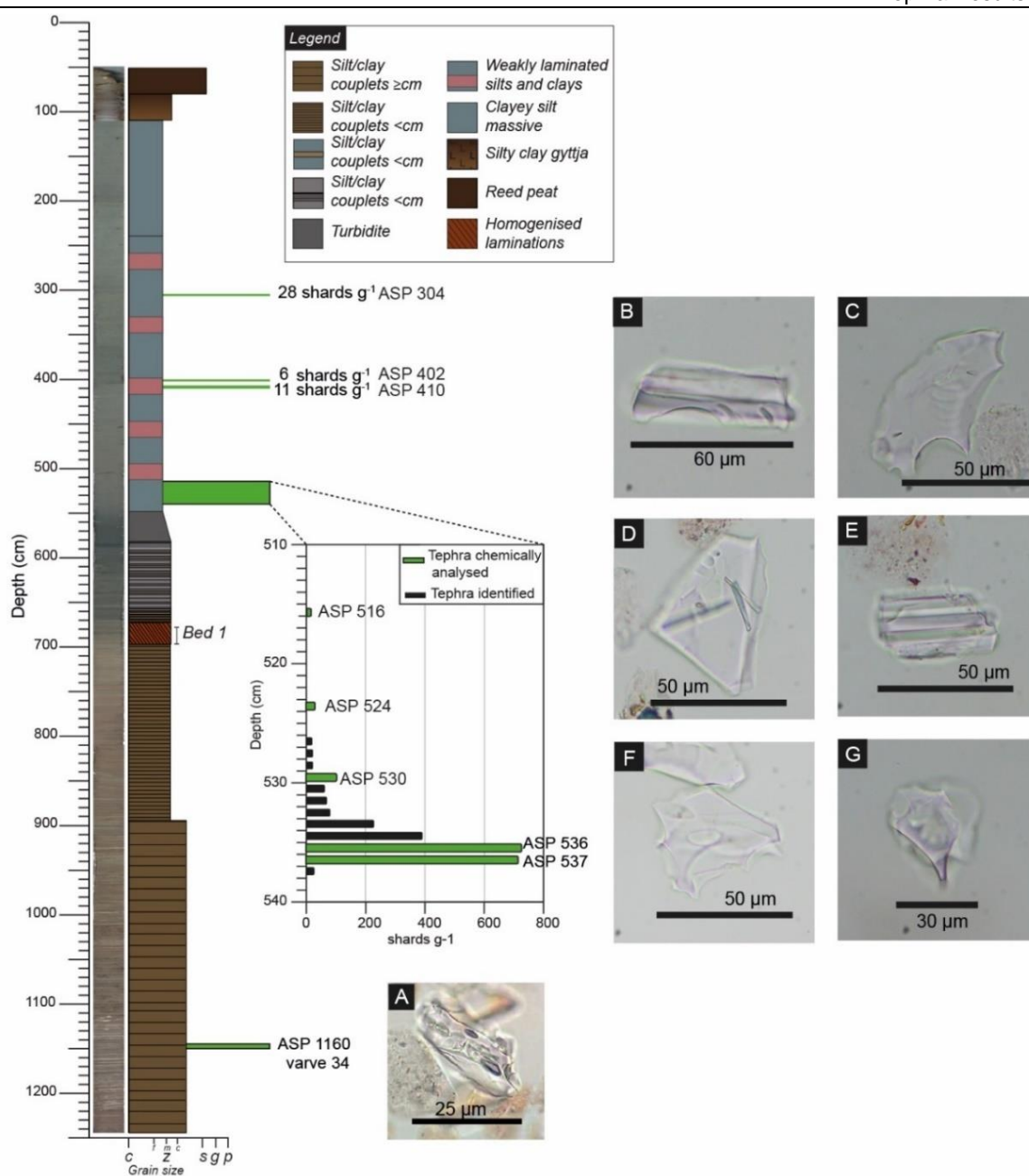


Figure 9-2. Asplången tephrostratigraphy.

(A) Tephra shard from ASP 1160 which displays open and closed vesicles and cusped edges. (B) Example of a fluted shard with cusped edge from ASP 537. (C) Example of a shard with cusped edges from ASP 536. (D) Example of a microlitic shard from ASP 537. (E) Fluted shard from ASP 530. (F) Shard with open vesicles and cusped edges from ASP 524. (G) Shard from ASP 516 with cusped edges and open vesicles.

Table 9-1. Raw and mean chemical data for Asplången, values expressed as weight % oxide.

Tephra Code	SiO₂	TiO₂	Al₂O₃	FeO	MnO	MgO	CaO	Na₂O	K₂O	P₂O₅	Total
ASP 1160	72.25	0.28	12.05	2.54	0.09	0.25	1.57	4.07	2.45	0.05	95.60
ASP 537	72.09	0.12	12.02	1.67	0.04	0.07	0.69	4.53	3.77	0.02	95.01
ASP 537	72.10	0.12	11.82	1.62	0.04	0.06	0.63	4.58	3.72	0.01	94.69
ASP 537	73.11	0.12	11.62	1.46	0.05	0.09	0.74	4.17	3.84	0.02	95.22
ASP 537	72.21	0.11	12.15	1.55	0.03	0.06	0.68	4.32	3.73	0.01	94.86
ASP 537	73.14	0.12	11.60	1.52	0.04	0.04	0.65	4.19	3.62	0.04	94.97
ASP 537	72.88	0.12	11.97	1.52	0.05	0.07	0.77	4.38	3.73	0.04	95.52
ASP 537	73.27	0.12	11.82	1.71	0.04	0.06	0.74	3.95	3.95	0.02	95.68
ASP 537	72.20	0.12	11.73	1.53	0.04	0.09	0.74	4.23	3.64	0.01	94.32
ASP 537	73.98	0.12	11.86	1.51	0.04	0.07	0.76	4.39	3.77	0.02	96.53
ASP 537	71.88	0.12	12.41	1.50	0.05	0.09	0.66	4.06	3.82	0.01	94.60
ASP 537	73.18	0.12	11.44	1.76	0.05	0.11	0.69	4.25	3.61	0.01	95.21
ASP 537	72.23	0.12	11.48	1.50	0.04	0.07	0.69	4.06	3.77	0.01	93.98
ASP 537	72.52	0.11	11.80	1.52	0.05	0.05	0.63	3.98	3.67	0.01	94.33
ASP 537	72.85	0.10	12.19	1.45	0.03	0.07	0.66	4.27	3.83	0.00	95.45
ASP 537	72.35	0.12	11.65	1.72	0.04	0.06	0.73	4.54	3.78	0.01	95.01
ASP 537	72.87	0.12	11.02	1.56	0.05	0.06	0.76	3.81	3.76	0.02	94.03
ASP 537	72.10	0.13	12.25	1.53	0.04	0.08	0.82	4.40	3.60	0.00	94.94
ASP 537	72.35	0.12	12.01	1.60	0.05	0.06	0.81	4.07	3.78	0.02	94.88
Mean	72.63	0.12	11.82	1.57	0.04	0.07	0.71	4.23	3.74	0.02	94.96
stdev. (n=18)	0.54	0.01	0.33	0.09	0.01	0.02	0.06	0.21	0.09	0.01	0.60

Tephra Code	SiO ₂	TiO ₂	Al ₂ O ₃	FeO	MnO	MgO	CaO	Na ₂ O	K ₂ O	P ₂ O ₅	Total
ASP 536	72.04	0.13	12.12	1.49	0.05	0.07	0.63	4.38	3.80	0.02	94.72
ASP 536	72.15	0.11	11.65	1.47	0.04	0.05	0.71	4.11	3.80	0.01	94.09
ASP 536	72.23	0.13	11.93	1.70	0.04	0.07	0.83	4.33	3.89	0.01	95.16
ASP 536	72.52	0.12	12.72	1.47	0.05	0.07	0.72	4.55	3.76	0.01	95.99
Mean	72.24	0.12	12.11	1.53	0.05	0.07	0.72	4.34	3.81	0.01	94.99
stdev. (n=4)	0.21	0.01	0.45	0.12	0.01	0.01	0.08	0.18	0.05	0.00	0.80
ASP 530	72.06	0.12	12.35	1.79	0.04	0.08	0.74	4.53	3.76	0.01	95.48
ASP 530	72.78	0.11	11.30	1.46	0.04	0.05	0.68	4.27	3.70	0.02	94.42
ASP 530	73.99	0.07	10.93	1.19	0.02	0.03	0.46	3.78	3.98	0.01	94.46
Mean	72.94	0.10	11.53	1.48	0.04	0.06	0.63	4.19	3.81	0.01	94.79
stdev. (n=3)	0.97	0.02	0.74	0.30	0.01	0.02	0.15	0.38	0.15	0.01	0.60
ASP 524	72.31	0.12	12.60	1.45	0.03	0.06	0.70	4.45	3.85	0.02	95.61
ASP 524	72.21	0.11	12.31	1.57	0.04	0.08	0.74	4.27	3.86	0.01	95.21
Mean	72.26	0.12	12.46	1.51	0.04	0.07	0.72	4.36	3.86	0.02	95.41
stdev. (n=2)	0.08	0.00	0.20	0.09	0.01	0.01	0.03	0.13	0.01	0.01	0.28
ASP 516	72.87	0.12	11.76	1.49	0.04	0.07	0.74	4.28	3.71	0.01	95.10
ASP 516	72.18	0.12	11.57	1.43	0.04	0.07	0.74	4.21	3.76	0.01	94.13
Mean	72.52	0.12	11.67	1.46	0.04	0.07	0.74	4.25	3.73	0.01	94.62
stdev. (n=2) pop. A	0.48	0.01	0.14	0.04	0.00	0.00	0.00	0.05	0.03	0.00	0.68

Tephra Code	SiO ₂	TiO ₂	Al ₂ O ₃	FeO	MnO	MgO	CaO	Na ₂ O	K ₂ O	P ₂ O ₅	Total
ASP 516	67.37	0.27	12.52	3.49	0.15	0.20	1.27	5.90	3.32	0.04	94.53
ASP 516	69.51	0.28	12.97	4.01	0.15	0.21	1.28	5.20	3.53	0.03	97.17
ASP 516	69.00	0.28	12.62	3.73	0.13	0.20	1.36	5.54	3.41	0.05	96.31
ASP 516	69.54	0.29	12.96	3.51	0.14	0.22	1.37	5.64	3.45	0.05	97.16
ASP 516	69.10	0.27	11.99	3.66	0.15	0.22	1.39	5.18	3.45	0.04	95.44
Mean	68.91	0.28	12.61	3.68	0.14	0.21	1.33	5.49	3.43	0.04	96.12
stdev. (n=5) pop. B	0.89	0.01	0.40	0.21	0.01	0.01	0.05	0.31	0.08	0.01	1.14
ASP 410	73.62	0.11	12.08	1.48	0.04	0.02	0.60	4.43	3.91	0.01	96.30
ASP 410	74.12	0.10	11.23	1.42	0.05	0.07	0.73	4.46	3.72	0.01	95.92
ASP 410	72.78	0.11	11.43	1.42	0.03	0.03	0.62	3.76	3.85	0.01	94.05
Mean	73.51	0.11	11.58	1.44	0.04	0.04	0.65	4.22	3.83	0.01	95.42
stdev. (n=3) pop. A	0.55	0.00	0.36	0.03	0.01	0.02	0.06	0.32	0.08	0.00	0.98
ASP 410 pop. B	68.35	0.27	12.37	3.69	0.16	0.20	1.28	4.92	3.49	0.04	94.78
ASP 402	67.43	0.31	13.49	3.97	0.16	0.19	1.41	5.86	3.44	0.07	96.31

9.4 Asplången tephra classification

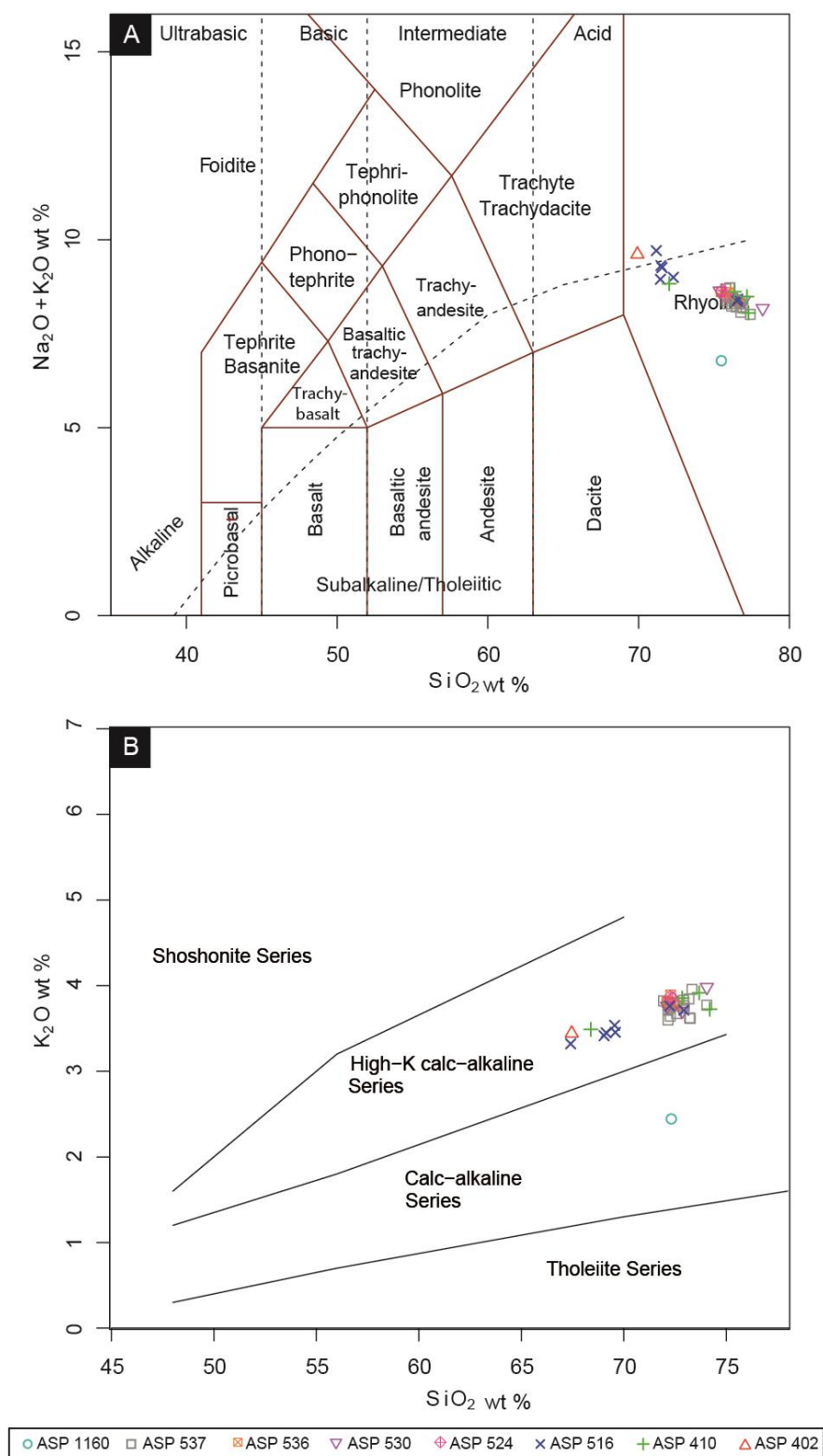


Figure 9-3. Asplången tephra classification.

Tephra samples plotted as (A) Total alkali vs Silica (Le Bas et al., 1986), (B) K-series (Peccerillo and Taylor, 1976).

9.4.1 ASP 1160

In varve 34 at Asplången one shard was successfully chemically analysed and is defined as a sub-alkaline rhyolite with medium potassium values (Figure 9-3). It is chemically characterised by Na₂O 4.07 wt%, CaO 1.57 wt% and FeO 2.54 wt%.

9.4.2 ASP 537 and ASP 536

Chemical analyses from ASP 537 and ASP 536 are defined as sub-alkaline rhyolites with high potassium values (Figure 9-3). Both samples are a homogenous population which is composed of shards with Na₂O values of ca 4.25 wt%, CaO totals of ca 0.72 wt% and FeO totals of ca 1.56 wt%.

9.4.3 ASP 530 and ASP 524

Chemical analyses from ASP 530 and ASP 524 are defined as sub-alkaline rhyolites with high potassium values (Figure 9-3). The shard from ASP 530 has Na₂O values of ca 4.19 wt%, CaO totals of ca 0.63 wt% and FeO totals of ca 1.48 wt%. The shard from ASP 524 is defined by Na₂O 4.36 wt%, CaO 0.72 wt% and FeO totals of ca 1.51 wt%.

9.4.4 ASP 516

Chemical analyses revealed two distinct populations; population A is obtained from 2 analyses from a single shard and is defined as a sub-alkaline rhyolite with high potassium values (Figure 9-3). The shard has Na₂O values of ca 4.25 wt%, CaO totals of ca 0.74 wt% and FeO totals of ca 1.46 wt%. Population B is obtained from 5 analyses from 2 shards and is defined as a sub-alkaline rhyolite with high potassium values (Figure 9-3). The shards have Na₂O values of ca 5.49 wt%, CaO totals of ca 1.33 wt% and FeO totals of ca 3.68 wt%.

9.4.5 ASP 410

ASP 410 is a mixed layer with two distinct populations; population A is obtained from 4 analyses from a single shard and is defined as a sub-alkaline rhyolite with high potassium values (Figure 9-3). The shard has Na₂O values of ca 4.22 wt%, CaO totals of ca 0.65 wt% and FeO totals of ca 1.44 wt%. Population B is obtained from 1 analysis of a single shard and is defined as a sub-alkaline rhyolite with high potassium values (Figure 9-3). The shard has Na₂O values of 4.92 wt%, CaO totals of 1.28 wt% and FeO totals of 3.69 wt%.

9.4.6 ASP 402

For ASP 402, 1 shard was picked and mounted with a single analysis obtained. The shard is defined as a sub-alkaline rhyolite with high potassium values (Figure 9-3). The shard has Na₂O values of 5.86 wt%, CaO totals of 1.41 wt% and FeO totals of 3.97 wt%.

9.5 Glottern tephrostratigraphy

Subsamples taken from borehole A and B were processed for tephra at contiguous 10 cm intervals, whilst in boreholes C and D two 10 cm samples were extracted from the central 20 cm of each core to account for overlaps. Volcanic glass shards were found in one range finder sample at 300-310 cm depth at the base of LF5 in unlaminated sediments (Figure 9-4). The horizon was refined to a 2 cm interval at 303-305 cm. In total two samples were taken for chemical analysis and analyses were obtained for both samples. Raw chemical data alongside mean and standard deviations are presented for each sample in Table 9-2.

9.5.1 GLO 304 and GLO 305

Shard concentrations were not calculated for the Glottern sequence. In both samples, the shards display open vesicles with cusped edges and there is some evidence of corrosion (Figure 9-4). In total 89 shards were identified, and 46 shards were picked and mounted for chemical analysis with 26 analyses obtained from two 1 cm samples: GLO 304 (n=11) and GLO 305 (n=15).

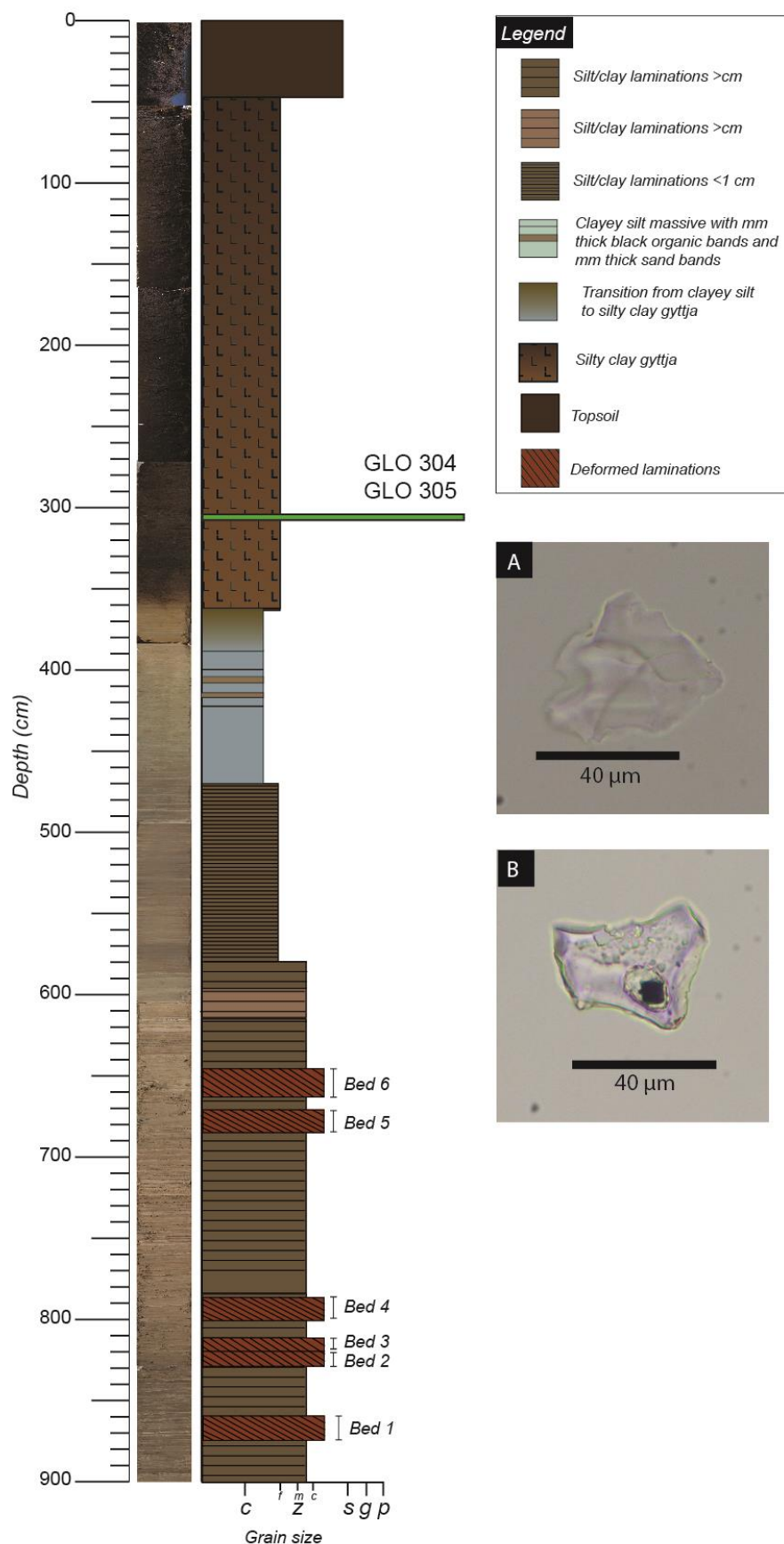


Figure 9-4. Glottern tepthrostratigraphy. (A) Example shard from GLO 304 with cusped edges and open vesicles. (B) Example of a weathered shard in GLO 305.

Table 9-2. Chemical data for GLO 304 and GLO 305, values expressed as weight % oxide.

Tephra Code	SiO ₂	TiO ₂	Al ₂ O ₃	FeO	MnO	MgO	CaO	Na ₂ O	K ₂ O	P ₂ O ₅	Total
GLO 304	74.05	0.30	12.71	2.52	0.08	0.22	1.50	4.53	2.45	0.05	98.42
GLO 304	74.04	0.29	12.48	2.68	0.07	0.26	1.48	4.65	2.54	0.04	98.52
GLO 304	73.65	0.30	11.92	2.49	0.07	0.24	1.53	4.16	2.55	0.05	96.96
GLO 304	73.91	0.30	12.68	2.51	0.09	0.26	1.68	4.41	2.49	0.05	98.36
GLO 304	74.51	0.31	12.25	2.40	0.08	0.24	1.63	4.53	2.49	0.05	98.50
GLO 304	74.54	0.30	12.85	2.67	0.09	0.23	1.61	4.76	2.51	0.05	99.61
GLO 304	73.67	0.30	12.52	2.49	0.09	0.25	1.52	4.52	2.52	0.05	97.92
GLO 304	74.46	0.29	12.06	2.42	0.10	0.26	1.51	4.37	2.48	0.04	97.99
GLO 304	74.19	0.28	11.75	2.55	0.08	0.22	1.67	4.76	2.55	0.04	98.11
GLO 304	73.59	0.30	12.41	2.36	0.08	0.23	1.58	4.90	2.50	0.04	97.99
GLO 304	72.84	0.30	12.33	2.45	0.09	0.25	1.52	4.59	2.43	0.04	96.83
Mean	73.95	0.30	12.36	2.50	0.08	0.24	1.56	4.56	2.50	0.05	98.11
stdev. (n=11)	0.50	0.01	0.34	0.10	0.01	0.01	0.07	0.21	0.04	0.01	0.76
GLO 305	73.30	0.29	12.43	2.49	0.10	0.22	1.65	4.61	2.50	0.05	97.65
GLO 305	74.55	0.29	12.88	2.63	0.08	0.26	1.51	4.44	2.45	0.05	99.15
GLO 305	75.45	0.30	12.47	2.43	0.08	0.24	1.59	4.31	2.58	0.04	99.50
GLO 305	74.40	0.29	11.99	2.55	0.10	0.22	1.50	4.43	2.55	0.04	98.08
GLO 305	74.12	0.30	11.94	2.42	0.09	0.26	1.41	4.40	2.46	0.05	97.44
GLO 305	74.85	0.29	12.42	2.53	0.10	0.26	1.56	3.99	2.54	0.05	98.58
GLO 305	76.06	0.31	13.13	2.47	0.07	0.26	1.61	4.08	2.58	0.06	100.63
GLO 305	72.68	0.29	11.89	2.50	0.09	0.26	1.55	4.38	2.38	0.04	96.06

Tephra Code	SiO₂	TiO₂	Al₂O₃	FeO	MnO	MgO	CaO	Na₂O	K₂O	P₂O₅	Total
GLO 305	73.36	0.30	12.03	2.60	0.08	0.23	1.56	4.26	2.61	0.04	97.07
GLO 305	73.46	0.30	11.34	2.46	0.08	0.26	1.55	4.65	2.52	0.04	96.65
GLO 305	73.40	0.30	11.66	2.43	0.09	0.25	1.54	4.88	2.47	0.05	97.06
GLO 305	73.93	0.30	12.49	2.37	0.10	0.25	1.64	4.38	2.58	0.04	98.10
GLO 305	73.85	0.30	13.12	2.45	0.09	0.25	1.63	4.25	2.43	0.04	98.40
GLO 305	72.86	0.30	12.27	2.52	0.08	0.23	1.48	4.74	2.42	0.05	96.95
GLO 305	72.26	0.30	12.08	2.46	0.08	0.23	1.44	4.50	2.50	0.05	95.90
Mean	73.90	0.30	12.28	2.49	0.09	0.25	1.55	4.42	2.50	0.05	97.81
stdev. (n=15)	1.04	0.00	0.51	0.07	0.01	0.02	0.07	0.24	0.07	0.01	1.30

9.6 Glottern tephra classification

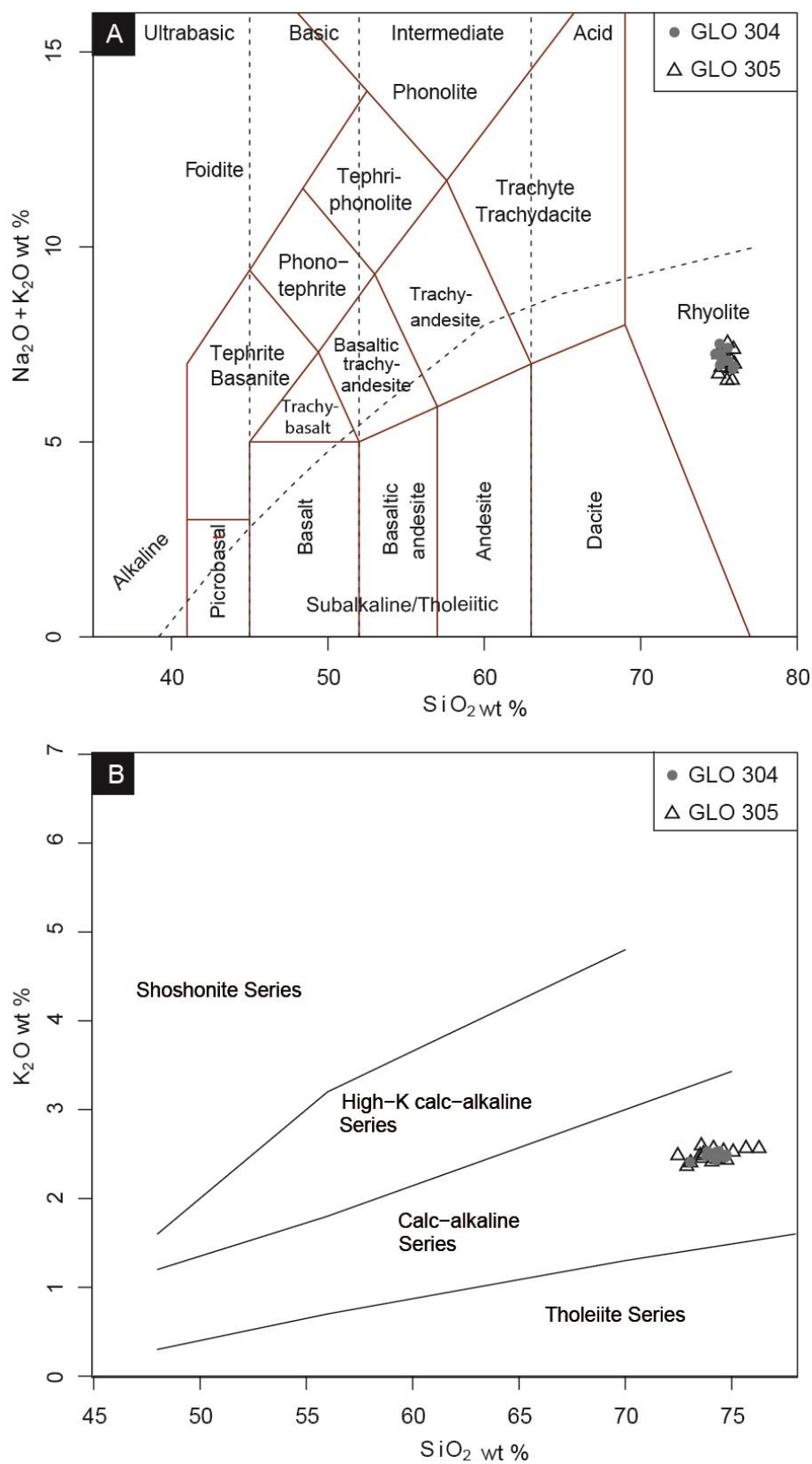


Figure 9-5. Glottern tephra classification. Tephra samples plotted as (A) Total alkali vs Silica (Le Bas et al., 1986), (B) K-series (Peccerillo and Taylor, 1976).

9.6.1 GLO 304 and GLO 305

Both tephra layers are defined as sub-alkaline rhyolites with medium potassium values (Figure 9-5). Chemically, the horizons are a homogenous population which is composed of shards with Na₂O values of ca 4.47 wt%, CaO totals of ca 1.56 wt% and FeO totals of ca 2.49 wt%. Raw and mean chemical data are presented in Table 9-2.

9.7 Tephra correlations

The following section presents: 1) correlations of the identified tephras within and between sites; 2) known tephras from the Lateglacial-early Holocene periods; 3) proposed correlations to known tephras for each sample; and 4) where applicable, implications of the proposed correlations for the published ages of the tephras.

9.7.1 Correlations within and between sites

The tephras generated in this thesis from the Asplången and Glottern records are characterised by three distinct chemical groups. Group 1 includes samples from both the Asplången and Glottern sequence: ASP 1160, GLO 304 and GLO 305. These shards have medium potassium values that are slightly lower than Groups 2 and 3. Group 2 includes samples ASP 537, ASP 536, ASP 530, ASP 524 and population A of samples ASP 516 and ASP 410. These shards have high potassium values and slightly higher silica values than Group 3. Group 3 includes population B of samples ASP 516 and ASP 410, and sample ASP 402. These shards have high potassium values and slightly lower silica values than Groups 1 and 2 (Figure 9-6).

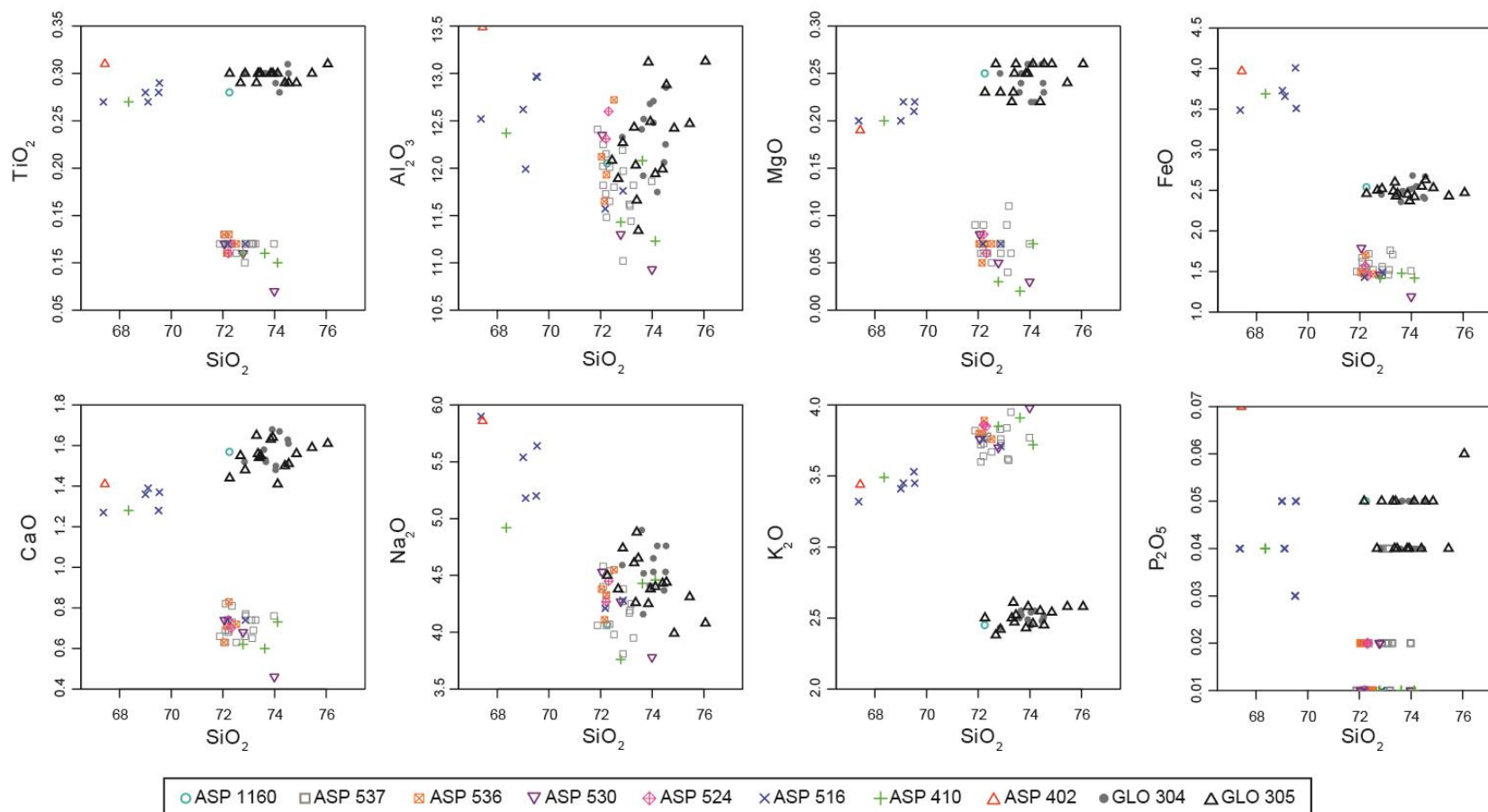


Figure 9-6. Harker variation plots for the Asplången and Glottern tephras.

Three chemical groups can be observed. Group 1: ASP 1160, GLO 304 and GLO 305, Group 2: ASP 537, ASP 536, ASP 530, ASP 524, population A of ASP 516 and population A of ASP 410, Group 3: population B of ASP 516, population B of ASP 410, ASP 402.

9.7.2 Correlations to known tephras

Multiple tephras have been identified throughout the Lateglacial and early Holocene periods across the North Atlantic region (Figure 9-7). The main sources of tephra to Sweden during this time period are the Icelandic and Eifel volcanic centres (e.g. Wastegård, 2005; Larsson and Wastegård, 2018).

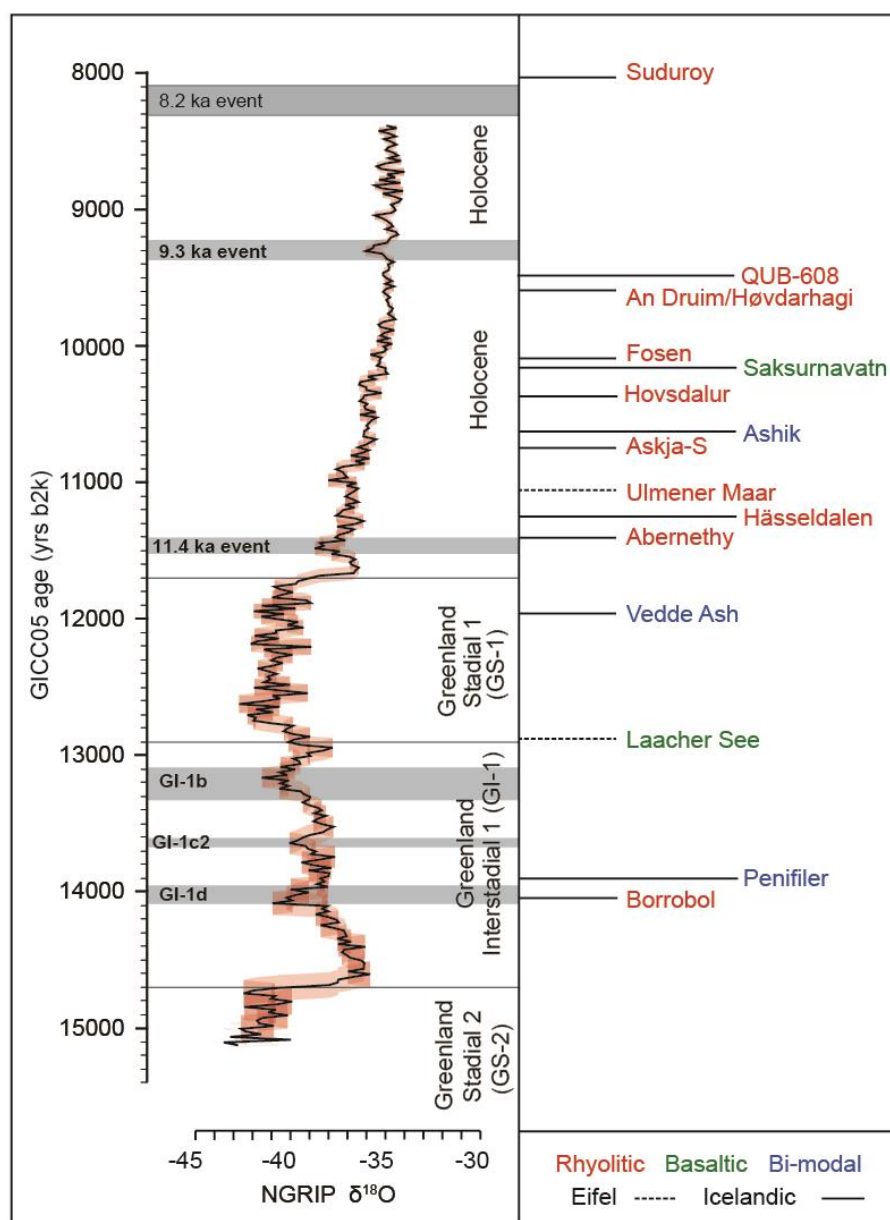


Figure 9-7. The $\delta^{18}\text{O}$ record and event stratigraphy from the NGRIP for the LGIT (Rasmussen et al., 2006, 2014) alongside key tephras from the Icelandic and Eifel volcanic centres that have been identified across the North Atlantic region. Modified from Timms et al. (2019).

The following ages in cal. yrs BP are used for the tephras. Borrobol $14,098 \pm 94$, Penifiler $13,919 \pm 132$, Laacher See $12,937 \pm 46$, Vedde Ash $12,023 \pm 86$, Abernethy $11,462 \pm 144$, Ulmener Maar $11,096 \pm 117$ (Bronk Ramsey et al., 2015). Hässeldalen $11,316 \pm 124$ (Wastegård et al., 2018), Askja-S $10,824 \pm 97$ (Kearney et al., 2018), Ashik $10,716 \pm 230$ (Timms et al., 2017), Hovsdalur $10,475 \pm 350$ (Wastegård, 2002), Sakurnavatn $10,210 \pm 35$ (Lohne et al., 2014), Fosen $10,139 \pm 116$ (Timms et al., 2017), An Druim/Høvdarhagi (Timms, 2016), QUB-608 ca 9,500 (Pilcher et al., 2005), Suduroy $8,073 \pm 192$ (Wastegård, 2002).

Since the tephra generated in this thesis are rhyolitic tephtras, the basaltic Saksurnavatn and Laacher See tephtras, as well as the basaltic components of the Vedde Ash and Ashik tephtras are not viable correlatives. With the exception of the Laacher See Tephra (Larsson and Wastegård, 2018), these basaltic tephtras have not been identified in sediment sequences in Sweden. Potential correlatives to the tephtras in this thesis can be further constrained using published chronological information. For example, the radiocarbon ages from the varved sediments at Glottern indicate a *ca* 12,500 cal. yrs BP age for the site (Wohlfarth *et al.*, 1998). Since samples GLO 304 and GLO 305 are located in gyttja sediments 1.88 m stratigraphically above glacial varves, tephtras older than *ca* 12,500 cal. yrs BP are also not viable correlatives (e.g. Penifiler and Borrobol tephtras). This is further supported by other chronological information (e.g. Hughes *et al.*, 2016; Stroeven *et al.*, 2016) that indicate a Younger Dryas deglaciation age for the Glottern and Asplången sites (see also Chapters 2 and 3). Therefore, only rhyolitic tephtras from the mid-Younger Dryas to the early Holocene are potential correlatives for the tephtra generated in this thesis, and these are plotted in Figure 9-8.

The tephtra groups identified in Figure 9-6 can be correlated to known rhyolitic tephtras from the Lateglacial and early Holocene periods. For Group 1 the chemical data suggest a correlation with the Askja-S tephtra, Group 2 a correlation with Borrobol-type tephtras and Group 3 a correlation to tephtras of a Katla origin with Vedde Ash-type chemistry (Figure 9-8). These correlations are discussed further in the following sections using other contextual information such as the stratigraphic position of each sample and varve spacing.

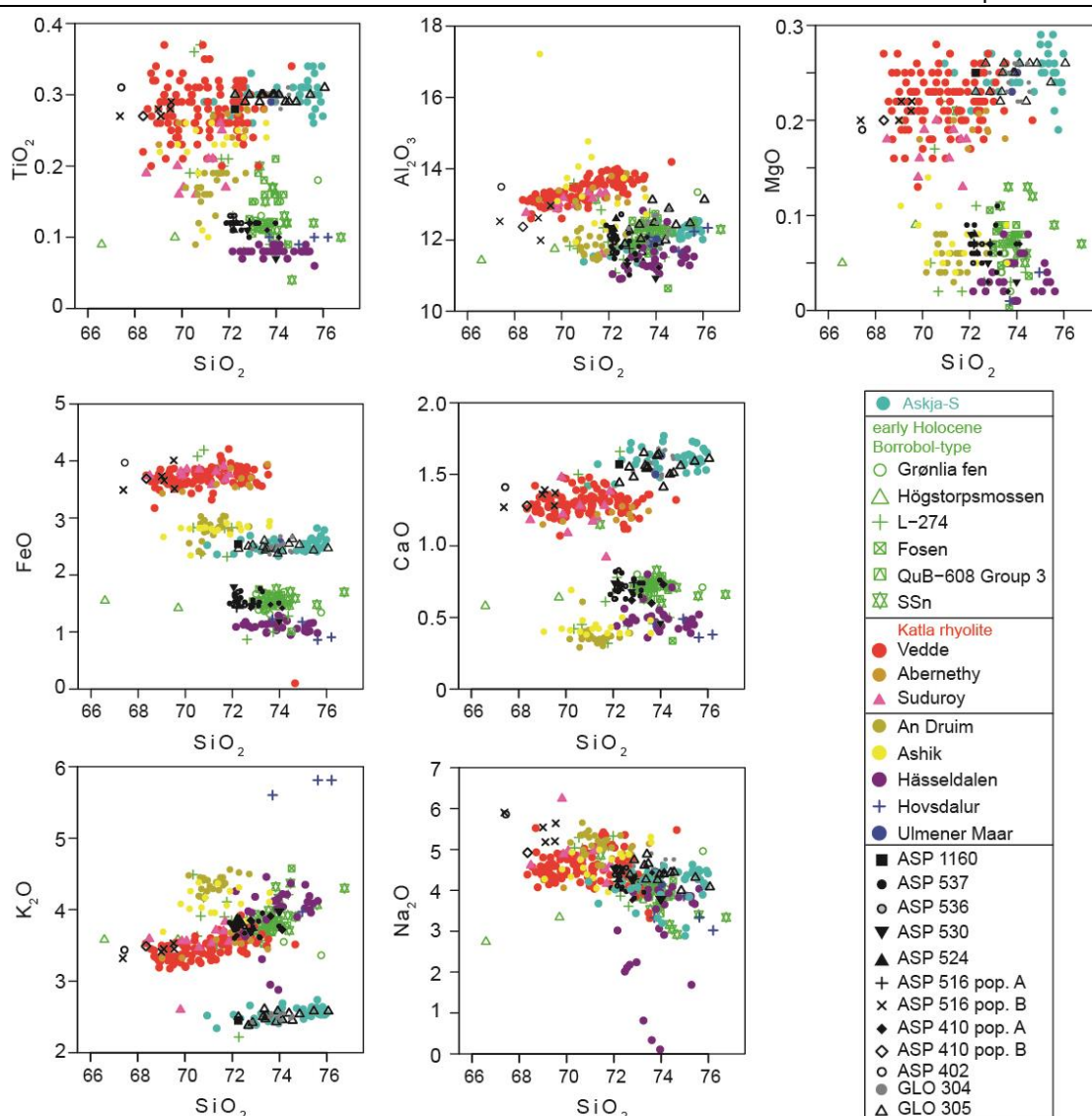


Figure 9-8. Harker variation diagrams for rhyolitic Lateglacial-early Holocene tephras and tephras from the Asplängen and Glottern sites.

The tephras from this study plot within the field of the Askja-S tephra, early Holocene Borrobol-type tephras and Katla rhyolites. All data are supplied in the appendices.

9.7.2.1 ASP 1160

The chemical data suggest a correlation with the Askja-S tephra which was derived from a Plinian eruption of the Askja caldera in the Dyngjuföll volcanic system, Iceland (Sigvaldason, 2002; Davies *et al.*, 2003). The Askja-S eruption occurred during glacial retreat in Iceland after the onset of Holocene warming and during this time only one eruption is known to have occurred from the Dyngjuföll volcanic centre. Proximal deposits have been identified along the north-eastern coast of Iceland (Sigvaldason, 2002; Gudmundsdóttir *et al.*, 2011) and distal deposits have been found across Europe. The first report of a distal Askja-S deposit in the form of a cryptotephra layer was reported by Davies *et al.* (2003) from Hässeldala port, Sweden. The Askja-S tephra has since

been identified across sites in north-western Europe in Borge, Norway (Pilcher *et al.*, 2005), Soppensee, Switzerland (Lane *et al.*, 2011), Lake Czechowskie, Poland (Wulf *et al.*, 2016), Pant-y-Llyn, Wales (Jones *et al.*, 2017), and most recently in the Retezat Mountains in Lakes Brazi and Lia, Romania (Kearney *et al.*, 2018).

Several ages have been proposed for the Askja-S. Similar age estimates were derived from sediment sequences at Hässeldala port (10,810±240 cal. yrs BP; Wohlfarth *et al.*, 2006) and Soppensee (10,846±276 cal. yrs BP; Lane *et al.*, 2011). However, Lind and Wastegård (2011) suggested a younger age of 10,425±75 cal. yrs BP from Høvdarhagi Bog, Faroe Islands and Ott *et al.* (2016) proposed an older age of 11,228±226 cal. yrs BP from the Lake Czechowskie varve record. At present the most robust age estimate for the Askja-S tephra is reported by Kearney *et al.* (2018) who proposed a modelled age of 10,824±97 cal. yrs BP. This was produced by integrating radiocarbon age models from multiple palaeoenvironmental records across Europe using a Bayesian cross-referencing approach. The approach follows that taken by Bronk Ramsey *et al.* (2015) but uses cross-referencing of Askja-S age estimates from Hässeldala port, Soppensee and Romania, to provide a more highly constrained age of the Askja-S. This approach is considered more comprehensive than the Bronk Ramsey *et al.* (2015) age which only uses modelled Askja-S ages from Hässeldala port and Soppensee. Therefore, the Kearney *et al.* (2018) age was initially used in this research to date varve 34 at Asplången to 10,824±97 cal. yrs BP. It is important to note that with only one chemical analysis, this correlation was initially tentative and so the stratigraphic position of other tephra layers at Asplången was also considered alongside the varve chronology.

9.7.2.2 ASP 537 and ASP 536

Both samples plot within the field of Borrobol-type tephtras (Figure 9-9). Given that each sample has a similar shard concentration, shard morphology and shard chemistry, ASP 537 and ASP 536 are considered to represent an isochronous tephra layer. Using the laws of superposition, the ASP 537/536 peak must be younger than the Askja-S eruption. There are several layers with the age and stratigraphic position of the early-Holocene that are younger than the Askja-S eruption and which are of the Borrobol-type tephra group (Lind *et al.*, 2016). To date, the Fosen tephra with age estimate of *ca* 10,177±136 cal. yrs BP (Timms *et al.*, 2017); the Högstorpssmossen tephra *ca* 10,200 cal. yrs BP (Björck and Wastegård, 1999); a component of the L-274 tephra layer *ca* 10,200 cal. BP detected in the Faroe Islands (Lind and Wastegård, 2011); population 3 of the QUB-608 *ca* 9,500 cal. yrs BP detected in Norway (Pilcher *et al.*, 2005); and also the younger SSn *ca* 7,300 cal. yrs BP tephra detected in Iceland (Boygale, 1999) have all been ascribed as

part of the early Holocene Borrobol-type tephra group. With the exception of the SSn, it has been proposed that these tephras represent the same eruption since their age estimates are similar (Lind *et al.*, 2013). However, at present only the Fosen tephra has been identified within several sequences, and is the only tephra of those with a robust age estimate (e.g. Timms *et al.*, 2017). Therefore the ASP 537/536 layer is correlated to the Fosen Tephra using the Timms *et al.* (2017) age $10,177 \pm 136$ cal. yrs BP.

Correlation to the Fosen tephra and Askja-S tephras is further supported by the varve chronology and lithostratigraphy at Asplången. A total of 792 varves (minimum estimate) were counted stratigraphically above the ASP 1160/Askja-S layer. Therefore, it is proposed that the ASP 537/536 layer is at least 792 years younger than the Askja-S tephra. At the time of thesis submission, a second varve count had not been conducted and so varve count errors are not reported. At Asplången, varve sedimentation ceases at 585 cm and glaciolacustrine sediments are sharply truncated by a turbidite from 585-552 cm (see Chapter 7) suggesting that sediments across this interval were deposited almost instantaneously. Following turbidite deposition, a further 15 cm of sediment accumulated between 552-537 cm before deposition of the ASP 537/536 tephra (Figure 9-10). The minimum varve count of 792 years does not account for varves which could have been eroded during turbidite emplacement, or the total time lapsed during deposition of Bed 1 (703.5-678 cm) which is interpreted as a zone of deformation due to localised slumping and sliding (section 6.2.6). To estimate the number of years represented by Bed 1, the most common method is to use varve interpolation. In the case of Bed 1 at Asplången, the sedimentation rate of the previous 100 varves was applied. Using the sedimentation rate of 0.35 cm/yr^{-1} , Bed 1 (678-703.5 cm) represents approximately 72 varve years. Until a second varve count is obtained for this sequence a 2% error of ± 2 vyrs has been applied to this interval. It is therefore estimated that the time lapsed from deposition of the ASP 1160/Askja-S layer to the ASP 537 layer is at least 792 years with a possible additional 72 ± 2 vyrs in Bed 1: ca 864 ± 2 vyrs. However, this estimate does not account for the time elapsed between turbidite emplacement and the Fosen tephra and so must be considered a minimum estimate.

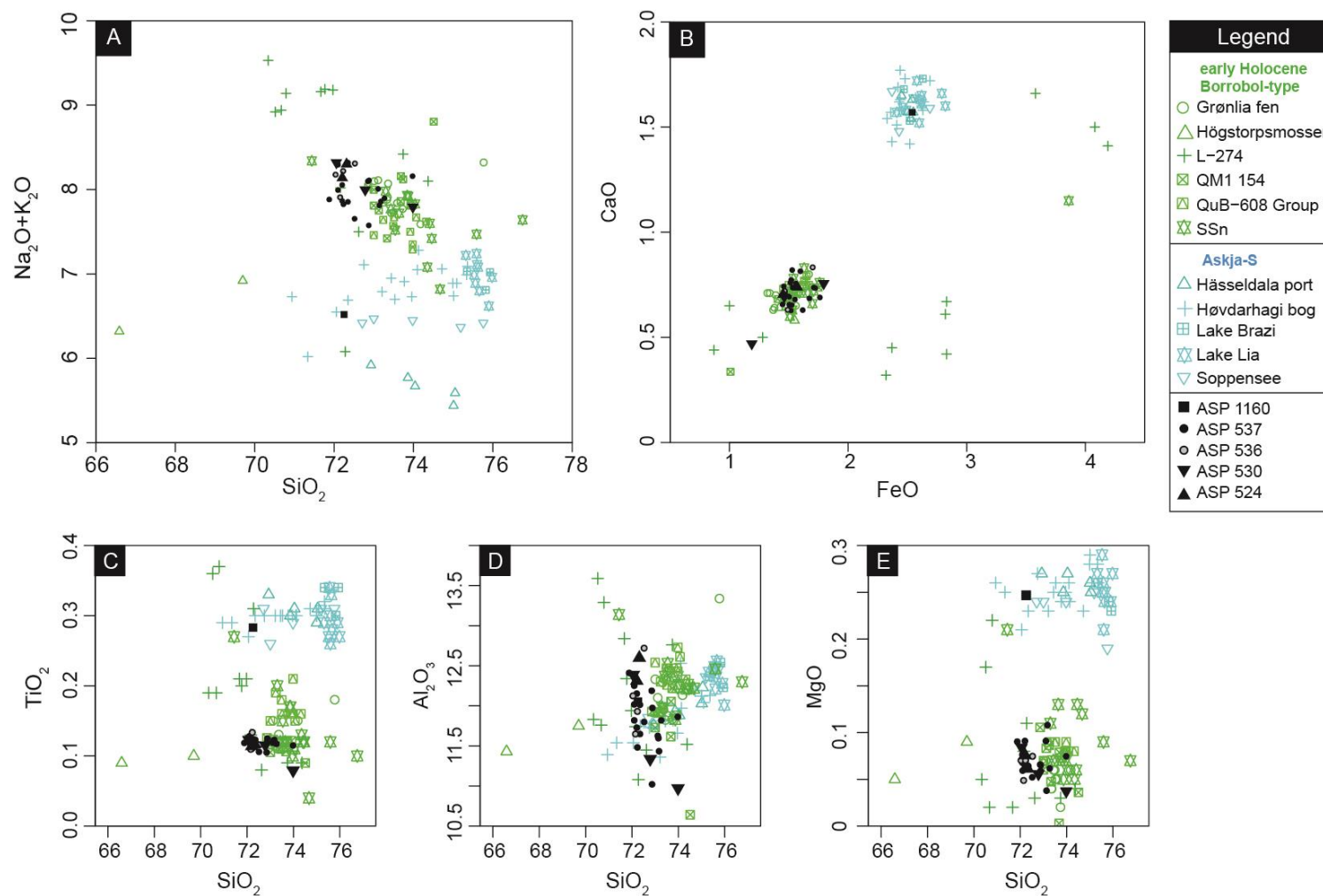


Figure 9-9. Asplängen tephra chemistry data alongside published data for the Askja-S and early Holocene Borrobol-type tephras. (A-B) Major element bi-plots and (C-E) Harker variation diagrams.

Given the Askja-S correlation at ASP 1160 is based on a small amount of chemical data there is perhaps some doubt in the strength of this correlation. However, there are several lines of evidence that support this correlation: 1) the stratigraphic position of the ASP 1160 tephra in relation to the Fosen tephra at ASP 537/536; 2) the absence of shards with a similar chemical composition within close stratigraphic proximity to the ASP 1160 layer; 3) the lack of other tephras with a similar chemistry in the early Holocene (Figure 9-8); and 4) the number of varves between the tephras is within statistical agreement of several published ages of both the Askja-S and Fosen Tephras (Figure 9-11). As such the correlations seem plausible and have been accepted.

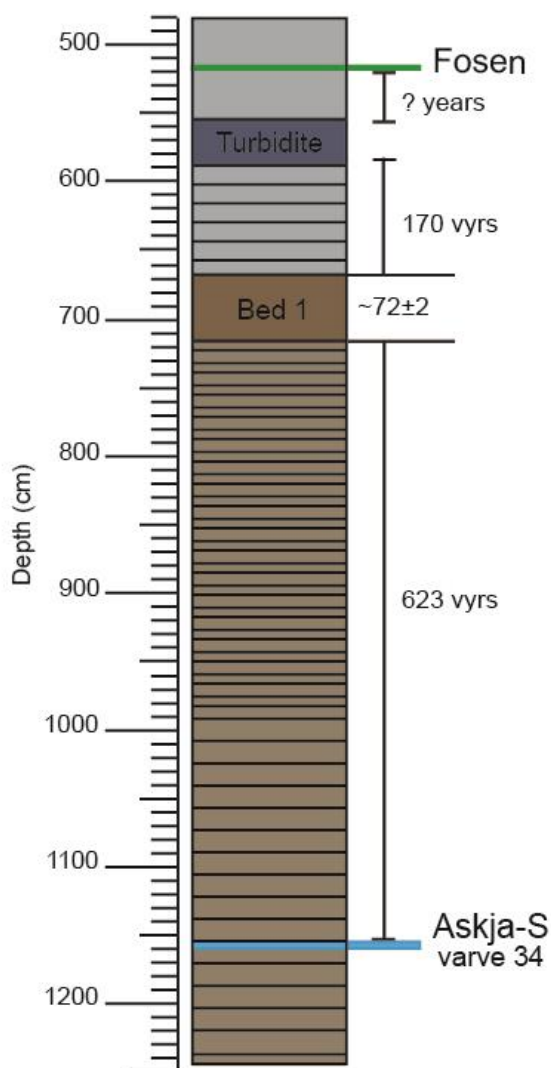


Figure 9-10. Asplången stratigraphic log from 480-1246 cm with identified tephra layers. The Fosen (536-537 cm) and the Askja-S (varve 34/1160 cm) tephras are highlighted with blue and green bars respectively. The number of varves between the tephra horizons is also highlighted. After deposition of the Askja-S tephra 623 varves accumulated before deposition of Bed 1. It is estimated that Bed 1 represents 72 ± 2 yrs of sedimentation using the annual sedimentation rate of the previous 100 varves and a 2% varve count error. After deposition of Bed 1, 170 varves accumulated before turbidite deposition. It is assumed that the turbidite was deposited almost instantaneously.

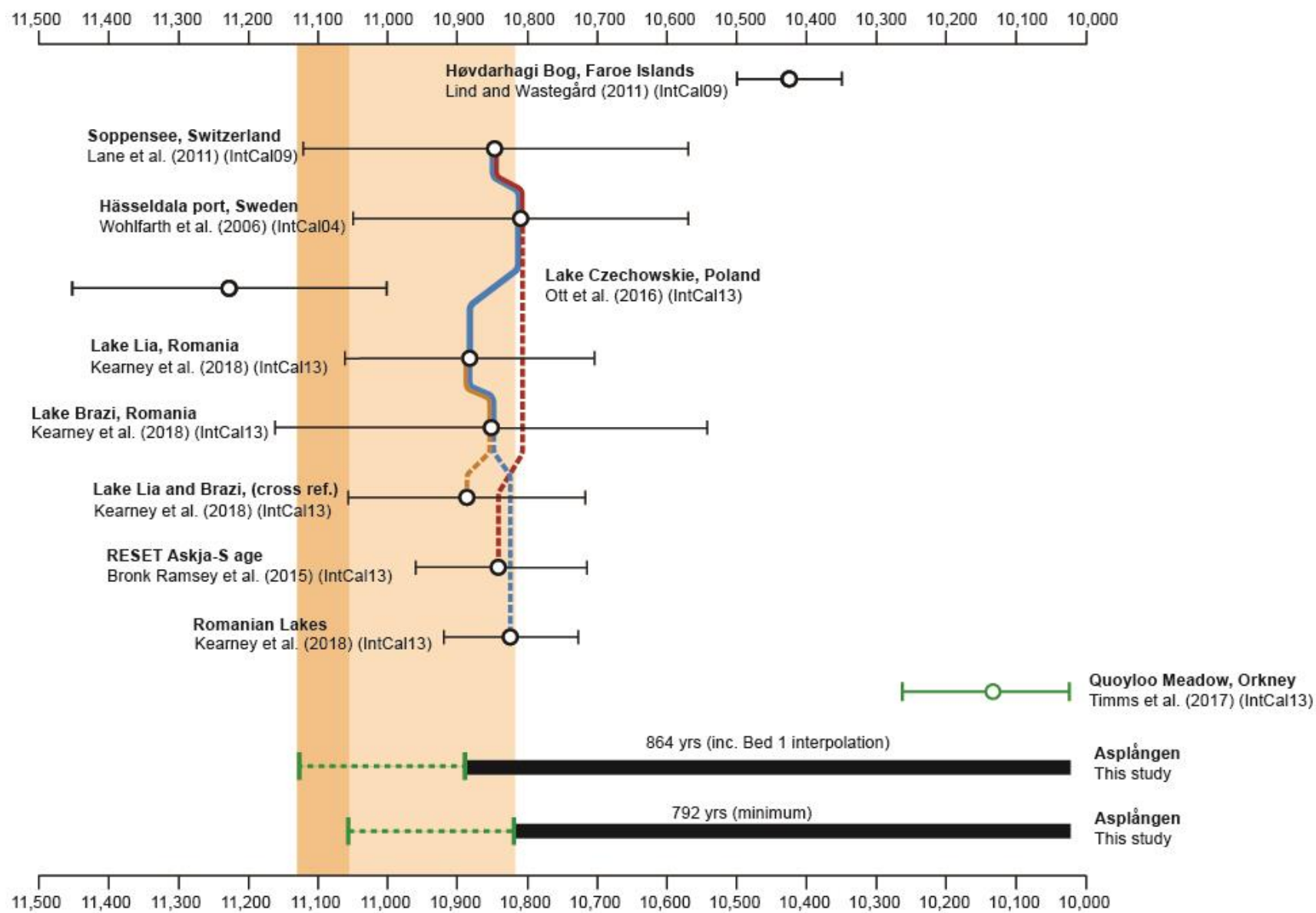


Figure 9-11. Diagram showing published ages of the Askja-S and Fosen tephtras and the Asplången varve record.

(Left; black error bars) Schematic representation of published age estimates for the Askja-S tephra. The red line indicates the sites cross-referenced in the Bayesian chronological modelling by Bronk Ramsey *et al.* (2015) to produce a refined Askja-S age estimate as part of the RESET tephra lattice; the orange line shows the age estimate from cross-reference Bayesian age modelling from Kearney *et al.* (2018) of Lakes Brazi and Lia only, the blue line indicates the sites cross-referenced in Kearney *et al.* (2018) that build upon the RESET model by Bronk Ramsey *et al.* (2015) with the incorporation of the data from Lakes Brazi and Lia. (Right; green error bar) Age estimate of the Fosen Tephra from Quoyloo meadow (Timms *et al.*, 2017). (Bottom; black bars) The varve record from Asplången presented as 1) 864 yrs which includes the number of varves counted and the years interpolated across Bed 1, and 2) 792 vvs which represents a minimum varve count. The Asplången record is placed at the youngest theoretical starting point based on the youngest age estimate of the Fosen Tephra (10,016 cal. yrs BP). The age range of the Fosen tephra is shown at the end of the varve chronology for illustrative purposes (dashed green error bars). The light orange box shows the overlap of the Asplången record with the Askja-S age estimates using the minimum varve count and the dark orange box shows the overlap if Bed 1 is included. In both scenarios, all published ages of the Askja-S, with the exception of Lind and Wastegård (2011), are within errors of the varve chronology at Asplången. Modified from Kearney *et al.* (2018).

9.7.2.3 ASP 530 and ASP 524

Both shards plot within the field of Borrobol-type tephtras (Figure 9-10). Given that both horizons are part of the tail of shards that continue from the peak at ASP 537/536, these samples are considered to represent the re-working of sediments in the catchment.

9.7.2.4 ASP 516

A few centimetres above the Fosen Tephra at 516 cm a single shard with Borrobol-Type chemistry (population A) is identified with some shards with Katla provenance (population B). The chemistry of population A correlates to the Fosen Tephra ca 10,200 cal. yrs BP, population 3 of the QUB-608 ca 9,500 cal. yrs BP detected in Norway (Pilcher *et al.*, 2005); and also, the younger SSn ca 7,300 cal. yrs BP tephra detected in Iceland (Boygles, 1999). The chemistry of population B falls into the chemical envelope of Katla, with a Vedde Ash-type chemistry. The youngest Katla rhyolite tephra reported from the North Atlantic region is the Suđuroy Tephra, which has an age ca 8000 cal. a BP. As two different chemical populations were identified in ASP 516 it seems possible that they are reworked shards of the Vedde Ash isochron, although it is also possible that the shards are from younger Katla eruptions, such as the Suđuroy Tephra. Though the absence of Vedde Ash throughout the rest of the sequence indicates that correlation to the Suđuroy tephra is more likely. The same can be said of the Borrobol-Type shard found within ASP 516. It is likely that this shard is the result of reworking of the previously deposited Fosen Tephra, but contribution from a younger eruption such as the QUB 608 or SSn tephtras is possible.

9.7.2.5 ASP 410 and ASP 402

ASP 410 is a mixed layer with Borrobol-Type chemistry (population A) is identified with some shards of Vedde-Type chemistry (population B). Again, population A correlates to the Fosen Tephra *ca* 10,200 cal. yrs BP, population 3 of the QUB-608 *ca* 9,500 cal. yrs BP detected in Norway (Pilcher *et al.*, 2005); and also, the younger SSn *ca* 7,300 cal. yrs BP tephra detected in Iceland (Boygale, 1999). The chemistry of population B falls into the chemical envelope of the Vedde Ash but could be correlated to the younger, Suđuroy Tephra, which has an age *ca* 8000 cal. yrs BP. As two chemical populations has been identified in ASP 410, and in the absence of other independent age constraints such as radiocarbon dates, it is not possible to determine if the Vedde-type shards are reworked shards of the Vedde Ash isochron or primary airfall of the Suđuroy Tephra. Though the absence of Vedde Ash throughout the rest of the sequence indicates that correlation to the Suđuroy tephra is more likely. Again, the Borrobol-Type shards found within ASP 410 could be a reworked Fosen Tephra, but contribution from a younger eruption such as the QUB 608 or SSn tephtras is again possible. If ASP 410 is correlated to the Suđuroy Tephra, this would explain the single shard of Vedde-type chemistry a few centimetres above at 402 cm as a reworked shard of the Suđuroy Tephra. However, at present the evidence is inconclusive and further work is needed to clarify the taphonomic context of these tephtras.

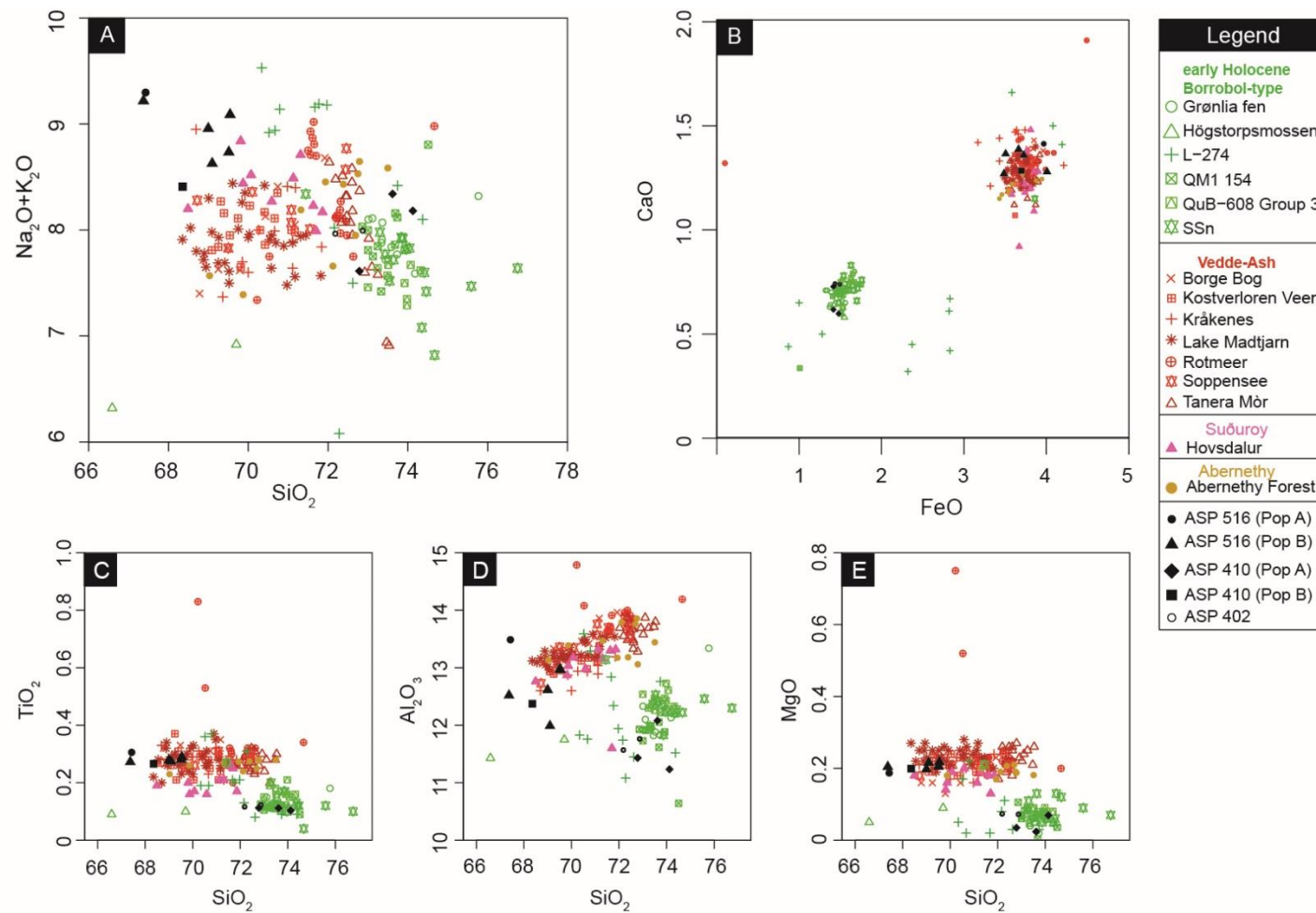


Figure 9-12. Asplången tephra chemistry data and published data for early Holocene Borrobol-type, Vedde Ash, Suðuroy and AF555 tephras. (A-B) Major element bi-plots and (C-E) Harker variation diagrams.

Table 9-3. Summary of the tephra layers identified in the Asplången sediment record

Tephra Code	Unit	Correlation	Age	Notes
ASP 1160	1	Askja-S	early Holocene	One shard analysed but is stratigraphically below the Fosen Tephra and separated by at least 792 varves.
ASP 537	4	Fosen	early Holocene	Stratigraphically above the Askja-S tephra and separated by at least 792 varves.
ASP 536	4	Fosen	early Holocene	Stratigraphically above the Askja-S tephra and separated by at least 792 varves.
ASP 530	4	Fosen	early Holocene	Reworking
ASP 524	4	Fosen	early Holocene	Reworking
ASP 516	4	Uncertain	Uncertain	Mixed layer with several potential correlatives – Borrobol-type population could be reworked Fosen or SSn or QUB 608. Population B could be reworked Vedde or Suđuroy tephra. Though the absence of Vedde Ash throughout the rest of the sequence indicates that correlation to the Suđuroy tephra is more likely.
ASP 410	4	Uncertain	Uncertain	Mixed layer with several potential correlatives – Borrobol-type population could be reworked Fosen or SSn or QUB 608. Population B could be reworked Vedde or Suđuroy tephra. Though the absence of Vedde Ash throughout the rest of the sequence indicates that correlation to the Suđuroy tephra is more likely.
ASP 402	4	Uncertain	Uncertain	Mixed layer with several potential correlatives – Borrobol-type population could be reworked Fosen or SSn or QUB 608. Population B could be reworked Vedde or Suđuroy tephra. Though the absence of Vedde Ash throughout the rest of the sequence indicates that correlation to the Suđuroy tephra is more likely.

9.7.2.6 GLO 304 and GLO 305

The chemical data suggest correlation with the Askja-S tephra (Figure 9-13) and given the published radiocarbon age estimate for the underlying varved sediments at Glottern of *ca* 12,400 cal. yrs BP (Wohlfarth *et al.*, 1998; Muschitiello *et al.*, 2016), a correlation to the Askja-S is accepted.

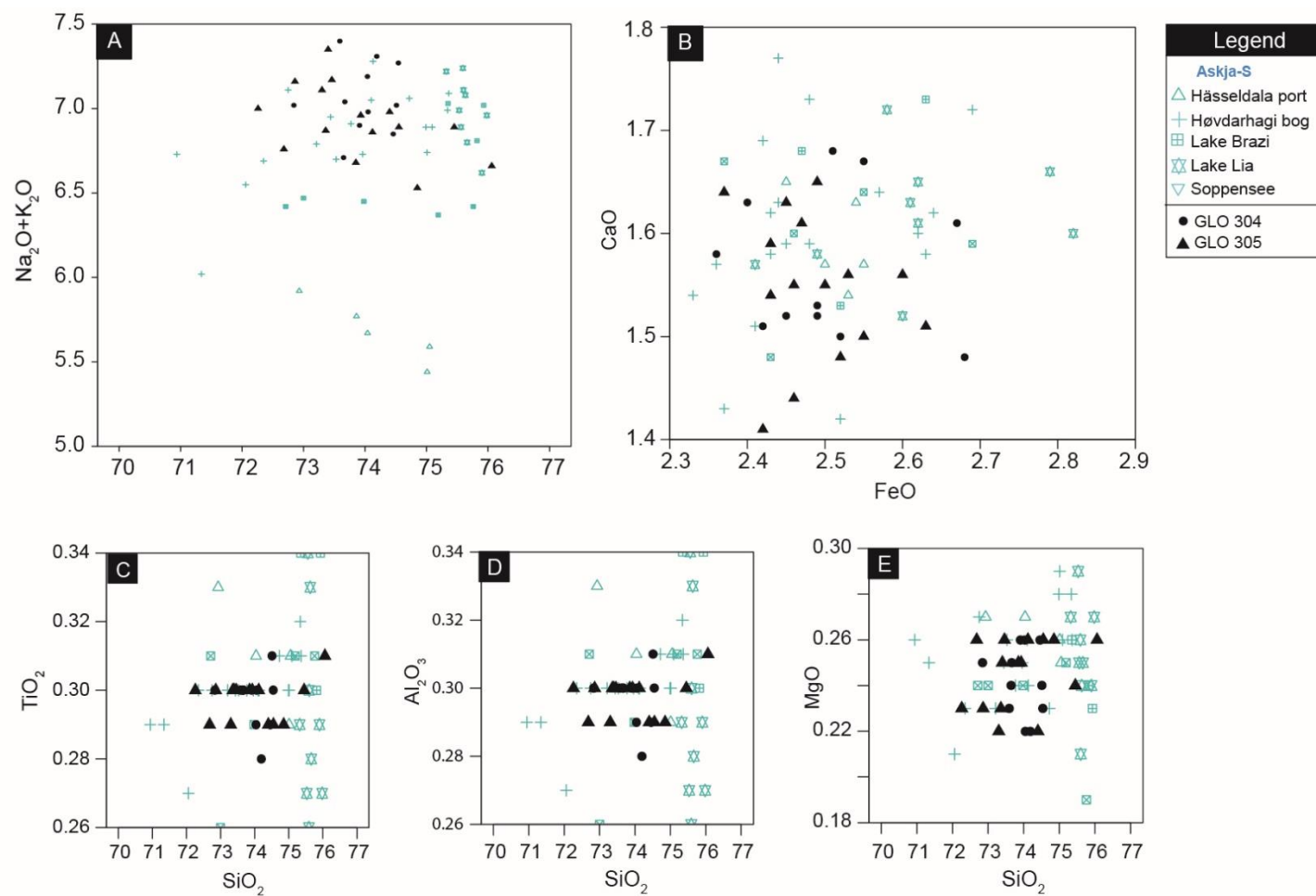


Figure 9-13. Glottern tephra chemistry data alongside published data for the Askja-S tephra. (A-B) Major element bi-plots and (C-E) Harker variation diagrams.

9.8 Implications for published tephra ages

The identification of the Askja-S tephra in glacial varves at the Asplången site has important implications for the published ages of this tephra. In the context of early Holocene tephras, the Askja-S tephra has a unique chemistry (Figure 9-8). This in addition to its highly constrained age estimate makes it a key isochron in early Holocene tephrostratigraphies (Wohlfarth *et al.*, 2006; Lane *et al.*, 2011; Bronk Ramsey *et al.*, 2015; Kearney *et al.*, 2018). The Askja-S tephra is often found in sedimentary sequences that also contain the Hässeldalen tephra (e.g. Wohlfarth *et al.*, 2006; Ott *et al.*, 2016). The current best age estimates of these tephras have been derived from Bayesian age models and date the Askja-S tephra to $10,824 \pm 97$ cal. yrs BP (Kearney *et al.*, 2018) and the Hässeldalen tephra to $11,387 \pm 270$ cal. yrs BP (Ott *et al.*, 2016).

The best age estimate of the Hässeldalen tephra is considered the 'model 2' age from Ott *et al.* (2016) which is a recalibration of the Wohlfarth *et al.* (2006) 'model B' age. However, there are several issues with the Hässeldalen tephra age that must first be considered. By accepting the age of the Hässeldalen tephra published by Ott *et al.* (2016) the original age proposed by Wohlfarth *et al.* (2006) must also be accepted. However, it is important to note that the age estimates from the Hässeldala port sequence (Wohlfarth *et al.*, 2006) might include sources of error related to the stratigraphy. For example, samples for radiocarbon dating were acquired from a different core (core 2) to the tephras (core 1). The cores were then correlated by wiggle matching total organic carbon (TOC) records despite slight variations between the individual TOC curves. The tephra layer was then dated by Bayesian probability age modelling using IntCal04 to $11,380 \pm 216$ cal. yrs BP (Davies *et al.*, 2003; Wohlfarth *et al.*, 2006) and was later recalibrated using IntCal13 to $11,387 \pm 270$ cal. yrs BP (Ott *et al.*, 2016).

Using the Kearney *et al.* (2018) Askja-S age and the Ott *et al.* (2016) Hässeldalen tephra age, the age difference between these two tephras would be 225 years. However, Ott *et al.* (2016) identified both tephras in the varved sediment sequence from Lake Czechowskie, Poland enabling a more precise estimate of the number of years between the tephras. The Lake Czechowskie varve record suggests that the age difference between the two tephras is $152 +11/-8$ varve years. By using the Hässeldalen tephra age of $11,380 \pm 216$ cal. yrs BP as an anchor, Ott *et al.* (2016) use the varve spacing from Lake Czechowskie to derive an age estimate for the Askja-S tephra of $11,228 \pm 226$ cal. yrs BP. This age estimate is substantially older than most

modelled Askja-S ages and is ultimately grounded in the assumption that the Hässeldalen tephra age is correct. As such a revision of tephra ages based on the 'floating' nature of the Lake Czechowskie varve chronology should be interpreted with caution.

Therefore, an independent means of assessing the age estimate of either of these tephras is required. For the Askja-S, one such approach would be to find younger tephras with well constrained ages within another varved sequence and test the age difference between the tephras against the range of proposed ages for the Askja-S. The Asplången sediment record provides an excellent opportunity to test this through counting the number of varves between the well-dated Fosen tephra and the Askja-S. The results in this thesis suggest that at least 792 varve years are observed between these tephras. Using the Timms *et al.* (2017) $10,177 \pm 136$ cal. yrs BP age of the Fosen Tephra as an anchor and adding the varve counts from Asplången, it is possible that the age of the Askja-S tephra could be between ca 11,105-10,833 cal. yrs BP. However, if the additional 72 years that are interpolated across Bed 1 are included then the Askja-S could be between ca 11,177-10,905 cal. yrs BP. In both scenarios, the varve chronology at Asplången suggests that previous estimates of the Askja-S could be too young and could be within the errors of the Ott *et al.* (2016) age as well as the younger ages (Figure 9-11). An outcome of the varve counts and tephra work at Asplången is the potential to test the ages associated with these key tephra layers, the results of which are presented in Chapter 10.

9.9 Chapter summary

Tephra shards were identified at all three sites in this research demonstrating the potential to find tephras within other varve records in the Swedish Timescale. At Glottern, the Askja-S does not constrain the existing radiocarbon-based age estimate for this site but it's stratigraphic position in gyttja sediments 1.88 m above the youngest glacial varve provides a minimum age of the underlying varved sediments.

Unfortunately, chemical data were not obtained from the Svinstadsjön tephras, however the presence of tephra in this sequence demonstrates the potential of tephrochronology for independent correlation between varve records within the STS since the Asplången and Svinstadsjön sites should overlap in age.

It was not expected that the Askja-S tephra would be found within glacial varves at Asplången since the early Holocene age of this tephra is in disagreement with the published age of the varve records in Östergötland (e.g. Brunnberg, 1995). However, data from this research permit correlation to the Askja-S for two key reasons: 1) thin

section analysis of the Asplången varves has enabled construction of an accurate varve chronology and the number of varves between the Askja-S and Fosen tephras is in agreement with published age estimates of these tephras, and 2) the Askja-S tephra has a unique chemistry and there are no other tephras across the North Atlantic region with a similar chemical profile that were deposited during the Lateglacial and early Holocene (Figure 9-8) (Timms *et al.*, 2017; Wastegård *et al.*, 2018). On this basis, correlation to the Askja-S tephra has been accepted. This research therefore extends the known distributions of the Askja-S and Fosen tephras. The Asplången record represents the first known occurrence of the Fosen tephra in Sweden and the first known occurrence of the Askja-S tephra in Swedish glaciolacustrine varves. In Chapter 10 the tephra and varve data from Svinstadsjön and Asplången are integrated within a Bayesian age model.

In Chapter 11 the tephra results are discussed with a focus on the usefulness of tephra for: 1) providing independent links between varve records in the STS, which enables; 2) testing of the traditional methodological approaches that have been employed to link varve thickness records; 3) providing independent age estimates for the varve records; and 4) testing the current deglaciation chronology.

Chapter 10. Bayesian age modelling

10.1 Introduction

Chapters 6, 7 and 8 present individual floating site varve chronologies and Chapter 9 presents the results of tephrostratigraphic and tephrochronology work from the three sequences. In this chapter, these datasets are integrated within a Bayesian age model with the goal of fixing the floating varve chronologies using absolute dates of the tephra horizons identified in the sequences. The approach of using glaciolacustrine varves and tephrochronology is becoming more widespread (e.g. MacLeod *et al.*, 2014) but utilising these data with Bayesian age modelling techniques is in its infancy (e.g. Bendle *et al.*, 2017) and has not been adopted when examining the Swedish Timescale. In this chapter, a detailed explanation of data selection and the steps required to construct the age model are presented, followed by a summary of the key sediment boundaries and phases that have been dated using this approach.

10.2 Data selection

Unfortunately, not all data from this study could be included in the age model. There appears to be an unpredicted gap in the varve sedimentation between Glottern and the other two sites, Asplången and Svinstadsjön. This is identified by two lines of evidence: 1) the existing radiocarbon age estimates from Glottern suggest that the uppermost 100 varves correspond to ca 12,400 cal. yrs BP placing this record within the early Younger Dryas cold period (Wohlfarth *et al.*, 1998), and 2) the Askja-S tephra in varve 34 in the Asplången varve chronology place this site within the early Holocene. Therefore, the Glottern and Asplången varve chronologies do not overlap in age (Figure 11-1). Despite the presence of the Askja-S tephra in the Glottern sequence, the stratigraphic position of this tephra layer 1.88 m above glaciolacustrine varves in gyttja sediments does not constrain, but supports the ca 12,400 cal. yrs BP age of the varved sediments presented by Wohlfarth *et al.* (1998). Consequently, the Bayesian age models that refine the chronology of deglaciation use data from Asplången and Svinstadsjön only. This is based on the likely varve thickness match between these two records, with vyr 1 in Asplången being visually and statistically matched to vyr 75 in Svinstadsjön, the Asplången varve chronology being fixed to an

absolute timescale with the Askja-S tephra, and the cessation of varve formation at Asplången being constrained by the Fosen tephra (Chapter 9).

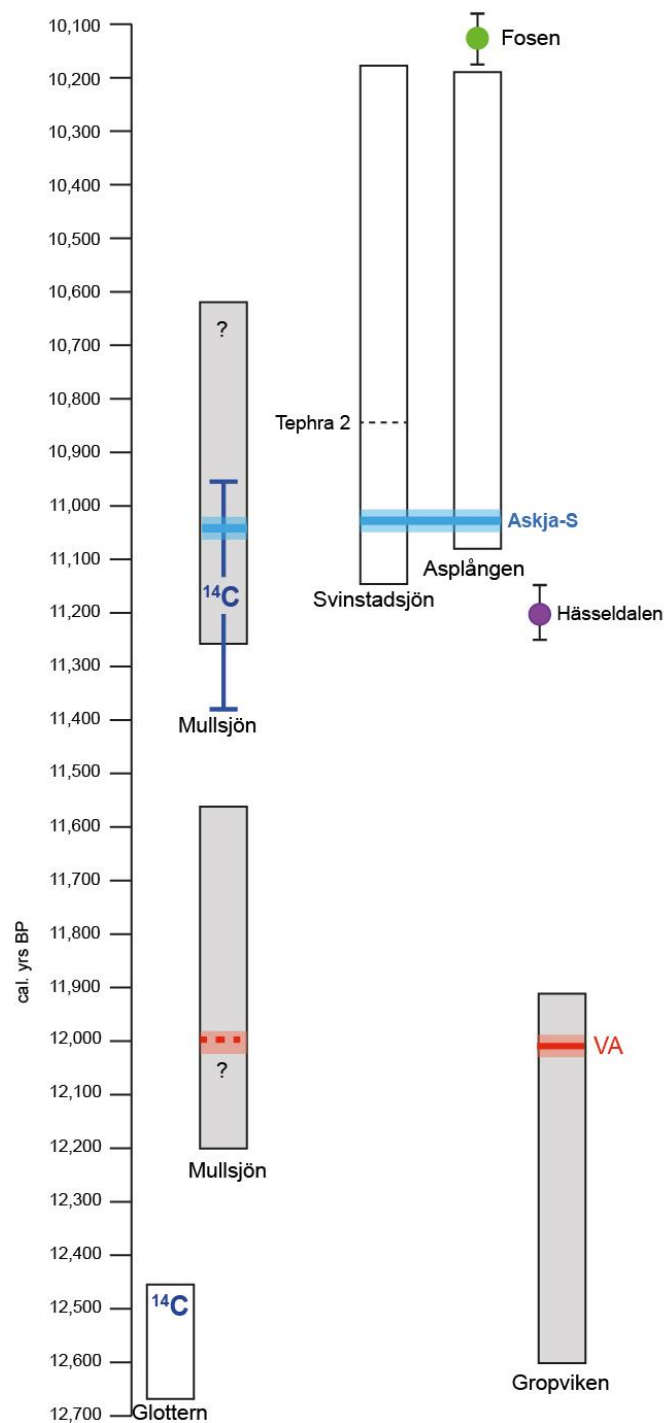


Figure 10-1. Schematic showing the new ages of the sites in this study alongside the Gropviken and Mullsjön varve records.

Revised ages of the sequences in this thesis based on the tephra. The age of the Glottern varve chronology remains the same as proposed by Wohlfarth et al. (1998) and the identification of the Askja-S in gyttja sediments above the varved sediments at Glottern confirm the ca 12,500 cal. yrs BP age. The Gropviken site remains anchored by the Vedde Ash. The Askja-S and Fosen tephras anchor the Asplången record and the varve thickness correlation between Asplången and Svinstadsjön suggest that Tephra 1 in the Svinstadsjön sequence is also the Askja-S. The remodelled age of the Hässeldalen tephra is also presented.

There are four steps to the process of fixing the varve chronologies to an absolute timescale:

- 1) Identify the currently understood best age estimates for the following tephras. Hässeldalen, Askja-S and the Fosen Tephra.
- 2) These ages are used in conjunction with the Asplången and Lake Czechowskie varve chronologies to derive likely age estimates for the tephra in Sweden. The Asplången varve chronology interval drives the calculation of the tephra ages through the more precise estimate of the years between the tephras.
- 3) This age model produces an absolute chronology for Asplången, which then includes the Svinstadsjön varve thickness data using the linking varve point between Asplången and Svinstadsjön.
- 4) The age estimates for events recorded in the varve thickness records and potential revised age estimates for the tephra horizons are presented.

The first stage in this study is to determine the best age estimate for each tephra. The Fosen tephra provides a younger limit to the age model and the age proposed by Timms *et al.* (2017) of $10,177 \pm 136$ cal. yrs BP is used. The most robust estimate for the Askja-S tephra is from Kearney *et al.* (2018), $10,824 \pm 97$ cal. yrs BP. For the Hässeldalen tephra, an adapted age following the Kearney *et al.* (2018) model was produced, running a new model including the varve and tephra data from Lake Czechowskie, Poland (previously discounted by Kearney *et al.* (2018)), to produce a new age of $11,297 \pm 66$ cal. yrs BP. Two component *Sequence* models were created with the purpose of each as follows:

Model 1 integrates the varve-count data and tephras from Asplången to anchor the record in time whilst also testing the existing tephra ages for this period. The model also provides age estimates for site deglaciation and key lithofacies changes.

Model 2 utilises the position of the varve thickness overlap between Asplången and Svinstadsjön and the varve count data to construct age estimates for site deglaciation and key lithofacies changes at Svinstadsjön.

10.3 Model assumptions

There are several assumptions to consider when interpreting the model outputs. First, for Model 1 at the time of thesis submission a second varve count had not been undertaken on the Asplången record. Varve count errors were only assigned to interval 4 which represents a section of deformed varves, all other intervals were

assigned a varve count error of ± 1 vyrs for each varve interval, which equates to 3% or less of a varve interval. Repeat varve counts are pending at the time of writing, however, if the varve count error in the Asplången record is similar to the Svinstadsjön record at 2.6% the current age model will not significantly change. We also use an uncertainty term in the modelling of the post-varve sediment to the Fosen tephra as this is unlaminated. A time period of 50 ± 50 years was used to encompass an error from zero to 100 years and to permit flexibility in the model, though this could be an under or overestimate. Radiocarbon dates from these sediments may constrain the estimate but terrestrial macrofossils were not found in these sediments during laboratory analyses.

A key limitation of Model 2 is that the Svinstadsjön varve record has no independent age constraint and relies on the varve thickness correlation to the Asplången sequence. Since a varve sequence has not been extracted from the Svinstadsjön site prior to this study, the overlap between the sites is based on the assumption that the ice margin lines proposed by Brunnberg (1995) and Kristiansson (1985) are somewhat accurate. Tracing the ice margin lines to the Svinstadsjön and Asplången sites suggests that Asplången was deglaciated *ca* 200 vyrs before Svinstadsjön (Chapter 5; section 5.2). It is not possible to directly compare the proposed overlap from this study with a published varve thickness overlap but the sites were expected to overlap in age based on their location (Brunnberg *pers. comm.*). The varve thickness overlap between the sites has the potential to change if geochemical data are obtained from the tephra horizons at Svinstadsjön. The implications of the current placement of the overlap and the potential tephra correlations at Svinstadsjön are discussed in Chapter 11.

10.4 Model 1 – Asplången

10.4.1 Model 1 input

In Model 1 the composite varve chronology from Asplången and Lake Czeckowskie was divided into 6 intervals. The first interval (section 1 in Figure 10-2) has a duration of 152 ± 12 vyrs and represents the number of vyrs accumulated between deposition of the Håsseldalen and Askja-S tephra at Lake Czeckowskie. Using the Askja-S as an anchor point between the Lake Czeckowskie and Asplången varve records, the overlap between the two records (Figure 10-2) has a duration of 33 ± 1 vyrs and represents the number of varve years before deposition of the Askja-S tephra at Asplången. Since the Askja-S tephra is found in a single varve in each record, this varve is termed a “link varve” between the two records. The following interval (section

2 in Figure 10-2) has a duration of 223 ± 1 yrs and represents the number of yrs accumulated in LF1. Varves in this interval have complex summer layers and are \geq cm-scale in thickness. Interval 3 (section 3 in Figure 10-2) has a duration of 399 ± 1 yrs and represents the number of varves accumulated in LF2. Varves in this interval are composed of a simple, single lamination summer layer. The following interval (section 4 in Figure 10-2) has a duration of 72 ± 1 yrs and corresponds to a zone of deformed varves that interrupts LF2. The duration of this interval is based on interpolation of the varve record using varve thickness data from the previous ($n=100$) varves. Interval 5 (section 5 in Figure 10-2) has a duration of 170 ± 1 yrs and is a continuation of varves equivalent to LF2 and these varves are grey unlike the preceding brown varves. The final interval (section 6 in Figure 10-2) has an approximate duration of 50 ± 50 years and represents the approximate number of years formed between the uppermost varve in Asplången and the Fosen tephra.

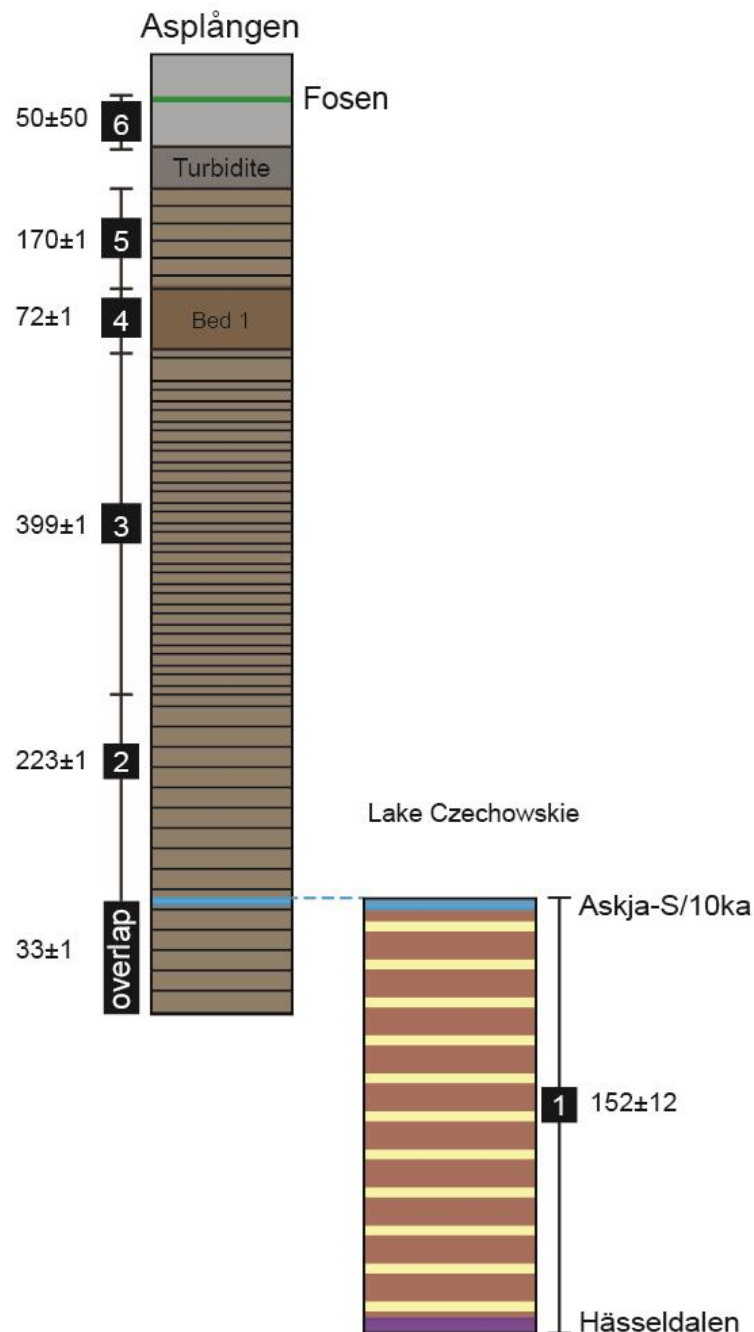


Figure 10-2. Schematic diagram showing the overlap between the Asplången and Lake Czechowskie varve records.

The Hässeldalen and Askja-S tephras bracket the Lake Czechowskie sequence and the Askja-S links the record with the Asplången sequence. There is an overlap of 33 yrs between the two varve chronologies. The Fosen tephra marks the younger limit in the Asplången sequence. Black numbered boxes show the sediment intervals that are used in Model 1. The duration of each interval and the uncertainty is also displayed.

10.4.2 Model 1 output

The model produces new age estimates of the tephras. The modelled age of the Fosen tephra $10,135 \pm 43$ cal. yrs BP is in good agreement with the published age by Timms *et al.*, (2017) of $10,177 \pm 136$ cal. yrs BP. The new age of the Askja-S tephra of

11,043±42 cal. yrs BP is older than the published age presented by Kearney *et al.* (2018) though this is unsurprising given the inclusion of the tephras and varve spacing from Asplången. The new modelled age of the Hässeldalen tephra of 11,197±42 cal. yrs BP is younger than published age estimates due to the new Askja-S age and Asplången varve spacing.

The identification of the Fosen tephra at Asplången enables that tephra to act as an anchor point. However, using the annual age estimate from the younger varves at Asplången below the Fosen would indicate that at least 792 yrs occur between the two tephras. Therefore, the mid-point and 1 sigma age of Kearney *et al.* (2018) is less likely to be correct. When combined with a varve count dataset from Lake Czechowskie this suggests that an older age of 11,043±42 cal. yrs BP is more likely and closely in line with the findings of Ott *et al.* (2016) (Chapter 9; Figure 9.7).

Table 10-1. Model 1 output.

Key events in the Asplången record and modelled ages of the Fosen, Askja-S and Hässeldalen tephras.

Event	Unmodelled cal. yrs BP (95.4%)	Unmodelled cal. yrs BP ($\mu \pm \sigma$)	Modelled cal. yrs BP (95.4%)	Modelled cal. yrs BP ($\mu \pm \sigma$)
Fosen	10,255-10,015	10,135±60	10,220-10,050	10,135±43
End of varve formation	-	-	10,265-10,095	10,180±43
Deformation end/ LF2 start/ colour change from brown to grey varves	-	-	10,435-10,265	10,350±43
LF2 break/ deformation start	-	-	10,507-10,337	10,421±42
LF1 end/ LF2 start	-	-	10,906-10,736	10,820±42
Askja-S	11,018-10,631	10,824±97	11,129-10,958	11,043±42
Start of varve formation (LF1)	-	-	11,164-10,092	11,077±42
Tephra				
Fosen	10,255-10,015	10,135±60	10,220-10,050	10,135±43
Askja-S	11,018-10,631	10,824±97	11,129-10,958	11,043±42
Hässeldalen	11,429-11,165	11,297±66	11,282-11,111	11,197±42

Model 1 also provides the likelihood distributions for deglaciation and lithofacies changes at Asplången (Table 10-1) and is a significant improvement on the previous estimates for deglaciation in the region. Model output from OxCal is shown in Figure 10-3. The integration of Model 1 with Model 2 provides a new reconstruction of ice margin position and timing of palaeoglaciolacustrine changes at Svinstadsjön.

OxCal v4.3.2 Bronk Ramsey (2017); r:5

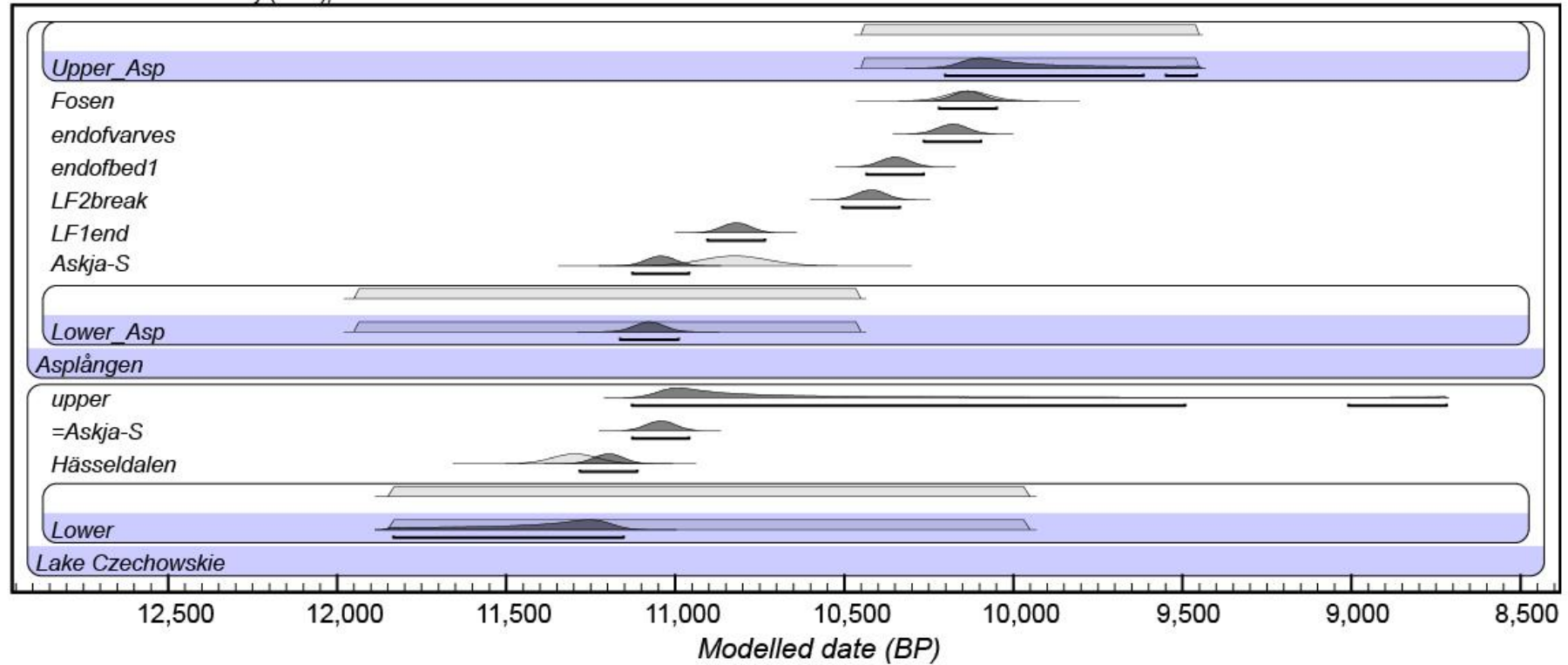


Figure 10-3. Model 1 OxCal output.

Model 1 output showing key events in the Asplången record and modelled ages of the Fosen, Askja-S and Hässeldalen tephras. The Askja-S tephra is used to link the Asplången record to the Lake Czechowskie record.

10.5 Model 2 – Svinstadsjön

10.5.1 Model 2 input

In Model 2 varve 1 in the Asplången chronology is statistically correlated to varve 75 in the Svinstadsjön sequence using Pearson's moment correlation. Statistical correlation indicates that the lowermost $n=657$ brown varves in the Asplången sequence (prior to deposition of Bed 1) can be correlated to the varve interval 75-731 yrs in the Svinstadsjön record with $r^2=0.55$ ($p<0.001$) (Figure 10-4).

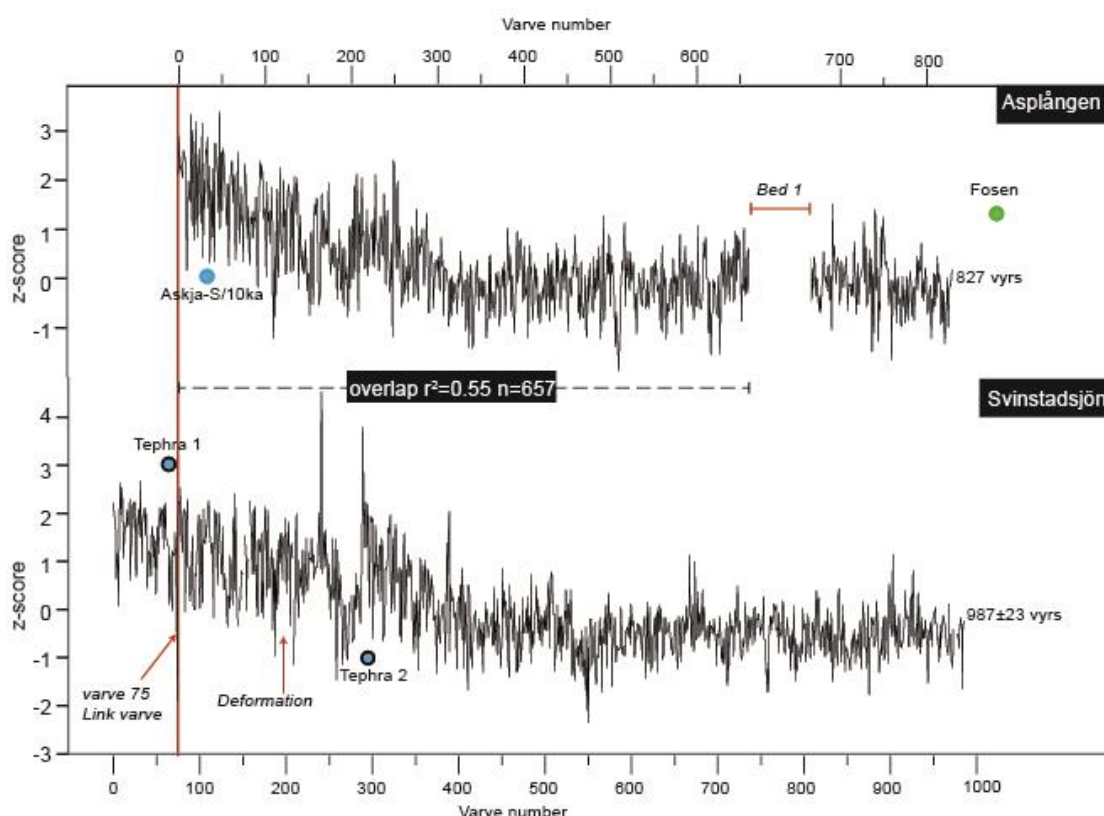


Figure 10-4. Varve thickness correlation between Svinstadsjön and Asplången. Varve 1 in the Asplången sequence corresponds to varve 75 in the Svinstadsjön record and is termed the “link varve”.

It is recognised that the r^2 value of 0.55 could be deemed too low to warrant a valid correlation between the records, but this is the highest r^2 value when correlating the varve thickness records. The current placement of the “link varve” between the Svinstadsjön and Asplången varve chronologies is further supported by the near-synchronous pattern in the Lamination Types at each site. In particular, the early occurrences of Lamination Types A and B appear to occur around the same time (Figure 10-4). Furthermore, given that the ice margin lines proposed by Brunnberg (1995) and Kristiansson (1985) indicate that the Asplången and Svinstadsjön varve

records should overlap in age, with approximately 200 yrs between the sites, the current placement of the overlap is deemed to be reliable given the available data.

In this model the varve chronology from Svinstadsjön was divided into 6 intervals. The first interval (section 1 in Figure 10-5) has a duration of 65 ± 1 yr and represents the number of yrs accumulated before deposition of Tephra 1 in LF1. The second interval (section 2 in Figure 10-5) has a duration of 10 ± 1 yr and represents the number of yrs between Tephra 1 and varve 75 which is the “link varve” between Svinstadsjön and Asplången. Interval 3 has a duration of 128 ± 5 yrs and represents yrs accumulated in LF1 prior to deposition of Bed 1. Interval 4 (section 4 in Figure 10-5) has a duration of 93 ± 2 yr and represents the uppermost varves accumulated in LF1 prior to deposition of Tephra 2. Varves in intervals 1-4 have complex summer layers and are \geq cm-scale in thickness. Following deposition of Tephra 2 is interval 5 (section 5 in Figure 10-5) which has a duration of 522 ± 17 yrs and represents continuous varve accumulation in LF2. Varves in this interval are comprised of a simple, single lamination summer layer. The start of this interval coincides with a decrease in varve thickness indicative of a rapid ice-margin retreat. The following interval (section 6 in Figure 10-5) has a duration of 169 ± 14 yrs and corresponds to continuous varve accumulation in LF3. Varves in this interval are composed of a simple, single lamination summer layer and are grey unlike the preceding brown varves.

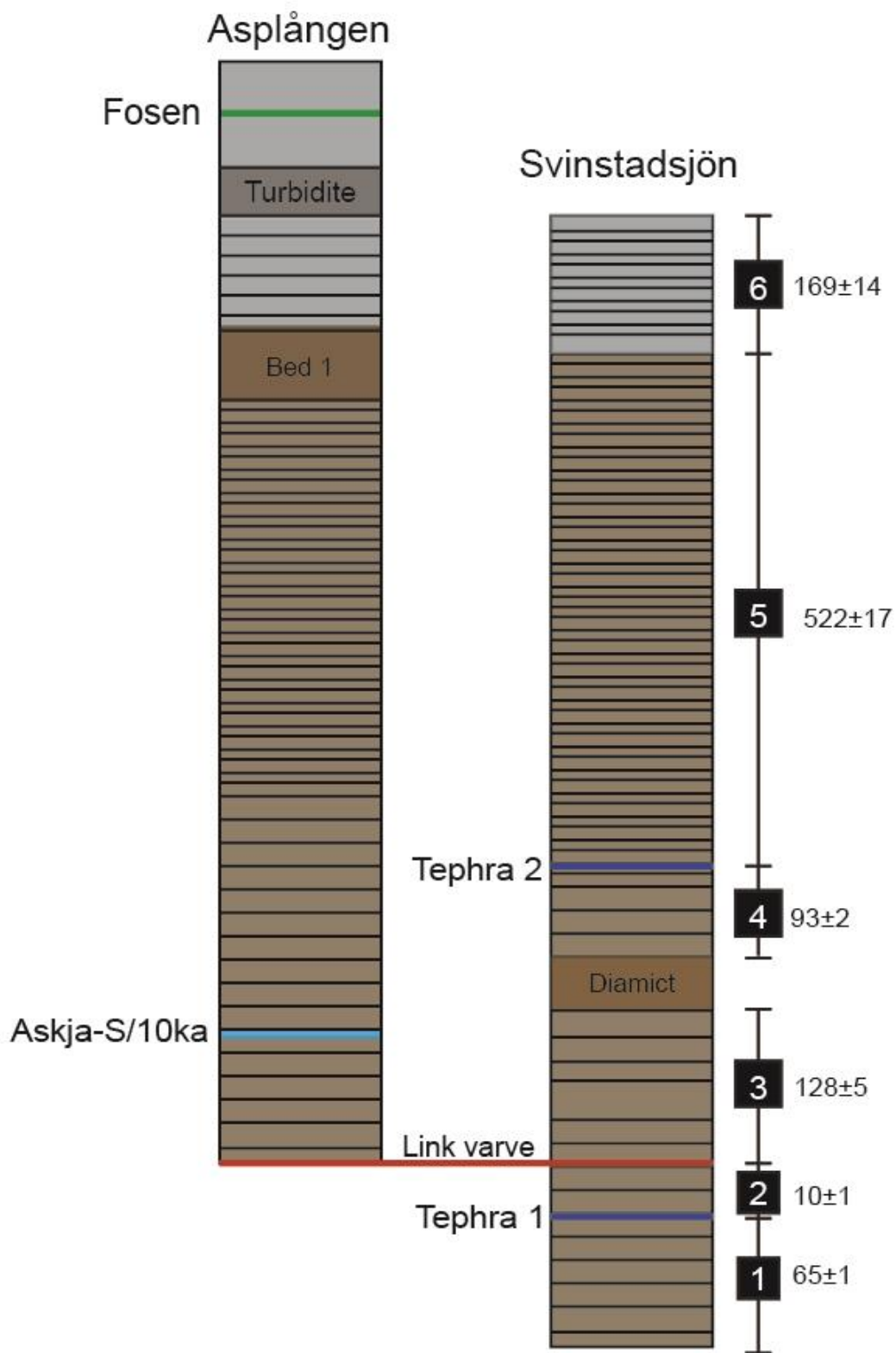


Figure 10-5. Schematic overlap between Asplången and Svinstadsjön varve records. The Askja-S tephra anchors the Asplången varve record. There is an overlap of 75 ± 2 yrs between the two varve chronologies. The Fosen tephra marks the younger limit in the Asplången sequence. Black numbered boxes show the sediment intervals that are used in Model 2. The duration of each interval and the uncertainty is also displayed.

10.5.2 Model 2 output

Model 2 provides the likely distributions for deglaciation, lithofacies changes and tephra ages at Svinstadsjön and differs from the previous estimates for the timing of deglaciation between Svinstadsjön and Asplången (Table 10-2). Model output from OxCal is also shown in Figure 10-3. The results of Bayesian age modelling indicate that the Svinstadsjön and Asplången sites were deglaciated around 11,153±41 cal. yrs BP and 11,077±42 cal. yrs BP respectively i.e. at the same time (within errors). Varve sedimentation also ceases simultaneously (within errors) at both sites: Svinstadsjön at 10,168±43 cal. yrs BP and at Asplången at 10,180±43 cal. yrs BP. However, the published ice margin lines suggests the Asplången site was deglaciated *ca* 200 yrs after Svinstadsjön (Kristiansson, 1986; Brunnberg, 1995). The implications of these new ages for deglaciation in Östergötland are explored in more detail in Chapter 11.

Table 10-2. Model 2 output.
Modelled likelihood ages of key events in the Svinstadsjön record.

Event	Unmodelled cal. yrs BP (95.4%)	Unmodelled cal. yrs BP ($\mu \pm \sigma$)	Modelled cal. yrs BP (95.4%)	Modelled cal. yrs BP ($\mu \pm \sigma$)
End of varve formation	-	-	10,255-10,083	10,168±43
LF2 end/LF3 start/colour change from brown to grey varves	-	-	10,422-10,252	10,337±43
Tephra 2/LF2 start	-	-	10,942-10,773	10,858±42
Deformation zone	-	-	11,034-10,868	10,951±42
Link varve	11,160-10,992	11,076±42	11,158-10,093	11,076±42
Tephra 1	-	-	11,172-11,005	11,089±42
Start of varve formation (LF1)	-	-	11,238-11070	11,153±41

OxCal v4.3.2 Bronk Ramsey (2017); r:5

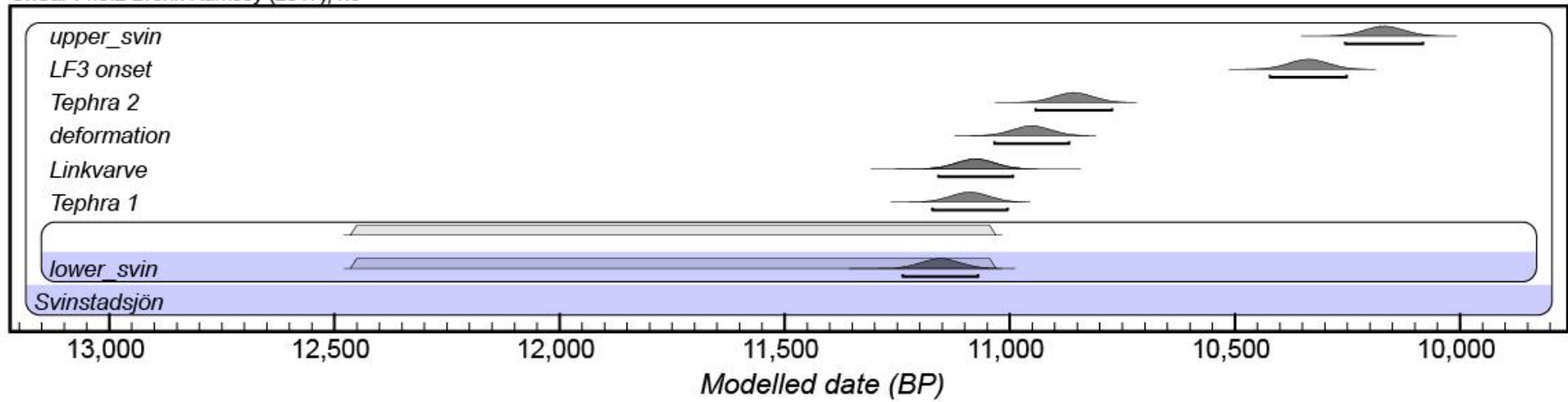


Figure 10-6. Model 2 OxCal output.

Model 2 output showing key events in the Svinstadsjön record and modelled ages of unknown Tephra 1 and Tephra 2.

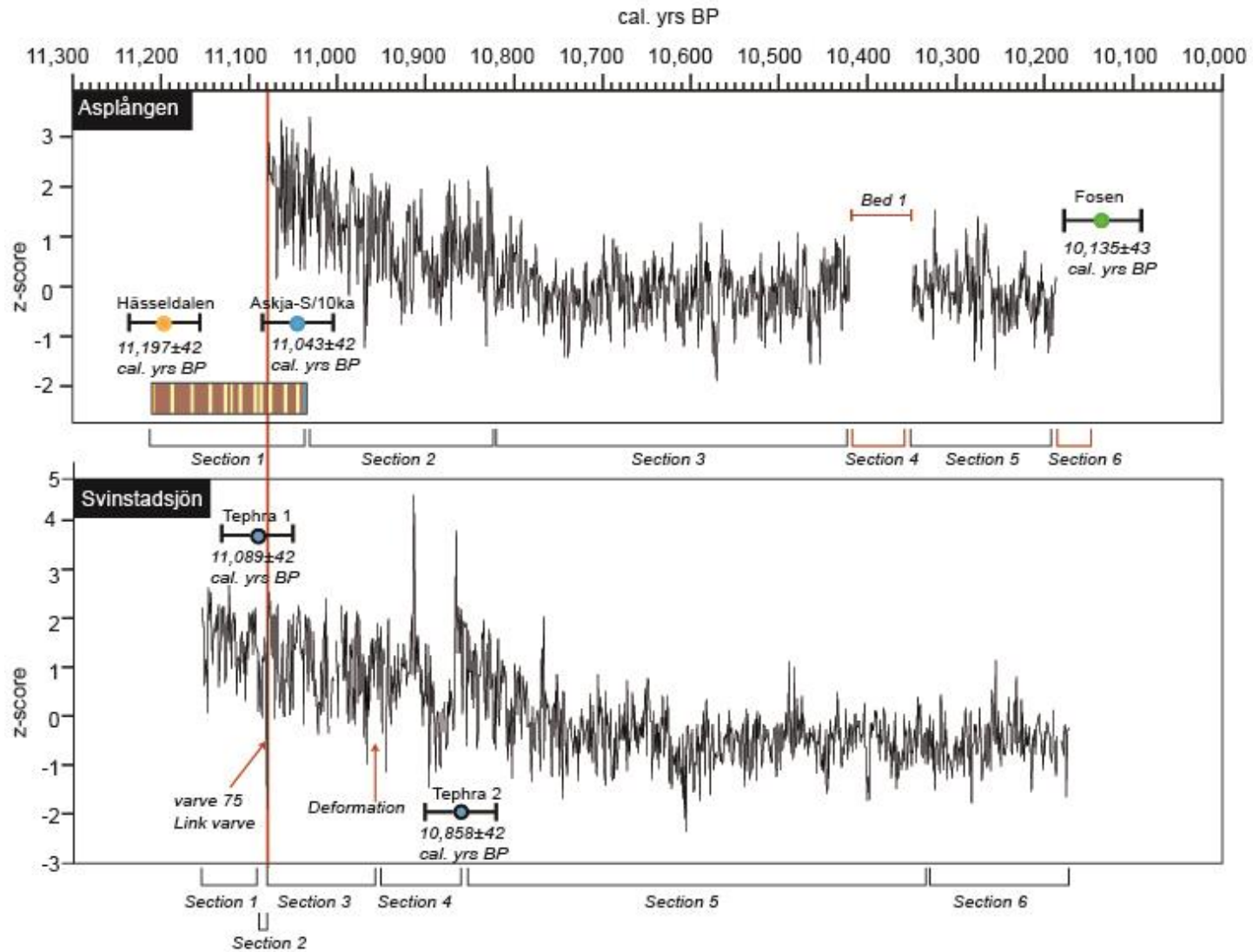
10.6 Summary

The data presented in this thesis offer new insights on the precise timing of deglaciation, tephra deposition and microfacies changes at Svinstadsjön and Asplången. The results from age modelling suggest that the Svinstadsjön and Asplången sites co-existed and the similarities between the varve thickness records suggest that the sites were influenced by common sedimentological processes. However, the presence of deformation zones that do not overlap in age between the sites also indicate that the sites were subject to local deformation processes and this further supports the difficulties in using deformation zones to verify site correlations.

The results of Bayesian age modelling have enabled revised age estimates for the Hässeldalen, Askja-S and Fosen tephtras that are constrained by varve spacing. Through varve thickness correlation between Asplången and Svinstadsjön, the “Tephra 1” horizon in the Svinstadsjön varve sequence has now been dated to $11,089 \pm 42$ cal. yrs BP which is within errors of the new modelled age of the Askja-S tephra. This supports a correlation of the Tephra 1 horizon in the Svinstadsjön record to the Askja-S (Figure 10-7). In the absence of geochemical analyses correlation to this tephra must remain speculative. However, if Tephra 1 is indeed the Askja-S tephra then it is likely that Tephra 2 is a reworked tephra. This is substantiated by the lack of known tephra deposits of this age within Sweden and the low shard abundance ($n=1$) for this horizon in comparison to the Tephra 2 horizon ($n=4$). Implications of the new site chronologies for the existing deglaciation chronology and potential links to the final Baltic Ice Lake drainage and early Holocene climatic events are discussed in Chapter 11.

Figure 10-7. Model 1 and Model 2 output: Asplången and Svinstadsjön varve chronologies presented on a modelled cal. yrs BP timescale.

Next page. Asplången varve chronology anchored by the Askja-S and Fosen tephtras. Non-varved sections are highlighted in red. Lake Czechowskie varve record is also displayed. Svinstadsjön varve chronology correlated to the Asplången varve chronology at varve 75 using varve thickness wiggle matches and Pearson’s moment correlation coefficient $r^2=0.55$. The modelled ages of unknown Tephra 1 and Tephra 2 are highlighted. The absolute timing of varve thickness variations is established through integration of the remodelled Hässeldalen, Askja-S and Fosen tephra ages.



Chapter 11. Discussion

11.1 Introduction

This chapter discusses the microfacies and tephra results presented in this thesis in the context of published literature. First the microfacies descriptions and varve thickness data that are presented in Chapters 6, 7 and 8 are revisited and integrated within the microfacies framework proposed by Palmer *et al.* (2019). This approach enables the Lamination Types and Sets to be placed within a location in the BIL in order to determine the proximal-distal relationships between the varved sediments at each site. The microfacies results are compared to microfacies analysis conducted by Ringberg and Erlström (1999) to assess the spatial extent of varve microfacies across the Baltic Ice Lake. The implications of these results for the construction of site and regional varve chronologies are also discussed. The varve chronologies obtained in this thesis from thin section analysis are then compared to the existing records that were obtained from macroscale varve analysis. A critical evaluation of the traditional macroscale-based varve counts is presented. The implications of the microfacies analysis for the construction of composite varve chronologies is explored through a critical evaluation of the correlation between the Svinstadsjön and Asplången chronologies.

The tephra results enable absolute dating of the varve records and comparisons are drawn between the tephra-based varve chronologies in this thesis and the published deglaciation chronology. The potential of tephrochronology for independent correlation of varve records is also presented. Finally, the results from this thesis are discussed in the context of the final drainage of the BIL and the existing deglaciation chronology is re-evaluated. Possible links to early Holocene climatic events are also proposed.

11.2 Microfacies analysis

With the exception of Ringberg and Erlström (1999) microfacies analysis has not been applied to the STS. The microfacies investigation of Swedish glacial varves by Ringberg and Erlström (1999) focussed on sediment description and depositional processes, rather than testing varve counts that were produced at the macroscale. There are several purposes of microfacies analysis in this thesis: 1) generate precise sediment descriptions; 2) understand depositional processes; 3) develop a varve sedimentation model; and 4) undertake precise varve thickness measurements and accurate varve

counts for the generation of robust varve chronologies. This section focuses on points 1 to 3 with point 4 addressed throughout the rest of the chapter.

This thesis presents the first detailed microfacies analysis of Swedish glaciolacustrine varves through the application of the descriptive framework proposed by Palmer *et al.* (2019). The descriptive protocol has enabled objective classification of laminated sediments at the microscale, interpretation of local-scale sediment processes and development of a varve model. This process has led to construction of highly accurate and precise varve chronologies for the Glottern, Svinstadsjön and Asplången sites. In this section, the local-scale sediment processes that underpin the Lamination Types and Lamination Sets presented in Chapters 6, 7 and 8 are revisited. The Lamination Sets, including varve thickness, are then linked to specific locations within the lake basin using the Lamination Set Assemblage framework outlined by Palmer *et al.* (2019). Comparisons are drawn between the sites in this thesis before comparisons are made with the varve microfacies that are identified in southern Sweden by Ringberg and Erlström (1999). This enables an assessment of the spatial and temporal changes in the sediment processes that operated across the Baltic Ice Lake. Understanding these processes has important implications for constructing varve chronologies in the STS and these are outlined in section 11.2.6.

11.2.1 Lamination Types

In Chapters 6, 7 and 8 different Lamination Types were identified at the microscale within the sediments at the Svinstadsjön, Asplången and Glottern sites. The coarse and fine-grained Lamination Types (LT) that comprise the Lamination Sets (LS) show the relative timing of sediment transport and deposition to the lake floor. Table 11-1 presents the 10 Lamination Types that were identified across the three sites in this study.

Table 11-1. Sedimentological properties of the Lamination Types (LT) observed in the microfacies of the glaciolacustrine sediments within this study.

Descriptions follow the format of Palmer et al. (2019). *asterisks denotes Laminations Types that are not identified by Palmer et al. (2019) and are unique to the Asplången and Svinstadsjön records. C = clay; VFZ = very fine silt; FZ = fine silt; MZ = medium silt; CZ = coarse silt; FS = fine sand. Ma = massive; NGr= normally graded. WS = well sorted; MS = moderately sorted; PS = poorly sorted. Sh = sharp; Gr = gradational. Dg = dropgrain; In = intraclast; WD = well-developed.

Lamination Type (LT)	Grain size (dominant)	Structure	Sorting	Upper Contact	Other
i	VFS/FS	Ma	WS	Sh	In/Dg
v	VFS/FS-MZ	NGr	WS	Sh	Dg
vi	VCZ-MZ	NGr	WS	Sh	Dg
vii	CZ-MZ	NGr	WS	Sh	Dg
viii	CZ-MZ	Single grain alternations	WS	Sh	Dg
ix	CZ/MZ-FZ/C	NGr	WS	Sh	Dg
xiv	CZ	Ma	PS/MS	Sh	Dg
xv	MZ	Ma	PS/MS	Sh	Dg
xvi	VFZ-C	NGr (short)	WS	Sh	Masepic WD
xix*	VFZ	Ma	WS	Gr	Dg

11.2.1.1 Depositional processes and Lamination Types

Using the microscopic characteristics of the sediments, depositional processes were established for each Lamination Type and are summarised below.

Lamination Type i is composed of massive well-sorted fine and very fine sand consistent with persistent flow (Palmer *et al.*, 2019). Within LT i there are sometimes clay intraclasts indicative of high energy underflows that eroded and ripped up previously deposited clay (Ringberg and Erlström, 1999). Lamination Types v, vi, vii, viii and ix are consistent with variable flows whereby the flow strength of a single input event varies over time. The normally graded nature of these Lamination Types suggests a decline in flow strength. The massive poorly sorted structure of Lamination Types xiv and LT xv with a medium or coarse silt matrix and occasional coarse grains is also indicative of variable flow with coarser grains sourced from low density underflows and finer grained material deposited from suspension settling (Palmer *et al.*, 2019). Lamination Type xvi is composed mostly of clay but displays normal grading from very fine silt to clay and is consistent with suspension settling through the water column.

Lamination Type xix is a new Lamination Type that has been identified in this study. The grain size is very fine silt and the massive structure suggests that there is a consistent supply of this sediment in the water column. The lack of coarser-grained material suggests that this Lamination Type was deposited via suspension settling. Further interpretation of Lamination Type xix is presented in section 11.2.3.4.

11.2.2 Lamination Sets

Repeating groups of Lamination Types were also identified under thin section and classified into distinct Lamination Sets (Table 11-2). The Lamination Sets show evidence of the different relative timing of sediment transport and deposition indicative of seasonal variations in sediment supply, these processes are summarised in Chapters 6, 7 and 8. Lamination Sets were therefore interpreted as glaciolacustrine varves.

Table 11-2. Lamination Sets identified within the Glottern, Svinstadsjön and Asplången sequences.

Lamination Set (LS)	Coarse-grained component LT	Fine-grained component LT
A	xix	xvi
B	xiv	xvi
C	xv	xvi
D	viii	xvi
E	vii, viii	xvi
F	i, v, ix	xvi
G	xv, xix	xvi
H	ix,xv	xvi

11.2.3 Lamination Set Assemblages

The categorisation of Lamination Sets into Lamination Set Assemblages is achieved by linking the Lamination Set properties (including varve thickness) to specific locations within the lake basin. The following section uses the classification scheme proposed by Palmer *et al.* (2019) and assigns each Lamination Set to a Lamination Set Assemblage. The Lamination Set Assemblages from Palmer *et al.* (2019) that were identified in this thesis are: 1) Proximal Intermediate; 2) Intermediate/Distal Lake Bottom; 4) Distal Lake Bottom; and 5) Ultra Distal/Nival (Figure 11-1). Lamination Set Assemblage 3, Distal Bottomset/subaqueous fan, was not identified in the sites in this study.

11.2.3.1 Lamination Set Assemblage 1

Lamination Set F is ascribed to Lamination Set Assemblage 1. These varves have an overall thickness >20 mm and the coarse component is thicker than the fine component. The coarse components are composed of a series of coarse grained Lamination Types (LT i, vi) that are either massive or normally graded and represent underflow sedimentation from turbidity currents (Ashley, 1975; Ridge *et al.*, 2012). The sharp contact to the fine-grained clay component is indicative of a sudden change in depositional process to suspension settling (Ringberg and Erlström, 1999). This

Lamination Set Assemblage represents varves that are deposited in a relatively proximal position to the glacier margin whereby all sediment is delivered directly from the glacier. These varves are referred to as Proximal Intermediate sediments (Palmer *et al.*, 2019).

11.2.3.2 Lamination Set Assemblage 2

Lamination Sets E, G and H are ascribed to Lamination Set Assemblage 2. These varves are between 10 and 20 mm in thickness and the coarse component is thicker than the fine component. The fine component is composed of very fine silt that normally grades to clay with a sharp upper contact (LT xvi). The coarse components are composed of normally graded Lamination Types of varying thickness and that grade from coarse silt to medium silt (LT v, vii, viii). The coarser-grained normally graded Lamination Types suggest sedimentation via quasi-continuous flows from the glacier (e.g. Bendle *et al.*, 2017; Palmer *et al.*, 2019). The Lamination Sets are a more distal version of the Proximal Intermediate varves with lower energy and/or lower sediment concentration in the flows. These varves are referred to as Intermediate/Distal lake bottom sediments (Palmer *et al.*, 2019).

11.2.3.3 Lamination Set Assemblage 4

Lamination Set D is ascribed to Lamination Set Assemblage 4. These varves are between 1-5 mm thickness and the coarse component is thinner than the fine component. The fine component is composed of very fine silt that normally grades to clay with a sharp upper contact (LT xvi). The coarse components are composed of single grain alternations between coarse and medium silt (LT viii). These alternations in grain size reflect sedimentation during the melt season from either single flow events, nival melt and/or precipitation events. These varves likely contain limited sediment sourced directly from the glacier margin and therefore were formed in distal locations within the lake basin. These varves are referred to as Distal Lake Bottom sediments (Palmer *et al.*, 2019).

11.2.3.4 Lamination Set Assemblage 5

Lamination Sets B and C are ascribed to Lamination Set Assemblage 5. These varves can be <1 mm thickness but are usually between 1-5 mm thickness. The coarse component is thinner than the fine component. The fine component is composed of very fine silt that normally grades to clay with a sharp upper contact (LT xvi). Whilst Palmer *et al.* (2019) report that these Lamination Sets are typically <1 mm thickness, the micro-sedimentology of Lamination Sets B and C are the same as those identified by Palmer *et al.* (2019) in Lamination Set Assemblage 5. The coarse components of LS B and C are composed of a single massive and poorly sorted coarse silt (LT xiv) or medium silt

with grains of coarse silt within the matrix (LT xv). These coarse silt grains were likely deposited as quasi-continuous underflows from high discharge events whereas the finer grained (fine and medium silt) sediments were deposited from suspension settling. These varves are likely the result of nival melt with little to no material supplied directly from the glacier margin. These varves are referred to as Ultra Distal/Nival sediments.

11.2.3.5 Lamination Set Assemblage 6

Lamination Set A does not fit into the descriptive framework proposed by Palmer *et al.* (2019) and so is ascribed to a new Lamination Set Assemblage that is, at present, unique to the Baltic Ice Lake. Lamination Set A are between 1-5 mm thickness and the coarse component is thinner than the fine component. The fine component is composed of very fine silt that normally grades to clay with a sharp upper contact (LT xvi). The coarse components are composed of massive fine to very fine silts and display a graded contact to the overlying fine component (LT xix). The fine grain sizes and the massive structure suggests that there is a consistent supply of this sediment in the water column. The lack of coarser-grained material that would be deposited from low density underflows suggests that these sediments were likely deposited due to suspension settling. Localised resuspension of fine-grained material at the lake bottom was likely caused by underflows which travelled across the basin floor. After the underflow waned, the fine- and very fine silts fall from suspension in the water column (e.g. Bendle *et al.*, 2017). These varves receive little to no input from nival melt, precipitation events or underflows and are therefore categorised as “Ultra Distal Baltic Ice Lake sediments” (Figure 11-1).

Lamination Set Assemblage	Melt Season (MS)				Non-Melt Season (NMS)		
	Varve Thickness (mm)	Particle Size (Sorting)	Structure	Upper Contact	Particle Size	Structure	Upper Contact
1	20 - 600 MS > NMS	VCZ - MZ (WS)	multi-lamination; f.u. (CZ-MZ); turbidites f.u. (CS-VFS)	sharp	C (VFZ) (WS)	graded: VFZ f.u. to clay from the first part of the lamination	sharp
2	2 - 20 MS ≥ NMS	VFS; CZ; MZ (WS)	multi-lamination; 1st input MZ; later f.u. (CZ-MZ)	sharp	C (VFZ) (WS)	graded: VFZ f.u. to clay from the first part of the lamination	sharp
4	1 - 5 MS ≤ NMS	MZ;CZ (WS)	multiple laminations; alternations of CZ and MZ; CZ sometimes single grain lineations	sharp	C (VFZ) (WS)	graded: VFZ f.u. to clay from the first part of the lamination	sharp
5	<1 MS ≤ NMS	MZ (PS)	single lamination or multi lamination; single grain lineations of CZ	appears graded	C (VFZ) (WS)	graded appearance due to contact from MZ from the NMS layer; f.u. to clay	sharp
6	1-5 MS ≤ NMS	VFZ/FZ (WS)	single lamination	appears graded	C (VFZ) (WS)	graded: VFZ f.u. to clay from the first part of the lamination	sharp

MS = Melt Season; NMS = Non Melt Season; FS = fine sand; VFS = very fine sand; VCZ = very coarse silt; CZ = coarse silt; MZ = medium silt; VFZ = very fine silt; C = clay; WS = well sorted; PS = poorly sorted; f.u. = fining upwards; QS = Quasi Steady; ST = surge type

Lamination Set Assemblage	Basinward Transport	Sediment Source	Lamination Set Assemblage Name	Microfacies Schematic
1	MS: QS underflow & ST for turbidites NMS: suspension settling	All glacier sourced sediment	Proximal Intermediate	
2	MS: QS underflow 1st input lower energy (spring melt from catchment) than subsequent laminae. NMS: suspension settling	High glacier sourced sediment	Intermediate / Distal Lake Bottom	
4	MS: QS underflow; only high discharge events recorded; element of suspension deposition. NMS: suspension settling	High fluvial (nival)/glaciofluvial; low ice contact glacial component	Distal Lake Bottom	
5	MS: QS underflow; flow velocity is low providing only suspended load. Some mixing of higher flow events NMS: suspension settling	High fluvial (nival) glaciofluvial; no ice contact component	Ultra Distal / Nival	
6	MS: suspension settling of localised reworked sediments NMS suspension settling	No fluvial (nival) glaciofluvial; no ice contact component localised reworked bottom sediments	Ultra Distal Baltic Ice Lake	

Key:
MS = Melt Season; NMS = Non Melt Season; QS = Quasi Steady; ST = surge type; sg = single grain

Melt season: massive, normally graded, normally graded

Non Melt season: grading at the very first part of the lamination, grading distributed evenly through the lamination

Thickness range of the microfacies (mm): 0, 2-20

Grain size on each log: c (clay); fz (fine silt); mz (medium silt); cz (coarse silt); vfs (very fine silt)

Figure 11-1. Lamination Set Assemblages in this study. Melt season and non-melt season characteristics, basinward transport, sediment source and microfacies schematic for each Lamination Set Assemblage (LSA). LSA 6 is highlighted in grey. Modified from Palmer et al. (2019).

11.2.4 Comparisons between sites

There are several Lamination Sets that are common to all three sites (e.g. Lamination Sets B, C, D, E and F) however, Lamination Set A is absent in the Glottern site (Figure 11-2), and Lamination Sets G and H are absent at Svinstadsjön (Figure 11-3) and Asplången (Figure 11-4). Table 11-3 summarises the Lamination Sets identified at each site.

Table 11-3. Lamination Sets that were identified at each site.

Lamination Set (LS)	Glottern	Svinstadsjön	Asplången
A	X	✓	✓
B	✓	✓	✓
C	✓	✓	✓
D	✓	✓	✓
E	✓	✓	✓
F	✓	✓	✓
G	✓	X	X
H	✓	X	X

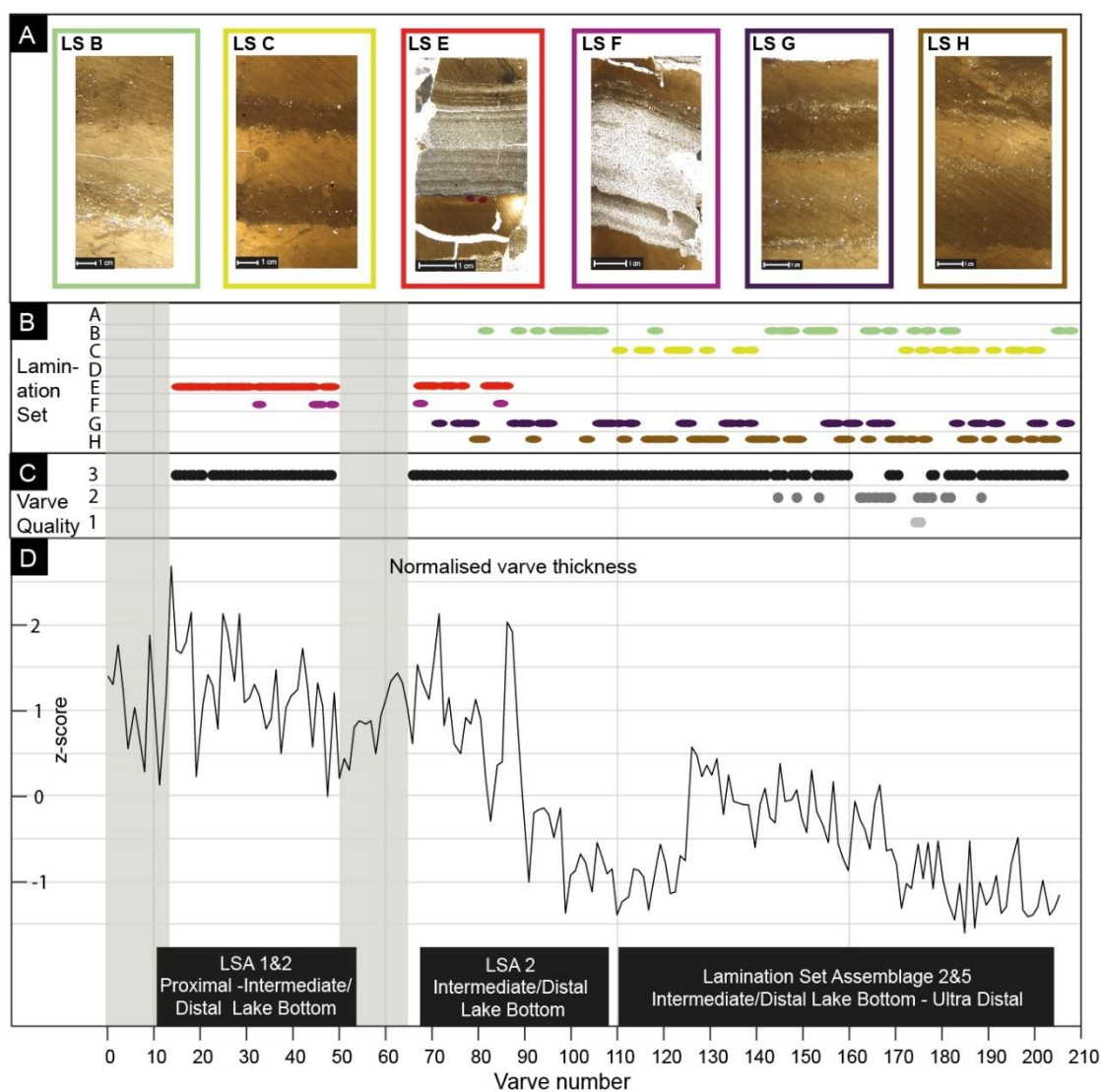


Figure 11-2. Lamination Sets and Lamination Set Assemblages in the Glottern sequence (A) Images of Lamination Sets identified in the Glottern sequence. (B) Distribution of Lamination Sets throughout the Glottern sequence. (C) Normalised varve thickness with Lamination Set Assemblages (LSA) labelled.

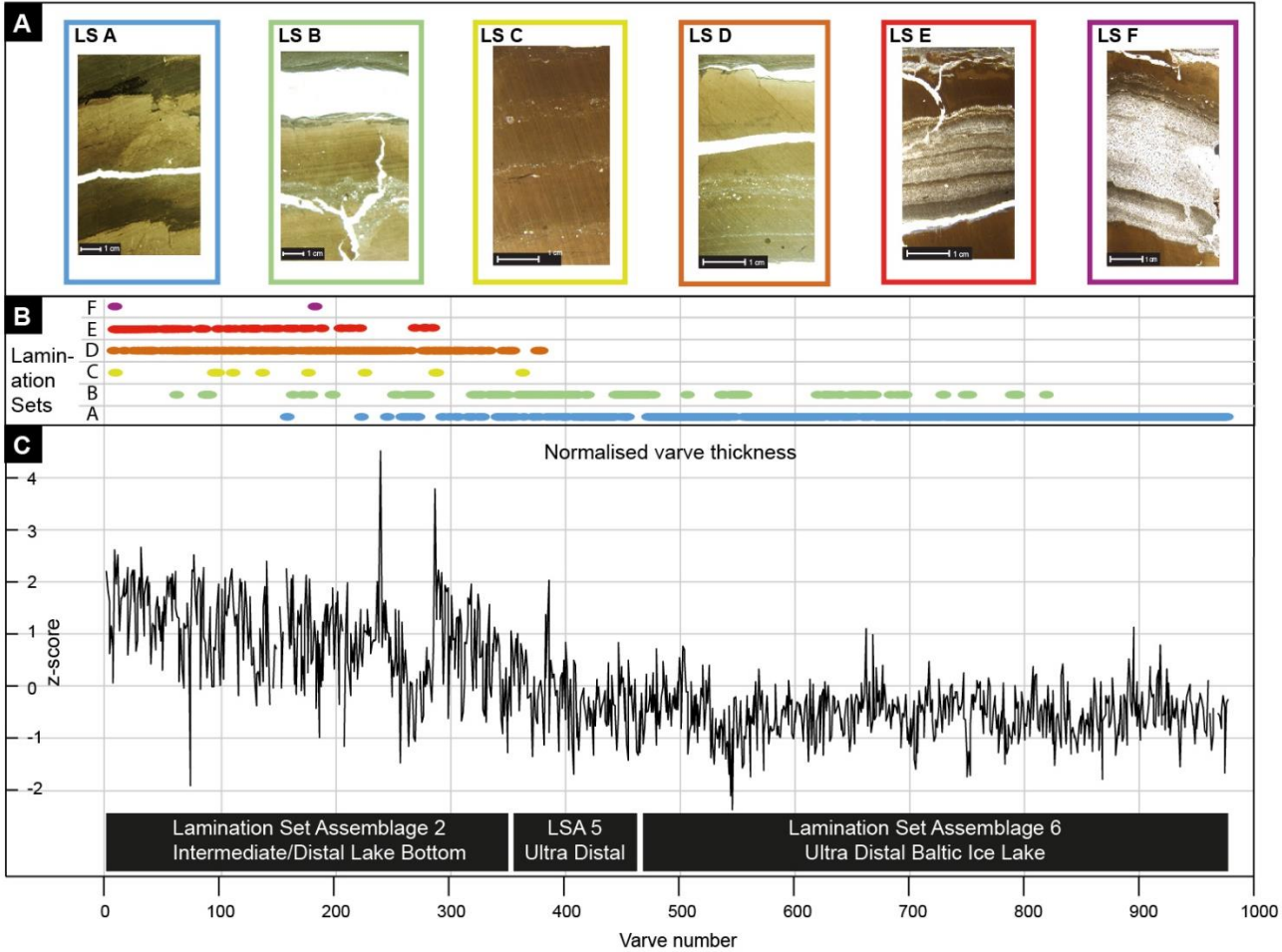


Figure 11-3. Lamination Sets and Lamination Set Assemblages in the Svinstadsjön sequence. (A) Images of Lamination Sets identified in the Svinstadsjön sequence. (B) Distribution of Lamination Sets throughout the Svinstadsjön sequence. (C) Normalised varve thickness with Lamination Set Assemblages (LSA) labelled.

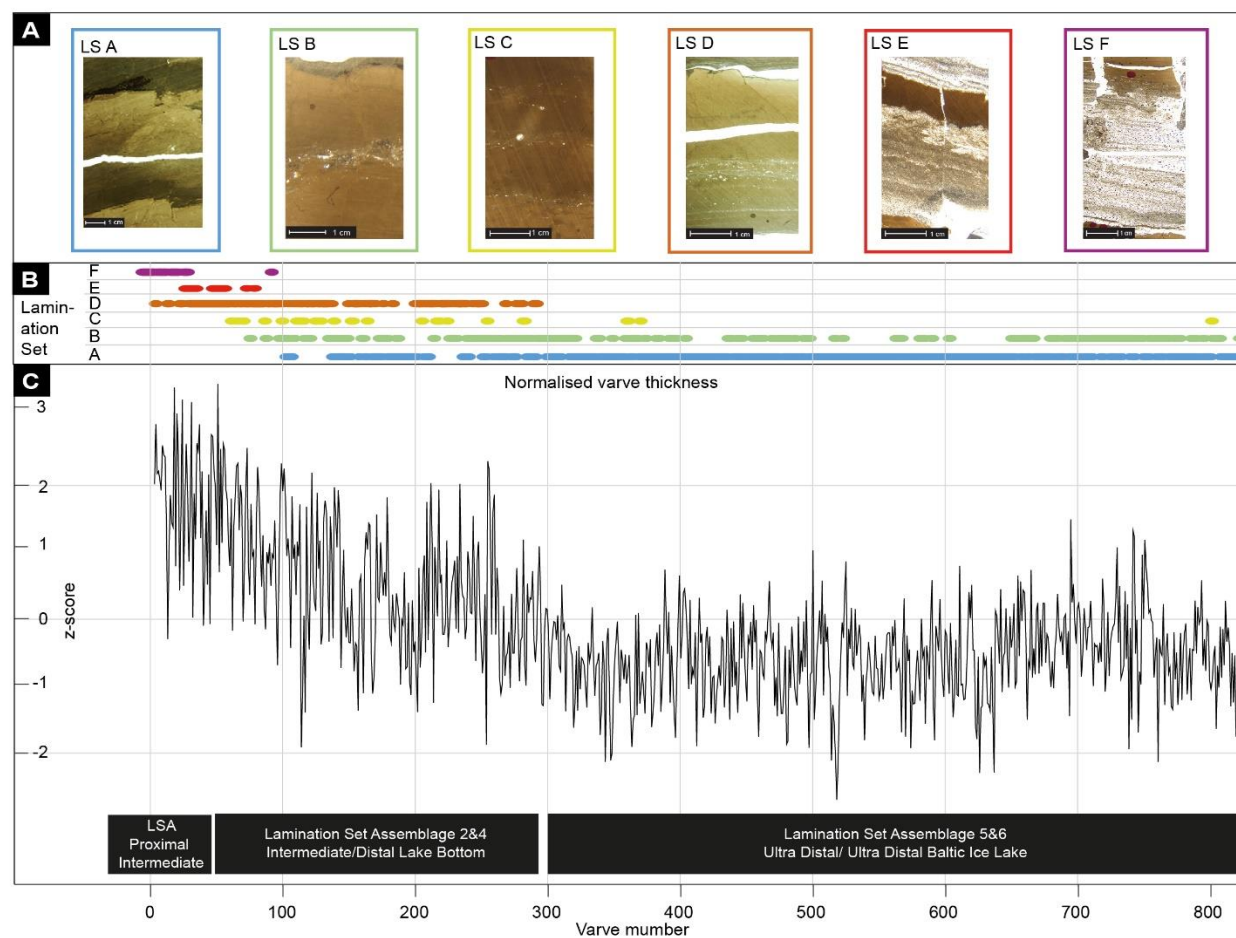


Figure 11-4. Lamination Sets and Lamination Set Assemblages in the Asplången sequence.

(A) Images of Lamination Sets identified in the Asplången sequence. (B) Distribution of Lamination Sets throughout the Asplången sequence. (C) Normalised varve thickness with Lamination Set Assemblages (LSA) labelled.

The absence of varves of Lamination Set A at the Glottern site is attributed to the different depositional environment. The Glottern site was located in an archipelago system with narrow valleys and shallow water depths (ca 30-50 m) (Wohlfarth *et al.*, 1993, 1998). The islands above the highest shoreline likely provided a source of sediment to the lake basin in addition to sediment sourced directly from the retreating ice margin. In contrast, the Asplången and Svinstadsjön sites are located further north outside of the archipelago system in the main Baltic Ice Lake, and varves were deposited in water depths ca 100 m (Brunnberg, 1995). The Asplången and Svinstadsjön sites are located further away from the lake edge than the Glottern site and as such, likely received little sediment from catchment meltwater streams. Therefore, the fine- to very fine silts that comprise Lamination Set A were likely deposited due to seasonal suspension settling of reworked sediments from the water column, with limited to no input from nival or glacier melt.

Similarly, the presence of Lamination Sets G and H at the Glottern site can also be related to the depositional environment. The presence of multiple laminations in the coarse component that are attributed to nival melt is likely due to the proximity of the Glottern site to the lake edge. The results from this thesis indicate that varves deposited in an archipelago system may contain more laminations in the coarse component than sites in the main Baltic Ice Lake (e.g. Svinstadsjön and Asplången). Additional microfacies analysis from sites within the Wohlfarth *et al.* (1998) regional varve chronology would be required to assess the spatial extent of these microfacies. The following section compares the Lamination Sets observed in this study with those identified by Ringberg and Erlström (1999) in order to make an assessment of the spatial distribution of varve microfacies across the Baltic Basin.

11.2.5 Comparisons with Ringberg and Erlström (1999)

Prior to this thesis, the only micromorphological description of glaciolacustrine varves in the Baltic Ice Lake is that of Ringberg and Erlström (1999). The authors identified four microfacies from sites in Skåne and Blekinge that were located at the southern margin of the FIS. Coarse component layer thicknesses range between 10 and 30 mm and are categorised as: 1) Bottom/Proximal varves; 2) Varves above bottom; 3) Varves of diffuse appearance; and 4) Distal varves. The Lamination Sets in this thesis are comparable to those identified by Ringberg and Erlström (1999) and demonstrate that similar processes operate across the BIL over spatial and temporal scales. A summary of these varve microfacies are presented in Table 11-4.

Table 11-4. Microfacies descriptions of Baltic Ice Lake varves by Ringberg and Erlström (1999).

Varve types described by Ringberg and Erlström (1999) alongside the corresponding Lamination Set from this thesis. Lamination Set Assemblage and name are also provided using the Palmer et al. (2019) classification scheme.

Varve type (Ringberg and Erlström, 1999)	Description	Corresponding Lamination Set in this study	Lamination Set Assemblage	Name (Palmer <i>et al.</i> , 2019)
Bottom/Proximal	<ul style="list-style-type: none"> • 0.5-20 cm thicknesses, $s > w$ • Coarse components contain multiple graded laminae and a layer of coarser sediment grains in the early melt season. • The early melt season layers exhibit a sharp and often erosional contact with the underlying winter layer. • Clay intraclasts are common in the coarse component. • Winter layer is homogenous clay 	F	1	Proximal Intermediate
Varves above bottom	<ul style="list-style-type: none"> • 0.5-20 cm; $s < w$ • Coarse component contains multiple graded laminae containing matrix supported silts and some clay. • Winter layer is normally graded from very fine silt to clay, some evidence of shear within the clays. 	C	2	Intermediate/ Distal lake bottom
Varves of diffuse appearance	<ul style="list-style-type: none"> • 1-3 cm; $s > w$ • Coarse component contains fewer multiple graded laminae, clay intraclasts, contact with the underlying winter layer is erosional. • Winter layer is normally graded from very fine silt to clay 	C	2	Intermediate/ Distal lake bottom
Distal varves	<ul style="list-style-type: none"> • 1-10 mm thickness; $s > w$ • Up to eleven graded laminae with sharp upper contacts observed in the summer component • Grain sizes of fine to coarse silt. • Winter layer is graded from very fine silt to clay and has a sharp and erosional upper contact 	E or G	4	Distal lake bottom

Ringberg and Erlström (1999) only describe varves with multiple laminations in the coarse component and do not describe varves that are composed of a single lamination within the coarse component such as Lamination Sets A, B and C that are presented in this thesis. This indicates that some varve processes may not be pervasive across the Baltic Ice Lake. The lack of Lamination Sets A, B and C in the Skåne and Blekinge varve records is comparable to the Glottern site presented in this thesis. This is unsurprising given that the varve sites in Skåne and Blekinge were located within an archipelago system, similar to Glottern. The lack of varves with a single-lamination coarse component is indicative of the proximity of those sites to the lake edge and/or small islands in the archipelago. This would have ensured a readily available supply of sediment to the lake basin from nival melt and/or precipitation. The implications of these findings for the construction of accurate varve chronologies in the STS is discussed in more detail in the following section.

11.2.6 Implications for constructing a composite varve chronology

The results from microfacies analysis demonstrate that several sedimentological processes underpin varve formation, and this varies spatially across the Baltic Ice Lake. The increased level of detail generated in this thesis indicates that these complexities are likely overlooked when analysing varves at the macroscale. Whilst varve characteristics are primarily driven by proximity to the glacier margin, the results from this thesis indicate that proximity to the lake edge and site-specific depositional processes may also control varve thickness.

The microfacies results demonstrate that whilst most of the Lamination Sets in this thesis can be categorised using the Palmer *et al.* (2019) framework there are Lamination Sets that show more complex sedimentological patterns across this part of the Baltic Basin. The varve structure of Lamination Set A is, to date, unique to the Baltic Ice Lake but is only identified in certain depositional settings. Moreover, there are regional differences in varve sediment processes across the Baltic Basin since Lamination Sets A, B and C were not identified by Ringberg and Erlström (1999) in southern Sweden. The spatial differences in the microfacies may explain, or partially explain, the difficulties encountered by some researchers when trying to link regional varve chronologies (e.g. Kristiansson, 1986; Brunnberg, 1995; Wohlfarth *et al.*, 1998).

In particular the presence of very thin, Lamination Set A structures that are derived from suspension settling processes could play an important role in matching varve thickness records. It was hypothesised that these varves would be of limited use for site correlations. This is explored in more detail in section 11.4 through analysis of the

Asplången and Svinstadsjön composite varve chronology where varves of Lamination Set A are observed in both varve chronologies.

11.3 Comparison of the varve records in this thesis with the existing varve records

This section presents a comparison between the varve counts and thickness records in this thesis with existing varve chronologies. The Svinstadsjön site has not been investigated prior to this thesis and so comparisons cannot be made with published literature. Therefore, comparisons will focus on the Glottern and Asplången records.

Varve records have been established at the Glottern site by Wohlfarth *et al.* (1998), and for the Asplången site an unpublished varve thickness record was provided by Dr Lars Brunnberg. Differences between this thesis and existing varve records are discussed in the context of the sedimentological processes at each site and the analytical methods that were applied to describe and identify the varved sediments. The section summarises by outlining the implications for the construction of site and regional varve chronologies in the STS, and by recommending a new approach for future analysis of STS varves.

11.3.1 Glottern

The varve thickness record generated in this thesis matches well with the “Core 2” record obtained by Wohlfarth *et al.* (1998), however there are some differences. More varves were counted under thin section (207 varves) than were identified from the macroscale analysis conducted by Wohlfarth *et al.* (1998) (198 varves). A *ca* 5% increase in total varves was recorded, despite the Wohlfarth *et al.* (1998) chronology containing 4 additional basal varves (Figure 11-5).

By visually aligning the varve records and applying Pearson’s moment correlation, it is possible to determine where the additional varves are located within the sequence. Figure 11-5 demonstrates that the additional varves are \geq cm thickness and are likely located in the lowermost part of the varve record in LF1. It was anticipated that if more varves were identified by thin section analysis that these would likely be thin (<mm-scale) varves that are difficult to identify at the macroscale. However, even the thinnest varves in the Glottern sequence were identifiable at the macroscale, likely due to their composition and thicknesses which are typically 2-10 mm. Microfacies analysis shows that the boundary between seasonal laminations is sharp, and they are also marked by a distinct colour change between seasonal components, aiding identification.

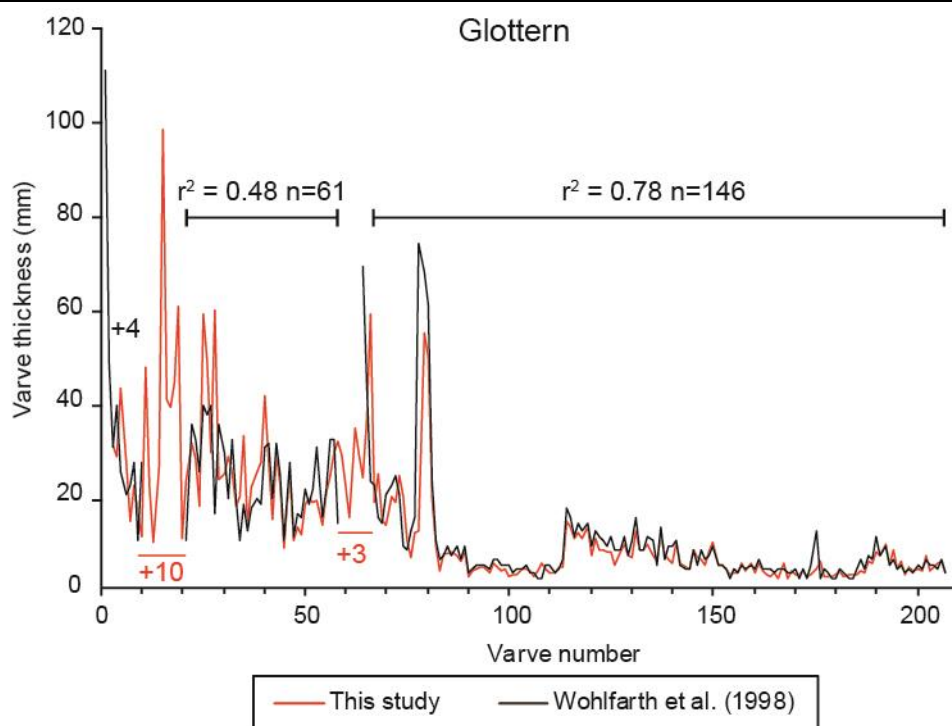


Figure 11-5. Glottern varve chronologies from this study and Wohlfarth *et al.* (1998).

The 13 additional varves that were identified in this study are cm-scale varves with multiple graded beds in the summer component (i.e. Lamination Set E and F). As discussed above, the varves at Glottern are readily identifiable at the macroscale, suggesting that the record obtained by Wohlfarth *et al.* (1998) was taken from a sub-optimal location at the Glottern site. A key finding from the sediment depth survey at Glottern is that the sediment bathymetry is highly variable across relatively short distances (Chapter 8). Indeed, Wohlfarth *et al.* (1998) report three varve records from Glottern with counts between 150 to 198 yrs (Table 11-5).

Table 11-5. Glottern varve count comparison

Devine (2019)	Wohlfarth <i>et al.</i> (1998)		
GLO1	Core 1	Core 2	Core 3
207±1	159	198	150

One hypothesis for the disparity between the number of proximal varves between different coring locations within the Glottern site is that the variable topography may prevent the progression of turbidity currents across the lake basin (e.g. Gustavson, 1975). For example, an esker, glacial boulder or a moraine may cause “blocking” of sediment density flows (e.g. Lundqvist, 1957). In the STS some researchers have reported that local-scale processes may impact varve formation (e.g. Kristiansson, 1986;

Strömberg, 1989), however this does not appear to have been considered during the original investigation at Glottern.

Another difference between the varve record obtained in this thesis versus the record obtained by Wohlfarth *et al.* (1998) is the presence of deformation structures. In total 6 zones of deformation were identified in LF1 which are absent in the original varve chronology. At present it is not possible to determine whether this is because the coring location in this thesis was susceptible to localised deformation processes, or whether deformation structures were observed by Wohlfarth *et al.* (1998) but “bridged” during the process of creating the site varve chronology. The authors report that site varve chronologies within their regional chronology were constructed from multiple overlapping core sections but the original data from each section is not available. Additional cores from the Glottern site would be required in order to test the extent of the observed deformation, and if particular events causing deformation are pervasive across the basin.

Of the deformation structures identified at Glottern, 2 of the 6 were not observed during macroscale analysis and were only identifiable from X-radiographs and from thin sections (Figure 11-6). These two deformation structures were misidentified as individual varves during macroscale counts. Since original varve records were analysed at the macroscale, this raises questions about the number of type 1 errors (false positives) included in the original Glottern varve chronology of Wohlfarth *et al.* (1998).

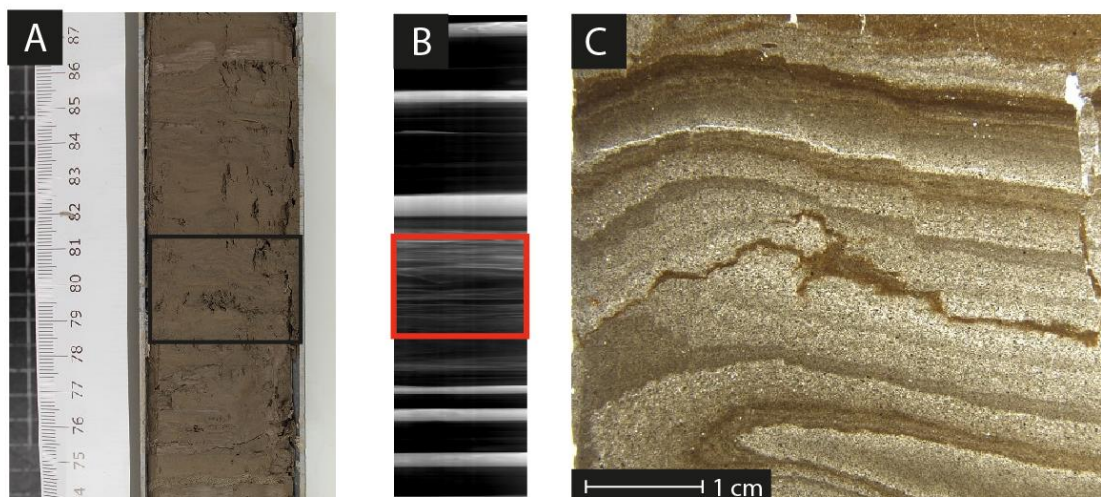


Figure 11-6. Example of a deformation zone observed from the core surface, under X-ray and under thin section.

The accuracy of the regional varve chronology produced by Wohlfarth *et al.* (1998) is supported by radiocarbon dating of macrofossils within the varved sediments (Wohlfarth *et al.*, 1995; 1998, later revised by Muschitiello *et al.*, 2016). However, the data presented in this thesis suggests that thorough basin surveys in combination with thin section

analysis holds the potential to further refine the existing varve counts and to enhance varve chronologies by providing a more accurate estimate of the varve spacing between each radiocarbon date. Moreover, since subsamples for radiocarbon dating comprised segments of 10-130 yrs, thin section analysis could further elucidate the precise number of varves represented by each date which, in turn, better highlight the underlying assumptions present within the Bayesian age model produced by Muschitiello *et al.* (2016).

11.3.2 Asplången

The Asplången varve chronology was extracted by Dr Lars Brunnberg in February 1997, with varve counts and thickness measurements conducted in April 1997. Measurements were made from core surfaces under laboratory conditions by rolling a paper strip next to the core and marking individual varves on the paper (Brunnberg, *pers comm*). The overall stratigraphy of the varve record obtained from this thesis is similar to the record obtained by Brunnberg in that there is a distinct colour change from brown to grey glacial varves observed in the upper part of both records. However, the varve counts are substantially different between the records and 218 fewer varves were counted by Brunnberg equating to a 27% difference in the varve counts. In this thesis, 657 brown varves and 170 grey varves were identified under thin section (827 yrs total). In contrast, Brunnberg counted 438 brown varves and 171 grey varves from macroscopic analysis of core surfaces (609 yrs total) (Table 11-6).

Table 11-6. Asplången varve counts from this study and Brunnberg.

Core section	This study	Brunnberg (unpublished)	Difference relative to Brunnberg
Brown glacial varves	657	438	+219
Grey glacial varves	170	171	-1
Total	827	609	+218

In the cm-scale varves a convincing correlation was possible and the lowermost 267 varves in the Brunnberg chronology can be visually and statistically correlated to the varve record obtained in this study. Varve 1 in the Brunnberg chronology is linked to varve 18 in the varve record in this thesis with an r^2 value of 0.48 (Figure 11-7). An additional 17 varves were found at the base of the sequence and microfacies analysis shows that the summer components of these varves are composed of multiple graded beds from sediment underflows (i.e. Lamination Set E and F). Similar to the Glottern site, it is unlikely that these varves were extracted by Brunnberg but missed during varve counts since these additional varves are clearly identifiable at the macroscale. Instead, the basin survey from Asplången demonstrates that sediment depth is highly variable

across short distances, and this may have impacted varve preservation. In other sites in Östergötland, Brunnberg (1995) describes difficulties correlating varve records from the same site due to variable varve thicknesses, and multiple cores had to be extracted in order to get a good correlation between individual cores (Brunnberg, *pers comm*). Whilst the effect of basin topography was considered by Brunnberg (1995), it is not clear precisely how individual or composite varve chronologies were created, or if a basin survey was undertaken in order to target a specific coring location.

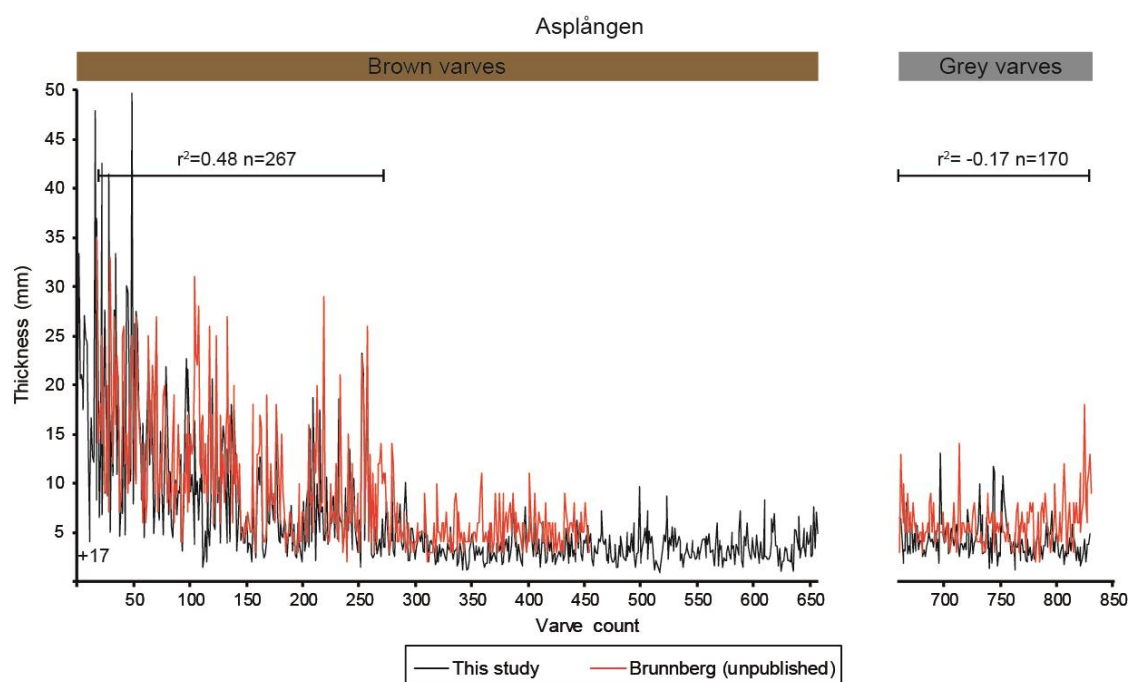


Figure 11-7. Asplången varve thickness record from this study and Brunnberg (unpublished).

It has not been possible to correlate the <cm-scale brown varves between the records (Table 11-7). This is primarily due to the difference between the varve counts, whereby 373 thin (<cm-scale) varves were counted in this thesis in comparison to 171 thin varves counted by Brunnberg.

Table 11-7. Correlation between this study and the Brunberg Asplången varve chronologies.

This study		Brunberg		Varve thickness	Varve colour	Correlation between this study and Brunberg (unpublished)
Varve number	No. of varves	Varve number	No. of varves			
1-17	17	N/A	N/A	≥cm-scale	Brown	N/A
18-284	267	1-267	267	≥cm-scale	Brown	$r^2=0.48$
285-657	373	268-438	171	<cm-scale	Brown	No correlation
658-827	170	439-609	171	<cm-scale	Grey	$r^2= -0.17$ statistical correlation and wiggle match are weak. Whilst varves could be correlated using the colour change from brown to grey varves, this requires independent testing

Comparisons between core surfaces and thin sections show that the <cm-scale brown varves are not identifiable at the macroscale, and that almost all correspond to Lamination Set A. Varves in Lamination Set A are typically <5 mm thickness, contain a fine- to very fine silt summer component and the winter component normally grades from very fine silt to clay. These characteristics mean that these varves are difficult to identify from core surfaces (Figure 11-8).

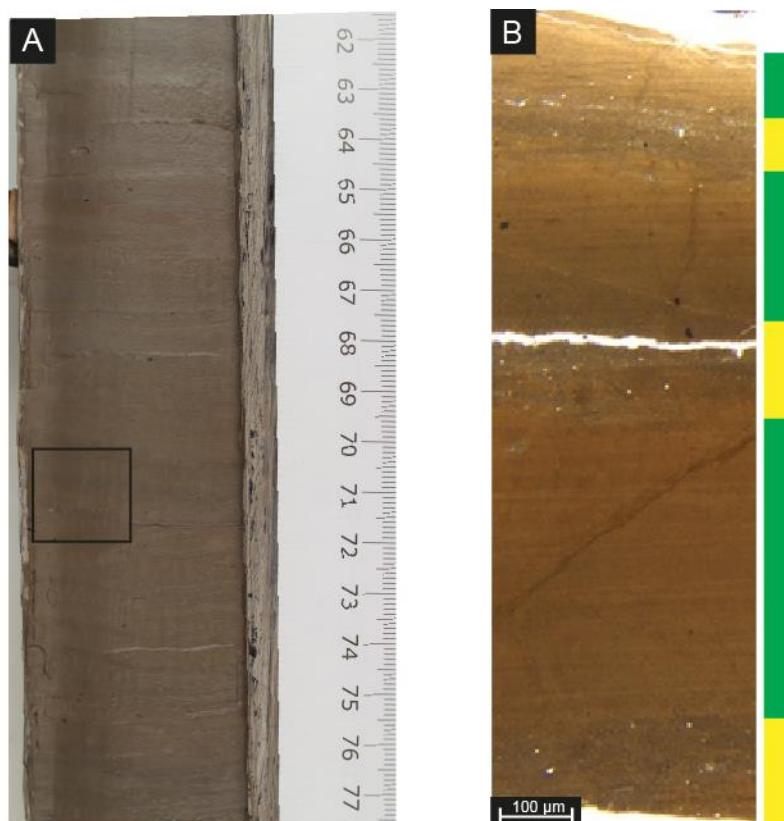


Figure 11-8. Example of varves in Lamination Set A in the Asplången sequence. (A) Core surface image from 662-677 cm. (B) Thin section image of the sediments highlighted in the black box in image A.

There is a distinct colour change from brown to grey glacial varves in the Asplången record. Since the number of grey varves is almost the same and both records were taken from the same site, it was expected that the thickness patterns in the grey varves would be similar. However, the thickness patterns are highly variable (Figure 11-7) and show weak negative correlation $r^2 = -0.17$. Difficulties correlating grey varves from the same site are described by Brunnberg (1995) in varve sites in the Södertörn peninsula, south of Stockholm. At present it is not clear whether difficulties correlating grey varves is because local processes control varve thickness patterns, or if the colour change represents an asynchronous event and should not be used to correlate records (Figure 11-9). Therefore, it is unclear whether the varve record in this thesis should be correlated to the Brunnberg record using varve thickness or colour changes. This problem is described by Brunnberg (1995) however, many site correlations in the regional varve chronology appear to be based on the mere presence of grey varves rather than convincing varve thickness correlations. This highlights the need for independent means of correlating varve records and raises questions about the validity of the existing regional varve chronologies that use colour changes for varve correlations (e.g. Brunnberg, 1995; Andrén *et al.*, 1999).

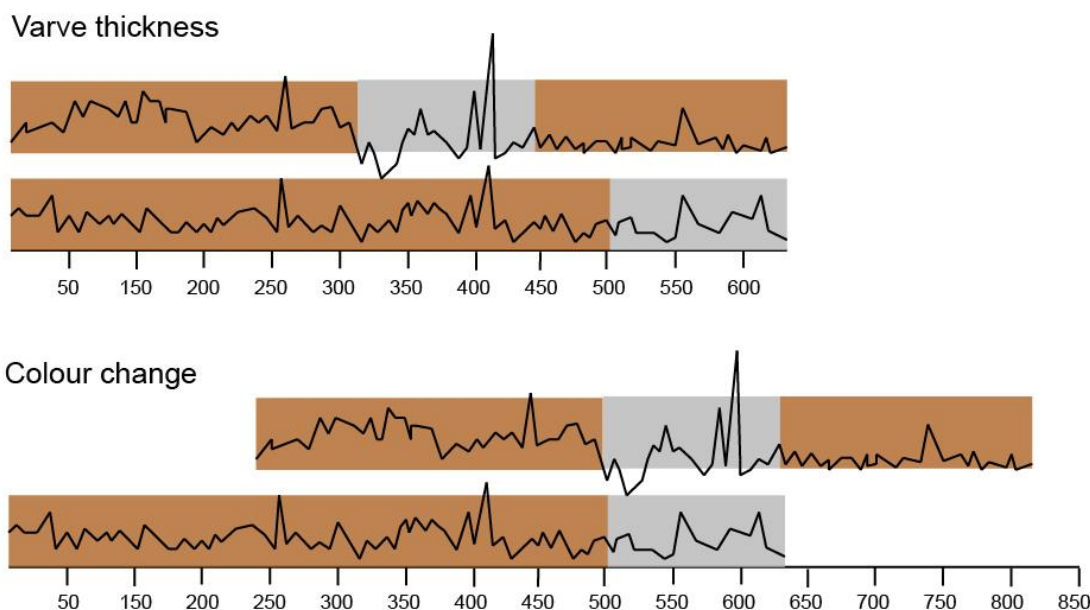


Figure 11-9. Hypothetical varve correlations using varve thickness wiggle matching (top) and colour changes (bottom).

If varve records are correlated by varve thickness, then colour changes are asynchronous. If varve records are correlated using colour changes then the varve thickness correlation is weak.

Whilst thin section analysis has led to improved precision and accuracy of the Asplången varve chronology, it is difficult to correlate the varve chronology from this thesis with the existing site chronology in the sections of <cm-scale brown varves and the grey varves.

For these sections both the traditional visual alignment and statistical correlations were unconvincing. These results are consistent with results from Holmqvist and Wohlfarth (1998) who found that sites in Östergötland near to Asplången could not be statistically correlated using varve thickness data. It is therefore recommended that if matches using colour changes and visual alignment/statistics are in disagreement then linking of varve records should be avoided or independently verified.

11.3.3 Summary

Through comparison of the results from this thesis with existing varve chronologies from Glottern and Asplången more varves are found at both sites. This is due to two key reasons; 1) sediment depth surveys enabled a targeted approach to coring location selection, and 2) microfacies analysis enabled detection of “hidden” varves that were not identifiable at the macroscale. At both sites additional \geq cm-scale ice-proximal varves were found as a result of a thorough basin survey with 13 additional varves identified at Glottern and 17 at Asplången. At the Asplången site a further 202 varves of Lamination Set A were identified under thin section, though at Glottern, varves of this nature are absent. These varves were the most difficult to identify at the macroscale due to subtle differences in texture and colour between the $<$ mm and mm-scale laminations within a single varve.

The absence of varves in Lamination Set A at the Glottern site is attributed to the different depositional environment (section 11.2.4). The Glottern site was located in an archipelago system whereas the Asplången site is located further north outside of the archipelago system in the main Baltic Ice Lake. The Glottern site likely received more sediments from nival melt in comparison to the Asplången site. The microfacies and varve count data suggest that depositional settings similar to the Glottern site are less prone to undercounting. However, in sites without varves of Lamination Set A, the risk of type 1 error (false positives) is greater at the macroscale. Future research could be targeted on a subset of sites where counts are likely to be less robust.

Given that sediments in Lamination Set A are composed of material derived from suspension settling processes rather than being driven by the extent and behaviour of the ice margin, it was hypothesised that these varves would be of limited use for site correlations. This is explored in section 11.4 in more detail through analysis of the Asplången and Svinstadsjön composite varve chronology where varves of Lamination Set A are observed in both site varve chronologies.

The difficulties faced when correlating the varve thickness record from this study with that of Brunberg, may simply be a product of the different analytical precision of the methods employed when identifying the varves i.e macro- versus microscale techniques.

Therefore, a key part of this thesis aimed to test varve correlations between two records that were both analysed under thin section. This is explored in more detail in the following section through analysis of the Svinstadsjön and Asplången correlation.

11.4 Assessing the correlation between the Svinstadsjön and Asplången varve records

This section discusses the correlation between the Svinstadsjön and Asplången varve chronologies. Since the varve records were both analysed under thin section, any difficulties when overlapping the varve thickness records cannot be related to different analytical methods. This enables discussion of other influences on the varve thickness records such as the impact of local and regional depositional processes. This section also discusses the impact of depositional processes on the construction of a composite varve chronology.

The current placement of the overlap between the site records shows that there is good visual and statistical agreement between the records, but this is more convincing in the basal \geq cm-scale varves than the uppermost $<$ cm-scale varves. Statistical correlation indicates that the lowermost $n=657$ brown varves in the Asplången sequence (prior to deposition of Bed 1) can be correlated to the varve interval 75-731 vyrs in the Svinstadsjön record with an $r^2=0.55$ ($p<0.001$). The uppermost $n=170$ grey varves from the Asplången record (after deposition of Bed 1) show weak statistical correlation with the Svinstadsjön sequence, with all possible correlations yielding r^2 values less than 0.1.

The link varve position cannot be supported by the temporal succession of Lamination Sets which is asynchronous between the sites. For example, around the position of the link varve, the progression of Lamination Sets D, E and F to Lamination Sets A, B and C is asynchronous (Figure 11-10). Since Lamination Sets D, E and F derive most of their sediment from the glacier margin (section 11.2) and Lamination Sets A, B and C are deposited in a more ice-distal location, their temporal progression at each site is likely a function of ice margin position. Therefore, it is unsurprising that the succession of Lamination Sets appears time-transgressive from Svinstadsjön to Asplången. However, this inference assumes that the position of the link varve is correct, which introduces an element of circularity when assessing its reliability. One way to independently test the current placement of the overlap would be to obtain chemical data for the Svinstadsjön tephtras, allowing the varve chronology to be independently dated. This is discussed further in section 11.5.3.

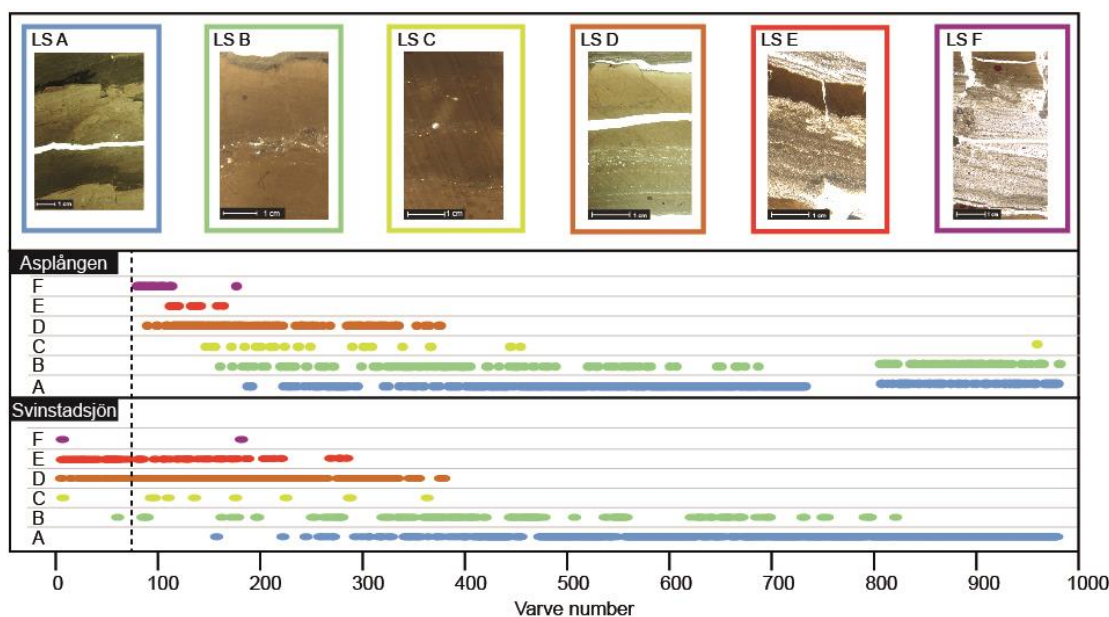


Figure 11-10. Lamination Sets in the Svinstadsjön and Asplången sequences aligned using the link varve (dashed line).

Despite the aforementioned assumptions, the current placement of the link varve is deemed the most reliable given the available data. The good statistical and visual correlation between the varve thickness records in the basal \geq cm-scale varves demonstrates that some sediment processes were common at both sites. The poor statistical and visual correlation between the records in the <cm-scale varves indicates that more localised sediment processes controlled varve thickness during deposition.

Microfacies analysis indicates that the basal sediments are ice-proximal and proximal-intermediate varves, whereby most sediment is delivered to the basin directly from the glacier as underflows. In contrast, the uppermost <cm-scale laminations are interpreted as ultra-distal varves that are produced by local-scale sediment processes. Critically, the effect of local-scale sediment processes appears to outweigh the influence of larger-scale processes, producing a considerable amount of noise in the varve thickness records. This suggests that the influence of localised sediment processes, which can lead to “noisy” varve thickness records leads to difficulties correlating site chronologies, even those in close proximity.

Given that ultra-distal varves are usually not identifiable at the macroscale, the identification of these so-called “hidden” varves may generate noise in varve thickness records. It is possible that reanalysis of other sites within the STS which are currently thought to have good correlation would show considerably weaker links if the varved sediments are re-examined under thin section and potentially ultra-distal varves are

identified. It is even possible that this reanalysis could suggest new links between sites, fundamentally changing the existing composite chronologies.

Thin section analysis demonstrates that it is not only thickness which makes certain varves difficult to identify, but also the internal composition of the varves such as grain size and structural differences between seasonal components. These differences are driven by the depositional processes at each site, and without thin section analysis it is not possible to make this observation. Critically, prior to this research, it has not been possible to assess the extent to which local-scale processes influence varve formation and it is apparent that if local-scale processes influence varve composition and thickness then these varve types may be of limited use for correlations between sites. The results from thin section analysis demonstrate that understanding sediment processes at the sub-annual scale is necessary for the development of robust varve chronologies. Yet with precise and accurate varve counts noise is enhanced and the process of correlation becomes more challenging.

11.4.1 Summary

One of the objectives of this thesis was to use thin section analysis to improve the accuracy of varve counts and the precision of thickness measurements. The driving factor for this is that several researchers reported difficulties correlating varve records in close proximity to one another (Kristiansson, 1986; Strömberg, 1989; Brunnberg, 1995; Wohlfarth *et al.*, 1998). Whilst thin section analysis has produced highly precise and accurate site varve chronologies, difficulties remain when correlating individual records to produce a composite varve chronology. It appears that thin section analysis has highlighted the genuine level of noise in varve thickness records which has, until now, been suppressed by the macroscale techniques employed. Thus, resolving the problems identified in the existing STS, regarding correlations between site chronologies, cannot necessarily be achieved with thin section analysis alone. The results presented here reinforce the need for other independent means of correlating varve records such as tephrochronology.

11.5 Tephrochronology

Tephra has been identified within glacial varves in two of the three sites in this thesis and identification of the Askja-S tephra in the Asplången sequence is the first identification of this tephra within Swedish glacial varves.

The identification of tephra in the sediment sequences in this thesis has been valuable for several reasons;

- 1) the presence of tephra in varved sediments demonstrates the potential to find tephra in other varve sequences in the STS,
- 2) the integration of tephra and varve data has enabled existing tephra ages to be remodelled within a Bayesian framework,
- 3) correlation to known tephras has enabled the Asplången and Svinstadsjön records to be placed on an absolute timescale and the previously reported ages of the varve sequences have been revised,
- 4) tephra data shows the potential for independent correlation between varve chronologies in the STS, and
- 5) the new ages of the varve chronologies have enabled the current deglaciation model to be tested.

The following section explores points 2-4 in more detail, with point 5 explored in section 11.7 alongside the implications for the published age estimates of the deglaciation chronology and final drainage of the BIL.

11.5.1 Bayesian age modelling of tephras

The approach of using glaciolacustrine varves and tephrachronology is becoming more widespread in varve research (e.g. MacLeod *et al.*, 2014), but utilising these data alongside Bayesian age modelling techniques is not widely established (e.g. Bendle *et al.*, 2017) and has not been adopted when examining the STS. A key outcome of the Bayesian age modelling in this thesis are the new re-modelled ages of the Hässeldalen, Askja-S and Fosen tephras.

The remodelled age of the Fosen tephra is in good agreement with the published age proposed by Timms *et al.* (2017), however the new age of the Hässeldalen tephra is several hundred years younger than previous estimates (e.g. Wohlfarth *et al.*, 2006; Wastegård *et al.*, 2018). For the Askja-S tephra, the re-modelled age is several hundred years older than the recently proposed best age estimates (e.g. Bronk Ramsey *et al.*, 2015; Kearney *et al.*, 2018).

The revised ages of the Hässeldalen and Askja-S tephras presented in this thesis are of importance to the wider palaeoclimate community since these tephras are considered to be key isochrons within early Holocene climate archives across northwest Europe (e.g. Davies *et al.*, 2003; Wohlfarth *et al.*, 2006). These tephras are particularly important since they bracket a brief period of climatic cooling during the early Holocene; the Preboreal Oscillation (PBO) (Wohlfarth *et al.*, 2006; Ott *et al.*, 2016). The early Preboreal climate across northwestern Europe was complex and accurate dating is often problematic due to the radiocarbon plateau during this time (Björck *et al.*, 1997). Consequently, the Hässeldalen and Askja-S tephras are important chronostratigraphic

marker layers for synchronising climate archives and assessing leads and lags in the climate system.

11.5.2 Absolute dating of varve sequences

It was anticipated that the Svinstadsjön and Asplången varve records would be of Younger Dryas age for several reasons. First, since the sites are located north of the Glottern site where the uppermost 100 varves have been radiocarbon dated to ca 12,500 cal. yrs BP (Wohlfarth *et al.*, 1998), the Svinstadsjön and Asplången sites should be younger than 12,500 cal. yrs BP. Second, the ice margin lines proposed by Kristiansson (1986) and Brunnberg (1995) place the Svinstadsjön site approximately 200 yrs younger than the base of the Glottern sequence. Third, it was expected that the Vedde Ash would be found within the Svinstadsjön and Asplången sequences based on the identification of the Vedde Ash in the Gropviken varve chronology from Östergötland (MacLeod *et al.*, 2014) and the purported Vedde ash within the Mullsjön varve chronology from Västergötland (Wohlfarth *et al.*, 1993) (Figure 11-11). Whilst there are questions regarding whether the Mullsjön tephra can be correlated to the Vedde Ash (Chapter 3), the ice lines proposed by Strömberg (1989), Kristiansson (1986) and Brunnberg (1995) indicate that the Mullsjön varve record can be correlated in age to the Gropviken site. Since the Asplången and Svinstadsjön sites are located on this same ice margin line, it was expected that the Vedde Ash would be found within these varve records.

Identification of the Vedde Ash would have placed the Asplången and Svinstadsjön varve chronologies within the Younger Dryas period, confirming the current placement of the ice margin lines and timing of deglaciation in Östergötland. However, the presence of the Askja-S tephra in the Asplången varve chronology, indicates that there is an unexpected gap between the Glottern and Asplången records of ca 1,000 yrs (Figure 11-11). There is also an unexpected gap between the Gropviken and Asplången varve records suggesting that the ice margin lines proposed by Brunnberg (1995) are incorrect. Since the ice margin lines are constructed using varve thickness data, there are likely fundamental flaws in the construction of the composite varve chronology in this region.

With regard to the Mullsjön site, since the tephra layer is linked to, but not chemically correlated to the Vedde Ash (Wohlfarth *et al.*, 1993), it is possible that this tephra could be the Askja-S tephra and not the Vedde Ash. This is supported by the younger of the two radiocarbon ages from the Mullsjön varve record (Table 11-8). The sample (AMS-12; Ua-2741) was taken from the base of the varve sequence and the tephra is located ca 200 yrs above this. When calibrated, the sample age is $10,966 \pm 249$ cal. yrs BP (1σ) and if correct would indicate an early Holocene age for the sequence. However, this

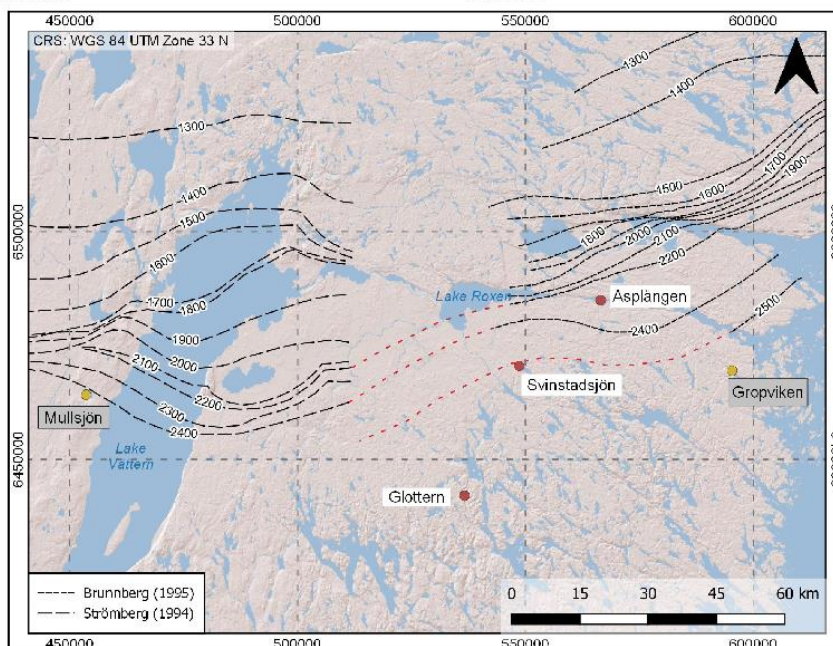
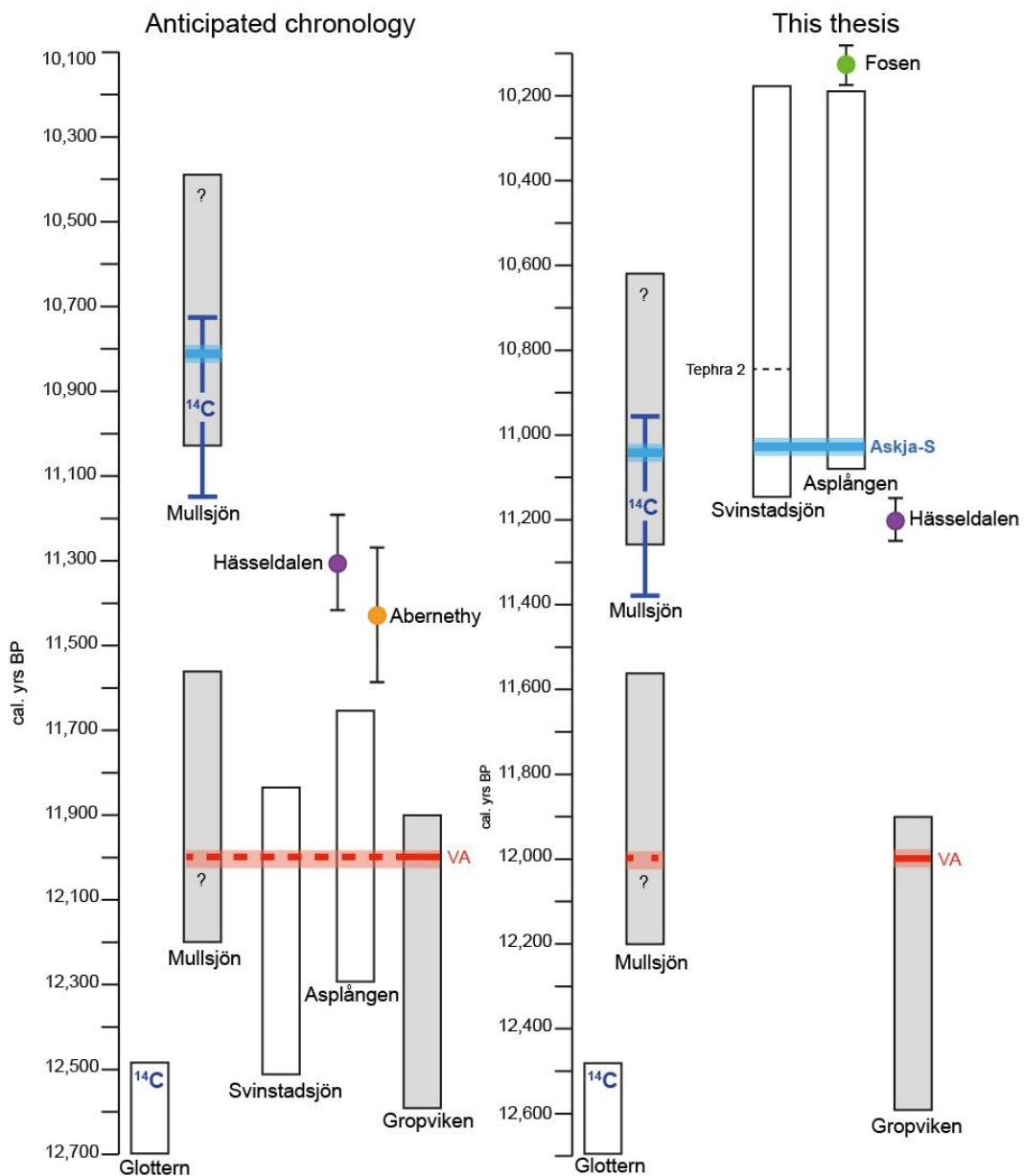
age was rejected since it does not align with the assumed Younger Dryas age of the sediment sequence based on macrofossil evidence and previous pollen investigations at the site (Björck and Digerfeldt, 1989). The recalibrated age of this sample is, however, similar to the modelled age of the Askja-S presented in this thesis and if the ice margin lines that connect Mullsjön to Asplången are correct, this would indicate that the Mullsjön tephra is the Askja-S.

Table 11-8. Radiocarbon data from the Mullsjön site (Wohlfarth et al., 1993). L = leaf, ff = fragment, ? = uncertain macrofossil identification.

Sample number	Lab. No.	No. of vyrs	vyr interval	Expected chronozone	Macrofossils submitted	AMS ¹⁴ C age BP
AMS-12	Ua-2741	105	510-615	Younger Dryas	? <i>Dryas octopetala</i> (L, ff)	9,640±190
AMS-16, 17	Ua-2744	50	210-260	Younger Dryas	? <i>Betula</i> (L, ff), ? <i>Salix</i> (L, ff)	9,945±115

It must be recognised that this hypothesis is also based on accepting the ice margin lines proposed by Strömberg (1989) in Västergötland, and that the link to the ice margin lines proposed by Kristiansson (1986) and Brunnberg (1995) in Östergötland is correct. Given the results from microfacies analysis in this thesis, there is also the potential for errors in the varve counts and thickness measurements in the Strömberg (1989) chronology. This casts doubt on the reliability of the ice margin lines and therefore, correlation of the Mullsjön tephra to the Askja-S tephra is a hypothesis that should be tested in the future.

Figure 11-11. Schematic of the expected and new ages of the varve chronologies. Next page. (Top left) Expected ages of the varve records in this thesis. The Vedde Ash is highlighted with a solid red line in the Gropviken record and a dashed red line in the Svinstadsjön and Asplången sequences. It was also anticipated that the Hässeldalen and/or Abernethy tephtras would be found in non-varved sediments stratigraphically above the varve records. (Top right) Revised ages of the sequences in this thesis based on the tephtras. The age of the Glottern varve chronology remains the same as proposed by Wohlfarth et al. (1998) and the identification of the Askja-S in gyttja sediments above the varved sediments at Glottern confirm the ca 12,500 cal. yrs BP age. The Gropviken site remains anchored by the Vedde Ash. The Askja-S and Fosen tephtras anchor the Asplången record and the varve thickness correlation between Asplången and Svinstadsjön suggest that Tephra 1 in the Svinstadsjön sequence is also the Askja-S. The remodelled age of the Hässeldalen tephra is also presented. (Bottom) Site locations in relation to 1) the ice margin lines proposed by Strömberg (1994) and Brunnberg (1995) and 2) the location of the Gropviken (MacLeod et al., 2015) and Mullsjön (Wohlfarth et al., 1993) sites that contain the Vedde Ash. Dashed red lines are inferred links between sites and are shown for illustrative purposes only.



The Askja-S tephra found at Asplången demonstrates that there are *ca* 1,000 “missing” varves between the Glottern and Asplången sites. The additional 1,000 yrs should be looked for in the varve records that are located between Glottern and Svinstadsjön i.e. the sites within the northern part of the Kristiansson (1986) regional varve chronology. The results from thin section analysis at Svinstadsjön and Asplången indicate that thin (<cm-scale) varves that are only discernible at the microscale may exist within the Kristiansson (1986) varve chronology, and this may account for, or at least partly account for, the missing years.

Alternatively, the radiocarbon age estimate for the Glottern sequence may be inaccurate. Wohlfarth *et al.* (1998) report substantially different radiocarbon ages from two different samples from overlapping varve intervals (Table 11-9). The radiocarbon age difference between the samples is *ca* 900 ¹⁴C yrs and the older of these dates was attributed to reworking of plant material. Due to the large variability in radiocarbon ages from the Glottern site, neither of the radiocarbon dates are included in the Muschitiello *et al.* (2016) Bayesian age model.

Table 11-9. Radiocarbon sample information from Glottern. Modified from Wohlfarth *et al.* (1998). L = leaves, Lf = leaf fragments, S = seeds.

Lab. No.	Local varve years	Macrofossils submitted for AMS measurement	AMS ¹⁴ C date yr BP	Wohlfarth <i>et al.</i> (1998) Estimated cal. yr BP	Used in the Muschitiello <i>et al.</i> (2016) Bayesian age model
Ua-4496	1856±50	Salix/Betula (Lf)	10,585±465	12,506	No
Ua-10180	1872±66	<i>Empetrum</i> (L), <i>Salix</i> indet (Lf), <i>Salix/Betula</i> (Lf), <i>Dryas oct.</i> (L), <i>Arenaria</i> (S), insects	11,550±300	12,522*	No

The idea that there may be problems with the Kristiansson (1986) regional varve chronology is not a new concept. Wohlfarth *et al.* (1998) suggested several revisions to the chronology. For example, radiocarbon ages from Wohlfarth *et al.* (1998) placed the Allerød/Younger Dryas boundary *ca* 100-250 yrs earlier than proposed by Kristiansson (1986) and Wohlfarth *et al.* (1998) suggested that deglaciation from Högsby to Linköping took approximately 1,300-1,700 yrs. This is considerably longer than the 900-1,000 yrs proposed by Kristiansson (1986). Using the upper estimate from Wohlfarth *et al.* (1998) of 1,700 yrs, and the lower estimate from Kristiansson (1986) of 900 yrs for the duration of ice margin retreat suggests that there may be up to 800 yrs missing in the Kristiansson (1986) chronology. The results from this thesis would support this inference and suggest that at least 1,000 yrs are missing in the Kristiansson (1986) chronology north of the Glottern site (Figure 11-12).

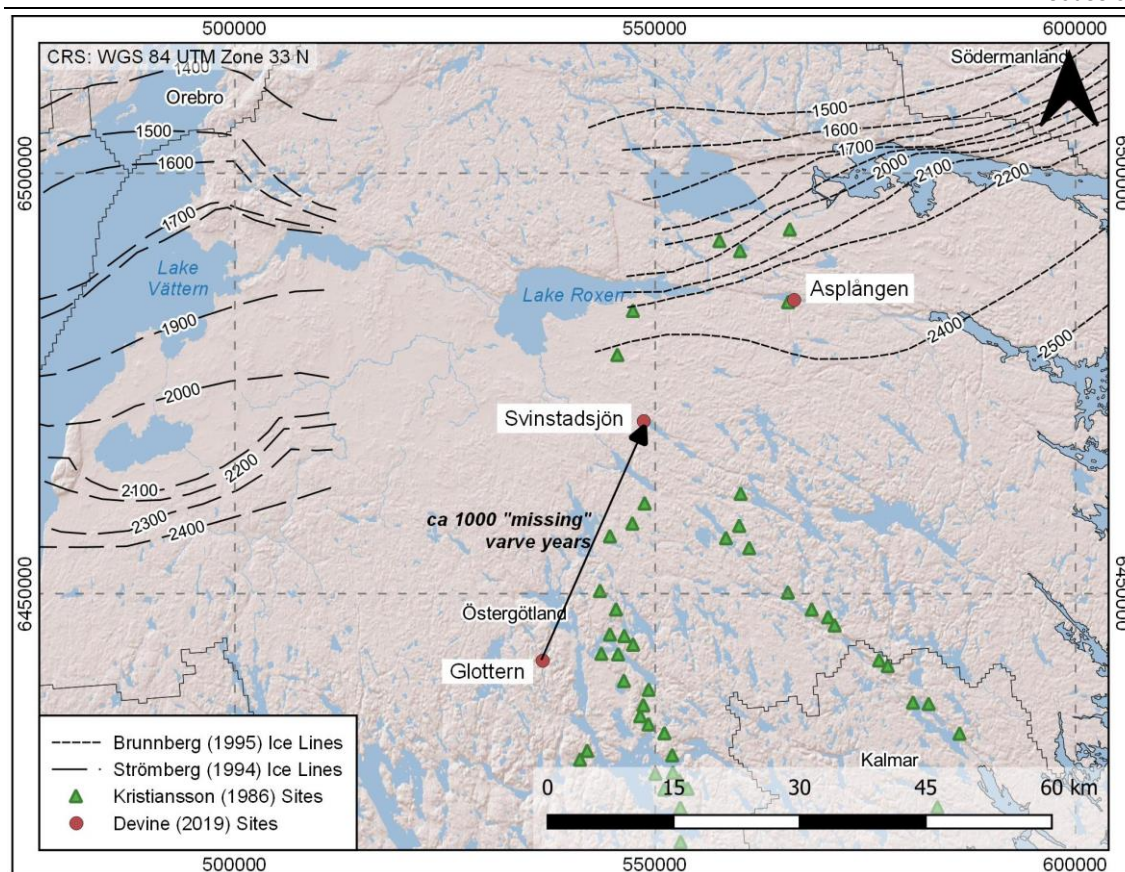


Figure 11-12. Location of “missing” varves between the Glottern and Svinstadsjön site in relation to the Kristiansson (1986) varve records.

The application of thin section analysis will be crucial in identifying the missing varves in the Kristiansson (1986) chronology. However, given the difficulties described by Kristiansson (1986) when correlating varve records in close proximity, the identification of tephra layers will also be fundamental in providing independent links between varve records. The identification of the Askja-S tephra within the base of the Asplången record demonstrates that other Lateglacial-early Holocene tephras could be found within sites further south of Asplången in the Kristiansson (1986) chronology. Moreover, the identification of the Fosen tephra stratigraphically above glaciolacustrine varves in the Asplången sequence, suggests that this tephra may be found within varved sediments to the north of the Asplången site. This would enable testing of the Bayesian age model presented in this thesis by providing an improved estimate of the number of varves between the Askja-S and Fosen tephras.

11.5.3 Tephra and varve thickness correlations in this thesis

The identification and chemical characterisation of the tephras in the Asplången sequence has enabled construction of a site age depth model (Model 1; Chapter 10). No tephra chemistry was obtained from the Svinstadsjön sequence, and so it is correlated to the Asplången varve chronology by statistical matching of the varve thickness records.

The varve chronologies and tephra data have been integrated within a Bayesian age model (Model 2; Chapter 10). Model 2 indicates that Tephra 1 (11,089±42 cal. yrs BP) in the Svinstadsjön sequence is the same age (within errors) as the Askja-S (11,043±42 cal. yrs BP). Tephra 2 in the Svinstadsjön sequence was deposited 231±7 vyrs later and has a modelled age of 10,858±42 cal. yrs BP. However, these interpretations assume that the placement of the overlap between the Svinstadsjön and Asplången records is correct. In the absence of chemical data from the Svinstadsjön tephra layers and given the limitations of the current placement of the overlap (section 11.4), the correlation of Tephra 1 to the Askja-S should be tested by obtaining chemical data for the Svinstadsjön tephtras.

Outlined in this section is a re-interpretation of the Svinstadsjön tephtras if the varve interval between the tephra layers is considered in isolation. In this regard, it is possible that the Svinstadsjön tephtras could be correlated to other Lateglacial-early Holocene tephtras. The purposes of this exercise are to: 1) emphasise the potential of tephrochronology for linking site varve chronologies, and 2) re-iterate the problems with linking varve records using varve thickness and/or colour changes.

In this exercise it is assumed that both tephra layers in the Svinstadsjön sequence were deposited from primary airfall and so the interval between the volcanic eruptions that produced the tephtras is 231±7 vyrs. This interval is consistent with the age difference between the modelled ages of the Abernethy, Hässeldalen and Askja-S tephtras (within errors) (Table 11-10). Therefore, several hypotheses could be considered for the correlation of the Svinstadsjön tephtras.

Table 11-10. Possible correlations for unknown tephra layers in the Svinstadsjön sequence. Using the varve interval spacing between Tephra 1 and Tephra 2 of 231±7 vyrs, several hypotheses are possible. The Abernethy tephra age is from Bronk Ramsey et al. (2015) and the modelled ages of the Hässeldalen and Askja-S tephtras are those proposed in this thesis. The current hypothesis proposed in this thesis is highlighted in italics.

Name	Tephra 1	Tephra 1 modelled age cal. yrs BP (2σ)	Tephra 2	Tephra 2 modelled age cal. yrs BP (2σ)	Age interval between the tephtras
Hypothesis 1	Abernethy	11,462±144	Hässeldalen	11,197±42	265±186
Hypothesis 2	Abernethy	11,462±144	Askja-S	11,043±42	419±186
Hypothesis 3	Hässeldalen	11,197±42	Askja-S	11,043±42	154±84
<i>Current correlation</i>	<i>Askja-S</i>	<i>11,043±42</i>	<i>Re-worked unknown</i>	<i>10,858±42</i>	<i>231±7 (varve interval)</i>

If either of the hypotheses proposed in Table 11-10 are correct, this would change the placement of the overlap between the Svinstadsjön and Asplången sequences. Figure 11-13 shows the position of the overlap for Hypotheses 1, 2 and 3. For every hypothesis the visual alignment between the varve chronologies is less convincing than the current

placement of the overlap. In addition, the position of the colour change from brown to grey varves would change given any of the proposed hypotheses. It is important to note that at present the colour change is synchronous (within errors) between the Asplången and Svinstadsjön sites, and none of the alternative hypotheses suggest that the colour change is a synchronous event. This demonstrates the fragility of the current placement of the overlap and that the colour change could be an asynchronous event. Therefore, its use as a time-synchronous anchor point between varve records could be flawed.

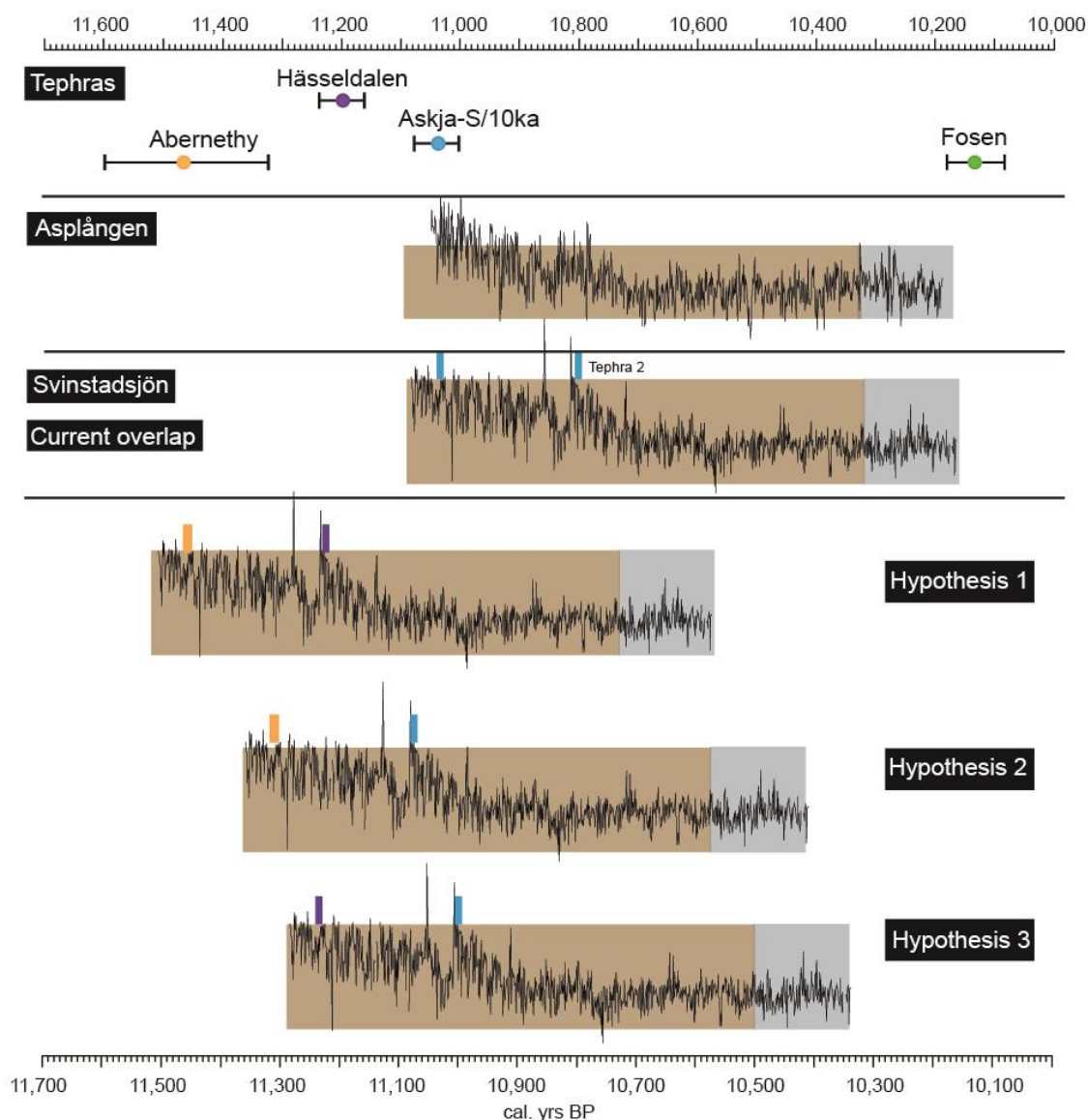


Figure 11-13. Hypothesised tephra correlations using varve spacing between Tephra 1 and Tephra 2 in the Svinstadsjön sequence.

The modelled ages of the Fosen, Askja-S and Hässeldalen tephras from this thesis are shown. The Bronk Ramsey et al. (2015) age of the Abernethy tephra is also shown. The Asplången record is fixed to the calendar year timescale using the current placement of the Svinstadsjön sequence. The hypothesised ages of the Svinstadsjön sequence based on the possible tephra correlations are presented and the coloured boxes above the varve record correspond to the colour-code for each tephra. The varve colour change from brown to grey varves is also highlighted and is asynchronous in any of the proposed hypotheses. Varve thickness correlation between the Asplången and Svinstadsjön sequence is also unconvincing for each hypothesis.

At present, the overlap between the varve records has been guided by the ice margin lines proposed by Brunnberg (1995) and Kristiansson (1986), corroborated by visually aligning the records and statistical correlation ($r^2=0.55$). The tephra data, however, demonstrate that the traditional means of correlating varve records using thickness variations, statistics and/or colour changes could be incorrect. The placement of the overlap between the Svinstadsjön and Asplången varve chronologies will change if chemical data are obtained for either of the tephra layers in the Svinstadsjön sequence.

In the absence of chemical data for the tephra, the current position of the overlap (Figure 11-13) is considered to be the most robust. The results of this exercise should therefore be viewed as the first step towards demonstrating the usefulness of tephrochronology for the construction of accurate and reliable composite varve chronologies in the STS.

11.6 Deglaciation chronology and timing of BIL drainage

This section discusses the implications of the microfacies-derived varve thickness chronologies combined with tephrochronology previously presented in this study. Particular emphasis is placed on whether the use of the colour change is viable as a stratigraphic marker within the STS and the impact of different interpretations on the BIL drainage. First, the current deglaciation and BIL drainage model is presented including the link between BIL drainage and the colour change from brown to grey varves. Second, the results from this thesis will be integrated with published literature to determine the sedimentological processes that likely caused the colour change. Finally, the correlation between the Svinstadsjön and Asplången records, and specifically the synchronicity/asynchronicity of the colour change, are discussed within the context of other STS records. Following this, the modelled age of the colour change within the Asplången and Svinstadsjön sequences will be compared to other age estimates for the change. The section finishes by considering a new age for the final drainage of the BIL and provides possible links to climatic events.

11.6.1 Overview of the final BIL drainage

The final BIL drainage marks the end of the Gotiglacial stage of the Baltic Ice Lake, and has long been considered to be more or less synchronous with the end of the Younger Dryas period and the beginning of the Holocene (Björck and Digerfeldt, 1984; Björck, 1995; Andrén *et al.*, 2011). It has been proposed that the drainage was a sudden lowering of the BIL level by 25 m (Svensson, 1989; Strömberg, 1992) and either occurred catastrophically over 1-2 years (Björck, 1995; Jakobsson *et al.*, 2007), or was initially a

gradual process over *ca* 90 yrs that ended in a final catastrophic outflow (Strömberg, 1992). A two-step final drainage has also been suggested (Bodén *et al.*, 1997).

The final drainage of the BIL has been placed in the late Younger Dryas pollen stratigraphy predating the early Holocene Preboreal vegetation transition (Figure 11-14). In southern Sweden the vegetational succession for the Younger Dryas to the Preboreal period is well documented by pollen analysis of lacustrine sediments in eastern central Sweden that were situated close to the FIS margin (Berglund, 1979; Björck and Digerfeldt, 1989; Svensson, 1989). The vegetational succession is characterised by a transition from tundra herbs and shrubs with *Artemisia* and *Poaceae*, to an open shrubland with *Betula*, *Empetrum* and *Juniperus*, and to *Betula* and *Pinus* woodlands (e.g. Berglund, 1995).

The drainage has been dated by radiocarbon dating to *ca* 10,300 ¹⁴C yrs BP (*ca* 11,700 cal. yrs BP; Björck *et al.*, 1997) or slightly younger (Svensson, 1989; Wohlfarth *et al.*, 1993) and through synchronisation of varve records in the Baltic Proper with the GRIP ice-core to 11,620 cal. yrs BP (Andrén *et al.*, 2002). The drainage has also been placed at *ca* 10,770 clay yrs BP and 1,474 to 1,501 v yrs on the De Geer timescale (Strömberg, 1994; Brunnberg, 1995) (Figure 11-14).

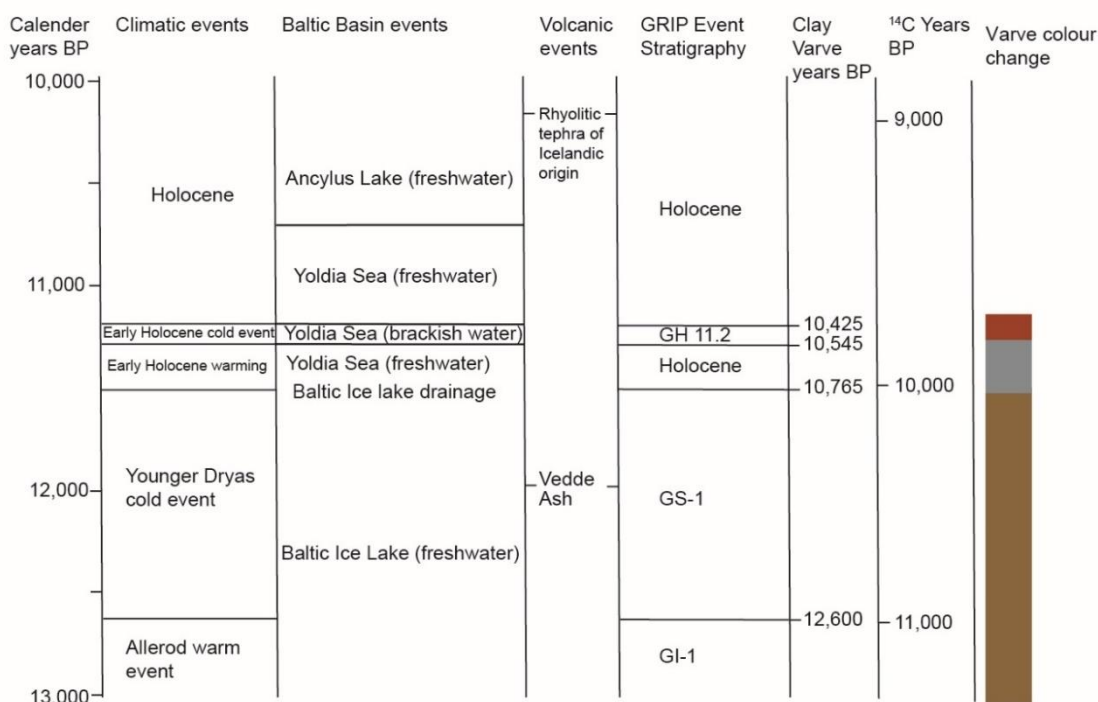


Figure 11-14. The Lateglacial-Holocene event stratigraphy for eastern middle Sweden. Modified from Björck *et al.* (2002).

11.6.2 Lithostratigraphic evidence

Lithostratigraphical evidence for the final drainage of the BIL varies spatially, with changes in grain size, unit thickness and sediment sorting indicative of a complex depositional event. Closer to the ice margin, which was situated *ca* 30 km south of Stockholm at the proposed time of drainage, a distinct colour change is observed in multiple varve records across eastern middle Sweden and the Baltic Proper (Björck and Digerfeldt, 1984; Kristiansson, 1986; Strömberg, 1989; Brunnberg, 1995; Andrén *et al.*, 1999; Johnson *et al.*, 2013). The colour change can be interspersed by other sediments, including sand to cobble sized drainage sediments (Johnson *et al.*, 2013) or till mixed with clay (Björck and Digerfeldt, 1984). South of Mt Billingen in Västergötland and to the east of Lake Vättern, drainage sediments are absent and varve records transition directly (Kristiansson, 1986; Strömberg, 1989; Brunnberg, 1995; Andrén *et al.*, 2002).

It is accepted that when brown glacial varves were accumulating in Östergötland and Västergötland the ice margin was either at Mt Billingen or retreating towards the final drainage position south of Götene (Strömberg, 1994; Brunnberg, 1995; Johnson and Ståhl, 2010; Johnson *et al.*, 2013) (Figure 11-15). The rapid colour transition from brown to grey is thought to indicate that the ice margin had retreated north of Mt Billingen, opening up the drainage pathway and leading to the catastrophic final drainage of the BIL (Björck and Digerfeldt, 1984; Strömberg, 1992; Andrén *et al.*, 2002).

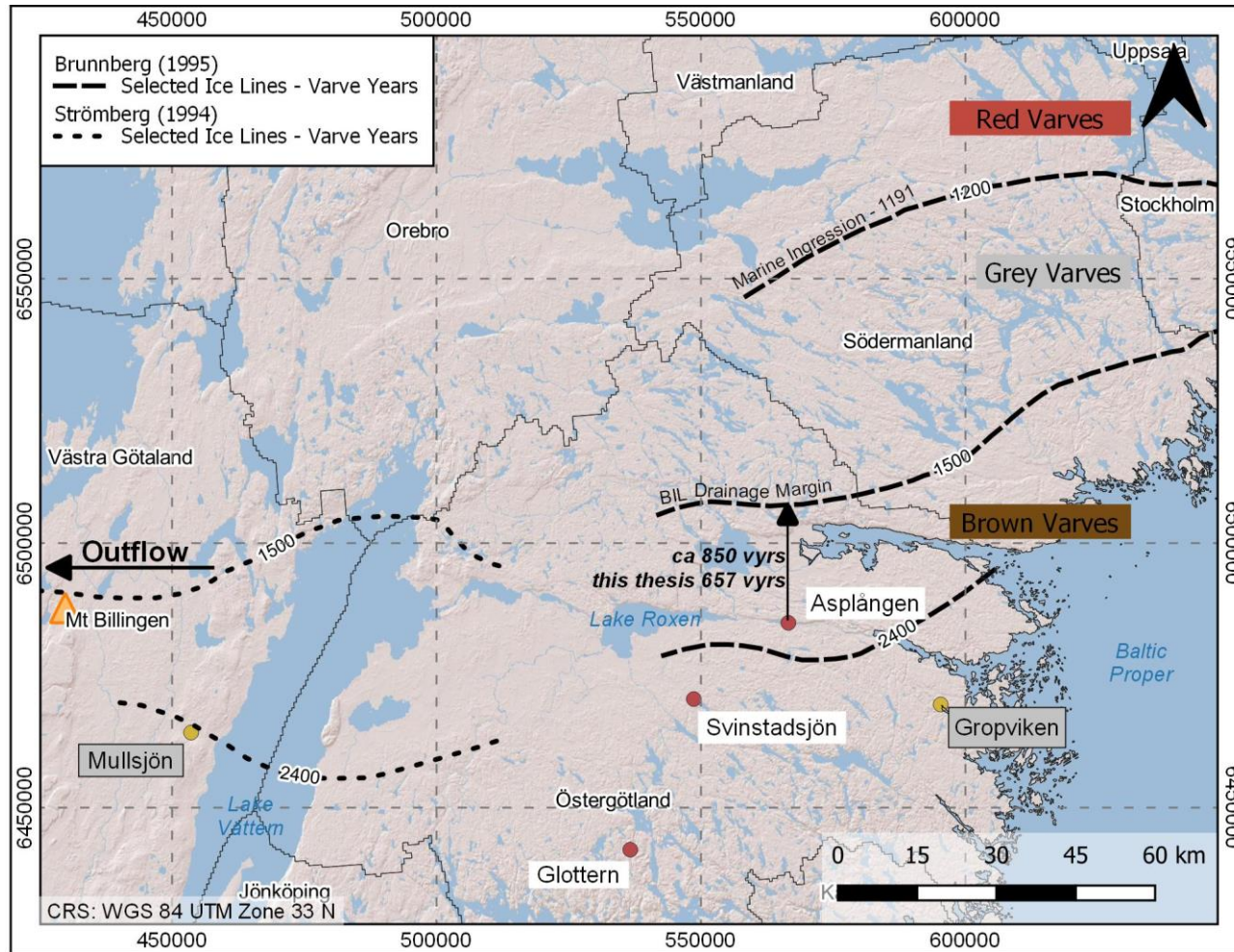


Figure 11-15. Location of sites in this thesis in relation to the BIL drainage and marine ingression ice margin lines (in De Geer years). Sites south of ice margin line 1,500 (BIL drainage) contain brown varves. Sites between 1,500 and 1,191 contain grey varves, sites above 1,200 contain reddish marine varves from the Yoldia Sea stage. Mt Billingen and direction of drainage outflow are also labelled.

In sites in Västergötland, the Södertörn peninsula and south of Stockholm there are grey glacial varves stratigraphically above the brown varves (Strömberg, 1989; Brunnberg, 1995; Björck *et al.*, 2001) (Figure 11-15). It has been suggested that the presence of these ca 300 grey glacial varves represents the duration of a freshwater Baltic phase, also referred to as the first freshwater sub-stage of the Yoldia Sea stage (Svensson, 1989; Wastegård *et al.*, 1995). This short-lived freshwater phase occurred immediately after the drainage of the BIL at Mt Billingen, but prior to the ingression of marine water in the Stockholm area (Strömberg, 1994; Brunnberg, 1995; Andrén *et al.*, 2011). The marine ingression is marked by another colour change from grey to reddish varves. The red varves contain fossils of the marine arctic mollusc *Portlandia (Yoldia) arctica* (e.g. De Geer, 1913, 1940; Brunnberg and Possnert, 1992) and more recently by findings of marine foraminifera and ostracods (e.g. Schoning and Wastegård, 1999).

A colour change from brown to grey varves is located within the Svinstadsjön and Asplången varve sequences, with 169 ± 23 grey varves identified in the Svinstadsjön sequence and 170 in the Asplången sequence. Red varves are not observed within either sequence and marine fossils such as those found in the Stockholm area are absent. This is consistent with other varve records in this part of Östergötland (Kristiansson, 1986; Brunnberg, 1995). The discussion therefore focuses on the transition from brown to grey varves observed in this thesis.

The results from thin section analysis and tephrochronology indicate that: 1) there is no difference in the varve microfacies between the grey varves and the preceding ($n=100$) brown varves at both sites; 2) the colour change is synchronous between the records and; 3) the colour change in both the Svinstadsjön and Asplången sequences occurs ca 1,000 cal. yrs BP later than the current age estimates from elsewhere in the STS. The following sections discuss the importance of these findings for the regional varve chronology, the deglaciation model and the final drainage of the BIL.

11.6.2.1 Spatial differences in the brown to grey colour change

It is first necessary to describe the chemical and physical differences between the brown and grey varves in order to understand the processes that may have caused the colour change. Understanding these processes enables assessment of the suitability of the colour change for correlating varve records and its suitability as a “proxy” for BIL drainage.

Kristiansson (1986) discusses the use of the colour change within the context of his regional varve chronology and factors that might lead to erroneous linking of sites. For example, Kristiansson (1986) links the colour to a change in texture in the varve series and also suggests that the colour change observed east of Mt Billingen in Östergötland

could be due to secondary or modern-day groundwater changes. However, identification of the same colour change within varved sediment in the Baltic Proper (Andrén *et al.*, 1999, 2002) indicates that the colour change, at least in the Baltic Sea, is unlikely to be due to groundwater changes.

Johnson *et al.* (2013) report a similar change in varve colour from brown to grey varves at the Länsmansgården site west of Mt Billingen. The two varve units are separated by a sand layer interpreted to be sediment deposited during BIL drainage. The uppermost grey varves are finer-grained (due to higher clay content) than the basal brown varves and this is attributed to the relative proximity of the ice margin. The authors propose that during accumulation of the basal brown varves the site was located outside of the BIL and following drainage and deposition of the sand layer, the site became part of the BIL and accumulated grey post-drainage varves. However, it is possible that because this site was located outside the BIL prior to drainage, the colour change was not caused by the same process that caused the colour change in sites located within the BIL (e.g. Brunnberg, 1995).

The grey post-drainage varves have been linked to an increase in organic matter content (De Geer, 1940; Johnson *et al.*, 2013), and/or a change in the chemical composition of the sediments (Antevs 1925). Johnson *et al.* (2013) found a slight difference in the elemental content between grey and brown varves with iron slightly more abundant in the grey varves, though this is likely a grain size signal since particle size analysis indicated that these had higher clay content. In contrast, X-ray diffraction analysis from samples of brown and grey varves in Östergötland shows no change in the minerals present (Brunnberg, 1995), though it is possible that there is a change in the relative proportions.

The role of salinity has also been discussed, however, evidence for salinity changes between the varve colour types varies by location. For example, Johnson *et al.* (2013) found no evidence of salinity changes between grey and brown varves near Mt Billingen. Yet marine fauna has been identified within both brown pre-drainage varves to the west of Mt Billingen in the Middle Swedish End Moraine Zone (Johnson and Ståhl, 2010) and grey post-drainage varves in eastern middle Sweden (Björck *et al.*, 2001).

In this thesis, thin section and particle size analysis show that there are no differences in the microfacies structures or grain size characteristics between the brown and grey varves at either site. The two varve colour types are interpreted as ultra-distal glaciolacustrine varves, and are consistent with the previous classification of these sediments as glaciolacustrine varves deposited in freshwater conditions (Strömberg,

1983, 1985, 1992; Kristiansson, 1986; Brunnberg, 1995). The differences between brown and grey varves are summarised in Table 11-11.

Table 11-11 Summary of differences between brown and grey varves. Information from this study highlighted in *italics*.

Difference observed between brown and grey varves	Analytical method	Comment	Location (site)	Reference
<i>No difference</i>	<i>Thin section and particle size analysis</i>	Brown and grey varves deposited in ultra-distal glaciolacustrine environment	Östergötland (Asplången, Svinstadsjön)	<i>This study</i>
No difference	X-ray diffraction	No change in mineralogy but could be a change in elemental concentration	Södertörn (Vidbynäs)	(Brunnberg, 1995)
Grain size	Macroscale analysis of core surface	Grey varves finer-grained than brown varves	Östergötland (Fjärdingstad)	(Kristiansson, 1986)
Grain size	Particle size analysis	Grey varves finer-grained than brown varves Brown and grey varves separated by sand layer	West of Mt Billingen (Länsmansgården)	(Johnson <i>et al.</i> , 2013)
Slight chemical different	μ XRF	Brown varves slightly more Si, K, Ca and Sr, grey varves slightly more Fe	West of Mt Billingen (Länsmansgården)	(Johnson <i>et al.</i> , 2013)
Chemical	Trace elements	Ratio of grey:red for Zn, Sr, Y and Zr shows no difference in Zn or Zr, but slight difference in Sr and Y	Southwest of Mt Billingen drainage outlet (Lake Lången)	(Olsson, 1991)

It has been proposed that because a colour change is observed at several sites that: 1) the colour change represents a common process; 2) the event which caused the colour change was of large enough magnitude to influence sediment records across the Baltic Basin; and 3) the colour change represents a synchronous or near-synchronous event (Strömberg, 1992; Brunnberg, 1995). For these reasons, it has been accepted that the change in sediment colour can be related to the drainage of the Baltic Ice Lake since it was a high-magnitude, basin-wide event (e.g. Björck and Digerfeldt, 1984; Strömberg, 1989; Brunnberg, 1995; Andrén *et al.*, 1999). However, the colour change appears not to have a consistent source and cannot consistently be determined sedimentologically or biostratigraphically. Therefore, it could be argued that this colour change is not reflective of a common change in the physical and chemical properties of the brown and

grey varves across the Baltic Basin. At present it is not possible to determine whether the colour change represents: 1) a single event that propagated differently in different locations; 2) local processes; 3) inconsistent application of different methodological approaches to describe the varves (Table 11-11); or 4) a combination of all factors.

11.6.2.2 Synchronicity/asynchronicity of the colour change

Many of the records where this colour change is observed either lack independent age estimates (Kristiansson, 1986; Brunnberg, 1995; Andrén *et al.*, 1999; Johnson *et al.*, 2013), or have questions regarding the accuracy of the existing chronology. Chronological issues at these sites are largely related to problems with: 1) radiocarbon dates based on bulk sediment samples or marine sediments/fossils (e.g. Björck and Digerfeldt, 1984; Johnson and Ståhl, 2010); 2) dates inferred from regional pollen stratigraphic zones (e.g. Kristiansson, 1986; Andrén *et al.*, 2002); 3) dating varve records through synchronising varve thickness records to the Greenland ice-core records (Andrén *et al.*, 1999); and more recently 4) the presence of the colour change has been used as a chronostratigraphic marker for the Younger Dryas/Holocene boundary (Svärd *et al.*, 2016) and has been used to correlate sequences from different sites; or 5) a combination of these techniques.

Prior to this research, an independent assessment of the synchronicity of the colour change has been lacking and as such there remains a propensity to rely on the colour change as a key anchor point in the construction of a site chronology. This makes it challenging to evaluate whether the colour change represents a single synchronous event, a single time-transgressive event, or several diachronous events occurring over a wide area.

The age modelling from this thesis suggests that the absolute age of the colour change is synchronous (within errors) between the Svinstadsjön and Asplången sites, occurring at $10,337 \pm 43$ cal. yrs BP at Svinstadsjön and at $10,350 \pm 43$ cal. yrs BP at Asplången. Whilst the absolute age of the colour change is synchronous, the colour change between the Svinstadsjön and Asplången records is separated by 13 yrs. This would indicate that the colour change at these sites in yrs is broadly synchronous, but ultimately asynchronous. However, the varve count uncertainty in the Svinstadsjön sequence of ± 23 yrs may account for this offset.

It is important to note that the near-synchronicity of the colour change is due to the placement of the overlap between the varve records, based on visual alignment and statistical correlations rather than tephra correlation. The tephra correlation hypotheses presented in section 11.5.3 demonstrate that whilst the current age model indicates that the colour change is broadly synchronous, there is also potential that it could be

asynchronous between the two sites. This casts some doubt on the robustness of using the colour change to link varve records and/or its use as a means of verifying varve thickness correlations between sites. Nevertheless, based on the available data the current placement of the overlap between the sites has been accepted and the colour change between the Asplången and Svinstadsjön sites is deemed to be synchronous or near-synchronous.

For the aforementioned reasons, it cannot be assumed that the colour change is a synchronous event across the rest of the Baltic Basin. Identification and chemical characterisation of tephra in other varve records that contain this colour change would be required to test this.

The results from this thesis indicate that there is a substantial difference between the modelled age of the colour change in this thesis and published age estimates from other sediment sequences in the Baltic Basin. The following section presents a critical evaluation of the existing ages for the colour change.

11.6.3 Dating the final BIL drainage

The colour change from brown to grey glacial varves is largely considered to be synonymous with the final drainage of the BIL. This is suggested to have occurred at the Younger Dryas-Preboreal transition at 11.7 ka BP and consequently at the onset of the Holocene (Björck *et al.*, 2001; Swärd *et al.*, 2016). Andrén *et al.* (1999) suggest that the drainage took place *ca* 30-40 years before the Younger Dryas-Preboreal transition. The Younger Dryas-Preboreal transition (11.7 ka BP) age for the colour change is based on several lines of evidence including: 1) using the age of the Middle Swedish End-Moraine Zone (MSEMZ) which has been dated by radiocarbon dating and pollen analysis, and 2) wiggle matching varve thickness records to the Greenland ice-cores (Björck *et al.*, 1996; Andrén *et al.*, 1999; Lundqvist and Wohlfarth, 2001). This section provides more detail on these dating techniques.

11.6.3.1 Morphostratigraphy

The age of the MSEMZ is used to constrain the timing of BIL drainage. The moraines are dated to the Younger Dryas based on: 1) radiocarbon dating (e.g. Johnson and Ståhl, 2010); 2) the moraines must be younger than the Levene Moraine which is dated to the Allerød/Younger Dryas pollen zone (Lundqvist and Wohlfarth, 2001); 3) further north of Mt Billingen there are very few ice marginal landforms suggesting rapid decay of the ice sheet that has been linked to early Holocene climatic warming (Lundqvist and Wohlfarth, 2001; Houmark-Nielsen and Kjær, 2003); and 4) the fact that Baltic Ice Lake drainage deposits, which have been ascribed to the period 30-40 years before the end of GS-1

(Andrén *et al.*, 2002), are younger than the northernmost MSEMZ ridge at Gullhammar, Västergötland (Johnson *et al.*, 2019). Therefore, the northernmost ridge represents the last glacial standstill during the Younger Dryas cold period (Andrén *et al.*, 1999, 2002; Lundqvist and Wohlfarth, 2001; Hughes *et al.*, 2016; Stroeven *et al.*, 2016) (Chapter 2).

11.6.3.2 Radiocarbon dating

Between the moraines in the MSEMZ are intermoraine flats that are composed of sands and gravel at the surface which are underlain by up to 25 m of glaciomarine varved clay (Johnson and Ståhl, 2010). The overlying sands and gravels have been interpreted as being partly derived from drainage sediments (Johansson, 1926; Johnson *et al.*, 2019) and so radiocarbon dates from marine ostracods and foraminifera in sediments in front of a moraine represent a minimum age of formation. These radiocarbon dates often have large uncertainties due to the difficulties associated with the marine reservoir effect (Björck and Digerfeldt, 1984; Johnson and Ståhl, 2010). Whilst Austin *et al.* (1995) concluded that during the Younger Dryas the reservoir effect was *ca* 700 years in the North Atlantic, it has been demonstrated that the marine reservoir effect was highly variable in the past (e.g. Wastegård and Schoning, 1997; Wastegård *et al.*, 1998; Mangerud *et al.*, 2006). Moreover, the modern-day marine reservoir ages in the current Baltic Sea range from *ca* 250-900 yrs (Table 2-1; Chapter 2). Nevertheless, radiocarbon dates from marine ostracods and foraminifera in the MSEMZ indicate formation during the Younger Dryas period (Johnson and Ståhl, 2010).

11.6.4 Pollen analysis and synchronisation of varve and GRIP ice-core records

The timing of the final BIL drainage has also been determined by pollen analysis across the colour change from brown to grey varves in the Baltic Proper (Björck and Digerfeldt, 1984; Andrén *et al.*, 1999). Pollen data suggest that the colour change occurred at the Younger Dryas-Preboreal transition (Figure 11-16) (Andrén *et al.*, 1999) which has been correlated to the onset of the Holocene in the Greenland ice-core records at $11,703 \pm 103$ yrs b2k (Rasmussen *et al.*, 2014), or $11,650 \pm 103$ yrs BP.

However, the colour change at the Asplången site occurs at $10,350 \pm 43$ cal. yrs BP, suggesting a discrepancy of *ca* 1,000 cal. yrs. At the Svinstadsjön site, the colour change has been dated to $10,337 \pm 43$ cal. yrs BP however there may be inaccuracies in this date, as highlighted in section 11.5.3, and so discussion will focus on the Asplången date only.

The following discussion uses the assumption that the colour change in this thesis is synchronous, or near-synchronous with the Baltic Proper varve chronology (Andrén *et al.*, 1999). This enables further exploration of the apparent *ca* 1,000 cal. yrs BP discrepancy between the different ages of the colour change. First the age proposed by Andrén *et al.* (1999) that is based on synchronisation of the varve-pollen record from the Baltic Proper will be critically evaluated.

Pollen analysis by Andrén *et al.* (1999) places the Baltic Proper varve chronology within the Younger Dryas and Preboreal pollen zones, with the colour change (interpreted as the final BIL drainage) occurring at 10,685 clay vyrs. The authors use the Younger Dryas-Preboreal transition at 10,650 vyrs BP and correlate this to the Younger Dryas-Preboreal transition in the GRIP ice-core. This is defined as $\delta^{18}\text{O}$ values above -40‰ and is dated to *ca* 11,525 cal. yrs BP (ss09 timescale) or *ca* 11,700 \pm 98 yrs b2k (GICC05 timescale; Seierstad *et al.*, 2014). Minimum values in the mean varve thickness at *ca* 10,685 and 10,670 vyrs BP correspond with minimum $\delta^{18}\text{O}$ values in the GRIP ice-core record at *ca* 11,560 and 11,545 cal. yrs BP (Figure 11-17).

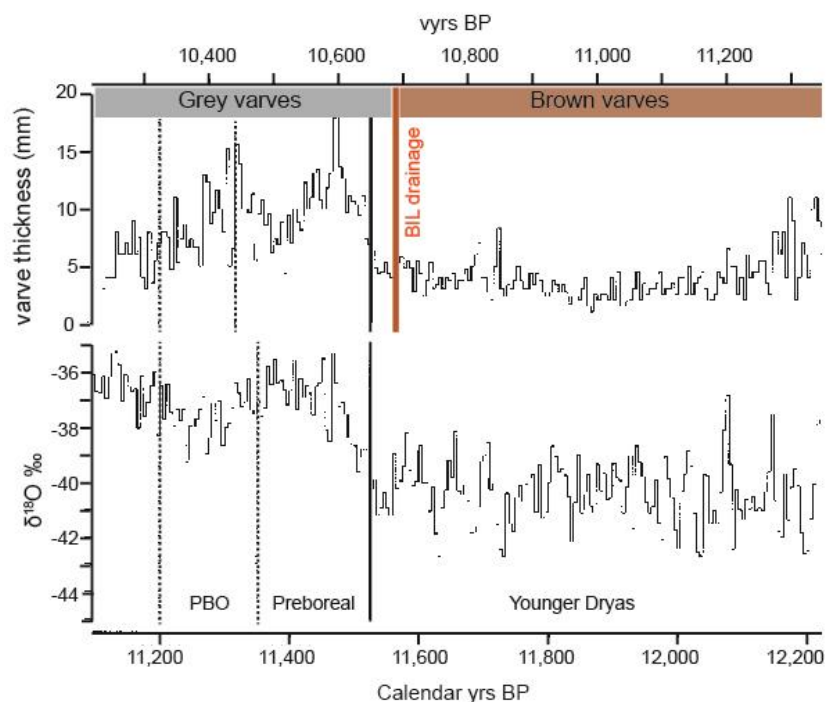


Figure 11-17. Correlation of the 5-yr mean varve thickness in the northwestern Baltic Proper and the 5-yr mean $\delta^{18}\text{O}$ record from the GRIP ice-core. Modified from Andrén *et al.* (1999). The solid line indicates the Younger Dryas–Preboreal transition, defined as $\delta^{18}\text{O}$ values above -40‰ . Dotted lines mark the age of the Preboreal oscillation. The red line indicates the final drainage of the BIL at *ca* 10,685 vyrs BP as a decrease in varve thickness and a change in colour from brown to grey varves.

By using the Younger Dryas-Preboreal transition period in the GRIP $\delta^{18}\text{O}$ ice-core chronology as an anchor point, Andrén *et al.* (1999) synchronised the varve thickness

record to the ice-core isotope record and age-information was transferred from the ice-core record to the STS (Figure 11-17). This suggested that the final drainage of the BIL, defined by the colour change, occurred ca 40 vyrs before the Younger Dryas-Preboreal climate shift, though this was later revised to 120 vyrs (Andrén *et al.*, 2002).

Prior to synchronisation of the Baltic Proper clay varve chronology with the GRIP ice-core record, the age of the colour change from brown to grey varves had previously been estimated to 10,740+100 to -250 vyrs BP 1950 (Strömberg, 1994). The wiggle match between the Baltic Proper varve chronology and the GRIP ice-core was used to demonstrate that there was an error in the STS of ca 875 vyrs (Andrén *et al.*, 1999). This was accepted and the clay varve timescale was updated to account for the offset. However, the original clay varve year proposed by Strömberg (1994) is similar to the modelled age of the colour change at Asplången of 10,350±43 cal. yrs BP. It appears that revision to the clay varve timescale was driven by the apparent link to Greenland $\delta^{18}\text{O}$ profiles and the expected synchronicity of biostratigraphic (pollen) data and the Greenland temperature record. The regional pollen zones and their inferred ages were imported into the STS ages rather than providing an alternative explanation for the offset.

There are two steps to the age estimate produced by Andrén *et al.* (1999): 1) the assignment of the Younger Dryas-Preboreal pollen zone, and 2) the transfer of age information for this time period from the GRIP ice-core to the Swedish varves using wiggle matching. There are several assumptions that have not been considered by Andrén *et al.* (1999) when adopting these approaches.

In southern Sweden the vegetational succession for the Younger Dryas to the Preboreal period is well documented by pollen analysis of lacustrine sediments in eastern central Sweden that were situated close to the FIS margin (Berglund, 1979; Björck *et al.*, 1988, 2002). The vegetational succession is characterised by a transition from tundra herbs and shrubs with *Artemisia* and *Poaceae*, to an open shrubland with *Betula*, *Empetrum* and *Juniperus*, and to *Betula* and *Pinus* woodlands (e.g. Berglund, 1995).

The pollen data from the Baltic Proper varves shows a decrease in *Artemisia* and *Poaceae* that coincides with an increase in varve thickness at 10,650 vyrs. BP. This event occurs 40 vyrs (revised to 120 vyrs by Andrén *et al.*, 2002) after a decrease in varve thickness and a change in colour from brown to grey varves (Figure 11-16). The increase in varve thickness and colour change is interpreted as the final BIL drainage.

By placing the colour change at the Younger Dryas-Preboreal transition, Andrén *et al.* (1999) interpret a later increase in *Artemisia* and *Poaceae* stratigraphically above the colour change as the Preboreal oscillation (PBO). This increase in cold climate taxa occurs ca 225-345 vyrs after the colour change from brown to grey varves and is

consistent with the *ca* 300 grey varves that are observed in terrestrial sequences (e.g. Brunnberg, 1995).

If the original clay varve age for the colour change is used (10,740±100 to -250 vrys BP 1950; Strömberg, 1994), then an increase in *Artemisia* and *Poaceae* would be dated to *ca* 10,600 – 10,150 vrys BP. This in theory, could be a response to another less well defined climatic oscillation in the early Holocene such as the 10.8 event or the 10.4 ka BP Erdalen events (Nesje *et al.*, 2001; Dahl *et al.*, 2002). However, to date these climatic events have not been recognised in pollen records in Sweden and at the time of publication these climatic events were unknown to Andrén *et al.* (1999). By wiggle matching the varve thickness record to the GRIP ice-core chronology, the colour change has been dated to the Younger Dryas-Preboreal transition and this “fits well” with the rest of the pollen stratigraphy.

Ultimately, by linking the pollen stratigraphy to the GRIP ice-core record, it has been assumed that the vegetation record is driven primarily by climatic changes. However, the pollen data may reflect a vegetation response to a larger-scale glacier advance or local-scale oscillation of the ice margin, rather than a climatic signal. Indeed, just before the second increase in *Artemisia* and *Poaceae* at *ca* 10,350-10,450 clay vrys BP which is correlated to the PBO (Figure 11-17), there is a marked increase and decrease in the varve thickness record in the C9106 core, indicative of an oscillating ice margin (Andrén *et al.*, 1999). This suggests that the vegetation record could in part be linked to the position of the ice margin and not just a climatic signal.

Whilst most investigations in Scandinavia indicate that there is one single cold event during the early Preboreal (Björck *et al.*, 1997), there is evidence in a few records that the Preboreal was more complex. For example, marine records off the western Swedish coast indicates that there were two Preboreal oscillations at 9,900 and 9,700 ¹⁴C yrs BP (Wastegård *et al.*, 1998), and evidence from stable isotopes of terrestrial lake systems outside Scandinavia and the ice-cores indicates that there were several warm and cold oscillations during this period (Whittington *et al.*, 1996; Rasmussen *et al.*, 2014). Several early Preboreal marginal moraines have been identified in western middle Sweden, although it is not clear whether the moraines formed in response to climatic or topographic changes (Lundqvist, 1988). More recently, Blockley *et al.*, (2018) identified two early Holocene climatic reversals at 11.4 cal. ka BP and 11.1 cal. ka BP at the Star Carr site in north-east England. To date, research indicates that there may be several PBO events, though their expression in climatic archives varies spatially across the North Atlantic region.

The strength of the correlation to the PBO lies in the correlation of the varve chronology to the GRIP ice-core record and the assumption that the varve counts that enable this are accurate. However, most of the varve thicknesses throughout the Baltic Proper chronology are <cm-scale and were measured at the macroscale. Indeed, Andrén *et al.* (1999) report an average varve thickness in the lowermost brown varves between 10,650-11,370 vrs BP of 4 mm. Given that there are 219 more varves in the Asplången sequence, and 360 more varves in the Svinstadsjön sequence when counted under thin section in comparison to macroscale observations, it is possible that there are large errors in the Andrén *et al.* (1999) varve counts.

Apart from the influence of climate and glacial proximity, other factors such as soil characteristics may play a role in vegetation change. For example, it is likely that across Fennoscandia there was a lag between the time of deglaciation and the stabilisation of soils, and the stabilisation of soils and the establishment of vegetation on the landscape. It is also logical to assume that these processes were time-transgressive across the Baltic Basin, following the retreat margin of the FIS. The influence of the ice margin position, stabilisation of soils, establishment of vegetation and the associated time lag is often not acknowledged when using pollen stratigraphy to date varve sequences in the STS (e.g. Björck and Digerfeldt, 1984; Andrén *et al.*, 1999)

Until recently, there has been no evidence in Scandinavia for a lag in proxy response to climatic oscillations, but Muschitiello and Wohlfarth (2015) have demonstrated that there is a mean temporal lag of *ca* 290 years in the proxy-inferred climatic change between sites in Denmark and southern Sweden. They suggest that the temporal lag between sites may be due to specific processes that operate at each site. For example, the influence of coastal sea ice during the Lateglacial may have influenced the timing of proxy response to climatic change in sites in Sweden and Norway, compared to sites in Ireland and Denmark. The authors also proposed that the FIS probably acted as a climatic buffer during the Younger Dryas and subdued the seasonal cycle and the amplitude of temperature fluctuations. Moreover, cold katabatic winds coming off the FIS likely had an impact on the proxy response to large-scale climatic changes (Muschitiello and Wohlfarth, 2015). In light of this research, the direct assignment of age information to varve records using pollen stratigraphic evidence requires caution, and age estimates that are determined on this basis require independent testing.

The second aspect to the approach taken by Andrén *et al.* (1999) concerns the synchronisation of the varve record in the Baltic Proper to the Greenland ice-cores using wiggle matching and transferring age information between archives. Since Strömberg (1994) proposed that there was no lag between the Younger Dryas climatic event and the associated FIS response, Andrén *et al.* (1999) correlated the vegetation record from

the Swedish varves to the ice-cores. The assumed absence of a lag between the vegetation, ice-sheet and climate system is the key justification for using the Greenland ice-core ages to date the assumed climatic changes within the Baltic Proper varve record. There are, however, various problems with correlating vegetation records to the ice-core records without independent means of correlation. For example, different proxies have different environmental and climatic sensitivities and do not necessarily change in phase with climatic transitions. Recent research has demonstrated that although climatic changes may appear abrupt at the local scale, climatic synchronicity across larger scales should not be assumed and local climatic changes may be time-transgressive across regional scales (Lane *et al.*, 2013; Muschitiello and Wohlfarth, 2015). Pennington (1986) demonstrated vegetation lags in arboreal taxa at the onset of the Holocene and Lateglacial period were between 500-1,500 years long, were primarily governed by the local soil development and were asynchronous with prevailing climatic conditions. More recently Blockley *et al.* (2018) demonstrate a lag of *ca* 500 years between local climatic amelioration into the Holocene and the establishment of 'warm' taxa in Northern England. While this lag is less time than might be required for Southern Sweden it should be noted this was identified in a lowland site without glaciation during the Younger Dryas period and with evidence of existing skeletal soils remaining through this period. Where local conditions are driven by ice retreat any lag is likely to be of much longer duration.

It is important to recognise that this research was undertaken at a time when wiggle matching and tuning proxy records to the Greenland ice-cores was commonplace. Since then, multiple authors have repeatedly warned against wiggle-matching and tuning proxy records (e.g. Walker *et al.*, 1999; Blaauw *et al.*, 2007; Blaauw, 2012), yet the age estimate for the final BIL drainage proposed by Andrén *et al.* (1999) is continually cited and used within FIS reconstructions without acknowledgement of the potential flaws in the methodological approach (Hughes *et al.*, 2016; Stroeve *et al.*, 2016; Swärd *et al.*, 2016). The final BIL drainage age proposed by Andrén *et al.* (1999) has become a key chronostratigraphic marker in FIS reconstructions (Andrén *et al.*, 2011; Hughes *et al.*, 2016; Stroeve *et al.*, 2016) however, the lack of independent testing of this long-accepted age estimate only serves to perpetuate the aforementioned problems.

The number of assumptions required to accept the current date of the colour change far outweighs the limitations of the approach taken in this thesis. Therefore, the age estimate proposed by Andrén *et al.* (1999) for the colour change of 11.5 ka yrs BP has not been robustly tested and the age presented in this thesis is considered the current best age estimate for the change (assuming it is a synchronous event).

11.6.5 Implications for the deglaciation chronology in Östergötland

The tephra data from this thesis demonstrate that glacial varves were accumulating in Östergötland during the early Holocene. By implication since glacial varves were accumulating in Östergötland with the ice margin in the MSEMZ, this suggests that an ice margin blocking the Mt Billingen drainage route also existed into the early Holocene. This inference is based on the published varve chronologies for the region. The varve records of Brunenberg have been chronologically linked to Strömberg's varve records to the east of Lake Vättern in the MSEMZ (Figure 11-18).

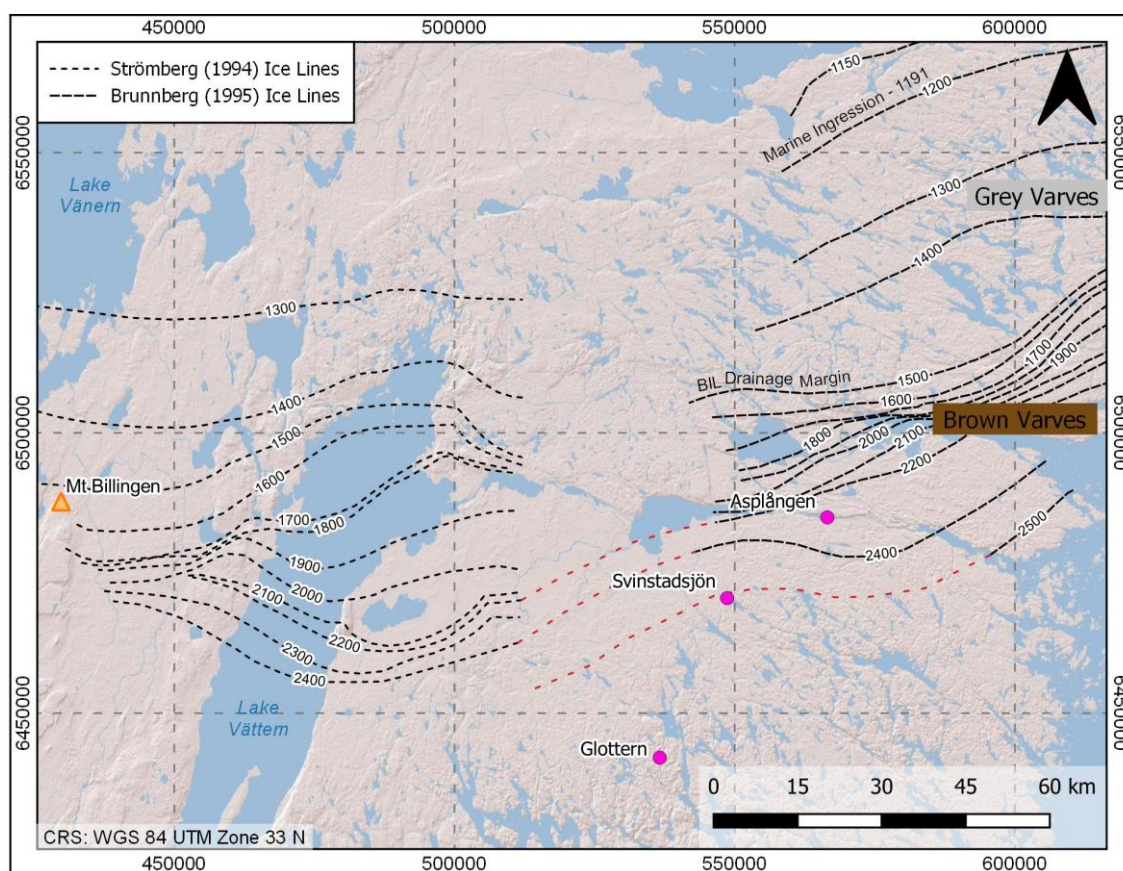


Figure 11-18. Strömberg (1994) and Brunenberg (1995) ice lines in relation to the sites in this study and Mt Billingen.

Dashed red lines are inferred links between sites and are shown for illustrative purposes only.

Given that Svinstadsjön and Asplången are located approximately along the trend of the ca -2500 and the ca -2300 ice lines respectively (Figure 11-18) and that the drainage ice line has been interpreted at ca -1500 line north of Mt Billingen (e.g. Strömberg, 1994; Brunenberg, 1995), then it can be inferred that varves were accumulating at these sites for ca 800 vyrs before drainage. Given that the Askja-S tephra is located 34 vyrs from the base of the Asplången site, then this tephra layer marks 34 vyrs after site

deglaciation. Therefore, these sites were accumulating varved sediments at the time of the Askja-S eruption during the early Holocene and prior to BIL drainage.

The BIL drainage line at ca -1500 is situated north of Mt Billingen and has been linked to the colour change from brown to grey varves in multiple varve records within the Brunnberg (1995) chronology (Figure 11-18). If the colour change is indeed a synchronous event that represents the final BIL drainage, this is marked at varve 657 in the Asplången sequence and is dated to 10,350±43 cal. yrs BP. However, the ca 800 yrs between deglaciation at Asplången and drainage proposed by Brunnberg (1995) is based on unconvincing varve thickness correlations that are mostly guided by the colour change. The results from thin section and tephra analysis in this thesis demonstrate that not only are varve thickness correlations likely to be inaccurate, but the colour change could be an asynchronous event. Therefore, the use of these approaches for the construction of the varve chronology is likely flawed.

Conclusions that have been made on the basis of accepting the varve chronologies in south-eastern Sweden (e.g. Brunnberg, 1995; Andrén *et al.*, 1999) such as: 1) using the colour change from brown to grey varves as a proxy for BIL drainage; 2) accepting that the colour change is a synchronous event; and 3) using the varve chronology to date the BIL drainage require reappraisal and independent testing.

11.6.6 Proposed timing of final BIL drainage

For the purposes of discussion, if the “colour change model” for the deglaciation chronology is correct, the final drainage of the BIL can be linked to the transition from brown to grey varves. This is dated to 10,337±43 cal. yrs BP at Svinstadsjön and 10,350±43 cal. yrs BP at the Asplången.

These ages, however, conflict with the current accepted age estimates for BIL drainage and moraine emplacement west of Mt Billingen. For example, the Skara and Skånings-Åsaka moraines that have been linked to the Younger Dryas have been dated to 12.6-11.5 ka BP. It has been suggested that the drainage of the BIL occurred just after the formation of these moraines and the northernmost moraine (Gullhammar) in the MSEMZ (Björck *et al.*, 2001; Lundqvist and Wohlfarth, 2001). It is considered unlikely that the ice margin occupied the area between the northernmost moraine and Mt Billingen (ca 5 km) for 1,200 years. Given the issues with the chronological approaches that have been adopted when dating these moraines (as discussed in section 11.6.3) it is proposed that the age of the moraines may require revision.

Given the potential issues in the accuracy of the published varve chronologies and the asynchronicity of the colour change across the Baltic Basin, the BIL drainage may not be represented by the brown to grey colour change. It is expected that the colour change

will be asynchronous across other varve records in south eastern Sweden though this must be tested with tephrochronology in varve records that are analysed using thin section analysis.

If the colour change is an asynchronous event, its use as a key marker within varve records as the BIL drainage cannot be correct and the drainage must have occurred, at a minimum, prior to the ingression of marine water (i.e. deposition of varves with abundant fossil evidence for saline ingression). The final drainage event therefore could have occurred as late as the uppermost varve in the Svinstadsjön and Asplången records since these varves are characteristically freshwater glaciolacustrine varves. The uppermost varve in each record is dated to $10,168 \pm 43$ cal. yrs BP at Svinstadsjön and $10,180 \pm 43$ cal. yrs BP at Asplången (i.e. synchronous within errors). Yet these dates conflict with other Baltic Sea phases that occurred after the BIL drainage such as the brackish phase of the Yoldia Sea stage.

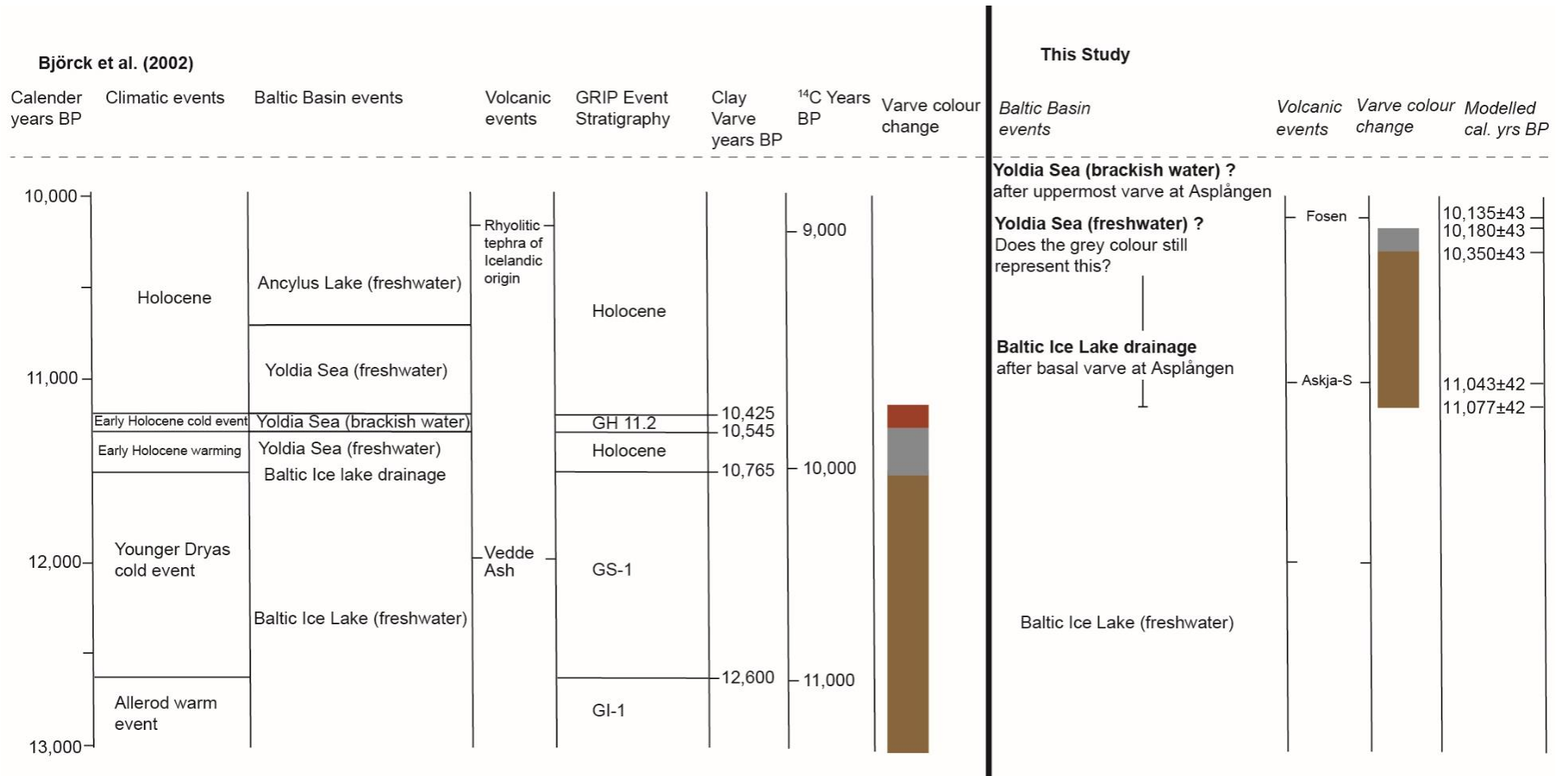


Figure 11-19. Event stratigraphy for the Lateglacial-Holocene transition in eastern middle Sweden alongside the chronology presented in this thesis. Modified from Björck et al. (2002).

11.6.7 Potential implications for the Yoldia Sea dates

The brackish phase of the Yoldia Sea stage has been identified in numerous sediment cores around the Baltic Basin by lithological changes (red brackish varves) and marine calcareous fossils and diatoms in the western and south eastern Baltic Sea (Svensson, 1989; Brunnberg, 1995; Schoning and Wastegård, 1999; Andrén *et al.*, 2002). This brackish phase has a duration of 120 vyrs in the mineral magnetic record of the north western Baltic Proper and a duration of 60-70 vyrs from the marine fossil record (Wastegård *et al.*, 1995). In the Baltic Proper, the presence of *ca* 200 symmetric varves represents the Yoldia Sea stage (Andrén *et al.*, 2002) with the onset of the marine ingression of the Yoldia Sea dated to *ca* 10,430 vyr BP (Strömberg, 1994; Brunnberg, 1995). There is also evidence of marine influence in the Lake Vättern basin *ca* 110-135 vyrs before the main marine ingression (Björck *et al.*, 2001; Swärd *et al.*, 2016). The influx of marine water has been radiocarbon dated in the main inlet of marine waters east of the Närke strait (Wastegård *et al.*, 1998) and in the Stockholm area (Brunnberg and Possnert, 1992).

Many of the radiocarbon ages for the Yoldia Sea stages are derived from marine sediments/marine fossils and it is possible that some, if not all of these ages, could be inaccurate. Inaccuracies could be due to: 1) problems estimating the marine reservoir offset; 2) incorporation of old carbon; or 3) the radiocarbon plateau during the early Holocene. Moreover, almost all radiocarbon dates contain age uncertainties that are longer than the duration of the event itself (Table 11-12).

Table 11-12. Summary of radiocarbon samples from Brunnberg and Possnert (1992). INS = insoluble fraction, SOL = soluble fraction. fr = fragment. * = analysed value from fragments of the same shell, ** = Measured value of a separate periostracum found 1990. *** = An average value of the three measurement shell carbonates. **** = Assumed value by Brunnberg and Possnert (1992).

Lab No	Material	$\delta^{13}\text{C}$	^{14}C age BP
Ua-2251	<i>Portlandia</i> (fr)	-3.2*	10,535±135
Ua-2252	<i>Portlandia</i> (fr)	-3.2*	11,565±135
Ua-2253	<i>Portlandia</i> (fr)	-3.2*	10,635±140
Ua-2254	Periostracum	-16.7**	9,145±290
Ua-2255	<i>Portlandia arctica</i>	-3.3***	10,740±145
Ua-2256	<i>Portlandia arctica</i>	-3.3***	11,060±135
Ua-2257	<i>Portlandia arctica</i>	-3.3***	11,405±210
Ua-2258	Periostracum	-16.7**	8,220±210
Ua-2259	<i>Portlandia</i> (fr)	-3.6	11,620±170
Ua-2260	<i>Portlandia</i> (fr)	-3.1**	11,450±185
Ua-2261	Periostracum	16.7****	8,425±260
Ua-2262	Sediment with shell (INS)	-25****	16,620±390

Lab No	Material	$\delta^{13}\text{C}$	^{14}C age BP
Ua-2263	Sediment with shell (SOL)	-25****	14,225±235
Ua-2264	Sediment above INS	-25****	22,450±570
Ua-2265	Sediment above SOL	-25****	16,485750
Ua-2266	Sediment below INS	-25****	19,700±420
Ua-1673	<i>Salmo alpinus</i>	-21****	8,665±115

To the west of the Närke Strait at Lake Vibysjön shell fragments, foraminifera and the bivalve *Portlandia arctica* were dated. Dates from *Portlandia arctica* yielded an age of 10,580±75 ^{14}C yrs BP and dates from foraminifera returned an age of 10,985±140 ^{14}C yrs BP (Wastegård *et al.*, 1998). These were considered older than expected, and there are questions over the marine reservoir offset which was set at 450 yrs. The marine reservoir offset during the Yoldia Sea Stage has been estimated at 1,000-1,500 years (Wastegård and Schoning, 1997) and 800-1,000 years (Wastegård *et al.*, 1998). In the North Atlantic it has been proposed that the marine reservoir offset was 700-800 yrs during the Younger Dryas (Bard *et al.*, 1994; Austin *et al.*, 1995), dropped rapidly at the Younger Dryas-Preboreal boundary to ca 300-400 yrs (Mangerud *et al.*, 2006) and may have been up to 700 yrs during the Preboreal (Haflidason *et al.*, 2000). In the modern Baltic Sea, the marine offset can range from 100-800 yrs over short distances (Chapter 2) meaning that quantifying the past marine reservoir offset remains a challenge.

Additional consideration with radiocarbon dates from this period is that the first part of the Preboreal is characterised by a plateau at 10,000 ^{14}C yrs BP (Björck *et al.*, 1996). Therefore radiocarbon dates are highly sensitive to the marine reservoir effect and dates between 11,000–10,500 ^{14}C yrs BP could yield an age of ca 10,000 ^{14}C yrs BP if a marine reservoir effect of 700-800 yrs is applied (Björck *et al.*, 2002).

It is beyond the scope of this research to re-appraise the timing of other Baltic Sea stages but given the limitations of marine radiocarbon dates and the tephra and thin section data from this thesis, existing chronologies for the Baltic Basin may require revision. Using the assumption that the chronology presented in this thesis is correct, the marine phase must have occurred after glaciolacustrine varve sedimentation ceased placing the Yoldia Sea stage after 10,180±43 cal. yrs BP (uppermost varve at Asplången). These ages are similar to the ca 10,430 yrs BP age that has been previously proposed for the main marine ingressions (Strömberg, 1994; Brunnberg, 1995; Andrén *et al.*, 2002), and the age proposed for the Lake Vättern basin (ca 110-135 yrs before the main marine ingressions) and would equate to ca 10,295-10,320 yrs BP (Björck *et al.*, 2001; Swärd *et al.*, 2016).

11.6.8 Comparison with existing deglaciation chronology

The key argument against deglaciation in Östergötland at ca 11 ka yrs BP and a BIL drainage during the early Holocene at ca 10.3 ka yrs BP is the existing deglaciation chronology which indicates that sites to the north of Asplången and Svinstadsjön deglaciated earlier (see reviews by Hughes *et al.*, 2016; Stroeven *et al.*, 2016) (Figure 11-20).

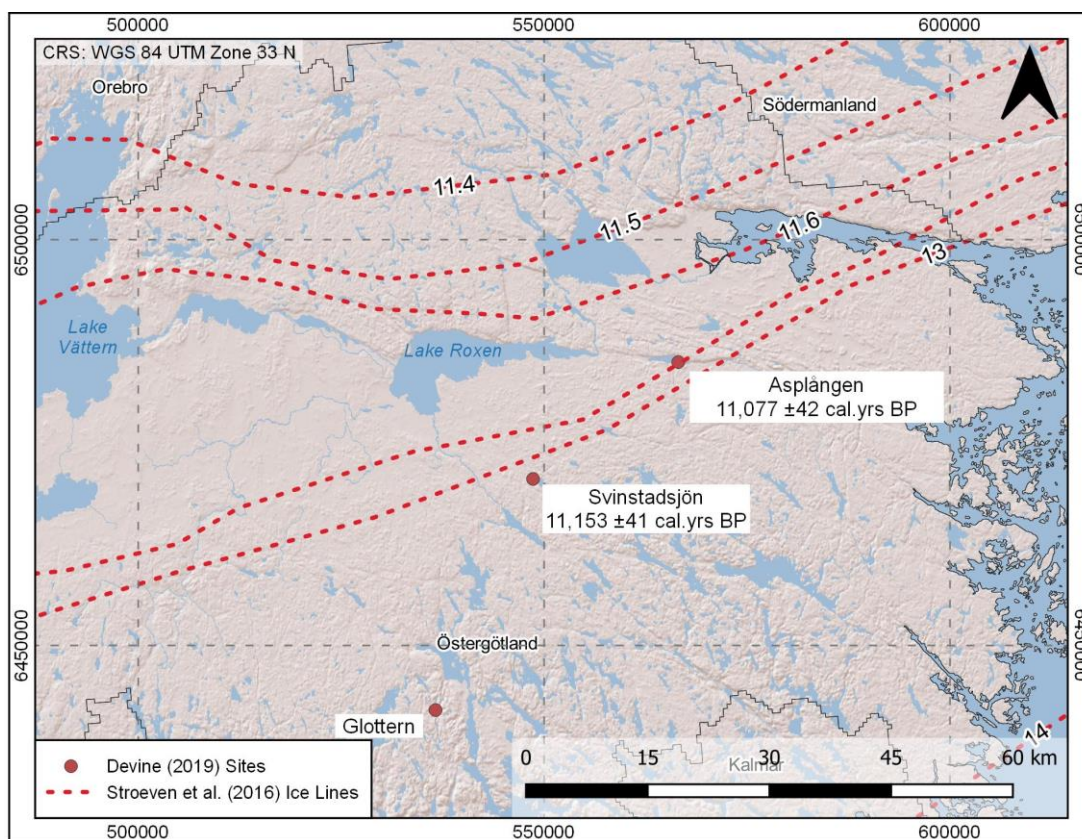


Figure 11-20. Deglaciation ages for the Svinstadsjön and Asplången sites proposed in this thesis in comparison to the deglaciation chronology proposed by Stroeven *et al.* (2016). Red dashed ice margin lines are in ka cal. yrs BP. Conversion to cal. yrs BP is based on the connection of the STS to the GRIP ice core chronology using the timing of the Baltic Ice Lake Drainage proposed by Andrén *et al.* (2002) (ca -1530 vryrs in the STS); which correlates to ca 11,620 cal. yrs BP in the GRIP ice core record. Asplången is located on the 12.7 ka cal. yrs BP ice margin and Svinstadsjön is located on the 13 ka cal. yrs BP ice margin.

It is important to note that the ages of the ice margin lines proposed by Stroeven *et al.* (2016) (Figure 11-21) for the Younger Dryas and early Holocene part of the STS were calculated using the 11,620 cal. yrs BP age of the BIL drainage proposed by Andrén *et al.* (2002). This age is derived from wiggle matching the Baltic Proper varve chronology to the GRIP ice core record originally outlined by Andrén *et al.* (1999), later revised by Andrén *et al.* (2002). Stroeven *et al.* (2016) then traced the published varve chronologies in the STS (e.g. De Geer, 1940; Bergström, 1968; Strömberg, 1985, 1989, 1994) to the varve-zero (-1530 De Geer vryrs) and assigned it an age of

ca 10,090 cal. yrs BP (Table 11-13). The age of the ice margin lines for the Younger Dryas and early Holocene in Sweden were then assigned using the new age of the varve-zero that is inherited from the GRIP ice-core record (Andrén *et al.*, 1999; 2002).

Table 11-13. Conversion of the STS to cal. yrs BP in Stroven *et al.* (2016).

STS De Geer yrs	Varve yrs BP	cal. yrs BP	Comment
+140	9,100	9,950	
±0	9,240	10,090	Varve-zero
-1400	10,640	11,490	
-1500	10,740	11,590	
-1530	10,770	11,620	BIL drainage
-2200	11,440	12,290	
-2250	11,490	12,340	
-3300	12,540	13,390	

Based on the aforementioned assumptions in the Andrén *et al.* (2002) age for BIL drainage (section 11.6.4) and using the assumption that the tephra-based chronology proposed in this thesis is accurate, the most recent deglaciation chronology may not be robust. Outlined in this section is a re-appraisal of the deglaciation ages across Fennoscandia using the dataset provided by Stroeven *et al.* (2016). The purposes of this process are to: 1) highlight the key dates which contradict the deglaciation ages proposed in this thesis; 2) highlight the underlying assumptions that have been made when constructing the deglaciation chronology; and 3) emphasise the potential of tephrochronology to test the existing deglaciation chronology.

A set of criteria were applied to the dataset in order to highlight dates that are unreliable, and these criteria are presented in the following section. Similar data-cleaning exercises have been undertaken by authors when reviewing chronological databases (e.g. Blockley and Pinhasi, 2011; Hughes *et al.*, 2016; Davies *et al.*, 2020), though filtering of dates using robust criteria does not appear to have been applied to the Stroeven *et al.* (2016) database.

11.6.8.1 Stroeven *et al.* (2016) data cleaning

The published database contains 335 radiocarbon, 727 cosmogenic nuclide and 138 OSL dates. Of these, 88 radiocarbon, 93 cosmogenic nuclide and 33 OSL dates have calibrated ages between 9,500-12,000 cal. yrs BP. Table 11-14 summarises the criteria that were adopted when assessing the reliability of these dates.

Table 11-14. Criteria for selecting deglaciation dates from the Stroeven et al. (2016) dataset.

Criteria	Radiocarbon	OSL	Cosmogenic nuclide
Extracted calibrated ages for deglaciation between 9,500-12,000 cal. yrs BP	✓	✓	✓
Removed dates with uncertainties that suggest deglaciation post 10,000 cal. yrs BP (as not a problem under the model proposed in this thesis)	✓	✓	✓
Removed dates from Russia, Latvia, and Finland as not directly relevant to the study location	✓	✓	✓
Removed dates above 67 degrees north (as the ice margin is to the north, east or west)	✓	✓	✓
Removed dates west of the Norwegian mountains as not directly relevant.	✓	✓	✓
Removed dates with unreported measurement errors	✓	✓	✓
Removed dates that are rejected by the original authors due to unreliable sample selection.	✓	✓	✓
Removed duplicate dates from the same core (always leaving the oldest date)	✓	X	X
Removed dates from marine shells and calcite concretions which have unknown reservoirs.	✓	X	X
Removed dates with 1 sigma uncertainties greater than 1,000 yrs since these dates cover the entire period of interest	X	✓	✓

After application of the criteria, 13 radiocarbon dates remain and only 5 are derived from terrestrial plant macrofossils with the remaining 8 from bulk material. It is recognised that the bulk dates may not necessarily be inaccurate, and may suffer from untestable mineral carbon errors (Walker, 2005).

The 13 radiocarbon dates were also ranked on their reliability using the replicability and reported sample data. Rank 1 dates appear to be robust. Rank 2 dates have some doubts over reliability but may be correct. Rank 3 dates are considered in error by either the author or show dispute between replicates in the same interval and/or contain limited information. After this process if only the Rank 1 and 2 dates are utilised the deglaciation chronology between 9,500-12,000 cal. yrs BP is dependent on 9 radiocarbon dates that are not in close proximity to the Asplången and Svinstadsjön sites (Figure 11-21). The filtering process also leaves 19 OSL and 20 cosmogenic nuclide ages which have relatively large uncertainties (Figure 11-22).

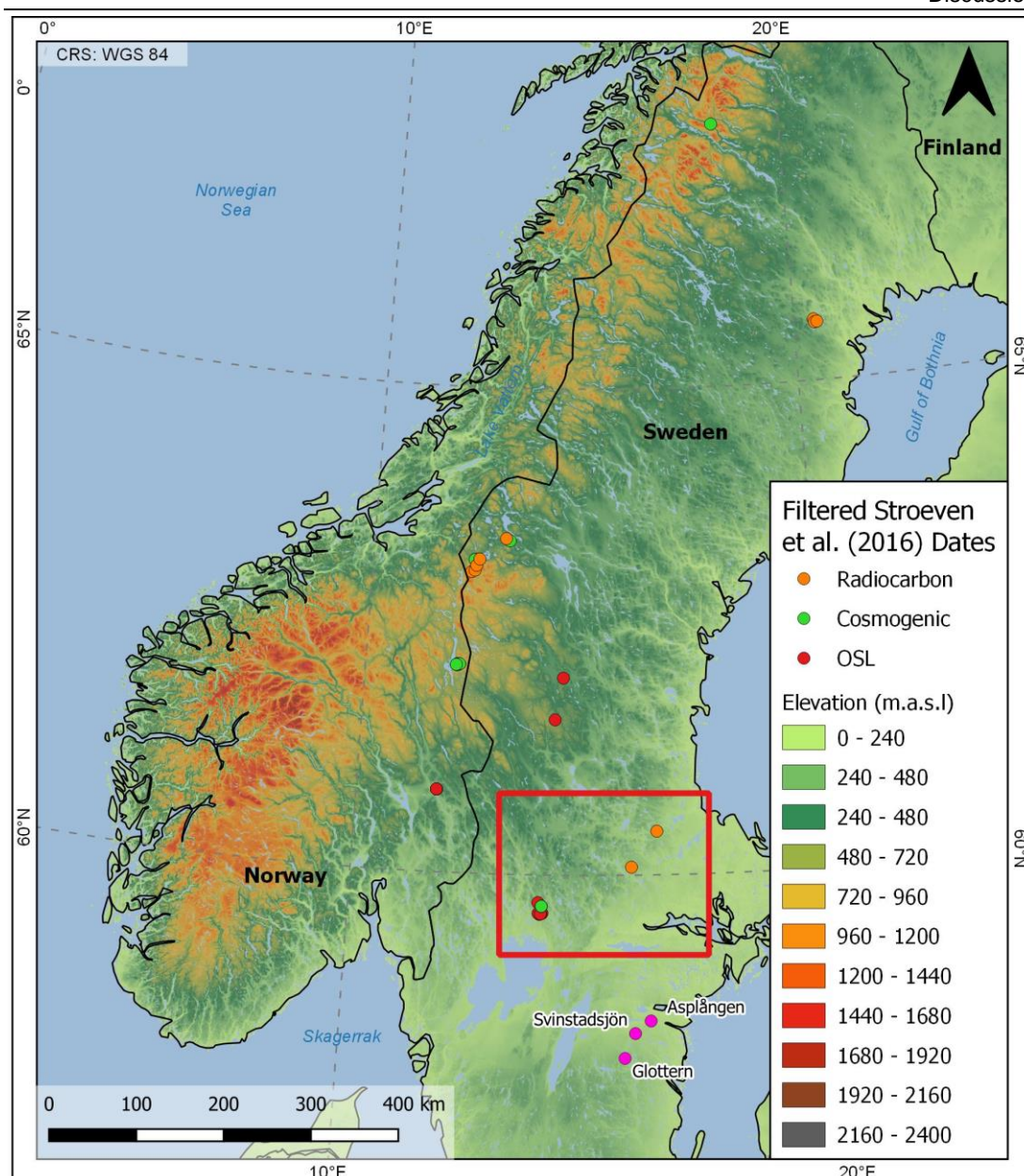


Figure 11-21. Map of the remaining dates after filtering the Stroeven et al. (2016) dataset. Red box marks the sites that are marked with an asterisk in Figure 11-22.

11.6.8.2 Re-evaluation of the deglaciation chronology

The remaining radiocarbon, OSL and cosmogenic nuclide ages were plotted alongside the minimum deglaciation age at Asplången ($11,044 \pm 43$ cal.yrs BP) and the end of glaciolacustrine varve formation at the site ($10,180 \pm 43$ cal. yrs BP) (Figure 11-22). The uppermost varve in the Asplången sequence likely indicates that the ice margin had retreated north of Mt Billingen since ultra-distal varves characterise the uppermost varves in the sequence.

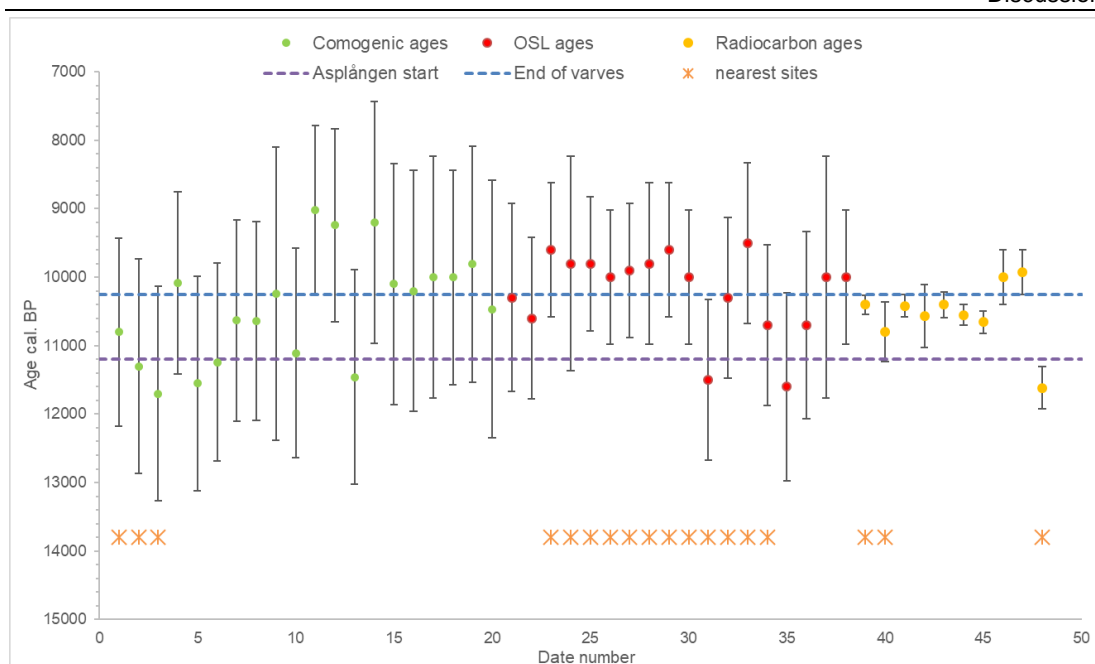


Figure 11-22. Deglaciation ages from the Stroeven *et al.* (2016) filtered dataset. The displayed dates are those that conform to the above criteria and the ones nearest to the study region are marked by an asterisk. All dates are given with 2 sigma uncertainties. All dates except one overlap or postdate the proposed deglaciation age at Asplången.

The results of this exercise indicate that the cosmogenic nuclide and OSL ages either post-date or overlap in age with deglaciation at Asplången (Figure 11-22). The radiocarbon dates from the filtered dataset of Stroeven *et al.* (2016) give the required precision to test the deglaciation age proposed in this thesis. With the exception of one date, all of the remaining radiocarbon ages fall after the proposed deglaciation of the Asplången site at $11,077 \pm 42$ cal. yrs BP. The single radiocarbon date which pre-dates the deglaciation age at Asplången is from an isolation basin and the authors suggest that this date may have an apparent older age due to low organic content in the bulk sediment sample (Lindén *et al.*, 2006). The remaining dates are still in support of deglaciation in higher altitude sites in northern Sweden around 10.2 ka, though this could be a result of ice sheet thinning.

Critically, this thesis demonstrates that current models of the deglaciation chronology are based on a small number of radiocarbon dates with broad periods constrained by other methods. These data have insufficient density to robustly test the alternative model proposed in this thesis. Therefore, it is plausible that Östergötland deglaciated during the early Holocene and that BIL drainage occurred, at a minimum, after $11,077 \pm 42$ cal. yrs BP. Additional tephra-based varve chronologies would be required to test the proposed deglaciation chronology presented in this thesis.

11.6.9 Early Holocene climatic events

The results from this thesis indicate that glacial varves were forming in Östergötland in the early Holocene from as late as $11,043 \pm 43$ cal. yrs BP, in disagreement with the current deglaciation model. Moreover, the results suggest issues in the use of the colour change to infer a final BIL drainage. On this basis it is not possible to provide a more precise estimate for the BIL drainage other than it occurred after formation of the northernmost moraine in the MSEMZ and likely occurred after $11,043 \pm 43$ cal. yrs BP.

If this inference regarding the timing of BIL drainage is correct, then this event could have delivered freshwater forcing to the North Atlantic which might have in turn driven some of the identified early Holocene climatic cooling events recorded in climate archives across the North Atlantic region, as previously suggested by Björck *et al.* (1997) and Jessen *et al.* (2008). At present, several early Holocene climatic cooling events have been identified such as the 10.8 ka BP event, the Erdalen events at 10.2 ka BP (Dahl *et al.*, 2002), and North Atlantic cooling identified in the Faroe Islands, centred on 10.6, 10.45, 10.3 ka BP (Jessen *et al.*, 2008). However, given that it is not currently possible to constrain the exact timing of the termination of the BIL this must remain speculative until: 1) chronological issues in the STS are resolved; 2) direct lithological evidence for BIL drainage is found and independently dated; and 3) there is evidence from proxy records in Sweden for freshwater forcing in the early Holocene.

11.7 Summary

The results from this thesis demonstrate that there may be errors in the STS that stem from the inaccurate identification of individual varves at the macroscale. The increased level of detail afforded by microfacies analysis has enabled scrupulous analysis of varve structures at the sub-seasonal scale. This approach has led to reconstructions of sediment processes in the BIL. Furthermore, microfacies analysis indicates that a combination of local and regional-scale sediment processes drive varve formation, and this varies spatially across the BIL. The microfacies analysis presented in this thesis indicate that varve thickness may be driven by the proximity of the site to the lake edge. When the ice margin retreats, sites in close proximity to the lake edge (e.g. Glottern) continue to accumulate complex, multi-laminated varves due to the readily available supply of sediment from areas above the highest shoreline. In contrast, sites which are located in the main Baltic Ice Lake

(Svinstadsjön and Asplången) accumulate simple, single laminations in the coarse component due to the lack of sediment input from nival melt.

Varve chronologies that have been constructed on the basis of macroscale analysis may overlook important sedimentological process information that has direct relevance to the construction of accurate varve chronologies. For example, the presence of ultra-distal varves at the Svinstadsjön and Asplången sites indicates that varve thickness is not necessarily primarily controlled by the ice margin position. As a consequence, it may not be possible to correlate these varves using varve thickness, even with multiple cores from the same site. Moreover, these varve types are difficult to identify at the macroscale, leading to consistent under counting, and at Svinstadsjön (40%) and Asplången (27%) fewer varves were counted at the macroscale in comparison to the microscale.

Whilst thin section analysis has produced precise varve thickness measurements and accurate varve counts, the resulting varve thickness records demonstrate the true amount of noise in the varve chronologies, which has, until now, been suppressed by macroscale analysis. These “noisy” varve thickness records are difficult to correlate, even between sites in close proximity. Thus, resolving the problems identified in the existing STS regarding correlations between site chronologies cannot necessarily be achieved with thin section analysis alone. The results presented here reinforce the need for other independent means of correlating varve records such as tephrochronology.

The presence of tephra within the Svinstadsjön and Asplången varve records demonstrate the potential to find other tephras in the STS. The combined application of tephra and varve count data has enabled the existing ages of the Askja-S, Fosen and Hässeldalen tephras to be integrated within a Bayesian age model. The remodelled ages of the tephras is of importance to the wider palaeoclimate community. Tephra data shows the potential for independent links between varve chronologies in the STS. The tephra data also indicates that the colour change from brown to grey varves may not be synchronous between sites and its use as a marker horizon for the construction of the regional varve chronologies could be flawed. It is recognised that whilst chemical data were not obtained for the Svinstadsjön tephras, the results should be viewed as an important first step in demonstrating the usefulness of tephrochronology for independent varve correlations.

The correlation to known tephras has enabled the Asplången and Svinstadsjön records to be placed on an absolute timescale and the varve spacing between the Askja-S and Fosen tephras is in agreement with the number of years between the

published ages of these tephras. The identification of the Askja-S within the proximal varves at Asplången is the first known occurrence of this tephra in glacial varves in Sweden.

Critically, the presence of the Askja-S in varve 34 at Asplången, indicates that the site was deglaciated during the early Holocene at ca 11.0 ka cal. yrs BP. This age is ca 1,200 years younger than the current deglaciation model which placed this site during the Younger Dryas period. This warranted further assessment of the reliability of the dates that underpin the deglaciation chronology, in particular the age of the colour change from brown to grey varves that has been linked to the BIL drainage.

Review of the biostratigraphic and lithological data indicates that the colour change from brown to grey varves appears not to have a consistent source and cannot consistently be characterised. Given the tephra data presented in this thesis, it has been concluded that the colour change from brown to grey varves may not represent the final drainage of the BIL and so direct dating of this event has not been proposed using the absolute age of the colour change in the Asplången and Svinstadsjön sequences.

One of the key arguments against Asplången deglaciating during the early Holocene is the published deglaciation chronology which indicates that sites to the north of Asplången became ice-free earlier. However, the published age of the varve records in Östergötland is based on the assumption that the colour change from brown to grey varves is synchronous with the same colour change in the varve records in the Baltic Proper. The Baltic Proper varve chronology has been dated to the Younger Dryas-Preboreal transition using pollen stratigraphy and aligning the varve thickness record to the GRIP ice-core chronology. For the reasons outlined in this chapter, this approach is considered unreliable and the Baltic Proper varve chronology requires testing via independent dating techniques, such as tephrochronology.

Despite the questions regarding the Baltic Proper varve chronology, dates from other sites to the north of Asplången appear to contradict the deglaciation age proposed in this thesis. However, upon further investigation of the Stroeven *et al.* (2016) deglaciation dataset, only 13 of the 88 published radiocarbon dates were deemed reliable, and of these only one contradicts the chronology proposed in this thesis. Additionally, the deglaciation chronology appears reliant on OSL and cosmogenic ages that have large uncertainties and do not necessarily disagree with the early Holocene age proposed in this thesis. Given the results of this thesis and the re-appraisal of the Stroeven *et al.* (2016) deglaciation chronology, it is proposed that sites in Östergötland deglaciated during the early Holocene and not during the

Younger Dryas. This hypothesis does come with large caveats and should be viewed as a hypothesis that requires testing.

At present it is not possible to provide a more precise estimate for the timing of BIL drainage since this research indicates that the colour change may not be a synchronous event. However, given that proximal varves were accumulating at Asplången around *ca* 11.0 ka cal. yrs BP, and by inference the ice margin was in the MSEMZ, the BIL likely drained sometime after the Asplången site was deglaciated. The links to early Holocene climatic events due to BIL drainage are somewhat speculative and demonstrate that the long-accepted deglaciation chronology may require testing. Recommendations for future research that would be required to test the hypotheses that are proposed in this thesis are presented in the following chapter.

Chapter 12. Conclusions

12.1 Introduction

The thesis has provided an opportunity to: 1) re-examine the traditional macroscale based methodological approaches that have been employed when creating the STS; 2) anchor the varve chronologies to an absolute timescale and re-assess the timing of retreat in the Swedish sector of the FIS during the Younger Dryas-early Holocene; and 3) critically assess the age of the final drainage of the Baltic Ice Lake and propose links to climate shifts across the North Atlantic region. Here the findings from this study are synthesised and future directions for the research are considered.

12.2 Key findings

With regards to point 1, the STS has been constructed using macroscale-based methodological approaches and as a consequence several, often overlooked, assumptions have been made previously when constructing this timescale. These assumptions include whether the existing descriptive protocols are capable of accurately and precisely defining varves at the macroscale that have implications for the accuracy of varve counts and whether repeat counts or varve count errors are incorporated into the STS. In addition, distinct sediment features in the STS such as colour changes, varve thickness or sand beds are reported as spatially-extensive features across the basin that were deposited synchronously. These assumptions have important implications for the construction of site varve chronologies and for correlating varve records to create composite varve chronologies.

At the outset of the thesis, sites were selected to cover the Younger Dryas-Preboreal (12.0-11.5 ka BP) period of the STS and the approach has been to examine optimal positions for core extraction in these basins or local depocentres. At least 20 depth probes were taken across areas of ca 50-100 m² at each site. This identified that the basins in areas adjacent to extant lakes tended to have undulating bottom topographies and core extraction is preferred from locations that are relatively flat and that bottom onto bedrock because this will produce the longest sediment records (high numbers of macroscopically-visible varves) and with the presence of relatively few zones of disturbance.

Further microfacies analysis focussing on the site of Svinstadsjön (Chapter 6) demonstrates that 40% more varves (987 ± 23 yrs) than were identified using macroscale analysis (619 yrs) with X-radiograph (488 yrs) and μ XRF (336 yrs) techniques yielding even fewer varves (section 6.6.4). The results illustrate that thin section analysis provides the most accurate identification and thickness measurement of varved and non-varved sediments in comparison to the other techniques. In this thesis, the application of robust descriptive protocols (Palmer *et al.*, 2019) has been used to explore the variation in sedimentary processes that lead to varve formation. This detailed approach to varve analysis has led to further development of sedimentological models of Swedish varves proposed by De Geer (1940) and Antevs (1926) using macroscale analysis and Ringberg and Erlström (1999) at the microscale. The prevailing sedimentological model suggests that sedimentation at a particular site is primarily driven by proximity to the ice margin, whereas the results from microfacies analysis in this thesis demonstrates that varve sedimentation in a sequence is driven by a combination of processes where the sediment source can be derived directly from the glacier margin (Lamination Sets E, F, G, and H), and, in some cases, other more local processes dominate the sediment source with minimal glacier-sourced material (e.g. Lamination Set A; see Chapters 6, 7, and 11).

Critically the varve thickness measurements and microfacies contribute to the formation of three new varve site chronologies from Asplången (826 yrs), Glottern (207 ± 1 yrs) and Svinstadsjön (987 ± 23 yrs). Whilst thin section analysis has produced precise varve thickness measurements and accurate varve counts, the resulting varve thickness records demonstrate the true amount of noise in the varve chronologies, which has, until now, been suppressed by macroscale analysis. These “noisy” varve thickness records are difficult to correlate, even between sites in close proximity, or between cores from the same site.

The presence of tephra in these varve records in this thesis reinforces the potential of discovering tephra in other varve sequences in Sweden. The chronological implications of this are discussed below, but importantly this finding demonstrates that there is the potential to be able to link varve records independently through geochemically distinct tephra horizons rather than being reliant on lithostratigraphic markers such as the colour change or distinctive varve thickness patterns. This will be of greater importance since the inherent noise within the varve thickness records using microscale analysis may prohibit statistical correlation using varve thickness measurements.

One of the key driving factors for this thesis was that several authors had proposed that there may be up to 700-900 yrs missing in the STS during the Lateglacial, early or mid-Holocene periods (e.g. Björck *et al.*, 1996; Wohlfarth *et al.*, 1997; Andrén *et al.*, 1999). It had been proposed that these missing years may be due to problems with the correlation between one or two regional varve chronologies (Wohlfarth *et al.*, 1997; Wohlfarth and Possnert, 2000) and that varve chronologies which are constructed from macroscale analysis contain little or no varve count errors. Therefore, identifying the source of the missing varves in the STS had been challenging. As detailed above, the missing STS years for this period may be represented within the additional years identified at the microscale and is therefore a product of mismatches made when comparing macroscale properties. Potentially this issue can be addressed with a more systematic approach to varve identification and tested through tephra analysis.

The second element of the thesis is addressed through the combination of robust site-based varve chronologies and the identification of tephra layers permit the placement of those records in absolute time. It highlights the potential for tephrochronology to link records and refine the STS therefore breaking away from the traditional methods (section 11.3 and 11.6) which assume either synchronous sedimentological or climatic shifts. While time-consuming and logistically difficult, tephra studies seem to be the most objective way to make progress in the process of linking varve studies and therefore elucidating the patterns and rates of deglaciation. The final combination of tephra and varves within a Bayesian age model has also permitted a reappraisal of the data used to constrain deglaciation.

Specific progress toward addressing the aims of this thesis has been made by achieving the following tephra results:

- 1) The first identification of the Askja-S tephra within glacial varves in Sweden.
- 2) The first identification of the Fosen tephra in non-varved sediments in Sweden.
- 3) At Asplången a rhyolitic tephra derived from the Katla volcano is reported from the sediments immediately above the Fosen tephra. If identified elsewhere this might be an important marker in the younger varved sediments north of Asplången.
- 4) The varves have provided refined ages for the tephra layers identified with the new age of the Askja-S being $11,043 \pm 42$ cal. yrs BP which supports the assessment of Ott *et al.* (2016).
- 5) The first placement of Swedish varve chronologies into the early Holocene using tephra layers

- 6) The presence of the Askja-S at Asplången indicates that the site was deglaciated during the early Holocene at $11,077 \pm 42$ cal. yrs BP. This age is ca 1,200 years younger than the current deglaciation model.

A review of the bio- and lithostratigraphic data indicates that the colour change from brown to grey varves appears not to have a consistent source and cannot be robustly characterised. Therefore, this colour change may not represent the final drainage of the BIL and so direct dating of this event has not been possible during this thesis.

The data presented here query the purported synchronicity of climatic events with glacial lake stages and this suggests the Greenland ice cores may not provide a direct template for the stages of deglaciation of the FIS. This viewpoint needs to be critically reappraised with additional studies to validate the findings outlined in Chapter 11.

The deglaciation chronology outlined in this thesis prompted a reappraisal of the absolute dating information for the most recent synthesis of FIS deglaciation (Stroeven *et al.* 2016). This review, focussed on 12.5-10.0 ka BP, indicates that this period is constrained by 89 published radiocarbon dates, of which only 13 meet robust standards (outlined in Table 11.13). Of the remaining 13 dates, six are based on bulk organic material and/or do not provide sufficient information to assess for hard water effects. One of the thirteen dates directly contradicts the chronology proposed in this thesis but the date (from an isolation basin) is disputed by the original authors due to low organic content in the bulk sediment sample. Additionally, the deglaciation chronology appears to be strongly supported by OSL and cosmogenic ages that have sufficiently large uncertainties that they permit the early Holocene ages proposed in this thesis. Addressing the areas with the least chronological information using dating tools that are able to address the deglaciation at sufficient precision is a priority for future work.

Finally, the work has highlighted the need for additional research in order to constrain the age of the final drainage of the Baltic Ice Lake and propose links to climate shifts across the North Atlantic region. Prior to this research the final drainage of the BIL is considered to have occurred shortly after sites in Östergötland became ice-free (e.g. Brunnberg, 1995) and this event had been attributed to the interval around the Younger Dryas-Preboreal transition (Andrén *et al.*, 1999; Björck *et al.*, 2002). Given the results of this thesis and the re-appraisal of the Stroeven *et al.* (2016) deglaciation chronology, the Asplången and Svinstadsjön sites deglaciated later than the period identified in the established model, during the early Holocene (ca 11.0 cal. ka BP). This is based on the presence of proximal varves at Asplången ca 11.0 cal. ka BP, and that by inference the ice margin was within the MSEMZ. Therefore, the BIL

drained after the Asplången site was deglaciated. This implies that BIL drainage and the consequent release of freshwater into the North Atlantic/Nordic Seas could be linked to short-lived early Holocene climatic events around the North Atlantic margins. These conclusions are made tentatively as no direct palaeoclimatic evidence has been obtained from these new varve thickness records. Therefore, these conclusions should be viewed as a hypothesis to be tested in the future.

Until present, the final drainage of the BIL has been inferred largely from glacial morphostratigraphy and chronologically-constrained by radiocarbon dates, pollen stratigraphy and climatic wiggle-matching to the Greenland ice-core chronology. The wealth of research on the climatic events that characterise the LGIT and the identification of these events within the Greenland ice-core records means that evidence of events found in Greenland are matched to other European archives often without sufficient chronological basis. Researchers may place emphasis around specific sediment boundaries, geomorphological features or time intervals where a climatic oscillation is expected to occur. For example, the colour change from brown to grey varves has been linked to the final drainage of the Baltic Ice Lake, and it has been proposed that this drainage caused freshwater forcing in the North Atlantic leading to abrupt climatic cooling (Björck *et al.*, 1996, 1997). As a result of this accepted but largely untested chain of events, it is possible to attribute the colour change in the varved sediments to a climatostratigraphic boundary. This problem of 'reinforcement syndrome' (Blaauw, 2012) is also apparent in the correlation of key ice-marginal landforms in southern Sweden to the climatic events that are observed in the Greenland ice-core chronology (e.g. Stroeve *et al.*, 2016).

A means of testing the synchronicity of glacial events and climatic change, as recorded in Greenland, is via independently dated high-resolution chronologies, but these dates are currently lacking in the context of the FIS deglaciation. This thesis demonstrates the potential of tephrochronology and varve chronology in resolving these issues. Below a series of priorities for future testing of these challenges are highlighted.

12.3 Ideas for future work:

These priorities for future research focus on increasing spatial and temporal precision in the STS. It is structured according to specific questions raised and relies on the refined knowledge gained from the construction of varve chronologies and tephrostratigraphy that has been developed in this thesis. It is recommended that this knowledge is applied for the next stage of research on the STS and is targeted at four key localities in southern Sweden:

1. sites in the northern part of the Kristiansson (1986) varve chronology,
2. sites *ca* 25 km north of Asplången,
3. varved sediments in the Baltic Proper that contain the colour change from brown to grey varves, and
4. varved sediment records in the MSEMZ.

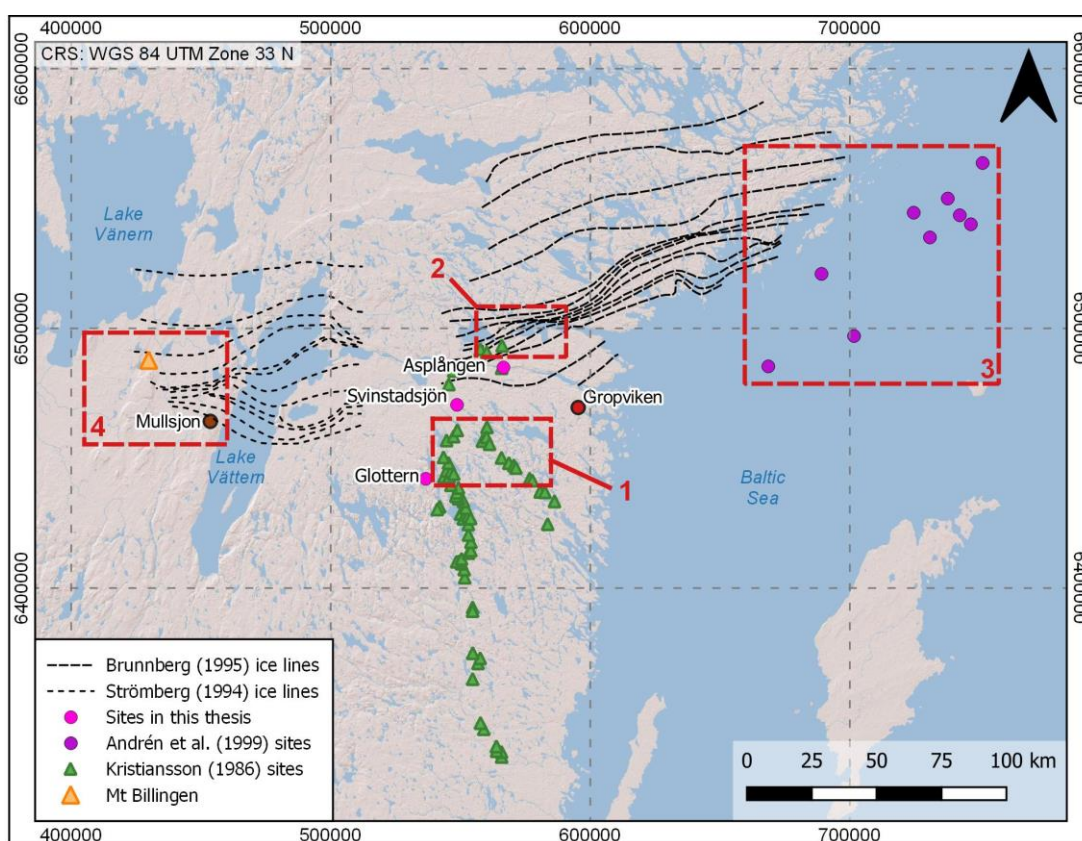


Figure 12-1. Target areas for future research on the STS.

1) Varve sites in the north of the Kristiansson (1986) chronology, 2) varve sites *ca* 25 km north of the Asplången site, 3) varve records from the Baltic Proper, 4) varve records in the MSEMZ, in particular the Mulsjön site.

12.3.1 Target area 1 – Refining the absolute chronology and identifying the ‘missing’ years in the STS (12.5 to 11 ka) using the northern Kristiansson (1986) varve records

The results from this thesis demonstrate that there are *ca* 1,200 yrs “missing” in the late Younger Dryas-Preboreal part of the STS. These varves are likely located in the varve records between Glottern and Svinstadsjön, i.e. the northern sites in the Kristiansson (1986) composite chronology (Figure 12-1). These “missing” varves are due to two key reasons that will be fundamental to the methodological approach that should be adopted in future research. These sites are likely to have thin (<cm-scale) varves that are unidentifiable at the macroscale and/or missing varves due to spatial differences in varve formation across the lake basin as a result of uneven basin bathymetry that may cause “blocking” of sediment density flows (Chapter 11, section 11.2.4). Therefore, it is pertinent that in future research thorough basin surveys are conducted in order to identify the spatial distribution of varves and to establish any missing varves. Secondly it is fundamental that varve records are analysed under thin section.

An additional consideration when targeting these sites will be the approach adopted in order to create a composite chronology. It is essential that this new composite chronology can be reliably linked to the Svinstadsjön and Asplången sites. Tephrostratigraphy and tephrochronology will be critical in this regard and tephra must be looked for in these varve records. In order to maximise the returns on time and financial investment in future research projects, long (>200 yrs, ideally >500 yrs) sequences should be targeted. Given that the Askja-S has been identified in the base of the Asplången sequence, and that varve sites to the south of Asplången will be older than the Askja-S (*ca* 11.0 cal. yrs BP), it is likely that other, older tephras will be found in the target area in the Kristiansson (1986) chronology. It is anticipated that the Askja-S will be found in the northernmost target sites, but also the southernmost sites in target area 1 (Figure 12-1) may contain the Hässeldalen, Abernethy and/or Vedde Ash tephras.

Whilst tephra has been found within the varved sediments at Svinstadsjön and Asplången, shard concentrations were extremely low. In order to maximise the likelihood of extracting sediment that will contain enough shards for chemical analysis, researchers will need to extract multiple (at least three) cores from each site. The extraction of multiple cores can also be used to assess the spatial distribution of varved sediments at each site to identify any missing varves.

12.3.2 Target area 2 – Extending the ‘known’ tephra lattice in varve records from sites north of Asplången (<11 ka)

This thesis demonstrates the potential to create a tephra lattice for the STS through identification of multiple tephtras within multiple varve records throughout the Lateglacial-Holocene periods. This will provide the required precision to test the existing deglaciation chronology and also test the chronology proposed in this thesis. The identification of the Fosen tephra stratigraphically above the uppermost varve in the Asplången site demonstrates an excellent opportunity to find the Fosen tephra within varved sediments. Since the Fosen tephra is no more than ca 200 yrs older than the uppermost varve in the Asplången sequence, this tephra could be found no more than 200 v yrs north of the Asplången sequence. Using the published ice margin lines as a broad guide, the Fosen tephra should in theory be located within glacial varves in sites located ca 25 km north of Asplången (Target area 2; Figure 12-1). Identification of this tephra within glacial varves will also enable the published ice margin lines to be tested as well as providing a more precise estimate of the number of varve years between the Fosen and Askja-S tephtras. Coincidentally, if the Fosen is indeed located ca 200 v yrs above the uppermost varve in the Asplången record, and the colour change model is correct, this would place the Fosen tephra within the red-coloured (brackish Yoldia Sea stage) varves that have been identified in the Östergötland and Stockholm area. This would in turn enable this Baltic Sea phase to be independently dated, thus providing a means of testing the existing marine radiocarbon dates for the Yoldia Sea stage (e.g. Brunnberg and Possnert, 1992).

12.3.3 Target area 3 – Constraining the timing of changes in state of the BIL from varve records in the Baltic Proper

The results from this thesis indicate that the colour change between the brown and grey varves in the STS may not be synchronous across the Baltic Ice Lake. Moreover, the climatic signal that has been derived from this colour change through synchronisation of the Baltic Proper pollen stratigraphy with the Greenland ice core chronology may also be inaccurate. If this hypothesis is correct, then the use of the colour change as a “proxy” for BIL drainage may also be flawed. In order to test the synchronicity of the colour change from brown to grey varves, tephrostratigraphy and tephrochronology must be applied to the Baltic Proper varve record. If the colour change in the Baltic Proper is indeed synchronous with the colour change identified in the Asplången and Svinstadsjön varve records, as previously proposed, it is expected that the Askja-S tephra should be located within the basal brown varves in the Baltic Proper varve chronology. Identification of tephtras within the Baltic Proper

varve chronology will also enable the assumed climatic synchronicity with Greenland to be tested and an assessment of potential leads and lags between vegetation response to climatic change. Fundamental to this approach will be the development of accurate varve counts which at present have been achieved through macroscale observations on core surfaces (Andrén *et al.*, 1999). Given that the mean varve thickness in the Baltic Proper record is 4 mm, and that in this thesis varves <cm-scale were consistently misidentified at the macroscale, thin section analysis will be essential when re-appraising the chronology. It is therefore recommended that the chronology (Target site 3, Figure 12-1) is re-examined using a combination of thin sections and tephrochronology.

12.3.4 Target area 4 – Accurate and precise timing of the final BIL drainage using varved sediment records in the MSEMZ

Re-appraisal of the deglaciation chronology in the MSEMZ indicates that robust, high-precision dates are lacking for this part of the deglaciation chronology. Given that this area is of vital importance for reconstructing the timing of BIL drainage, future research should focus on the varve records within the MSEMZ (Target area 4; Figure 12-1). A key record that will enable the deglaciation of the FIS prior to BIL drainage to be more accurately assessed is the varve record from Lake Mullsjön (Figure 12-1). Since volcanic ash has been reported, but not chemically characterised from this site, the Mullsjön varve chronology (Wohlfarth *et al.*, 1993) is of high importance for future STS research. Identification and chemical characterisation of tephra in the Mullsjön site will enable the varve record to be anchored to an absolute timescale, thus providing a means to test the existing site chronology which is largely based on unreliable radiocarbon dates (Table 3-3) and biostratigraphy (Chapter 3). Tephrochronology will again, enable the use of pollen stratigraphy as a chronostratigraphic marker to be re-examined and the synchronicity/asynchronicity of vegetation and climate to be assessed. In addition, the chemical characterisation of tephra within the Mullsjön varve record will enable the ice margin lines proposed by Strömberg (1994) and Brunnberg (1995) to be tested since this site has been correlated to the Asplången varve record. Fundamental to this work will be the development of an accurate varve chronology and so thin section analysis should also be applied to this record.

References

- Abbott, P. M. and Davies, S. M. (2012) 'Volcanism and the Greenland ice-cores: The tephra record', *Earth-Science Reviews*. Elsevier B.V., 115(3), pp. 173–191.
- Agrell, H., Friberg, N. and Oppgård, R. (1976) 'The Vimmerby line - an ice-margin zone in north-eastern Småland', *Svensk Geografisk Årsbok*, 52, pp. 71–91.
- Aitchison, J. (1982) 'The statistical analysis of compositional data', *Journal of the Royal Statistical Society: Series B Methodological*, 44(2), pp. 139–177.
- Alexanderson, H. and Murray, A. S. (2012) 'Problems and potential of OSL dating Weichselian and Holocene sediments in Sweden', *Quaternary Science Reviews*. Elsevier Ltd, 44, pp. 37–50.
- Alexandrin, M. Y., Darin, A. V., Kalugin, I. A., Dolgova, E. A., Grachev, A. M. and Solomina, O. N. (2018) 'Annual Sedimentary Record From Lake Donguz-Orun (Central Caucasus) Constrained by High Resolution SR-XRF Analysis and Its Potential for Climate Reconstructions', *Frontiers in Earth Science*.
- Alley, R. B. (2007) 'Wally was right: predictive ability of the North Atlantic "conveyor belt" hypothesis for abrupt climate change', *Annual Review of Earth and Planetary Science*, 35, pp. 241–272.
- Alley, R. B. and Ágústsdóttir, A. M. (2005) 'The 8k event: Cause and consequences of a major Holocene abrupt climate change', *Quaternary Science Reviews*, 24(10–11), pp. 1123–1149.
- Amann, B., Mauchle, F. and Grosjean, M. (2014) 'Quantitative high-resolution warm season rainfall recorded in varved sediments of Lake Oeschinen, northern Swiss Alps: calibration and validation AD 1901-2008', *Journal of Paleolimnology*, 51, pp. 375–391.
- Andersen, B. G. (1979) 'The deglaciation of Norway 15,000-10,000 BP', *Boreas*, 8, pp. 79–87.
- Andersen, B. G., Mangerud, J., Sørensen, R., Reite, A., Sveian, H., Thoresen, M. and Bergstrøm, B. (1995) 'Younger Dryas ice-marginal deposits in Norway', *Quaternary International*, 28, pp. 147–169.
- Andersson, G. (1998) 'Deglaciation pattern and dynamics in the Bolmen area, southwestern Sweden', *LUNDQUA Thesis*, 42, pp. 1–22.
- Andrén, T. (1990) 'Till Stratigraphy and Ice Recession in the Bothnian Bay', *Research*

Report 18 University of Stockholm Department of Quaternary, pp. 1–59.

Andrén, T., Björck, J. and Johnsen, S. (1999) 'Correlation of Swedish glacial varves with the Greenland (GRIP) oxygen isotope record', *Journal of Quaternary Science*, 14(4), pp. 361–371.

Andrén, T., Björck, S., Andrén, E., Conley, D., Zillén, L. and Anjar, J. (2011) 'The Development of the Baltic Sea Basin During the Last 130 ka', in Harff, J., Björck, S. and Hoth, P. (eds) *the Baltic Sea Basin. Central and Eastern European Development Studies (CEEDES)*. Heidelberg, Berlin: Springer, pp. 165–188.

Andrén, T., Lindeberg, G. and Andrén, E. (2002) 'Evidence of the final drainage of the Baltic Ice Lake and the brackish phase of the Yoldia Sea in glacial varves from the Baltic Sea', *Boreas*, 31(3), pp. 226–238.

Anjar, J., Larsen, N. K., Håkansson, L., Moller, P., Linge, H., Fabel, D. and Xu, S. (2014) 'A ^{10}Be -based reconstruction of the last deglaciation in southern Sweden', *Boreas*, 43, pp. 132–148.

Antevs, E. (1922) 'On the late-glacial and post-glacial history of the Baltic', *American Geographical Society*, 12, pp. 602–612.

Antevs, E. (1931) 'Late Glacial clay chronology of North America: Annual Report of the Board of Regents of the Smithsonian Institution for the Year Ended June 30', pp. 313–326.

Antevs, E. (1935) 'Telecorrelations of varve curves', *Geologiske Foreningens i Stockholm Forhandlingar*, 57(1), pp. 47–58.

Antevs, E. (1954) 'Chronology of the deglacial and neothermal ages: a reply', *Journal of Geology*, 62(5), pp. 516–521.

Arnold, J. R. and Libby, W. F. (1949) 'Age determination by radiocarbon content: Check with samples of known age', *Science*, 110, pp. 678–680.

Van Asch, N., Lutz, A. F., Duijkers, M. C. H., Heiri, O., Brooks, S. J. and Hoek, W. Z. (2012) 'Rapid climate change during the Weichselian Lateglacial in Ireland: Chironomid-inferred summer temperatures from Fiddaun, Co. Galway', *Palaeogeography, Palaeoclimatology, Palaeoecology*. Elsevier B.V., 315–316, pp. 1–11.

Ashley, G. M. (1975) 'Rhythmic sedimentation in Glacial Lake Hitchcock, Massachusetts Connecticut', in Jopling, A. V and McDonald, B. C. (eds) *Society of Economic Paleontologists and Mineralogists Special Publication*. 23rd edn, pp. 304–320.

- Austin, W. E. N., Bard, E., Hunt, J. B., Kroon, D. and Peacock, J. D. (1995) 'The 14C age of the Icelandic Vedde Ash: implications for Younger Dryas marine reservoir age corrections', *Radiocarbon*, 37(1), pp. 53–62.
- Avşar, U., Jónsson, S., Avşar, Ö. and Schmidt, S. (2016) 'Journal of Geophysical Research: Solid Earth', *Journal of Geophysical Research: Solid Earth*, 121, pp. 1183–1201.
- Bakke, J., Dahl, S. O. and Nesje, A. (2005) 'Lateglacial and early Holocene palaeoclimatic reconstruction based on glacier fluctuations and equilibrium-line altitudes at northern Folgefonna, Hardanger, western Norway', *Journal of Quaternary Science*, 20(2), pp. 179–198.
- Bakke, J., Lie, Ø., Heegaard, E., Dokken, T., Haug, G., Birks, H., Dulski, P. and Nilsen, T. (2009) 'Rapid oceanic and atmospheric changes during the Younger Dryas cold period', *Nature Geoscience*, 2, pp. 202–205.
- Balascio, N., Zhang, Z., Bradley, R., Perren, B., Dahl, S. and Bakke, J. (2011) 'A multi-proxy approach to assessing isolation basin stratigraphy from the Lofoten Islands, Norway', *Quaternary Research*, 75, pp. 288–300.
- Baltrūnas, V., Švedas, K. and Pukelytė, V. (2007) 'Palaeogeography of South Lithuania during the last ice age', *Sedimentary Geology*, 193(1–4), pp. 221–231.
- Bard, E., Arnold, M. and Duplessy, J.-C. (1991) 'Reconciling the sea level record of the last deglaciation with 18O spectra from deep sea cores', *Radiocarbon Dating: Recent Applications and Future Potential*, 1, pp. 67–73.
- Bard, E., Arnold, M., Mangerud, J., Paterne, M., Labeyrie, L., Duprat, J., Mélières, M. A., Sønsteegaard, E. and Duplessy, J. C. (1994) 'The North Atlantic atmosphere-sea surface 14C gradient during the Younger Dryas climatic event', *Earth and Planetary Science Letters*, 126(4), pp. 275–287.
- Le Bas, M. J., Maitre, R. W. L., Streckeisen, A. and Zanettin, B. (1986) 'A chemical classification of volcanic rocks based on the total alkali-silica diagram', *Journal of Petrology*, 27(3), pp. 745–750.
- Battarbee, R., Juggins, S., Gasse, F., Anderson, N., Bennion, H., Cameron, N., Ryves, D., Pailles, C., Chalieu, F. and Telford, R. (2001) 'An Information System for Palaeoenvironmental Reconstruction', *European Diatom Database (EDDI)*, 81, pp. 1–94.
- Bendle, J. M. (2017) 'The timing, dynamics and palaeoclimatic significance of ice sheet deglaciation in central Patagonia, southern South America'.

- Bendle, J. M., Palmer, A. P. and Carr, S. J. (2015) 'A comparison of micro-CT and thin section analysis of Lateglacial glaciolacustrine varves from Glen Roy, Scotland', *Quaternary Science Reviews*, 114, pp. 61–77.
- Bendle, J. M., Palmer, A. P., Thorndycraft, V. R. and Matthews, I. P. (2017) 'High-resolution chronology for deglaciation of the Patagonian Ice Sheet at Lago Buenos Aires (46.5°S) revealed through varve chronology and Bayesian age modelling', *Quaternary Science Reviews*, 177, pp. 314–339.
- Benn, D. I. (1996) 'Subglacial and subaqueous processes near a glacier grounding line: sedimentological evidence from a former ice-dammed lake, Achnasheen, Scotland', *Boreas*, 25, pp. 23–36.
- Bennett, M. R., Huddart, D. and Thomas, G. S. P. (2002) 'Facies architecture within a regional glaciolacustrine basin: Copper River, Alaska', *Quaternary Science Reviews*, 21(20–22), pp. 2237–2279.
- Berglund, B. E. (1979) 'The deglaciation of southern Sweden 13,000-10,000 BP', *Boreas*, 8, pp. 89–117.
- Berglund, M. (1995) 'The Late Weichselian deglaciation, vegetational development and shore displacement in Halland, southwestern Sweden', *LUNQUA Thesis*, 35, pp. 1–115.
- Bergström, R. (1968) 'Stratigrafi och isrecesion i södra Västerbotten', *Sveriges Geologiska Undersökning*, C-634, pp. 1–76.
- Björck, J., Andrén, T., Wastegård, S., Possnert, G. and Schoning, K. (2002) 'An event stratigraphy for the Last Glacial-Holocene transition in eastern middle Sweden: Results from investigations of varved clay and terrestrial sequences', *Quaternary Science Reviews*, 21(12–13), pp. 1489–1501.
- Björck, J., Possnert, G. and Schoning, K. (2001) 'Early holocene deglaciation chronology in Västergötland and Närke, southern Sweden - Biostratigraphy, clay varve, 14C and calendar year chronology', *Quaternary Science Reviews*, 20(12), pp. 1309–1326.
- Björck, J. and Wastegård, S. (1999) 'Climate oscillations and tephrochronology in eastern middle Sweden during the last glacial-interglacial transition', *Journal of Quaternary Science*, 14(5), pp. 399–410.
- Björck, S. (1995) 'A review of the history of the Baltic Sea, 13.0-8.0 ka BP', *Quaternary International*, 27(C), pp. 19–40.
- Björck, S. (1995) 'A review of the history of the Baltic Sea, 13.0– 8.0 BP', *Quaternary*

International, 27, pp. 19–40.

Björck, S. (2008) 'The late Quaternary development of the Baltic Sea basin', in The BACC author team (ed.) *Assessment of climate change for the Baltic Sea Basin*. Heidelberg, Berlin: Springer.

Björck, S., Bennike, O., Possnert, G., Wohlfarth, B. and Digerfeldt, G. (1998) 'A high-resolution ¹⁴C dated sediment sequence from southwest Sweden: age comparisons between different components of the sediment', *Journal of Quaternary Science*, 13, pp. 85–89.

Björck, S., Berglund, B. E. and Digerfeldt, G. (1988) 'New aspects on the deglaciation chronology of South Sweden', *Geographica Polonica*, 55, pp. 37–49.

Björck, S. and Digerfeldt, G. (1982) 'Late Weichselian shore displacement at Hunneberg, southern Sweden, indicating complex uplift', *Geologiska Föreningens i Stockholm Förhandlingar*, 104, pp. 131–155.

Björck, S. and Digerfeldt, G. (1984) 'Climatic changes at Pleistocene/Holocene boundary in the Middle Swedish endmoraine zone, mainly inferred from stratigraphic indications', in Mörner, N.-A. and Karlén, W. (eds) *Climatic Changes on a Yearly to Millennial Basis*. Dordrecht: Reidel Publishing Company, pp. 37–56.

Björck, S. and Digerfeldt, G. (1986) 'Late Weichselian-Early Holocene shore displacement west of Mt. Billingen within the Middle Swedish end-moraine zone', *Boreas*, 15, pp. 1–18.

Björck, S. and Digerfeldt, G. (1989) 'Lake Mulsjön – a key site for understanding the final stage of the Baltic Ice Lake east of Mt Billingen', *Boreas*, 18, pp. 209–219.

Björck, S. and Digerfeldt, G. (1991) 'Allerød–Younger Dryas sea level change in southwestern Sweden and their relation to the Baltic Ice Lake development', *Boreas*, 20, pp. 115–133.

Björck, S. and Håkansson, S. (1982) 'Radiocarbon dates from Late Weichselian lake sediments in South Sweden as a basis for chronostratigraphic subdivision', *Boreas*, 11, pp. 141–150.

Björck, S., Koç, N. and Skog, G. (2003) 'Consistently large marine reservoir ages in the Norwegian Sea during the last deglaciation', *Quaternary Science Reviews*, 22, pp. 429–435.

Björck, S., Kromer, B., Johnsen, S., Bennike, O., Hammarlund, D., Lemdahl, G., Possnert, G., Rasmussen, T. L., Wohlfarth, B., Hammer, C. U. and Spurk, M. (1996) 'Synchronized terrestrial-atmospheric deglacial records around the North Atlantic',

Science, 274(5290), pp. 1155–1160.

Björck, S. and Möller, P. (1987) 'Late Weichselian environmental history in southeastern Sweden during the deglaciation of the Scandinavian ice sheet', *Quaternary Research*, 28(1), pp. 1–37.

Björck, S., Rundgren, M., Ingólfsson, Ó. and Funder, S. (1997) 'The Preboreal oscillation around the Nordic Seas: terrestrial and lacustrine responses', *Journal of Quaternary Science*, 12(6), pp. 455–465.

Björck, S., Walker, M. J. C., Cwynar, L. C., Johnsen, S., Knudsen, K. L., Lowe, J. J. and Wohlfarth, B. (1998) 'An event stratigraphy for the last termination in the North Atlantic region based on the Greenland ice-core record: a proposal by the INTIMATE group', *Journal of Quaternary Science*, 13(4), pp. 283–292.

Björnsjö, N. (1949) 'Israndstudier i södra Bohuslän', *Sveriges Geologiska Undersökning C*, 504, p. 321.

Blaauw, M. (2012) 'Out of tune: the dangers of aligning proxy archives', *Quaternary Science Reviews*, 36, pp. 38–49.

Blaauw, M., Christen, J. A., Mauquoy, D., van der Plicht, J. and Bennett, K. D. (2007) 'Testing the timing of radiocarbon-dated events between proxy archives', *The Holocene*, 17(2), pp. 283–288.

Blake, K. P. and Olsen, L. (1999) 'Deglaciation of the Svartisen area, northern Norway, and isolation of a large ice mass in front of the Fennoscandian Ice Sheet', *Norsk Geografisk Tidsskrift*, 53(1), pp. 1–16.

Blockley, S., Candy, I., Matthews, I., Langdon, P., Langdon, C., Palmer, A., Lincoln, P., Abrook, A., Taylor, B., Conneller, C., Bayliss, A., MacLeod, A., Deepprose, L., Darvill, C., Kearney, R., Beavan, N., Staff, R., Bamforth, M., Taylor, M. and Milner, N. (2018) 'The resilience of postglacial hunter-gatherers to abrupt climate change', *Nature Ecology and Evolution*. Springer US, 2(5), pp. 810–818.

Blockley, S. P. ., Bourne, A. J., Brauer, A., Davies, S. M., Hardiman, M., Harding, P. R., Lane, C. S., MacLeod, A., Matthews, I. P., Pyne-O'Donnell, S. D. F., Rasmussen, S. O., Wulf, S. and Zanchetta, G. (2014) 'Tephrochronology and the extended intimate (integration of ice-core, marine and terrestrial records) event stratigraphy 8–128ka b2k', *Quaternary Science Reviews*, 106, pp. 88–100.

Blockley, S. P. E., Lane, C. S., Hardiman, M., Rasmussen, S. O., Seierstad, I. K., Steffensen, J. P., Svensson, A., Lotter, A. F., Turney, C. S. M. and Bronk Ramsey, C. (2012) 'Synchronisation of palaeoenvironmental records over the last 60,000

years, and an extended INTIMATE 1 event stratigraphy to 48,000 b2k', *Quaternary Science Reviews*, 36, pp. 2–10.

Blockley, S. P. E. and Pinhasi, R. (2011) 'A revised chronology for the adoption of agriculture in the Southern Levant and the role of Lateglacial climatic change', *Quaternary Science Reviews*. Elsevier Ltd, 30(1–2), pp. 98–108.

Blockley, S. P. E., Pyne-O'Donnell, S. D. F., Lowe, J. J., Matthews, I. P., Stone, A., Pollard, A. M., Turney, C. S. M. and Molyneux, E. G. (2005) 'A new and less destructive laboratory procedure for the physical separation of distal glass tephra shards from sediments', *Quaternary Science Reviews*, 24, pp. 1952–1960.

Blockley, S. P. E., Ramsey, C. B., Lane, C. S. and Lotter, A. F. (2008) 'Improved age modelling approaches as exemplified by the revised chronology for the Central European varved lake Soppensee', *Quaternary Science Reviews*, 27(1–2), pp. 61–71.

Bloemsa, M., Croudace, I., Daly, J. S., Edwards, R. J., Francus, P., Galloway, J. M., Gregory, B. R. B., Steven Huang, J. J., Jones, A. F., Kylander, M., Löwemark, L., Luo, Y., Maclachlan, S., Ohlendorf, C., Patterson, R. T., Pearce, C., Profe, J., Reinhardt, E. G., Stranne, C., Tjallingii, R. and Turner, J. N. (2018) 'Practical guidelines and recent advances in the Itrax XRF core-scanning procedure', *Quaternary International*. Elsevier, 514, pp. 16–29.

Blunier, T., Chappellaz, J., Schwander, J., Dällenbach, A., Stauffer, B., Stocker, T. F., Raynaud, D., Jouze, J., Clausen, H. B., Hammer, C. U. and Johnsen, S. J. (1998) 'Asynchrony of Antarctic and Greenland climate change during the last glacial period', *Nature*, 394, pp. 739–743.

Bodén, P., Fairbanks, R. G., Wright, J. D. and Burckle, L. H. (1997) 'High- resolution stable isotope records from southwest Sweden: the drainage of the Baltic Ice Lake and Younger Dryas ice marginal oscillation', *Paleoceanography*, 12, pp. 39–49.

Boës, X., Rydberg, J., Martinez-Cortizas, A., Bindler, R. and Renberg, I. (2011) 'Evaluation of conservative lithogenic elements (Ti, Zr, Al, and Rb) to study anthropogenic element enrichments in lake sediments', *Journal of Paleolimnology*, 46(1), pp. 75–87.

Bond, G., Broecker, W., Johnsen, S., McManus, J., Labeyrie, L., Jouzel, J. and Bonani, G. (1993) 'Correlations between climate records from North Atlantic sediments and Greenland ice', *Nature*, 365(6442), pp. 143–147.

Bond, G., Showers, W., Cheseby, M., Lotti, R., Almasi, P., DeMenocal, P., Priore, P., Cullen, H., Hajdas, I. and Bonani, G. (1997) 'A pervasive millennial-scale cycle in

- North Atlantic Holocene and glacial climates', *Science*, 278(5341), pp. 1257–1266.
- Borgström, I. (1989) 'Meddelanden från Naturgeografiska institutionen vid Stockholms universitet Terrängformerna och den glaciala utvecklingen i södra fjällen: Geomorphology and Glacial History of the Middle Swedish Mountains', *Department of Physical Geography. Stockholm University, Stockholm*, A234, pp. 1–133.
- Boygle, J. (1999) 'Variability of tephra in lake and catchment sediments, Svinavatn, Iceland', *Global and Planetary Change*, 21(1–3), pp. 129–149.
- Boyle, J. F., Chiverrell, R. C. and Schillereff, D. (2015) 'Approaches to water content corrections and calibration for μ XRF core scanning: Comparing x-ray scattering with simple regression of element concentrations', in Rothwell, G. and Croudace, I. (eds) *Micro-XRF Studies of Sediment Cores, Development in Paleoenvironmental Research*. Springer, pp. 373–390.
- Brauer, A. (2004) 'Annually laminated lake sediments and their palaeoclimatic relevance.', in Fischer, H., Kumke, T., Lohmann, G. and Negendank, J. (eds) *The Climate in Historical Times*. Springer, pp. 109–127.
- Brauer, A. and Casanova, J. (2001) 'Chronology and depositional processes of the laminated sediment record from Lac d'Annecy, French Alps', *Journal of Paleolimnology*, 25, pp. 163–177.
- Brauer, A., Dulski, P., Mangili, C., Mingram, J. and Liu, J. (2009) 'The potential of varves in high-resolution paleolimnological studies', *PAGES news*, 17(3), pp. 96–98.
- Brauer, A., Endres, C. and Negendank, J. F. W. (1999) 'Lateglacial calendar year chronology based on annually laminated sediments from Lake Meerfelder Maar, Germany', *Quaternary International*, 61(1), pp. 17–25.
- Brauer, A., Haug, G. H., Dulski, P., Sigman, D. M. and Negendank, J. F. W. (2008) 'An abrupt wind shift in western Europe at the onset of the Younger Dryas cold period', *Nature Geoscience*, 1(8), pp. 520–523.
- Breckenridge, A. (2015) 'The Tintah-Campbell gap and implications for glacial Lake Agassiz drainage during the Younger Dryas cold interval', *Quaternary Science Reviews*, 117, pp. 124–134.
- Broecker, W. S. (1998) 'Paleocean circulation during the last deglaciation: a bipolar seesaw?', *Paleoceanography*, 13, pp. 119–121.
- Broecker, W. S. (2006) 'Was the Younger Dryas triggered by a flood?', *Science*, 312, pp. 1146–1148.

- Broecker, W. S., Kennett, J. P., Flower, B. P., Teller, J. T., Trumbore, S., Bonani, G. and Wolfli, W. (1989) 'Routing of meltwater from the Laurentide Ice', 341, pp. 318–321.
- Bronk Ramsey, C. (2008) 'Deposition models for chronological records', *Quaternary Science Reviews*, 27(1–2), pp. 42–60.
- Bronk Ramsey, C. (2009) 'Bayesian Analysis of Radiocarbon Dates', *Radiocarbon*, 51(1), pp. 337–360.
- Bronk Ramsey, C., Albert, P. G., Blockley, S. P. E., Hardiman, M., Housley, R. A., Lane, C. S., Lee, S., Matthews, I. P., Smith, V. C. and Lowe, J. J. (2015) 'Improved age estimates for key Late Quaternary European tephra horizons in the RESET lattice', *Quaternary Science Reviews*, 118, pp. 18–32.
- Bronk Ramsey, C., Staff, R. A., Bryant, C. L., Brock, F., Kitagaw, H., van der Plicht, J., Schlolaut, G., Marshall, M. H., Brauer, A., Lamb, H. F., Payne, R. L., Tarasov, P. E., Haraguchi, T., Gotanda, K., Yonenobu, H., Yokoyama, Y., Tada, R. and Nakagawa, T. (2012) 'A Complete Terrestrial Radiocarbon Record for 11.2 to 52.8 kyr B.P.', *Science*, 338(6105), pp. 370–374.
- Brooks, S. J. and Langdon, P. G. (2014) 'Summer temperature gradients in northwest Europe during the Lateglacial to early Holocene transition (15-8 ka BP) inferred from chironomid assemblages', *Quaternary International*. Elsevier Ltd and INQUA, 341, pp. 80–90.
- Brooks, S. J., Langdon, P. G. and Heiri, O. (2007) *The Identification and Use of Palaeartic Chironomidae Larvae in Palaeoecology. Technical Guide No. 10*.
- Brunnberg, L. (1995) 'Clay-varve chronology and deglaciation during the Younger Dryas and Pre-boreal in the easternmost part of the Middle Swedish Ice Marginal Zone', *PhD Thesis. Stockholm University*, pp. 1–94.
- Brunnberg, L. and Possnert, G. (1992) 'Radiocarbon dating of the Goti-Finiglacial boundary of the Swedish Time Scale', *Boreas*, 21(1), pp. 89–96.
- Burpee, B. T., Anderson, D. and Saros, J. E. (2018) 'Assessing ecological effects of glacial meltwater on lakes fed by the Greenland Ice Sheet: The role of nutrient subsidies and turbidity', *Arctic, Antarctic, and Alpine Research*. Taylor & Francis, 50(1), pp. 1–15.
- Caldenius, C. (1924) 'Ragundasjön stratigrafi och geokronologi', *Sveriges Geologiska Undersökning*, Cu 12, p. 91.
- Caldenius, C. (1932) 'Las glaciaciones Cuaternarias en la Patagonia Y Tierra del

- Fuego', *Geografiska Annaler: Series A, Physical Geography*, pp. 1–164.
- Caldenius, C. (1942) 'Gotiglaciala israndsstadier och jökelbäddar i Haland. Förelöpande meddelande', *Geologiska Föreningens i Stockholm Förhandlingar*, 63, pp. 163–183.
- Caldenius, C. (1944) 'Baltiska issjöns sänkning till Västerhavet. En geokronologisk studie', *Geologiska Föreningens i Stockholm Förhandlingar*, 66(366–382).
- Capron, E., Landais, A., Lemieux-Dudon, B., Schilt, A., Masson-Delmotte, V., Buiron, D., Chappellaz, J., Dahl-Jensen, D., Johnsen, S., Leuenberger, M., Louergue, L. and Oerter, H. (2010) 'Synchronising EDML and NorthGRIP ice cores using d18O of atmospheric oxygen (d18O_{atm}) and CH₄ measurements over MIS5 (80-123 kyr)', *Quaternary Science Reviews*, 29, pp. 222–234.
- Cato, I. (1985) 'The definitive connection of the Swedish geochronological time scale with the present, and the new date of the zero year in Döviken, northern Sweden', *Boreas*, 14(2), pp. 117–122.
- Cato, I. (1987) 'On the definitive connection of the Swedish Time Scale with the present', *Sveriges Geologiska Undersökning*, 68, pp. 1–55.
- Cato, I. (1992) 'Shore displacement data based on lake isolation confirm the postglacial part of the Swedish Geochronological Time Scale', *Sveriges Geologiska Undersökning*, Ca 81, pp. 75–80.
- Cheel, R. J. and Rust, B. R. (1986) 'A sequence of soft-sediment deformation (dewatering) structures in Late Quaternary subaqueous outwash near Ottawa, Canada.', *Sedimentary Geology*, 47, pp. 77–93.
- Church, M. and Gilbert, R. (1975) 'Proglacial Fluvial and Lacustrine Environments', *Glaciofluvial and Glaciolacustrine Sedimentation*, pp. 22–100.
- Clark, J., McCabe, A. M., Bowen, D. Q. and Clark, P. U. (2012) 'Response of the Irish Ice Sheet to abrupt climate change during the last deglaciation', *Quaternary Science Reviews*, 35, pp. 100–115.
- Clark, P. U., Marshall, S. J., Clarke, G. K. C., Hostetler, S. W., Licciardi, J. M. and Teller, J. T. (2001) 'Freshwater forcing of abrupt climate change during the last glaciation', *Science*, 293, pp. 283–287.
- Clark, P. U., Pisias, N. G., Stocker, T. J. F. and Weaver, A. J. (2002) 'The role of the thermohaline circulation in abrupt climate change', *Nature*, 415, pp. 863–869.
- Clement, A. and Peterson, L. (2006) 'Mechanisms of abrupt climate change of the last glacial period', *Reviews of Geophysics*, 46, p. RG4002.

- Cockburn, J. M. H. and Lamoureux, S. F. (2008) 'Inflow and lake controls on short-term mass accumulation and sedimentary particle size in a High Arctic lake: Implications for interpreting varved lacustrine sedimentary records', *Journal of Paleolimnology*, 40(3), pp. 923–942.
- Collins, M., Knutti, R., Arblaster, J., Dufresne, J.-L., Fichet, T., Friedlingstein, P., Gao, X., Gutowski, W. J., Johns, T., Krinner, G., Shongwe, M., Tebaldi, C., Weaver, A. J. and Wehner, M. (2013) 'Long-term Climate Change: Projections, Commitments and Irreversibility', in Stocker, T. ., Qin, D., Plattner, G.-K., Tignor, M., Allen, S. K., Boschung, J., Nauels, A., Xia, Y., Bex, V. and Midgley, P. M. (eds) *Climate Change 2013: The Physical Science Basis. Contribution of Working Group I to the Fifth Assessment Report of the Intergovernmental Panel on Climate Change*. Cambridge, United Kingdom and New York, NY, USA: Cambridge University Press, pp. 1029–1136.
- Cook, E., Davies, S. M., Guðmundsdóttir, E. R., Abbott, P. M. and Pearce, N. J. G. (2018) 'First identification and characterization of Borrobol-type tephra in the Greenland ice cores: new deposits and improved age estimates', *Journal of Quaternary Science*, 33(2), pp. 212–224.
- Coope, G. R. and Lemdahl, G. (1995) 'Regional differences in the Lateglacial climate of northern Europe based on coleopteran analysis', *Journal of Quaternary Science*, 10, pp. 391–395.
- Coope, G. R., Lemdahl, G., Lowe, J. J. and Walkling, G. (1998) 'Temperature gradients in northern Europe during the last glacial–Holocene transition (14–9 14C kyr BP) interpreted from coleopteran assemblages', *Journal of Quaternary Science*, 13(5), pp. 419–433.
- Crookshanks, S. and Gilbert, R. (2008) 'Continuous, diurnally fluctuating turbidity currents in Kluane lake, Yukon Territory, Canada', *Journal of Earth Science*, 45(10), pp. 1123–1138.
- Croudace, I. W., Rindby, A. and Rothwell, R. G. (2008) 'ITRAX: description and evaluation of a new multi-function X-ray core scanner', *Geological Society, London, Special Publications*, 267(1), pp. 51–63.
- Cuven, S., Francus, P. and Lamoureux, S. F. (2010) 'Estimation of grain size variability with micro X-ray fluorescence in laminated lacustrine sediments, Cape Bounty, Canadian High Arctic', *Journal of Paleolimnology*, 44, pp. 803–817.
- Czymzik, M., Brauer, A., Dulski, P., Plessen, B., Naumann, R., von Grafenstein, U. and Scheffler, R. (2013) 'Orbital and solar forcing of shifts in Mid- to Late Holocene

flood intensity from varved sediments of pre-alpine Lake Ammersee (southern Germany)', *Quaternary Science Reviews*, 61, pp. 96–110.

Van Daele, M., Moernaut, J., Silversmit, G., Schmidt, S., Fontijn, K., Heirman, K., Vandoorne, W., De Clercq, M., Van Acker, J., Wolff, C., Pino, M., Urrutia, R., Roberts, S. J., Vincze, L. and De Batist, M. (2014) 'The 600 yr eruptive history of Villarrica Volcano (Chile) revealed by annually laminated lake sediments', *Bulletin of the Geological Society of America*, 133, pp. 130–146.

Dahl, S. O., Lie, Ø., Fjordheim, K., Nesje, A., Lie, Ø. and Matthews, J. A. (2002) 'Timing, equilibrium-line altitudes and climatic implications of two early-Holocene glacier readvances during the Erdalen Event at Jostedalbreen, western Norway', *Holocene*, 12(1), pp. 17–25.

Davies, B. J., Darvill, C. M., Lovell, H., Bendle, J. M., Dowdeswell, J. A., Fabel, D., García, J. L., Geiger, A., Glasser, N. F., Gheorghiu, D. M., Harrison, S., Hein, A. S., Kaplan, M. R., Martin, J. R. V., Mendelova, M., Palmer, A., Pelto, M., Rodés, Á., Sagredo, E. A., Smedley, R. K., Smellie, J. L. and Thorndycraft, V. R. (2020) 'The evolution of the Patagonian Ice Sheet from 35 ka to the present day (PATICE)', *Earth-Science Reviews*. Elsevier, 204(September 2019), p. 103152.

Davies, S. J., Lamb, H. F. and Roberts, S. J. (2015) 'Micro-XRF Core Scanning in Palaeolimnology: Recent Developments', in Croudace, I. and Rothwell, R. (eds) *Micro-XRF Studies of Sediment Cores, Development in Paleoenvironmental Research*. Dordrecht: Springer, pp. 188–226.

Davies, S. M. (2015) 'Cryptotephra: the revolution in correlation and precision dating', *Journal of Quaternary Science*, 30, pp. 114–130.

Davies, S. M., Wastegård, S. and Wohlfarth, B. (2003) 'Extending the limits of the Borrobol Tephra to Scandinavia and detection of new early Holocene tephras', *Quaternary Research*, 59(3), pp. 345–352.

Dean, J. M., Kemp, A. E. S., Bull, D., Pike, J., Patterson, G. and Zolitschka, B. (1999) 'Taking varves to bits: Scanning electron microscopy in the study of laminated sediments and varves', *Journal of Paleolimnology*, 22, pp. 121–136.

Demidov, I. N., Houmark-Nielsen, M., Kjær, K. H. and Larsen, E. (2006) 'The last Scandinavian Ice Sheet in northwestern Russia: ice flow patterns and decay dynamics', *Boreas*, 35, pp. 425–443.

Deschamps, P., Durand, N., Bard, E., Hamelin, B., Camoin, G., Thomas, A. L., Henderson, G. M., Okuno, J. and Yokoyama, Y. (2012) 'Ice-sheet collapse and sea-level rise at the Bølling warming 14,600 years ago', *Nature*, 483, pp. 559–563.

- Desloges, J. R. and Gilbert, R. (1994) 'Sediment source and hydroclimatic inferences from glacial lake sediments: the postglacial sedimentary record of Lillooet Lake, British Columbia', *Journal of Hydrology*, 159, pp. 375–393.
- Devine, R. M. and Palmer, A. P. (2017) 'A new varve thickness record from Allt Bhraich Achaidh Fan, middle Glen Roy, Lochaber: implications for understanding the Loch Lomond Stadial glaciolacustrine varve sedimentation trends', *Proceedings of the Geologists' Association*, 128, pp. 136–145.
- Diatoms of North America (no date) 'Diatoms of North America [WWW Document], n.d. URL <https://diatoms.org/> (accessed 8.30.19).'
- Dokken, T. M., Nisancioglu, K. H., Li, C., Battisti, D. S. and Kissel, C. (2013) 'Dansgaard-Oeschger cycles: Interactions between ocean and sea ice intrinsic to the Nordic seas', *Paleoceanography*, 28(3), pp. 491–502.
- Donner, J. (1951) 'Pollen-analytical studies of late-glacial deposits in Finland.', *Comptes Rendus de la Société géologique de Finlande*, 24, pp. 1–92.
- Donner, J. (2010) 'The younger dryas age of the salpausselkä moraines in Finland', *Bulletin of the Geological Society of Finland*, 82(2), pp. 69–80.
- Dowling, T. P. F., Alexanderson, H. and Moller, P. (2013) 'The new high-resolution LiDAR digital height model ('Ny Nationell Höjdmodell') and its application to Swedish Quaternary geomorphology', *GFF*, 135, pp. 145–151.
- Dulski, P., Brauer, A. and Mangili, C. (2015) 'Combined μ -XRF and Microfacies Techniques for Lake Sediment Analyses', in.
- Duphorn, K., Kogler, F.-C. and Stay, B. (1979) 'Late-glacial varved clays in the Bornholm Basin and Hano Bay', *Boreas*, 8, pp. 137–140.
- Duplessy, J. C., Shackleton, N. J., Fairbanks, R. G., Labeyrie, L., Oppo, D. and Kallel, N. (1988) 'Deepwater source variations during the last climatic cycle and their impact on the global deepwater circulation', *Paleoceanography*, 3(3), pp. 343–360.
- Evans, D. J. A. and Benn, D. I. (2004) *A practical guide to the study of glacial sediments*. Routledge.
- Fernlund, J. M. R. (1988) 'The Halland Coastal Moraines: are they end moraines or glaciotectonic ridges?', in Croot, D. G. (ed.) *Glaciotectonics. Forms and Processes*. A. A. Balkema, pp. 77–90.
- Fernlund, J. M. R. (1993) 'The long-singular ridges of the Halland Coastal Moraines, south-western Sweden.', *Journal of Quaternary Science*, 8, pp. 67–78.
- Flower, B. P., Oppo, D. W., McManus, J. F., Venz, K. A., Hodell, D. A. and Cullen, J.

- L. (2000) 'North Atlantic intermediate to deep water circulation and chemical stratification during the past 1 Myr', *Paleoceanography*, 15(4), pp. 388–403.
- Fortin, D., Francus, P., Gebhardt, A. C., Hahn, A., Kliem, P., Lisé-Pronovost, A., Roychowdhury, R., Labrie, J. and St-Onge, G. (2013) 'Destructive and non-destructive density determination: Method comparison and evaluation from the Laguna Potrok Aike sedimentary record', *Quaternary Science Reviews*, 71, pp. 147–153.
- Francus, P. (2004) *Image Analysis, Sediments and Paleoenvironments, Developments in Paleoenvironmental Research*. vol. 7. Edited by P. Francus. Dordrecht: Springer.
- Francus, P., Bradley, R. S., Abbott, M. B., Patridge, W. and Keimig, F. (2002) 'Paleoclimate studies of minerogenic sediments using annually resolved textural parameters', *Geophysical Research Letters*, 29(20), pp. 59-1-59–4.
- Francus, P., Kanamaru, K. and Fortin, D. (2015) 'Standardization and Calibration of X-Radiographs Acquired with the ITRAX Core Scanner', in Croudace, I. W; Rothwell, R. G. (ed.) *Micro-XRF Studies of Sediment Cores, Developments in Palaeoenvironmental Research*. 17th edn. Springer, pp. 491–505.
- Fredén, C. (1975) 'Subfossil finds of arctic whales and seals in Sweden', *Sveriges Geologiska Undersökning*, C710, p. 72.
- Fredén, C. (1988) 'Marine life and deglaciation chronology of the Vänern basin, southwestern Sweden', *Sveriges Geologiska Undersökning Ca*, 71, p. 80.
- Fredén, C. (1990) 'Beskrivning till jordartskartan Borås NO', *Sveriges Geologiska Undersökning Ae*, 107, p. 90.
- Fredin, O., Rubensdotter, L., van Welden, A., Larsen, E. and Lyså, A. (2012) 'Distribution of ice marginal moraines in NW Russia', *Journal of Maps*, 8, pp. 236–241.
- Fuhrmann, R. (2012) 'Atlas quartärer und rezenter Ostrakoden Mitteldeutschlands', *Altenburger Naturwissenschaftliche Forschungen*, 15, pp. 1–320.
- Gavelin, A. and Munthe, H. (1907) 'Beskrivning till kartbladet "Jönköping"', *Geological Survey of Sweden*, Serie Aa 1.
- De Geer, G. (1884) 'Om möjligheten af att införa en kronologi för Istiden', *Geologiska Föreningens i Stockholm Förhandlingar*, 7(3).
- De Geer, G. (1896) 'Skandinaviens geografiska utveckling efter istiden', *Sveriges Geologiska Undersökning*, 161, pp. 1–60.

- De Geer, G. (1909) 'Dal's Ed Some stationary Ice-borders of the last Glaciation', *Geologiska Föreningens i Stockholm Förhandlingar*, 31, pp. 511–556.
- De Geer, G. (1912) 'Gechronologie der letzten 12000 Jahre', *Geologische Rundschau*, III, pp. 457–471.
- De Geer, G. (1913) 'Finiglaciala Yoldia relikter', *Geologiska Föreningens i Stockholm Förhandlingar*, 35, pp. 307–309.
- De Geer, G. (1926) 'On the Solar Curve: As Dating the Ice Age, the New York Moraine, and Niagara Falls through the Swedish Timescale', *Geografiska Annaler*, 8, pp. 252–284.
- De Geer, G. (1927) 'Late glacial clay varves in Argentina measured by Dr. Carl Caldenius, dated and connected with the solar curve through the Swedish timescale', *Geografiska Annaler*, 9, pp. 1–8.
- De Geer, G. (1932) 'Stockholmstraktens kvartärgeologi', *Sveriges Geologiska Undersökning*, Ba 12, p. 89.
- De Geer, G. (1940) 'Geochronologia Suecia Principes', *Kungliga Svenska Vetenskapsakademiens Handlingar Bd*, 18(6).
- Gherardi, J.-M., Labeyrie, L., Nave, S., Francois, R., McManus, J. F. and Cortijo, E. (2009) 'Glacial-interglacial circulation changes inferred from 231Pa/230Th sedimentary record in the North Atlantic region', *Paleoceanography*, 24, p. PA2204.
- Gibbard, P. L., Head, M. J., Walker, M. J. C. and The Subcommittee on Quaternary Stratigraphy (2010) 'Formal ratification of the Quaternary System/Period and the Pleistocene Series/Epoch with a base at 2.58 Ma', *Journal of Quaternary Science*, 25, pp. 96–102.
- Goehring, B. M., Brook, E. J., Linge, H., Raisbeck, G. M. and Yiou, F. (2008) 'Beryllium-10 exposure ages of erratic boulders in southern Norway and implications for the history of the Fennoscandian Ice Sheet', *Quaternary Science Reviews*, 27, pp. 320–336.
- Goslar, T., Arnold, M., Tisnerat-Laborde, N., Hatté, C., Paterne, M. and Ralska-Jasiewiczowa, M. (2000) 'Radiocarbon calibration by means of varves versus 14C ages of terrestrial macrofossils from lake Gosciadz and Lake Perespilno, Poland', *Radiocarbon*, 42(3), pp. 335–348.
- Goslar, T., Wohlfarth, B., Björck, S., Possnert, G. and Björck, J. (1999) 'Variations of atmospheric 14C concentrations over the Alleröd-Younger Dryas transition', *Climate Dynamics*, 15, pp. 29–42.

- Greenwood, S. L., O'Regan, M., Swärd, H., Flodén, T., Ananyev, R., Chernykh, D. and Jakobsson, M. (2015) 'Multiple re-advances of a Lake Vättern outlet glacier during Fennoscandian Ice Sheet retreat, south-central Sweden', *Boreas*, 44(4), pp. 619–637.
- Gudmundsdóttir, E. R., Eiríksson, J. and Larsen, G. (2011) 'Identification and definition of primary and reworked tephra in Late Glacial and Holocene marine shelf sediments off North Iceland', *Journal of Quaternary Science*, 26(6), pp. 589–602.
- Guiry, M. D. and Guiry, G. M. (2018) *AlgaeBase. World-wide electronic publication [WWW Document] URL <http://www.algaebase.org> (accessed on 09-08-2018)*.
- Gustavson, T. C. (1975) 'Bathymetry and sediment distribution in proglacial Malaspina Lake, Alaska', *Journal of Sedimentary Petrology*, 45, pp. 450–461.
- Hafliðason, H., Eiríksson, J. and van Kreveld, S. (2000) 'The tephrochronology of Iceland and the North Atlantic region during the middle and late Quaternary: a review', *Journal of Quaternary Science*, 15(3), p. 22.
- Hajdas, I., Ivy, S. D., Beer, J., Bonani, G., Imboden, D., Lotted, A. F., Sturm, M. and Suter, M. (1993) 'AMS radiocarbon dating and varve chronology of Lake Soppensee: 6000 to 12000 14C years BP', *Climate Dynamics*, 9(3), pp. 107–116.
- Haltia-Hovi, E., Saarinen, T. and Kukkonen, M. (2007) 'A 2000-year record of solar forcing on varved lake sediment in eastern Finland', *Quaternary Science Reviews*, 26(5–6), pp. 678–689.
- Hang, T. (2003) 'A local clay-varve chronology and proglacial sedimentary environment in glacial Lake Peipsi, eastern Estonia', *Boreas*, 32, pp. 416–426.
- Hang, T., Gurbich, V., Subetto, D., Strakhovenko, V., Potakhin, M., Belkina, N. and Zobkov, M. (2019) 'A local clay-varve chronology of Onega Ice Lake, NW Russia', *Quaternary International*. Elsevier, 524(November 2018), pp. 13–23.
- Hardy, D. R., Bradley, R. S. and Zolitschka, B. (1996) 'The climatic signal in varved sediments from Lake C2, northern Ellesmere Island, Canada', *Journal of Paleolimnology*, 16(2), pp. 227–238.
- Hättestrand, C. (1997) 'Ribbed moraines in Sweden - Distribution pattern and palaeoglaciological implications', *Sedimentary Geology*, 111(1–4), pp. 41–56.
- Hättestrand, C. (1998) 'The glacial geomorphology of central and northern Sweden', *Sveriges Geologiska Undersökning*, Ca 85, pp. 1–47.
- Hättestrand, C. and Clark, C. D. (2006) 'Reconstructing the pattern and style of deglaciation of Kola Peninsula, NE Fennoscandian Ice Sheet', in Knight, P. G. (ed.)

- Glaciology and Earth's Changing Environment*. Oxford: Blackwell, pp. 199–201.
- Hättestrand, C and Clark, C. D. (2006) 'The glacial geomorphology of Kola Peninsula and adjacent areas in Murmansk Region, Russia', *Journal of Maps*, pp. 30–42.
- Hättestrand, C., Kolka, V. and Stroeven, A. P. (2007) 'The Keiva ice marginal zone on the Kola Peninsula, northwest Russia: a key component for reconstructing the palaeoglaciology of the northeastern Fennoscandian Ice Sheet', *Boreas*, 36, pp. 352–370.
- Hättestrand, C. and Stroeven, A. P. (2004) 'A relict landscape in the centre of Fennoscandian glaciation: geomorphological evidence of minimal Quaternary glacial erosion', *Geomorphology*, 44, pp. 127–143.
- Hays, J. D., Imbrie, J. and Shackleton, N. J. (1976) 'Variations in the earth's orbit: Pacemaker of the ice ages', *Science*, 194(4270), pp. 1121–1132.
- Hayward, C. (2012) 'High spatial resolution electron probe microanalysis of tephras and melt inclusions without beam-induced chemical modification', *The Holocene*, (22), pp. 119–125.
- Hebrand, M. and Åmark, M. (1989) 'Esker formation and glacier dynamics in eastern Skåne and adjacent areas, southern Sweden', *Boreas*, 18, pp. 67–81.
- Hegerl, G. C. and Bindoff, N. L. (2005) 'Warming the world's oceans', *Science*, 309, pp. 254–255.
- Heideman, M., Menounos, B. and Clague, J. J. (2015) 'An 825-year long varve record from Lillooet Lake, British Columbia, and its potential as a flood proxy', *Quaternary Science Reviews*. Elsevier Ltd, 126, pp. 158–174.
- Heier-Nielsen, S., Heinemeir, J., Nielsen, H. L. and Rud, N. (1995) 'Recent reservoir ages for Danish fjords and marine waters', *Radiocarbon*, 37, pp. 875–882.
- Heine, K., Reuther, A. U., Thieke, H. U., Schulz, R., Schlaak, N. and Kubik, P. W. (2009) 'Timing of Weichselian ice marginal positions in Brandenburg (northeastern Germany) using cosmogenic in situ ^{10}Be ', *Zeitschrift für Geomorphologie*, 53(4), pp. 433–454.
- Hilldén, A. (1979) 'Deglaciationen i trakten av Berghemsmoränen öster om Göteborg', *University of Lund, Department of Quaternary Geology, Thesis*, 6, pp. 1–130.
- Hillefors, Å. (1975) 'Contribution to the knowledge of the chronology of the deglaciation of western Sweden with special reference to the Gothenburg moraine', *Svensk Geografisk Årsbok*, 51, pp. 70–81.
- Hillefors, Å. (1979) 'Deglaciation models from the Swedish West Coast', *Boreas*, 8,

pp. 153–169.

Holmqvist, B. and Wohlfarth, B. (1998) 'An evaluation of the late weichselian swedish varve chronology based on cross-correlation analysis', *Gff*, 120(1), pp. 35–46.

Houmark-Nielsen, M. (1987) 'Pleistocene stratigraphy and glacial history of the central part of Denmark', *Bulletin of the Geological Society of Denmark*, 36, pp. 1–189.

Houmark-Nielsen, M. and Kjær, K. H. (2003) 'Southwest Scandinavia, 40-15 kyr BP: Palaeogeography and environmental change', *Journal of Quaternary Science*, 18(8), pp. 769–786.

Houmark-Nielsen, M., Linge, H., Fabel, D., Schnabel, C., Xu, S., Wilcken, K. M. and Binnie, S. (2012) 'Cosmogenic surface exposure dating the last deglaciation in Denmark: Discrepancies with independent age constraints suggest delayed periglacial landform stabilisation', *Quaternary Geochronology*, 13, pp. 1–17.

Hughen, K. A., Overpeck, J. T. and Anderson, R. F. (2000) 'Recent warming in a 500-year palaeotemperature record from varved sediments, Upper Soper Lake, Baffin Island, Canada', *Holocene*, 10, pp. 9–19.

Hughes, A. L. C., Gyllencreutz, R., Lohne, Ø. S., Mangerud, J. and Svendsen, J. I. (2016) 'The last Eurasian ice sheets - a chronological database and time-slice reconstruction, DATED-1', *Boreas*, 45(1), pp. 1–45.

Hunt, J. B. and Hill, P. G. (1993) 'Tephra geochemistry: a discussion of some persistent analytical problems', *The Holocene*, 3(3), pp. 271–278.

Imbrie, J., Berger, A. and Shackleton, N. J. (1993) 'Role of orbital forcing: a two-millionyear perspective', in Eddy, J. . and Oeschger, H. (eds) *Global Changes in the Perspective of the Past*. Chichester and New York: Wiley, pp. 263–277.

Imbrie, J. and Imbrie, K. P. (1979) *Ice Ages: Solving the Mystery*. London: Macmillan.

Iversen, J. (1954) 'The late-glacial flora of Denmark and its relation to climate and soil', *Danmarks geologiske undersøgelse*, 2, pp. 87–119.

Iversen, J. (1973) 'The development of Denmark's nature since the Last Glacial', *Geological Survey of Denmark, Series 7-C*, p. 122.

Jakobsson, M., Björck, S., Alm, G., Andrén, T., Lindeberg, G. and Svensson, N.-O. (2007) 'Reconstructing the Younger Dryas ice dammed lake in the Baltic Basin: bathymetry, area and volume', *Global and Planetary Change*, 57, pp. 355–370.

Janoušek, V., Farrow, C. M. and Erban, V. (2006) 'Interpretation of whole-rock geochemical data in igneous geochemistry: introducing Geochemical Data Toolkit

- (GCDkit)', *Journal of Petrology*, 47(6), pp. 1255–1259.
- Järnefors, B. (1963) 'Lervarvskronologien och isrecessionen I östra Mellansverige', *Sveriges Geologiska Undersökning*, C-594, pp. 1–67.
- Jennings, A. E., Hald, M., Smith, M. and Andrews, J. T. (2006) 'Freshwater forcing from the Greenland ice sheet during the Younger Dryas: Evidence from southeastern Greenland shelf cores 2', *Quaternary Science Reviews*, 25, pp. 82–298.
- Jessen, C. A., Rundgren, M., Björck, S., Andresen, C. S. and Conley, D. J. (2008) 'Variability and seasonality of North Atlantic climate during the early Holocene: Evidence from Faroe Island lake sediments', *Holocene*, 18(6), pp. 851–860.
- Jessen, K. (1935) 'Archaeological dating in the history of North Jutland's vegetation', *Acta Archaeologica*, 5, pp. 185–214.
- Johansson, B. T. (1982) 'Deglaciationen av norra Bohuslän och södra Dalsland', *Chalmers Tekniska Högskola Göteborgs Universitet, Geologiska Institutionen Publ. A*, 38, p. 180.
- Johansson, S. (1926) 'Baltiska issjöns tappning', *Geologiska Föreningens i Stockholm Förhandlinga*, 48, pp. 186–263.
- Johnsen, T. F., Alexanderson, H., Fabel, D. and Freeman, S. P. H. T. (2009) 'New ^{10}Be cosmogenic ages from the Vimmerby Moraine confirm the timing of Scandinavian ice sheet deglaciation in southern Sweden', *Geografiska Annaler: Series A, Physical Geography*, 91, pp. 113–120.
- Johnson, M. D. and Clayton, L. (2003) 'Supraglacial landsystems in lowland terrain', in Evans, D. J. A. (ed.) *Glacial landsystems*. London: Arnold, pp. 228–258.
- Johnson, M. D., Kylander, M. E., Casserstedt, L., Wiborgh, H. and Björck, S. (2013) 'Varved glaciomarine clay in central Sweden before and after the Baltic Ice Lake drainage: A further clue to the drainage events at Mt Billingen', *Gff*, 135(3–4), pp. 293–307.
- Johnson, M. D. and Ståhl, Y. (2010) 'Stratigraphy, sedimentology, age and palaeoenvironment of marine varved clay in the Middle Swedish end-moraine zone', *Boreas*, 39(2), pp. 199–214.
- Johnson, M. D., Wedel, P. O., Benediktsson, Í. and Lenninger, A. (2019) 'Younger Dryas glaciomarine sedimentation, push-moraine formation and ice-margin behavior in the Middle Swedish end-moraine zone west of Billingen, central Sweden', *Quaternary Science Reviews*, 224.
- Johnsson, G. (1956) 'Glacialmorfologiska studier i södra Sverige. Med särskild

- hänsyn till glaciala riktningselement och periglaciala frostfenomen. , Vol. 31, 407 pp.', *Meddelanden från Lunds Universitets Geografiska Institution, Avhandlingar*, 31, pp. 1–407.
- Jones, G., Davies, S. M., Farr, G. J. and Bevan, J. (2017) 'Identification of the Askja-S Tephra in a rare turlough record from Pant-y-Llyn, south Wales', *Proceedings of the Geologists' Association*. The Geologists' Association., 128(4), pp. 523–530.
- Jowsey, P. C. (1966) 'An Improved Peat Sampler', *New Phytologist*, 65(2), pp. 245–248.
- Kalm, V. (2012) 'Ice-flow pattern and extent of the last Scandinavian Ice Sheet southeast of the Baltic Sea', *Quaternary Science Reviews*, 44, pp. 51–59.
- Kalugin, I., Darin, A., Tretyakov, G., Rogozin, D., Kholodova, L. and Maksimova, N. (2013) 'Geochemical Signals of Paleoclimate in the varved clastic and carbonate lake sediments', in *Air Pollution and Climate Change*.
- Karlsson, V. (1882) 'Några ord till Upplysning om bladet "Wasterås"', *Sveriges Geologiska Undersökning*, Aa, p. 16.
- Kearney, R., Albert, P. G., Staff, R. A., Pál, I., Veres, D., Magyari, E. and Bronk Ramsey, C. (2018) 'Ultra-distal fine ash occurrences of the Icelandic Askja-S Plinian eruption deposits in Southern Carpathian lakes: New age constraints on a continental scale tephrostratigraphic marker', *Quaternary Science Reviews*, 188, pp. 174–182.
- Kinder, M., Tylmann, W., Enters, D., Piotrowska, N., Poreba, G. and Zolitschka, B. (2013) 'Construction and validation of calendar-year time scale for annually laminated sediments - an example from Lake Szurpiły (NE Poland)', *Gff*, 135(3–4), pp. 248–257.
- Kjær, K. H., Demidov, I. N., Larsen, E., Murray, A. and Nielsen, J. K. (2003) 'Mezen Bay—a key area for understanding Weichselian glaciations in northern Russia', *Journal of Quaternary Science*, 18, pp. 73–93.
- Kjær, K., Lagerlund, E., Adrielsson, L., Thomas, P. J., Murray, A. and Sandgren, P. (2006) 'The first independent chronology for Middle and Late Weichselian sediments from southern Sweden and the Island of Bornholm', *GFF*, 128, pp. 209–220.
- Kleman, J. (1972) 'The palimpsest glacial landscape in northwestern Sweden - late Weichselian deglaciation landforms and traces of older west-centered ice sheets', *Geografiska Annaler: Series A, Physical Geography*, 74A, pp. 305–325.
- Kleman, J. (1994) 'Preservation of landforms under ice sheets and ice caps Geomorphology', *Geomorphology*, 9, pp. 19–32.

- Kleman, J., Hättestrand, C., Borgström, I. and Stroeven, A. (1997) 'Fennoscandian paleoglaciology reconstructed using a glacial geological inversion model', *Journal of Glaciology*, 43, pp. 283–299.
- Kramarska, R. (1998) 'Origin and development of the Odra Bank in the light of the geologic structure and radiocarbon dating', *Geology Quarterly*, 42, pp. 277–288.
- Krammer, K. (2002) *Diatoms of Europe. Diatoms of the European Inland Waters and Comparable Habitats*. Volume 3. Germany: Cymbella.
- Krammer, K. and Lange-Bertalot, H. (1986) *Bacillariophyceae. 1: Teil: Naviculaceae, Süßwasserf.* Stuttgart, New York: Gustav Fischer Verlag.
- Krammer, K. and Lange-Bertalot, H. (1988) *Süßwasserflora von Mitteleuropa, 2/2 Bacillariophyceae, 2. Teil: Bacillariaceae, Epithemiaceae, Surirellaceae*. Stuttgart, New York: Gustav Fischer Verlag.
- Krammer, K. and Lange-Bertalot, H. (1991a) *Süßwasserflora von Mitteleuropa, 2/3 Bacillariophyceae, 3. Teil: Centrales, Fragilariaceae, Eunotiaceae*. Berlin: Gustav Fischer Verlag.
- Krammer, K. and Lange-Bertalot, H. (1991b) *Süßwasserflora von Mitteleuropa, 2/4 Bacillariophyceae, 4. Teil: Achnanthaceae Kritische Ergänzungen zu Achnanthes s.l., Navicula s.str., Gomphonema*. Berlin: Gustav Fischer Verlag.
- Kristiansson, J. (1986) 'The ice recession in the south-eastern part of Sweden. A varve-chronological time scale for the latest part of the Late Weichselian', *University of Stockholm, Department of Quaternary Research, Report*, 7, p. 149.
- Kylander, M. E., Ampel, L., Wohlfarth, B. and Veres, D. (2011) 'High-resolution X-ray fluorescence core scanning analysis of Les Echets (France) sedimentary sequence: New insights from chemical proxies', *Journal of Quaternary Science*, 26(1), pp. 109–117.
- Lagerlund, E. (1987) 'An alternative Weichselian glaciation model, with special reference to the glacial history of Skåne, South Sweden', *Boreas*, 16(4), pp. 433–459.
- Lagerlund, E. and Houmark-Nielsen, M. (1993) 'Timing and pattern of the last deglaciation in the Kattegat region, southwest Scandinavia', *Boreas*, 22, pp. 337–347.
- Lambert, A. and Hsü, K. J. (1979) 'Non-annual cycles of varve-like sedimentation in Walensee, Switzerland', *Sedimentology*, 26(3), pp. 453–461.
- Lamoureux, S. F. (1994) 'Embedding unfrozen lake sediments for thin section preparation', *Journal of Paleolimnology*, 10, pp. 141–146.

- Lamoureux, S. F. (2001) 'Varve chronology techniques', *Kluwer Academic Publishers*, pp. 247–258.
- Lamoureux, S. F. and Bradley, R. S. (1996) 'A late holocene varved sediment record of environmental change from northern Ellesmere Island, Canada', *Journal of Paleolimnology*, 16(2), pp. 239–255.
- Lamoureux, S. F. and Gilbert, R. (2004) 'A 750-yr record of autumn snowfall and temperature variability and winter storminess recorded in the varved sediments of Bear Lake, Devon Island, Arctic Canada', *Quaternary Research*, 61, pp. 134–147.
- Lane, C. S., Blockley, S. P. E., Bronk Ramsey, C. and Lotter, A. F. (2011) 'Tephrochronology and absolute centennial scale synchronisation of European and Greenland records for the last glacial to interglacial transition: A case study of Soppensee and NGRIP', *Quaternary International*, 246(1–2), pp. 145–156.
- Lane, C. S., Brauer, A., Blockley, S. P. E. and Dulsk, P. (2013) 'Volcanic ash reveals time-transgressive abrupt climate change during the Younger Dryas', *Geology*, 41(12), p. 1254.
- Lane, C. S., Brauer, A., Martín-Puertas, C., Blockley, S. P. E., Smith, V. C. and Tomlinson, E. L. (2015) 'The Late Quaternary tephrostratigraphy of annually laminated sediments from Meerfelder Maar, Germany', *Quaternary Science Reviews*. Elsevier Ltd, 122, pp. 192–206.
- Lane, C. S., Cullen, V. L., White, D., Bramham-Lawa, C. W. F. and Smith, V. C. (2014) 'Cryptotephra as a dating and correlation tool in archaeology', *Journal of Archaeological Science*. Elsevier Ltd, 42(1), pp. 42–50.
- Lange-Bertalot, H. (2001) *Diatoms of Europe: Diatoms of the Europe inland waters and comparable habitats. Volume 2: Navicula sensu stricto, 10 Genera separated from Navicula sensu lato, Frustulia*. Edited by H. Lange-Bertalot. Germany: Ganter Verlag.
- Lapointe, F., Francus, P., Lamoureux, S. F., Saïd, M. and Cuvén, S. (2012) '1750 years of large rainfall events inferred from particle size at East Lake, Cape Bounty, Melville Island, Canada', *Journal of Paleolimnology*, 48(1), pp. 159–173.
- Larsen, E., Lysa, A., Demidov, I., Funder, S., Houmark-Nielsen, M., Kjaer, K. H. and Murray, A. S. (1999) 'Age and extent of the Scandinavian ice sheet in northwest Russia', *Boreas*, 28, pp. 115–132.
- Larsen, N. K., Knudsen, K. L., Krohn, C. F., Ronborg, C., Murray, A. S. and Nielsen, O. B. (2009) 'Late Quaternary ice sheet, lake and sea history of southwest

- Scandinavia – a synthesis', *Boreas*, 38, pp. 732–761.
- Larsen, N. K., Linge, H., Håkansson, L. and Fabel, D. (2012) 'Investigating the last deglaciation of the Scandinavian Ice Sheet in southwest Sweden with ^{10}Be exposure dating', *Journal of Quaternary Science*, 27(2), pp. 211–220.
- Larsson, S. A. and Wastegård, S. (2018) 'The Laacher See Tephra discovered in southernmost Sweden', *Journal of Quaternary Science*, 33(5), pp. 477–481.
- Lasberg, K. and Kalm, V. (2013) 'Chronology of Late Weichselian glaciation in the western part of the East European Plain', *Boreas*, 42, pp. 995–1007.
- Lewis, T., Gilbert, R. and Lamoureux, S. F. (2002) 'Spatial and Temporal Changes in Sedimentary Processes at Proglacial Bear Lake, Devon Island, Nunavut, Canada', *Arctic, Antarctic, and Alpine Research*, 34(2), pp. 119–129.
- Li, C., Battisti, D. S. and Bitz, C. M. (2010) 'Can North Atlantic sea ice anomalies account for Dansgaard-Oeschger climate signals?', *Journal of Climate*, 23(20), pp. 5457–5475.
- Li, Y. K., Harbor, J., Stroeven, A. P., Fabel, D., Kleman, J., Fink, D., Caffee, M. and Elmore, D. (2005) 'Ice Sheet erosion patterns in valley systems in northern Sweden investigated using cosmogenic nuclides', *Earth Surface Processes and Landforms*, 30, pp. 1039–1049.
- Licciardi, J. M., Teller, J. T. and Clark, P. U. (1999) 'Freshwater routing by the Laurentide Ice Sheet during the last deglaciation', in Clark, P. U., Webb, R. S. and Keigwin, L. D. (eds) *Mechanisms of Global Climate Change at Millennial Time Scales*, pp. 177–202.
- Lidén, R. (1913) 'Geokronologiska studier öfver det finiglaciala skedet i Ångermanland', *Sveriges Geologiska Undersökning*, Ca-9, pp. 1–39.
- Lidén, R. (1938) 'Den senkvartära strandförskjutningens förlopp och kronologi i Ångermanland', *Geologiska Föreningens i Stockholm Förhandlingar*, 60, pp. 397–404.
- Lind, E. M., Lilja, C., Wastegård, S. and Pearce, N. J. G. (2016) 'Revisiting the Borrobol Tephra', *Boreas*, 45(4), pp. 629–643.
- Lind, E. M. and Wastegård, S. (2011) 'Tephra horizons contemporary with short early Holocene climate fluctuations: New results from the Faroe Islands', *Quaternary International*, 246(1–2), pp. 157–167.
- Lind, E. M., Wastegård, S. and Larsen, J. J. (2013) 'A Late Younger Dryas-Early Holocene tephrostratigraphy for Fosen, Central Norway', *Journal of Quaternary*

Science, 28(8), pp. 803–811.

Lindén, M., Möller, P., Björck, S. and Sandgren, P. (2006) 'Holocene shore displacement and deglaciation chronology in Norrbotten, Sweden', *Boreas*, 35, pp. 1–22.

Lippstreu, L., Beiträgen von Brose, F. and Marcinek, J. (1995) 'Brandenburg', in Benda, L. (ed.) *Das Quartär Deutschlands*. Stuttgart: Borntraeger.

Lisiecki, L. E. and Raymo, M. E. (2005) 'A Pliocene-Pleistocene stack of 57 globally distributed benthic δ 18O records', *Paleoceanography*, 20(1), pp. 1–17.

Litt, T., Schölzel, C., Kühl, N. and Brauer, A. (2009) 'Vegetation and climate history in the Westeifel Volcanic Field (Germany) during the past 11 000 years based on annually laminated lacustrine maar sediments', *Boreas*, 38, pp. 679–690.

Lohne, Ø. S., Bondevik, S., Mangerud, J. and Svendsen, J. I. (2007) 'Sea-level fluctuations imply that the Younger Dryas ice-sheet expansion in western Norway commenced during the Allerød', *Quaternary Science Reviews*, 26, pp. 2128–2151.

Lohne, Ø. S., Mangerud, J. and Birks, H. H. (2014) 'IntCal13 calibrated ages of the Vedde and Saksunarvatn ashes and the Younger Dryas boundaries from Kråkenes, western Norway', *Journal of Quaternary Science*, 29(5), pp. 506–507.

Longva, O. and Thoresen, M. K. (1991) 'Iceberg scours, iceberg gravity craters and current erosion marks from a gigantic Preboreal flood in southeastern Norway', *Boreas*, 20, pp. 47–62.

Lotter, A. F. and Lemcke, G. (1999) 'Methods for preparing and counting biochemical varves', *Boreas*, 28(2), pp. 243–252.

Lougheed, B., Filipsson, C. H. L. and Snowball, I. (2013) 'Large spatial variations in coastal 14C reservoir age - a case study from the Baltic Sea', *Climate of the Past*, 9, pp. 1015–1028.

Lowe, D. J. (2011) 'Tephrochronology and its application: A review', *Quaternary Geochronology*, 6, pp. 107–153.

Lowe, J. J., Rasmussen, S. O., Björck, S., Hoek, W. Z., Steffensen, J. P., Walker, M. J. C. and Yu, Z. C. (2008) 'Synchronisation of palaeoenvironmental events in the North Atlantic region during the Last Termination: a revised protocol recommended by the INTIMATE group', *Quaternary Science Reviews*, 27(1–2), pp. 6–17.

Lowe, J. J. and Walker, M. J. C. (2000) 'Radiocarbon dating the Last Glacial-Interglacial Transition (ca 14-9 14C ka BP) in terrestrial and marine records: the need for new quality assurance protocols.', *Radiocarbon*, 42(1), pp. 53–68.

- Lowe, J. J. and Walker, M. J. C. (2014) *Reconstructing Quaternary Environments*. Third Edit. London: Routledge.
- Lowe, J. J. and Walker, N. J. (2015) *Reconstructing Quaternary Environments*. 3rd Edn. London: Routledge.
- Löwemark, L., Chen, H. F., Yang, T. N., Kylander, M., Yu, E. F., Hsu, Y. W., Lee, T. Q., Song, S. R. and Jarvis, S. (2011) 'Normalizing XRF-scanner data: A cautionary note on the interpretation of high-resolution records from organic-rich lakes', *Journal of Asian Earth Sciences*, 40(6), pp. 1250–1256.
- Lundqvist, G. (1959) 'Description to accompany the map of the Quaternary deposits of Sweden', *Sveriges Geologiska Undersökning Ae*, Ba 17, pp. 1–116.
- Lundqvist, J. (1957) 'Geokronologiska undersökningar i Värmland', *Sveriges Geologiska Undersökning*, C 551, p. 28.
- Lundqvist, J. (1972) 'Ice-lake types and deglaciation pattern along the Scandinavian mountain range', *Boreas*, 1, pp. 27–54.
- Lundqvist, J. (1987) 'Beskrivning till jordartskarta över Västernorrlands län och förutvarande Fjällsjö k:n', *Sveriges Geologiska Undersökning*, Ca 55, pp. 1–270.
- Lundqvist, J. (1988) 'Younger Dryas-Preboreal moraines and deglaciation in southwestern Värmland, Sweden', *Boreas*, 17, pp. 301–316.
- Lundqvist, J. (1995) 'The Younger Dryas icemarginal zone in Sweden.', *Quaternary International*, 28, pp. 171–176.
- Lundqvist, J. (2007) 'Surging ice and break-down of an ice dome - a deglaciation model for the Gulf of Bothnia', *GFF*, 129, pp. 329–336.
- Lundqvist, J. and Wohlfarth, B. (2001) 'Timing and east-west correlation of south Swedish ice marginal lines during the Late Weichselian', *Quaternary Science Reviews*, 20(10), pp. 1127–1148.
- Lunkka, J. P., Saarnisto, M., Gey, V., Demidov, I. and Kiselova, V. (2001) 'Extent and age of the Last Glacial Maximum in the southeastern sector of the Scandinavian Ice Sheet', *Global and Planetary Change*, 31, pp. 407–425.
- Lüthgens, C. and Böse, M. (2011) 'Age of the Pomeranian ice-marginal position in northeastern Germany determined by Optically Stimulated Luminescence (OSL) dating of glaciofluvial sediments', *Boreas*, 40, pp. 598–615.
- Lyså, A., Larsen, E., Buylaert, J.-P., Fredin, O., Jensen, M. A., Kuznetsov, D., Murray, A. S., Subetto, D. A. and van Welden, A. (2014) 'Late Pleistocene stratigraphy and sedimentary environments of the Severnaya Dvina-Vycheгда region in northwestern

Russia', *Boreas*, 43, pp. 759–779.

MacAyeal, D. R. (1992) 'Irregular oscillations of the West Antarctic ice sheet', *Nature*, 359, pp. 29–35.

MacLeod, A. (2010) 'The potential for developing an annually-resolved chronology of events in Scotland during the last glacial-interglacial transition (16-8 ka BP)', *PhD Thesis, Royal Holloway, University of London*, pp. 1–514.

MacLeod, A., Brunnberg, L., Wastegård, S., Hang, T. and Matthews, I. P. (2014) 'Lateglacial cryptotephra detected within clay varves in Östergötland, south-east Sweden', *Journal of Quaternary Science*, 29(7), pp. 605–609.

MacLeod, A., Matthews, I. P., Lowe, J. J., Palmer, A. P. and Albert, P. G. (2015) 'A second tephra isochron for the Younger Dryas period in northern Europe: The Abernethy Tephra', *Quaternary Geochronology*. Elsevier B.V, 28, pp. 1–11.

MacLeod, A., Palmer, A., Lowe, J., Rose, J., Bryant, C. and Merritt, J. (2011) 'Timing of glacier response to Younger Dryas climatic cooling in Scotland', *Global and Planetary Change*, (79), pp. 264–274.

Magri, D. and Tzedakis, P. C. (2000) 'Orbital signatures and long-term vegetation patterns in the Mediterranean', *Quaternary International*, 73/74, pp. 69–78.

Mäkinen, J., Kajuutti, K., Palmu, J., Ojala, A. and Ahokangas, E. (2017) 'Triangular-shaped landforms reveal subglacial drainage routes in SW Finland.', *Quaternary Science Reviews*, 164, pp. 37–53.

Mangerud, J. A. N., Andersen, S. T., Berglund, B. E. and Donner, J. J. (1974) 'Quaternary stratigraphy of Norden, a proposal for terminology and classification', *Boreas*, 3, pp. 109–126.

Mangerud, J., Bondevik, S., Gulliksen, S., Karin Hufthammer, A. and Høisæter, T. (2006) 'Marine 14C reservoir ages for 19th century whales and molluscs from the North Atlantic', *Quaternary Science Reviews*, 25(23–24), pp. 3228–3245.

Mangerud, J., Gyllencreutz, R., Lohne, Ø. and Svendsen, J. I. (2011) 'Glacial history of Norway', *Developments in Quaternary Science*, 15(5007), pp. 279–298.

Marshall, J. D., Lang, B., Crowley, S. F., Weedon, G. P., van Calsteren, P., Fisher, E. H., Holme, R., Holmes, J. A., Jones, R. T., Bedford, A. and Brooks, S. J. (2007) 'Terrestrial impact of abrupt changes in the North Atlantic thermohaline circulation: Early Holocene, UK', *Geology*, 7, pp. 639–642.

Marshall, M., Schlolaut, G., Nakagawa, T., Lamb, H., Brauer, A., Staff, R., Ramsey, C. B., Tarasov, P., Gotanda, K., Haraguchi, T., Yokoyama, Y., Yonenobu, H. and

- Tada, R. (2012) 'A novel approach to varve counting using μ XRF and X-radiography in combination with thin-section microscopy, applied to the Late Glacial chronology from Lake Suigetsu, Japan', *Quaternary Geochronology*, 13, pp. 70–80.
- Martin-Puertas, C., Brauer, A., Dulski, P. and Brademann, B. (2012) 'Testing climate-proxy stationarity throughout the Holocene: An example from the varved sediments of Lake Meerfelder Maar (Germany)', *Quaternary Science Reviews*, 58, pp. 56–65.
- Martin-Puertas, C., Matthes, K., Brauer, A., Muscheler, R., Hansen, F., Petrick, C., Aldahan, A., Possnert, G. and Van Geel, B. (2012) 'Regional atmospheric circulation shifts induced by a grand solar minimum', *Nature Geoscience*. Nature Publishing Group, 5(6), pp. 397–401.
- Maslin, M. A. and Ridgwell, A. J. (2005) 'Mid-Pleistocene revolution and the 'eccentricity myth'', *Geological Society, London, Special Publications*, 247(1), pp. 19–34.
- Matthews, I. P. (2008) 'The potential of tephrostratigraphy in the investigation of wetland archaeological records', *PhD Thesis, Royal Holloway, University of London*.
- Matthews, I. P., Birks, H. H., Bourne, A. J., Brooks, S. J., Lowe, J. J., Macleod, A. and Pyne-O'Donnell, S. D. F. (2011) 'New age estimates and climatostratigraphic correlations for the borrobol and penifiler tephras: Evidence from Abernethy Forest, Scotland', *Journal of Quaternary Science*, 26(3), pp. 247–252.
- Mayewski, P. A., Rohling, E. E., Stager, J. C., Karlén, W., Maasch, K. A., Meeker, L. D., Meyerson, E. A., Gasse, F., van Kreveld, S., Holmgren, K., Lee-Thorp, J., Rosqvist, G., Rack, F., Staubwasser, M., Schneider, R. R. and Steig, E. J. (2004) 'Holocene climate variability', *Quaternary Research*, 62(3), pp. 243–255.
- McClain, M. E., Boyer, E. W., Dent, C. L., Gergel, S. E., Grimm, N. B., Groffman, P. M., Hart, S. C., Harvey, J. W., Johnston, C. A., Mayorga, E., McDowell, W. H. and Pinay, G. (2003) 'Biogeochemical hot spots and hot moments at the interface of terrestrial and aquatic ecosystems', *Ecosystems*, 6(4), pp. 301–312.
- McManus, J. F., Francois, R., Gherardl, J. M., Kelgwin, L. and Drown-Leger, S. (2004) 'Collapse and rapid resumption of Atlantic meridional circulation linked to deglacial climate changes', *Nature*, 428(6985), pp. 834–837.
- Mees, F., Swennen, R., Geet, M. V and Jacobs, P. (2003) 'Applications of X-ray computed tomography in the geosciences', *Geological Society, London, Special Publications*, 215, pp. 1–6.
- Merkt, J. (1971) 'Zuverlässige Auszählungen von Jahresschichten in Seesedimenten

- mit Hilfe von Groß-Dünnschliffen', *Archiv für Hydrobiologie*, 69, pp. 145–154.
- Mesoella, K. J., Matthews, R. K., Broecker, W. S. and Thurber, D. L. (1969) 'The astronomical theory of climate change: Barbados data', *Journal of Geology*, 77(3), pp. 250–274.
- Möller, P. (1987) 'Moraine morphology, till genesis, and deglaciation pattern in the Åsnen area, south-central Smaland, Sweden', *Lundqua Thesis 20*.
- Möller, P. (2010) 'Melt-out till and ribbed moraine formation, a case study from south Sweden', *Sedimentology*, 232, pp. 161–180.
- Monecke, K., Anselmetti, F. S., Becker, A., Sturm, M. and Giardini, D. (2004) 'The record of historic earthquakes in lake sediments of Central Switzerland', *Tectonophysics*, 394(1–2), pp. 21–40.
- Moreno, A., Lopéz-Merino, L., Leira, M., Marco-Barba, M., González-Sampériz, P., Valero-Garcés, B. L., Lopéz-Saez, J., Santos, L., Mata, P. and Ito, E. (2011) 'Revealing the last 13,500 years of environmental history from the multi-proxy record of a mountain lake (Lago Enol, northern Iberian Peninsula)', *Journal of Paleolimnology*, 40, pp. 943–961.
- Mörner, N. A. (1969) 'The Late Quaternary History of the Kattegatt Sea and the Swedish West Coast. Deglaciation, shorelevel displacement, chronology, isostasy and eustasy', *Sveriges Geologiska Undersökning C*, 640, p. 487.
- Mörner, N. A. (1979) 'The Fennoscandian uplift and Late Cenozoic geodynamics: geological evidence', *GeoJournal*, 3, pp. 287–318.
- Mörner, N. A. (1996) 'Liquefaction and varve deformation as evidence of paleoseismic events and tsunamis. The autumn 10,430 bp case in Sweden', *Quaternary Science Reviews*, 15(8–9), pp. 939–948.
- Mörner, N. A. (2011) 'Paleoseismology: The application of multiple parameters in four case studies in Sweden', *Quaternary International*. Elsevier Ltd and INQUA, 242(1), pp. 65–75.
- Mulder, T. and Alexander, J. (2001) 'The physical character of subaqueous sedimentary density flow and their deposits', *Sedimentology*, 48, pp. 269–299.
- Murton, J. B., Bateman, M. D., Dallimore, S. R., Teller, J. T. and Yang, Z. (2010) 'Identification of Younger Dryas outburst flood path from Lake Agassiz to the Arctic Ocean', *Nature*. Nature Publishing Group, 464(7289), pp. 740–743.
- Muschitiello, F., Lea, J. M., Greenwood, S. L., Nick, F. M., Brunnberg, L., MacLeod, A. and Wohlfarth, B. (2016) 'Timing of the first drainage of the Baltic Ice Lake

- synchronous with the onset of Greenland Stadial 1', *Boreas*, 45(2), pp. 322–334.
- Muschitiello, F., Pausata, F. S. R., Lea, J. M., Mair, D. W. F. and Wohlfarth, B. (2017) 'Enhanced ice sheet melting driven by volcanic eruptions during the last deglaciation', *Nature Communications*. Springer US, 8(1).
- Muschitiello, F., Pausata, F. S. R., Watson, J. E., Smittenberg, R. H., Salih, A. A. M., Brooks, S. J., Whitehouse, N. J., Karlatou-Charalampopoulou, A. and Wohlfarth, B. (2015) 'Fennoscandian freshwater control on Greenland hydroclimate shifts at the onset of the Younger Dryas', *Nature Communications*. Nature Publishing Group, 6(1), p. 8939.
- Muschitiello, F. and Wohlfarth, B. (2015) 'Time-transgressive environmental shifts across Northern Europe at the onset of the Younger Dryas', *Quaternary Science Reviews*. Elsevier Ltd, 109, pp. 49–56.
- Nakagawa, T., Gotanda, K., Haraguchi, T., Danhara, T., Yonenobu, H., Brauer, A., Yokoyama, Y., Tada, R., Takemura, K., Staff, R. A., Payne, R., Bronk Ramsey, C., Bryant, C., Brock, F., Schlolaut, G., Marshall, M., Tarasov, P. and Lamb, H. (2012) 'SG06, a fully continuous and varved sediment core from Lake Suigetsu, Japan: Stratigraphy and potential for improving the radiocarbon calibration model and understanding of late Quaternary climate changes', *Quaternary Science Reviews*, 36, pp. 164–176.
- Nesje, A., Matthews, J. A., Dahl, S. O., Berrisford, M. S. and Andersson, C. (2001) 'Holocene glacier fluctuations of Flatebreen and winter-precipitation changes in the Jostedalbreen region, western Norway, based on glaciolacustrine sediment records', *Holocene*, 11(3), pp. 267–280.
- Neugebauer, I., Brauer, A., Dräger, N., Dulski, P., Wulf, S., Plessen, B., Mingram, J., Herzsuh, U. and Brande, A. (2012) 'A Younger Dryas varve chronology from the Rehwiese palaeolake record in NE-Germany', *Quaternary Science Reviews*, 36, pp. 91–102.
- Neugebauer, I., Brauer, A., Schwab, M. J., Waldmann, N. D., Enzel, Y., Kitagawa, H., Torfstein, A., Frank, U., Dulski, P., Agnon, A., Ariztegui, D., Ben-Avraham, Z., Goldstein, S. L. and Stein, M. (2014) 'Lithology of the long sediment record recovered by the ICDP Dead Sea Deep Drilling Project (DSDDP)', *Quaternary Science Reviews*, 102, pp. 149–165.
- Nilsson, E. (1968) 'Södra Sveriges senkvartära historia. Geokronologi, issjöar och landhöjning. Kungl', *Svenska Vetenskapsakademiens Handlingar IV*, 12(1), pp. 1–117.

- Ohlendorf, C., Niessen, F. and Weissert, H. (1997) 'Glacial Varve Thickness and 127 Years of Instrumental Climate Data: A Comparison', *Climatic Change*, 36, pp. 391–411.
- Ojala, A. E. K. and Francus, P. (2002) 'Comparing X-ray densitometry and BSE-image analysis of thin section in varved sediments', *Boreas*, 31(1), pp. 57–64.
- Ojala, A. E. K., Launonen, I., Holmström, L. and Tiljander, M. (2015) 'Effects of solar forcing and North Atlantic oscillation on the climate of continental Scandinavia during the Holocene', *Quaternary Science Reviews*, 112, pp. 153–171.
- Ojala, A. E. K. and Saarnisto, M. (1999) 'Comparative varve counting and magnetic properties of the 8400-yr sequence of an annually laminated sediment in Lake Valkiajarvi, Central Finland', *Journal of Paleolimnology*.
- Oldfield, F., Wake, R., Boyle, J., Jones, R., Nolan, S., Gibbs, Z., Appleby, P., Fisher, E. and Wolff, G. (2003) 'The late-Holocene history of Gormire Lake (NE England) and its catchment: a multiproxy reconstruction of past human impact', *The Holocene*, 13, pp. 677–690.
- Olsson, S. (1991) 'Geochemistry, mineralogy, and pore water composition in uplifted, Late Weichselian-Early Holocene clays from southern Sweden', *Lundqua thesis*, 28, p. 89.
- Orsi, T. H., Edwards, C. M. and Andersson, A. L. (1994) 'X-ray computed tomography: a nondestructive method for quantitative analysis of sediment cores', *Journal of Sedimentary Research*, 64, pp. 690–693.
- Ott, F., Wulf, S., Serb, J., Słowiński, M., Obremska, M., Tjallingii, R., Błaszczewicz, M. and Brauer, A. (2016) 'Constraining the time span between the Early Holocene Hässeldalen and Askja-S Tephra through varve counting in the Lake Czechowskie sediment record, Poland', *Journal of Quaternary Science*, 31(2), pp. 103–113.
- Ovenshine, A. (1970) 'Observations on iceberg rafting in Glacier Bay, Alaska and the identification of ice-rafted deposits', *Geological Society of America Bulletin*, 81, pp. 891–894.
- Påhlsson, I. and Bergh Alm, K. (1985) 'Pollen-Analytical Studies of the Cores 14103-3 and 14102-1 from the Western Baltic', *Striae*, 23, pp. 74–82.
- Palmer, A. P. (2005) 'The Micromorphological Description, Interpretation and Palaeoenvironmental Significance of Lacustrine Clastic Lamination Sediments', *PhD thesis, University of London*.
- Palmer, A. P., Bendle, J. M., MacLeod, A., Rose, J. and Thorndycraft, V. R. (2019)

'The micromorphology of glaciolacustrine varve sediments and their use for reconstructing palaeoglaciological and palaeoenvironmental change', *Quaternary Science Reviews*. Elsevier Ltd, 226, p. 105964.

Palmer, A. P., Carr, S. and Lee, A. (2008) 'Revised Laboratory Procedures for the Preparation of Thin Sections from Unconsolidated Material', *Royal Holloway, University of London Technical Report*.

Palmer, A. P., Rose, J., Lowe, J. J. and MacLeod, A. (2010) 'Annually resolved events of younger dryas glaciation in lochaber (Glen Roy and Glen Spean), Western Scottish Highlands', *Journal of Quaternary Science*, 25(4), pp. 581–596.

Palmer, A. P., Rose, J., Lowe, J. J. and Walker, M. J. C. (2008) 'Annually laminated Late Pleistocene sediments from Llangorse Lake, South Wales, UK: a chronology for the pattern of ice wastage', *Proceedings of the Geologists' Association*, 119, pp. 245–258.

Palmer, A. P., Rose, J. and Rasmussen, S. O. (2012) 'Evidence for phase-locked changes in climate between Scotland and Greenland during GS-1 (Younger Dryas) using micromorphology of glaciolacustrine varves from Glen Roy', *Quaternary Science Reviews*, 36, pp. 114–123.

Påsse, T. (1992) 'Erratic flint along the Swedish west coast', *Geologiska Föreningens i Stockholm Förhandlingar*, 114, pp. 271–210.

Peccerillo, A. and Taylor, S. R. (1976) 'Geochemistry of eocene calc-alkaline volcanic rocks from the Kastamonu area, Northern Turkey', *Contributions to Mineralogy and Petrology*, 58(1), pp. 63–81.

Peglar, S. M., Fritz, S. C. and Birks, H. J. B. (1989) 'Vegetation and land-use history at Diss, Norfolk', *Journal of Ecology*, 77, pp. 203–222.

Pennington, W. (1986) 'Lags in adjustment of vegetation to climate caused by the pace of soil development. Evidence from Britain', *Plant Ecology*, 67, pp. 105–118.

Peterson, G. and Johnson, M. D. (2018) 'Hummock corridors in the south-central sector of the Fennoscandian ice sheet, morphometry and pattern', *Earth Surface Processes and Landforms*, 43(4), pp. 919–929.

Peterson, G., Johnson, M. D., Dahlgren, S., Pålsson, T. and Alexanderson, H. (2018) 'Genesis of hummocks found in tunnel valleys: an example from Hörda, southern Sweden', *Gff*, 140(2), pp. 189–201.

Peterson, G., Johnson, M. D. and Smith, C. A. (2017) 'Glacial geomorphology of the south Swedish uplands – focus on the spatial distribution of hummock tracts', *Journal*

of Maps, 13(2), pp. 534–544.

Petit, J. R., Jouzel, J., Raynaud, D., Barkov, N. I., Barnola, J. M., Basile, I., Bender, M., Chappellaz, J., Davis, M., Delaygue, G., Delmotte, M., Kotlyakov, V. M., Legrand, M., Lipenkov, V. Y., Lorius, C., Pepin, L., Ritz, C., Saltzman, E. and Stievenard, M. (1999) 'Climate and atmospheric history of the past 420,000 years from the Vostok ice core, Antarctica', *Nature*, 399(6735), pp. 429–436.

Petterson, G., Renberg, I., Geladi, P., Lindberg, A. and Lindgren, F. (1993) 'Spatial uniformity of sediment accumulation in varved lake sediments in northern Sweden', *Journal of Paleolimnology*, 9(3), pp. 195–208.

Pike, J. H. (2015) 'Detailed sedimentological and tephrochronological study of annually-laminated deposits at Svärdsklova, Southeastern, Sweden.', *Unpublished MSc thesis, University of London*.

Pilcher, J., Bradley, R. S., Francus, P. and Anderson, L. (2005) 'A Holocene tephra record from the Lofoten Islands, Arctic Norway', *Boreas*, 34(2), pp. 136–156.

Pisias, N. G. and Shackleton, N. J. (1984) 'Modelling the global climate response to orbital forcing and atmospheric carbon dioxide changes', *Nature*, 319, pp. 757–759.

Pollard, A. M., Blockley, S. P. E. and Lane, C. S. (2006) 'Some numerical considerations in the geochemical analysis of distal microtephra', *Applied Geochemistry*, 21(10), pp. 1692–1714.

Poraj-Górska, A. I., Żarczyński, M. J., Ahrens, A., Enters, D., Weisbrodt, D. and Tylmann, W. (2017) 'Impact of historical land use changes on lacustrine sedimentation recorded in varved sediments of Lake Jaczno, northeastern Poland', *Catena*.

Putkinen, N., Lunkka, J. P., Ojala, A. E. K. and Kosonen, E. (2011) 'Deglaciation history and age estimate of the Younger Dryas end moraines in the Kalevala region, NW Russia', *Quaternary Science Reviews*, 30, pp. 3812–3822.

Rach, O., Brauer, A., Wilkes, H. and Sachse, D. (2014) 'Delayed hydrological response to Greenland cooling at the onset of the Younger Dryas in western Europe', *Nature Geoscience*. Nature Publishing Group, 7(2), pp. 109–112.

Rahmstorf, S. (2002) 'Ocean circulation and climate during the past 120,000 years', *Nature*, 419, pp. 207–214.

Rahmstorf, S., Crucifix, M., Ganopolski, A., Goosse, H., Kamenkovich, I., Knutti, R., Lohmann, G., Marsh, R., Myzak, L. A., Wang, Z. and Weaver, A. J. (2005) 'Thermohaline circulation hysteresis: A model intercomparison', *Geophysical*

Research Letters, 32(23), pp. 1–5.

Rasmussen, S. O., Andersen, K. K., Svensson, A. M., Steffensen, J. P., Vinther, B. M., Clausen, H. B., Siggaard-Andersen, M. L., Johnsen, S. J., Larsen, L. B., Dahl-Jensen, D., Bigler, M., Röthlisberger, R., Fischer, H., Goto-Azuma, K., Hansson, M. E. and Ruth, U. (2006) 'A new Greenland ice core chronology for the last glacial termination', *Journal of Geophysical Research Atmospheres*, 111(6), pp. 1–16.

Rasmussen, S. O., Bigler, M., Blockley, S. P., Blunier, T., Buchardt, S. L., Clausen, H. B., Cvijanovic, I., Dahl-Jensen, D., Johnsen, S. J., Fischer, H., Gkinis, V., Guillevic, M., Hoek, W. Z., Lowe, J. J., Pedro, J. B., Popp, T., Seierstad, I. K., Steffensen, J. P., Svensson, A. M., Vallelonga, P., Vinther, B. M., Walker, M. J. C., Wheatley, J. J. and Winstrup, M. (2014) 'A stratigraphic framework for abrupt climatic changes during the Last Glacial period based on three synchronized Greenland ice-core records: Refining and extending the INTIMATE event stratigraphy', *Quaternary Science Reviews*. Elsevier Ltd, 106, pp. 14–28.

Rasmussen, S. O., Vinther, B. M., Clausen, H. B. and Andersen, K. K. (2007) 'Early Holocene climate oscillations recorded in three Greenland ice cores', *Quaternary Science Reviews*, 26(15–16), pp. 1907–1914.

Regnéll, C., Hafliðason, H., Mangerud, J. and Svendsen, J. I. (2019) 'Glacial and climate history of the last 24 000 years in the Polar Ural Mountains, Arctic Russia, inferred from partly varved lake sediments', *Boreas*, 48(2), pp. 432–443.

Reimer, P. J., Baillie, M. G. L., Bard, E., Bayliss, A., Beck, J. W., Bertrand, C. J. H., Blackwell, P. G., Buck, C. E., Burr, G. S., Cutler, K. B., Damon, P. E., Edwards, R. L., Fairbanks, R. G., Friedrich, M., Guilderson, T. P., Hogg, A. G. and Hughen, C. E. (2004) 'INTCAL04 terrestrial radiocarbon age calibration, 0–26 cal kyr BP.', *Radiocarbon*, 46, pp. 1029–1058.

Reimer, P. J., Bard, E., Bayliss, A., Beck, J. W., Blackwell, P. G., Ramsey, C. B., Buck, C. E., Cheng, H., Edwards, R. L., Friedrich, M., Grootes, P. M., Guilderson, T. P., Hafliðason, H., Hajdas, I., Hatté, C., Heaton, T. J., Hoffmann, D. L., Hogg, A. G., Hughen, K. A., Kaiser, K. F., Kromer, B., Manning, S. W., Niu, M., Reimer, R. W., Richards, D. A., Scott, E. M., Southon, J. R., Staff, R. A., Turney, C. S. M. and Plicht, J. van der (2013) 'IntCal13 and Marine13 radiocarbon age calibration curves 0–50,000 years cal BP', *Radiocarbon*, 55(4), pp. 1869–1887.

Renberg, I. and Segerström, U. (1981) 'The initial points on a shoreline displacement curve for southern Västerbotten, dated by varve- counts of lake sediments', in Königsson, L.-K. and Paabo, K. (eds) *Florilegium Florinis Dedicatum*, pp. 174–176.

- Ridge, J. C., Balco, G., Bayless, R. L., Beck, C. C., Carter, L. B., Dean, J. L., Voytek, E. B. and Wei, J. H. (2012) 'The new north american varve chronology: A precise record of southeastern laurentide ice sheet deglaciation and climate, 18.2-12.5 KYR BP, and correlations with greenland ice core records', *American Journal of Science*, 312(7), pp. 685–722.
- Ringberg, B. (1971) 'Glacialgeologi och isavsmältning i östra Blekinge', *Sveriges Geologiska Undersökning*, C 661, pp. 1–174.
- Ringberg, B. (1979) 'Varve chronology of the glacial sediments in Blekinge and northeastern Skåne, southeastern Sweden', *Boreas*, 8, pp. 209–215.
- Ringberg, B. (1984) 'Cyclic lamination in proximal varves reflecting the length of summers during the Late Weichsel in southernmost Sweden', in Mörner, N.-A. and Karlén, W. (eds) *Climate Changes on a Yearly to Millennial Basis*. Reidel Publishing Company, pp. 57–62.
- Ringberg, B. (1991) 'Late Weichselian clay varve chronology and glaciolacustrine environment during deglaciation in southeastern Sweden', *Sveriges Geologiska Undersökning*, Ca-79, pp. 1–42.
- Ringberg, B., Björck, J. and Hang, T. (2003) 'Correlation of stadial and interstadial events in the south Swedish glacial varves with the GRIP oxygen isotope record', *Boreas*, 32(2), pp. 427–435.
- Ringberg, B. and Erlström, M. (1999) 'Micromorphology and petrography of Late Weichselian glaciolacustrine varves in southeastern Sweden', *Catena*, 35(2–4), pp. 147–177.
- Ringberg, B., Hang, T. and Kristiansson, J. (2002) 'Local clay-varve chronology in the Karlskrona-Hultsfred region, southeast Sweden', *GFF*.
- Ringberg, B. and Rudmark, L. (1985) 'Varve chronology based upon glacial sediments in the area between Karlskrona and Kalmar, southeastern Sweden', *Boreas*, 14, pp. 107–110.
- Rinterknecht, V. R., Clark, P. U., Raisbeck, G. M., Yiou, F., Bitinas, A., Brook, E. J., Marks, L., Zelcs, V., Lunkka, J.-P., Pavlovskaya, I. E., Piotrowski, J. A. and Raukas, A. (2006) 'The last deglaciation of the southeastern sector of the Scandinavian Ice Sheet', *Science*, 311, pp. 1449–1453.
- Rinterknecht, V. R., Clark, P. U., Raisbeck, G. M., Yiou, F., Brook, E. J., Tschudi, S. and Lunkka, J. P. (2004) 'Cosmogenic ^{10}Be dating of the Salpausselkä I Moraine in southwestern Finland', *Quaternary Science Reviews*, 23(23–24), pp. 2283–2289.

- Rinterknecht, V. R., Marks, L., Piotrowski, J. A., Raisbeck, G. M., Yiou, F., Brook, E. J. and Clark, P. U. (2005) 'Cosmogenic ^{10}Be ages on the Pomeranian moraine, Poland', *Boreas*, 34(3), pp. 186–191.
- Robock, A. (2000) 'Volcanic Eruptions and Climate', *Reviews of Geophysics*, 38(2), pp. 191–219.
- Ronnert, L. (1989) 'The deglaciation of the Berghem area, south-western Sweden', *Chalmers Tekniska Högskola – Göteborgs Universitet, Geologiska Institutionen Publ. A*, 64, pp. 1–14.
- Rothwell, G. and Croudace, I. (2015) 'Micro-XRF Studies of Sediment Cores: A Perspective on Capability and Application in the Environmental Sciences', in Rothwell, G. and Croudace, I. (eds) *Micro-XRF Studies of Sediment Cores, Development in Paleoenvironmental Research*. Springer, pp. 1–21.
- Ruddiman, W. F. (1997) *Tectonic Uplift and Climate Change*. Boston, MA: Springer.
- Ruddiman, W. F. (2006a) 'Orbital changes and climate', *Quaternary Science Reviews*, 25(23), pp. 3092–3112.
- Ruddiman, W. F. (2006b) 'Ice-driven CO_2 feedback on ice volume', *Climate of the Past*, 2, pp. 43–55.
- Ruddiman, W. F. and Kutzbach, J. E. (1991) 'Plateau uplift and climate change', *Scientific American*, 264(3), pp. 66–75.
- Ruddiman, W. F., Raymo, M. E., Lamb, H. H. and Andrews, J. T. (1988) 'Northern Hemisphere Climate Regimes During the Past 3 Ma : Possible Tectonic Connections [and Discussion]', *Philosophical Transactions of the Royal Society of London. Series B, Biological Science*, 318(1191), pp. 411–430.
- Ruddiman, W. F., Raymo, M. and McIntyre, A. (1986) 'Matuyama 41,000-year cycles: North Atlantic Ocean and northern hemisphere ice sheets', *Earth and Planetary Science Letters*, 80(1–2), pp. 117–129.
- Rupf, I. and Radons, G. (2004) 'New approaches for automated data processing of annually laminated sediments', *Nonlinear Processes in Geophysics*, 11, pp. 599–607.
- Saarnisto, M. and Saarinen, T. (2001) 'Deglaciation chronology of the scandinavian ice sheet from the Lake Onega Basin to the Salpausselkä End Moraines', *Global and Planetary Change*, 31, pp. 387–405.
- Saks, T., Kalvans, A. and Zelcs, V. (2012) 'OSL dating of Middle Weichselian age shallow basin sediments in Western Latvia, Eastern Baltic', *Quaternary Science Reviews*, 44, pp. 60–68.

- Sandgren, P., Snowball, I. F., Hammarlund, D. and Risberg, J. (1999) 'Stratigraphic evidence for a high marine shore-line during the Late Weichselian deglaciation on the Kullen Peninsula, southern Sweden', *Journal of Quaternary Science*, 14, pp. 223–237.
- Sauramo, M. (1918) 'Geochronologische Studien über die spätglaziale Zeit in Südfinnland', *Fennia*, 41, pp. 1–44.
- Sauramo, M. (1923) 'Studies on Quaternary varve sediments in southern Finland', *Bulletin Commission geologique*, 44(1), p. 164.
- Sauramo, M. (1929) 'The Quaternary geology of Finland', *Bulletin de la Commission géologique de Finlande*, 86, p. 110.
- Schenk, F., Väiliranta, M., Muschitiello, F., Tarasov, L., Heikkilä, M., Björck, S., Brandefelt, J., Johansson, A. V., Näslund, J. O. and Wohlfarth, B. (2018) 'Warm summers during the Younger Dryas cold reversal', *Nature Communications*. Springer US, 9(1).
- Schenk, F. and Vinuesa, R. (2019) 'Results in Engineering Enhanced large-scale atmospheric flow interaction with ice sheets at high model resolution', *Results in Engineering*. Elsevier Ltd, 3(June), p. 100030.
- Schlolaut, G., Marshall, M. H., Brauer, A., Nakagawa, T., Lamb, H. F., Staff, R. A., Bronk Ramsey, C., Bryant, C. L., Brock, F., Kossler, A., Tarasov, P. E., Yokoyama, Y., Tada, R. and Haraguchi, T. (2012) 'An automated method for varve interpolation and its application to the Late Glacial chronology from Lake Suigetsu, Japan', *Quaternary Geochronology*, 13, pp. 52–69.
- Schlolaut, G., Staff, R. A., Brauer, A., Lamb, H. F., Marshall, M. H., Bronk Ramsey, C. and Nakagawa, T. (2018) 'An extended and revised Lake Suigetsu varve chronology from ~50 to ~10 ka BP based on detailed sediment micro-facies analyses', *Quaternary Science Reviews*, 200.
- Schoning, K. (2001) 'Marine conditions in middle Sweden during the Late Weichselian and Early Holocene as inferred from foraminifera, Ostracods and stable isotopes', *Quaternaria Series A:8 thesis*, Stockholm University, Department of Physical Geography and Quaternary Geology, p. 26.
- Schoning, K. (2002) 'Palaeohydrography and marine conditions in the south-western part of the Vänern basin during the Younger Dryas and Early Preboreal', *GFF*, 124, pp. 1–12.
- Schoning, K. and Wastegård, S. (1999) 'Ostracod assemblages in late Quaternary

varved glaciomarine clay of the Baltic Sea Yoldia stage in eastern middle Sweden', *Marine Micropaleontology*, 37, pp. 313–321.

Seierstad, I. K., Abbott, P. M., Bigler, M., Blunier, T., Bourne, A. J., Brook, E., Buchardt, S. L., Buizert, C., Clausen, H. B., Cook, E., Dahl-Jensen, D., Davies, S. M., Guillevic, M., Johnsen, S. J., Pedersen, D. S., Popp, T. J., Rasmussen, S. O., Severinghaus, J. P., Svensson, A. and Vinther, B. M. (2014) 'Consistently dated records from the Greenland GRIP, GISP2 and NGRIP ice cores for the past 104ka reveal regional millennial-scale $\delta^{18}\text{O}$ gradients with possible Heinrich event imprint', *Quaternary Science Reviews*, 106, pp. 29–46.

Shackleton, N. J. and Opdyke, N. D. (1973) 'Oxygen isotope and Paleomagnetic stratigraphy of equatorial Pacific core V28-238: Oxygen Isotope Temperatures and Ice Volumes on a 105 Year and 106 Year Scale', *Quaternary Research*, 55, pp. 39–55.

Shaw, J. and Archer, J. (1978) 'Winter turbidity current deposits in Late Pleistocene glaciolacustrine varves, Okanagan Valley, British Columbia, Canada', *Boreas*, 7, pp. 123–130.

Siddall, M., Chappell, J. and Potter, E. K. (2007) '7. Eustatic sea level during past interglacials', *Developments in Quaternary Science*, 7(C), pp. 75–92.

Sigvaldason, G. E. (2002) 'Volcanic and tectonic processes coinciding with glaciation and crustal rebound: An early Holocene rhyolitic eruption in the Dyngjufjöll volcanic centre and the formation of the Askja caldera, north Iceland', *Bulletin of Volcanology*, 64(3–4), pp. 192–205.

Singh, H. A., Battisti, D. S. and Bitz, C. M. (2014) 'A heuristic model of dansgaard-oeschger cycles. part i: Description, results, and sensitivity studies', *Journal of Climate*, 27(12), pp. 4337–4358.

Słowiński, M., Zawiska, I., Ott, F., Noryśkiewicz, A. M., Plessen, B., Apolinarska, K., Rzodkiewicz, M., Michczyńska, D. J., Wulf, S., Skubała, P., Kordowski, J., Błaszkiwicz, M. and Brauer, A. (2017) 'Differential proxy responses to late Allerød and early Younger Dryas climatic change recorded in varved sediments of the Trzechowskie palaeolake in Northern Poland', *Quaternary Science Reviews*, 158, pp. 94–106.

Smith, N. D. and Ashley, G. M. (1985) 'Proglacial lacustrine environment', in Ashley, G. M., Shaw, J. and Smith, N. D. (eds) *Glacial Sedimentary Environments*. Tulsa, OK: Society of Palaeontologists and Mineralogists, pp. 135–212.

Sørensen, R. (1979) 'Late Weichselian deglaciation in the Oslofjord area, south

Norway', *Boreas*, 8, pp. 241–246.

Sørensen, R. (1992) 'The physical environment of Late Weichselian deglaciation of the Oslofjord region, southeastern Norway', *Sveriges Geologiska Undersökning Ca*, 81, pp. 339–346.

Srokosz, M. A. and Bryden, H. L. (2015) 'Observing the Atlantic Meridional Overturning Circulation yields a decade of inevitable surprises', *Science*, 348(6241).

St-Onge, G., Mulder, T., Francus, P. and Long, B. (2007) 'Continuous physical properties of cored marine sediments', in Hillaire-Marcel, C. and De Varnal, A. (eds) *Developments in Marine Geology*. Volume 1. Amsterdam: Elsevier, pp. 63–98.

Stauch, G. and Gualtieri, L. (2008) 'Late Quaternary glaciations in northeastern Russia', *Journal of Quaternary Science*, 23, pp. 545–558.

Steffensen, J. P., Andersen, K. K., Bigler, M., Clausen, H. B., Dahl-Jensen, D., Fischer, H., Goto-Azuma, K., Hansson, M., Johnsen, S. J., Jouzel, J., Masson-Delmotte, V., Popp, T., Rasmussen, S. O., Rothlisberger, R., Ruth, R., Stauffer, B., Siggaard-Andersen, M. L., Sveinbjornsdottir, A. E., Svensson, A. and White, J. W. (2008) 'High-resolution Greenland ice-core data show abrupt climate change happens in few years', *Science*, 321(5889), pp. 680–684.

Stevens, R. (1985) 'Glaciomarine varves in late-Pleistocene clays near Göteborg, southwestern Sweden', *Boreas*, 14, pp. 127–132.

Stocker, T. F. and Wright, D. G. (1991) 'Rapid transitions of the ocean's deep circulation induced by changes in surface water fluxes', 351, pp. 729–732.

Stolpe, P. (1911) 'En sydsvensk israndlinje och dess geografiska betydelse.', *Göteborgs kungliga vetenskaps och vitterhetssamhälles handlingar*, Fjärde föl.

Stroeven, A. P., Hättstrand, C., Kleman, J., Heyman, J., Fabel, D., Fredin, O., Goodfellow, B. W., Harbor, J. M., Jansen, J. D., Olsen, L., Caffee, M. W., Fink, D., Lundqvist, J., Rosqvist, G. C., Strömberg, B. and Jansson, K. N. (2016) 'Deglaciation of Fennoscandia', *Quaternary Science Reviews*, 147, pp. 91–121.

Strömberg, B. (1969) 'Den mellansvenska israndzonen. Översiktlig naturvårdsinventering med hänsyn till kvartärgeologisk-naturgeografiska värden', *Stockholms Universitet, Naturgeografiska Institutionen, Forskningsrapport*, 6, p. 56.

Strömberg, B. (1983) 'The Swedish varve chronology', in Ehlers, J. (ed.) *Glacial Deposits in North- West Europe*. Balkema, Rotterdam, pp. 97–105.

Strömberg, B. (1985) 'Revision of the lateglacial Swedish varve chronology', *Boreas*, 14(2), pp. 101–105.

- Strömberg, B. (1989) 'Late Weichselian deglaciation and clay-varve chronology in east-central Sweden', *Sveriges Geologiska Undersökning*, Ca 73, pp. 1–70.
- Strömberg, B. (1990) 'A connection between the clay varve chronologies in Sweden and Finland', *Annales Academiae Scientiarum Fennicae A III*, 153, p. 32.
- Strömberg, B. (1992) 'The final stage of the Baltic Ice Lake', *Sveriges Geologiska Undersökning*, Ca 81, pp. 347–353.
- Strömberg, B. (1994) 'Younger Dryas deglaciation at Mt. Billingen, and clay varve dating of the Younger Dryas/Preboreal transition', *Boreas*, 23, pp. 177–193.
- Stuiver, M., Reimer, P. J., Bard, E., Beck, J. W., Burr, G. S., Hughen, K. A., Kromer, B., McCormac, G., van der Plicht, J. and Spurk, M. (1998) 'INTCAL98 Radiocarbon age calibration, 24,000-0 cal BP', *Radiocarbon*, 40(1), pp. 1041–1083.
- Sturm, M. (1979) 'Origin and composition of clastic varves', in Schlüchter, C. (ed.) *Moraines and Varves: Origin, Genesis, Classification*. Rotterdam, The Netherlands: A.A. Balkema, pp. 281–285.
- Sun, Y., Clemens, S. C., An, Z. and Yu, Z. (2006) 'Astronomical timescale and palaeoclimate implication of stacked 3.6-Myr monsoon records from the Chinese Loess Plateau', *Quaternary Science Reviews*, 25, pp. 33–48.
- Sun, Y., Kutzbach, J., An, Z., Clemens, S., Liu, Z., Liu, W., Liu, X., Shi, Z., Zheng, W., Liang, L., Yan, Y. and Li, Y. (2015) 'Astronomical and glacial forcing of East Asian summer monsoon variability', *Quaternary Science Reviews*, 115, pp. 132–142.
- Svendsen, J. I., Alexanderson, H., Astakhov, V. I., Demidov, I., Dowdeswell, J. A., Funder, S., Gataullin, V., Henriksen, M., Hjort, C., Houmark-Nielsen, M., Hubberten, H. W., Ingólfsson, Ó., Jakobsson, M., Kjær, K. H., Larsen, E., Lokrantz, H., Lunkka, J. P., Lyså, A., Mangerud, J., Matiouchkov, A., Murray, A., Möller, P., Niessen, F., Nikolskaya, O., Polyak, L., Saarnisto, M., Siegert, C., Siegert, M. J., Spielhagen, R. F. and Stein, R. (2004) 'Late Quaternary ice sheet history of northern Eurasia', *Quaternary Science Reviews*, 23(11–13), pp. 1229–1271.
- Svensson, N.-O. (1989) 'Late Weichselian and early Holocene shore displacement in the central Baltic, based on stratigraphical and morphological records from eastern Småland and Gotland, Sweden', *Quaternary Sciences, Department of Geology, Lund University*, 195 s(LUNDQUA Thesis).
- Swärd, H., O'Regan, M., Ampel, L., Ananyev, R., Chernykh, D., Floden, T., Greenwood, S. L., Kylander, M. E., Mörth, C. M., Preto, P. and Jakobsson, M. (2016) 'Regional deglaciation and postglacial lake development as reflected in a 74 m

sedimentary record from Lake Vättern, southern Sweden', *Gff. Taylor Francis*, 138(2), pp. 336–354.

Talling, P. J., Masson, D. G., Sumner, E. J. and Malgesini, G. (2012) 'Subaqueous sediment density flows: Depositional processes and deposit types', *Sedimentology*, 59, pp. 1937–2003.

Tarasov, L., Dyke, A. S., Neal, R. M. and Peltier, W. R. (2012) 'A data-calibrated distribution of deglacial chronologies for the North American ice complex from glaciological modeling', *Earth and Planetary Science Letters*. Elsevier B.V., 315–316, pp. 30–40.

Teller, J. T., Leverington, D. W. and Mann, J. D. (2002) 'Freshwater outburst to the oceans from glacial Lake Agassiz and their role in climate change during the last deglaciation', *Quaternary Science Reviews*, 21, pp. 879–887.

Thomas, G. S. P. and Connell, R. J. (1985) 'Iceberg drop, dump and grounding structures from Pleistocene glaciolacustrine sediments, Scotland', *Journal of Sedimentary Research*, 55, pp. 243–249.

Thornalley, D. J. R., Elderfield, H. and McCave, I. N. (2010) 'Intermediate and deep water paleoceanography of the northern North Atlantic over the past 21,000 years', *Paleoceanography*, 25.

Thornalley, D. J. R., Oppo, D. W., Ortega, P., Robson, J. I., Brierley, C. M., Davis, R., Hall, I. R., Moffa-Sanchez, P., Rose, N. L., Spooner, P. T., Yashayaev, I. and Keigwin, L. D. (2018) 'Anomalously weak Labrador Sea convection and Atlantic overturning during the past 150 years', *Nature*, 556(7700), pp. 227–230.

Tiljander, M., Ojala, A., Saarinen, T. and Snowball, I. (2002) 'Documentation of the physical properties of annually laminated (varved) sediments at a sub-annual to decadal resolution for environmental interpretation', *Quaternary International*. Pergamon, 88(1), pp. 5–12.

Timms, R. G. O. (2016) 'Developing a refined tephrostratigraphy for Scotland, and constraining abrupt climatic oscillations of the Last Glacial-Interglacial Transition (ca 16-8 ka BP) using high resolution tephrochronologies', *PhD Thesis, University of London*, p. 494.

Timms, R. G. O., Matthews, I. P., Lowe, J. J., Palmer, A. P., Weston, D. J., MacLeod, A. and Blockley, S. P. E. (2019) 'Establishing tephrostratigraphic frameworks to aid the study of abrupt climatic and glacial transitions: a case study of the Last Glacial-Interglacial Transition in the British Isles (c. 16-8 ka BP)', *Earth-Science Reviews*. Elsevier, 192(November 2018), pp. 34–64.

- Timms, R. G. O., Matthews, I. P., Palmer, A. P., Candy, I. and Abel, L. (2017) 'A high-resolution tephrostratigraphy from Quoyloo Meadow, Orkney, Scotland: Implications for the tephrostratigraphy of NW Europe during the Last Glacial-Interglacial Transition', *Quaternary Geochronology*, 40, pp. 67–81.
- Tjallingii, R., Röhl, U., Kölling, M. and Bickert, T. (2007) 'Influence of the water content on X-ray fluorescence corescanning measurements in soft marine sediments', *Geochemistry, Geophysics, Geosystems*, 8(2), pp. 1–12.
- Tomkins, J. D., Lamoureux, S. F. and Sauchyn, D. J. (2008) 'Reconstruction of climate and glacial history based on a comparison of varve and tree-ring records from Mirror Lake, Northwest Territories, Canada', *Quaternary Science Reviews*, 27, pp. 1426–1441.
- Torres, V., Hooghiemstra, H., Lourens, L. and Tzedakis, P. C. (2013) 'Astronomical tuning of long pollen records reveals the dynamic history of montane biomes and lake levels in the tropical high Andes during the Quaternary', *Quaternary Science Reviews*, 63, pp. 59–72.
- Tröften, P. E. and Mörner, N. A. (1997) 'Varved clay chronology as a means of recording paleoseismic events in southern Sweden', *Journal of Geodynamics*, 24(1–4), pp. 249–258.
- Tschudi, S., Ivy-Ochs, S., Schüchter, C., Kubik, P. and Rainio, H. (2000) '10Be dating of Younger Dryas Salpausselkä I formation in Finland', *Boreas*, 29, pp. 287–293.
- Tylmann, K., Rinterknecht, V. R., Woźniak, P. P., Bourlès, D., Schimmelpfennig, I., Guillou, V., Aumaître, G. and Keddadouche, K. (2019) 'The Local Last Glacial Maximum of the southern Scandinavian Ice Sheet front: Cosmogenic nuclide dating of erratics in northern Poland', *Quaternary Science Reviews*, 219, pp. 36–46.
- Tylmann, W., Kinder, M., Żarczyński, M. and Poraj-Górska, A. (2017) 'Preliminary characteristics of laminations in recent sediments from lakes Kamendul and Perty in the Suwałki Landscape Park, northeastern Poland', *Limnological Review*, 16(4), pp. 237–245.
- Waelbroeck, C., Duplessy, J.-C., Michel, E., Labeyrie, L., Paillard, D. and Duprat, J. (2001) 'The timing of the last deglaciation in North Atlantic climate records', *Nature*, 412, pp. 724–727.
- Waldemarson, D. (1986) 'Weichselian lithostratigraphy, depositional processes and deglaciation pattern in the southern Vättern basin, south Sweden', *LUNDQUA Thesis*, 17, p. 128.

- Walker, M. J. C. (2005) *Quaternary Dating Methods*. Wiley.
- Walker, M. J. C., Berkelhammer, M., Björck, S., Cwynar, L. C., Fisher, D. A., Long, A. J., Lowe, J. J., Newnham, R. M., Rasmussen, S. O. and Weiss, H. (2012) 'Formal subdivision of the Holocene Series/Epoch: A Discussion Paper by a Working Group of INTIMATE (Integration of ice-core, marine and terrestrial records) and the Subcommittee on Quaternary Stratigraphy (International Commission on Stratigraphy)', *Journal of Quaternary Science*, 27(7), pp. 649–659.
- Walker, M. J. C., Björck, S., Lowe, J. J., Cwynar, L. C., Johnsen, S., Knudsen, K. L. and Wohlfarth, B. (1999) 'Isotopic "events" in the GRIP ice core: A stratotype for the Late Pleistocene', *Quaternary Science Reviews*, 18(10–11), pp. 1143–1150.
- Walker, M. J. C., Bryant, C., Coope, G. R., Harkness, D. D., Lowe, J. J. and Scott, E. M. (2001) 'Towards a radiocarbon chronology for the Lateglacial: sample selection strategies', *Radiocarbon*, 43, pp. 1007–1020.
- Wastegård, S. (2002) 'Early to middle Holocene silicic tephra horizons from the Katla volcanic system, Iceland: new results from the Faroe Islands', *Journal of Quaternary Science*, 17, pp. 723–730.
- Wastegård, S. (2005) 'Late Quaternary tephrochronology of Sweden: A review', *Quaternary International*, 130(1), pp. 49–62.
- Wastegård, S., Andrén, T., Sohlenius, G. and Sandgren, P. (1995) 'Different phases of the Yoldia Sea in the north-western Baltic Proper', *Quaternary International*, 27(C), pp. 121–129.
- Wastegård, S., Björck, S., Possnert, G. and Wohlfarth, B. (1998) 'Evidence for the occurrence of Vedde Ash in Sweden: radiocarbon and calendar age estimates', *Journal of Quaternary Science*, 13(3), pp. 271–274.
- Wastegård, S., Gudmundsdóttir, E. R., Lind, E. M., Timms, R. G. O., Björck, S., Hannon, G. E., Olsen, J. and Rundgren, M. (2018) 'Towards a Holocene tephrochronology for the Faroe Islands, North Atlantic', *Quaternary Science Reviews*, 195, pp. 195–214.
- Wastegård, S. and Schoning, K. (1997) 'Calcareous fossils and radiocarbon dating of the saline phase of the Yoldia Sea stage', *GFF*, 119, pp. 245–248.
- Wastegård, S., Turney, C. S. M., Lowe, J. J. and Roberts, S. J. (2000) 'New discoveries of the Vedde Ash in southern Sweden and Scotland', *Boreas*, 29, pp. 72–78.
- Weber, M. E., Reichelt, L., Kuhn, G., Pfeiffer, M., Korff, B., Thurow, J. and Ricken, W.

- (2010) 'BMPix and PEAK tools: New methods for automated laminae recognition and counting-Application to glacial varves from Antarctic marine sediment', *Geochemistry, Geophysics, Geosystems*, 11, pp. 1–18.
- Wedel, P. O. (1971) 'The Gothenburg moraine', *Geologiska Föreningens i Stockholm Förhandlinga*, 93, pp. 525–536.
- Weltje, G. J., Bloemsa, M. R., Tjallingii, R., Heslop, D., Röhl, U. and Croudace, I. W. (2015) 'Prediction of Geochemical Composition from XRF Core Scanner Data: A New Multivariate Approach Including Automatic Selection of Calibration Samples and Quantification', in Croudace, I. W. and Rothwell, R. G. (eds) *Micro-XRF Studies of Sediment Cores, Developments in Palaeoenvironmental Research*. Berlin Heidelberg: Springer, pp. 507–534.
- Weltje, G. J. and Tjallingii, R. (2008) 'Calibration of XRF core scanners for quantitative geochemical logging of sediment cores: Theory and application', *Earth and Planetary Science Letters*, 274(3–4), pp. 423–438.
- Whittington, G., Fallick, A. E. and Edwards, K. J. (1996) 'Stable oxygen isotope and pollen records from eastern Scotland and a consideration of late-glacial and early Holocene climate change for Europe', *Journal of Quaternary Science*, 11, pp. 327–340.
- Wohlfarth, B. (1996) 'The chronology of the last termination: A review of radiocarbon-dated, high-resolution terrestrial stratigraphies', *Quaternary Science Reviews*, 15(4), pp. 267–284.
- Wohlfarth, B., Björck, S. and Cato, I. (1996) 'A new middle Holocene varve diagram from the river Ångermanälven, northern Sweden: indications for a possible error in the Holocene varve chronology', *Boreas*, 37, pp. 347–359.
- Wohlfarth, B., Björck, S., Cato, I. and Possnert, G. (1997) 'A new middle Holocene varve diagram from the river Ångermanälven, northern Sweden: Indications for a possible error in the Holocene varve chronology', *Boreas*, 26(4), pp. 347–353.
- Wohlfarth, B., Björck, S., Holmqvist, B., Lemdahl, G. and Ising, J. (1994) 'Ice recession and depositional environment in the Blekinge archipelago of the Baltic Ice Lake', *GFF*, 116, pp. 3–12.
- Wohlfarth, B., Björck, S. and Possnert, G. (1995) 'The Swedish time scale: a potential calibration tool for the radiocarbon time scale during the Late Weichselian', *Radiocarbon*, 37(2), pp. 347–359.
- Wohlfarth, B., Björck, S., Possnert, G. and Holmquist, B. (1998) 'An 800-year long,

radiocarbon-dated varve chronology from south-eastern Sweden', *Boreas*, 27(4), pp. 243–257.

Wohlfarth, B., Björck, S., Possnert, G., Lemdahl, G., Brunnberg, L., Ising, J., Olsson, S. and Svensson, N.-O. (1993) 'AMS dating Swedish varved clays of the last glacial/interglacial transition and the potential difficulties of calibrating Late Weichselian "absolute" chronologies', *Boreas*, 22(2), pp. 113–128.

Wohlfarth, B., Blaauw, M., Davies, S. M., Andersson, M., Wastegård, S., Hormes, A. and Possnert, G. (2006) 'Constraining the age of Lateglacial and early Holocene pollen zones and tephra horizons in southern Sweden with Bayesian probability methods', *Journal of Quaternary Science*, 21(4), pp. 321–334.

Wohlfarth, B. and Possnert, G. (2000) 'AMS radiocarbon measurements from the Swedish varved clays', *Radiocarbon*, 42(3), pp. 323–334.

Wooling, T., Lockwood, M., Masato, G., Bell, C. and Gray, L. (2010) 'Enhanced signature of solar variability in Eurasian winter climate.', *Geophysical Research Letters*, 37, p. L20805.

Wulf, S., Dräger, N., Ott, F., Serb, J., Appelt, O., Gudmundsdóttir, E., van den Bogaard, C., Słowiński, M., Błaszkiwicz, M. and Brauer, A. (2016) 'Holocene tephrostratigraphy of varved sediment records from Lakes Tiefer See (NE Germany) and Czechowskie (N Poland)', *Quaternary Science Reviews*, 132, pp. 1–14.

Wulf, S., Ott, F., Słowiński, M., Noryskiewicz, A. M., Dräger, N., Martin-Puertas, C., Czymzik, M., Neugebauer, I., Dulski, P., Bourne, A. J., Błaszkiwicz, M. and Brauer, A. (2013) 'Tracing the Laacher See Tephra in the varved sediment record of the Trzechowskie palaeolake in central Northern Poland', *Quaternary Science Reviews*, 76, pp. 129–139.

Żarczyński, Maurycy, Szymańda, J. and Tylmann, W. (2019) 'Grain-Size Distribution and Structural Characteristics of Varved Sediments from Lake Żabińskie (Northeastern Poland)', *Quaternary*, 2(1), p. 8.

Żarczyński, M., Tylmann, W. and Goslar, T. (2018) 'Multiple varve chronologies for the last 2000 years from the sediments of Lake Żabińskie (northeastern Poland) – Comparison of strategies for varve counting and uncertainty estimations', *Quaternary Geochronology*, 47(June), pp. 107–119.

Żarczyński, M., Wacnik, A. and Tylmann, W. (2019) 'Tracing lake mixing and oxygenation regime using the Fe/Mn ratio in varved sediments: 2000 year-long record of human-induced changes from Lake Żabińskie (NE Poland)', *Science of the Total Environment*.

Zillén, L. M., Wastegård, S. and Snowball, I. F. (2002) 'Calendar year ages of three mid-Holocene tephra layers identified in varved lake sediments in west central Sweden', *Quaternary Science Reviews*, 21(14–15), pp. 1583–1591.

Zolitschka, B., Brauer, A., Negendank, J. F. ., Stockhausen, H. and Lang, A. (2000) 'Annually dated late Weichselian continental paleoclimate record from the Eifel, Germany', *Geology*, 28(9), pp. 783–786.

Zolitschka, B., Francus, P., Ojala, A. E. K. and Schimmelmann, A. (2015) 'Varves in lake sediments - a review', *Quaternary Science Reviews*, 117, pp. 1–41.

Appendices

For appendices please refer to the included memory stick.